



Investigation of human C12orf65 and mtRF1, members of the mitochondria translation release factor family

Ana-Mădălina Ion

BSc, MRes

Supervisors:

Professor Zofia Chrzanowska-Lightowers

Professor Robert Lightowers

This thesis is submitted for the degree of

Doctor of Philosophy

Wellcome Centre for Mitochondrial Research,

Biosciences Institute,

Newcastle University

June 2021

Abstract

Mitochondria contain their own DNA (mtDNA) and protein synthesis machinery. Human mtDNA encodes for two rRNAs, 22 tRNAs and 13 polypeptides. Those polypeptides are subunits of complexes involved in oxidative phosphorylation and their translation is driven by the mitoribosome. Translation consists of four phases - initiation, elongation, termination and mitoribosome recycling- with translation factors required at each step.

My work focused on termination, which requires the action of release factors. In human mitochondria, there are four proteins in the release factor family: mRF1a, ICT1, mtRF1 and C12orf65. Termination occurs once a release factor recognises a stop codon (UAA or UAG) in the A site of the mitoribosome. This changes the mitoribosome conformation, inducing the polypeptide's release. Only mtRF1a recognizes stop codons and terminates translation for all the 13 mtDNA-encoded polypeptides. However, all four members contain the GGQ motif involved in peptide release. ICT1 is a component of the mitoribosome large subunit. My research focused on the functions of mtRF1 and C12orf65 which are yet unknown, although it was observed that patients with *C12orf65* pathogenic variants show impaired mitochondria translation.

My research hypothesis was that C12orf65 and mtRF1 initiate termination in mitoribosomes that stall during translation. Stalling has multiple causes including mRNA pseudoknot structures, defective tRNA or insufficient amino acids. Release factors would recognise mRNA targets to the same effect as stop codons.

To test this, I aimed to identify mRNA targets specific to mtRF1. I also aimed to detect proteins C12orf65 interacted with to confirm whether it was involved in termination. I used cross-linking and immunoprecipitation of the mitoribosome, BioID2 and CRISPR-Cas9 techniques. Thus, I obtained and characterized two BioID2 cell lines that helped locate C12orf65 interactors involved in translation. Moreover, I established a C12orf65 knockout cell line that presents a growth defect, further demonstrating C12orf65's involvement in cell viability.

Acknowledgements

First, I would like to thank my supervisors Prof. Zofia Chrzanowska-Lightowlers and Prof. Robert Lightowlers for choosing me to pursue this PhD project, which enabled me to grow both professionally and personally. In particular, I am grateful to Prof. Zofia Chrzanowska-Lightowlers for guidance in preparing this manuscript, proof-reading of chapters and inspiring suggestions.

Moreover, I would like to thank my collaborators, Professor Hans Spelbrink (Radboud Centre for Mitochondrial Medicine, Radboud University Medical Centre, Nijmegen, the Netherlands), and Prof. Matthias Trost (Newcastle University Biosciences Institute) for granting me the use of their resources for my mass-spectrometry results.

Towards Professor Hans Spelbrink, I am grateful for welcoming me in his lab during my REMIX secondment and for making me feel that I belong there despite the short time. From the Radboud team, I owe a big ‘thank you’ to my REMIX colleague Alisa Potter and to Dr. Alfredo Cabrera-Orefice for technical help, help with troubleshooting and for fruitful discussions about my BioID2 samples. Thank you as well Helga, Selma, Andrei, Madhuria and Zeinab for kindly enhancing my cultural exchange.

Towards Professor Matthias Trost, I am grateful for the advice regarding my mass-spectrometry samples and making himself available for further questions. From his group, I would further mention Dr. Frédérique Lamoliatte and Dr. Akshada Gajbhiye who analysed my BioID samples and patiently answered my unclarities. Special thanks to Anetta, Paul, Abeer and Tiaan, for their kindness and friendship. Sharing a meal or a hot chocolate became beautiful memories.

To all the past and present members of the Lightowlers lab- thank you for your support during my PhD journey. I am privileged I met you. Thank you, Yasmin- you were the best buddy and a constant inspiration. Thank you Agata for your help with the mtRF1 project and for all the time you offered me, despite being in your final months of contract. Thank you, Reece, for help with cloning and cell transfection for the BioID2 project and thank you Christin for suggestions about data analysis. Thank you, Rawaa, Fei, Richard, and Shreya: you provided an immense emotional support, as well as excellent technical expertise when I needed it, throughout the entire project, even from outside the lab.

Gareth, Iffath, Olga and Viviana- it was a pleasure being your colleague. Although we were not involved in the same projects, all the chats we had broadened my horizon. I cannot forget ‘the

boys from the office'- Adam, Matt and Shane. Thank you for making me laugh on rainy days, for teaching me Geordie and for creating a joyful atmosphere.

My gratitude extends towards all the past and present members of the MRG, towards everyone who helped me with all the little things that make a difference. Thank you, Tom and Katja for advice about BioID2 and for being open to discuss science, teaching and the right to ask questions. Thank you, Monika and Amy Vincent, for encouragement and technical support in key moments. Thank you Nuria and Marie Eleni for technical tips and believing in me when I didn't. Thank you, Rui Ban, Tianhong, Kamil, Darroch, Ash, Fiona, Nana-Jane and Peta for being such good friends through my ups and downs. Thank you, Julie and Lyndsey, for making me a part of the public engagement events you organized.

Thank you, all my REMIX colleagues, and especially Petra, Mujeeb, Vivek and Pamella for all the beautiful memories we made together during our meetings and conferences.

A big thank you goes as well to the members of the Newcastle University Archery Club. You taught me consistency, resilience and, most importantly, to keep shooting even if I knew my arrow would never reach the target. Special thanks to Catherine for always being by my side, on the range and outside it.

To my parents and my sister – there are no words to thank you enough. You rebuilt me from small pieces, you kept my ambition alive and made every difficulty seem small. You surrounded me with love and showed an immense patience through all those years, especially during my writing period. I dedicate this thesis to you.

Last but not least, I would like to thank the European Union's Horizon 2020 research and innovation programme for funding this project. I was a Marie Curie ITN REMIX fellow, under the Marie Skłodowska-Curie grant agreement No 721757. Their funding made my PhD possible and the training I received contributed to my growth as a scientist.

Table of Contents

Abstract.....	iii
Acknowledgements.....	iv
Table of Contents	vi
List of Figures.....	ix
List of Tables	xii
Abbreviations	xiv
Chapter 1 Introduction.....	1
1.1 Mitochondria-general aspects	2
1.1.1 Origin and evolution of mitochondria.....	2
1.1.2 Mitochondria structure	3
1.2 Import of nuclear-encoded mitochondrial proteins.....	8
1.3 Mitochondrial functions	11
1.3.1 The oxidative phosphorylation process (OXPHOS).....	11
1.3.2 Other mitochondrial functions	16
1.4 Mitochondrial genome	21
1.5 Replication of mtDNA	23
1.6 Transcription and post-transcriptional modifications in human mitochondria	26
1.7 Translation in human mitochondria	31
1.7.1 Human mitochondrial ribosome.....	32
1.7.2 Initiation	37
1.7.3 Elongation	41
1.7.4 Termination	44
1.7.5 Recycling	50
1.8 Defects of translation in mitochondria.....	52
1.8.1 Defects of mtDNA	52
1.8.2 Defective mt-tRNA modifying enzymes	53
1.8.3 Defects of the mitochondrial ribosome	54
1.8.4 Defects of translation initiation	55
1.8.5 Defects of translation elongation	56
1.8.6 Defects of C12orf65.....	57
1.9 Systems of translation quality control.....	59
1.9.1 Ribosome recycling and rescue mechanisms in bacteria	59
1.9.2 Ribosome recycling and rescue mechanisms in eukaryotes	62
1.10 Research hypothesis	64
Chapter 2 Materials and Methods.....	67
2.1 Cell Culture	68
2.1.1 mtRF1 cell line.....	68
2.1.2 BioID2-HA cell lines	68
2.1.3 Cell harvesting	68
2.1.4 Cell storage and thawing.....	69
2.1.5 Mycoplasma testing	69

2.1.6 DSP treatment.....	69
2.1.7 Stable transfection of HEK293-Flp-In T-RExTM cells	70
2.1.8 KO of C12orf65 in HEK293-Flp-In T-RExTM cells.....	71
2.2 Bacterial culture.....	72
2.2.1 Bacterial propagation and storage	72
2.2.2 Transformation of competent cells	72
2.2.3 Detection of transformed bacterial clones	73
2.2.4 Preparation of glycerol stocks	73
2.3 Protein Manipulations.....	73
2.3.1 Cell lysis	73
2.3.2 Measurement of protein concentration	73
2.3.3 Isokinetic Sucrose Gradient Separation.....	74
2.3.4 Precipitation of sucrose gradient fractions with TCA	75
2.3.5 Immunoprecipitation with anti-FLAG antibody	76
2.3.6 Mitochondria isolation.....	77
2.3.7 Mitochondrial subfractionation	78
2.3.8 Precipitation of postmitochondrial supernatant with TCA.....	79
2.3.9 SDS-PAGE, western blotting and detection.....	80
2.4 DNA Manipulations	82
2.4.1 Extraction of plasmid DNA.....	82
2.4.2 Measurement of DNA concentration.....	82
2.4.3 DNA agarose electrophoresis	82
2.4.4 Digestion of the pcDNA5/FRT/TO/C12orf65-BioID2-HA vector	83
2.4.5 Gel extraction of C12orf65 DNA fragment.....	83
2.4.6 Digestion of the pcDNA5/FRT/TO/Linker-BioID2-HA vector.....	83
2.4.7 Dephosphorylation of the pcDNA5/FRT/TO/Linker-BioID2-HA vector.....	83
2.4.8 Purification and precipitation of plasmid DNA.....	84
2.4.9 Ligation of the Linker plasmid with the C12orf65 fragment	84
2.4.10 Ligation of gRNA targeting C12orf65 into PX458.....	85
2.4.11 Plasmid sequencing	86
2.4.12 DNA extraction from HEK cells	86
2.4.13 Real-time PCR (qPCR).....	87
2.4.14 Sequencing of potential C12orf65 KO HEK cells	88
2.5 RNA Manipulations.....	89
2.5.1 RNA isolation from the FLAG-immunoprecipitate	89
2.5.2 RNA isolation from the eluate after FLAG-immunoprecipitation	90
2.5.3 Reverse-transcription.....	90
2.6 Sample preparation for mass-spectrometry	90
2.6.1 Isolation of crude mitochondria for mass-spectrometry analysis.....	90
2.6.2 Mitochondria lysis and streptavidin-affinity purification performed at Newcastle University	92
2.6.3 Mitochondria lysis and streptavidin-affinity purification performed at Radboud University, Nijmegen, The Netherlands	94

Chapter 3 Investigation of mtRF1 function.....	96
3.1 Introduction	97
3.2 Results.....	103
3.2.1 mtRF1 transiently interacts with the mitoribosome	103
3.2.2 Mitochondrial mRNA can be isolated by mtRF1-FLAG immunoprecipitation ...	107
3.3 Discussion	115
Chapter 4 C12orf65-BioID2-HA, an initial cell model to investigate C12orf65 function using the BioID2 approach.....	119
4.1 Introduction	120
4.2 Results.....	125
4.3 Discussion	134
Chapter 5 C12orf65-Linker-BioID2-HA, a second cell model to investigate C12orf65 function using the BioID2 approach.....	136
5.1 Introduction	137
5.2 Results.....	138
5.3 Discussion	146
Chapter 6 Identification of C12orf65 protein interactors by BioID2	152
6.1 Introduction	153
6.2 Results.....	159
6.2.1 Non-specific biotinylation versus endogenously biotinylated proteins	159
6.2.2 Interactors identified in Newcastle	162
6.2.3 Interactors identified in Nijmegen, the Netherlands	174
6.2.4 Interactors identified in Newcastle using an improved methodology.....	177
6.1 Discussion	192
6.1.1 Comparison between the mass-spectrometry experiments	192
6.1.2 Integration of C12orf65 BioID2 results in the context of current research	199
Chapter 7 Generation of a C12orf65 knockout cell line using CRISPR-Cas9	205
7.1 Introduction	206
7.2 Results.....	212
7.3 Discussion	229
Chapter 8 Final conclusions	233
Appendices.....	238
Appendix-A Antibodies.....	239
Appendix-B Plasmid details	241
Appendix-B.1 C12orf65-BioID2-HA in pcDNA5/FRT/TO (6,305bp)	241
Appendix-B.2 Linker-BioID2-HA in pcDNA5/FRT/TO (6,064bp)	243
Appendix-B.3 C12orf65-Linker-BioID2-HA in pcDNA5/FRT/TO (6,512bp)	244
Appendix-B.4 PX458 C12orf65 gRNA (9,290bp).....	245
Appendix-C Details of mass-spectrometry experiments	246
Appendix-D Sequencing of KO control HEK clones.....	251
Appendix-E List of hits identified using BioID2	256
References	294

List of Figures

Figure 1-1. Original electron micrographs of mitochondria from an acinar cell of rat pancreas	4
Figure 1-2. Structure of a mitochondrion	5
Figure 1-3. Structure of the MICOS-SAM complex in human mitochondria.....	7
Figure 1-4. The mammalian oxidative phosphorylation system	13
Figure 1-5. Structure of mitochondrial ATP synthase.....	15
Figure 1-6. Iron metabolism in mitochondria.....	17
Figure 1-7. Nutrient catabolism in the mitochondrial matrix	18
Figure 1-8. Mitochondrial involvement in urea cycle	19
Figure 1-9. The human mitochondrial genome	22
Figure 1-10. Replication of mtDNA.....	25
Figure 1-11. Transcription of mtDNA.....	27
Figure 1-12. Structure of the human mitochondrial ribosome	35
Figure 1-13. Translation initiation in mammalian mitochondria (taken from (Khawaja et al., 2020)).....	40
Figure 1-14. Translation elongation in mammalian mitochondria	42
Figure 1-15. Alignment between bacterial and human mitochondrial release factors	46
Figure 1-16. Translation termination and recycling in mammalian mitochondria.....	48
Figure 2-1. Binding sites for the primers used for <i>C12orf65</i> sequencing after KO	89
Figure 3-1. Alignment between RF1 from <i>E. coli</i> and release factors from different organisms (taken from (Zhang and Spremulli, 1998)).....	97
Figure 3-2. Alignment of bacterial RF with human mtRF1 and mtRF1a	101
Figure 3-3. Chemical structure of DSP	103
Figure 3-4. Separation of mtRF1-FLAG HEK cell lysate on sucrose gradient.....	105
Figure 3-5. Separation of cross-linked mtRF1-FLAG HEK cell lysate on sucrose gradient ..	106
Figure 3-6. Mean Ct values obtained after RNA isolation from immunoprecipitate	108
Figure 3-7. Test of FLAG expression in the samples used for immunoprecipitation	109
Figure 3-8. Proof of principle: elution of mtRF1-FLAG.....	111
Figure 3-9. Immunoprecipitation followed by elution of mtRF1-FLAG in DSP treated samples	113
Figure 3-10. Mean Ct values obtained after RNA isolation from eluate.....	114
Figure 3-11. Elution of mtRF1-FLAG using different batches of FLAG peptides	115

Figure 4-1. Principle of biotinylation and promiscuous biotin-ligases	122
Figure 4-2. Determination of HA expression in C12orf65-BioID2-HA HEK cells	125
Figure 4-3. Mitochondria isolation from C12orf65-BioID2-HA HEK cells	128
Figure 4-4. Cartoon depicting the steps of mitochondria subfractionation.....	129
Figure 4-5. Example of mitochondria subfractionation of a C12orf65-BioID2-HA clone ...	130
Figure 4-6. Comparison between mitochondria subfractionation of different C12orf65-BioID2-HA clones.....	131
Figure 4-7. Sucrose gradient of C12orf65-BioID2-HA clone 3	133
Figure 5-1. Cartoon depicting the cloning of C12orf65-Linker-BioID2-HA plasmid	139
Figure 5-2. Production of the C12orf65 DNA fragment.....	140
Figure 5-3. Digestion and dephosphorylation of the Linker-BioID2-HA pcDNA5 plasmid	141
Figure 5-4. Digestion of the C12orf65-Linker-BioID2-HA pcDNA5 plasmid	142
Figure 5-5. Determination of HA expression in C12orf65-Linker-BioID2-HA HEK cells ..	143
Figure 5-6. Isolation and subfractionation of mitochondria from C12orf65-Linker-BioID2-HA HEK cells	144
Figure 5-7. Sucrose gradient of C12orf65-Linker-BioID2-HA clone 9	146
Figure 5-8. Examples of different phenotypes observed in Linker clones	148
Figure 5-9. C12orf65 primary sequence	150
Figure 6-1. Application of the BioID2 principle to study C12orf65	158
Figure 6-2. Biotin induces non-specific biotinylation in BioID2 clones	160
Figure 6-3. Western blot results for NCL1 affinity purification.....	164
Figure 6-4. Filtering steps performed in Perseus version 1.6.5.0	166
Figure 6-5. Analysis of BioID2 interactors identified in NCL1	168
Figure 6-6. Biotinylated MRPs identified in NCL1	171
Figure 6-7. Localization of NCL1 hits on mtSSU	173
Figure 6-8. Western blot results for the Nijmegen affinity purification	176
Figure 6-9. Western blot results for NCL2 affinity purification.....	178
Figure 6-10. Analysis of COX8-MTS-BioID2-HA interactors identified in NCL2.....	180
Figure 6-11. Analysis of C12orf65-BioID2-HA interactors identified in NCL2	184
Figure 6-12. Biotinylated MRPs identified in C12orf65-BioID2-HA (NCL2) samples	186
Figure 6-13. Analysis of C12orf65-Linker-BioID2-HA interactors identified in NCL2	189
Figure 6-14. Biotinylated MRPs identified for C12orf65-Linker-BioID2-HA (NCL2).....	191
Figure 6-15. Structure of MRPL34 (close view)	195
Figure 6-16. Primary sequence of human C12orf65	198

Figure 7-1. Mechanism of action for CRISPR-Cas9	208
Figure 7-2. Localisation of the CRISPR-Cas9 target sequence on the reference C12orf65 ..	213
Figure 7-3. The results of DNA sequencing of mutant cells from sample 5N- allele 1	216
Figure 7-4. Predicted polypeptide encoded by 5N allele 1	217
Figure 7-5. The results of DNA sequencing of mutant cells from sample 5N- allele 2	218
Figure 7-6. Predicted polypeptide encoded by 5N allele 2	219
Figure 7-7. The results of DNA sequencing of mutant cells from sample 15N – allele 1	221
Figure 7-8. Predicted polypeptide encoded by 15N allele 1	222
Figure 7-9. DNA sequencing and polypeptide prediction of sample 15N – allele 2.....	223
Figure 7-10. The results of DNA sequencing of mutant cells from sample 22F – allele 1	226
Figure 7-11. Predicted polypeptide encoded by 22F allele 1	227
Figure 7-12. The results of DNA sequencing of mutant cells from sample 22F- allele 2.....	228
Figure 7-13. Predicted polypeptide encoded by 22F allele 2	229
Figure Apx 1. Map of the C12orf65-BioID2-HA/pcDNA5/FRT/TO plasmid	242
Figure Apx 2. Map of the Linker-BioID2-HA/pcDNA5/FRT/TO plasmid	243
Figure Apx 3. Map of the C12orf65-Linker-BioID2-HA/pcDNA5/FRT/TO plasmid	244
Figure Apx 4. Map of the C12orf65 gRNA PX458 plasmid.....	245
Figure Apx 5. Test of trypsinization efficiency performed in Nijmegen	249
Figure Apx 6. Total ion chromatogram of BSA positive control.....	250
Figure Apx 7. Binding sites of the C12orf65 primers used for sequencing	251
Figure Apx 8. Sequencing results of 4E, control sample for CRISPR-Cas9	252
Figure Apx 9. Alignment of 4E control sequence against the human genome	253
Figure Apx 10. Sequencing results of 12E, control sample for CRISPR-Cas9	254
Figure Apx 11. Alignment of 12E control sequence against the human genome	255

List of Tables

Table 1-1. Details of several complete ribosomal structures resolved up to current date	34
Table 2-1. Lysis buffer	73
Table 2-2. Bradford standard curve	74
Table 2-3. Sucrose gradient buffer.....	74
Table 2-4. Lysis buffer for sucrose gradient	75
Table 2-5. Dissociation buffer	76
Table 2-6. Homogenisation buffer 1 (HB1) complete	77
Table 2-7. Homogenisation buffer 2	79
Table 2-8. SDS-PAGE gel components (1 gel with 0.75 mm spacers)	80
Table 2-9. Solutions used for SDS-PAGE	81
Table 2-10. Ligation mixes for Linker plasmid and C12orf65 fragment.....	85
Table 2-11. Combined digestion/ligation reaction mix	86
Table 2-12. Primers used for pcDNA5 plasmid sequencing.....	86
Table 2-13. Sequences of primers used in Real Time PCR.....	87
Table 2-14. Profile and analysis condition for LightCycler® Nano software	88
Table 2-15. Sequences of primers used for sequencing of KO clones	88
Table 2-16. Hypotonic buffer.....	91
Table 2-17. 2.5X MSH buffer	92
Table 2-18. 1X MSH buffer	92
Table 2-19. Mitochondria lysis buffer	93
Table 2-20. Wash Buffer 2.....	93
Table 5-1. Predicted MMPs for C12orf65	150
Table 6-1. Mammalian biotin-dependent carboxylases	161
Table 6-2. NCL1 biotinylated proteins identified by multiple UniProt codes.....	170
Table 6-3. Biotinylated proteins from NCL1 involved in mitochondrial gene expression....	171
Table 6-4. Biotinylated proteins identified in Nijmegen	175
Table 6-5. Biotinylated proteins from NCL2 involved in mitochondrial gene expression....	181
Table Apx 1. Primary antibodies used for western blotting in Newcastle University.....	239
Table Apx 2. Secondary antibodies used for western blotting in Newcastle University.....	240

Table Apx 3. Primary and secondary antibodies used for western blotting in Radboud University, Nijmegen, The Netherlands	240
Table Apx 4. Primers used for C12orf65 insert generation.....	241
Table Apx 5. Primers used for sequencing of the C12orf65 region after ligation	241
Table Apx 6. Primers used for generation of the <i>Linker-BioID2</i> insert	243
Table Apx 7. Biotinylated proteins identified by multiple UniProt codes in COX8-MTS control (NCL2)	246
Table Apx 8. Biotinylated proteins identified by multiple UniProt codes in C12orf65-BioID2 samples (NCL2).....	247
Table Apx 9. Biotinylated proteins identified by multiple UniProt codes in C12orf65-Linker-BioID2 samples (NCL2).....	248
Table Apx 10. NCL1 mitochondria	257
Table Apx 11. NCL1 adjacent.....	261
Table Apx 12. NCL2 COX8 mitochondria	267
Table Apx 13. NCL2 COX8 adjacent	271
Table Apx 14. NCL2 C12-BioID2 mitochondria.....	274
Table Apx 15. NCL2 C12-BioID2 adjacent.....	278
Table Apx 16. NCL2 C12-Linker-BioID2 mitochondria.....	282
Table Apx 17. NCL2 C12-Linker-BioID2 adjacent.....	289

Abbreviations

Å	Angstrom
<i>A. aeolicus</i>	<i>Aquifex aeolicus</i>
aa	Amino acid(s)
ABC	ATP-binding cassette
ACC	Acetyl-CoA carboxylase
ADP	Adenosine diphosphate
AGC	Automatic gain control
AIF	Apoptosis-inducing factor
APAF1	Protease activating factor 1
APEX	Ascorbic acid peroxidase
approx.	Approximatively
APS	Ammonium persulphate
ArfA	Alternative ribosome factor A
ArfB	Alternative ribosome factor B
Arg	Arginine
A-site	Aminoacyl-tRNA site within the ribosome
ATP	Adenosine triphosphate
ATPase	Adenosine triphosphatase
AURKAIP1	Aurora kinase A interacting protein 1
BFDR	Bayesian false discovery rate
BioID	Proximity-dependent biotin identification
BN-PAGE	Blue Native polyacrylamide gel electrophoresis
b	base(s)
bp	Base pair(s)
BSA	Bovine serum albumin
CBB	Coomassie brilliant blue
cDNA	Complementary DNA
CL	Cell lysate
CO ₂	Carbon dioxide
CoA	Coenzyme A
COX	Cytochrome c oxidase
CPEO	Chronic progressive external ophthalmoplegia
CRISPR	Clustered regularly interspaced short palindromic repeats
crRNA	CRISPR-derived RNA
Cryo-EM	Cryo-electron microscopy
CsCl	Cesium chloride
Ct	Threshold cycle
C-terminus	Carboxyl-terminus
Cu	Copper
Cyt c	Cytochrome c
DAP3	Death associated protein 3
ddH ₂ O	Double distilled water

DEPC	Diethyl pyrocarbonate
dH ₂ O	Distilled water
D-loop	Displacement loop
DMEM	Dulbecco's modified Eagle's medium
DMSO	Dimethyl-sulphoxide
DNA	Deoxyribonucleic acid
dNTP	Deoxynucleotide triphosphate
Doxy	Doxycycline
dsDNA	double-stranded DNA
DSB	Double stranded breaks
DSP	Dithiobis (succinimidyl propionate)
DTT	Dithiothreitol
<i>E. coli</i>	<i>Escherichia coli</i>
e.g.	For example
EDTA	Ethylene diamine tetra-acetic acid
EF(-G/-Ts/-Tu)	Elongation factor (-G/-Ts/-Tu)
EGTA	Ethylene glycol tetra-acetic acid
EJC	Exon junction complex
EK	Eukaryotic
EndoG	Endonuclease G
ER	Endoplasmic reticulum
eRF1/3	Eukaryotic release factor 1/3
E-site	Exit site within the ribosome
ex.	Exon
ETC	Electron transport chain
FACS	Fluorescence activated cell sorting
FAD	Flavin adenine dinucleotide
FADH ₂	Reduced flavin-adenine dinucleotide
FBS	Foetal bovine serum
Fe-S	Iron-Sulphur
fMet	Formylmethionine
FRT	Flp recombination target
g	Gram
g	Centrifugal force
GDP	Guanosine diphosphate
GFP	Green fluorescent protein
gRNA	Guide RNA
GTP	Guanosine triphosphate
GTPase	Guanosine triphosphatase
h	Hour
H	Heavy strand
HCl	Hydrochloric acid
HDR	Homology-directed repair
HEK	Human embryonic kidney
HEK293T	Human embryonic kidney 293 Flip-In TM /TREx TM cells
HEPES	4-(2-hydroxyethyl)-1-piperazineethanesulfonic acid

HPLC	High-performance liquid chromatography
HRP	Horseradish peroxidase
<i>H. sapiens</i>	<i>Homo sapiens</i>
Hsp	Heat-shock protein
HSP	Heavy strand promoter
HUPRA	HyperUricemia, pulmonary hypertension, renal failure and alkalosis
IBM	Inner boundary membrane
ICS	Intracristal space
ICT1	Immature colon carcinoma transcript 1
IF	Initiation factor
IMM	Inner mitochondrial membrane
IMS	Intermembrane space
In	Input
kb	Kilo base
KCl	Potassium chloride
kDa	Kilo-Dalton
KO	Knockout
L	Light strand
LB	Luria-Bertani
LBSL	Leukoencephalopathy with brainstem and spinal cord involvement
LC MS/MS	Liquid chromatography - tandem mass spectrometry
LRPPRC	Leucine-rich pentatricopeptide-repeat containing protein
LSP	Light strand promoter
LTBL	Leukoencephalopathy involving the thalamus and brainstem with high lactate
Lys	Lysine
M	Molar
MAP	Mitogen-activated protein
MCC	3-methylcrotonyl-CoA carboxylase
MCS	Multiple cloning site
MELAS	Mitochondrial encephalomyopathy with lactic acidosis and stroke-like episodes
Met	Methionine
mg	Milligram
Mg(CH ₃ COO) ₂	Magnesium acetate
MgCl ₂	Magnesium chloride
MIB	Mitochondrial intermembrane space bridging complex
MICOS	Mitochondrial contact site and cristae organizing system
MIDD	Maternally inherited diabetes and deafness
min	Minute(s)
MMP	Matrix metalloproteinase
MPP	Mitochondrial processing peptidase
MRG	Mitochondrial RNA granules
mRNA	Messenger RNA
MRP	Mitochondria ribosomal protein
MRPL/S	Mitochondria ribosomal protein of the large/small subunit
mt	Mitochondria
mtDNA	Mitochondrial genome

MTERF1	Mitochondrial termination factor 1
MTFMT	Mitochondrial methionyl-tRNA formyltransferase
mtLSU	mitochondrial large subunit
MTPAP	Mitochondrial poly(A) polymerase
MTRES1	Mitochondrial transcription rescue factor 1
MTS	Mitochondria targeting sequence
mtSSB	Mitochondrial single-stranded binding protein
mtSSU	Mitochondrial small subunit
MW	Molecular weight
MWM	Molecular weight marker
N-terminus	Amino-terminus
NaCl	Sodium chloride
NAD	Nicotinamide adenine dinucleotide
NEAA	Non-essential amino acids
ng	Nanogram
NGD	No-go decay
NH ₄ Cl	Ammonium chloride
NHEJ	Non-homologous end joining
NHS	N-hydroxysuccinimide
nm	Nanometer
NMD	Nonsense-mediated decay
NP-40	Nonidet P-40, octyl phenoxy-polyethoxy-ethanol
NSD	Non-stop decay
NT	siRNA non-targeting negative control
O _H	Origin of replication for the heavy strand
O _L	Origin of replication for the light strand
OMM	Outer mitochondrial membrane
Opa1	Optic atrophy protein
ORF	Open-reading frame
OXPHOS	Oxidative phosphorylation
PAM	Protospacer adjacent motif
PBS	Phosphate buffered saline
PC	Pyruvate carboxylase
PCC	Propionyl-CoA carboxylase
PCR	Polymerase chain reaction
Phe	Phenylalanine
Pi	Inorganic phosphate
PMSF	Phenylmethylsulphonyl fluoride
PMSN	Postmitochondrial supernatant
POLRMT	Mitochondrial RNA polymerase
P-site	Peptidyl site within the ribosome
PTC	Peptidyl transferase center
PTH	Peptidyl-tRNA hydrolase
PTM	Post-translational modification
PVDF	Polyvinylidene difluoride
qPCR	Quantitative Polymerase chain reaction

RC	Respiratory complex
RF	Release factor(s)
RITOLS	Ribonucleotide incorporation throughout the lagging strand
RNase	Ribonuclease
ROS	Reactive oxygen species
rpm	Rotations per minute
RRF	Ribosome recycling factor
rRNA	Ribosomal RNA
S	Sedimentation coefficient
<i>S. cerevisiae</i>	<i>Saccharomyces cerevisiae</i>
<i>S. pombe</i>	<i>Schizosaccharomyces pombe</i>
SAM	Sorting and assembly machinery
SDH	Succinate dehydrogenase
SDS	Sodium dodecyl sulphate
SDS-PAGE	Sodium dodecyl sulphate polyacrylamide gel electrophoresis
sec	Seconds
siRNA	Small interfering RNA
SLIRP	Stem-loop interacting RNA-binding protein
SmpB	Small protein B
SN	Supernatant
STAGE	Stop And Go Extraction
STED	Stimulated emission depletion
<i>T. thermophilus</i>	<i>Thermus thermophilus</i>
Ta	Temperature of annealing
TAE	Tris-acetate EDTA
TALEN	Transcription activator-like effector nucleases
TBS-T	Tris-buffered saline and Tween-20
TCA	Trichloroacetic acid
TCA cycle	Tricarboxylic acid
TCEP	Tris(2-carboxyethyl)phosphine
TEFM	Transcription elongation factor of mitochondria
TEMED	N, N, N', N'-tetramethylethylene-diamine
Tet	Tetracycline
TFAM	Transcription factor A, mitochondrial
TFB2M	Transcription factor B2, mitochondrial
THF	Tetrahydrofolate
TIM	Translocase of the inner membrane
Tm	Temperature of melting
tmRNA	Transfer messenger tRNA
TOM	Translocase of the outer membrane
Top1	Topoisomerase 1
tracrRNA	Triggering pre-crRNA
Tris	2-Amino-2-hydroxymethyl-propane-1,3-diol
Triton-X 100	Polyethylene glycol p-(1,1,3,3-tetramethylbutyl)-phenyl ether
tRNA	Transfer RNA
TRNT1	tRNA nucleotidyl transferase 1

Tween-20	Polyoxyethylene sorbitanmonolaurate
U	Uracil
U	unit of enzymatic activity
Un	Unbound material
UTR(s)	Untranslated region(s)
UV	Ultraviolet
V	Volt
Val	Valine
VDAC	Voltage-dependent anion channel
WT	Wild-type
XIAP	X-linked inhibitor of apoptosis protein
ZFN	Zinc finger nucleases
μ	Micro

Chapter 1

Introduction

1.1 Mitochondria-general aspects

1.1.1 *Origin and evolution of mitochondria*

The discovery of mitochondria is attributed to the German pathologist Richard Altman who, in 1890, described ubiquitous structures vital for cellular function, that he considered ‘elementary organisms’ and named ‘bioblast’ (Altmann, 1890). The term ‘mitochondria’ was introduced in 1898, by Carl Benda, and was based on their shape during spermatogenesis, from the Greek ‘mithos’ (thread) and ‘chondros’ (granule) (Ernster and Schatz, 1981). Since 1898, numerous efforts were made to isolate them and understand their structure and function. Like other organelles, mitochondria research was strongly dependent on the development of scientific techniques and equipment. This research continued despite the Second World War and culminated with the discovery that mitochondria contain the enzymes of the citric acid cycle, fatty acid oxidation, and oxidative phosphorylation (1948-1951). Those reactions were deeply investigated during the 1950s, when the respiratory chain was reconstituted (Ernster and Schatz, 1981).

In the 1960s were made two remarkable discoveries: the existence of a mitochondrial DNA (mtDNA) as well as the independent translation system of the organelle (Nass and Nass, 1963). The presence of an extranuclear, functional DNA opened different avenues of research. The fact that mitochondria were not seen only as headquarters of biochemical reactions, but as genetic entities, raised the question of their origin. The 1970s were the scene of a fierce debate on this issue (Archibald, 2015, Sapp, 2007).

The first hypothesis on the mitochondria origin was emitted in 1970, when Lynn Margulis proposed that mitochondria evolved from bacteria that were engulfed by an eukaryotic host cell and lived in symbiosis (Margulis, 1970). This was contradicted by Richard Klein and Arthur Cronquist (Richard M. Klein, 1967) and by Tom Cavalier Smith (Cavalier-Smith, 1975), who believed that mitochondria had evolved within a photosynthetic eukaryotic cell, which in its turn had evolved from a cyanobacterium-like prokaryote. Several other authors adopted different points of view, which stayed in contradiction with both Margulis theory and with each other’s theories (Bogorad, 1975, Raff and Mahler, 1972, Uzzell and Spolsky, 1974). What they had in common was the belief that the endosymbiosis was too radical and that mitochondria evolved through intracellular compartmentalization. For this reason, in 1974 their theory was defined as ‘autogenous’ (Taylor, 1974).

During the past five decades, several discoveries came in support of the endosymbiotic theory. Early sequencing studies showed that rRNA from the mitochondria small ribosomal subunit had a significant sequence homology with rRNA from the bacterial small subunit, but not with the rRNA from the cytosolic small subunit (Bonen et al., 1977). Further investigations revealed that the sequence of mitochondria rRNA from the small subunit was similar with the homologous rRNA sequence from *Agrobacterium tumefaciens*, a species belonging to the α subdivision of the purple photosynthetic bacteria (Yang et al., 1985). The sequencing of the *Rickettsia prowazekii* genome, another member of the α subdivision, identified no genes necessary for glycolysis, but many genes involved in the tricarboxylic acid cycle and the respiratory-chain, two key functions of mitochondria (Andersson et al., 1998). Ultimately, the scientific community rejected the autogenous hypothesis, considering *Rickettsia*, the aetiologic agent of typhus and obligatory intracellular bacteria, as the closest relative of mitochondria (Gray, 2014).

Mitochondria evolution was characterised by adaptation of the α -protobacterium to the host, via endosymbiotic gene transfer (Burger et al., 2003) and genome reduction. Most mitochondrial proteins are encoded by the nuclear DNA, a phenomenon explained by a major loss of genes in the original α -proteobacteria and the transfer of those genes to the nucleus. The transfer possibly occurred through phagolysosomes or via RNA intermediates. When phagolysosomes degraded mitochondria, the DNA content was released and it integrated in the nuclear DNA (Thorsness and Fox, 1990). Studies on yeast revealed the possibility that gene transfer also functioned in the opposite direction: "a large number of novel mitochondrial genes were recruited from the nuclear genome to complement the remaining genes from the bacterial ancestor" (Karlberg et al., 2000). Elimination of redundant genes also played a role in evolution: either the genes were no longer needed because the host genome already contained similar genes, or they were not needed at all because the environment did not require them (Gray et al., 2001). The earliest organisms in terms of mitochondria evolution are considered the jakobid flagellates, with the protist *Reclinomonas americana* having the largest mitochondrial genome (69,034 bp), containing the highest number of genes, and the most similar to bacteria (Lang et al., 1997).

1.1.2 Mitochondria structure

The technical advances and development of electron microscopy lead to the publication of the official 'mitochondria portrait' by G.E. Palade, in 1952 (Palade, 1952). Palade studied mitochondria from various cell types and tissues of adult, new-born, or embryonic albino rats.

He was the first to show that mitochondria shape, structure and position within the cell depended on the tissue and cell type. On the high-resolution electron micrographs that he acquired, one can already distinguish the cristae, named 'lamellae' in the article (Figure 1-1). Mitochondria size and number are difficult to assess. Palade appreciated the mitochondria length between 7-12 μm and diameter between 0.2-12 μm , depending on cell type, but he noted

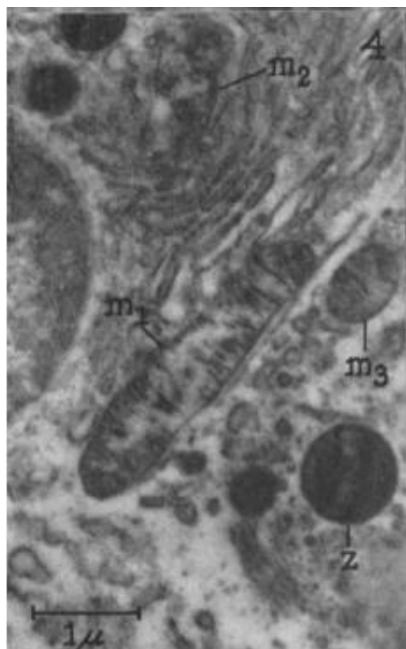


Figure 1-1. Original electron micrographs of mitochondria from an acinar cell of rat pancreas

Labels, as described by the author, are: m1 - obliquely sectioned mitochondrion; m2 and m3 - profiles of less well-preserved mitochondria; Z - sectioned zymogen granule. Magnification: X 21,000, X 15,750. (taken with permission from (Palade, 1952), RightsLink license number 4832540417223)

that the dimensions varied with the pH during fixation (Palade, 1952). Also, the organelles are highly dynamic, they fuse and split depending on their functional status or the cellular demand (Scott and Youle, 2010) and they form networks in the cytoplasm. It is therefore difficult to set a size or a number of mitochondria per cell, with few exceptions: the red blood cells, the parasitic protists, and some anaerobic organisms. The red blood cells lack mitochondria, which are eliminated via autophagy during reticulocyte maturation (Schweers et al., 2007). Several parasitic protists, like *Toxoplasma gondii*, *Plasmodium falciparum* and *Trypanosoma brucei*, contain a single mitochondrion per cell (Voleman and Doležal, 2019). Two anaerobic organisms have recently been discovered to either completely lack

mitochondria - microbial eukaryote *Monocercomonoides* sp. (Karnkowska et al., 2016) - or lack mtDNA and transcription/replication mechanisms - parasite Cnidaria *Henneguya salminicola* (Yahalomi et al., 2020). For all the other aerobic eukaryotes, mitochondrial content is referred to as mitochondria DNA copy number per cell or mitochondria mass (Robin and Wong, 1988).

The electron microscopy studies performed from 1952 onwards made possible the elucidation of the mitochondria structure (Figure 1-2). The organelle is delimited by two membranes, the outer membrane (OMM) and the inner membrane (IMM) separated by the intermembrane space (IMS). The IMM is folded into parallel structures that protrude towards the interior of the

organelle, perpendicular to the long axis, named cristae. The inner space enclosed by the cristae is the matrix (Palade, 1953, Sjöstrand, 1956).

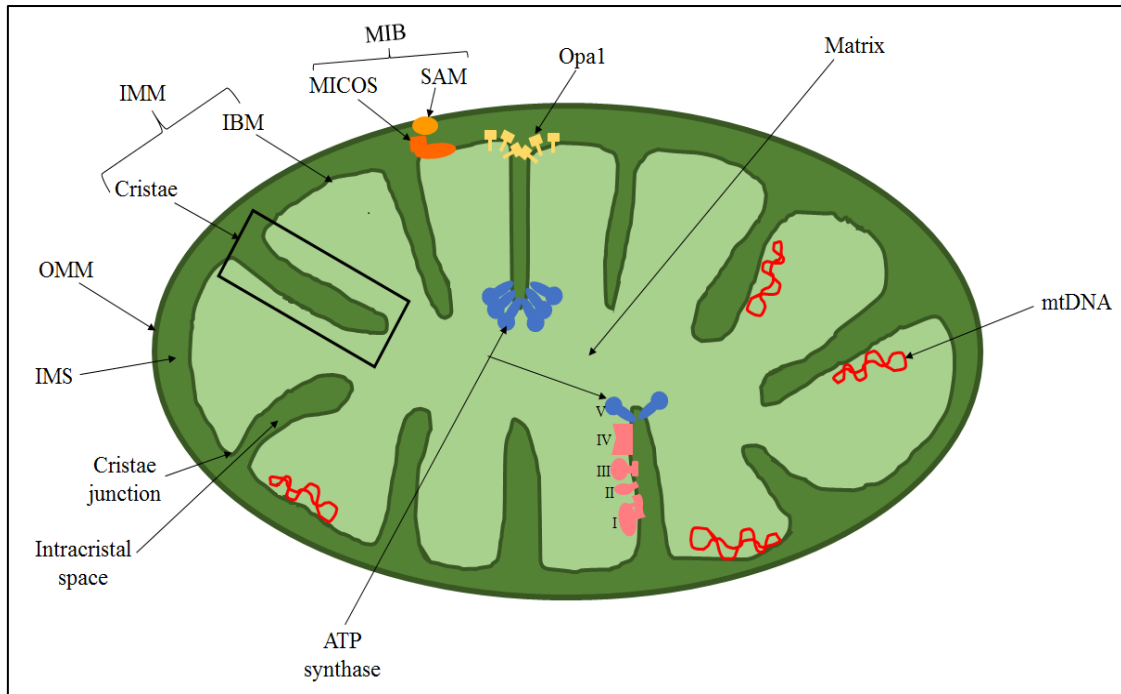


Figure 1-2. Structure of a mitochondrion

A 2D cartoon drawing depicting the mitochondrial compartments
 OMM-outer mitochondrial membrane, IMM-inner mitochondrial membrane, IMS-intermembrane space, IBM-inner boundary membrane, MICOS-mitochondrial contact site and cristae organizing system, SAM-sorting and assembly machinery, MIB-mitochondrial intermembrane space bridging complex, I-IV respiratory complexes, V-ATP synthase

The unfolded part of IMM, which runs parallel to the OMM, is the inner boundary membrane (IBM). If cristae unfolded, the IMM surface would be four times bigger than the OMM surface. This is particularly important, because IMM contains all the respiratory complexes and the ATP synthase involved in oxidative phosphorylation (OXPHOS). Therefore, a higher IMM surface results in a higher ATP production (Ikon and Ryan, 2017).

The regions where IBM becomes discontinuous and cristae begin invaginating are known as cristae junctions (Perkins et al., 1997, Perkins et al., 1998). Cristae junctions are narrow, tubular openings of approximately 12–40 nm diameter that delimitate the intracristal space (ICS) and might act as gates that regulate the flux of metabolites towards/from the cristae (Vogel et al., 2006, Kondadi et al., 2019). For example, during apoptosis, release of cytochrome *c* from the ICS to the cytosol leads to caspase activation and cell death (Scorrano et al., 2002).

The mitochondria sub-division allows each compartment to have its characteristic function. The biochemical composition and permeability of OMM and IMM differs. The OMM is relatively permeable; it contains the voltage-dependent anion channel (VDAC) that allows the passing of

cations (K^+ , Na^+ and Ca^{2+}) and anions (ATP, ADP, Pi) and of small metabolites to/from mitochondria. OMM does not have membrane potential but is voltage-dependent (Camara et al., 2017). In contrast, IMM contains transporter proteins specific for each ion or molecule that is necessary to cross to/from the matrix. It also contains all the respiratory complexes and the ATP synthase involved in OXPHOS. The respiratory complexes pump protons outside the IMM membrane and ATP synthase shuttles them back into the matrix, thus creating a membrane potential of 180 mV. A common feature that both OMM and IMM have is translocases, proteins involved in transport of nuclear encoded mitochondrial proteins from the cytosol to the correct mitochondrial compartment. The mitochondrial matrix is the compartment where two key metabolic processes take place: Krebs cycle and β -oxidation of fatty acids, both involved in ATP production. It also contains mtDNA and all the proteins necessary for mtDNA replication, transcription and subsequent translation (Kühlbrandt, 2015). The IMS contains proteins involved in apoptosis (apoptosis-inducing factor, Smac/DIABLO), scavenger of reactive oxygen species (Glutaredoxin 1, Sod1) and several types of cytochrome *c* molecules (Herrmann and Riemer, 2010).

The existence of cristae is strongly dependent on the protein complexes that maintain the IMM folded: the MICOS (mitochondrial contact site and cristae organizing system)-SAM (sorting and assembly machinery) complex (Huynen et al., 2016), Opa1 (Cogliati et al., 2013) and ATP synthase (Paumard et al., 2002). The MICOS-SAM complex and Opa1 act at the cristae junctions, while the ATP synthase acts at the tip of the cristae. The ATP synthase dimerises in an angular association of monomers (Dudkina et al., 2005), which induces the strong curvature of the IMM. The dimers arrange in long rows (approx. 1 μ m) at the apex of cristae (Strauss et al., 2008). They keep maintaining their function as part of the OXPHOS and their ATP production is not affected by their role in cristae structure, on the contrary: clustering of ATP synthase dimers and the IMM curvature generates a proton trap, which facilitates ATP production (Jonckheere et al., 2012).

The MICOS complex (also known as MINOS or MitOS) is a large protein system anchored in the IMM that stretches through the intermembrane space to reach the OMM (Kozjak-Pavlovic, 2017). In human, it has the size of 1,279 kDa (John et al., 2005) and consists of nine subunits, the largest ones being Mic60 and DnaJC11 (Figure 1-3). Mic60 (also known as mitofillin) resides in the intermembrane space, with only the N-terminus being embedded in the IMM, and localizes close to cristae junctions (Odgren et al., 1996, Jans et al., 2013).

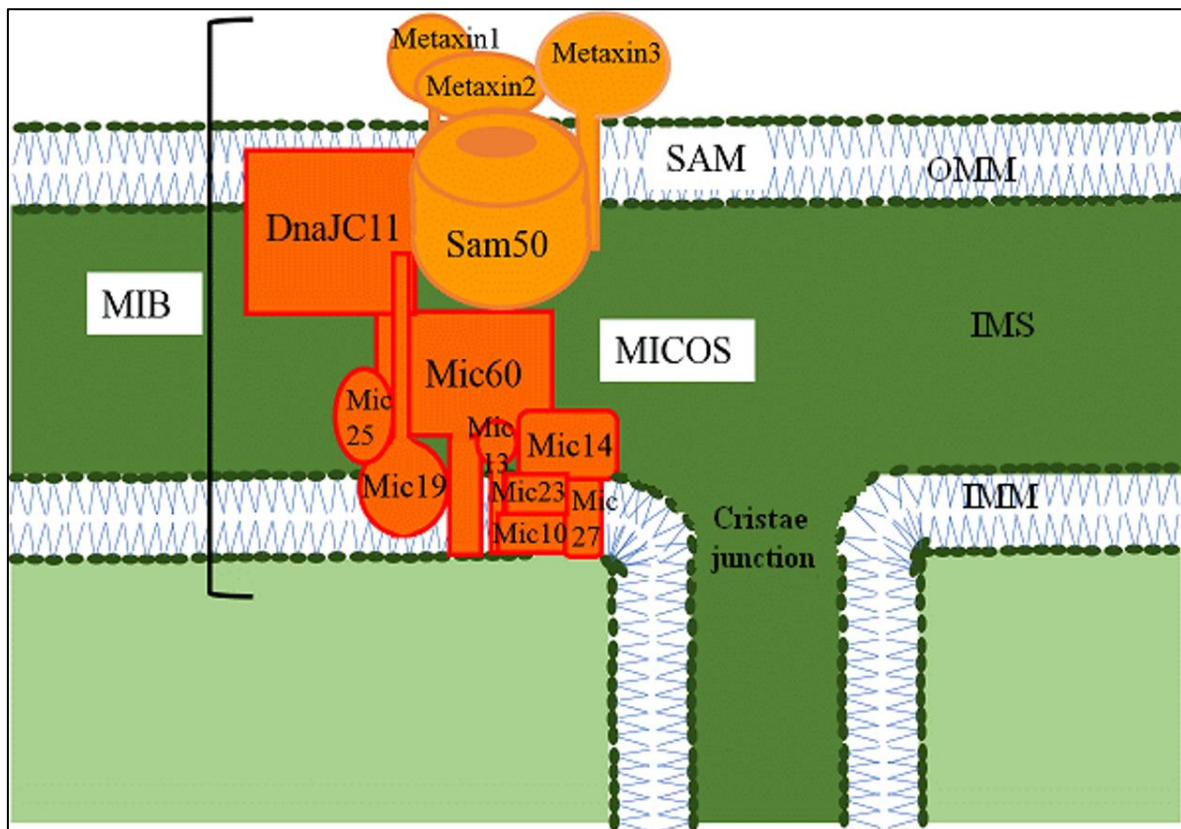


Figure 1-3. Structure of the MICOS-SAM complex in human mitochondria

Schematic representation of the interaction between MICOS and SAM complexes at the cristae junction; MICOS-mitochondrial contact site and cristae organizing system, SAM-sorting and assembly machinery, MIB-mitochondrial intermembrane space bridging complex

It is the central subunit of MICOS, strongly associated with mitochondria structure. Mic60 depletion causes the complete loss of cristae and the change of IMM shape, which appears like concentric membrane stacks (John et al., 2005). Mic60 and DnaJC11 interact with the Sam50 subunit of the sorting and assembly machinery (SAM), a protein complex embedded in the OMM that inserts β -barrel proteins in the OMM (Ott et al., 2012, Ott et al., 2015). It was shown that Mic60 knockdown also induces a decrease in the protein levels of the SAM complex subunits (Ott et al., 2015), as well as other MICOS subunits and Opa1 (Ding et al., 2015). Together, MICOS and SAM form the mitochondrial intermembrane space bridging complex (MIB) (Ott et al., 2012).

Opa1 is a complex protein with eight human isoforms (Del Dotto et al., 2018). Pathogenic variants in the *Opa1* gene cause autosomal dominant optic atrophy, a hereditary neuropathy resulting in progressive loss of sight. There are two types of Opa1 isoforms: long, which contain the N-terminal transmembrane domain and are inserted in the IMM, facing the IMS (Olichon et al., 2002); and short, which are soluble in the IMS (Cipolat et al., 2006). Although only 8% of Opa1 localizes near cristae junctions (Gripasic et al., 2004), its role in cristae remodelling is

crucial. Knockdown of Opa1 causes an aberrant cristae morphology in mammals and yeast (Olichon et al., 2002), while overexpression of Opa1 increases cristae number and reduces cristae width (Varanita et al., 2015). In addition to cristae maintenance, Opa1 plays a role in mitochondria dynamics: the long isoforms regulate IMM fusion (Cipolat et al., 2004, Song et al., 2009), while the short isoforms are associated with mitochondria fission (Anand et al., 2014).

1.2 Import of nuclear-encoded mitochondrial proteins

Only 1% of the approximatively 1,200 mitochondrial proteins are encoded by mtDNA (Calvo et al., 2016). The rest are encoded by nuclear DNA and need to be imported in the organelle in order to fulfill their function.

The SAM complex is only one of the five protein import pathways described in mitochondria. The classical import mechanism is the presequence pathway, specific to matrix and IMM proteins (Wiedemann and Pfanner, 2017). It is required by the majority of mitochondrial proteins (60%) and is based on the existence of a cleavable mitochondria targeting sequence at the N-terminus of the pre-protein (Vögtle et al., 2009). This cleavable sequence usually contains 15-50 aa and adopts the structure of an amphipathic α -helix, with one hydrophobic face and one positively charged face (Roise et al., 1986).

The hydrophobic face of the presequence is recognized by the receptor Tom20, a subunit of the translocase of the outer membrane (TOM) complex (Abe et al., 2000). Then, the positively charged face is bound by the receptor Tom22, a subunit that crosses the OMM, starting from the cytosolic surface and protruding in the intermembrane space (Yamano et al., 2008). Tom22 plays an important role in the TOM maturation by assembling the Tom40 subunits in the complex. Tom40 is the transmembrane channel of the complex formed by a single molecule, a β -barrel protein that is part of the VDAC/porin superfamily (Bayrhuber et al., 2008, Lackey et al., 2014). Tom22 subunits form a central cluster that links the Tom40 subunits (1-3 per complex) together to form a mature TOM (Shiota et al., 2015). Tom40 is the entry channel for the pre-proteins that contain an N-terminal amphipathic presequence. On the inside, the channel contains separate hydrophilic and hydrophobic regions which interact specifically with the hydrophilic (ex: matrix) and hydrophobic (ex: carriers) pre-proteins (Esaki et al., 2003, Melin et al., 2014). Once the pre-protein translocates through Tom40, the N-terminal presequence binds to the intermembrane space domain of Tom22 (Moczko et al., 1997), then to the receptor Tim50, a subunit of the translocase of the inner membrane (TIM) complex (Rahman et al., 2014). Tim50 also interacts with the N-terminal domain of the Tim23 channel. If no

presequence is bound, Tim50 maintains Tim23 closed. Once the presequence is present, Tim23 is activated and the pre-protein is translocated through the channel (Meinecke et al., 2006). What happens after this step depends on the destination of the pre-protein.

Some of the proteins which upon maturation must be embedded in the IMM contain an additional sorting signal, a hydrophobic stop-transfer sequence (Glick et al., 1992). This sequence is bound by Mgr2, a small protein that interacts with the Tim23 channel (Ieva et al., 2014) and facilitates the lateral sorting of the pre-protein from Tim23 to IMM (Botelho et al., 2011). This is the case for cytochrome *c1*, for example (Glick et al., 1992). The translocation is driven by the membrane potential, which is negative on the matrix side and attracts the positively charged N-terminal presequence (Martin et al., 1991). It also activates Tim23 by inducing a conformational rearrangement (Truscott et al., 2001, Malhotra et al., 2013). The N-terminal pre-sequence is cleaved during translocation through Tim23 by a heterodimeric peptidase located in the matrix, MPP (Hawlitschek et al., 1988). The hydrophobic stop-transfer sequence is cleaved by the inner-membrane peptidase (IMP) (Popov-Čeleketić et al., 2008, Gomes et al., 2017, Bharadwaj et al., 2014). The cleaved presequences are degraded in the matrix by the presequence protease (PreP) or Cym1 (Johnson et al., 2006, Mossmann et al., 2014).

If the pre-protein being translocated through Tim23 is destined to the mitochondria matrix, the membrane potential is not sufficient. The process requires ATP, the nucleotide exchange factor Mge1 and an additional import machinery named PAM. The mitochondrial heat-shock protein 70 (mtHsp70) (Kang et al., 1990, Horst et al., 1997), a component of PAM, is a chaperon with an ATP hydrolysis domain and a peptide binding domain. The mtHsp70 is connected to the Tim23 channel via Tim44; the latter binds the pre-protein emerging at the matrix side of Tim23 and transfers it to the peptide binding domain of mtHsp70 (Banerjee et al., 2015). From this step, there are two models that try to explain how the import continues. In the trapping model (Horst et al., 1997), several molecules of mtHsp70 bind consecutively to the pre-protein, preventing it from returning in the Tim23. The pre-protein is imported step by step, with each mtHsp70 that binds to it. In the pulling model (De Los Rios et al., 2006), the pre-protein is actively pulled inside the matrix by mtHsp70, which suffers a conformational change while hydrolyzing ATP. Wiedemann and Pfanner consider that both mechanisms occur, and both ensure the translocation into the matrix (Wiedemann and Pfanner, 2017). Next, a soluble form of mtHsp70 prevents the misfolding and aggregation of the pre-protein (Kang et al., 1990), which is further retrieved and folded by the mtHsp60-Hsp10 complex in an ATP-dependent manner (Ostermann et al., 1989).

A particular case of N-terminal presequence protein sorting is the so-called conservative mechanisms, via Tim23-PAM and Oxa1. The pre-protein is transported to the matrix as described above, but it is re-imported into the IMM through Oxa1 (Hartl et al., 1986, Rojo et al., 1995). This is specific to multispanning IMM proteins, as opposed to single-spanning IMM proteins that are laterally sorted via Tim23-Mgr2 (Park et al., 2013). Several mitochondrial proteins are imported in the IMM using both conservative and lateral-sorting mechanisms: the ATP-binding cassette (ABC) transporter Mdl1, Tim18 and Sdh3 (Bohnert et al., 2010, Stiller et al., 2016). In yeast, Oxa1 and Mba1 are also responsible for the co-translational IMM insertion of the mtDNA-encoded proteins by binding to the large subunit of the mitochondria ribosome, (Pfeffer et al., 2015). In human as well, Oxa1L was reported to bind to the large subunit of the mitoribosome (Haque et al., 2010). Recently, it was shown that Oxa1L has three contact sites with the mitoribosome and this interaction allows the exit and co-translational insertion of the polypeptide chain (Itoh et al., 2021).

There are four transport pathways that do not require the N-terminal sequence but are rather based on internal sorting signals. This is the case of metabolite carriers, hydrophobic proteins from the IMM formed by six α -helix transmembrane sequences (Saraste and Walker, 1982, Nelson et al., 1998). The carrier pre-proteins are delivered to the Tom70 receptor by the cytosolic chaperons Hsp70 and Hsp90 (Young et al., 2003, Bhangoo et al., 2007). From Tom70, they are transferred to the Tom22 receptor and then inserted in the Tom40 channel (Wiedemann et al., 2001). To facilitate transport, the N-terminal segment of Tom40 moves from the cytosolic side through the channel to the intermembrane space (Qiu et al., 2013, Shiota et al., 2015), where it recruits the Tim9-Tim10 complex and the Tim12 chaperons (Gebert et al., 2008, Lionaki et al., 2008). These chaperons prevent the pre-proteins from aggregation in the intermembrane space and deliver them to the Tim54 receptor (Gebert et al., 2008, Wagner et al., 2008), from which they are transported through the Tim22 channel. The carrier is then inserted in the IMM via lateral sorting, using the membrane potential (Rehling et al., 2003).

The intermembrane space proteins also lack the N-terminal presequence. Instead, they contain cysteine motifs that form intramolecular disulfide bonds. The pre-proteins are translocated in their reduced state (Durigon et al., 2012) from the cytosol to the intermembrane space through the Tom40 channel without the involvement of any TOM receptors (Naoé et al., 2004, Gornicka et al., 2014). When emerging from the channel, they are bound by Mia40 (Chacinska et al., 2004), a protein that recognizes the signal formed by the hydrophobic residues and the cysteine residue (Peleh et al., 2016). Mia40 also has a disulfide isomerase activity, which promotes the

formation of the native intramolecular disulfide bonds and the correct folding of the protein in the intermembrane space (Koch and Schmid, 2014).

The SAM complex is involved in the sorting of β -barrel proteins to the OMM (ex: Tom40, VDAC, Sam50) (Paschen et al., 2003). The β -barrel pre-proteins do not possess an N-targeting sequence, having a β -hairpin element instead (Jores et al., 2016). They are recognized by Tom20 (Jores et al., 2016) and translocated through the Tom40 channel (Jores et al., 2016) and bound by the small Tim chaperon proteins once they reach into the intermembrane space. The Tim chaperons protect the β -barrel pre-proteins from aggregation and deliver it to the SAM complex (Wiedemann et al., 2004, Hoppins and Nargang, 2004). The β strand from the C-terminus of the precursor is recognized by the receptor Sam35 and by the channel Sam50 (Kutik et al., 2008). Subsequently, Wiedemann and Pfanner propose that the precursor is translocated through the channel and inserted into OMM via lateral sorting, by opening of the lateral gate of Sam50 (Wiedemann and Pfanner, 2017).

The last mitochondria sorting pathway that does not involve an N-terminal presequence is the insertion of α -helix proteins into the OMM. These proteins can be divided in signal-anchored (contain an α -helical transmembrane segment at the N-terminus), tail-anchored (the α -helical segment is at the C-terminus) and multispanning. The signal-anchored and multispanning proteins are inserted via the MIM complex (Dimmer et al., 2012), by a mechanism not yet fully understood. It is known however that the multispanning proteins are recognized by the Tom70 receptor prior to being transferred to the MIM insertase (Becker et al., 2011b). The tail-anchored proteins are directly inserted into MOM because it has a low-ergosterol content (Krumpe et al., 2012), no import complex being identified (Kemper et al., 2008).

1.3 Mitochondrial functions

1.3.1 *The oxidative phosphorylation process (OXPHOS)*

A key function of mitochondria is to convert simple nutrients in adenosine 5'-triphosphate (ATP), a high energy molecule which functions as a currency that fuels all the metabolic reactions in the cell. The entire process is called oxidative phosphorylation and was first proposed by Peter Mitchell in 1961 (Mitchell, 1961). Peter Mitchell realised that ATP is produced by phosphorylation of ADP, and that this phosphorylation is coupled to an electron transport system and a proton transfer across an ion-impermeable membrane (chemiosmotic coupling hypothesis).

The synthesis of ATP from ADP is based on the electron transport chain (four respiratory complexes) and the ATP synthase (F_1F_0 ATPase or complex V). The four respiratory complexes are complex I (NADH: ubiquinone oxidoreductase), complex II (succinate: ubiquinone oxidoreductase), complex III (ubiquinol: cytochrome c reductase) and complex IV (cytochrome c oxidase) (Nelson, 2017). The complexes I-IV and the ATP synthase are large enzymes localized in the IMM, organised into supercomplexes (also named respirasomes). The three respirasomes described so far are formed by complexes I, III and IV, by complexes I and III only, or by complexes III and IV (Schägger and Pfeiffer, 2000, Schägger and Pfeiffer, 2001).

There are two main metabolic pathways that provide the electron transport chain with the reduction equivalents necessary for electron generation: tricarboxylic acid (TCA) cycle (Krebs cycle) and β -oxidation. TCA cycle is involved in the catabolism of carbohydrates (glucose, fructose, galactose) and amino acids, while β -oxidation is required for the catabolism of fatty acids. Both processes take place in the mitochondrial matrix and lead to the production of NADH and $FADH_2$ (Bartlett and Eaton, 2004, Fernie et al., 2004). NADH is oxidized by the respiratory complex I to NAD^+ and $FADH_2$ is oxidized by the respiratory complex II to FAD, which results in free electrons that are transferred between the respiratory complexes (Figure 1-4). These electrons are transferred to ubiquinone (coenzyme Q), which is reduced to ubiquinol, then further transferred to complex III. From complex III, they are transferred to cytochrome c in the intermembrane space, and from there to complex IV. The final electron acceptor is oxygen, resulting in the production of water.

The electron transport transduces the energy, which is used by the respiratory complexes I, III and IV to pump protons from the matrix to the intermembrane space. The protons that accumulate at this site tend to travel in the matrix in order to equilibrate the concentrations on both sides of the inner membrane (Berg JM, 2002). Since the inner membrane is very hydrophobic and does not permit diffusion, the only way protons can travel towards the matrix is through the ATP synthase (complex V). The electrochemical gradient resulted from proton shuttle fuels ATP synthase with energy, used to catalyze the addition of a phosphate group to ADP to form ATP. The process is very efficient: it produces 38 ATP molecules from one molecule of glucose. In comparison, glycolysis only produces 2 ATP molecules (Reece, 2011).

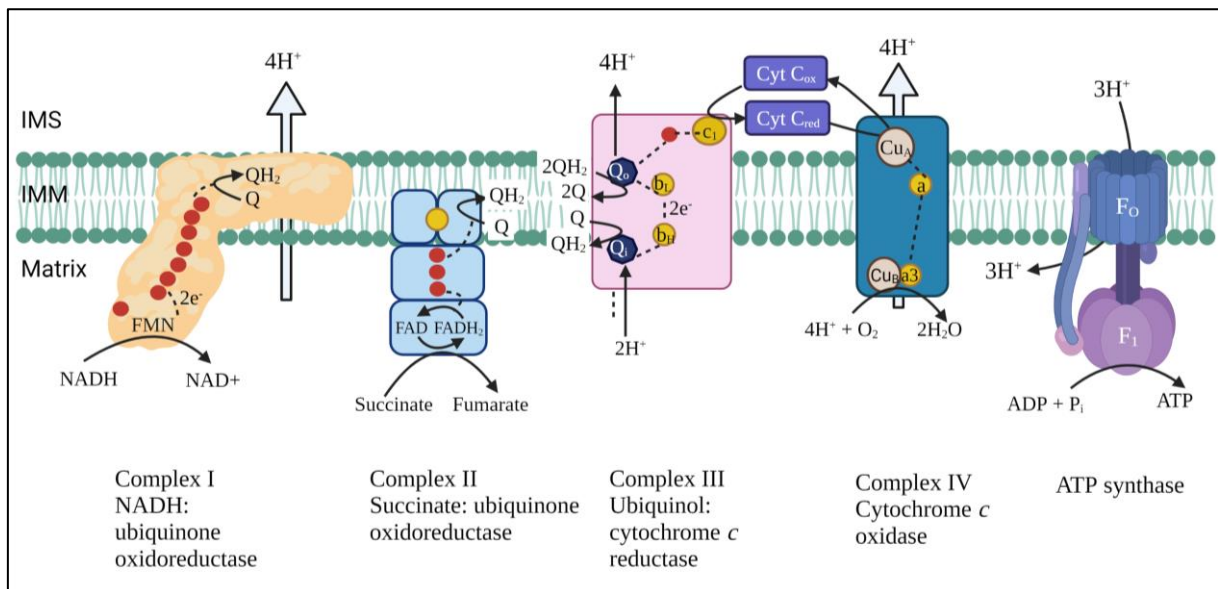


Figure 1-4. The mammalian oxidative phosphorylation system

From left to right, this cartoon (not to scale) depicts the five OXPHOS complexes from IMM: four complexes of the respiratory chain and the ATP synthase. Complex I and II collect electrons that they further release to ubiquinone (Q) which delivers them to complex III. Complex III transfers them to the cytochrome c in the IMS, from where they are finally delivered to complex IV, where oxygen (O_2) is the final acceptor, being reduced to water (H_2O). Complexes I, III and IV pump protons in the IMS, which are shuttled in the matrix by the F_0 domain of ATP synthase. This generates an electrochemical gradient used by the F_1 domain of ATP synthase for ATP production. IMS – intermembrane space, IMM – inner mitochondrial membrane, Fe-S cluster – red circle, NAD – nicotinamide adenine dinucleotide, FAD – flavin adenine dinucleotide, FMN – flavin mononucleotide, heme – yellow circle, quinol binding sites – dark blue octagon, Cyt C – cytochrome c, oxi – oxidised, red – reduced, Cu centre – light brown circle, Q – ubiquinone, QH_2 – ubiquinol, e – electron, P_i – inorganic phosphate. Figure made using BioRender (www.biorender.com)

Complex I: NADH: ubiquinone oxidoreductase is the first complex of the electron transport chain (ETC). It is also the largest complex: it has a molecular weight of approx. 980 kDa and contains a total of 46 subunits in mammals, of which 7 are encoded by the mtDNA (ND1-ND6, ND4L). Cryo-electron microscopy (cryo-EM) studies performed starting from bovine heart showed that complex I has an L-shape and is composed of two domains: a hydrophilic arm that protrudes in the matrix and a hydrophobic arm that is inserted in the IMM (Carroll et al., 2003). At the top of the hydrophilic arm is situated a flavin mononucleotide (FMN) which oxidises the NADH resulted from TCA cycle or β -oxidation. The two electrons released in the oxidation reaction are transferred through a chain of seven consecutive iron-sulphur (Fe-S) clusters until they reach ubiquinone, which is reduced to ubiquinol (Vinothkumar et al., 2014, Zickermann et al., 2015). An eight Fe-S is present close to FMN, but it does not contribute to electron transport and has a yet unknown function (Birrell et al., 2013). The hydrophobic arm is involved

in pumping of protons towards the intermembrane space (four protons for each molecule of NADH) (Jones et al., 2017).

Complex II: Succinate: ubiquinone oxidoreductase, also known as succinate dehydrogenase (SDH), is the only complex that does not pump protons across IMM and the only complex that is entirely encoded by nuclear DNA. It is composed of four subunits: SDHA, SDHB (hydrophilic, protrude in the matrix) and SDHC, SDHD (hydrophobic, embedded in the IMM) (Sun et al., 2005). SDHA is also a component of the TCA cycle: it oxidises succinate to fumarate, thus linking mitochondrial metabolic reactions with OXPHOS. SDHA contains the cofactor flavin (FAD), which accepts the two electrons resulted from succinate oxidation and transfers them to the three consecutive Fe-S clusters in SDHB. The electrons eventually reduce ubiquinone to ubiquinol. SDHA also contains a heme group in the hydrophobic domain, but its role is unclear, as it is not an element of the electron transport (Iverson, 2013).

Complex III: ubiquinol: cytochrome *c* reductase (also known as cytochrome *bc1* complex), is a symmetrical dimer that contains 11 subunits per monomer of which only cytochrome *b* subunit is encoded by mtDNA (Vázquez-Acevedo et al., 1993). Cytochrome *b* is involved in electron transfer and contains two heme groups, *b*_L (lower potential heme) and *b*_H (higher potential heme), as well as two binding sites for quinone (Q_O and Q_i). The other subunits involved in electron transport are cytochrome *c1* and the Rieske protein. Cytochrome *c1* contains a heme type *c1*, while Rieske protein contains a Fe-S cluster in the hydrophilic C-terminus and interacts with the intermembrane space (Zhang et al., 1998). The ubiquinol resulted from complex I and complex II binds at the Q_O site and is oxidized to ubiquinone, releasing two electrons in the process. One electron is transferred to the Fe-S cluster, from where it reduces heme *c1*, then is finally transferred to the cytochrome *c* in the intermembrane space. The second electron is transferred to the Q_i site via *b*_L and *b*_H. At the Q_i site, ubiquinone is reduced to ubiquinol, thus completing the Q cycle. The process of transferring electrons from ubiquinol to cytochrome *c* results in pumping of four protons in the intermembrane space (Link and Iwata, 1996, Brandt, 1998).

Complex IV: cytochrome *c* oxidase is the last enzyme of ETC. In mammals, it is composed of 13 subunits (Tsukihara et al., 1996, Kadenbach and Hüttemann, 2015), out of which three are encoded by mtDNA: COX1, COX2 and COX3 (Anderson et al., 1981). The first two are involved in oxygen reduction: COX1 contains a molecule of heme *a* and a heme *a3/Cu_B* centre, while COX2 contains a Cu_A centre. Cu_A receives four electrons from cytochrome *c*, which are then transferred to heme *a* and further transferred to the heme *a3/Cu_B* centre. The heme *a3/Cu_B* centre also binds O₂, which is reduced by the four electrons to two molecules of water, marking

the end of the ETC (Yoshikawa et al., 2006). The process is coupled with proton translocation (Wikstrom, 1977).

ATP synthase (Figure 1-5) is the last complex of OXPHOS and is responsible for phosphorylation of ADP to ATP. ATP synthases form dimers in the mammalian IMM. The dimers are V-shaped and assemble into rows at the tip of the cristae, maintaining the cristae structure (Dudkina et al., 2005, Strauss et al., 2008).

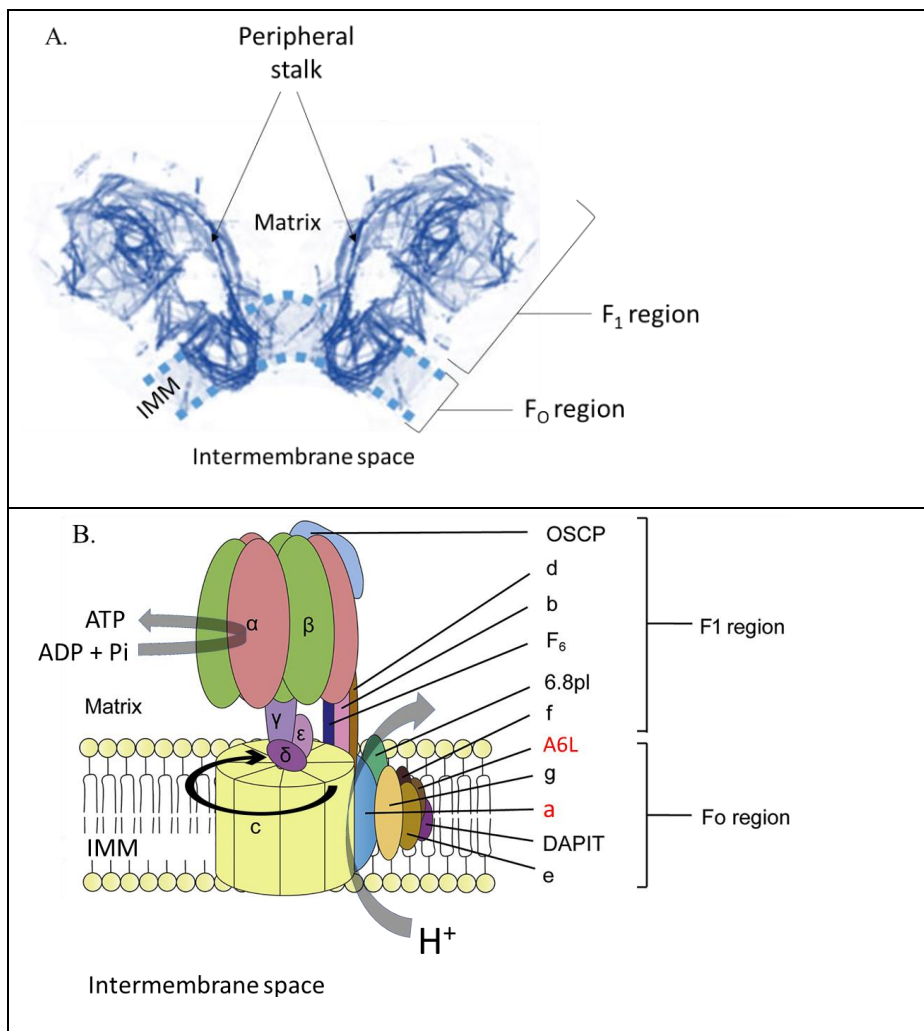


Figure 1-5. Structure of mitochondrial ATP synthase

- A. Mitochondrial ATP synthase forms dimers that fold the IMM at the tip of cristae (figure taken from (Almendro-Vedia et al., 2021) under a Creative Commons license)
- B. The mitochondrial ATP synthase is composed of two regions: F₀, situated inside the IMM, and F₁, that protrudes in the matrix. The two regions are connected by the peripheral stalk. The subunits a and A6L (red font) from F₀ are encoded by mtDNA. Protons from the intermembrane space pass through F₀ into the matrix, which induces the rotation of central stalk (hexamer of c subunit) and subsequent production of ATP by F₁ (figure adapted from (Wang et al., 2021) under a Creative Commons license).

Each monomer is formed by an F₁ domain, situated in the matrix, and an F₀ domain, immersed in the IMM. The two portions are connected by the central and peripheral stalk (Zhou et al.,

2015). Each monomer of the mammalian ATP synthase is composed of 17 subunits, with two encoded by the mtDNA: subunit a (encoded by *ATP6*) and subunit A6L (encoded by *ATP8*) (Anderson et al., 1981), both situated in the F_O domain (Zhou et al., 2015). F_O forms a channel through which the protons pumped by complexes I, III and IV to the intermembrane space are reimported in the matrix. This proton gradient generates a proton-motive force that rotates the central stalk and triggers rotation of F₁, providing energy for ATP synthesis (Watt et al., 2010).

1.3.2 Other mitochondrial functions

Although the ATP production is a key function of mitochondria, it is not the only one. Some artificially created cells (Rho⁰) can survive without mtDNA and therefore with no respiratory complexes and OXPHOS, because they rely on glycolysis for energy production (King and Attardi, 1989). Another essential function of mitochondria is the production of Fe-S clusters. Fe-S clusters are small inorganic cofactors that exist in all organisms and are involved in numerous cellular processes such as heme synthesis, anti-viral response, ribosome assembly, DNA repair and respiration (Lill and Mühlenhoff, 2008). No cell can survive without Fe-S clusters, and they are the only mitochondrial function that can be found in all species (Lill, 2009). Fe-S synthesis (Figure 1-6A) takes place in the mitochondrial matrix, where iron is transported from the cytosol by mitoferrin proteins. As iron is toxic as free element, in the matrix it is bound by frataxin (FXN) (Tsai and Barondeau, 2010) then by the scaffold protein ISCU (Mühlenhoff et al., 2003). The enzyme cysteine desulfurase (NFS1) in complex with ISD11 removes sulphur from L-cysteine and delivers it to ISCU (Van Vranken et al., 2016). The Fe-S cluster is undertaken by consecutive chaperons that deliver it to recipient apoproteins (ex. lipoic acid synthase, aconitase, subunits of respiratory complexes I-III) (Cardenas-Rodriguez et al., 2018).

Another synthetic pathway that involves iron metabolism in mitochondria is the production of heme (Figure 1-6B). Heme is a protein cofactor that plays the role of electron carrier in haemoglobin and myoglobin (involved in O₂ transport), catalases and peroxidases (ROS scavengers) and cytochromes (Reedy et al., 2008). It is composed from a protoporphyrin IX macrocycle with a coordinated iron in the centre. Heme synthesis starts in the mitochondrial matrix, with the synthesis of 5-aminolevulinic acid from succinyl-CoA and glycine (catalysed by the enzyme 5-aminolevulinate). The 5-aminolevulinic acid is transported in the cytosol, where is used as starting molecule for the synthesis of coproporphyrinogen III, an intermediary that is transported back in the mitochondria. Here, this intermediary is maturated and in the

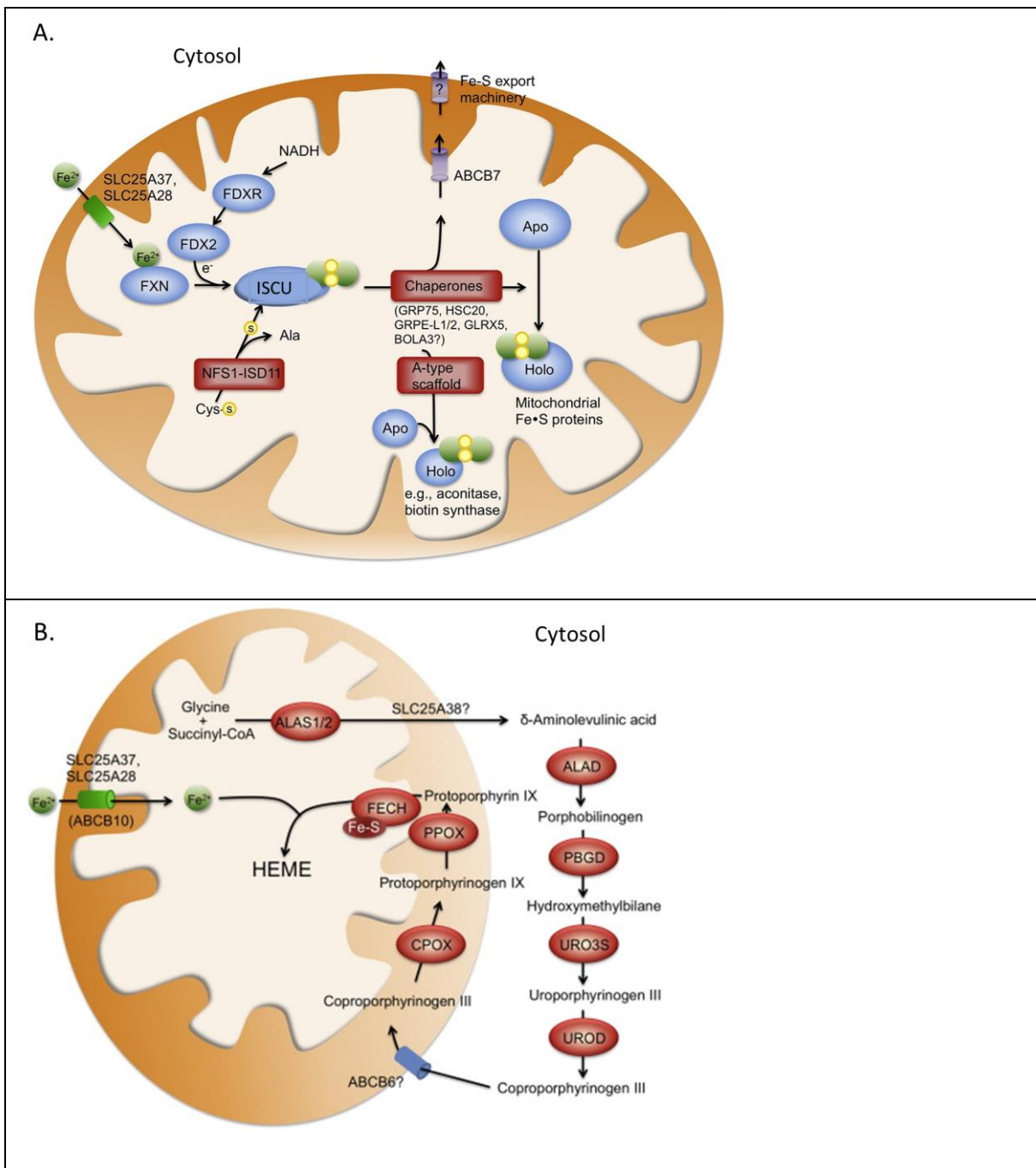


Figure 1-6. Iron metabolism in mitochondria

A. Iron is imported from the cytosol and bound by frataxin (FXN) in the matrix, then transferred to ISC1. Sulphur is taken from cysteine by the NFS1-ISD11 complex and delivered to ISC1 as well. ISC1 assembles the Fe-S clusters, which are taken in charge by mitochondrial chaperones. Eventually, the Fe-S clusters are either exported in the cytosol, or used inside the matrix as enzyme cofactors; adapted from (Xu et al., 2013) with permission, RightsLink license number 5273980270144

B. The first and last steps of heme synthesis are localized in mitochondria. The δ (or δ)-aminolevulinic acid is synthesized there, then exported in the cytosol, where it is used for the synthesis of coproporphyrinogen III. Coproporphyrinogen III is imported in the mitochondria, metabolized to protoporphyrin IX and eventually transformed into heme by coordination of iron in the centre of protoporphyrin IX; taken from (Xu et al., 2013) with permission, RightsLink license number 5274020714517

final step, iron is inserted by the enzyme ferrochelatase (Piel et al., 2019).

The mitochondrial matrix is also the headquarters of essential metabolic pathways like the TCA cycle, β -oxidation and (partially) urea cycle. Catabolism of nutrients initially starts in the cytosol, but downstream metabolic intermediates are imported in the mitochondrial matrix (Figure 1-7).

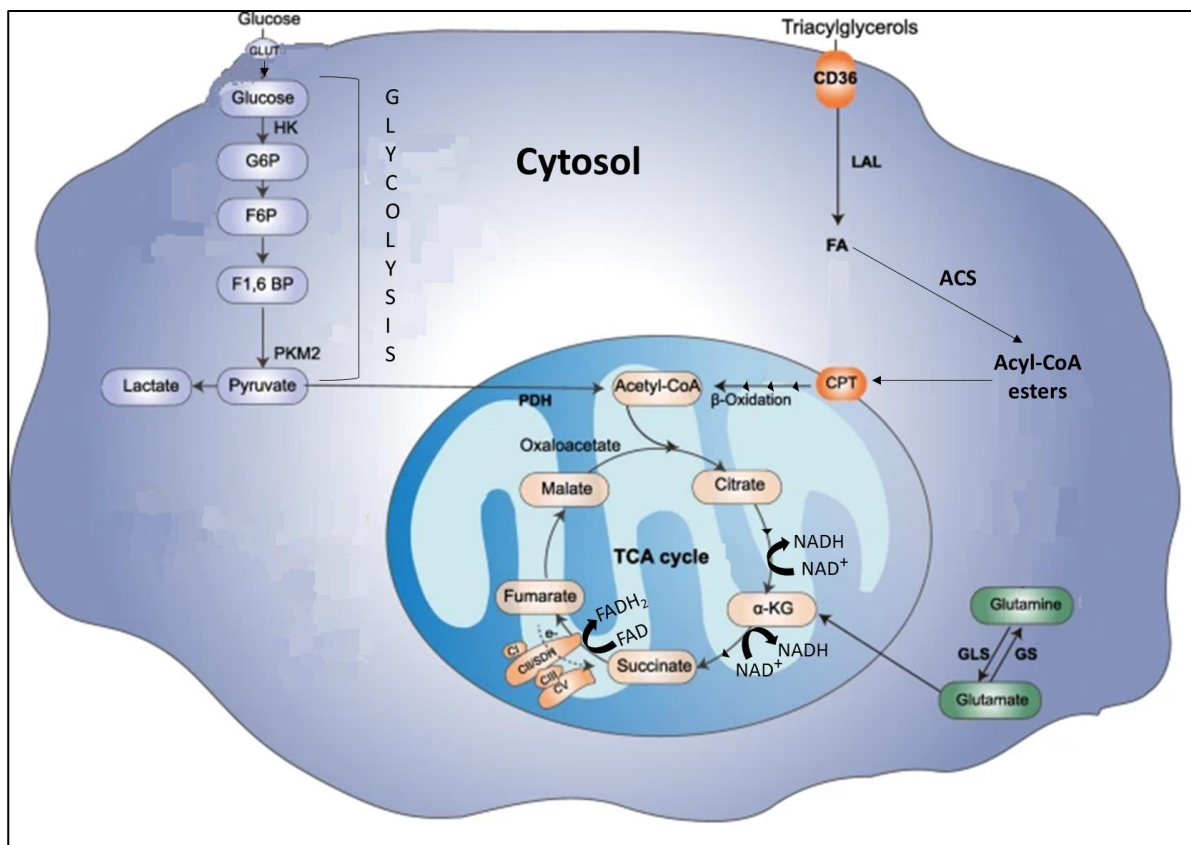


Figure 1-7. Nutrient catabolism in the mitochondrial matrix

Glucose from cytosol enters glycolysis and is metabolised to pyruvate. Pyruvate is transported in the matrix, where it is converted into acetyl-CoA by the pyruvate dehydrogenase (PDH). Triacylglycerols are metabolized into fatty acids (FA) by the lysosomal acid lipase (LAL), which are activated by acyl-CoA synthetases (ACS) to acyl-CoA esters. These esters are transported inside the matrix by the carnitine palmitoyltransferase (CPT), where they are subjected to consecutive reactions that remove two carbons at each step, until they are entirely metabolized to acetyl-CoA. Acetyl-CoA enters the Krebs cycle. Krebs cycle produces NAD^+ and FADH_2 which are used in the electron transport chain. The Krebs cycle is supplied by glutamine metabolism, which produces the intermediary alpha-ketoglutarate ($\alpha\text{-KG}$). Figure adapted from (Liu et al., 2021) with permission under a Creative Commons Attribution 4.0 (<https://creativecommons.org/licenses/by/4.0/>)

During glycolysis, glucose is oxidized to pyruvate, which is transported into the matrix (Bricker et al., 2012). Here, the pyruvate dehydrogenase complex facilitates the reaction with coenzyme A (CoA) and converts pyruvate into acetyl-CoA (Patel et al., 2014), an important intermediary in the TCA cycle. Another TCA cycle intermediate is succinate, which is oxidized to fumarate

by SDHA subunit of complex II (Vakifahmetoglu-Norberg et al., 2017). During fatty acid catabolism, the fatty acid molecules are activated to acyl-CoA esters by acyl-CoA synthetases from the cytosol. The acyl-CoA esters are transported through the mitochondrial membranes via carnitine binding, as acyl-carnitine intermediates. In the mitochondrial matrix, the long fatty acid chains are shortened during successive rounds in which two carbon atoms are cleaved each round (β -oxidation). The final metabolic product of β -oxidation is acetyl-CoA, which enters the TCA cycle (Bartlett and Eaton, 2004). During amino acid catabolism, the free ammonium ions that are produced are conjugated to bicarbonate in the liver mitochondria, resulting in carbamoyl phosphate (Figure 1-8). Carbamoyl phosphate is further conjugated to ornithine, resulting in L-citrulline, which is transported in the cytosol. L-citrulline undergoes a series of metabolic reactions in the cytosol, until it reaches the intermediary state of ornithine and is transported back in the mitochondria. The cycle results in the release of an urea molecule (Adeva et al., 2012).

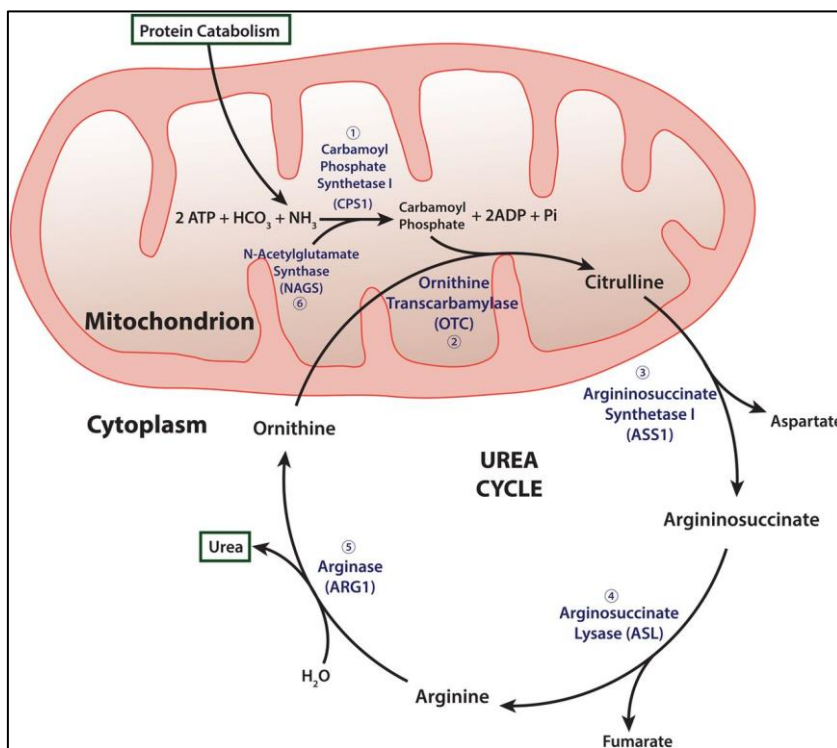


Figure 1-8. Mitochondrial involvement in urea cycle

The first and last steps of urea formation take place in the matrix. In the first step, ammonia resulted from protein catabolism is conjugated to bicarbonate by the carbamoyl phosphate synthetase. The carbamoyl phosphate is transferred to ornithine, resulting in citrulline that is exported. In the cytosol, citrulline is metabolized to ornithine, which is re-imported in the mitochondria; taken from (Blair et al., 2015) with permission, RightsLink license number 5274501044085

Mitochondria are also involved in cell survival and apoptosis. Through a series of cytosolic reactions, apoptotic stimuli (DNA damage, oxidative stress or excess of calcium) induce the

permeabilization of OMM (Shimizu et al., 1999). This leads to the release of the mitochondrial proteins: cytochrome c, AIF (apoptosis-inducing factor), EndoG (endonuclease G), Smac/DIABLO and Omi/HtrA2 (Kilbride and Prehn, 2013). Cytochrome c binds apoptotic protease activating factor 1 (APAF1) in the cytosol, which oligomerizes and activates caspase 9, a cysteine protease involved in degradation of cell components, that further activates caspases 3 and 7 (Goldstein et al., 2000, Zou et al., 1997). AIF and EndoG induce apoptosis via caspase-independent mechanisms. After release from the intermembrane space, AIF translocates to the nucleus, where it binds DNA irrespective of nucleotide sequence, to induce DNA fragmentation and chromatin condensation (Ye et al., 2002). EndoG, a mitochondrial nuclease, acts in a similar manner with AIF: released from the intermembrane space, it translocates to the nucleus and induces DNA fragmentation (Li et al., 2001). In mammals, EndoG collaborates with DNase I to generate double-strand DNA breaks (Widlak et al., 2001). Smac/DIABLO and Omi/ HtrA2 both bind to X-linked inhibitor of apoptosis protein (XIAP) and prevent it from inhibiting caspases (Srinivasula et al., 2001, Yang et al., 2003, Du et al., 2000), thus promoting apoptosis (Eckelman et al., 2006).

One cause for apoptosis is production of excessive reactive oxygen species (ROS), of which mitochondria are the main source (Redza-Dutordoir and Averill-Bates, 2016). Approximately 1% of the total oxygen used in respiration is converted to superoxide radical anions (O_2^-), hydrogen peroxide (H_2O_2) and hydroxyl radicals ($-HO\cdot$) (Chen et al., 2003, Murphy, 2008). Those are highly reactive molecules derived from incomplete reduction of oxygen that can cause oxidative stress. They can damage DNA, proteins and lipids and trigger the opening of the mitochondrial permeability transition pore, initiating apoptosis (Petronilli et al., 1994). Complexes I and III are the main ROS generators: in total, they contain 11 ROS production sites, and generate 45% of total H_2O_2 (Wong et al., 2019, Brand, 2016). As an adaptive response, cells use scavenger enzymes to eliminate ROS: superoxide dismutase (SOD), glutathione peroxidase, catalase, and peroxiredoxin. SOD, present both in the cytosol and IMS, converts ROS in H_2O_2 (Okado-Matsumoto and Fridovich, 2001) then glutathione peroxidase converts H_2O_2 in water by using glutathione as reducing substrate (Deponte, 2013). Catalase uses two molecules of H_2O_2 to produce molecular oxygen and water (Kirkman et al., 1999), while peroxiredoxin reduces H_2O_2 or alkyl hydroperoxide to alcohol and water (Chae et al., 1994). As long as their levels remain in equilibrium with the capacity of the scavenger enzymes, ROS are part of the normal physiology of the cell (Clément and Pervaiz, 2001). They activate cell survival signaling pathways (UPR, Nrf2) and are involved in angiogenesis, autophagy and activation of immune cells (Valko et al., 2007, Fukai and Ushio-Fukai, 2020). However, due to

environmental factors (smoking, pollution, UV irradiation, heavy metals) and ageing, the ROS production can exceed the scavenger capacities of those enzymes, resulting in a large spectrum of disorders like cancer, diabetes, Parkinson's disease and cardiovascular disease (Valko et al., 2007, Al Shahrani et al., 2017).

In addition to all the above-mentioned functions, mitochondria are also involved in calcium homeostasis (Rizzuto et al., 2012) and thermogenesis (Li et al., 2020b). All the enzymes responsible for non-OXPHOS functions are encoded by the nucleus and are imported into mitochondria via different pathways described at 1.2.

1.4 Mitochondrial genome

One aspect that makes mitochondria unique among mammalian organelles is having their own mitochondrial DNA (mtDNA). Studies performed in rat estimate 2-10 mtDNA molecules per mitochondrion (Wiesner et al., 1992), but the number varies depending on cell type (Dickinson et al., 2013). Organization of mtDNA is similar to bacterial DNA: mtDNA is packed into protein aggregates named 'nucleoids' that lack histones. Mitochondrial nucleoids are ellipsoid structures, with a diameter of approx. 110 nm (Dlasková et al., 2018), that are tightly associated with IMM (Brown et al., 2011) and contain a single copy of mtDNA each (Kukat et al., 2015). MtDNA is very tightly packed in the nucleoids, more tightly than the bacterial or nuclear DNA, as the 110 nm nucleoid diameter would correspond to a 300 bp segment (Brown et al., 2011, Bogenhagen, 2012). The main factor responsible for mtDNA packaging is TFAM (transcription factor A, mitochondrial), a very abundant protein (1,000 TFAM molecules per 1 molecule of mtDNA) that covers the entire genome (Alam et al., 2003, Kukat et al., 2011).

The complete sequence of human mtDNA was solved for the first time by Anderson and colleagues (Anderson et al., 1981), then revised by Andrews and colleagues (Andrews et al., 1999). The molecule is circular, double-stranded and small (16,569 bp). It encodes for 37 genes: 2 rRNAs (12S and 16S), 22 tRNAs and 13 polypeptides, the last being subunits of OXPHOS complexes I, III, IV and V (Figure 1-9). The two complementary strands were defined as heavy (H) and light (L), based on nucleotide composition: H is guanine rich, while L is cytosine rich. For this reason, after denaturation, the two strands could be separated by ultracentrifugation in cesium chloride (CsCl) density gradient (Borst et al., 1967). The genes are not equally distributed among the H and L strands: H strand encodes for 14 tRNAs, 12 polypeptides, and 2 rRNAs, while the L strand encodes for 8 tRNAs and only one polypeptide.

Distribution of genes is very efficient. MtDNA lacks introns and contains overlapping genes: *MT-ND4* and *MT-ND4L* (encoding for complex I subunits ND4 and ND4L), *MT-ATP6* and *MT-ATP8* (ATPase subunits 6 and 8) as well as *mt-tRNA^{Tyr}*/*mt-tRNA^{Cys}*. One non-coding region is the displacement loop (D-loop), with approx. 1.1 kb length, situated between the genes encoding for tRNA^{Phe} and tRNA^{Pro}. The D-loop contains the origin of replication for the H strand (O_H) and the transcription promoters for H and L strands (HSP1, HSP2 and LSP). A third DNA strand has been identified in the D-loop: a stably incorporated 7S DNA, which does not occur in every single mtDNA molecule and currently has an unknown function (Walberg and Clayton, 1981, Nicholls and Minczuk, 2014). Another non-coding region contains the origin of replication for the L strand (O_L) and is sandwiched between five tRNA genes (Anderson et al., 1981).

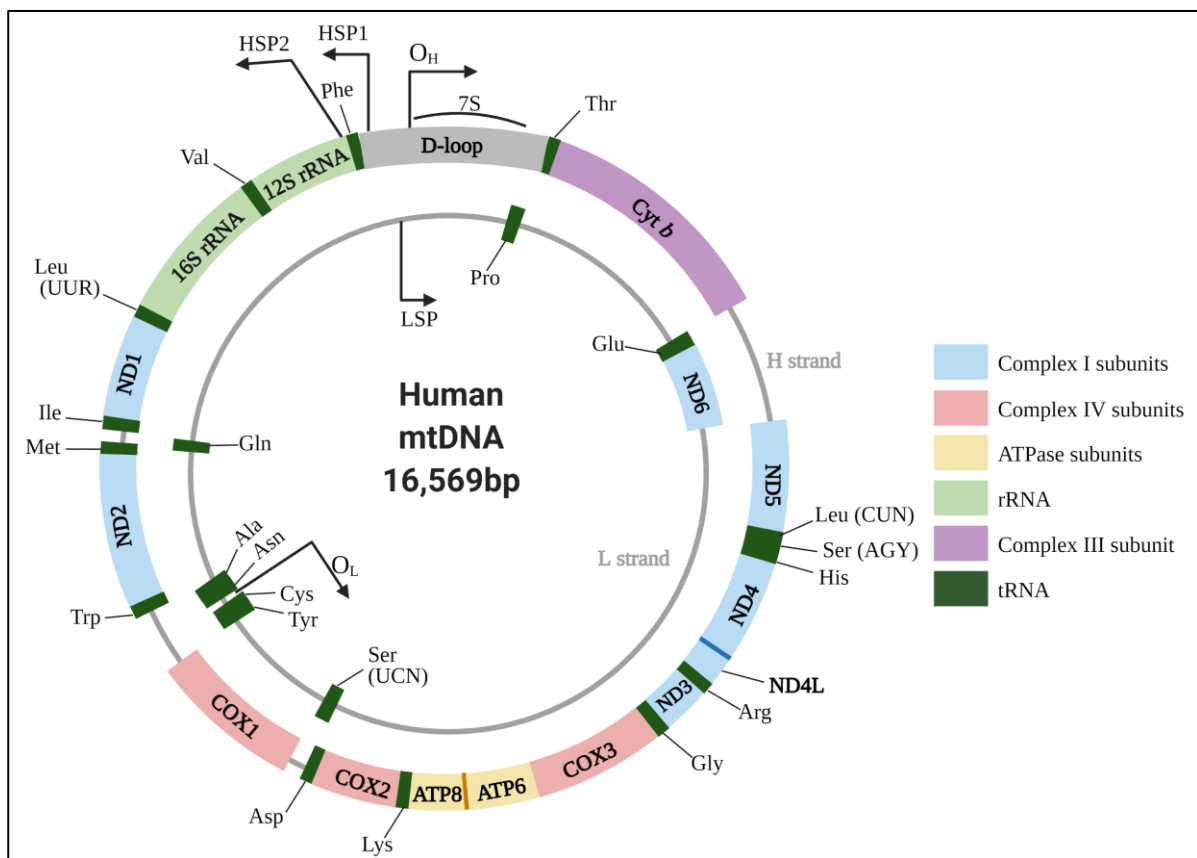


Figure 1-9. The human mitochondrial genome

The diagram illustrates the organisation of human mtDNA as a circular double stranded molecule. Heavy (H) and light (L) strands encode for a total of 37 genes, corresponding to 13 polypeptides that become subunits of the respiratory complexes, 2 rRNAs (light green) and 22 tRNAs (dark green). Non-coding DNA is in grey. The origins of replication (O_H and O_L) and transcription promoters (HSP1, HSP2, LSP) are indicated by bent black arrows. Figure made using BioRender (www.biorender.com)

Mitochondrial genetic code deviates from the universal code. For example, AUA encodes for methionine instead of isoleucine and UGA, usually a stop codon, encodes for tryptophan. There

are two codons that signal the start of translation: AUG (for 10 genes) and AUA (for 3 genes) and only two of the three universal stop codons are retained: UAA and UAG (Anderson et al., 1981). Two genes terminate in codons that usually encode for arginine: *MTCO1* terminates in AGA, while *MTND6* in AGG. During translation of the *MTCO1* and *MTND6* transcripts, the mitochondrial ribosome performs a -1 frameshifting, to allow the presence of a universal stop codon in the A site (Temperley et al., 2010a). In addition, the number of tRNAs encoded by mtDNA is almost equal to the number of amino acids, and only leucine and serine can be recognized by two tRNAs each (Christian and Spremulli, 2012). In contrast, the universal genetic code uses 61 codons for amino acids, and less tRNAs (approx. 40-50, (Goodenbour and Pan, 2006)) to recognize them. According to “the Wobble hypothesis”, the anticodon of a single tRNA can pair with more than one codon (Crick, 1966).

MtDNA is maternally inherited (Hutchison et al., 1974). Maturation of reproductive cells has different effects on the mtDNA copy number: during spermatogenesis, the number of mtDNA molecules decreases until approx. 100 copies in the mature sperm cell, localized mostly in the midpiece, while the mature oocyte has over 150,000 copies (Larsson et al., 1997, Wai et al., 2010). In addition, the paternal mtDNA that enters the oocyte after fertilisation is rapidly degraded by different mechanisms (Sato and Sato, 2013, Yu et al., 2017).

MtDNA is more prone to defects than nuclear DNA. One possible cause resides in the high concentrations of guanine in the mitochondria, compared to other dNTPs, which decrease the accuracy of mtDNA polymerase gamma, causing mismatches (Song et al., 2005). Another cause is oxidative stress, exacerbated by the lack of protective histones; since mtDNA is associated with IMM, it becomes proximal to OXPHOS, and more prone to oxidative damage caused by ROS (Richter et al., 1988). Recent studies suggest that the first cause, rather than ROS, is the main cause of pathogenic variants (Szczepanowska and Trifunovic, 2017). Variants do not occur in every single mtDNA molecule from a cell; instead, the same cell contains different percentages of mutant and healthy mtDNA (heteroplasmy), which contributes to the heterogeneity of mitochondrial disorders (Stewart and Chinnery, 2015).

1.5 Replication of mtDNA

Replication of mtDNA is distinct from nuclear DNA replication. Mitochondria have their own replication machinery, with proteins encoded by the nucleus, that must be imported in the organelle (Falkenberg, 2018). The minimum components necessary for this process, as identified by *in vitro* replication, are mtDNA polymerase γ (Poly γ), Twinkle helicase, and mitochondrial single-stranded binding protein (mtSSB) (Korhonen et al., 2004). Poly γ is the only

DNA polymerase specific for mitochondria (Ropp and Copeland, 1996). Because this enzyme cannot use double stranded DNA as a template, the mtDNA is first unwound by the Twinkle helicase and maintained unwound by mtSSB (Korhonen et al., 2004). Twinkle is a 5' → 3' DNA helicase efficient at unwinding short stretches of dsDNA (20 bp); its activity is strongly stimulated by mtSSB (Spelbrink et al., 2001, Korhonen et al., 2003).

Additional proteins involved in mtDNA replication are mitochondrial RNA polymerase (POLRMT), exonuclease RNase H1 and DNA ligase III (Falkenberg, 2018). POLRMT synthesizes the RNA primers required for initiation of replication (Fusté et al., 2010). Once Poly starts the elongation of DNA chain, RNase H1 digests the RNA primers from the RNA-DNA hybrids, as they are no longer necessary (Holmes et al., 2015) (Holt and Reyes, 2012). When replication finishes, the ends of the newly formed DNA strands are ligated by DNA ligase III (Lakshmipathy and Campbell, 1999, Puebla-Osorio et al., 2006).

The exact mechanism of replication is still a matter of debate, and three models had been proposed (Gustafsson et al., 2016) (Figure 1-10).

The first model is the strand displacement model, proposed in 1972 by (Robberson et al., 1972). According to it, replication of each strand is continuous, but not simultaneous. It first initiated at O_H and continues for two-thirds of genome length, passing O_L. During this process, the H strand is covered by mtSSB (Miralles Fusté et al., 2014), which prevents POLRMT from binding it (Wanrooij et al., 2008). However, when the replication fork passes O_L, the single H strand adopts a stem-loop structure that prevents mtSSB from binding (Martens and Clayton, 1979). The single stranded DNA remains exposed, which allows POLRMT to bind to O_L and synthesize a 25 b primer, at which point Poly starts replication of the L strand in the opposite direction (Wong and Clayton, 1985, Falkenberg, 2018).

The second model is known as RITOLS (Ribonucleotides Incorporated Through Out the Lagging Strand). It has common aspects with the strand displacement model, like predicting the two DNA strands are not synthesized at the same time, and that replication starts from O_H (Holt and Reyes, 2012). By contrast, RITOLS predicts that segments of RNA are successively hybridized to the H-strand, only to be matured into DNA at a later stage (Yang et al., 2002) (Yasukawa et al., 2006). The RNA/DNA hybrids have been identified in mitochondria using specific antibodies (Pohjoismäki et al., 2010), but the putative enzymes involved in this process are unknown (Reyes et al., 2013).

The last model is the strand-coupled replication, proposed by Holt et al. (Holt et al., 2000). The authors used ethidium bromide to induce mtDNA depletion in mammalian cells, then allowed

them to recover. In order to compensate for the mtDNA loss, cells increased replication. In those cells, they identified double-stranded DNA intermediates that indicate a synchronous bidirectional replication of the H and L strands. The start of replication was not O_H , but rather a broad region spanning over genes *Cytb*, *NAD5* and *NAD6* (Bowmaker et al., 2003).

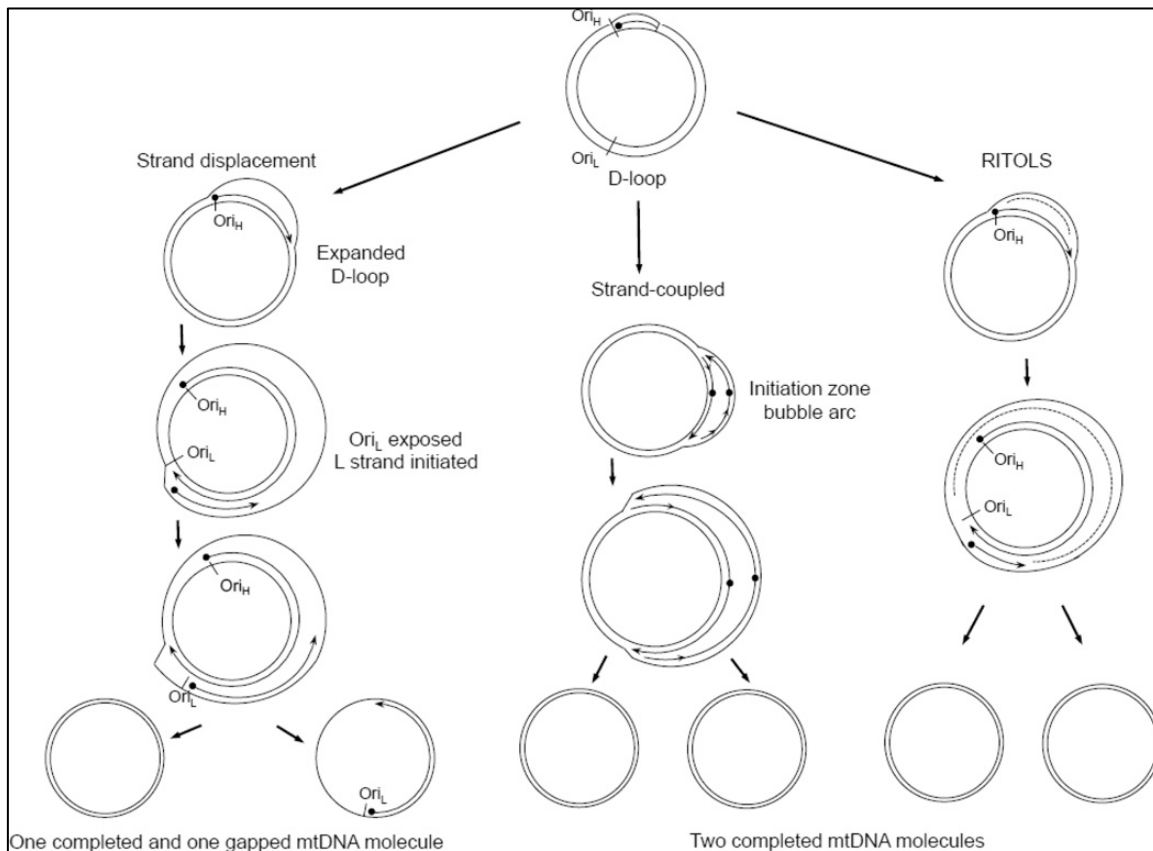


Figure 1-10. Replication of mtDNA

Currently there are three models that explain the mtDNA replication. The strand displacement model (left panel) states that replication of the two strands is asynchronous. First starts the replication of the H strand, from O_H . Replication continues for two thirds of the genome, then initiates in the opposite direction for the L strand, from O_L . In the strand-coupled model (middle panel), replication is synchronous and bidirectional; the origin is neither O_H nor O_L , but a broader initiation zone. According to the RITOLS model (right panel) replication is asynchronous and starts from the O_H on the H strand, but the L strand is transcribed into RNA and re-converted into DNA at a later stage. Figure taken from (Kasiviswanathan et al., 2012) with permission, RightsLink license number 5275090476041

1.6 Transcription and post-transcriptional modifications in human mitochondria

Replication and transcription are mutually exclusive (Fontanesi et al., 2020). Transcription of mtDNA starts from both strands and results in long polycistronic transcripts that undergo processing and maturation. Transcription promoters are localized in the D-loop, and serve different genes from each strand (Chang and Clayton, 1984). Initial experiments performed in the '80s by Montoya et al. used radiolabeled mitochondrial transcripts that were mapped to mtDNA by DNA–RNA hybridization. Based on them it was established an initial model that included three promoters, as it follows:

1. LSP- L strand, initiates a transcript that contains 8 tRNAs and *MT-ND6* (Montoya et al., 1982)
2. HSP1- H strand, initiates a transcript that contains 2 tRNAs (tRNA^{Phe} and tRNA^{Val}) and the 12S and 16S rRNA (Montoya et al., 1982)
3. HSP2- H strand, initiates a transcript that contains all the remaining genes (Montoya et al., 1983)

However, later experiments questioned the existence of HSP2. In a recombinant *in vitro* transcription system, Litonin et al. used synthetic templates that contained the HSP1, HSP2 or LSP promoters, but only identified an RNA product for HSP1 and LSP (Litonin et al., 2010). The authors repeated the experiments using a longer template that contained both HSP1 and HSP2, but only HSP1 initiated transcription. No transcription activity was identified for HSP2, possibly because it was not recognized by the mitochondrial RNA polymerase (POLRMT) (Litonin et al., 2010). Subsequently, it is currently considered that transcription of the H strand starts from a single promoter (D'Souza and Minczuk, 2018, Rebelo-Guiomar et al., 2019).

The enzyme that drives transcription is POLRMT, a single subunit protein which has a similar structure with the RNA polymerase from T7 bacteriophage. However, the domains that in T7 would melt DNA have a different position in human POLRMT, which makes it unable to melt DNA alone. Therefore, to fulfil its activity, POLRMT associates with TFAM and mitochondrial transcription factor B2 (TFB2M) and forms an initiation complex (Ringel et al., 2011) (Figure 1-11).

TFAM plays a role in both DNA packaging and transcription. As DNA packaging factor, it binds DNA irrespectively of the nucleoid sequence (Fisher and Clayton, 1988). As transcription factor, TFAM binds 10-35 bases upstream from the transcription start site (Fisher et al., 1987),

on both strands, and bends the promoter DNA in a U-shape (Ngo et al., 2011, Rubio-Cosials et al., 2011). This change in DNA structure facilitates binding of POLRMT to TFAM, via the N-terminus of the polymerase, and forms a pre-initiation complex (Gaspari et al., 2004, Morozov et al., 2014). TFB2M binds to this complex and separates the DNA strands, allowing transcription to initiate (Posse and Gustafsson, 2017). TFB2M binds to the dsDNA and to the POLRMT, inducing a conformational change of this enzyme and DNA opening. Via its positively charged N-terminus, TFB2M traps the non-template DNA strand and thus keeps the two strands apart (Hillen et al., 2017a).

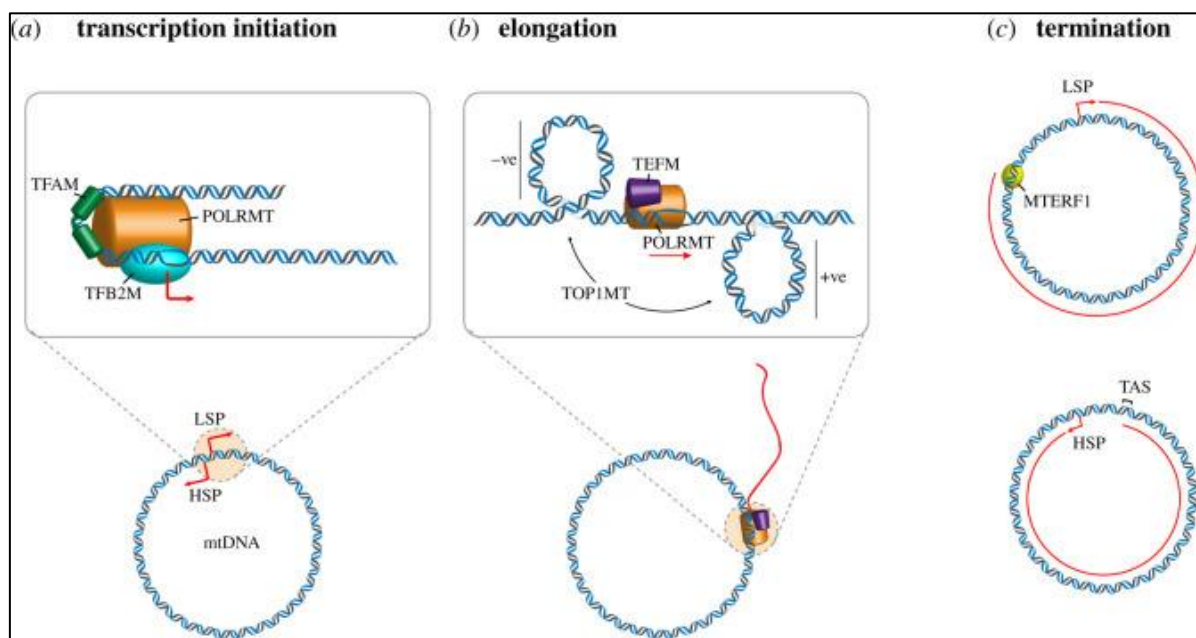


Figure 1-11. Transcription of mtDNA

During transcription initiation, TFAM binds the mtDNA upstream from the start site and binds the promoter region (LSP or HSP), which allows the binding of POLRMT and TFB2M. TFB2M separates the DNA strands, which allows POLRMT to start the synthesis of RNA. During elongation, TEFM binds to POLRMT and enhances the enzyme processivity. Top1MT maintains the mtDNA in a supercoiled state. During termination, MTERF1 binds at the mt-tRNA^{Leu(UUR)} site on the L-strand and blocks the POLRMT, which leaves the mtDNA. Transcription termination for the H strand is unclear, but some reports have identified a termination-associated sequence (TAS) in the non-coding region of mtDNA (Freyer et al., 2010). Figure taken from (Menger et al., 2021) with permission under the terms of the Creative Commons Attribution License (<http://creativecommons.org/licenses/by/4.0/>)

During transition from transcription initiation to elongation, TFAM and TFB2M leave the complex (Hillen et al., 2017a), which allows the binding of TEFM (transcription elongation factor of mitochondria) at the catalytic region of POLRMT (Minczuk et al., 2011). Two molecules of TEFM bind at the C-terminus to form a dimer that interacts with POLRMT at the DNA-RNA hybrid cavity. The point of interaction is the intercalating hairpin of POLRMT, a mobile element from N-terminus responsible for the separation of the nascent RNA from the

DNA template. At the same time, TEFM interacts with the dsDNA upstream as well as downstream from elongation site and traps the non-template DNA strand (Hillen et al., 2017b).

TEFM binding to POLRMT enhances the enzyme processivity (Minczuk et al., 2011). *In vitro* transcription reactions that use ssDNA templates show that POLRMT alone is only capable to synthesize short RNA fragments (25-75 nucleotides), while the length of polycistronic transcripts of mammalian mitochondria is in the order of kilobases (Wanrooij et al., 2008, Minczuk et al., 2011). When TEFM is added to the mixture, the amount of long RNA products (200-400 nucleotides) becomes double (Minczuk et al., 2011). Moreover, when using dsDNA templates of different lengths, the presence of TEFM in the reaction mixture accelerates the production of long transcripts by POLRMT. Concomitantly, silencing of TEFM using RNA interference in human cells leads to a decrease in steady-state levels for promoter-distal mitochondrial transcripts, for both H and L strands (Minczuk et al., 2011).

Further *in vitro* studies show that transcription of long DNA templates is stimulated by increased concentrations of TEFM and that, in its absence, the long transcripts represent a small fraction of the total transcript levels (Posse et al., 2015). In addition, it is observed that POLRMT pauses at various sites on the DNA template, and the presence of TEFM resumes transcription after the pause, including after oxidative lesions (Posse et al., 2015).

Recent *in vivo* studies performed in mice also confirm that TEFM promotes POLRMT processivity: knockout of TEFM results in a drastic decrease of promoter-distal transcripts from both strands (16S rRNA, all mt-mRNAs and most mt-tRNAs) and an increase of short, prematurely terminated transcripts (Jiang et al., 2019).

TEFM is an important factor in the switch between replication and transcription, as POLRMT is responsible for synthesis of RNA primers for replication. In the absence of TEFM, POLRMT terminates transcription approx. 120 bp downstream from the LSP promoter, at a G-rich region named conserved sequence block II (CSBII). This region is situated close to O_H, and the short transcript is used to start replication of the H strand. In the presence of TEFM, POLRMT passes CSBII and synthesizes long transcripts (Agaronyan et al., 2015).

At the end of transcription, POLRMT leaves the mtDNA template. The factor responsible for transcription termination is mitochondrial termination factor 1 (MTERF1), identified for the first time in 1989 by Attardi group (Kruse et al., 1989). Based on previous observations that mt-rRNA genes, situated close to HSP promoter, are transcribed at a rate 16-60 times higher than the protein coding genes, located distant from the promoter (Gelfand and Attardi, 1981), the authors hypothesized that transcription is attenuated somewhere between 16S rRNA and

tRNA^{Leu} genes (Kruse et al., 1989). Using an *in vitro* transcription termination system where mitochondria isolated from HeLa cells were programmed with a DNA template containing the HSP promoter and the termination site between *16S rRNA* and *tRNA^{Leu}*, the authors identified MTERF1 by DNase footprinting (Kruse et al., 1989). Further *in vitro* transcription assays that used recombinant human MTERF1 confirmed that the factor terminates transcription efficiently, and that it acts as a monomer (Asin-Cayuela et al., 2005). However, complete termination was not observed when MTERF1-binding site was in the same orientation as HSP, being detected only with the site in the reverse orientation (Asin-Cayuela et al., 2005). Studies of MTERF1 structure using X-ray crystallography provided a model for its mechanism of action. MTERF1 binds the dsDNA at a specific G-rich region in the *tRNA^{Leu(UUR)}* gene and causes the molecule to bend. It unwinds the DNA and induces the flipping of three bases, which in turn increases the binding stability. It was proposed that because of this strong DNA binding, MTERF1 acts as a barrier for the advancing POLRMT, which leaves the DNA (Yakubovskaya et al., 2010, Jiménez-Menéndez et al., 2010).

The hypothesis that MTERF1 terminates transcription for the H strand was rejected by *in vivo* and *in vitro* studies. The mechanism of transcription termination for the H strand is still unknown. Based on assays that used randomized DNA sequences, it was shown that MTERF1 recognizes the L strand in preference to the H strand (Nam and Kang, 2005). In addition, transcription termination was more efficient in LSP orientation than in HSP (Asin-Cayuela et al., 2005, Yakubovskaya et al., 2010). Studies performed in HEK cells in which MTERF1 was over-expressed or downregulated showed that the factor prevents the accumulation of antisense transcripts of the rRNA (Hyvärinen et al., 2010). Knockout of MTERF1 in mice did not affect mt-rRNA expression, as expected if the factor bound the H strand: the steady-state levels of 12S rRNA, 16S rRNA, and various mt-mRNAs were normal. However, it was identified an increased level of antisense transcripts of the rRNA (Terzioglu et al., 2013). The current view regarding MTERF1 role is that the factor terminates transcription from the LSP by binding at the 3' end of the mRNA sequence, which prevents the transcription of antisense rRNA. The initial observation from Attardi and colleagues (Gelfand and Attardi, 1981) regarding the high levels of rRNA transcripts in mitochondria is attributed to the increased stability of those transcripts (D'Souza and Minczuk, 2018).

After transcription, maturation of the long polycistronic transcripts takes place inside membrane-less foci called RNA granules (MRG) (Jourdain et al., 2016). Like mtDNA, MRGs are associated with IMM (Rey et al., 2020). They are fluid and dynamic, being capable to fusion and exchange components. As unveiled by immunofluorescence microscopy, MRGs are

punctate structures with ellipsoid shape, with RNA compacted inside, surrounded by proteins (Rey et al., 2020). MRG associated proteins are involved in RNA processing and maturation and ribosome biogenesis (Antonicka and Shoubridge, 2015).

The polycistronic transcripts contain tRNA transcripts intercalated among the mRNA and rRNA. According to the ‘tRNA Punctuation Model’, the tRNA transcripts are excised from the transcripts and separated from mRNA and rRNA (Ojala et al., 1981). The endonucleases responsible for the excision are RNase P at the 5' and RNase Z (ELAC2) at the 3' (Holzmann et al., 2008, Brzezniak et al., 2011). The mitochondrial RNase P has no RNA component, like the cytoplasmic and bacterial RNase P, and is formed by three protein subunits: TRMT10C (MRPP1), HSD17B10 (SDR5C1, MRPP2), and PRORP (MRPP3) (Holzmann et al., 2008). The PRORP is the catalytic subunit, while TRMT10C is a tRNA methyltransferase that adds one methyl group to positions G9 and A9 (Vilardo et al., 2012, Fontanesi et al., 2020). RNase Z has dual localization, nuclear and mitochondrial, depending if its translation starts from the first AUG (and includes the MTS) or from the second AUG (nuclear form) (Rossmanith, 2011). Transcript processing starts first from the 5' end, then continues from the 3' end, as shown by *in vitro* (Manam and Van Tuyle, 1987) and *in vivo* (Rackham et al., 2016) experiments.

There are four instances in which mRNAs are not flanked by tRNAs: the 3' end of *MTND6*, the 5'ends of *MTCO1* and *MTCYB*, and the junction between *MTATP6/MTCO3* (Figure 1-9). Their mechanism of excision is currently unknown. Several Fas-activated serine/threonine kinase (FASTK) proteins, which localize to MRG, were suggested to be involved in the process, but a detailed mechanism is lacking (Jourdain et al., 2015, Boehm et al., 2017, Jourdain et al., 2017).

After separation, tRNAs, rRNAs and mRNAs undergo modifications independently. The enzyme tRNA nucleotidyl transferase 1 (TRNT1) adds the conserved CCA sequence responsible for binding the amino acids at the 3'-end of tRNAs (Nagaike et al., 2001). All the mRNAs -apart from *MT-ND6*- are polyadenylated in the 3' end (Slomovic et al., 2005, Rebelo-Guiomar et al., 2019) by the poly(A) polymerase MTPAP (Tomecki et al., 2004). Addition of a poly(A) tail completes the stop codon in the case of seven mRNAs. Apart from that, the effect of polyadenylation on stability is specific to each transcript: when MTPAP was affected by a missense variant, the steady-state levels of the transcripts identified in human fibroblasts were either decreased (*MTCO*, *ATP6/ATP8*), increased (*MTND1*) or unaffected (*MTND3*) (Wilson et al., 2014).

The mRNAs, rRNAs and tRNAs undergo base modifications as well. Those modifications have been identified for all four nucleotides, with preponderance for uridine, and they can occur at the nucleobase or at the ribose. Modifications consist of addition of a new chemical group (ex. methyl), as well as chemical modifications of the nucleotides, like substitution, oxidation, reduction or isomerisation (Rebelo-Guiomar et al., 2019). Isomerisation of uridine to pseudouridine, for example, reduces the flexibility of nucleobases and maintains RNA stability. It is the most abundant RNA modification, found in all organisms, and can form stable pairs with all the RNA nucleosides, not only adenine (Kierzek et al., 2013). Pseudouridylation of mitochondrial tRNAs was also described in *S. cerevisiae* (Behm-Ansmant et al., 2004) and plants (Fey et al., 2002).

Different nucleotide modifications can be found in mRNA, tRNA and rRNA molecules, usually at sites important for translation. For example, the 16S rRNA is methylated and pseudouridylated at sites that form the peptidyl transferase centre (PTC) or the peptide exit tunnel of the mitoribosome. Also, methylation of mRNA represses translation, by a yet unknown mechanism (Safra et al., 2017, Li et al., 2017). The molecules of tRNA are heavily modified, which is essential for their stability and folding, but also for the interaction with various proteins involved in translation. The modifications localized at the first nucleotide of the anticodon allow non-canonical base pairing and facilitate codon recognition. They are vital for translation, since mitochondria only has 22 tRNA molecules that must recognize 60 codons (Rebelo-Guiomar et al., 2019).

1.7 Translation in human mitochondria

Following transcription and RNA maturation, 11 mRNA molecules enter translation: 9 monocistronic and 2 bicistronic (*ATP6/ATP8*, *ND4/ND4L*), resulting in 13 proteins that are assembled into respiratory complexes (Anderson et al., 1981). The site of translation is separate from the nucleoid and MRGs. Using a combination of click chemistry with confocal microscopy and super resolution STED nanoscopy, Zorkau et al. (Zorkau et al., 2021) show that translation takes place at the cristae membrane.

The process of protein synthesis is performed by the mitochondrial ribosome (55S) and consists of four steps: initiation, elongation, termination and recycling. Despite their α -proteobacterial origin, mitochondria possess unique characteristics of protein synthesis, that distinguish them from bacteria.

1.7.1 Human mitochondrial ribosome

The molecular machinery that performs the protein synthesis is the mitochondrial ribosome (mitoribosome). Like in all organisms, it is composed from a small subunit (mtSSU) and a large subunit (mtLSU), each having its own function: mtSSU to bind the mRNA and mtLSU to catalyse the peptidyl-transferase reaction (De Silva et al., 2015). However, despite its eubacterial origin, the mitoribosome is different from the bacterial and cytosolic ribosomes and has different characteristics for each species. The mitoribosome is unique because it is expressed from two genomes – nuclear and mitochondrial.

Mitochondrial ribosomes are attached to the IMM by MRL45/Mba1, a protein from the mtLSU (Englmeier et al., 2017). The first structures of the mitoribosome were obtained at 13.5 Å resolution and used bovine ribosomes. These structures lead to the identification of important differences between the mitochondrial ribosomes and the bacterial and cytosolic counterparts. Mammalian mitoribosome has the lowest sedimentation coefficient (55S) compared to other ribosomes, despite having a higher mass than bacterial ribosome, due to its porous structure (Sharma et al., 2003). The bovine structures were followed by more detailed structures, obtained at a higher resolution, of human (3.5 Å, (Amunts et al., 2015)), porcine (3.8 Å, (Greber et al., 2015)) and yeast (3.3 Å, (Desai et al., 2017a)) mitoribosomes (Table 1-1).

The human mitoribosome (55S) is composed of 83 proteins (MRPs), all encoded by the nuclear genome, and three RNA molecules, all encoded by the mitochondrial genome: 16S rRNA, 12S rRNA and tRNA^{Val}. The small subunit (28S) contains a single rRNA molecule (12S) while the large subunit (39S) contains the 16S rRNA and the tRNA^{Val} (Figure 1-12). The mtSSU and mtLSU are connected by 15 intersubunit bridges, formed between RNA-RNA, RNA-protein or protein-protein (Brown et al., 2014, Amunts et al., 2015).

The most striking difference regarding human (and mammalian) mitoribosomes when compared to bacteria and cytosolic ribosomes is the inverted protein:RNA ratio. In bacteria, there is a 1:2 ratio for protein:RNA components, but in the mammalian mitoribosome, the RNA component was reduced and partially replaced with proteins during evolution, resulting in a 2:1 protein:RNA ratio (Sharma et al., 2003, De Silva et al., 2015). The 12S and 16S rRNAs are both reduced by half when compared to their bacterial counterparts (Amunts et al., 2015, Brown et al., 2014). The mitoribosomes retained some bacterial protein homologues in their structure, but those homologues have extended N and C termini; in addition, some proteins are mitochondria specific. For example, in bacteria, mRNA contain a specific sequence (Shine-Dalgarno) that base-pairs with the 3' end of the 16S rRNA from the SSU at the start of translation (Yusupova et al., 2001). In mitochondria, mRNAs do not contain this sequence

(Montoya et al., 1981), and the corresponding rRNA region is deleted: the 3' end of 12S rRNA from the mtSSU is stably bound by MRPS37 (mS37, alias CHCHD1) (Amunts et al., 2015).

Table 1-1. Details of several complete ribosomal structures resolved up to current date

	Bacterial ribosome (<i>T. thermophilus</i> , PDB 4V5J)	Human cytosolic ribosome (PDB 4V6X)	Human mitochondrial ribosome (PDB 3J9M, 3J7Y)	Yeast mitochondrial ribosome (PDB 5MRC, 3J6B)	Porcine mitochondrial ribosome (PDB 5AJ3, 4CE4)
Sedimentation coefficient	70S	80S	55S	74S	55S
Molecular weight (MDa)	2.3	4	2.8	3	2.7
RNA:protein	2:1	2:1	1:2	1:1	1:2
Small subunit	30S	40S	28S	37S	28S
	16S rRNA	18S rRNA	12S rRNA	15S rRNA	16S rRNA
	21 proteins	32 proteins	30 proteins	34 proteins	30 proteins
			(14 proteins mitochondria specific)	(14 proteins mitochondria specific)	(15 proteins mitochondria specific)
Large subunit	50S	60S	39S	54S	39S
	23S rRNA	28S rRNA	16S rRNA	21S rRNA	16S rRNA
	5S rRNA	5S rRNA	tRNA (Val)	N/A	tRNA (Phe)
	34 proteins	5.8 S rRNA	53 proteins	39 proteins	52 proteins
		47 proteins	(21 proteins mitochondria specific)	(13 proteins mitochondria specific)	(22 proteins mitochondria specific)
Reference	(Jin et al., 2010)	(Anger et al., 2013)	(Brown et al., 2014, Amunts et al., 2015)	(Amunts et al., 2014, Desai et al., 2017a)	(Greber et al., 2014b, Greber et al., 2015)

Another example is the complete loss of 5S rRNA in the mammalian and yeast mitoribosomes. In bacteria and cytosolic ribosomes, the LSU contains one molecule of 5S rRNA in the central protuberance, responsible for coordination with SSU during translation (Dontsova and Dinman, 2005). In yeast mitoribosomes, this is completely absent and is replaced by extended segments of the 21S rRNA (Amunts et al., 2014). In mammalian mitoribosomes, at the central protuberance is present a tRNA molecule that compensates for the loss of 5S: tRNA^{Val} (human) or tRNA^{Phe} (porcine) (Brown et al., 2014, Greber et al., 2014b) . Interestingly, Rorbach et al. showed that when the tRNA^{Val} steady-state levels are scarce, the human mitoribosome integrates a tRNA^{Phe} at the same site (Rorbach et al., 2016).

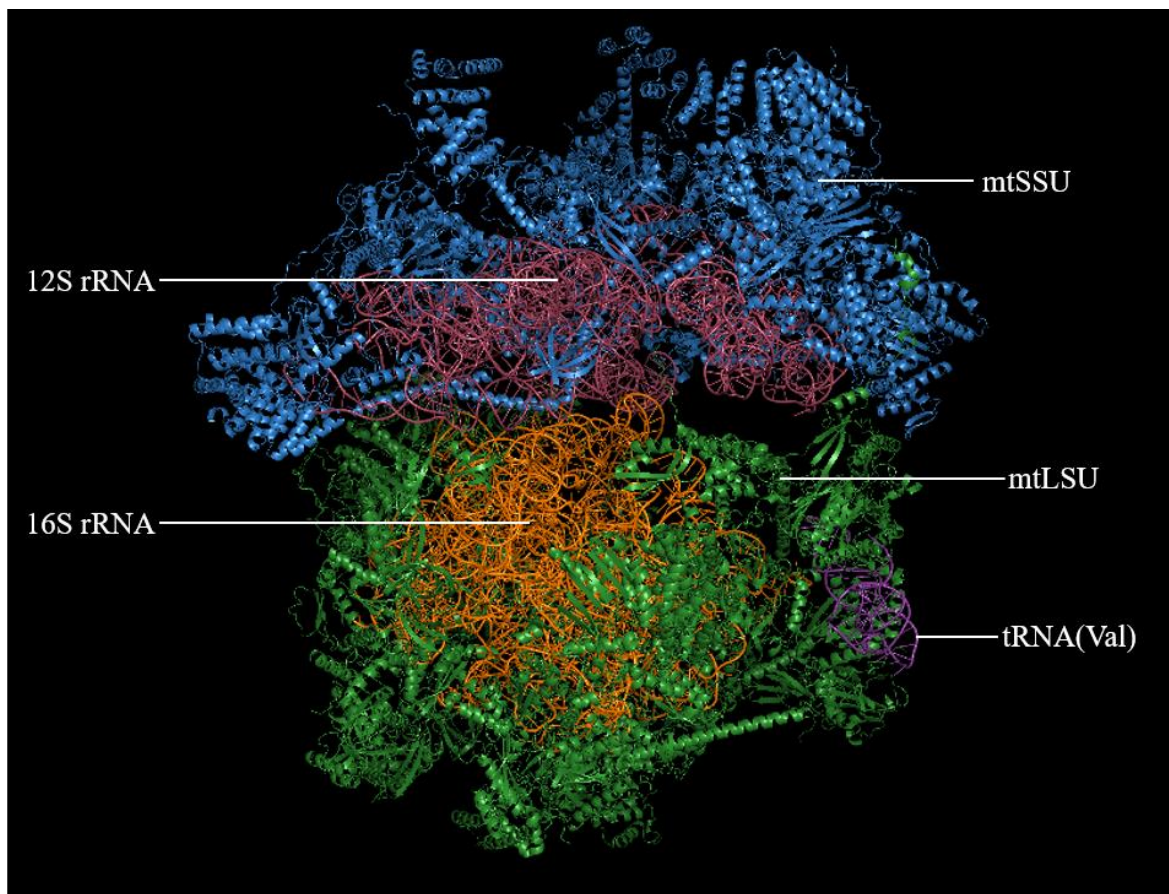


Figure 1-12. Structure of the human mitochondrial ribosome

The human mitochondrial ribosome is composed from a small (mtSSU) and a large (mtLSU) subunit. The structure PDB file 6zm5 (Itoh et al., 2021) was imported into PyMOL and coloured as it follows: sky blue – all the proteins of mtSSU; salmon pink- 12S rRNA (mtSSU), forest green- all the proteins of mtLSU; orange -16S rRNA (mtLSU); purple- tRNA(Val) (mtLSU)

The mRNA channel in the mtSSU was also remodelled during evolution. The loss of bacterial uS4 and the deletion of the C-terminal domain of uS3 resulted in a wider entry (15 Å diameter compared to 9 Å in bacteria), but the average diameter of the channel is smaller than the bacterial one. The mRNA is forced to enter as a single strand, and is bound by MRPs rich in

positive amino acids, like MRPS5 (uS5m) and MRPS39 (mS39, alias PTCD3) (Amunts et al., 2015).

In mtLSU, structural modifications affect the polypeptide exit tunnel and the tRNA binding sites. The polypeptide exit tunnel is paved with hydrophobic residues, since the polypeptides that pass through it are highly hydrophobic in order to integrate in the IMM as part of the OXPHOS complexes. Some proteins were lost from the A and P site when compared to bacteria, and some 16S rRNA segments were lost from the E site. This is in accord with the unique structure of mt-tRNAs, which lack the D- and/or T-loops that form the elbow, and results in a more loose binding of the tRNAs (Brown et al., 2014).

The section that was neither deleted nor reduced is the peptidyl transferase centre (PTC), the catalytical core of all ribosomes. PTC is responsible for the formation of peptide bond during translation and is remarkably conserved among species (Petrov et al., 2018). In mammalian mitoribosomes, PTC is formed by the folding of 16S rRNA in the mtLSU and is stabilised by MRPL36 (bL36m) (Brown et al., 2017).

Biogenesis of the human mitoribosome is a complicated process that starts at the nucleoids and continues in the RNA granules (Bogenhagen et al., 2014, Antonicka and Shoubridge, 2015). It is a lengthy process- it takes 2-3 h (Bogenhagen et al., 2018) compared to only 2 min in bacteria (Chen et al., 2012) - and is likely to take place in contact with the IMM (Kummer and Ban, 2021). The core of each subunit is the mature rRNA, around which are assembled the MRPs, imported from the cytosol. Positioning the rRNA inside the mitoribosome, covered by proteins, is thought to protect the rRNA from mitochondrial ROS (Koc and Koc, 2012). MRPs are imported in excess and degraded if not used. They respect a certain hierarchy during assembly, with clusters of early binding proteins attaching to the rRNA molecules and facilitating the binding of the intermediary proteins, which in turn facilitate the binding of late assembly proteins. This hierarchy is abandoned in certain situations that are essential for translation. For example, MRPL45 (mL45) also binds early, despite not having a direct contact with the 16S rRNA, to anchor the mtLSU (and subsequent mitoribosome) to the IMM (Bogenhagen et al., 2018). Also, folding of the 16S rRNA to form the PTC is a late-assembly step (Brown et al., 2017).

Ribosome biogenesis is a multi-step process that depends on numerous ribosome assembly factors, like guanosine triphosphate hydrolases (GTPases), RNA helicases, pseudouridine synthases, methyltransferases or endonucleases. They can be specific to one ribosomal subunit or they can act on both. Some of them reside in the RNA granules and regulate the folding of

12S and 16S rRNAs (Jourdain et al., 2016, Lopez Sanchez et al., 2021). The RNA binding assembly factors are not restricted to the initial steps of biogenesis. For example, methyltransferases MRM2 and MRM3, which methylate the ribose moieties of 16S rRNA (position U1369 and G1370, respectively) at the PTC, were found to be associated with mtLSU at late stages of assembly (Maiti et al., 2020, Rorbach et al., 2014). Also, two assembly factors can act at the same site, like TFB1M (analogous to transcription factor TFB2M) and RBFA. They both bind at the 3' terminus of 12S rRNA and both are involved in methylation of A936 and A937 towards the end of assembly (Liu et al., 2019b, Rozanska et al., 2017). RBFA also regulates the association with mtLSU (Rozanska et al., 2017). Importantly, the residues A936 and A937 are protected by GTPase ERAL1 during mtSSU assembly, which dissociates at the end of the process to allow RBFA binding (Dennerlein et al., 2010, Rozanska et al., 2017).

Other factors, like the RNA helicases DDX28 and DHX30, do not have a clear mechanism of action. DDX28 and DHX30 were found in the MRGs and appeared to be involved in mtLSU assembly (Antonicka and Shoubridge, 2015). DDX28 was found to bind 16S rRNA during the early steps of assembly (Tu and Barrientos, 2015), and depletion of DHX30 affected the formation of mtLSU and of the monosome (Antonicka and Shoubridge, 2015).

1.7.2 Initiation

Initiation of translation in human mitochondria is currently not fully understood. According to the model that best fits the current knowledge, mRNA is bound by mtSSU, and the start codon positioned in the P site is recognized by the initiator tRNA (Kummer and Ban, 2021). Based on the endosymbiotic origin of mitochondria, it was expected that mitochondrial and bacterial translation are similar. There are common characteristics- like the initiator tRNA, which is the formyl-methionyl-tRNA^{Met} (fMet-tRNA^{Met}) in both mitochondria and bacteria, in contrast to the cytosolic translation that uses Met-tRNA^{Met} (Spencer and Spremulli, 2004). However, as described for the mitoribosomes, the process per ensemble is unique. Mitochondria translation has diverged from bacterial translation (Ayyub and Varshney, 2020).

In bacteria there are three factors involved in translation initiation: IF1, IF2 and IF3. IF1 binds to the SSU and blocks the A site, ensuring that the initiator tRNA binds to the P site. IF2 recruits the fMet-tRNA^{Met} to the P site using GTP hydrolysis. IF3 prevents the premature association of LSU and adjusts the start codon to the P site (Rodnina, 2018). Because they have homologues in both Archaea and the cytosol, IF1 and IF2 are considered universal (Roll-Mecak et al., 2001). Despite that, IF1 is absent from mitochondria. Instead, the mitochondria IF2 (mtIF2) contains

a 37 aa insertion that interacts with the same region where IF1 would bind, and blocks the A site (Yassin et al., 2011).

A challenging question of mitochondria translation initiation was how the mt-mRNA is recruited, how the start codon is positioned at the P site and how it is recognized as the initiation point of translation. Mitochondrial mRNAs do not possess a sequence to signal the position of the start codon, as in bacteria and cytosolic transcripts (Christian and Spremulli, 2012). In bacteria, the Shine–Dalgarno sequence, containing the conserved sequence AGGAG, is localized at the transcript 5'end, upstream from the start codon, and is recognized by the anti-Shine–Dalgarno sequence of the rRNA from the small subunit. In this manner, the start codon is correctly positioned in the P site of the bacterial ribosome (Rodnina, 2018). In cytosolic translation, transcripts possess a 5'cap 7-methylguanosine (m7G) and the start codon is contained in the Kozak sequence (Kozak, 1986). The 5'cap recruits the pre-initiation complex, which scans the transcript until it recognizes the Kozak sequence (Hinnebusch, 2014). Mitochondria transcripts do not have a 5'cap or anything similar to a Kozak sequence (Montoya et al., 1981).

This question was initially solved in yeast: the mitochondrial transcripts are recognized by translation activators that bind to their 5'UTR regions, as well as to the mtSSU, and direct initiation of translation (Herrmann et al., 2013). However, mammalian transcripts do not have UTRs (Temperley et al., 2010b) and artificial addition of nucleotides upstream from the start codon inhibits translation (Christian and Spremulli, 2010). The only translation activator identified so far- TACO1- was shown to bind only the COX1 mRNA (Weraarpachai et al., 2009). In addition, in a mouse model, TACO1 was shown to bind at multiple regions of the transcript, and not to be required for the transcript recruitment to the mitoribosome (Richman et al., 2016).

The use of cryo-EM shed light on the translation initiation process. Kummer et al. (Kummer et al., 2018) applied this technique to study an initiation complex formed by porcine mitoribosomal subunits and human mtIF2, *MT-COX3* mRNA and fMet-tRNA^{Met}. Their results show that mtIF2 only interacts with the mitoribosome and not with the mRNA. MtIF2 binds the A site of the mtSSU and also interacts with the mtLSU- more exactly the PTC and MRPL12 (bL12m)- and the 3'-CCA end of fMet-tRNA^{Met}. They find that mRNA binds MRPS39 (mS39), a pentatricopeptide repeat (PPR) protein specific to mitochondrial ribosomes, situated close to the mRNA entry channel in the mtSSU. The authors note that the 11 mitochondrial transcripts contain U-rich sequences that start from the seventh codon and suggest that those sequences could bind the PPR motif in MRPS39. They also observe that MRPS5 (uS5m) forms the

opening of the mRNA channel and consider that the positively charged amino acids from MRPS5 attract the negatively charged mRNA, which MRPS5 guides towards the P site. Importantly, the authors show that the N-terminus of MRPL45 blocks the polypeptide exit tunnel during initiation of translation.

In a later cryo-EM study, Aibara et al. (Aibara et al., 2020) identified the LRPPRC-SLIRP complex associated with the translating mitoribosome in human cells. This interaction was specific to mitoribosome particles that contained a mt-mRNA and a mt-tRNA in the P-site. LRPPRC is a protein with 33 predicted PPR motifs involved in RNA binding. It preferentially binds mt-mRNAs, relaxing the secondary structures and exposing certain sites for translation (Siira et al., 2017). Based on their observations, Aibara et al. (Aibara et al., 2020) conclude that LRPPRC-SLIRP delivers the mRNA to the mitoribosome, binding MRPS39 at the entrance channel, to ensure correct accommodation of the mRNA.

Koripella et al. (Koripella et al., 2019) obtained the cryo-EM structure of the bovine mtSSU in complex with human mtIF3. The mtIF3 sequence is only 20-25% homologous to its bacterial counterpart (Koc and Spremulli, 2002). Both N and C termini contain mitochondria specific extensions. MtIF3 has the shape of two globular domains (corresponding to N and C terminus) connected by a flexible helical region (Bhargava and Spremulli, 2005). Koripella et al. (Koripella et al., 2019) mapped each domain on the mtSSU and found that the N-terminus strongly anchors the factor to the subunit, while the C-terminus prevents the binding of the mtLSU. The N-terminus forms multiple interactions with MRPS11 (uS11) as well as helix 23 (h23) and h24 of the 12S rRNA. The C-terminus binds close to the P-site and forms most contact points with h24, but also contacts h44 and h45. From this position, it interferes with the formation of two conserved intersubunit bridges.

Interestingly, the authors noticed that the mitochondrial specific extension of the C-terminus does not interact with the 28S subunit. When they superimposed their mtIF3-28S structure with the structure of the initiating complex from Kummer et al. (Kummer et al., 2018), they observed that this mitochondrial specific extension would clash with both the tRNA acceptor arm and mtIF2. The Koripella (Koripella et al., 2019) structure does not contain a mRNA, and it was previously shown that mtIF3 destabilizes the fMet-tRNA^{Met} from the P site in the absence of a mRNA molecule (Bhargava and Spremulli, 2005).

Reconstitution of pre-initiation complexes using human mtSSU also shows that mtIF3 and the fMet-tRNA^{Met} cannot be present at the same time on the same mtSSU particle (Khawaja et al., 2020). Binding of mtIF3 is also incompatible with MRPS37 (mS37), a protein from the mRNA

exit site that controls rotation of the mtSSU. The authors suggest that mtIF3 binding restricts mtSSU rotation and induces a conformation that allows mtIF2 binding. As a result, the conformations of both mtIF2 and mtSSU (particularly h44) are rearranged, which allows binding of mtLSU and exchange of mtIF3 for fMet-tRNA^{Met} and mRNA. The mt-mRNA molecules were not detected on the mtSSU and were only found in the monosome. In the new translation initiation model proposed (Khawaja et al., 2020), mt-mRNA binds to the monosome that contains attached an mtIF2 molecule, necessary for recruitment of fMet-tRNA^{Met} (Figure 1-13). Binding to the monosome seems to be favoured by the lack of any 5' signal sequence in mt-mRNA and has been previously shown to occur in bacterial ribosomes that translate leaderless mRNA (Udagawa et al., 2004, Moll et al., 2004).

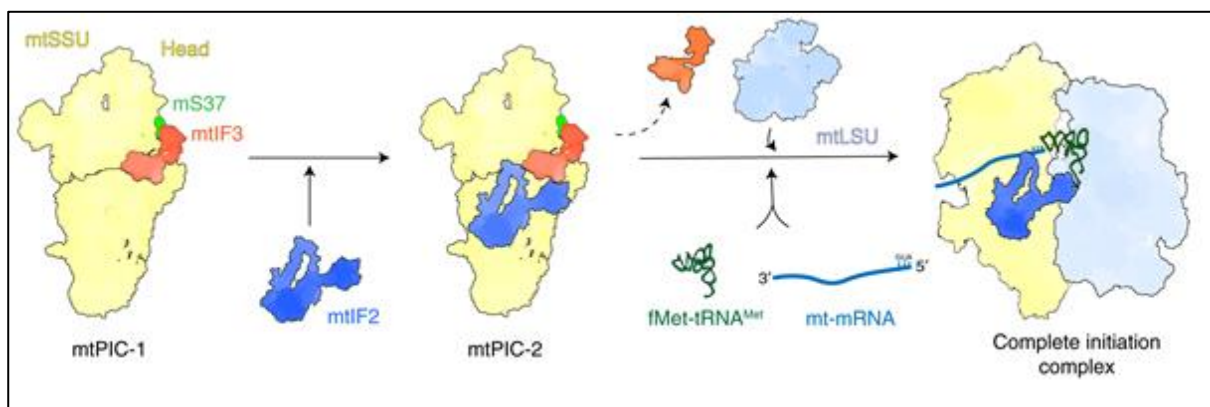


Figure 1-13. Translation initiation in mammalian mitochondria (taken from (Khawaja et al., 2020)

Binding of mtIF3 to mtSSU causes MRPS37 (mS37) to restrain subunit rotation (first pre-initiation complex, mtPIC-1) and to maintain a conformation that favours mtIF2 binding (second pre-initiation complex, mtPIC-2). Next, mtLSU binds and mtIF3 leaves the complex. Finally, mRNA binds to the monosome and the initiator tRNA (fMet-tRNA^{Met}) is recruited by mtIF2; permission to use this figure was granted because the original article is licensed under a Creative Commons Attribution 4.0 International License

<http://creativecommons.org/licenses/by/4.0/>

Mitochondria use the canonical start codon AUG but can start translation from AUA and AUU as well (Montoya et al., 1981). The three codons are recognized by the same tRNA^{Met} molecule, which is modified at the first nucleotide in the anticodon (wobble base) with formylcytosine (f⁵C34) (Bilbille et al., 2011). Currently, it is still unknown how they are recognized as start codons. One possibility could be that they are recognized based on proximity to the transcript 5' end, which is maintained unwound by LRPPRC-SLIRP, as suggested by Siira et al. (Siira et al., 2017). However, there are two bicistronic transcripts in human mitochondria (ATP6/ATP8, ND4/ND4L) which contain an internal start codon, and how they are recognized is also a mystery (Kummer and Ban, 2021).

1.7.3 Elongation

Elongation is the most conserved step of mitochondria translation, as the factors involved have orthologs in bacteria and cytosol. During elongation, the polypeptide is formed by successive addition of amino acids while the mitoribosome moves on the mRNA codon by codon. The process can be divided in three steps: decoding, peptide bond formation and translocation (Kummer and Ban, 2021).

During decoding step, the codon that arrives on the A site is recognized by the corresponding aminoacyl-tRNA. The aminoacyl-tRNAs are synthetized by aminoacyl-tRNA synthetases, which form an ester bond between the adenine from 3' acceptor stem of the tRNA and the corresponding amino acid (Boczonadi et al., 2018a). In mitochondria exists only one tRNA^{Met} that is used both to initiate translation and to deliver methionine residues to the A site during elongation (Tucker et al., 2011). The MTFMT enzyme adds a formyl group to the Met-tRNA^{Met} (Takeuchi et al., 1998), which is then recruited to the P site to initiate translation. The Met-tRNA^{Met} that remains non-formylated is recognized by the mitochondrial elongation factor EF-Tu and used in elongation (Spencer and Spremulli, 2004).

Mitochondrial EF-Tu GTP-activated binds an aminoacyl-tRNA and delivers it to the A site. If the codon: anticodon base-pairing occurs, GTP is hydrolysed and the EF-Tu-GDP is released from the mitoribosome. The guanine exchange factor mtEF-Ts then recycles EF-Tu-GDP to EF-Tu-GTP (Schwartzbach and Spremulli, 1989, Cai et al., 2000) (Figure 1-14).

Peptide bond formation is catalyzed by the PTC in the large subunit. PTC is a ribozyme formed by interconnected sections of 16S rRNA, which interacts with the 3'CCA ends of tRNAs from the P and A site during elongation (Brown et al., 2017). In the first reaction, the nucleophilic amino group of the amino acid from the A site attacks the electrophilic carbonyl carbon of the ester bond that links the nascent polypeptide to the tRNA from the P site, breaking the ester bond. In the second reaction, the PTC catalyses the condensation between the amino group of the amino acid bound to the A site tRNA and the carboxyl terminus of the polypeptide chain, resulting in a new peptide bond. At the end of this reaction, the P site contains a deacylated tRNA, the A site contains the nascent polypeptide and the E site is empty (Rodnina, 2013). For translation to continue, the A site must become empty, to accommodate a new aminoacyl-tRNA.

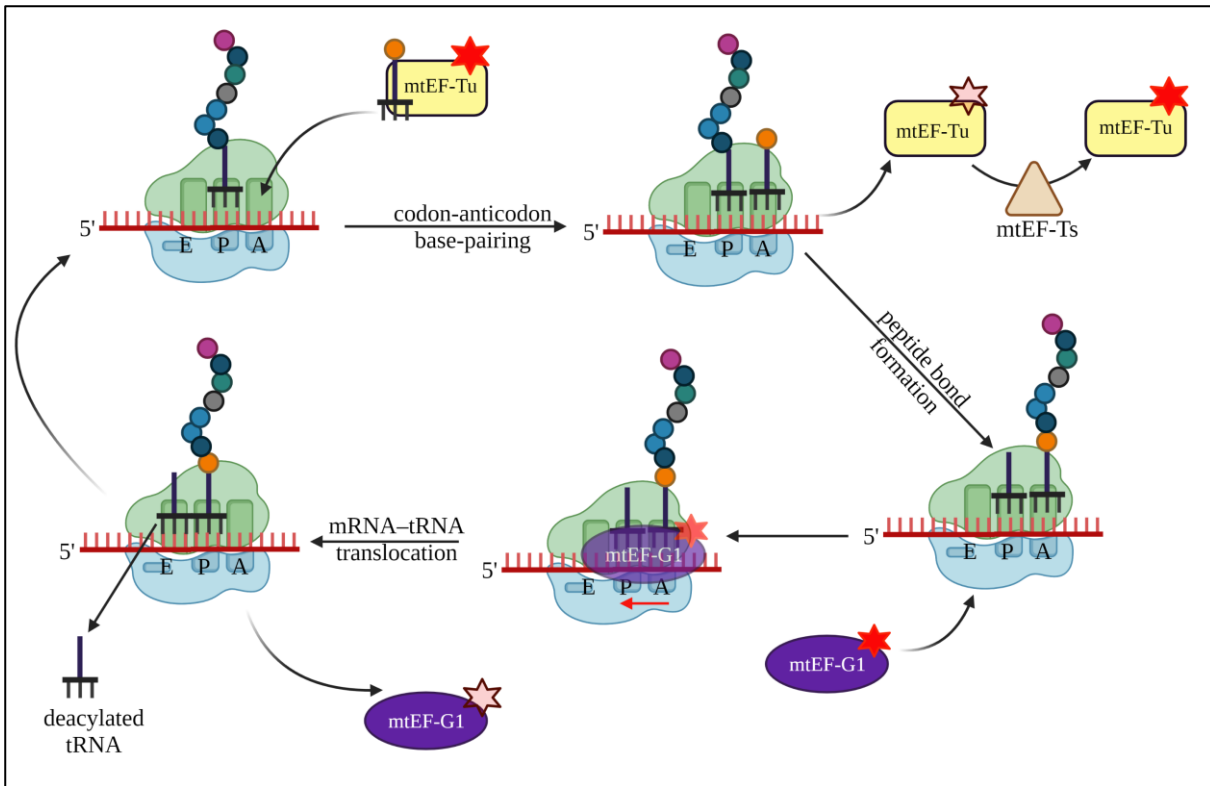


Figure 1-14. Translation elongation in mammalian mitochondria

A new aminoacyl-tRNA is bound by mtEF-Tu GTP-activated and delivered to the A site. Once the recognition between codon and anticodon takes place, mtEF-Tu-GDP leaves the mitoribosome and is recycled by mtEF-Ts. The PTC in the mtLSU catalyses the formation of the peptide bond between the carboxyl terminus of the P site polypeptide and the amino group of the newly delivered amino acid from the A site, resulting in an intermediary state where the peptidyl-tRNA occupies the A site. Binding of mtEF-G1 GTP-activated induces the mRNA-tRNA translocation with one codon, so that peptidyl-tRNA relocates to the P site, A site remains empty and the deacylated tRNA occupies the E site, from where it is ejected. Pale green subunit = mtLSU; pale blue subunit = mtSSU; dark magenta circle = N-formyl-methionyl; red star = GTP; pale brown star = GDP; cartoon not on scale; made using BioRender, www.biorender.com

During translocation, the mitoribosome advances by one codon and the mRNA and tRNA molecules are repositioned, so that the deacylated tRNA moves to the E site, the peptidyl-tRNA to the P site and the A site remains empty. The factor that catalyses the mRNA-tRNA translocation is the GTPase mtEF-G1 (Chung and Spremulli, 1990), a homologous of bacterial EF-G and cytosolic EF-2 (Hammarsund et al., 2001) (Figure 1-14). The movement is made possible by the rotation of the mtSSU head (Kummer and Ban, 2020, Koripella et al., 2020) and the risk of frameshifting is avoided thanks to specific contacts between mtEF-G1 and mRNA, tRNA and the mitoribosome. In the so called ‘classical’ state, the tRNAs are bound to the mtSSU with their anti-codon stem loops, and their acceptor stems protrude towards the mtLSU. In this manner, a tRNA occupies the same site (A or P) on both mtSSU and mtLSU. When mtSSU starts to rotate, the tRNAs are initially repositioned only in the mtLSU (from A site to

P site and from P site to E site) and keep their original sites in the mtSSU, which results in a ‘hybrid’ state (Kummer and Ban, 2020). Binding of mtEF-G1 stabilizes this hybrid state and prevents the tRNAs from slipping back, while the mtSSU head swivels around its own axis and repositions the tRNAs on mtSSU (from A to P site and from P site to E site) (‘chimeric’ state). Eventually, the tRNAs are repositioned on their new sites on both mtSSU and mtLSU, resulting in a ‘classical’ state in which both the anticodon stem loop and the acceptor stem of the same tRNA occupy the same site (P and E, respectively) (Kummer and Ban, 2020).

The human mtEF-G1 is 45% identical with bacterial EF-G, but also contains some unique characteristics, like a mitochondrial targeting signal (36 aa) which is cleaved, and mitochondrial-specific extensions, like the 11 aa extension from the C-terminus (Bhargava et al., 2004). Cryo-EM studies helped identify the binding sites of mtEF-G1 and established that interaction with the mitoribosome stabilizes the factor in a catalytic conformation (Kummer and Ban, 2020, Koripella et al., 2020). MtEF-G1 is likely to be recruited by the C-terminal domain of MRPL12 (uL12m) (Koripella et al., 2020). The mitochondria-specific extension of mtEF-G1 C-terminus is involved in translocation of the acceptor stem of the tRNA from the A site. The extension overlaps with the 3’CCA of the tRNA from the A site, pushing it to move towards the P site, and in the same time interacts with h71 of 16S rRNA, preventing the tRNA from translocating back to the A site (Koripella et al., 2020). After translocation, mtEF-G1 interacts with the mRNA-tRNA codon–anticodon region at the P site and helps stabilizing it. Two conserved consecutive glycine residues of the factor (G544 and G545) form the tip of a loop that sterically fits in the minor groove of the mRNA-tRNA, while two conserved polar residues (Q542 and H617) contact the tRNA backbone to prevent it from slipping (Kummer and Ban, 2020). The deacylated tRNA which arrives on the E site is weakly bound to the mitoribosome, due to the loss of two bacterial rRNA helices from mt-rRNA. The mtSSU rotates back, MRPS7 (uS7m) dislocates the E-site tRNA from the mRNA, and the deacylated tRNA is eventually ejected from the mitoribosome (Kummer and Ban, 2020).

During initiation, the polypeptide exit tunnel was blocked by the N-terminus of MRPL45 (Kummer et al., 2018). During elongation, upon mtEF-G1 binding, Koripella et al. (Koripella et al., 2020) observed that a conserved adenine from a loop region of 16S rRNA (A2725) intercalates between the N terminus of the nascent polypeptide and the N-terminus of MRPL45. This induces a conformational change that results in retraction of MRPL45, allowing the polypeptide to accommodate in the exit tunnel.

The nascent polypeptide is inserted in the IMM co-translationally, through the Oxa1L insertase, which has three contact sites with the mitoribosome (Itoh et al., 2021). The interaction

mitoribosome - IMM and the insertion of the polypeptide chain are facilitated by cardiolipin, a mitochondria specific phospholipid (Lee et al., 2020). The protein that orchestrates the insertion is MRPL45. The N-terminus of MRPL45 enters the exit channel, where it prevents the polypeptide from premature folding and directs it towards the channel opening. In addition, MRPL45 regulates the positioning of the channel opening with respect to the Oxa1L and maintains a gap between the two, to allow access for polypeptide modifications prior to insertion. First, the formyl group from the polypeptide N-terminus is removed by the mitochondrial peptidyl deformylase, then the starter methionine is removed by the methionine aminopeptidase (Serero et al., 2003, Leszczyniecka et al., 2006). Finally, the unfolded polypeptide chain enters the Oxa1L.

Apart from mtEF-Tu, mtEF-Ts and mtEF-G1, another translation elongation factor has been identified: mtEF4 (named GUF1 in yeast), a homologous of bacterial LepA. Bauerschmitt et al. show that in yeast mitochondria, GUF1 is associated with the IMM and binds the mitoribosome using GTP hydrolysis (Bauerschmitt et al., 2008). The factor promotes protein synthesis in stress conditions, like starvation or a too low/too high growth temperature, but not under physiological conditions. A similar result was obtained in *Caenorhabditis elegans*: at cold temperature, mitochondria translation was reduced and complex IV assembly was disrupted in the absence of mtEF4 (Yang et al., 2014). Moreover, mtEF4 is essential for spermatogenesis in mice (Gao et al., 2016). MtEF4 localizes to mitochondria and interacts with mitoribosomes in human cells, where it regulates apoptosis (Zhu et al., 2018). They find that the factor is upregulated in several cancer cells, which dysregulates mitochondria translation and promotes tumour progression. Cryo-EM studies revealed that mtEF4 promotes the back-translocation of tRNAs on the *E. coli* ribosome, similarly to LepA, to allow the ribosome to translocate the tRNAs correctly (Connell et al., 2008).

1.7.4 Termination

Translation terminates when the ribosome reaches a stop codon (UAA, UAG and UGA in bacteria and cytosolic translation) at the A site. In this case, instead of a tRNA, the stop codon is recognized by translation release factors that induce the hydrolysis of the nascent polypeptide (Nakamura et al., 1996). Two classes of release factors have been described. Class I factors contain a codon recognition motif that enters the empty A site and a highly conserved GGQ motif that interacts with the PTC to induce peptide release. In bacteria, there are two class I factors: RF1, that recognises UAA and UAG codons, and RF2 that recognises UAA and UGA (Rodnina, 2018), while in eukaryotic translation there is only one factor (eRF1) that recognizes

all three stop codons (Konecki et al., 1977, Frolova et al., 1999). Class II factors (RF3 in bacteria, eRF3 in cytosolic translation) are GTPases that catalyze the dissociation of class I factors from the ribosome (Freistroffer et al., 1997, Alkalaeva et al., 2006).

Release factors cannot exert peptide release activity independently, but only in the context of the ribosome (Jin et al., 2010, Weixlbaumer et al., 2008, Korostelev et al., 2008). They have a structural element that interacts with the nucleotides of the stop codon (recognition loop, sometimes called ‘anticodon’ loop); this element is formed by the 3D interaction between the N-terminal tip of helix α 5 and a conserved tripeptide (Figure 1-15, regions 1 and 2) (Ito et al., 2000, Petry et al., 2005). The tip of the helix α 5 contacts the uracil from the first position of the stop codon (Petry et al., 2005), while the tripeptide motif recognizes the nucleotides from the second position. In bacteria, release factors have different tripeptides: RF1 has a conserved PXT to recognize the adenine in the second position of the stop codon, while RF2 has a SPF tripeptide that can recognize either A or G at the second position (Ito et al., 2000). The third nucleotide of the stop codon is unstacked from the first two and recognized by other conserved amino acid residues from the anticodon loop: Gln-181 and Thr-194 (RF1, (Laurberg et al., 2008)) or Val-203 and Thr-216 (RF2, (Korostelev et al., 2008), aa numbering according to *Thermus thermophilus*).

When a release factor recognizes the stop codon, it undergoes a structural rearrangement and adopts an open conformation that directs the GGQ domain into the PTC, which in turn induces the peptidyl-tRNA hydrolysis (Polacek and Mankin, 2005). The two glycine residues confer flexibility to the GGQ motif, while glutamine forms interactions with PTC. Glutamine interacts with the 3' terminus of the tRNA from the P site as well as with key nucleotides from rRNA, forming a pocket that can accommodate a water molecule. The water molecule is necessary for the hydrolysis of the ester bond between the nascent peptide and peptidyl-tRNA. For glutamine to form the correct bonds, it requires N⁵-methylation (Zeng and Jin, 2018, Mora et al., 2007).

Figure 1-15. Alignment between bacterial and human mitochondrial release factors

Primary sequences of *T. thermophilus* RF1 (UniProt ID Q72HB8), RF2 (UniProt ID Q5SM01) and human mtRF1a (RF1ML, UniProt ID Q9UGC7), mtRF1 (RF1M, UniProt ID O75570), ICT1 (UniProt ID Q14197) and C12orf65 (MTRFR, UniProt ID Q9H3J6) were retrieved in FASTA format and aligned using Clustal Omega from EMBL-EBI (Goujon et al., 2010, Sievers et al., 2011). The codon recognition domains are indicated by rectangles 1 and 2. Rectangle 3 indicates the domain responsible for peptidyl-tRNA hydrolysis containing the GGQ motif. The conserved aa are classified as: identical (*), conserved (:) and semi-conserved (.) The percent identity matrix shows the percentage of identity between any two proteins of the alignment. The identity between a protein and itself is 100.00.

Mammalian mitochondria only contain two stop codons: UAA (used by nine transcripts) and UAG (used by *MTCO2* and *MTATP8*). For seven transcripts, the UAA stop codons are formed by polyadenylation, and two transcripts end in codons that usually encode for arginine (AGA, AGG) (Anderson et al., 1981). The search for the release factor that would recognize them started with the alignment between bacterial release factors and the human database. In 1998 it was identified a RF orthologue with a strong similar sequence to bacterial RF1, named mtRF1 (Zhang and Spremulli, 1998). The factor presented an almost identical GGQ motif with the one from RF1, but the recognition loop was different (Figure 1-15, regions 1 and 2). MtRF1 was more similar to RF1 than to RF2, which was in agreement with the two stop codons from mitochondria. However, despite proven to be a mitochondrial protein, mtRF1 showed no peptidyl-tRNA hydrolase (PTH) activity neither *in vitro*, using *E. coli* ribosomes, nor *in vivo*, since it failed to rescue *S. cerevisiae* or *S. pombe* lacking mitochondrial RFs (Soleimanpour-Lichaei et al., 2007).

Further bioinformatic approaches identified three other proteins that showed a sequence similar to bacterial RF1: mtRF1a, C12orf65 and ICT1. They, together with mtRF1, were classified as the mitochondrial translation release factor family (Chrzanowska-Lightowers et al., 2011). Only mtRF1a was proven to induce peptide release in mitochondria at the end of translation. Lightowers' group showed that mtRF1a was imported in the mitochondria and released tritiated formyl-Met only when UAA or UAG, but not UGA, were used in the assay (Soleimanpour-Lichaei et al., 2007). In addition, when used on yeast strains (*S. cerevisiae* and *S. pombe*) that lacked the mitochondrial homologue of RF1, mtRF1a restored the growth phenotype by promoting protein synthesis. Regarding the AGA and AGG codons, it was shown that the mitoribosome performs a -1 frameshift when encounters them, which results in the canonical UAG stop codon (Temperley et al., 2010a). Therefore, mtRF1a terminates translation for all the 13 mitochondrially encoded proteins (Chrzanowska-Lightowers et al., 2011) (Figure 1-16).

Analysis of mtRF1a primary sequence reveals the presence of the conserved GGQ as well as a typical codon recognition motif. The codon recognition motif contains the PXT tripeptide, same as bacterial RF1, and has a very similar helix a5 (Figure 1-15), like a classical release factor. Comparison with mtRF1, which is believed to have resulted from a gene duplication (Young et al., 2010), shows that the codon recognition motif is different: mtRF1 contains an extension of three peptides adjacent to the PXT motif, as well as two additional nucleotides in the a5 region. The role of this factor is currently unknown. Based on the extended motif, on the presence of the GGQ and on 3D modelling studies, Huynen et al. (Huynen et al., 2012) hypothesised that

mtRF1 could be implicated in translation termination of a truncated mRNA, when the A site would be empty.

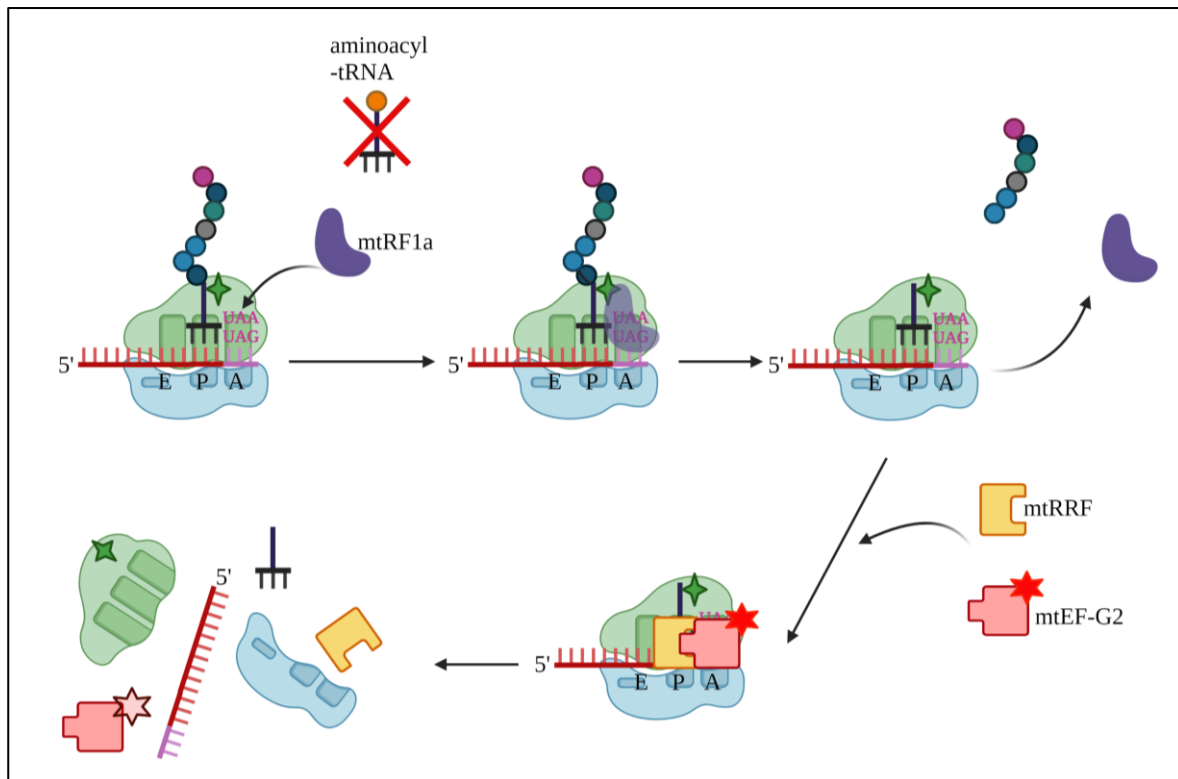


Figure 1-16. Translation termination and recycling in mammalian mitochondria

When a stop codon arrives at the A site of the mitoribosome, in the absence of a compatible aminoacyl-tRNA, it is recognized by mtRF1a. The anticodon loop of mtRF1a binds the nucleotides from the stop codon, while the GGQ motif interacts with the PTC (bright green morning star) in the mtLSU and induces the release of the nascent polypeptide from the P site. The mitoribosome is subsequently bound by recycling factors mtRRF and mtEF-G2 which split the large and the small subunit. GTP hydrolysis is required for mtEF-G2 to leave from the split subunits. Pale green subunit = mtLSU; pale blue subunit = mtSSU; dark magenta circle = N-formyl-methionyl; red star = GTP; pale brown star = GDP; cartoon not on scale; made using BioRender, www.biorender.com

The other two members of the mitochondria release family – C12orf65 and ICT1 – contain the GGQ motif, but not the codon recognition motif. When comparing their primary structure with the primary structures of mtRF1/mtRF1a, one can notice that few amino acids are present in the N-terminus half. This suggests that their PTH activity, conferred by the GGQ motif, should be codon-independent, and raises questions regarding the achievement of an open conformation in the absence of a codon- ‘anticodon loop’ recognition.

ICT1 (immature colon carcinoma transcript 1) was initially named DS-1 and was identified in human colon carcinoma, where it appeared upregulated in immature cells and downregulated during *in vitro* differentiation (Van Belzen et al., 1995). Later, Richter et al. (Richter et al., 2010a) showed that ICT1 is a mitochondrial protein that is cleaved upon import and confirmed

its involvement in translation. Loss of ICT1 reduced *de novo* synthesis of mitochondria-encoded proteins and decreased the levels of complex I, complex IV and MRPL3. Importantly, the authors proved that ICT1 is a component of mtLSU in human cells and that free ICT1 maintains the PTH activity. Purified ICT1, incubated with *E. coli* ribosomes, synthetic codons and tritiated f-Met-tRNA^{Met}, induced the release of formyl-Met from the P-site tRNA, irrespective of the codons used, and only when the ribosome was added in the reaction. In addition, the release activity was lost when the GGQ was mutated, but the factor was still assembled in the mitoribosome. Further cryo-EM studies confirmed that ICT1 is integrated in the mtLSU and renamed it accordingly, first as MRPL58 (Koc et al., 2013), then as MRPL62 (Greber et al., 2014a, Ban et al., 2014). However, the ICT1 position in the mitoribosome is incompatible with its release activity, since it resides away from the A site and cannot access the polypeptide chain at the P site (Greber et al., 2014b).

ICT1 was found to be a homologous of bacterial YaeJ (also named ArfB), a rescue factor of stalled ribosomes (Kogure et al., 2013). The GGQ domains of the two factors are identical, but the N-termini differ. Human ICT1 can rescue bacterial ribosomes stalled on non-stop mRNAs by promoting the hydrolysis of the polypeptide from the P-site tRNA as efficiently as YaeJ (Kogure et al., 2013, Feaga et al., 2016). However, YaeJ targeted to mitochondria did not integrate in the mtLSU and only showed transient interactions with the mitoribosome, suggesting that ICT1 and YaeJ could be involved in ribosome rescue, but they act by different mechanisms (Wesolowska et al., 2014). Analysis of ICT1 solution structure confirmed the existence of a cluster formed by positively-charged amino acids, consistent with RNA binding, and indicated that ICT1 could enter the A site (Handa et al., 2010). It was therefore suggested that the factor might have different functions in the mitochondria: one - to contribute at mtLSU structure, and two - to rescue stalled mitoribosomes as a ‘free’ protein in excess (Handa et al., 2010).

Interestingly, Antonicka et al. (Antonicka et al., 2010) overexpressed the members of the translation release factors family in a cell line derived from a patient with a C12orf65 pathogenic variant ([NM_152269](#): c.248delT p. (Leu84*)). Only ICT1 overexpression was capable of partially suppressing the variant effects, consistent with free ICT1 playing a role in peptidyl-tRNA hydrolysis. ICT1 increased COX activity with 50% and improved assembly of respiratory complexes.

Like ICT1, C12orf65 lacks the codon recognition motif and retains the GGQ motif. However, in an *in vitro* assay that used bacterial ribosomes, C12orf65 was unable to release tritiated formyl-Met from tRNA^{Met} regardless of the codons used. The absence of a codon had the same

effect (Antonicka et al., 2010). The authors concluded that C12orf65 might still have release activity but require 55S ribosomes instead of bacterial ones.

At the start of my project, the data available on mtRF1, C12orf65 and ICT1 could not explain the exact functions of those factors, and their role in mitochondria translation remained unclear. Recently, research done in parallel by other groups shows that C12orf65 and ICT1 rescue stalled mitoribosomes. C12orf65 forms a dimer with MTRES1 to release the nascent polypeptide from mtLSU, after dissociation of mtSSU (Desai et al., 2020). The authors renamed C12orf65 as mtRF-R, but, for simplicity, the old name will be used in the current manuscript. ICT1 rescues mitoribosomes that have arrived at the 3'end of a truncated mRNA that lacks a stop codon; instead of an anticodon loop, ICT1 positions its C-terminus in the A site devoid of mRNA (Kummer et al., 2021).

1.7.5 Recycling

Once the nascent polypeptide is released, the mitoribosomal subunits are split by two factors: mitochondrial ribosome recycling factor (mtRRF) and mtEF-G2 (Figure 1-16).

MtRRF was first identified by searching for human homologues of the bacterial RRF, using bioinformatic approaches (Zhang and Spremulli, 1998). In bacteria, RRF together with elongation factor EF-G were already known to split the ribosome at the end of translation (Janosi et al., 1996), but no eukaryotic homologues had been identified. The eukaryotic recycling factor was identified much later as the ATP-binding cassette protein ABCE1 (Pisarev et al., 2010). Human mtRRF appeared to have 25-30% identity with the bacterial homologue and, although the subcellular localization prediction tool suggested it should be mitochondrial, the factor did not show a clear mitochondrial targeting sequence (Zhang and Spremulli, 1998).

The proof that mtRRF is a mitochondrial protein responsible for 55S recycling came from Rorbach et al. (Rorbach et al., 2008). The authors showed that the factor is imported into mitochondria and that possesses an extended N-terminus presequence. In addition, mtRRF bound to *E. coli* ribosomes *in vitro* as well as to human 55S ribosomes *in vivo*. Depletion of mtRRF in HeLa cells caused monosomes to accumulate and to form aggregates and increased ROS production. Also, transfection of human mtRRF into *S. pombe* strains that lacked the endogenous homologue restored the yeast growth on non-fermentable carbon sources and the steady-state levels of mitochondria-encoded cytochromes and COX2 protein.

Cryo-EM studies of human mtRRF bound to the human 55S ribosome (Koripella et al., 2019) revealed that the factor binds to the monosome when the mtSSU is rotated. The factor adopts

an L-shape that allows it to fit between the two subunits. The long arm of the ‘L’ (domain I) overlaps with the binding positions of the A- and P-site tRNA molecules and disrupts their binding in the ‘classical’ structure. The tip of domain I contains three well-conserved amino acids that interact with three nucleotides from the PTC. The short arm of the ‘L’ (domain II) interacts with MRPS12. Interestingly, the mitochondrial targeting sequence is not cleaved upon matrix import; it becomes the apical region of domain I and establishes additional interactions with 16S rRNA helices and with N-terminus of MRPL27. Interaction with mtRRF induces a conformational change in MRPL27 that obstructs the binding of the acceptor arm of the peptidyl-tRNA to the mtLSU (Koripella et al., 2019).

The other recycling factor, mtEF-G2, is a parologue of mtEF-G1 (Hammarsund et al., 2001) that only acts during recycling and has no translocation activity (Tsuboi et al., 2009). It requires the presence of mtRRF to perform subunit dissociation. If both factors are present, they can replace the endogenous RRF and EF-G in *E. coli* during *in vivo* experiments. MtEF-G2 is a GTPase but, counterintuitively, GTP hydrolysis is not required for splitting the two subunits, but for factor dissociation from the split subunits (Tsuboi et al., 2009).

The structures of mtEF-G1 and mtEF-G2 explain the distinct functions of the two factors: mtEF-G1 contains some highly conserved amino acids that are not present in mtEF-G2, amino acids that recognize the codon–anticodon base-pairing during elongation (Kummer and Ban, 2020). Also, mtEF-G2 lacks the C-terminal extension from mtEF-G1, which would clash with mtRRF. In addition, mtEF-G2 contains a surface that specifically interacts with mtRRF, while the same site in mtEF-G1 contains amino acids that would repulse mtRRF (Kummer et al., 2021).

Recently, an additional translation recycling factor has been identified: GTPBP6 (Lavdovskaia et al., 2020). GTPBP6 is a GTPase homologous to the bacterial GTPase HflX, a factor that dissociates 70S ribosomes under heat stress (Zhang et al., 2015b). GTPBP6 localizes to the mitochondria matrix and induces dissociation of the 55S ribosome but is also required for mtLSU biogenesis. On one hand, overexpression of GTPBP6 causes an accumulation of separated subunits and decreases mtDNA-protein synthesis. On the other hand, *Gtpbp6*^{−/−} cells show an accumulation of 39S assembly intermediates blocked at later stages of maturation, after all MRPLs had been assembled. It is currently unclear how the factor can perform both functions and what relationship it has with mtRRF and mtEF-G2 (Lavdovskaia et al., 2020).

1.8 Defects of translation in mitochondria

Defects in mitochondrial translation are responsible for mitochondrial diseases characterised by decreased activities of OXPHOS complexes. The clinical presentation is very diverse, with multiple organs affected, mainly brain, liver, skeletal muscle and heart, and disease progression is often fatal (Boczonadi and Horvath, 2014, Boczonadi et al., 2018b). There are currently no treatments available for mitochondrial translation defects, which is in part due to an incomplete understanding of the process. In some particular cases, the mitochondrial phenotype could be alleviated *in vitro* (Bartsakouli et al., 2016). Attempts to increase the cellular level of NAD⁺, to induce mitochondrial turnover or to modulate ROS production were successful in mice, but the translation to human seems problematic due to substantial side effects. Several clinical trials using drugs already approved for other diseases are currently undergoing, but there is no mitochondria-specific drug (Russell et al., 2020).

The causes of mitochondrial translation diseases are either mitochondrial (variants in mtDNA) or nuclear: variants in the genes encoding for mitochondrial tRNA synthetase, translation initiation, elongation and termination factors, or mitochondria ribosomal protein subunits and assembly factors. The pathogenic mtDNA variants that affect translation are transmitted maternally, while the nuclear variants are transmitted recessively and are often identified in patients from consanguineous families. The histology analysis presents ragged red fibres, COX negative fibres (Rötig, 2011).

1.8.1 Defects of mtDNA

MtDNA defects are responsible for a broad range of diseases characterized by accumulation of lactate in the blood. Patients present with various clinical manifestations and the disease severity depends on the heteroplasmy level. The most common are large-scale mtDNA deletions and pathogenic mtDNA variants (Greaves et al., 2012), although mtDNA duplications have been identified as well (Rygiel et al., 2016). Mitochondrial deletions have been reported in Pearson's syndrome (Lee et al., 2007), Kearns–Sayre syndrome (Degoul et al., 1991) and chronic progressive external ophthalmoplegia (CPEO) (López-Gallardo et al., 2009). Pearson's syndrome and Kearns–Sayre syndromes are both developed mainly in infancy; they affect multiple organs and are often fatal (Komulainen et al., 2015, Park, 2015, González-Halphen, 2002). CPEO is developed in adulthood and is characterized by external ophthalmoplegia, ptosis and hearing loss (Heighton et al., 2017).

Pathogenic mtDNA variants are usually maternally inherited (Stewart and Chinnery, 2015), but they can also be acquired sporadically during healthy aging (Baines et al., 2014). Their accumulation is associated with diseases like cancer (Ju et al., 2014) and Parkinson's (Coxhead et al., 2016) and contributes to muscle fibre loss (Herbst et al., 2007). The mechanisms responsible for the sporadic accumulation of pathogenic mtDNA variants are a matter of debate: initially, it was considered that mtDNA is damaged by ROS produced in the respiratory chain (Miquel et al., 1980), but more recent studies suggest that errors made by Poly and spontaneous cytosine deamination to uracil (resulting in a G>A transition) are more likely to be involved (Zheng et al., 2006).

One of the most common mtDNA pathogenic variants is m.3243A>G in the *MT-TL1* (mt-tRNA^{Leu (UUR)}) and a second common pathogenic variant is m.8344A>G in the *MT-TK* (mt-tRNA^{Lys}) (Greaves et al., 2012). Studies performed in Finland indicated that m.3243 A>G *MT-TL1* affect 1 in 6,000 individuals (Majamaa et al., 1998), while birth prevalence studies in England recorded a frequency of 0.14% for the same variant (Elliott et al., 2008). A more recent study conducted at Newcastle University that involved adults with suspected mitochondrial disease also found m.3243A>G *MT-TL1* to be the most common variant, followed by m.8344A>G *MT-TK* (Gorman et al., 2015). Variant m.3243A>G *MT-TL1* is involved in maternally-inherited diabetes and deafness (MIDD) and mitochondrial encephalomyopathy with lactic acidosis and stroke-like episodes (MELAS). Variant m.8344A>G *MT-TK* is associated with myoclonic epilepsy with ragged-red fibres (MERRF) (Shoffner et al., 1990).

1.8.2 Defective mt-tRNA modifying enzymes

Posttranscriptional modifications of mt-tRNA were found as well to be associated with mitochondrial translational defects. For example, a missense variant in pseudouridine synthase 1 (*PUS1*) was found to cause MLASA syndrome (mitochondrial myopathy and sideroblastic anaemia), a rare, autosomal recessive disorder characterized by defects in OXPHOS and iron metabolism which primarily affects skeletal muscle and bone marrow (Bykhovskaya et al., 2004). Also, pathogenic variants in the 5-methylaminomethyl-2-thiouridylate methyltransferase (*TRMU*) are associated with reversible infantile respiratory chain deficiency and reversible infantile hepatopathy. *TRMU* catalyses the 2-thiouridylation of the mt-tRNA^{Glu}, mt-tRNA^{Gln} and mt-tRNA^{Lys}. *In vitro* supplementation of patient cells with L-cysteine, which *TRMU* can use as source of sulphur, can rescue complex I and IV activities with 20 and 30%, respectively (Boczonadi et al., 2013). Moreover, recessive pathogenic variants in *MTO1* were proven to cause reduced respiratory activity in mitochondria in two paediatric siblings

presenting hypertrophic cardiomyopathy and lactic acidosis (Ghezzi et al., 2012). MTO1 and its partner GTPBP3 are responsible for the formation of 5-taurinomethyluridine at the wobble position (U34) of mt-tRNA^{Gln}, mt-tRNA^{Glu}, mt-tRNA^{Leu}, mt-tRNA^{Trp} and mt-tRNA^{Lys} (Asano et al., 2018).

1.8.3 Defects of the mitochondrial ribosome

Mitoribosomes are affected by pathogenic mtDNA variants of the rRNA and pathogenic nuclear variants of MRPs. Variants in the 12S rRNA are more common than variants in 16S rRNA and are associated with hearing loss (Mohamed et al., 2020, Xing et al., 2007). The most common variants in 12S rRNA, m1555A>G and m1494C>T, affect decoding at the A site, and cause hearing loss particularly after treatment with aminoglycoside antibiotic (Guan, 2011, Wei et al., 2013). In one case, a patient suffering from CPEO had pathogenic variants in both rRNAs: a mC960del in 12S rRNA and a homozygous m2835C>T in 16S rRNA (Lv et al., 2017).

Pathogenic variants in MRPs can occur in both the small and the large subunit. Pathogenic variants in the small subunit are more numerous than in the large subunit and are spread through the entire subunit, being identified in MRPS2 (Gardeitchik et al., 2018), MRPS7 (Menezes et al., 2015), PTCD3 (Borna et al., 2019), MRPS25 (Bugiardini et al., 2019), MRPS34 (Richman et al., 2015). In some cases, pathogenic variants in MRPS are so severe that the phenotype starts to manifest *in utero*. For example, a recessive variant – NM_014018.2:c.356A>G p.(Lys119Arg) – in *MRPS28*, encoding the protein bS1m that forms the mRNA exit channel (Amunts et al., 2015) led to the loss of exon 2; this affected mtSSU assembly, decreased translation and caused intrauterine growth retardation and craniofacial dysmorphism (Pulman et al., 2019). In another case, a homozygous recessive variant – c.509G>A p.(Arg170His), current variant ID 3-139069025-G-A (GRCh37) and current RefSeq ENSG00000175110.7 – caused the replacement of a conserved arginine residue by histidine in MRPS22, a mitochondria specific protein; the foetuses showed generalized oedema and died in the first month after birth (Saada et al., 2007). Interestingly, this *MRPS22* variant caused a massive decrease of 12S rRNA content (10% of the control), even if the 12S rRNA gene was normal. A similar situation occurred for *MRPS16*, where a recessive substitution that introduced a premature stop codon – BC021106.1:c331C>T p.(Arg111*) reduced the steady-state level of 12S rRNA to 12% (Miller et al., 2004).

Only three proteins from the 39S subunit are known to cause mitochondrial diseases: MRPL3, MRPL12 and MRPL44. A missense variant – GenBank X06323.1:c.950C>G p.(p.Pro317Arg) – and a large-scale deletion identified in *MRPL3* were associated with hypertrophic

cardiomyopathy and psychomotor retardation (Galmiche et al., 2011). In *MRPL12*, a pathogenic variant –NM_002949.3:c.542C>T p.(Ala181Val) – led to the substitution of a conserved alanine residue by a valine, which most likely affected the interaction with mtEF-G1 (Serre et al., 2013, Korpella et al., 2020). A decreased level of MRPL12 was observed, together with a defective integration in the mtLSU. The patient suffered from general hypotrophy, hypotonia, psychomotor retardation and cerebellar ataxia and died aged 2. *MRPL44* is involved in infantile cardiomyopathy. A pathogenic variant –NM_022915.3:c.467T>G p.(Leu156Arg) – causes the substitution of a conserved leucine residue by an arginine, leading to instability of *MRPL44* and defects in the assembly of the large ribosomal subunit (Carroll et al., 2013).

In both *MRPL12* and *MRPL44* cases, the patients' conditions aggravated and became fatal following an acute infection. This can be due to the cross-reactivity of translation-targeted antibiotics (used against bacterial ribosomes) with mitochondrial ribosomes. Antibiotic treatment of fibroblasts obtained from patients with mitochondria translation defects inhibits cell growth (Jones et al., 2009). In particular, the use of gentamicin (an aminoglycoside that binds to the decoding site of the bacterial ribosome) reduced the growth of MRPS22 mutant cells (Miller et al., 2004) with 60% compared to wild-type cells and of MRPS16 mutated cells (Saada et al., 2007) with 70%. A similar effect was found for tetracycline and doxycycline, two largely-used antibiotics that bind to the 30S ribosomal subunit (Jones et al., 2009).

1.8.4 Defects of translation initiation

Translation initiation is affected by pathogenic variants in the genes coding for *MTFMT* and *TACO1*. *MTFMT* variants cause Leigh syndrome, as found by two separate groups in unrelated patients (Tucker et al., 2011) or in two sisters (Neeve et al., 2013). The variants, transmitted recessively, caused decreased levels of f-Met-tRNA^{Met} as well as decreased complex I and complex IV. The levels were rescued after transduction with *WT-MTFMT* in patients' fibroblast. Variants in *TACO1* were also associated with Leigh syndrome. A recessive insertion (NP_057444: c. 472_473insC p.(Arg165*)) caused complete loss of *TACO1* in the fibroblasts from a paediatric patient with Leigh syndrome isolated COX deficiency. Like for *MTFMT*, overexpression of *TACO1* rescued the COX I assembly, synthesis and activity (Weraarpachai et al., 2009).

1.8.5 Defects of translation elongation

Translation elongation is mainly affected by pathogenic variants in mitochondrial tRNA synthetases, which cause disorders of the central nervous system, heart, muscle and kidney (Sissler et al., 2017). Variants in the mitochondrial aspartyl-tRNA synthetase 2 (*DARS2*) cause LBSL syndrome (leukoencephalopathy with brainstem and spinal cord involvement) (Scheper et al., 2007), variants in arginyl-tRNA synthetase 2 (*RARS2*) cause pontocerebellar hypoplasia (Edvardson et al., 2007) and variants in the glutamyl-tRNA synthetase (*EARS2*) cause LTBL (leukoencephalopathy involving the thalamus and brainstem with high lactate) (Steenweg et al., 2012). Variants in *AARS2* (encoding the alanyl-tRNA synthetase) affect the heart rather than the brain, being associated with fatal early onset cardiomyopathy (Götz et al., 2011). Some cases of kidney and ovarian dysfunction have been described as well: variants in the mitochondrial seryl-tRNA synthetase 2 (*SARS2*) cause HUPRA syndrome (HyperUricemia, Pulmonary hypertension, Renal failure and Alkalosis) (Belostotsky et al., 2011) while variants in the mitochondrial histidyl-tRNA synthetase 2 (*HARS2*) and leucyl-tRNA synthetase 2 (*LARS2*) cause ovarian dysgenesis and sensorineural hearing loss (Perrault syndrome) (Pierce et al., 2013, Pierce et al., 2011). Also, variants in tyrosyl-tRNA synthetase 2 (*YARS2*) cause MLASA2 syndrome, characterized by myopathy, lactic acidosis, and sideroblastic anaemia (Riley et al., 2010).

In addition to all the aspects described above, mitochondria translation deficiencies are associated with pathogenic variants in elongation and recycling factors (Rötig, 2011). Elongation factors mtEF-Tu, mtEF-Ts and mtEF-G1, termination factor C12orf65 and recycling factor mtEF-G2 have been associated with mitochondrial diseases (Pearce et al., 2013, Glasgow et al., 2017, Perli et al., 2019).

A recessive variant reported in *TUFM* gene – [NM_003321:c.964G>A p. \(Gly322Arg\)](#) – leads to the replacement of a glycine by an arginine, making mtEF-Tu be unable to bind aminoacyl-tRNAs. The Gly322 residue is highly conserved and is required for GTP binding to mtEF-Tu. The identified patient had high levels of TCA cycle intermediates in urine, persistent lactic acidosis, decreased complex I and complex IV in muscle and decreased complex V in fibroblasts (Di Nottia et al., 2017). Similarly, a recessive *TUFM* variant –[NM_003321:c.1016 G>A p.\(Arg339Gln\)](#)– leads to the conversion of an arginine residue into a glutamine, which disrupts the tRNA binding domain of mtEF-Tu (Valente et al., 2007). The patients identified by the two groups had similar symptoms; they were new-born, female, and presented microcephaly, poor motility and delayed development.

Variants in *EFG1* cause different phenotypes and affect preferentially the liver. One study identifies tissue-specific variants, that affect only the liver and not the muscle and fibroblasts (Ravn et al., 2015). The variants are an insertion combined with a deletion (NM_024996.5: c.130_137delinsAAAAAAA, p.E44_Ile46delinsLysLysLys) and two missense variants, NM_024996.5: c.964G>A p.(Glu322Lys) and NM_024996.5: c.1655T>G p.(Val552Gly) identified in three patients that showed lactic acidosis and signs of liver dysfunction. MtEF-G1 was absent from fibroblasts in all patients. In muscle and fibroblasts, the activities of complexes I-IV were either normal or slightly decreased, but in liver they were severely decreased. Liver-specificity was also identified by Antonicka et al. who consider that the different relative ratios that elongation factors have in different tissues could determine translational efficiency (Antonicka et al., 2006). Different tissues possess different mechanisms of changing those ratios in response to dysfunction of the mitochondrial translation machinery (Antonicka et al., 2006). This is in agreement with Perli et al. who identified one frameshift variant, c.408_409delGT p.(Leu137Glyfs*24) and a missense variant, c.505C>T p.(Leu169Phe) in the *TSFM* gene (NM_001172697.1, encoding for mtEF-Ts) in an adult patient that had severe cardiomyopathy and underwent cardiac transplant (Perli et al., 2019). In the fibroblasts, the low level of mtEF-Ts was complemented by an upregulation of mtEF-Tu and the cells had normal oxygen consumption rate.

Valente et al. identified a case of *EFG1* defects that showed classical mitochondria phenotype: a new-born with microcephaly, generalized axial hypotonia, limb spasticity and nystagmus (Valente et al., 2007). Synthesis of mitochondrial-encoded proteins was severely reduced in muscle biopsies and fibroblasts, in contrast to later findings (Ravn et al., 2015). Two *EFG1* (NM_024996) variants were identified: c. 139C>T p.(Arg47*) which caused the replacement of Arg47 with a stop codon, and c. 1478T>G p.(Met496Arg). Authors suspected that second variant causes a structural rearrangement that either destabilizes mtEF-G1 or hinders its binding to the mitoribosome (Valente et al., 2007).

1.8.6 Defects of *C12orf65*

Finally, an important factor found to be associated with mitochondria translation defects is *C12orf65*. The first cases described in literature involved two paediatric patients, non-related (Antonicka et al., 2010). The first patient (female) had a recessive deletion in the *C12orf65* gene - [NM_152269](#): c.248delT p. (Leu84*), which led to a premature stop codon at position 84 of the aa sequence. She presented decreased complex IV activity in fibroblasts, severe assembly

defects in complexes I, IV, and V and a general decrease synthesis of the mtDNA-encoded proteins. From a clinical point of view, she suffered from psychomotor retardation, ataxia, severe optic atrophy and was diagnosed with Leigh syndrome. The second patient (male) also had a recessive deletion -[NM_152269](#):c.210delA p.(Leu84*)- in the *C12orf65* gene, which led to a premature stop codon at the same position. He presented the same biochemical and clinical characteristics as the first patient.

Since then, numerous variants of *C12orf65* were associated with mitochondrial diseases all over the world. In two Japanese patients, a homozygous nonsense variant -[NM_152269](#):c.394C>T p.(Arg132*)- was associated with autosomal recessive hereditary spastic paraplegia. This variant lead to a reduced protein synthesis in mitochondria and defects in respiratory complexes I and IV. A truncated form of the protein was detected (Shimazaki et al., 2012). In addition, another recessive variant -([NM_152269](#): c.346delG p.(Val116*)- was identified in two Indian patients. The patients were female monozygotic twins diagnosed with Leigh syndrome and presented optic atrophy, ophthalmoplegia, spastic paraparesis and intellectual disability (Imagawa et al., 2016).

In China, a large clinical study of children with mitochondrial disease revealed *C12orf65* as one of the causative nuclear genes (Fang, 2017). A compound heterozygous variant was identified in a Chinese girl with optic atrophy and distal motor neuropathy (Fang et al., 2017). It is the same variant - c.394C>T p.(Arg132*), current Ensemble Gene ID ENSG00000130921.3- identified by the Japanese group (Shimazaki et al., 2012) and has been inherited from the mother, while the c.6_7delCA p.(Thr3Argfs*4) variant (leading to a premature stop codon) is novel and has been inherited from the father.

C12orf65 pathogenic variants were also reported in three Irish patients and one patient of Hungarian Roma ethnic origin. The variants caused childhood-onset Behr's syndrome in all four patients, characterized by optic atrophy and ophthalmoparesis, spastic paraparesis, ataxia, peripheral neuropathy and intellectual disability. The three Irish patients all presented the same recessive truncating variant predicted to cause the complete loss of the protein: NM 152269: c.96_99dupATCC p.(Pro34Ilefs*25). The Hungarian Roma patient presented a homozygous NM 152269: c.282 G>A p.(Lys94Lys) variant that leads to the loss of a splice site and retention of an intron in the mature mRNA (Pyle et al., 2014).

Pathogenic variants in *C12orf65* were not reported only in children, but in adults as well. Three members of a consanguineous Indian family were all affected by a recessive *C12orf65* deletion leading to a premature stop codon: NM_001143905: c.346delG p.(Val116*). All presented

symptoms since childhood but were reported to the clinic at 35. Clinical symptoms included cognition impairment, axonal neuropathy and optic atrophy and measurements performed in lymphocytes showed a reduced oxygen consumption rate and mitochondrial membrane potential (Tucci et al., 2014). In addition, a recessive deletion was identified in a male patient that developed Leigh syndrome at 45-years-old: NM_152269.4: c.210delA p.(Gly72Alafs *13). The deletion induced a truncated protein, with the loss of the highly conserved GGQ motif. The patient presented decreased levels of complex IV and complex I and defects in assembly of complexes I, IV and V (Wesolowska et al., 2015).

1.9 Systems of translation quality control

1.9.1 Ribosome recycling and rescue mechanisms in bacteria

As no system is perfect, not every single mRNA molecule is translated. Approx. 2-4% of all translation events in *E. coli* fail (Ito et al., 2011). To ensure a maximal efficiency of the translation process, organisms have developed systems of quality control. In bacteria, transcription and translation are coupled. This provides bacteria with a high adaptability to environmental changes, but in the same time prevents processing and proof-reading of the synthetized mRNA. Often, the transcripts are truncated (lack the stop codon at the 3' end). Truncation has different causes: lesions of the DNA template (due to UV, gamma irradiation or reactive oxygen species) (Merrikh et al., 2012), premature termination of transcription or excessive nuclease activity (Keiler and Feaga, 2014). To overcome this issue, bacteria have developed systems that regulate translation when it arrives at a standstill.

The ribosome stalls when it encounters a truncated mRNA, because the translation termination (RF1 and RF2) and recycling (RFF and EF-G) factors can function only if the stop codon is present (Buskirk and Green, 2017). Stalling is problematic for the bacterium, because ribosomes are sequestered in a non-stop complex in which mRNA is present and the P site is occupied by peptidyl-tRNA, but the A site is empty. Therefore, the translation is unable to continue, the polypeptide synthetized so far is defective and the ribosomes are not available for the translation of other transcripts (Keiler and Feaga, 2014). If the peptide synthetized before stalling is shorter than five aa, the peptidyl-tRNA can exit through the E-site (de Valdivia and Isaksson, 2005). This is not possible for longer polypeptides and bacteria have developed other mechanisms to cope with stalling.

The most common rescue mechanism is the *trans*-translation process, performed by transfer-messenger RNA (tmRNA, encoded by the gene *ssrA*) and small protein B (SmpB) (Guyomar

and Gillet, 2019). TmRNA is a specialized RNA molecule that resembles both a tRNA and a mRNA. The structure of its 5' and 3' ends resembles the structure of alanyl-tRNA, while the middle is composed of four pseudoknot structures and an encoding sequence (messenger-like domain) that is decoded during trans-translation (Himeno et al., 2015) (Keiler and Feaga, 2014). The messenger-like domain contains a degradation target sequence and a stop codon, while the 3' end contains the conserved CCA (Komine et al., 1994). The small SsrA binding protein (SmpB) binds to the tRNA-like domain to form a complex that mimics a full-tRNA. The enzyme alanyl-tRNA synthetase charges the 3'CCA end of the tmRNA – SmpB complex with alanine and the complex is then recognized by EF-Tu-GTP, which delivers it to the empty A site of the ribosome as if it was a regular alanyl-tRNA (Gutmann et al., 2003). Here, the C-terminal tail of SmpB enters the empty mRNA channel and, because SmpB contains a globular domain that mimics a codon-anticodon pairing, the tRNA-like domain of tmRNA charged with alanine is accommodated in the A site. In the next step, the PTC catalyzes the formation of a peptide bond between the alanine brought by tmRNA – SmpB and the truncated peptide chain. Then, elongation factor EF-G translocates the tRNA-like domain of the tmRNA from the A site to the P site. The messenger-like domain of tmRNA is placed into the A site and, because it contains a stop codon, translation terminates as usually, by recruitment of RF1 and RF2 (Huter et al., 2017b). The truncated peptide that is released contains a degradation tag at the C-terminus and is degraded by the Clp protease system (Gottesman et al., 1998), while the non-stop mRNA is degraded by RNase R (Venkataraman et al., 2014).

To avoid translation impairment at maximum, bacteria developed back-up mechanisms for *trans*-translation. One is the ArfA protein, which rescues stalled ribosomes from non-stop codons by recruitment of RF2. It was discovered in *E. coli*, where is essential for bacterial viability (Garza-Sánchez et al., 2011). When *trans*-translation system is active, ArfA is degraded, but when the *ssrA* gene is deleted, ArfA is stable. Previous studies showed that ArfA can promote hydrolysis of peptidyl-tRNA and recycling of the ribosome with the help of RF2 (Chadani et al., 2010). The binding site of ArfA on the small subunit is delimitated by three helices of 16S rRNA and the S12 protein, a position that allows ArfA C-terminus to extend inside the mRNA entry channel (Huter et al., 2017c). ArfA binding induces a specific conformation (flipped *anti* conformation) of G530 of the 16S rRNA in the small subunit, the same conformation that the nucleotide adopts when a stop codon is present at the A site. The N-terminus of ArfA interacts with RF2 and recruits it to the A site. The interaction is made with an alpha-helix structure (α7) rather than the SPF motif of RF2. ArfA bound to RF2 induces a conformational change that directs the GGQ motif of RF2 in the PTC, resulting in hydrolysis of the nascent peptide (Demo et al., 2017). The exact mechanisms by which the empty A site is

recognized or RF2 is recruited are not completely understood (Keiler and Feaga, 2014, Huter et al., 2017b).

If both *trans*-translation and ArfA are unavailable, a third back-up system comes to the rescue of stalled ribosomes: ArfB (or YaeJ), discovered in *E. coli*. This protein can function as rescue factor by itself, since it contains the GGQ motif that confers PTH activity. YaeJ was shown to bind to stalled ribosomes via its C-terminal domain and to induce the release of the aberrant polypeptide *in vitro*. The PTH activity was abolished when the GGQ residues were mutated (Chadani et al., 2011, Handa et al., 2011). The C-terminal tail of YaeJ is rich in basic residues which form a helical structure that is inserted into the mRNA channel downstream from the A-site. In this manner, the factor identifies the empty A site of the stalled ribosome. The GGQ motif is situated in the globular N-terminus of YaeJ. Binding of the C-terminus to the mRNA channel induces a conformational change that positions the GGQ motif in the PTC, adjacent to the 3'CCA of the P-site tRNA. In addition, a particular arginine residue from the C-terminal tail (R118) interacts with nucleotide G530 of 16S rRNA and switches the nucleotide conformation from *syn* to *anti*, in the same way as the third nucleotide of the stop codon would do (Gagnon et al., 2012).

Importantly, in contrast to RF1 and RF2, YaeJ has no codon specificity. It was shown to rescue ribosomes stalled on mRNAs without an in-frame stop codon as well as on mRNAs that extended downstream from the A site (Shimizu, 2012). This suggests that YaeJ could act in stalling situations that do not require a truncated mRNA. Stalling can also occur due to amino acid starvation, insufficient or immature tRNAs, or when the mRNA is mutated or forms stable pseudoknot structures. *Trans*-translation and ArfA would not function in those situations. However, YaeJ promiscuity towards mRNA raises the question whether it could interfere with normal translation (Ayyub and Varshney, 2020).

A fourth translation rescue mechanism- ArfT- was discovered in *Francisella tularensis*, a species that does not encode ArfA or ArfB. Overexpression of ArfT rescued the growth phenotype in bacteria where *trans*-translation had been inhibited. This factor does not have peptidyl-tRNA hydrolysis activity, but is capable to recruit either RF1 or RF2 to induce peptide release (Goralski et al., 2018).

In addition, proline was found to favour stalling, since polyproline sequences arrest translation by destabilizing the P-site tRNA (Huter et al., 2017a). A special protein, elongation factor P (EF-P), comes to rescue in this case. EF-P has an L-shape that mimics the structure of a tRNA. It binds between the A and P sites of the 70S ribosome. It has no GGQ motif, but interacts with

the PTC via a particular loop from the N-terminus, which contains two highly conserved residues (arginine and lysine) that bind the 23S rRNA and the tRNA from the P-site (Blaha et al., 2009).

1.9.2 Ribosome recycling and rescue mechanisms in eukaryotes

Ribosome stalling can occur in cytosolic translation as well, but the rescue mechanisms are different from the ones described in bacteria and no tmRNA homologous have been found. Like in bacteria, normal eukaryotic translation termination is followed by recycling. After peptide release, the 80S ribosome is still attached to mRNA, to eRF1 and to the now-deacylated tRNA in the P site. Unlike bacteria, eukaryotes do not possess a homolog of RRF. Instead, ribosome recycling is promoted by a series of proteins that also take part in the no-go and non-stop decay pathway, two mechanisms of translation quality control (Dever and Green, 2012).

No-go (NGD) and non-stop decay (NSD) pathways are reactions that lead to degradation of the stalled ribosome-mRNA complexes in eukaryotes and are commonly known as “mRNA surveillance”. NGD occurs at sense codons. Ribosomes stalling at sense codons can be caused by damage of the RNA bases or subtle defects in mRNA secondary structure, like stable stem-loops, pseudoknots or GC-rich sequences (Schuller and Green, 2018). NSD occurs at mRNAs that lack the stop codon, which implies two situations: either mRNA is truncated, in which case the ribosome arrives at the end of the template, or mRNA lacks the stop codon but maintains the poly(A) tail (Shoemaker and Green, 2012). In the latter case, translation of poly(A) sequences into poly-lysine causes stalling because the poly-lysine, which is positively charged, interacts with the exit channel of the ribosome which is negatively charged. It was shown that stalling occurs after translation of only 18 adenosine nucleotides (in comparison, yeast transcripts have 70 and human 200 adenosine nucleotides) (Ito-Harashima et al., 2007, Eckmann et al., 2011).

The end goal of both NGD and NSD is the degradation of the aberrant mRNA and polypeptide product and the recycling of the ribosome. In yeast, mRNA is eliminated by two exonucleases: Xrn1 (specific to the 5'-3' direction) and the Ski complex (specific to the 3'-5' direction) (Anderson and Parker, 1998). In mammals, mRNA degradation results from a collaboration between different enzymes involved in decapping, deadenylating and exonucleolytic degradation. Decapping is performed by Dcp2 and the actual mRNA degradation takes place in both senses, via the exonucleases Rat1 or Xrn1 (5'→3') and PM/Scl100 (3'→5') (Lejeune et al., 2003). The aberrant polypeptide is degraded by polyubiquitylation, a process which involves two specific E3 ligases: Not4 and Ltn1 (Rkr1 in yeast) (Dimitrova et al., 2009).

There are two key proteins that interact to recycle the ribosome during NGD and NSD: Dom34 (yeast)/Pelota (mammals) and Hbs1 (Buskirk and Green, 2017). Dom34/Pelota have a similar structure and sequence to eRF1, but lack the codon recognition domain and the GGQ motif (Graillie et al., 2008). Hbs1 is homologous to the GTPase eRF3 (Carr-Schmid et al., 2002). Dom34-Hbs1 (yeast) and Pelota-Hbs1 (higher eukaryotes) resemble to the eRF1-eRF3 complex formed at the end of eukaryotic translation. They bind to the A site of the 80S ribosome similarly to eRF1-eRF3, but the N-terminus of Hbs1 extends in the empty mRNA channel (Becker et al., 2011a). This interaction makes that Dom34-Hbs1/Pelota-Hbs1 induce subunit dissociation preferentially when a 3' truncated mRNA is found in the A site (Pisareva et al., 2011) (Shoemaker et al., 2010).

Dom34-Hbs1/Pelota-Hbs1 complexes associate with ABCE1 (Rli1 in yeast), a member of the ATP-binding cassette (ABC) family of proteins, which is essential for dissociation of the ribosome and release of peptidyl-tRNA (Pisareva et al., 2011). Rli1/ABCE1 also binds to eRF1 to promote its release and 80S recycling during normal translation termination. Dissociation of 80S results in the free 60S subunit and the 40S subunit bound to the deacylated tRNA and to the mRNA (Shoemaker and Green, 2011, Pisarev et al., 2010). Rli1/ABCE1 is an ATPase that contains an N-terminal domain with two [4Fe-4S] clusters and two nucleotide-binding sites. Interactions between the Fe-S clusters and nucleotide-binding sites are involved in ATP-binding, which induces a conformational change of the factor, as well as provides the energy necessary for 80S dissociation (Karcher et al., 2008). ABCE1-induced dissociation is also Mg^{2+} dependent; at low Mg^{2+} concentrations, dissociation is induced by initiator factors eIF3, eIF1 and eIF1A (Shoemaker et al., 2010).

In a yeast model of stalling, Dom34-Hbs1 interacts with the ribosome and promotes subunit dissociation followed by release of intact peptidyl-tRNA in a codon-independent manner (Shoemaker et al., 2010), since Dom34 has no codon recognition or GGQ motif (Lee et al.). Although not obligatory, association of Rli1 to the Dom34-Hbs1 complex increases subunit dissociation by 20-fold (Shoemaker and Green, 2011). After dissociation of 60S, the mRNA that remains attached to the 40S subunit can be released by initiator factors eIF3, eIF1 and eIF1A or by ligatin (Pisarev et al., 2007, Skabkin et al., 2010).

1.10 Research hypothesis

The aim of my PhD project was to understand the role that two members of the mitochondria release factor family- mtRF1 and C12orf65- play in protein synthesis. I believe that unveiling their functions is important not only from the fundamental scientific perspective, but also from the clinical perspective, as this could contribute to a better understanding of mitochondrial protein synthesis defects and eventually of mitochondrial diseases.

The *bona fide* factor that terminates protein synthesis for all the 13 mtDNA-encoded proteins was proved to be mtRF1a (Soleimanpour-Lichaei et al., 2007). However, as seen in bacteria and eukaryotes, no translation is 100% efficient- and there is no evidence to suggest that mitochondria would make exception. My research hypothesis is that mtRF1 and C12orf65 are involved in translation quality control in mitochondria.

Truncated mRNA and ribosome stalling have already been reported in mitochondria. Truncated mRNAs appear due to several processes: excessive activity of exonuclease enzymes, defects in transcription, incorrect processing of RNA transcripts or disturbances in polyadenylation (Borowski et al., 2010). For example, downregulation of hSuv3 helicase resulted in aberrant truncated transcripts (Szczesny et al., 2010). Also, a deletion in mtDNA from a patient with mitochondrial disease caused the loss of stop codon for the bicistronic RNA unit encoding ATPase 8 and 6 (Temperley et al., 2003). The lack of a stop codon results in an empty A site, a P site holding the peptidyl-tRNA and a stalled mitoribosome. This condition impairs translation because it reduces the availability of mitoribosomes and tRNA molecules. In addition, genetic defects in tRNA^{Trp} caused ribosome stalling at tryptophan codons (Rooijers et al., 2013)

A mechanism for mitoribosome rescue is therefore necessary, but no such pathway has been described so far (Wesolowska et al., 2014). Following the endosymbiotic hypothesis (Gray, 2014), one would expect that mitochondria follow bacterial pathways. However, there are no tmRNA, ArfA or EF-P homologues in mammalian mitochondria (Wesolowska et al., 2014, Ayyub et al., 2020). There is a homologue of bacterial YaeJ (ArfB)- ICT1, another member of the mitochondria release factor family (Kogure et al., 2013)- but it had been recruited to the mtLSU, where it has no peptidyl-tRNA hydrolysis activity (Richter et al., 2010a).

Like ICT1, mtRF1 and C12orf65 have the GGQ motif required for peptide release and are essential for cell viability. However, neither C12orf65 nor mtRF1 showed peptidyl-tRNA hydrolysis (Soleimanpour-Lichaei et al., 2007, Antonicka et al., 2010) and they are not

structural components of the mitoribosome. Why would the GGQ motif prevail in a protein that could not release the polypeptide during *in vitro* translation assays? The absence of peptidyl-tRNA hydrolysis could be due to technical reasons (the use of bacterial ribosomes in the assays, for example) but it could also be due to scientific reasons: the two proteins might play a role in a particular situation during translation, not captured by the assay.

I started my project from the hypothesis that mtRF1 and C12orf65 perform translation quality control, but function in different situations. The supposition was that C12orf65 interacts with the mitoribosome and rescues it when stalling occurs at a defective mRNA, while mtRF1 acts when stalling occurs at a truncated mRNA, with an empty A site.

The sequence of mtRF1 is 39% identical with mtRF1a sequence, the main difference being the extended codon recognition motif of mtRF1 (Huynen et al., 2012). However, mtRF1 was not proved to recognize the stop codons, possibly because the tip of its helix $\alpha 5$ is too large and causes a steric hindrance at the A site. Still, mtRF1 could be a mitochondria release factor that does not act on stop codons. 3D structural modelling predicted that mtRF1 could bind to the large subunit of the mitoribosome if the A site were empty. An empty A site would occur only if a truncated mt-mRNA, without a stop codon, were blocked inside the mitoribosome (Huynen et al., 2012). As mtRF1 retains the GGQ motif and the 3D modelling suggested that the PTH activity is possible after binding the empty A site, Huynen et al. envisioned a new function for mtRF1 (Huynen et al., 2012). Their conclusion- which became the hypothesis of my research- was that mtRF1 binds to the mitoribosome when it is blocked on a truncated mt-mRNA and rescues it using the PTH activity, allowing translation to continue.

C12orf65 has no codon recognition motif, similar to ICT1 (Richter et al., 2010a). *In vitro* experiments did not show any peptidyl-tRNA hydrolysis for C12orf65, but they were performed using bacterial ribosomes (Antonicka et al., 2010). It could be that the factor can only function on human mitoribosomes. The importance of C12orf65 cannot be denied, since defects in the coding gene were identified in patients of different ages, with different ethnicities, manifesting different symptoms (detailed at 1.8). What all those patients had in common was a decrease in mitochondrial protein synthesis (Buchert et al., 2013). Also, missense variants that led to the loss of the GGQ motif were associated with more severe phenotypes, further emphasizing the role of this domain for protein function. Considering that ICT1 partially rescued a mutant C12orf65 in patient fibroblasts, it is likely that the two proteins act in a similar manner (Antonicka et al., 2010), but different from mtRF1, since mtRF1 maintains the codon recognition motif.

The aim of my PhD project, therefore, was to uncover the role of C12orf65 and mtRF1 in translation termination in mitochondria, more exactly to demonstrate or refute the hypothesis that the two factors rescue stalled mitochondrial ribosomes. To this end, I had two objectives:

1. Identify the truncated mRNA (if any) that remains protected inside the stalled mitoribosome that mtRF1 binds (the mRNA target).
2. Identify proteins that interact with C12orf65 transiently, because they could provide clues about its function.

Chapter 2

Materials and Methods

2.1 Cell Culture

2.1.1 *mtRF1* cell line

HEK 293T FLP-In T-Rex cells capable of inducibly expressing the FLAG-tagged version of wild-type mtRF1 protein were grown in Dulbecco's Modified Eagle's Medium (DMEM, Sigma D6429) supplemented with 10% FBS, 50 µg/ml uridine and 1X non-essential amino acids (NEAA, Sigma-Aldrich, M7145). Cells were sub-cultured in 75 cm² flasks at approximately 90% confluence and were propagated in 15 ml supplemented DMEM, at 37°C, in 5% CO₂, humidified atmosphere. Blasticidin^S (final concentration of 10 µg/ml, Melford, B12150-0.020) was used every third feed.

The expression of mtRF1-FLAG protein was induced by addition of doxycycline (final concentration 5 ng/ml) in 20 ml supplemented DMEM. For separation on isokinetic sucrose gradient, cells were induced for a period of 3.5 days, with media being changed after 2.5 days and doxycycline re-added. For immunoprecipitation experiments, cells were induced with doxycycline (final concentration 10 ng/ml) for 48 h.

2.1.2 *BioID2-HA* cell lines

HEK 293T FLP-In T-Rex capable of inducibly expressing C12orf65-BioID2-HA, C12orf65-Linker-BioID2-HA or COX8-MTS (Mitochondrial Targeting Sequence)-BioID2-HA were grown in identical conditions as described in 2.1.1. The DNA construct pcDNA5/FRT/TO-COX8-MTS-BioID2-HA was a gift (Professor Maria Falkenberg, Gothenburg University, Sweden) and was used to transfect HEK FLP-In T-Rex cells (performed by Yasmin Proctor-Kent). The stock cultures were maintained in 75 cm² flasks. For testing the HA expression, cells were grown in 6-well plates and induced with tetracycline (final concentration of 1 µg/ml) for 16-18 h.

2.1.3 Cell harvesting

When cells reached approximately 80% confluence, the media was removed, and cells were harvested in PBS/1 mM EDTA. The quantity used depended on the dimensions of the flask: 1 ml for a 6-well, 5 ml for 75 cm², 20 ml for 300 cm². Cell suspensions were centrifuged at 230 g for 4 min at room temperature. The supernatant was removed, and the cell pellet was resuspended in pre-warmed fresh medium and reseeded in new flasks.

2.1.4 Cell storage and thawing

For long term storage cells were frozen and kept in liquid nitrogen. Cells were harvested, the pellet was resuspended in 0.5 ml of FBS containing 10% (v/v) DMSO, transferred to a CryoPure tube (Sarstedt, Ref. 72.380.006) and stored for 24 h in a ‘temperature controlled’ cryo-box at -80°C prior to being transferred to liquid nitrogen.

For defrosting, the cells were removed from liquid nitrogen storage and placed directly onto a 37°C metallic heat block inside the tissue culture hood. Once defrosted, 5 ml pre-warmed media was gradually added to the cells: 100 µl, then 250 µl, then 500 µl, 1 ml and 2 ml, with 1 min waiting step in-between additions. The cell suspension was subsequently pelleted at 230 g for 4 min, resuspended in fresh pre-warmed media and transferred to a new flask.

2.1.5 Mycoplasma testing

Mycoplasma testing was performed using a commercial Mycoplasma Detection Kit (MycoAlert® Lonza). The test was performed every three months. If found positive, cells were treated with Plasmocin (1:1000, Invivogen, code ant-mpt) for minimum 2 weeks then re-tested.

2.1.6 DSP treatment

A stock concentration of 100 mM DSP (Pierce/Thermo Scientific, ref 22585) was prepared by dissolving the DSP powder in DMSO (Sigma-Aldrich). The solution was then diluted in PBS to obtain a final concentration of 1 mM. After removing the old medium, the cells were treated with 10 ml/75 cm² flask of 1 mM DSP solution (in pre-warmed PBS) and kept at 37°C in the incubator for 5 min. Then, the solution was removed, and the reaction quenched with 10 ml/75 cm² flask of 1X TBS (Table 2-9) for 10 min at room temperature.

After treatment, the 1X TBS solution was removed and cells were harvested with PBS/1 mM EDTA solution and mechanically detached using a scraper. Cells were then centrifuged (4 min, 230 g, room temperature), the supernatant was removed, and the pellet was washed with 1 ml cold PBS and the sample centrifuged again then kept on ice.

Following DSP treatment, cells were either used for sucrose gradient (2.3.3) or immunoprecipitation (2.3.5). As starting material was used one 75 cm² flask of approx. 90% confluence (DSP- sucrose gradient) or one 225 cm² (DSP- immunoprecipitation) per sample.

2.1.7 Stable transfection of HEK293-Flp-In T-RexTM cells

To generate a stable cell line with inducible expression of the C12orf65-Linker-BioID2-HA, HEK293-Flp-InT-REx cells were transfected with the pcDNA5/FRT/TO/C12orf65-Linker-BioID2-HA and pOG44 plasmids. Untransfected cells were seeded in a 6-well plate the day before transfection, to reach a 30-60% confluence on the day of the experiment. A mix consisting of 2 µg total plasmid DNA (1.8 µg of pOG44 and 0.2 µg pcDNA5/FRT/TO/C12orf65-Linker-BioID2-HA, ratio 9:1) was prepared in 100 µl DMEM lacking FBS, antibiotics, uridine and non-essential amino acids. The plasmid mix was then combined with SuperFect transfection reagent (Qiagen, ref. 301305, Germany) in two DNA:transfection reagent ratios: 1:5 (2 µg total plasmid DNA as 100 µl plasmid mix and 10 µl SuperFect) and 1:7.5 ratio (2 µg total plasmid DNA as 100 µl plasmid mix and 14 µl SuperFect). The transfection mixes were gently pipetted five times and incubated at room temperature for 10 min. Each plasmid/SuperFect ratio was used for a different well of the 6-well plate. To prepare the cells for transfection, media was removed, and each well was washed once with PBS. A volume of 600 µl supplemented DMEM was added to the plasmid DNA/SuperFect mix by gently pipetting two times, then the entire transfection mix was added to the cells from each well. The cells were cultured for 3 h, then the transfection mix was removed. The cells were washed two times with 1 ml PBS/well, fed with 2 ml supplemented DMEM/well, then returned to the incubator. Two non-transfected controls were prepared for each plate: one well without antibiotic and another one with the same antibiotic treatment as the transfected cells.

After 2-3 days post-transfection, the media was removed, and the cells were washed with 1 ml PBS/well and refed with 2 ml supplemented DMEM/well. The Blasticidin^S treatment was maintained every third fed and the selection of transfected cells was performed by addition of Hygromycin^B (final concentration: 100 µg/ml, Formedium Ltd, ref. HYG1000, England, stock kept at 4°C). Blasticidin^S resistance is conferred by the Tet repressor, which is expressed from the pcDNA6/TR vector that was already integrated in the HEK293-Flp-InT-REx cell line. Hygromycin^B resistance is conferred by the integration of the pcDNA5/FRT/TO/C12orf65-Linker-BioID2-HA into the genome of HEK293-Flp-In-REx cell line.

Hygromycin^B selection was maintained and cell growth was monitored for minimum a month. When cells started to die following antibiotic selection, media was changed, the remaining cells were gently washed with 1 ml PBS/well and then refed with 2 ml supplemented DMEM/well. The PBS wash was repeated each time the cells were refed.

Transfection was considered successful when all the untransfected and selective antibiotic treated HEK293-Flp-In T-Rex cells were dead. At this time point, the small colonies of

transfected cells which were kept under selection were considered C12orf65-Linker-BioID2-HA HEK clones. The colonies were identified under the microscope, then manually picked with a 1 ml pipette tip and moved to a well of a new 6-well plate, with 2 ml supplemented media.

When grown to at least 50% confluence in the 6-well plate, the colonies were individually harvested with 1 ml PBS/1 mM EDTA and transferred to a 25 cm² flask, then expanded. For expression tests, cells were grown in a 6-well plate and induced with tetracycline (final concentration 1 µg/ml) for 16 h, then harvested and lysed as described in 2.3.1. Cell lysates (50 µg) were later used for SDS-PAGE followed by immunoblotting using anti-HA antibody, as described in 2.3.8.

2.1.8 KO of C12orf65 in HEK293-Flp-In T-RexTM cells

KO of C12orf65 was performed with the Amaxa Cell Line Nucleofector Kit V (Lonza) according to the manufacturer's protocol. The gRNA was designed against exon1 and cloned in the pSpCas9(BB)-2A-GFP (PX458) plasmid (Appendix-B.4) by Mr. Reece Farren, MRes. The following transfection reactions were performed:

- HEK 293T Flp-In T-Rex + empty vector
- HEK 293T Flp-In T-Rex + PX458
- C12orf65-FLAG HEK 293T Flp-In T-Rex non-induced + PX458
- C12orf65-FLAG HEK 293T Flp-In T-Rex induced + PX458

All cell types were grown in supplemented media with Blasticidin^S (final concentration of 10 µg/ml, Melford, B12150-0.020) added every third feed. A quantity of 2 µg plasmid DNA was used for each transfection reaction. At the time of transfection, the C12orf65-FLAG HEK cells were induced with tetracycline (final concentration 1 µg/ml). The tetracycline treatment was maintained up to the point when single cell colonies have covered an entire well of a 6-well plate, when tetracycline was replaced by doxycycline (10 ng/ml).

After transfection, cells were grown in a 6-well plate for two days. In the second day, the cells were harvested and gently resuspended in 1 ml of 2% FCS solution prepared in PBS and filter sterilized. GFP-positive cells were identified by FACS and separated as single cell colonies in 96-well plates, one cell/well. For each transfected cell type were used two 96-well plates with 100 µL supplemented DMEM/well. The sorting was performed by technician Loredana Trevi at the Newcastle University Flow-Cytometry Facility.

Cells were maintained in culture until they formed colonies which could be visible with the naked eye. At this point, media was changed, and the colonies were kept under observation to determine the ideal time when to be moved to a 48-well plate. The arbitrary time chosen was the point when a single colony occupied as much as possible from the well surface without cells from its top starting to come off. The single colonies were moved one scale up each time they have occupied the current dish in which they were growing.

2.2 Bacterial culture

2.2.1 *Bacterial propagation and storage*

E. coli strains containing either the pcDNA5/FRT/TO/C12orf65-BioID2-HA or the pcDNA5/FRT/TO/C12orf65-Linker-BioID2-HA plasmid were grown in LB media (5 g NaCl, 5 g bacto-tryptone, 2.5 g yeast extract prepared in 500 ml dH₂O, pH adjusted to 7.4 and autoclaved). LB plates were prepared using 3% agar and 100 µg/ml final concentration of ampicillin (added to liquid media before solidification).

2.2.2 *Transformation of competent cells*

Alpha-Select Bronze Efficiency chemically competent bacterial cells (Bioline, BIO-85025) were transfected with either the pcDNA5/FRT/TO/C12orf65-BioID2-HA plasmid (made previously by Mr Reece Farren, MRes student in Lightowers group) or with the pcDNA5/FRT/TO/C12orf65-Linker-BioID2-HA plasmid (made by myself). Cells (40 µl) were thawed on ice and then mixed with 4 µl of plasmid DNA. They were incubated on ice for 30 min, then subjected to a heat-shock at 42°C for 45 sec (without shaking) and placed on ice again for 2 min. Next, a volume of 900 µl SOC media was added to the cells and they were incubated at 37°C for 60 min with shaking, then pelleted for 1 min at room temperature, 5,000 g. The supernatant was discarded, and the cell pellet was resuspended in 100 µl SOC media. From this, 80 µl were plated onto a single ampicillin (100 µg/ml final concentration) agar plate and 20 µl were plated onto another. To prepare the SOC media, a solution of 0.05% NaCl, 2% bacto-tryptone, 0.5% yeast extract, and 2.5 mM KCl (final concentrations) was sterilized by autoclaving, allowed to cool to less than 50°C, filtered and then completed by addition of 10 mM MgCl₂ and 20 mM glucose (final concentrations).

2.2.3 Detection of transformed bacterial clones

The C12orf65-Linker-BioID2-HA bacterial stock colonies were grown on LB ampicillin plates. The C12orf65-Linker-BioID2-HA plasmid was isolated as described (2.4.1) and then digested with the restriction enzymes BamH1 and Xho1 (300 ng plasmid/ reaction). Products of digestion were subjected to DNA agarose electrophoresis on 1% agarose gels (described in 2.4.3). Successful cloning was assessed by the detection of the C12orf65 fragment.

2.2.4 Preparation of glycerol stocks

For long term storage, each stock was prepared in duplicate. The bacterial clone was grown on two LB plates containing 100 µg/ml final concentration of ampicillin, at 37°C, for 18 h. The bacterial lawn from each plate was harvested in 1 ml of sterilised LB containing 18% glycerol, transferred to an Eppendorf tube and stored at -80°C.

2.3 Protein Manipulations

2.3.1 Cell lysis

Cells were harvested as described in 2.1.3, resuspended in 1 ml ice-cold PBS, transferred to a clean Eppendorf tube and centrifuged at 200 g, 4°C, 4 min. Lysis was performed using 50 µl per 10 mg pellet of lysis buffer (Table 2-1), prepared in 10 ml final volume, aliquoted (500 µl) and kept at -20°C. Samples were vortexed for 30 sec, then incubated on ice for 20 min and finally centrifuged at 500 g, 4°C for 2 min. The supernatant was collected for western blot analysis. If not used immediately, it was snap frozen in liquid nitrogen and kept at -80°C.

Table 2-1. Lysis buffer

Component	Final concentration
Tris-HCl pH 7.5	50 mM
NaCl	130 mM
MgCl ₂	2 mM
NP-40	1%
Protease Inhibitor Cocktail (Roche) EDTA-free	1 tablet/10 ml
PMSF (added immediately before use)	1 mM

2.3.2 Measurement of protein concentration

Protein concentration was measured using the Bradford assay. The BSA stock solution (1 mg/ml) used for the standard curve was aliquoted and kept at -20°C. The volumes used to

determine the standard concentration points of the curve can be found in Table 2-2. The experimental samples were prepared of cell lysate (1 μ l) and ddH₂O (799 μ l) and mixed with Bradford reagent (200 μ l, BioRad, kept at 4°C). All samples were vortexed and incubated at room temperature for 5 min. A 200 μ l aliquot of each sample was added into a 96-well plate. The OD reading was performed at 595 nm on a SpectraMax H3 microplate reader (Molecular Devices). All experimental samples and different BSA standard concentrations were prepared in duplicate.

Table 2-2. Bradford standard curve

ddH ₂ O (μ l)	BSA stock (μ l)	Final BSA concentration (μ g/ μ l)	Bradford reagent
800	0	0	200 μ l
798	2	2	200 μ l
795	5	5	200 μ l
790	10	10	200 μ l
785	15	15	200 μ l
780	20	20	200 μ l

2.3.3 Isokinetic Sucrose Gradient Separation

The 10% and 30% solutions of sucrose were prepared in 1X sucrose gradient buffer. The sucrose gradient buffer was prepared as a 10X stock (Table 2-3), divided in 1 ml aliquots, and kept at -20°C. To prepare the sucrose gradient, a volume of 500 μ l 10% sucrose solution was added to a 1 ml ultracentrifuge tube (Open-top Thickwall Polycarbonate, Beckman Coulter, ref 343778). Then, 500 μ l of 30% sucrose solution was delivered under the 10% sucrose solution using a 1 ml syringe and needle. The tubes were then rotated on the Biocomp Gradient Maker 107 using the programme TL55 (short sucrose, 10-30% S1/1, 0:55/85.0/22) and kept at 4°C for a minimum of 1 h.

Table 2-3. Sucrose gradient buffer

Component	Final concentration for 10X
Tris-HCl pH 7.2	0.5 M
Mg(CH ₃ COO) ₂	0.1 M
NH ₄ Cl	0.4 M
KCl	1 M
PMSF	1 mM (added to 1X immediately before use)
Chloramphenicol	50 μ g/ml (added to 1X immediately before use)

The cell pellet was lysed using 50 μ l per 10 mg wet weight of lysis buffer for sucrose gradient (Table 2-4), with rotation at 4°C for 30 min. The lysate was centrifuged for 10 min at 4°C, 12,000 g. The pellet containing the cell debris was discarded. The supernatant was recovered and used for protein concentration measurement with Bradford reagent. An aliquot (20-50 μ g) was kept for western blotting.

Table 2-4. Lysis buffer for sucrose gradient

Component	Final concentration
Tris-HCl pH 7.4	50 mM
NaCl	150 mM
EDTA	1 mM
Triton X-100	1%
Protease Inhibitor Cocktail (Roche) EDTA-free	1 tablet/10 ml
MgCl ₂ (added immediately before use)	10 mM
PMSF (added immediately before use)	1 mM

A quantity of 700 μ g of cell lysate (maximum volume: 100 μ l) was slowly loaded on the top of the sucrose gradient. The samples were centrifuged at 100,000 g for 2 h 15 min at 6°C and 11 fractions (100 μ l) were collected from each sample: fraction 1 was the first from the top. Aliquots of each fraction were kept for immunoblotting analysis (10 μ l) or TCA precipitation (50 μ l). The remainder of the fractions were snap frozen in liquid nitrogen and kept at -80°C.

2.3.4 Precipitation of sucrose gradient fractions with TCA

A 20% aqueous solution of trichloroacetic acid (VWR Chemicals) was prepared and kept at 4°C. For each sucrose fraction an equal volume of TCA solution was added followed by 30 min incubation on ice and centrifugation at 15,800 g, 15 min, 4°C. The supernatants were discarded, and the pellets were washed three times with 100% ice-cold acetone. Each wash consisted of addition of 1 ml of 100% cold acetone, followed by centrifugation and removal of supernatant. After the first wash, the pellets were scattered inside the microcentrifuge tubes. To ensure their precipitation at the bottom of the tube, the pellets were scraped off with a 1 ml pipette tip after addition of the 1 ml 100% cold acetone. After the last wash, the pellets were left to air dry and then resuspended in 10-20 μ l/pellet of 1X dissociation buffer (Table 2-5) for immunoblotting detection. When not used immediately, the samples were stored at -20°C.

Table 2-5. Dissociation buffer

1X dissociation buffer	4X dissociation buffer
10% glycerol	40% glycerol
2% SDS	8% SDS
0.125 M Tris pH 6.8	0.5 M Tris pH 6.8
0.0025% bromophenol blue	0.01% bromophenol blue
50 mM DTT	200 mM DTT

2.3.5 Immunoprecipitation with anti-FLAG antibody

All the solutions and buffers were prepared in 0.1% DEPC-treated water. The samples used were mtRF1-FLAG HEK293T cells, induced with doxycycline (final concentration 10 ng/ml, 48 h) or non-induced, both treated with DSP (final concentration 1 mM) for 5 min. For this experiment, the cells were grown in 225 cm² flasks for each condition. The immunoprecipitation was performed using the FLAG Immunoprecipitation Kit (FLAGIPT1, Sigma) which contains agarose beads coated with the monoclonal antibody anti-FLAG-M2. Since 10 µl of packed gel volume binds more than 1 µg FLAG fusion protein, a volume of 90 µl was used per two immunoprecipitation reactions (non-induced and doxycycline-induced samples). The slurry was pulsed for a maximum of 3 sec, the supernatant was removed, and the remaining agarose beads were washed three times, at room temperature, with 1 ml of 1X washing buffer (150 mM NaCl, 50 mM Tris-HCl pH 7.4, 20 mM MgCl₂). To minimize non-specific binding, the agarose beads were blocked in 1 ml of blocking solution (20 mg/ml BSA, 100 µg/ml heparin, 200 µg/ml *E. coli* tRNA prepared in 1 ml of 1X washing buffer) overnight at 4°C on the rotating wheel.

The following day after blocking, the beads were pulsed down, the blocking buffer was removed and the beads were washed three times (1X washing buffer, room temperature). The aliquot of beads was divided in two and each half was incubated (3 h, at 4°C, with rotation) with cell lysate (3 mg) obtained from either induced or non-induced cells.

Cells were harvested and resuspended in cold lysis buffer (150 mM NaCl, 50 mM Tris-HCl pH 7.4, 20 mM MgCl₂, 1 mM EDTA, 1% Triton X-100) to which were added right before use: 1 mM PMSF, protease inhibitor cocktail EDTA-free (1 tablet /10 ml, Roche) and RNA guard (1 µl for 10 ml). After lysis, samples were centrifuged at 564 g, 4 min, at 4°C. The supernatant (cell lysate) was kept and the protein concentration was determined using Bradford assay. An aliquot of lysate (20-50 µg) was retained as input sample for western blotting.

After incubation of the beads with the lysate (3 h, at 4°C, with rotation), the beads were pulsed down (maximum 3 sec) and the supernatant retained to be used for western blot. The beads were then washed three times in 1X washing buffer with 1 mM PMSF and RNA guard and were used later for RNA isolation.

The 3X FLAG peptide (Sigma, F4799) was used to elute mtRF1-FLAG from the beads prior to RNA isolation. The beads were incubated (45 min, at 4°C, with rotation) with 20 µg of 3X FLAG peptide in a total volume of 100 µl washing buffer (with 1 mM PMSF and RNA guard) after which beads were pelleted, and the supernatant was transferred to a clean tube. An aliquot (10 µl) of supernatant was mixed with 4X dissociation buffer (Table 2-5) and the remainder was used for RNA isolation. The beads were washed three times and then mixed with 1X dissociation buffer (Table 2-5) for western blot analysis.

2.3.6 Mitochondria isolation

Mitochondria isolation was performed from C12orf65-BioID2-HA or C12orf65-Linker-BioID2-HA FLP-In T-Rex HEK 293T cells grown in 75 cm² flasks to 80% confluency. After harvesting, the cell pellet was washed with 1 ml ice-cold PBS and resuspended in 1 ml HB1 complete (with PMSF and BSA, Table 2-6) using a cut tip.

Table 2-6. Homogenisation buffer 1 (HB1) complete

Component	Final concentration
Mannitol	0.6 M
EGTA	1 mM
Tris-HCl pH 7.4	10 mM
BSA (powder)	0.1%
PMSF	1 mM

The pellet was transferred in a chilled glass homogenizer (Cole-Parmer instrument CO, 04368-40) previously washed with 100% ethanol. To collect as much material as possible, the pellet tube was rinsed with 0.5 ml of HB1 complete which was also added to the homogenizer. Cell disruption was achieved by homogenization (15 strokes), performed on ice, by turning the homogenizer manually. After the last stroke, the solution was moved to a new 1.5 ml tube using a 230 mm glass Pasteur pipette and centrifuged at 400 g, 10 min, 4°C. The supernatant was transferred to a pre-chilled tube labelled S1. The pellet was homogenized again and centrifuged as described above. The second supernatant was transferred to a pre-chilled tube labelled S2. Both S1 and S2 were centrifuged (400 g, 10 min, 4°C) and the supernatants containing

mitochondria were transferred each to a new cold tube. To pellet the mitochondria, the supernatants were centrifuged at 11,000 g, 10 min, 4°C. The new supernatants were collected in a single 15 ml tube and kept as control for cytosolic proteins (postmitochondrial supernatant, PMSN). The pellets containing mitochondria were combined by resuspension in 400 µl of HB1 without PMSF and BSA. To increase the yield of mitochondria isolation, the tubes which had contained S1 and S2 were washed with an extra 400 µl HB1 (no PMSF, no BSA) which were added to the previous, resulting 800 µl of mitochondria in suspension. This suspension was centrifuged again (11,000 g, 10 min, 4°C) and the pelleted mitochondria were resuspended in 40 µl of HB1 (no PMSF, no BSA) and used for Bradford assay.

2.3.7 Mitochondrial subfractionation

Mitochondrial subfractionation was performed on C12orf65-BioID2-HA or C12orf65-Linker-BioID2-HA HEK FLP-In T-Rex HEK 293T grown in 300 cm² flasks at 80% confluence and treated with tetracycline (final concentration: 1 µg/ml) overnight prior to harvesting. Harvesting and mitochondria isolation were performed as described (2.3.6). During the entire process of subfractionation, the HB1 was used without BSA and without PMSF.

An amount of protein (360 µg) was resuspended in 90 µl HB1. From this, 15 µl (60 µg) were mixed with 5 µl 4X dissociation buffer (Table 2-5) and snap frozen in liquid nitrogen. This was labelled as “Sample A” – whole mitochondria – and retained for subsequent immunoblotting.

The remaining mitochondria sample was treated with 1.5 µg of proteinase K (20 mg/ml stock, Invitrogen, ref.25530-049, diluted in HB1) and incubated on ice for 30 min. Next, PMSF (5 mM final concentration) was added, the sample was centrifuged (11,000 g, 10 min, 4°C), and the pellet was resuspended in 75 µl of HB1; 15 µl (60 µg) were mixed with 5 µl 4X dissociation buffer and snap frozen in liquid nitrogen. This was labelled as “Sample B” – shaved mitochondria – and used later for immunoblotting.

The remaining sample was centrifuged at 11,000 g, 10 min, 4°C and the supernatant was discarded. The following steps of subfractionation were performed on ice, in the cold room. The pellet was resuspended in 900 µl of 10 mM Tris-HCl pH 7.4 and divided into two 1.5 ml tubes, 450 µl/tube. The tubes were labelled as ‘Y’ and respectively ‘Z’ and 0.6 µg of proteinase K were added only to sample Z. Both samples were incubated on ice for 30 min then both were mixed with 5 mM PMSF and an equal volume of homogenisation buffer 2 (Table 2-7).

Table 2-7. Homogenisation buffer 2

Component	Final concentration
Mannitol	1.2 M
EGTA	2 mM
Tris-HCl pH 7.4	10 mM

Both Y and Z samples were centrifuged (12,000 g, 10 min, 4°C) and each pellet was resuspended in 30 µl of HB1. A volume of 15 µl (60 µg) of each sample was mixed with 5 µl 4X dissociation buffer and snap frozen in liquid nitrogen. They were labelled as “Sample C” – mitoplasts – and “Sample D” – shaved mitoplasts – respectively and used later for immunoblotting.

A volume of 435 µl of HB1 was added to the remaining sample Z (for a 450 µl final volume), the sample was centrifuged (12,000 g, 10 min, 4°C) and the pellet was dissolved in 600 µl of 100 mM Na₂CO₃ and incubated on ice for 30 min. The sample was then centrifuged at 100,000 g, 15 min, 4°C and the pellet was resuspended in 15 µl of HB1 and mixed with 5 µl 4X dissociation buffer. This was labelled as “Sample E” – inner mitochondria membrane – snap frozen in liquid nitrogen and used later for immunoblotting.

2.3.8 Precipitation of postmitochondrial supernatant with TCA

The postmitochondrial supernatant (2.3.6) was concentrated by precipitation with TCA. The percentage of PMSN sample used for precipitation was equal to the percentage of mitochondria sample used for western blot. For example, if, for 50 µg of mitochondria sample was necessary 25% of the total sample volume, then the percentage of PMSN subject to precipitation was also 25% of its total volume.

The protocol was performed in the chemical hood. For precipitation, an equal volume of 20% TCA was added over PMSN, followed by incubation on ice for 30 min. The sample was then centrifuged at 15,800 g, 5 min, at 4°C. The supernatant was removed, and the pellet was washed two times with 100% ice-cold acetone, scraping the tube after the first wash as described previously (2.3.4).

The pellet was left to air dry very briefly, to avoid it becoming difficult to resuspend. Finally, it was resuspended in 20 µl of 1X dissociation buffer and boiled at 95°C for 10 min, under agitation, to improve resuspension. The sample was kept at -20°C and later used for western blotting.

2.3.9 SDS-PAGE, western blotting and detection

SDS-PAGE was performed using the Hoefer Mighty Small™ (GE Healthcare) or Bio-Rad Mini Protean Tetra® Cell systems. Proteins were separated on polyacrylamide gels consisting of a 12% or 10% resolving gel and a 3.75% stacking gel (Table 2-8). The percentage of resolving gel was chosen according to the molecular weight of the proteins to be separated. The components of the resolving gel were mixed at room temperature then poured in between the two glass plates. On top was added either dH₂O or isopropanol to isolate the gel from air and prevent inhibition of polymerisation. When the resolving gel solidified, the dH₂O or isopropanol was removed and the stacking gel was poured, followed by the immediate insertion of the comb. After polymerisation, the comb was removed, and the resulting wells were washed with dH₂O.

Table 2-8. SDS-PAGE gel components (1 gel with 0.75 mm spacers)

Stock reagent	12% Resolving Gel	10% Resolving Gel	3.75% Stacking Gel
30% 29:1 acrylamide: bisacrylamide	2 ml	1.667 ml	0.625 ml
3.75 M Tris-HCl pH 8.5	0.5 ml	0.5 ml	-
dH ₂ O	2.395 ml	2.726 ml	3.02 ml
0.5 M Tris-HCl pH 6.8	-	-	1.25 ml
10% SDS	50 µl	50 µl	50 µl
TEMED	5 µl	5 µl	5 µl
10% APS	50 µl	50 µl	50 µl

The samples were mixed with 4X dissociation buffer (Table 2-5) in ratio 3:1 and boiled at 95°C for 3 min prior to loading onto the gel. The broad-range molecular weight coloured protein ladder (CSL-BBL, Cleaver Scientific Ltd) was used as a marker. Separation was performed in 1X running buffer (Table 2-9) at 20 mA through the stacking gel and 30 mA through the resolving gel.

After separation, the proteins were transferred on a PVDF membrane (Immobilon-P, Millipore Corporation) by wet transfer in the Mini Trans-Blot module (BioRad). Prior to transfer, the membrane was activated in 100% methanol (20 sec, room temperature) then washed in dH₂O and incubated in 1X transfer buffer (Table 2-9). The resolving gel, gauze pads, sponges, and double thickness 3 MM Whatman filter papers were also incubated in 1X transfer buffer. All the components were added to the transfer sandwich in this order: black gauze pad with sponges at the bottom, followed by two Whatman filter papers, then the gel, the PVDF membrane on

top of the gel, two other Whatman filter papers on top of the membrane, followed by the second sponge and the transparent gauze pad.

Table 2-9. Solutions used for SDS-PAGE

Immunoblotting buffer solutions	Components (final concentrations)
10X Running buffer	1.92 M Glycine 250 mM Tris 1% SDS
1X Transfer buffer	25 mM Tris 192 mM Glycine 0.02% SDS 15% Methanol
1X TBS	20 mM Tris 0.5 M NaCl Adjusted to pH7.6 with HCl
CBB Staining solution	45% Methanol 10% Acetic Acid 0.2% Coomassie Blue R
CBB Distaining Solution	45% Methanol 10% Acetic Acid
Ponceau S solution	5% Acetic Acid 1 g/L Ponceau S powder

The transfer was carried out at 4°C, 100 V (constant) for 1 h in transfer buffer mixed constantly. Subsequently, the membrane was stained with Ponceau S solution and the gel with Coomassie Brilliant Blue (CBB) staining solution (Table 2-9) at room temperature. The gel was incubated for 15 min in staining solution then washed three times in destaining solution (Table 2-9), 10 min/wash. The membrane was incubated for 5 min in Ponceau solution, then quickly washed in TBS (Table 2-9) with 0.1% Tween 20 (TTBS). The gel and membrane were visualised with white light on the Chemi-Doc Imaging System (Bio-Rad) using ImageLab software.

Following Ponceau staining, the membrane was blocked in 20 ml solution of 5% skimmed milk in TTBS for 1 h with agitation at room temperature. Next, the membrane was incubated with primary antibodies prepared in 5% milk-TTBS solution overnight at 4°C with agitation. For biotinylation experiments, a buffer containing 5% BSA in TTBS was used instead of 5% skimmed milk. The list of primary and secondary antibodies can be found in Appendix-A, Tables Apx 1-3. Exceptions from the overnight incubation were the primary antibodies: VDAC1 (3 h, room temperature), GAPDH, NDUFS3 and SDHA (1-2 h, room temperature). To remove the excess of primary antibody, the membrane was washed in TTBS three times, 5 min/wash, prior to incubation with the secondary antibody for 1 h, with agitation. For protein

signal detection, the membrane was washed as previous and incubated with Amersham ECL Detection Reagent (GE Healthcare) as indicated by the manufacturer. The chemiluminescent signals were visualised on the Chemi-Doc Imaging System (Bio-Rad) using ImageLab software.

2.4 DNA Manipulations

2.4.1 Extraction of plasmid DNA

Single colonies were picked from the LB ampicillin plate and inoculated in 5 ml LB broth (described in 2.2.1) supplemented with 100 µg/ml final concentration of ampicillin. Inoculated broths were then incubated overnight in an orbital shaker at 37°C, 180 rpm. Plasmids were extracted using the Monarch® Plasmid Miniprep Kit (New England Biolabs, T1010S) according to manufacturer's protocol. The isolated plasmid was kept at -20°C.

2.4.2 Measurement of DNA concentration

DNA concentration was measured using Nanodrop Spectrophotometer ND-1000. The measurement was done for 1 µl of purified DNA, at 260 nm. Purity was estimated by 260 nm/280 nm ratio and verified by electrophoresis of 1 µl of purified DNA on a 1% agarose gel.

2.4.3 DNA agarose electrophoresis

DNA samples were verified on 1% or 2% agarose gels depending on their size. The gels were prepared by dissolving agarose (NBS-Biologicals, NBS-AG500) in 1X Tris-Acetate-EDTA (TAE) buffer (40 mM Tris-base, 1 mM EDTA) prepared from 50X stock solution (12.1 g Trizma base, 2.86 ml glacial acetic acid, 5 ml EDTA 0.5 M). The solution was boiled in the microwave until the agarose was completely dissolved. It was then left to cool until the temperature reached 45°C and ethidium bromide was added (0.5 µg/ml final concentration). The cooled gel was poured into a mould and when solid moved to an agarose tank and covered with 1X TAE buffer. DNA samples were loaded using 1 µl of 6X loading dye (3% glycerol, 0.025% bromophenol blue, 0.025% xylene cyanol). The ladder Gene Ruler 1 kb Plus (Thermo Fisher Scientific) was used as molecular weight reference. Samples were electrophoresed at 60-80 V.

2.4.4 Digestion of the pcDNA5/FRT/TO/C12orf65-BioID2-HA vector

The isolated pcDNA5/FRT/TO/C12orf65-BioID2-HA plasmid was digested with the enzymes Fast Digest BamH1 (FD0054) and Fast Digest Xho1 (FD0694) from Thermo Fisher Scientific, used with Fast Digestion Buffer 10X stock provided by the same company (suitable for all Fast Digest enzymes, working dilution 1:10). A short diagnostic digestion (1 h) was performed to test the efficacy of the enzymes and the presence of the C12orf65 DNA fragment. For the diagnostic digestion were used 200 ng/μl - 400 ng/μl plasmid in up to 20 μl total volume.

A long preparative digestion (overnight, 37°C) was performed to isolate the C12orf65 DNA fragment. For this were used 10 μg of plasmid in up to 50 μl total volume. The total amount of enzymes did not exceed 10% of the total reaction volume.

2.4.5 Gel extraction of C12orf65 DNA fragment

After separation on agarose electrophoresis (described in 2.4.3), the C12orf65 DNA fragment was excised from the gel with a sharp blade under UV light, in the dark room, and placed in an Eppendorf tube. The slice was weighted and the extraction of the DNA from the gel was performed using the Monarch® DNA Gel Extraction Kit (New England Biolabs, T1020S) according to the manufacturer's protocol. The isolated fragment was kept at -20°C.

2.4.6 Digestion of the pcDNA5/FRT/TO/Linker-BioID2-HA vector

Two clones of the plasmid vector pcDNA5/FRT/TO/Linker-BioID2-HA have been previously generated in Lightowlers' group by Mr. Reece Farren, MRes. Each clone was digested (3 h) at 37°C using the Fast Digest BamH1 (FD0054) and Fast Digest Xho1 (FD0694) enzymes from Thermo Fisher Scientific, used with Fast Digestion Buffer 10X (working dilution 1:10). A quantity of 10 μg plasmid (clone 1) or 6 μg plasmid (clone 2) were used in up to 50 μl reaction volume. To check if the digestion was successful, a DNA agarose electrophoresis was performed using 1 μl reaction mix on a 1% agarose gel.

2.4.7 Dephosphorylation of the pcDNA5/FRT/TO/Linker-BioID2-HA vector

The reaction mixes resulted from double digestion were dephosphorylated in order to prevent re-ligation of the Linker plasmid. A volume of 2.5 μl 10% SDS (for a final concentration of 0.005%), a volume of 9 μl of 1 M Tris pH 9 (for 0.175 M final concentration) and the appropriate volume of alkaline phosphatase were added to the entire reaction mixture. 1 U of

alkaline phosphatase (Roche, Ref. 10108146001, 1 U/μl stock) was used for each 1 μg of DNA. Afterwards, the samples were incubated first for 30 min at 37°C and then for 50 min at 50°C.

2.4.8 Purification and precipitation of plasmid DNA

After dephosphorylation, digested mixes were adjusted to 50 μl. An equal volume of phenol pH 7.4 was added, samples were vortexed and then centrifuged at 15,700 g, for 2 min, room temperature. The supernatant was collected, measured and mixed with an equal volume of 25:24:1 phenol:chloroform:isoamylalcohol. After vortexing, samples were centrifuged again at 15,700 g, for 2 min, room temperature. The new supernatant was collected, measured and mixed with an equal volume of 24:1 chloroform:isoamylalcohol. The samples were vortexed and centrifuged once more at 15,700 g, for 2 min, room temperature and the supernatants were collected. This final supernatant was measured and mixed with a tenth of the volume of 3 M sodium acetate pH 5.3, two times the volume of 100% ethanol and 1 μl of linear acrylamide. The samples were incubated at -80°C for 20 min, then centrifuged at 15,000 g, 4°C for 30 min to pellet the DNA. After this final centrifugation, the supernatant was discarded and the pellet was briefly air dried, then resuspended in 20 μl of sterile deionized water. The purified plasmids were kept at -20°C.

2.4.9 Ligation of the Linker plasmid with the C12orf65 fragment

The ligation of the dephosphorylated, purified Linker plasmids with the C12orf65 fragment extracted from the agarose gel (2.4.5) was performed using the Rapid DNA Ligation Kit from Thermo Fisher Scientific (Ref. K1422), according to the manufacturer's protocol. For each Linker plasmid clone, a ligation reaction with no insert was used as a control for successful dephosphorylation. The reaction mixes prepared for ligation can be found in Table 2-10

Table 2-10. Ligation mixes for Linker plasmid and C12orf65 fragment

Linker clone 1 control	Linker clone 1 insert	Linker clone 2 control	Linker clone 2 insert
120 ng plasmid	120 ng plasmid	100 ng plasmid	100 ng plasmid
-	25 ng insert (1 µl)	-	25 ng insert (1 µl)
4 µl ligation buffer 5X			
1 µl T4 DNA ligase			
ddH ₂ O	ddH ₂ O	ddH ₂ O	ddH ₂ O
up to 20 µl			

Reaction mixes were incubated at room temperature for 5 min. Ligation was followed by bacterial transformation as described previously (2.2.2).

2.4.10 Ligation of gRNA targeting C12orf65 into PX458

All the steps that resulted in the pSpCas9(BB)-2A-GFP (PX458) plasmid containing the gRNA targeted to exon 1 of *C12orf65* were performed by Mr. Reece Farren, MRes. The oligonucleotides used for single gRNA synthesis were designed using the OMICTOOLS website (www.omictools.com) (Henry et al., 2014) and commercially synthesized by Eurogentec (sequences in Appendix-B.4). The annealing reaction contained the complementary oligonucleotides (0.5 µM final concentration for each), 10X T4 DNA ligation buffer (Thermo Scientific) and nuclease free water covered by a small volume of mineral oil to prevent evaporation.

The reaction mixture was first heated in a thermoblock (95°C, 5 min), then the thermoblock was turned off to allow a slow decrease to room temperature. Insertion of the gRNA into the PX458 plasmid (Figure Apx 4) was done using the BbsI restriction enzyme and the T4 DNA ligase in a combined digestion/ligation reaction optimised by Dr. Fei Gao in the host lab. The components of the combined digestion/ligation can be found in Table 2-11. The reaction mixture was incubated at 37°C for 2 h and transformed into bacteria as described in 2.2.2. Plasmid DNA was extracted from bacterial clones (2.4.1) and screened by double digestion with BbsI and ApaI enzymes.

Table 2-11. Combined digestion/ligation reaction mix

Component	Volume (μl)
PX458	1 (100 ng)
Annealed oligos	1 (0.5 μM)
BbsI (Thermo Scientific)	1
Fast Digest Buffer 10 X	2
T4 DNA ligase (Thermo Scientific)	1
ATP 1 mM	2
Nuclease free H ₂ O	12
Total	20

2.4.11 Plasmid sequencing

Plasmids were sequenced by Sanger sequencing, which was kindly performed by genetic technologist Sarah Smith from the Newcastle Mitochondrial Highly Specialised Service laboratory. For each reaction were used: 450 ng of plasmid DNA resuspended in 6 μl of sterile deionized water, 1 μl of forward primer (10 μM), 1 μl of reverse primer (10 μM). The primers used for sequencing can be found in Table 2-12.

Table 2-12. Primers used for pcDNA5 plasmid sequencing

Primer	Sequence from 5' to 3'	Tm
CMV Forward Seq	CGC AAA TGG GCG GTA GGC GTG	65°C
BIOID SEQ reverse	GTT CAG CAG GAA GCT GAA GTA CAG GCC G	66°C

2.4.12 DNA extraction from HEK cells

Cells from a 25 cm² flask were harvested and pelleted as described in 2.1.3. On top of the pellet were added: 400 μl TE buffer (10 mM Tris-HCl pH 7.4, 1 mM EDTA pH 8.0), 50 μl 10% SDS, 50 μl proteinase K (20 mg/ml stock, Invitrogen, ref 100005393). The mix was incubated at 37°C, overnight, with mild shaking.

The following day samples were briefly centrifuged, then mixed with 500 µl/sample of phenol pH 7.3 in the chemical hood. Samples were vortexed for about 30 sec at room temperature, then centrifuged for other 15 min at 15,800 g. The upper aqueous phase was carefully transferred to a new tube and then mixed with 150 µl phenol and 150 µl chloroform:isoamylalcohol 24:1. Samples were rotated and centrifuged as previously, the supernatant was recovered and mixed as described. The samples were centrifuged again, the supernatant was recovered, measured, and mixed with an equal volume of chloroform only. The samples were centrifuged as previously; the upper phase containing DNA was recovered and mixed with 3 M sodium acetate pH 5.3 (a tenth of its volume) and 100% ethanol (two times the volume). The samples were kept at -80°C for at least one hour, then centrifuged at 20,000 g, 4°C, for 30 min. The pellet containing DNA was washed with ice-cold 75% ethanol, centrifuged again (20,000 g, 4°C, 30 min) and resuspended in 20-40 µl ddH₂O. DNA concentration was measured at NanoDrop (2.4.2).

2.4.13 Real-time PCR (qPCR)

The reactions were performed using the Fast start Essential DNA Green Master SYBR Green I - kit (Roche, reference 06402712001). All reactions were made up in 20 µl volume with the following components: 2 µl of template (1:10 dilution cDNA), 10 µl of SYBR green mix, forward and reverse primers (0.5 µM final concentration for each, Table 2-13) and ddH₂O. I used 2 µl of ddH₂O as negative control and 10 ng total genomic DNA as positive control for each experiment. The LightCycler® Nano (Roche) instrument and the affiliated computer program were used for the reaction conditions described in Table 2-14. The parameters ‘Analysis: automatic quantification, Tm calling’ were selected in the software.

Table 2-13. Sequences of primers used in Real Time PCR

Primer	Sequence from 5' to 3'	Tm	Ta
COX 2 forward	CCT AGA ACA GGC GAC	52°C	45°C
COX 2 reverse	GTC GTG TAG CGG TGA A	48°C	
12S forward	ACA CTA CGA GCC ACA G	50°C	47°C
12S reverse	ACC TTG ACC TAA CGT C	50°C	
16S forward	CCA ATT AAG AAA GCG TTC AAG	58°C	57°C
16S reverse	CAT GCC TGT GTT GGG TTG ACA	64°C	

Table 2-14. Profile and analysis condition for LightCycler® Nano software

Stage	Temperature	Ramp (°C/sec)	Time
Hold	95°C	5	600 sec
45 cycles	95°C	5	10 sec
	60°C	4	10 sec
	72°C	5	15 sec *
Melting: initiation	65°C	4	50 sec
Melting: final	95°C	0.1	1
Hold	4°C	-	-

* data collected after this step

2.4.14 Sequencing of potential *C12orf65* KO HEK cells

To determine if the KO was successful, single colonies were sequenced by Sanger sequencing. First, DNA was isolated from a 25 cm² flask using phenol-chloroform extraction (2.4.12), then the target region was amplified by PCR, performed using the Phusion High-Fidelity PCR Master mix (Thermo Fisher Scientific) according to the manufacturer's instructions. The primers can be found in Table 2-15 and the primer binding sites on *C12orf65* (NCBI Reference Sequence NG_027517.1) are in Figure 2-1.

Table 2-15. Sequences of primers used for sequencing of KO clones

Primer	Sequence from 5' to 3'	Tm	Ta
C12orf65 ex1 forward	GGG CAG ATG CCT CTT ACT G	62.4°C	63°C
C12orf65 ex1 reverse	CAG CAC CAC GCA GTT GC	66°C	

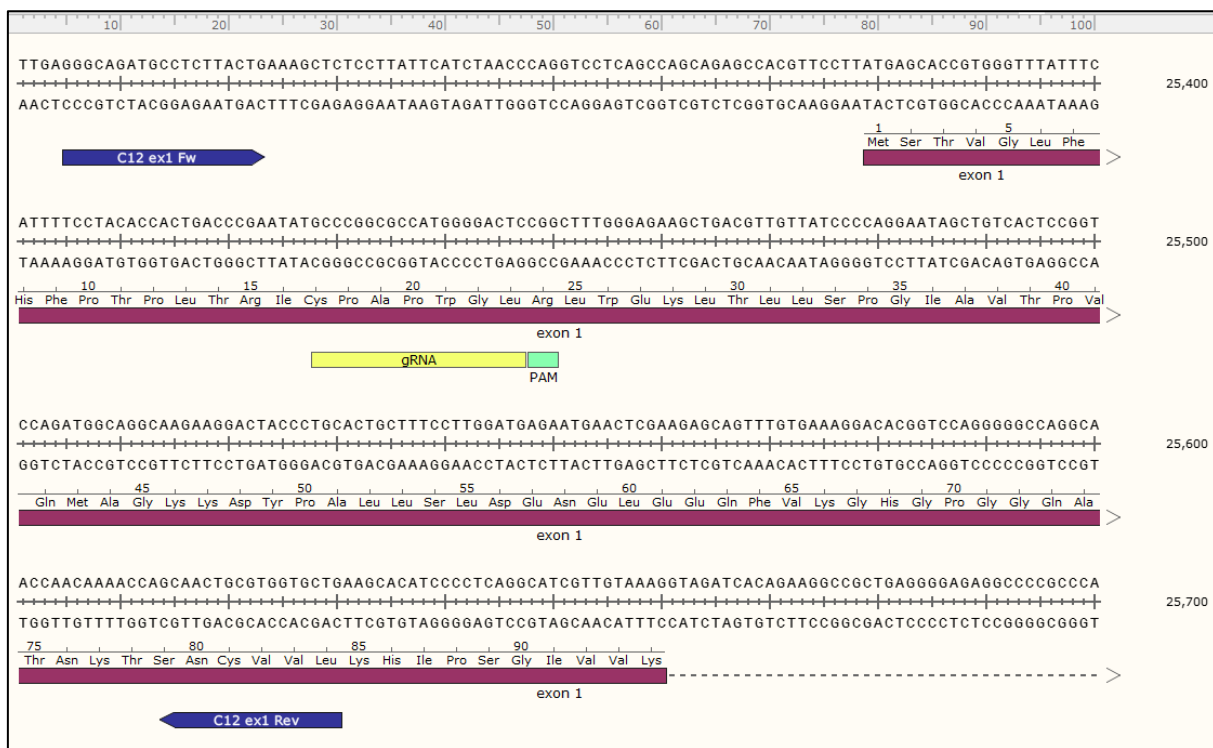


Figure 2-1. Binding sites for the primers used for *C12orf65* sequencing after KO

The primers used to sequence *C12orf65* (NCBI Reference Sequence NG_027517.1) bind to the exon 1 region: forward primer binds 74 bp upstream from the start of the exon and the reverse primer binds towards the end. Figure made using the software SnapGene version 5.1.6.

A volume of 5 μ l from the product of amplification (326 bp) was sent to be sequenced to the Newcastle Mitochondrial Highly Specialised Service laboratory. Due to Covid-19 outbreak and shortage of equipment and staff, the sequencing was done only with the forward primer. The sequencer used was ABI 3130 (Applied Biosystems) and sequencing was performed by genetic technologist Sarah Smith. The software SnapGene was used to visualize the samples chromatograms and retrieve the base calling. The sequences were analysed and compared using the Mutation Surveyor Software v5.1.2 from SoftGenetics.

2.5 RNA Manipulations

2.5.1 RNA isolation from the FLAG-immunoprecipitate

The RNA bound to the agarose beads after immunoprecipitation was isolated using TRIzol (100 μ l, Thermo Fisher Scientific) following manufacturer's instructions. Because the starting sample was small, GlycoBLUE Pellet Paint NF Co-Precipitant (1 μ l; Novagen, Cat.No. 70748-3) was added to the final aqueous phase together with 50 μ l of isopropanol/sample. The final RNA pellet was resuspended by adding 10 μ l of sterile DEPC-treated water over the pellet,

without pipetting up and down in order to avoid losing the RNA in the pipette tip. The samples were vortexed for 30 sec, then kept on ice for 5 min. This step was repeated three times. After optimization, prior to RNA resuspension, the RNA pellet was washed three times with 50 μ l cold 75% ethanol (in DEPC water).

Measurements of RNA concentration were performed at Nanodrop Spectrophotometer ND-1000, using a millimolar extinction coefficient of 40. The RNA was stored at -80°C.

2.5.2 RNA isolation from the eluate after FLAG-immunoprecipitation

Extraction of RNA from the eluate was performed with TRIzol LS (Thermo Fisher Scientific), according to the manufacturer's procedure. Briefly, the sample was dissociated using TRIzol LS, then RNA was extracted with chloroform. RNA was precipitated with isopropanol, washed with 75% ethanol, and finally resuspended in 10 μ l sterile water.

2.5.3 Reverse-transcription

The reverse transcription reaction was used to synthesise a cDNA from isolated RNA. Following the random primer protocol, RNA (5 ng-300 ng RNA/reaction) was first mixed with 50 ng of random hexamers and 1 μ l of 10 μ M dNTP (of each dNTP) to a final volume of 14.5 μ l. The mix was then incubated at 65°C for 5 min and on ice for 1 min. Next, 4 μ l of 5X buffer (Fermentas), 0.5 μ l of RiboLock RNase Inhibitor and 1 μ l reverse transcriptase enzyme Maxima H Minus (Thermo Fisher Scientific, ref Epo752) were added followed by incubation for 10 min at 25°C, then 30 min at 50°C and finally 5 min at 85°C. The resulting cDNA was kept at -20°C.

2.6 Sample preparation for mass-spectrometry

2.6.1 Isolation of crude mitochondria for mass-spectrometry analysis

Isolation of crude mitochondria was performed from C12orf65-BioID2-HA clone 3, C12orf65-Linker-BioID2-HA clone 9 and COX8-MTS (Mitochondrial Targeting Sequence)-BioID2-HA HEK cells. COX8-MTS-BioID2-HA HEK cells were kindly provided by my colleague Yasmin Proctor-Kent. Initially, for each sample, the starting material was 3* 300 cm² flasks of approximatively 80% confluence. To increase yield, during the last experiments, 2* cell factories of 500 cm² each (Nunc TripleFlask, Thermo Fisher, catalogue number 132913) were

used per sample. For each cell type, two samples were prepared: one induced with tetracycline for 16 h (final concentration 1 μ g/ml) and another both induced and fed with biotin (Sigma, B4501-1G, final concentration 50 μ M).

To isolate crude mitochondria, the cells for each sample (treated as described above) were harvested into a 50 ml tube. The pellet was washed in cold PBS and centrifuged (4°C, 230 g, 5 min), then weighted and resuspended in 9 volumes of hypotonic buffer (0.8 ml hypotonic buffer, Table 2-16, used per 1 g of cells).

Table 2-16. Hypotonic buffer

Component	Final concentration
1 M HEPES pH 8.0	20 mM
1 M KCl	5 mM
1 M MgCl ₂	1.5 mM
1 M DTT	2 mM, added immediately before use
100 mg/ml BSA	1 mg/ml, added immediately before use
Protease Inhibitor Cocktail (Roche) EDTA-free	1 tablet for 10 ml, added immediately before use

Following 10 min of incubation on ice, the cells were manually homogenized with 10 strokes, using a glass homogenizer (Cole-Parmer instrument CO, 04368-40). The homogenate was transferred to a 50 ml tube and 2.5X MSH buffer (Table 2-17) was added to it (2 ml of 2.5X MSH buffer to every 3 ml of hypotonic buffer used).

The sample was centrifuged at 1,600 g for 10 min, at 4°C. The pellet consisting of nuclei and cell debris was discarded and the supernatant was centrifuged again in the same conditions. The new supernatant was centrifuged at 10,000 g, 4°C for 10 min. The PMSN (cytosol) was stored at -20°C and the pellet (mitochondria) was washed in 5 ml of 1X MSH buffer (Table 2-18) and centrifuged (10,000 g, 10 min, 4°C). The pellet was resuspended in 1 ml of 1X MSH buffer, transferred to a 1.5 Eppendorf tube and centrifuged in the same conditions. After discarding the supernatant, the pellet was snap-frozen in liquid nitrogen and stored at -80°C.

Table 2-17. 2.5X MSH buffer

Component	Final concentration
Mannitol	525 mM
Sucrose	175 mM
1 M HEPES pH 8.0	20 mM
0.5 M EDTA	10 mM
1 M DTT	2 mM, added immediately before use
Protease Inhibitor Cocktail (Roche) EDTA-free	1 tablet for 10 ml, added immediately before use

Table 2-18. 1X MSH buffer

Component	Final concentration
Mannitol	210 mM
Sucrose	70 mM
1 M HEPES pH 8.0	20 mM
0.5 M EDTA	2 mM
1 M DTT	2 mM, added immediately before use
Protease Inhibitor Cocktail (Roche) EDTA-free	1 tablet for 10 ml, added immediately before use

2.6.2 Mitochondria lysis and streptavidin-affinity purification performed at Newcastle University

Mitochondria pellet was carefully resuspended in 1 ml of lysis buffer (Table 2-19) and left to rotate for 10 min at room temperature in 2 ml low-binding tubes (Eppendorf). Those tubes were used during the entire procedure of streptavidin-affinity purification.

After rotation were added 100 µl of 20% NP-40 and 900 µl of pre-chilled 50 mM Tris-Cl pH 7.4, the mixture was centrifuged (16,500 g, 10 min, 4°C) and the supernatant was collected. An aliquot (10-30 µg) of this was used for western blot detection (input) while the rest was incubated with streptavidin-coated magnetic beads (Dynabeads MyOne Streptavidin C1, Invitrogen, Thermo Fisher Scientific, catalogue number 65001).

Table 2-19. Mitochondria lysis buffer

Component	Final concentration
0.5 M Tris pH 7.5	50 mM
5 M NaCl	500 mM
10% SDS	0.2%
1 M DTT	1 mM, added immediately before use
Protease Inhibitor Cocktail (Roche) EDTA-free	1 tablet for 10 ml, added immediately before use

The beads were first equilibrated in binding buffer (1:1 mixture of room temperature lysis buffer and room temperature 50 mM Tris-HCl pH 7.4). They were vortexed and allowed to incubate for 5 min, then put on a magnetic separation rack (New England Biolabs, S1506S) and the buffer was removed once the beads had accumulated on the magnetic side. This step was performed twice, then the beads were resuspended in binding buffer and distributed equally among the samples (50-100 μ l beads suspension/sample).

The incubation between samples and beads was performed in the cold room, with rotation, overnight. Next, the beads were put in the magnetic stand for 5 min and the supernatant (unbound) was collected and stored at -20°C. A volume of unbound equal to the input volume was used for western blot detection. The beads were subjected to several consecutive washes, each wash consisting of resuspension in 1.5 ml buffer, vortex, rotation for 8 min, separation by standing in the magnetic rack for 5 min. The first two washes were done with 2% SDS, the next two with wash buffer 2 (Table 2-20) and the next seven with 50 mM Tris pH 7.5. The last three washes were removed with gel-loading tips.

Table 2-20. Wash Buffer 2

Component	Final concentration
5% Deoxycholic acid	0.10%
0.5 M EDTA pH 8.0	1 mM
20% Triton-X 100	1%
1 M HEPES pH 7.5	50 mM

A final wash with 1 ml of 50 mM ammonium bicarbonate/sample was done before the beads were resuspended in 100 μ l of 50 mM ammonium bicarbonate.

Proteins were reduced by addition of 1 mM TCEP (final concentration) to the beads, followed by 30 min incubation at room temperature. Next, samples were alkylated with 5 mM (final concentration) chloroacetamide and incubated at room temperature for 30 min in the dark. On-beads digestion was done by the addition of 5 ng/ μ l final concentration trypsin (Trypsin Gold, Mass-Spectrometry Grade, Promega V5280) and incubation overnight at 37°C in the thermomixer. The following day the samples were quickly pulsed down, then left in the magnetic stand for 5 min at room temperature. The supernatant containing digested peptides was collected and mixed with 2 μ l of 10% formic acid. The samples were kept at -80°C before being handed-in to Dr. Frédérique Lamoliatte or Dr. Akshada Gajbhiye, my colleagues from Newcastle University Mass-spectrometry facility (Prof. Matthias Trost's group). They worked with my samples from this step onwards. Peptides were analysed by nanoflow-LC-MS/MS using a Fusion Lumos Tribrid Orbitrap mass spectrometer or Orbitrap Q-Exactive HF Mass Spectrometer (Thermo Scientific) (Thermo Fisher Scientific) coupled to a Dionex Ultimate 3000.

2.6.3 Mitochondria lysis and streptavidin-affinity purification performed at Radboud University, Nijmegen, The Netherlands

During the secondment at Radboud University, the process of streptavidin-affinity purification was undertaken slightly different. The mitochondria were lysed and left to rotate as previously described, but instead of 100 μ l 20% NP-40 were used 100 μ l 20% Triton X-100. Following the incubation with mitochondria lysate overnight, the beads (50 μ l) were washed six times: two washes with 2% SDS, the next two with wash buffer 2 (Table 2-20) and two with 50 mM Tris pH 7.5. After the last wash was removed, the beads were further resuspended in 50 μ l/sample of 8 M urea prepared in 50 mM ammonium bicarbonate. Both solutions were prepared fresh every time, using HPLC water. Next, samples were reduced with 10 mM DTT (final concentration) for 30 min on the Eppendorf thermomixer (1,000 RPM, room temperature). Reduction was followed by alkylation with 50 mM chloroacetamide (20 min at room temperature in the dark, 1,000 RPM). A predigestion step was performed by addition of 1 μ g of lysyl endopeptidase C (LysC, WAKO Chemicals, 125-02543) and incubation on the thermomixer for at least 3 h at room temperature. Samples were diluted 8X with 50 mM ammonium bicarbonate. On-beads digestion was done by the addition of 1 μ g sequencing grade

modified trypsin (Promega, Madison, U.S., reference V511C), overnight, at 37°C on the thermomixer. Samples were acidified using trifluoroacetic acid (2% final concentration).

The resulting peptide samples were concentrated and desalted by ‘Stop And Go Extraction (STAGE) tips’ technique (Rappsilber et al., 2003) and the peptide sample was further purified by Pierce Detergent Removal Spin Columns (Thermo Fisher Scientific, reference 87777) according to the manufacturer’s protocol. Up to this stage, the experiment was performed by me. The preparation of the C18 separation column and sample injection was done by my colleague Alisa Potter under the supervision of Dr. Alfredo Cabrera Orefice.

Mass spectrometry measurements were performed by Dr. Alfredo Cabrera Orefice from Radboud University Mass-spectrometry facility using a nanoLC 1000 (Thermo Fisher Scientific) chromatography coupled online to a Q Exactive hybrid quadrupole-Orbitrap mass spectrometer (Thermo Fisher Scientific). Measurements and data analysis were done as previously described (Hensen et al., 2019).

Chapter 3

Investigation of mtRF1 function

3.1 Introduction

The protein mtRF1, one of the four members of the mitochondria translation release factor family in human, was first identified *in silico* by Zhang and Spremulli (Zhang and Spremulli, 1998). The authors used the primary sequence of *E. coli* RF1 to search for similar protein sequences in human and identified mtRF1, observing that it contains the conserved GGQ motif specific to translation release factors (Figure 3-1). They measured the length (445 aa) and molecular weight (52 kDa) of the protein and identified potential sites of N-terminal cleavage. A clear mtRF1 presequence however could not be identified.

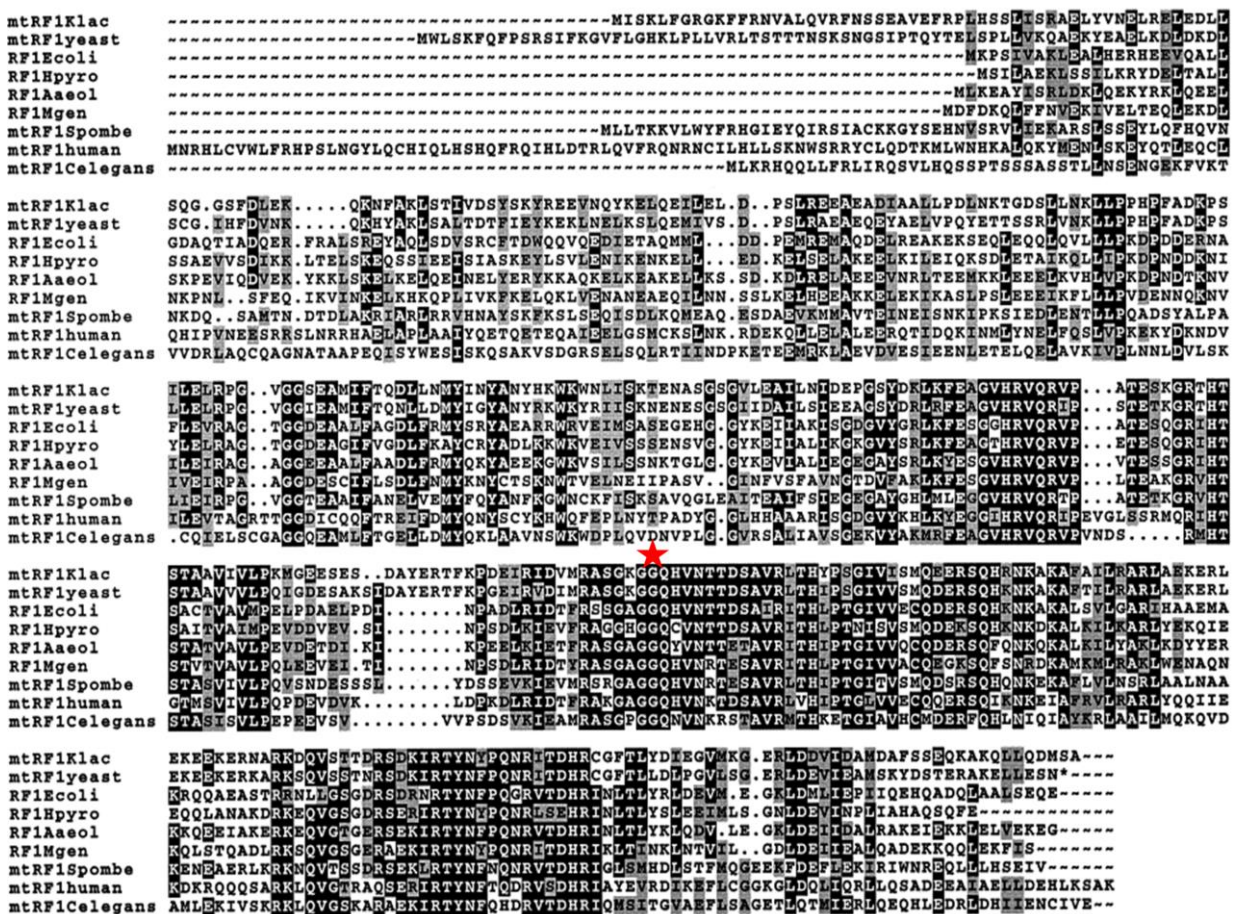


Figure 3-1. Alignment between RF1 from *E. coli* and release factors from different organisms (taken from (Zhang and Spremulli, 1998))

The authors used the primary sequence of *E. coli* RF1 (third from the top) and aligned it with corresponding sequences from other organisms including human (second from the bottom). The GGQ motif is indicated by a red star. As described in the original article, the alignment was made using the Genetics Computer Group (GCG) software program PILEUP and the alignment was displayed using BoxShade. Figure reproduced with permission, RightsLink license number 5255660712788

The subsequent biochemical studies which aimed to demonstrate that mtRF1 functions as translation release factor generated a surprising result: despite being imported in the human mitochondria, mtRF1 showed no release activity *in vitro* with *E. coli* ribosomes (Soleimanpour-Lichaei et al., 2007, Nozaki et al., 2008). Both studies used different variants of N-terminal cleaved mtRF1 to mimic the mature protein, but no release factor activity was detected. In addition to Nozaki et al. (Nozaki et al., 2008), Soleimanpour-Lichaei et al. (Soleimanpour-Lichaei et al., 2007) performed *in vivo* studies on two yeast strains (*S. cerevisiae* and *Schizosaccharomyces pombe*) that lacked the endogenous mitochondrial RF1($\Delta mrf1$). They expressed the human *mtRF1* cDNA in both strains, but the expression could not compensate for the loss of the yeast homologue. The *S. cerevisiae* $\Delta mrf1$ strains were still unable to grow on glycerol substrate (to prevent fermentation) and *S. pombe* $\Delta mrf1$ strains stopped growing on galactose (used to force OXPHOS), despite both expressing the human mtRF1.

The *bona fide* release factor identified in human mitochondria was mtRF1a (also named mtRF1L), which has a primary sequence 42% identical with mtRF1 and is imported in the organelle (Soleimanpour-Lichaei et al., 2007) (Nozaki et al., 2008). The protein mtRF1a showed release activity for both mitochondrial stop codons UAA and UAG in *in vitro* assays that used *E. coli* ribosomes (Soleimanpour-Lichaei et al., 2007, Nozaki et al., 2008). No release activity was registered with the UGA codon, which in mitochondria encodes for tryptophan (Barrell et al., 1979). In addition to the universally conserved GGQ motif, mtRF1a contains a stop codon recognition motif (PXT) that is more similar to the one from bacterial RF1 (PKT) compared to mtRF1 (Soleimanpour-Lichaei et al., 2007). *In vivo* studies performed in $\Delta mrf1$ yeast showed that expression of mtRF1a restored growth for *S. cerevisiae* as well as *S. pombe*. Moreover, mtRF1a was identified only in mitochondria, in different human cell lines, including skeletal muscle (Soleimanpour-Lichaei et al., 2007).

The natural question following those studies is: if mtRF1a specifically recognizes both UAA and UAG in human cells, then what is the role of mtRF1? This question is more ardent as the two proteins are 42% identical and have primary sequences more similar to eubacterial RF1 than to RF2 sequences. Bioinformatic analysis of vertebrate mtRF1 and mtRF1a suggest that mtRF1 emerged from a gene duplication in the early evolution of vertebrates (Young et al., 2010), pointing towards a similar function.

Initially, it was hypothesised that mtRF1 acts in addition to mtRF1a by recognizing two specific mitochondrial stop codons: AGG and AGA (Soleimanpour-Lichaei et al., 2007), codons that usually encode for arginine (Barrell et al., 1979) and were not recognized by mtRF1a. AGG is a stop codon for *MTND6* transcript and AGA for *MTCO1*. The majority of human mitochondria

ORFs are terminated by UAA and UAG is used only by *MTCO2* and *MTATP8* (Anderson et al., 1981).

However, subsequent studies from Temperley et al. proved that AGG and AGA are in fact not used as stop codons (Temperley et al., 2010a). When the human 55S ribosome arrives at either AGG or AGA, it employs a -1 frameshift which, as both codons are preceded by a 'U', results in a standard UAG stop codon that takes place in the A site. Therefore, mtRF1a terminates the translation for *MTND6* and *MTCO1* as it does for the other 11 ORFs from human mitochondria (Lightowlers and Chrzanowska-Lightowlers, 2010).

The study of mtRF1 was the subject of Dr. Aleksandra Pajak's thesis, prior to my arrival in the lab. To gain insight into its role, she used siRNA to deplete mtRF1 in HeLa and HEK cells and noticed a significantly lower growth rate in siRNA-mtRF1 samples compared to siRNA non-targeting negative control (NT). Also, mitochondria morphology was affected in both cell lines: mitochondria network was disrupted and appeared fragmented in comparison to the NT control (Pajak, 2013). To rescue the phenotype, Dr. Pajak used the siRNA treated cells to express an inducible mtRF1-FLAG with either a WT GGQ motif or a modified one (GSQ or AGQ). Only the expression of mtRF1-GGQ-WT-FLAG rescued the growth phenotype and re-established the healthy morphology. The mtRF1-GSQ-FLAG and mtRF1-AGQ-FLAG mutants did not have any effect on cell growth or morphology. On the contrary, they caused a more decreased growth rate which eventually lead to cell death.

Her results showed that mtRF1 is important for cell growth and that the GGQ motif is essential for its function. This information is crucial, especially because no *mtRF1* patients have been identified so far, so there is no other proof that mtRF1 is responsible for cell viability. However, no conclusions could be drawn with respect to the actual function of mtRF1. Depletion of mtRF1 did not change the level of mitochondrial encoded protein COX II or the nuclear encoded proteins mtRF1a, POLRMT or NDUFB8. There was no change in the MRPs levels either, and the migration of mitoribosomes on sucrose gradients was not altered. The level of mitochondrial encoded transcripts was also not affected (Pajak, 2013). Regarding a possible interaction with the 55S ribosome, immunoprecipitation of mtRF1-FLAG did not show any MRP in the eluate (Pajak, 2013). Similarly, immunoprecipitation of the 55S ribosome via ICT1-FLAG did not identify mtRF1 (Richter et al., 2010b).

The *in silico* study from Huynen et al. provided a new hypothesis for mtRF1 function (Huynen et al., 2012). The authors used multiple sequence alignment to separate the mtRF1 subfamily from the mtRF1a subfamily. Then, they compared the two subfamilies and identified the amino

acids that are conserved within each subfamily but are different between mtRF1 and mtRF1a. Moreover, they built a 3D model of mtRF1 and mtRF1a bound to the A-site of *T. thermophilus* ribosome. They compared the 3D model with the already known structure of RF1 bound to the 70S ribosome.

The results of this comparison showed that there are 24 critical aa residues that differ between mtRF1 and mtRF1a, with 20 of them being located in the codon recognition motif (Huynen et al., 2012). In particular, there are two insertions conserved in mtRF1 factors of vertebrate species studied in the article: RT and GLS (Figure 3-2), both located in the codon recognition motif.

In the 3D modelling of mtRF1 bound to the A-site of *T. thermophilus* ribosome, the RT insertion from mtRF1, localized in the tip of helix a5, is oriented outwards from the codon recognition site. In *T. thermophilus* RF1, the two amino acids that flank the RT insertion of mtRF1 interact with the universally conserved A-1493 of rRNA. This interaction occurs only if a stop codon is present in the A site and stabilizes the catalytic conformation of RF1 (Korostelev et al., 2010). The RT insertion of mtRF1 would clash with A-1493 if a stop codon were present. The second insertion, GLS, is located immediately after the PXT motif. In the 3D modelling, GLS is also oriented outwards from the codon recognition site. It forms a surface loop that extends towards the rRNA.

In addition to the above, the authors make two important observations, that lead to a new hypothesis regarding the mtRF1 role (Huynen et al., 2012). First, in mtRF1, the polar amino acids involved in



Figure 3-2. Alignment of bacterial RF with human mtRF1 and mtRF1a

Primary sequences of *T. thermophilus* RF2 (UniProt ID Q5SM01), RF1 (UniProt ID Q72HB8), and human mtRF1 (RF1M, UniProt ID O75570) and mtRF1a (RF1ML, UniProt ID Q9UGC7) were retrieved in FASTA format and aligned using Clustal Omega from EMBL-EBI (Sievers et al., 2011, Goujon et al., 2010). The codon recognition domains are indicated by rectangles 1 and 2. Rectangle 3 indicates the domain responsible for peptidyl-tRNA hydrolysis containing the GGQ motif. The conserved aa are classified as: identical (*), conserved (:) and semi-conserved (.). The percent identity matrix shows the percentage of identity between any two proteins of the alignment. The identity between a protein and itself is 100.00.

binding the nucleotides of the stop codon at the A site were replaced by hydrophobic amino acids. Second, the 3D modelling shows that mtRF1 is capable of self-stabilization in the catalytical conformation. Therefore, the authors advance the hypothesis that mtRF1 is a mitochondria translation release factor that binds to the A site of the 55S ribosome when no stop codon is present, rescuing it from stalling.

The lack of a stop codon is possible in several scenarios: a truncated mRNA (Huynen et al., 2012), pathogenic variants in the mitochondrial genome (Temperley et al., 2003) or aberrant mRNA processing (Szczesny et al., 2010). Temperley et al. describe a pathogenic 2 bp deletion in the mtDNA, located at the junction between *MTATP6* and *MTCO3*, that is predicted to remove the stop codon of *MTATP6* (Temperley et al., 2003). Despite that, *MTATP6* could still be translated, and the generated protein was stable and correctly integrated into FoF₁-ATP synthase. The ATP synthesis was not affected, suggesting the presence of a mechanism to ensure that translation occurred even if the stop codon was absent (Chrzanowska-Lightowers et al., 2004). In addition, Szczesny et al. reported 3' truncated transcripts in a study of ATP-dependent helicase hSuv3p, a protein involved in RNA degradation (Szczesny et al., 2010). The expression of a mutant hSuv3p lead to an increased accumulation of aberrant transcripts, but they were also detected in the control cells, although at a low level. The study shows that truncated mRNA exists in mitochondria, which can cause the mitoribosome to stall. As prolonged stalling decreases the availability of mitoribosomes for new translation cycles, which can eventually lead to cell death (Ayyub et al., 2020), a quality control mechanism is necessary for mitochondria translation.

The aim of my project was to identify the role of mtRF1. Since mtRF1 is imported in mitochondria and contains the universally conserved GGQ motif which is necessary for cell survival, and based on the 3D modelling studies (Huynen et al., 2012), I considered mtRF1 as the best candidate to rescue mitochondrial ribosomes stalled on empty A sites.

To test this hypothesis, I had to answer two research questions:

1. Does mtRF1 interact with the 55S ribosome?
2. Which, if any, is the mRNA target of mtRF1?

Previous studies from my host lab do not exclude the possibility of a transient interaction, that could not be identified by immunoprecipitation. To determine whether such interaction is possible, I used a cross-linker to ensure mtRF1 and the mitoribosome remain attached. I used cells expressing mtRF1-FLAG and, after cross-linking, I separated cellular components by sucrose gradient and identified the mitoribosome and mtRF1-FLAG with specific antibodies.

To determine whether truncated mRNA species are present in the mitoribosomes where mtRF1 is bound, I isolated the mtRF1-FLAG cross-linked to the mitoribosome by FLAG-immunoprecipitation. I isolated RNA from the immunoprecipitate and attempted to identify the transcripts by reverse-transcription and qPCR.

3.2 Results

3.2.1 *mtRF1 transiently interacts with the mitoribosome*

To assess whether mtRF1 rescues stalled mitochondrial ribosomes, it was first necessary to verify if mtRF1 interacts with the mitoribosome. For this, I used an approach that involved a cross-linker: dithiobis (succinimidyl propionate), on short called DSP. The chemical structure of DSP comprises a disulphuric bond and two N-hydroxysuccinimide (NHS) esters (Figure 3-3). The two NHS esters are separated by eight atoms, which span over a 12 Å range (Hermanson, 2013). Each ester reacts with a primary amine group of a lysine residue, forming stable amide bonds. In this manner, DSP crosslinks proteins that are in close proximity (Finel, 1987, Mattson et al., 1993). If one ester reacts with a primary amine from mtRF1-FLAG and the second ester reacts with a primary amine from the mitoribosome proteins, then mtRF1 and the mitoribosomal protein will be bound by the disulphuric bond.

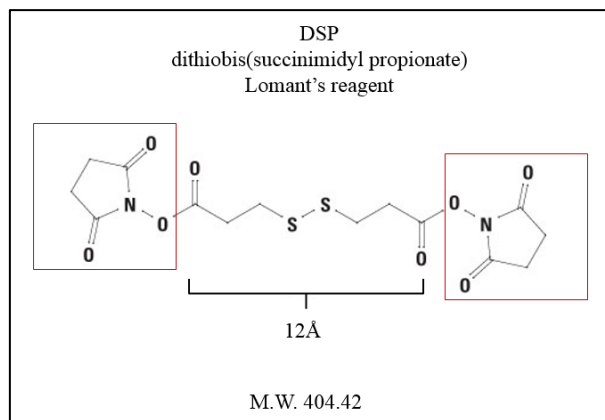


Figure 3-3. Chemical structure of DSP

Dithiobis (succinimidyl propionate), also known as Lomant's reagent, has a 12 Å spacer arm and two N-hydroxysuccinimide (NHS) esters, indicated by the red square.

I used HEK 293T cells and induced mtRF1-FLAG expression with doxycycline (5 ng/µL for 3.5 d), then treated them with DSP (1 mM, 5 min) prior to harvesting. The concentration of compounds and duration of treatment had been previously established in the lab. Duration of DSP treatment was optimized to ensure stabilization of transient interactions while avoiding protein aggregation in the cells. After harvesting, cells were lysed and the total cell lysate was loaded on a 10-30% sucrose gradient. The lysate was separated by ultracentrifugation due to the different density of the sucrose solutions and 11 fractions were collected. To concentrate the total protein amount, each fraction was precipitated with TCA. Fractions were denatured and loaded on SDS-PAGE. The addition of 50 mM DTT in the dissociation buffer ensured that the disulphuric bonds were reduced, including the ones created between proteins by the DSP cross-linking. Hence, if mtRF1 interacts with the mitoribosome, the two remain cross-linked when fractions are collected, but they are separated inside the fractions prior to SDS-PAGE, so they can migrate individually. The proteins of interest were visualized by immunoblotting using the anti-FLAG antibody (for mtRF1-FLAG) and antibodies specific for the mtSSU (DAP3, MRPS26) and for the mtLSU (MRPL3, MRPL45).

Without cross-linking, it was expected that mtRF1-FLAG and the mitoribosome subunits would appear in separate fractions. Indeed, for the sucrose samples not treated with DSP, mtRF1 accumulates in the higher fractions (1-3), while the mitoribosome subunits accumulate in the middle fractions: MRPS26 (small subunit) in fractions 4-6 and MRPL3 (large subunit) in fractions 6-8 (Figure 3-4).

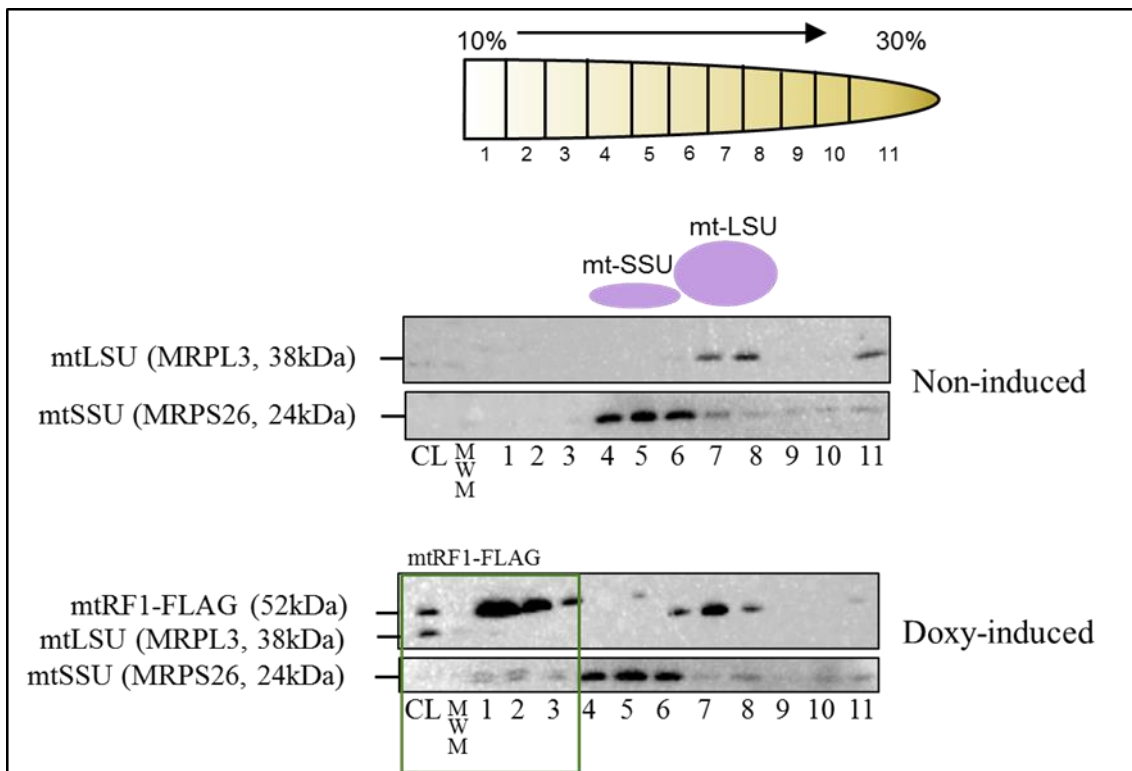


Figure 3-4. Separation of mtRF1-FLAG HEK cell lysate on sucrose gradient

Cells induced for mtRF1-FLAG expression and control cells were lysed and the components were separated on a 10-30% sucrose density gradient in 11 fractions. The fractions were TCA precipitated, then analysed by western blot (12% gel) using antibodies against the FLAG tag, the small subunit (MRPS26) and the large subunit (MRPL3) of the mitoribosome. The green rectangle highlights the position of free mtRF1-FLAG. CL-cell lysate; MWM-molecular weight marker (kDa); representative figure of 3 independent experiments

With cross-linking, I expected to observe a shift in the positions of mtRF1 and MRPs on the sucrose gradients. MRPs become denser when they are cross-linked with each other, with mtRF1-FLAG or with other proteins in their proximity. They shift towards the bottom of the tube during ultracentrifugation, therefore appearing in different fractions compared to the control without DSP. As can be seen in (Figure 3-5), the signal of DAP3, (mtSSU marker) shifts towards the bottom (fractions 4-9). The same is true for MRPL45 (upper panel) and MRPL3 (lower panel), two mtLSU marker proteins that migrate to fractions 6-10. Importantly, the FLAG signal migrates towards the lower fractions as well, which shows that DSP treatment was efficient and mtRF1 was cross-linked to the mitoribosome. MtRF1-FLAG appears together with the small mitoribosomal subunit in fractions 4-5 and with the monosome in fractions 7-9. The DSP treatment allows the cross-linking of the small and large subunit and maintains the monosome (fractions 7,8,9).

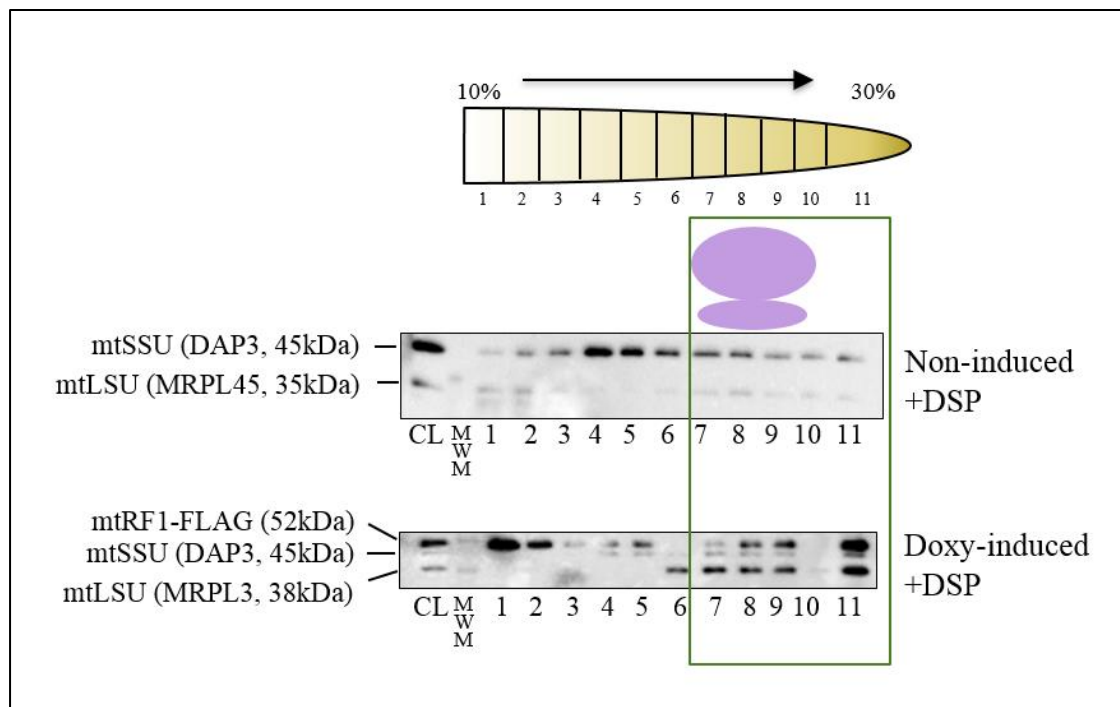


Figure 3-5. Separation of cross-linked mtRF1-FLAG HEK cell lysate on sucrose gradient

Cells induced for mtRF1-FLAG expression and control cells were treated with DSP (1 mM, 5 min). Cells were then lysed and separated on a 10-30% sucrose density gradient in 11 fractions. The fractions were TCA precipitated, then analysed by western blot (12% gel) using antibodies against the FLAG tag, the small subunit (DAP3) and the large subunit (MRPL45, MRPL3) of the mitoribosome. The green rectangle highlights the position of the monosome. CL-cell lysate; MWM-molecular weight marker (kDa); representative figure of 3 independent experiments

3.2.2 Mitochondrial mRNA can be isolated by mtRF1-FLAG immunoprecipitation

My results show that mtRF1 can be cross-linked to the mitoribosome, suggesting a transient interaction between the two. This agrees with mtRF1 being a translation rescue factor. In order to further investigate my work hypothesis, I aimed to identify the mRNA targets of mtRF1. This would help clarify whether truncated mRNA species are indeed associated with mtRF1, and if they are, whether there is any transcript that appears truncated more prevalently than other transcripts.

The putative mRNA target would be protected by the mitoribosome. To separate it from the other transcripts being translated, I cross-linked mtRF1-FLAG to the mitoribosome, then immunoprecipitated the mitoribosome via the FLAG-tag. This would ensure that the mitoribosomes are isolated only if mtRF1 was already bound (or was about to bind) to them. Also, it would maintain the monosome by cross-linking the small and the large subunit. The immunoprecipitated mitoribosome could then be used for RNA isolation followed by reverse-transcription, to identify the RNA species protected by it.

DSP treatment caused a severe decrease in total protein concentration. This was a recurrent problem during the sucrose gradient experiments, when I would constantly observe a lower protein concentration in the cell lysates of DSP treated samples than in the control, despite starting from the same amount of cells. For this reason, I increased the starting material of the immunoprecipitation experiments from a 75 cm^2 to a 225 cm^2 flask per sample. I induced mtRF1-FLAG expression and treated both non-induced and induced cells with 1 mM DSP for 5 min prior to harvesting. I lysed the cells and performed immunoprecipitation using anti-FLAG coated agarose beads. A small amount of the cell lysate was used to test FLAG expression by western blot, while the rest was incubated with the beads. I expected mtRF1-FLAG to bind the beads and carry over the mitoribosome and the mRNA inside it.

Another difficulty was that the cells had the tendency to either lose the FLAG expression after 3-4 months, or to become ‘leaky’ (express the FLAG in the absence of the inducer). To prevent this, I tested the FLAG expression and froze down several vials of cells with strong FLAG expression, at an early passage. I used those cells if the ones in culture would become problematic. Also, I doubled the concentration of inducer (from $5\text{ ng}/\mu\text{L}$ to $10\text{ ng}/\mu\text{L}$) and reduced the duration of induction (from 3.5 d to 48 h) to prevent the cells from becoming antibiotic resistant.

In a first attempt, I isolated RNA from the agarose beads immediately after immunoprecipitation. I reverse-transcribed the RNA and used the cDNA obtained for relative qPCR, using as primers 12S (marker for the small subunit), 16S (marker for the large subunit) and COX2 (as a possible mRNA protected inside the mitoribosome). I was expecting to obtain low Ct values, corresponding to a high quantity of RNA isolated, in the induced samples and high Ct values in the non-induced samples, where no mtRF1-FLAG was expressed to facilitate the immunoprecipitation.

However, the Ct values of all the three genes tested were low in the non-induced samples and the difference between induced and non-induced was small, if existent (Figure 3-6).

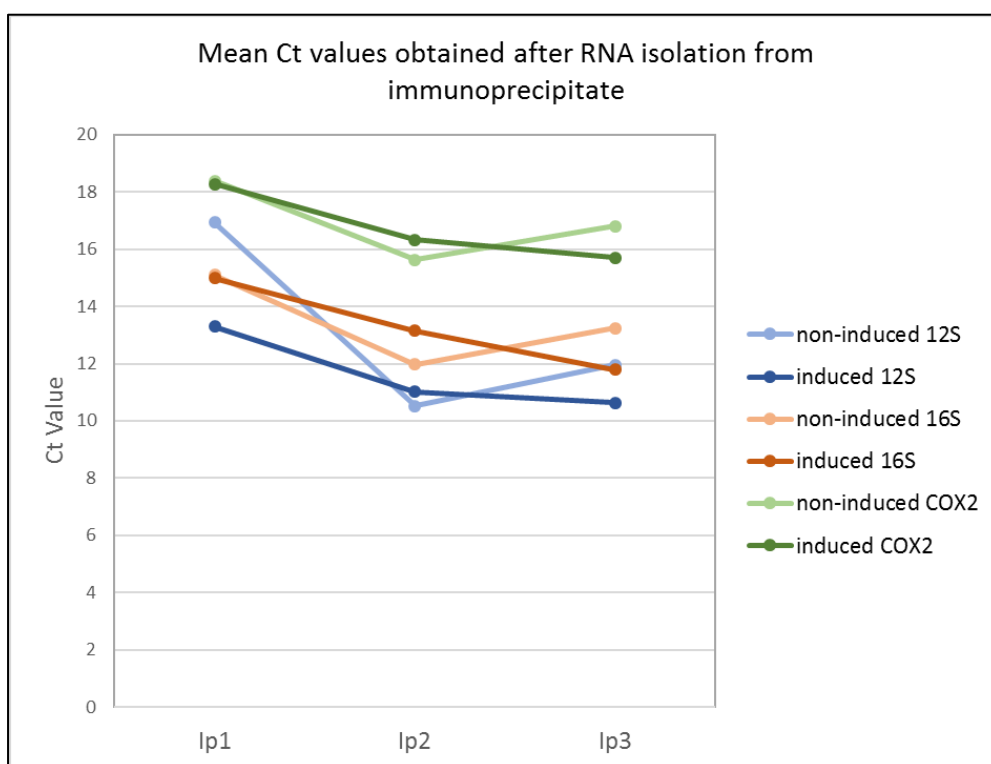


Figure 3-6. Mean Ct values obtained after RNA isolation from immunoprecipitate

RNA isolated from immunoprecipitation (Ip) was reverse-transcribed and the cDNA amplified by qPCR. The graph depicts the mean Ct values obtained in each experiment (N=3) for 12S (blue), 16S (orange) and COX2 (green). Each dot represents one Ct value measured for one experiment. A higher Ct value corresponds to a lower amount of RNA.

In addition, the levels of 12S and 16S did not correlate and were not consistent among the three independent experiments. As the two molecules are in 1:1 ratio in the monosome, I was expecting to obtain similar Ct values for 12S and 16S of the same sample, and similar

differences between induced and non-induced samples. More importantly, I was not expecting to obtain RNA from the non-induced samples.

The rationale behind using 12S and 16S rRNA was to have a positive control for RNA isolation from the immunoprecipitate. Their identification, as well as the identification of COX2 mRNA, proves that technically the experiment was successful. The surprising result however was the isolation of RNA from non-induced samples. To find the reason behind it, I tested the FLAG expression by western blot for each triplicate, but the results failed to provide an explanation. For two experiments, the western blot confirmed mtRF1-FLAG expression only in induced samples (Figure 3-7). No FLAG signal was detected in the second immunoprecipitation, suggesting a failed induction, but the qPCR showed a two-fold increase in 16S expression. The western blot and the qPCR results could not be correlated, which suggested a very high background level.

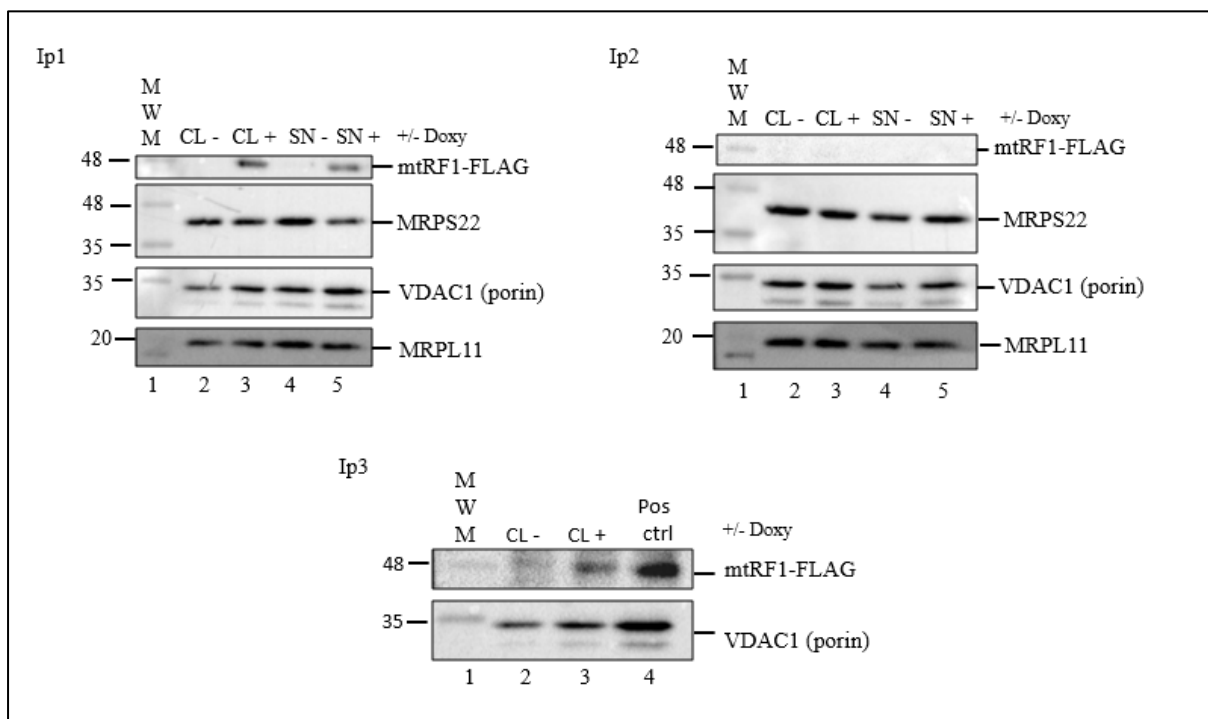


Figure 3-7. Test of FLAG expression in the samples used for immunoprecipitation

MtRF1-FLAG HEK 293T cells were induced (10 ng/ml doxycycline, 48 h) and treated with DSP prior to harvesting. 25 µg of input (CL, cell lysate incubated with anti-FLAG coated beads) and supernatant (SN, unbound) were loaded per lane. VDAC1 (porin) was used as loading control. MWM-molecular weight marker (kDa); 10% gel

Assuming that the high level of RNA expression in non-induced samples was given by the non-specificity of the beads, I optimized the experiment by introducing an elution step. I used the 3X FLAG peptide to elute the mtRF1-FLAG (cross-linked to the mitoribosome) attached to beads and isolate RNA from the eluate. This approach was designed to eliminate any non-specific binding to the beads. As the 3X FLAG peptide has a higher affinity for the anti-FLAG coated beads than mtRF1-FLAG, it should compete with the latter and remove it from the beads. Therefore, in the eluate of induced samples, I would expect to obtain only mtRF1-FLAG attached to the mitoribosome. Ct values reflecting the isolated RNA should be much lower for induced sample comparing to non-induced.

Before attempting the optimized protocol, I tested that mtRF1-FLAG is eluted from the beads after immunoprecipitation, using samples without DSP. I checked the presence of mtRF1-FLAG in the eluate by western blot, using anti-mtRF1 and anti-FLAG antibodies. The anti-mtRF1 antibody identified the protein in both input samples (Figure 3-8, lines 4 and 10) but weakly in the eluate. The FLAG signal from eluate was identified by the anti-FLAG antibody, only in the induced sample (line 15). No signal was identified in the three washes that followed beads incubation, showing mtRF1-FLAG is not lost.

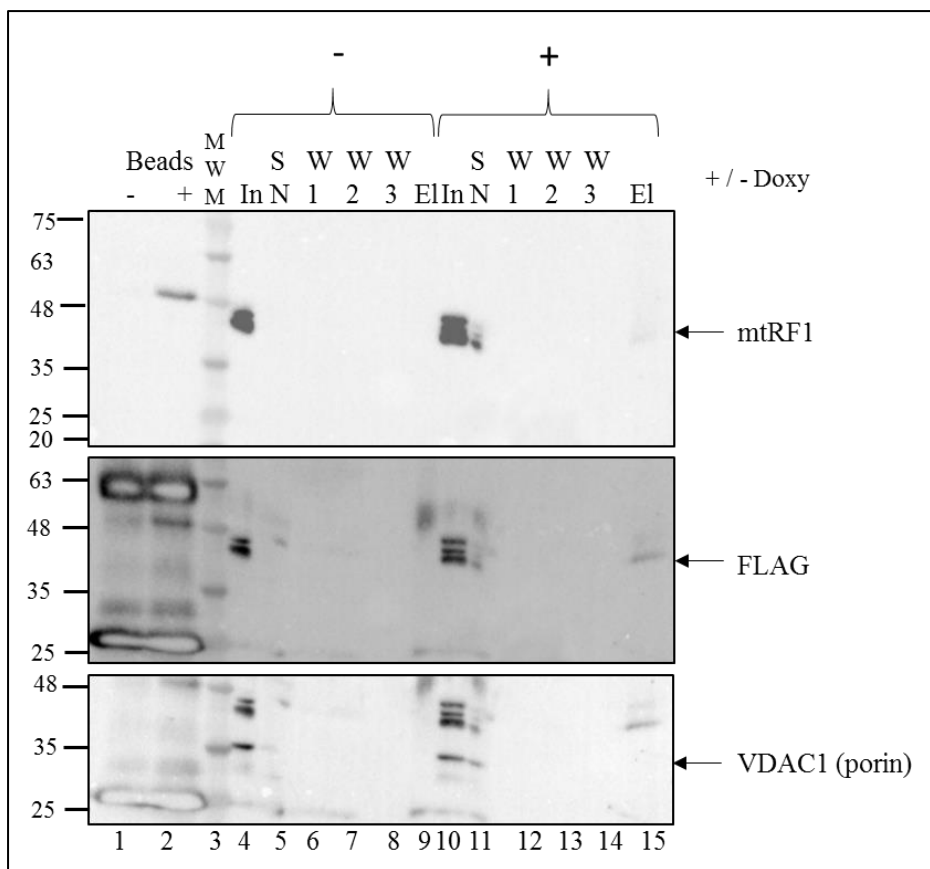


Figure 3-8. Proof of principle: elution of mtRF1-FLAG

MtRF1-FLAG HEK 293T cells were induced with doxycycline (10 ng/ml, 48 h), lysed and incubated with anti-FLAG coated beads. 20 µg of input (In, cell lysate incubated with the beads) and supernatant (SN, unbound) were loaded per lane. The three washes post-immunoprecipitation (W1-W3) and the eluate (El) were concentrated using TCA and loaded entirely. VDAC1 (porin) was used as loading control. 300 µg total input; 10% gel; MWM- molecular weight marker (kDa); N=1

After the successful elution of mtRF1-FLAG from the beads, I used this step for the DSP treated samples. I proceeded as before, but, instead of isolating RNA from the beads, I eluted the mtRF1-FLAG cross-linked to the mitoribosome and isolated RNA from the eluate. To test the efficiency of induction, as well as to determine if there was any mtRF1-FLAG in the eluate or if it has remained on the beads, I performed an SDS-PAGE and incubated the membrane with the anti-FLAG antibody. I used the cell lysate from induced and non-induced samples to check induction. The supernatant remained after beads incubation was used as an indicator that the beads bound mtRF1-FLAG from the cell lysate. To confirm that mtRF1-FLAG was eluted I used only 10 µl of the eluate (1/10 of the total volume), to ensure I have a sufficient quantity for RNA isolation. I also checked the beads after elution to confirm if mtRF1-FLAG was

detached from them. As a positive control for FLAG expression, I used a cell lysate from mtRF1-FLAG induced cells that I have tested previously.

Although the FLAG signal appeared in the positive control (Figure 3-9, lane 1), as well as in the cell lysate (lane 4) and the supernatant (lane 6) of the induced samples, it did not appear in the eluate (lane 8) or on the beads (lane 10). The Ponceau staining also did not show any coloration in the eluate. The only signal that was visible on the beads, with anti-FLAG and Ponceau staining, corresponded to the heavy and light chains of the antibody that coats the beads. The two antibodies used as marker for the small (MRPS22, 41 kDa) and large subunit (MRPL11, 21 kDa) did not show any signal in the beads or in the eluate.

Isolation of RNA from eluate did not improve the qPCR results. In two consecutive experiments, the background level remained high, despite elution (Figure 3-10). The only improvement consisted in similar levels of 12S and 16S rRNA, per experiment; in the first experiment, theoretically, there were twice more 12S and 16S molecules in the induced samples compared to non-induced, while in the second experiment there was no difference at all. However, a two-fold change in expression between induced and non-induced, that could not be reproduced, is not a trustable result. It may not reflect a real change in expression, and only shows that the background level is high.

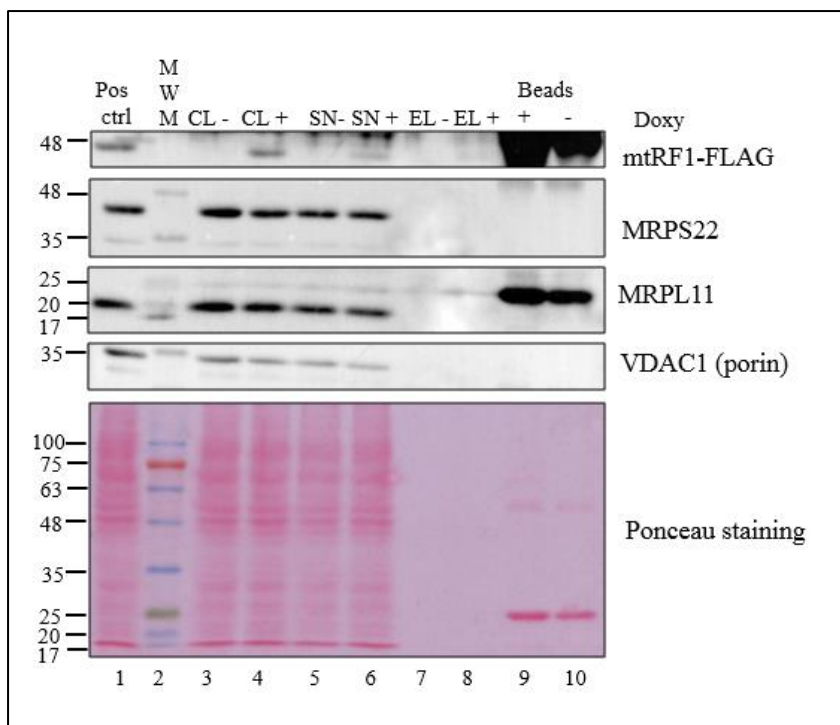


Figure 3-9. Immunoprecipitation followed by elution of mtRF1-FLAG in DSP treated samples

MtRF1-FLAG HEK 293T cells were induced with doxycycline and treated with DSP prior to harvesting. The input (CL, cell lysate incubated with anti-FLAG beads), supernatant (SN, unbound), eluate (EL) and beads, as well as a FLAG positive control (pos ctrl) were separated by SDS-PAGE (10% gel) and probed with anti-FLAG, anti-MRPS22 and anti-MRPL11 antibodies. VDAC1 was used as loading control. The positive control was a sample previously tested as positive for induction. Loaded per lane: 50 µg (lanes 1, 3, 4, 5, 6) or 10 µl (eluate). The strong bands that appear with Ponceau coloration (lanes 9-10) correspond to the heavy (upper band) and light (lower band) chains of the anti-FLAG antibody that coated the beads. MWM=molecular weight marker; N=2

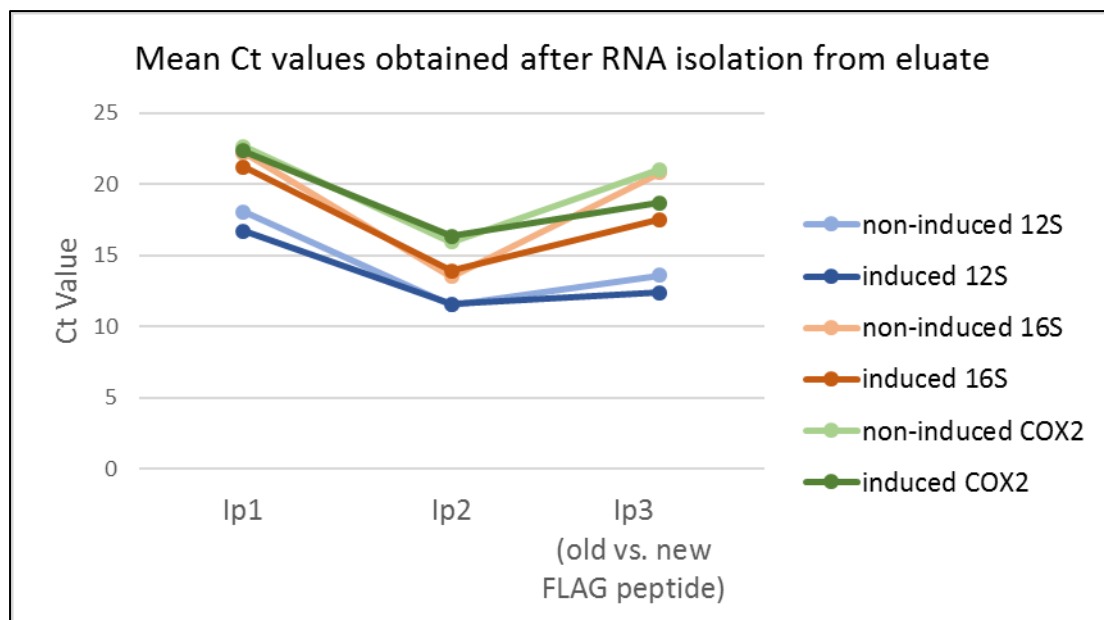


Figure 3-10. Mean Ct values obtained after RNA isolation from eluate

RNA was isolated from the eluate after immunoprecipitation (Ip), reverse-transcribed and the cDNA amplified by qPCR. During one experiment (Ip3) elution was performed only from induced cells with two different batches of FLAG peptide, to exclude the batch as a potential cause for the close Ct values. The graph depicts the mean Ct values obtained in each experiment (N=3) for 12S (blue), 16S (orange) and COX2 (green). For Ip3, the light colour shade corresponds to the old FLAG peptide and the dark shade corresponds to the new one. Each dot represents one Ct value measured for one experiment. A higher Ct value corresponds to a lower amount of RNA.

In a final attempt to optimize the experiment, I performed one immunoprecipitation using a different batch of 3X FLAG peptide for elution. Knowing that immunoprecipitation experiments followed by elution had been previously done in the lab, I used an aliquot of 3X FLAG peptide previously tested. I compared the efficiency of the ‘old’ aliquot with the ‘new’ one that I have been using. I prepared only one sample of induced cells, that I treated with DSP, then lysed. The lysate was split in two and each half was incubated with anti-FLAG beads. Following immunoprecipitation, half of the sample was eluted with an old batch of FLAG peptide and the other half with the batch currently used. Western blot analysis confirmed the FLAG expression in the input, but could not detect it in the eluate, with either peptide batch (Figure 3-11). The Ct values obtained using the old aliquot were higher than the ones obtained with the new one (Figure 3-10), suggesting that the RNA isolation was less efficient and that the new 3X FLAG peptide used so far had been the best option.

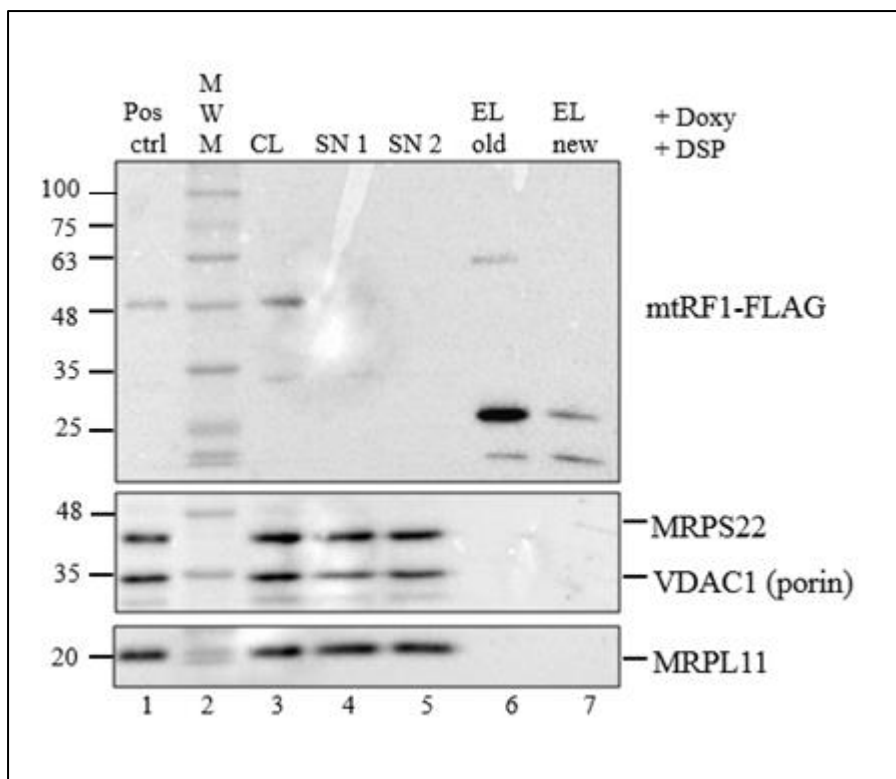


Figure 3-11. Elution of mtRF1-FLAG using different batches of FLAG peptides

MtRF1-FLAG HEK 293T cells were doxycycline-induced and DSP-treated prior to harvesting and lysis. The input (CL, cell lysate incubated with anti-FLAG beads), supernatants (SN1 and SN2, unbound), eluates (EL) and a FLAG positive control (pos ctrl) were separated by SDS-PAGE (10% gel) and probed with anti-FLAG, anti-MRPS22 and anti-MRPL11 antibodies. VDAC1 was used as loading control. Loaded per lane: 25 µg (lanes 1, 3) or 10 µl (eluates). MWM = molecular weight marker (kDa); N=1

Despite the efforts to optimize the RNA isolation, there was no difference between the induced and non-induced samples. The putative mRNA target of mtRF1 remained unidentified. However, my results showed that it is technically possible to isolate mitochondrial mRNA from immunoprecipitate and from eluate.

3.3 Discussion

Contrary to what was expected, there was no difference in RNA levels between the induced and non-induced samples. Only induced samples expressed mtRF1-FLAG, which facilitated the immunoprecipitation. Because of the cross-linking, the mitoribosome would also become attached to the beads, providing the material for RNA extraction. The qPCR experiments showed that this step was possible, and RNA could be isolated by this method. However, it

should have not been possible for non-induced samples, because they do not express the FLAG-tag, so the immunoprecipitation should not, in theory, be possible.

However, the Ct value obtained for background (non-induced) was low. One possible cause, strictly technical, could be the non-specificity of the beads. It could happen that the agarose beads have a non-specific affinity for ribosomes. Replacing them with magnetic beads could solve the problem. Another issue is the cells susceptibility to use mtRF1-FLAG. The cell model used overexpresses mtRF1-FLAG when induced, but it is not more prone to stalling. According to working hypothesis, mtRF1 would go to mitochondria to rescue stalled mitoribosomes. If the level of stalled mitoribosomes is similar in induced comparing to non-induced cells, then, even if I have a higher quantity of mtRF1-FLAG produced by induction, the quantity required for rescue remains the same as without induction. In consequence, the amount of RNA obtained from immunoprecipitation would be the same.

Regarding the western blot results, the FLAG signal was not visible after elution with the 3X FLAG peptide for both eluate and beads. However, this is not a proof that elution was not successful. Western blot is semiquantitative, and the Ct values obtained from qPCR, a more sensitive method, confirm that RNA was present in the eluate. In addition, the elution test experiment (Figure 3-8) detected mtRF1-FLAG in the eluate.

The quantity of eluate used for immunoblotting was only 1/10 of the total volume, comparing to 9/10 used for RNA extraction. There is still the possibility that mtRF1-FLAG bound to the mitoribosome was present in the eluate, but in such a small amount that it could not be detected. The same explanation stands for the lack of signal for the small (MRPS22) and large (MRPL11) mitoribosome subunits on the western blot. It is reasonable to assume that stalling does not occur very often, so the number of cross-linked mitoribosomes should be very small comparing to the total. In *E. coli*, for example, approx. 0.4% of translation events require ribosome rescue (Moore and Sauer, 2005). I would therefore expect the amount of mtRF1-FLAG bound to the mitoribosome to be scarce even in the total volume of eluate.

Unfortunately, the strong signal produced by the small and large chains of the antibody prevented me from observing if mtRF1-FLAG remained attached to the beads. As can be seen in Figure 3-9, the signal at 50 kDa, corresponding to the large chain, hides any possible FLAG signal on the beads, because mtRF1 has a similar molecular weight (52 kDa theoretical, including an unknown mitochondrial targeting sequence).

Another aspect that needs to be discussed is the fact that I was not able to test the efficiency of the DSP treatment, which cannot be determined from the immunoprecipitation. To do so, it would have been necessary to run the cell lysate on a sucrose gradient, but this was not possible due to insufficient material to accomplish both. Cross-linking caused the cells to adhere to the flask, which required manual scraping to harvest them. This could cause protein loss due to unintentional cell tearing. Although I have increased the starting material from a 75 cm² to a 225 cm² flask for each sample, there was still not sufficient material to perform both sucrose gradients and immunoprecipitation from one sample. Although I cannot prove that DSP treatment was efficient in the RNA isolation experiments, the sucrose gradients show that a 1 mM concentration and 5 min duration of treatment are enough for cross-linking mtRF1-FLAG to the monosome. Since I used the same conditions in the RNA experiments, it is unlikely that a failed DSP cross-linking causes the high background. The 12S, 16S and COX2 Ct values were low in the non-induced for all the experiments presented. If DSP failed in any of them, I would expect to see a high value for the Ct values (40-45), corresponding to no RNA isolated from the beads. Without cross-linking, only free mtRF1 would bind the beads.

Although I do not consider that a failed cross-linking caused the high RNA background, the treatment can still be improved. Kotrys et al. used a different methodology for DSP cell treatment (Kotrys et al., 2019). Instead of coating the cells with the 1 mM DSP solution, like I did, they resuspended the cells in PBS and added DSP to the cell suspension, at a 0.5 mM final concentration. They allowed the cells to incubate with DSP for 30 min with rotation and quenched the reaction with 50 mM Tris-HCl pH 7.4 for 15 min, also with rotation. In addition, they performed the incubation at 4°C, while I performed mine in the incubator. On one hand, I consider that their method reduces protein loss, because the cells are not collected by scraping. Also, during rotation, all cellular surface comes into contact with the DSP solution, which could increase cross-linking efficiency. Elimination of the scraping step would allow to increase the number of cells at the start of the experiment, because they could be grown in 500 cm² cell factories. A higher amount of starting material could lead to a better capture of mitochondrial RNA from induced cells, decreasing the background. On the other hand, keeping the cells at 4°C for 30 min might induce artefacts due to cellular response to cold. It would be interesting to apply the Kotrys' DSP methodology (Kotrys et al., 2019), then isolate RNA from the immunoprecipitate and compare those results with the current results obtained.

Although it was not possible to identify the mRNA target of mtRF1, my results show that this factor is capable of interacting with the mitoribosome in a transient manner. As shown by the

migration pattern on the sucrose gradients, the protein is free in the mitochondrial matrix, but can be chemically cross-linked to the mitoribosome. This is in agreement with Dr. Pajak's conclusions, who in addition showed that the GGQ motif of mtRF1 is essential for cell growth (Pajak, 2013). Recently, experiments performed in my host lab showed that knockout of mtRF1 leads to upregulation of C12orf65, another member of the mitochondria release factor family. Also, the overexpression of C12orf65 in a mtRF1 knockdown model improved cell growth (Dr. Shreya Ayyub, unpublished data). As C12orf65 was recently shown to rescue stalled mitochondrial ribosomes (Desai et al., 2020), it is possible that mtRF1 has a similar function. Taken together, the results obtained by myself and my colleagues indicate that mtRF1 could be involved in mitochondria translation, albeit the true function of the factor remains unknown.

Chapter 4

C12orf65-BioID2-HA, an initial cell model to investigate

C12orf65 function using the BioID2 approach

4.1 Introduction

The function of C12orf65 remains elusive, despite the presence of the conserved GGQ motif that suggests peptidyl-hydrolase activity (Ayyub et al., 2020). The patients with C12orf65 defects present with different symptoms and have different backgrounds, making the protein characterization even more difficult. Pathogenic *C12orf65* gene variants have been associated with optic atrophy and Leigh syndrome (Heidary et al., 2014, Imagawa et al., 2016), reviewed by (Finsterer, 2020), spastic paraplegia type SPG55 (Shimazaki et al., 2012), reviewed by (Kumar et al., 2015), neuropathy (Fang et al., 2017, Tucci et al., 2014), Behr's syndrome (Pyle et al., 2014) and intellectual disability (Antonicka et al., 2010). Patients have different ethnicities- from Japanese (Nishihara et al., 2017) and Chinese (Fang et al., 2017) to Irish/English (Pyle et al., 2014) and Indian (Tucci et al., 2014). The pathogenic variants are transmitted recessively and are identified as homozygous (Perrone et al., 2020) or compound heterozygous (Fang et al., 2017). Although the majority are pediatric, an adult-onset form of Leigh syndrome has been reported (Wesolowska et al., 2015).

The common denominator of all those patients is the involvement of GGQ motif: in its absence, the symptoms are aggravated, and mitochondrial translation is severely impaired, leading to defects in OXPHOS assembly. In a study by Buchert et al. the authors compare the premature stop gain that they have found at position 139, caused by a homozygous c.415C>T p.(Gln139*), current Ensemble Gene ID ENSG00000130921.3, with two truncating variants reported previously which occur upstream, at positions 84 (caused by a homozygous NM_152269: c.248delT p.(Leu84*)) and 132 (caused by a homozygous c.394C>T p.(Arg132*), current Ensemble Gene ID ENSG00000130921.3) (Buchert et al., 2013). They confirm a genotype–phenotype correlation between the variant locus and the severity of the symptoms: the symptoms correlated with the truncation from position 84 were exacerbated (intellectual disability, encephalomyopathy, optic atrophy, and ophthalmoplegia) compared to the ones reported by the other authors (mild intellectual disability, spastic paraplegia, but no impairment of hearing and vision and no epilepsy). Their conclusion is later reiterated by Spiegel et al. (Spiegel et al., 2014) who in addition define three major symptoms characteristic for pathogenic *C12orf65* variants: optic atrophy, axonal neuropathy and spastic paraparesis.

The importance of the GGQ motif indicates a potential role of C12orf65 in the termination step of mitochondria translation. However, this protein showed no peptidyl-tRNA hydrolase activity in an *in vitro* assay with *E. coli* 70S ribosomes (Antonicka et al., 2010) and it lacks the

codon-recognition motif. Also, mtRF1a has already been assigned as the translation termination factor in human mitochondria (Soleimani-pour-Lichaei et al., 2007). Therefore, the function of C12orf65 remains unknown. The aim of my project was to gain insight into this function by identifying possible C12orf65 interacting partners.

Previous studies done in Lightowlers' group by Dr. Aleksandra Pajak showed that C12orf65 is free, soluble in the mitochondria matrix, and does not stably associate with the mitochondria ribosome (Pajak, 2013). The immunoprecipitation experiment that she performed did not identify any C12orf65 binding partners, pointing towards a possible transient interaction with the mitoribosome ((Pajak, 2013), Figure 7.11 of the citation). In order to identify possible interacting partners, but not necessarily binding partners, I used a proximity-labelling method named BioID2.

BioID2 is the improved version of the BioID method (Kim et al., 2016a). BioID was developed in 2012 by Brian Burke's lab at the University of South Dakota and is based on a modified biotin-ligase from *E. coli* (Roux et al., 2012). Normally, in *E. coli*, the biotin-ligase (BirA) uniquely biotinylates the acetyl CoA carboxylase, an enzyme that catalyzes the rate-limiting step in the fatty acid biosynthesis pathway (Figure 4-1). ATP combines with biotin to form biotinoyl-5'-AMP ('activated biotin') (Lane et al., 1964) which is captured by BirA and released only to biotinylate the acetyl CoA carboxylase. The biotinylation reaction occurs at the primary amine of a lysine residue from a particular recognition sequence called Biotin Acceptor Tag (BAT), formed of at least 14 aa (Beckett et al., 1999). The reaction is very specific to this substrate and the process is tightly regulated at gene level as well: in addition to the biotin binding domain, BirA has a DNA binding domain and functions as a transcriptional repressor for the biotin biosynthetic operon (Chapman-Smith and Cronan, 1999, Satiaputra et al., 2016).

In BioID, BirA was mutated (p.Arg118Gly), which cancelled both the DNA binding capacity and the specificity to acetyl CoA carboxylase (Kwon et al., 2000). This reduced the affinity for biotinoyl-5'-AMP (Kwon and Beckett, 2000), making the biotin-ligase release the 'activated biotin' instead of holding it. As a consequence the 'activated biotin' binds any primary amines from any proteins, including itself, regardless of their species origin (Choi-Rhee et al., 2004, Cronan, 2005). This promiscuous form of BirA is used to study protein-protein interactions: by attaching a protein of interest to BirA, the proteins that come in proximity to the protein of interest on an approx. 10 nm radius (Kim et al., 2014) are biotinylated. They can be therefore

immunoprecipitated with streptavidin and analyzed using mass-spectrometry. In Brian Burke's lab, this method successfully detected multiple proteins that interact with lamin-A and identified a new protein associated with the nuclear lamina (Roux et al., 2012).

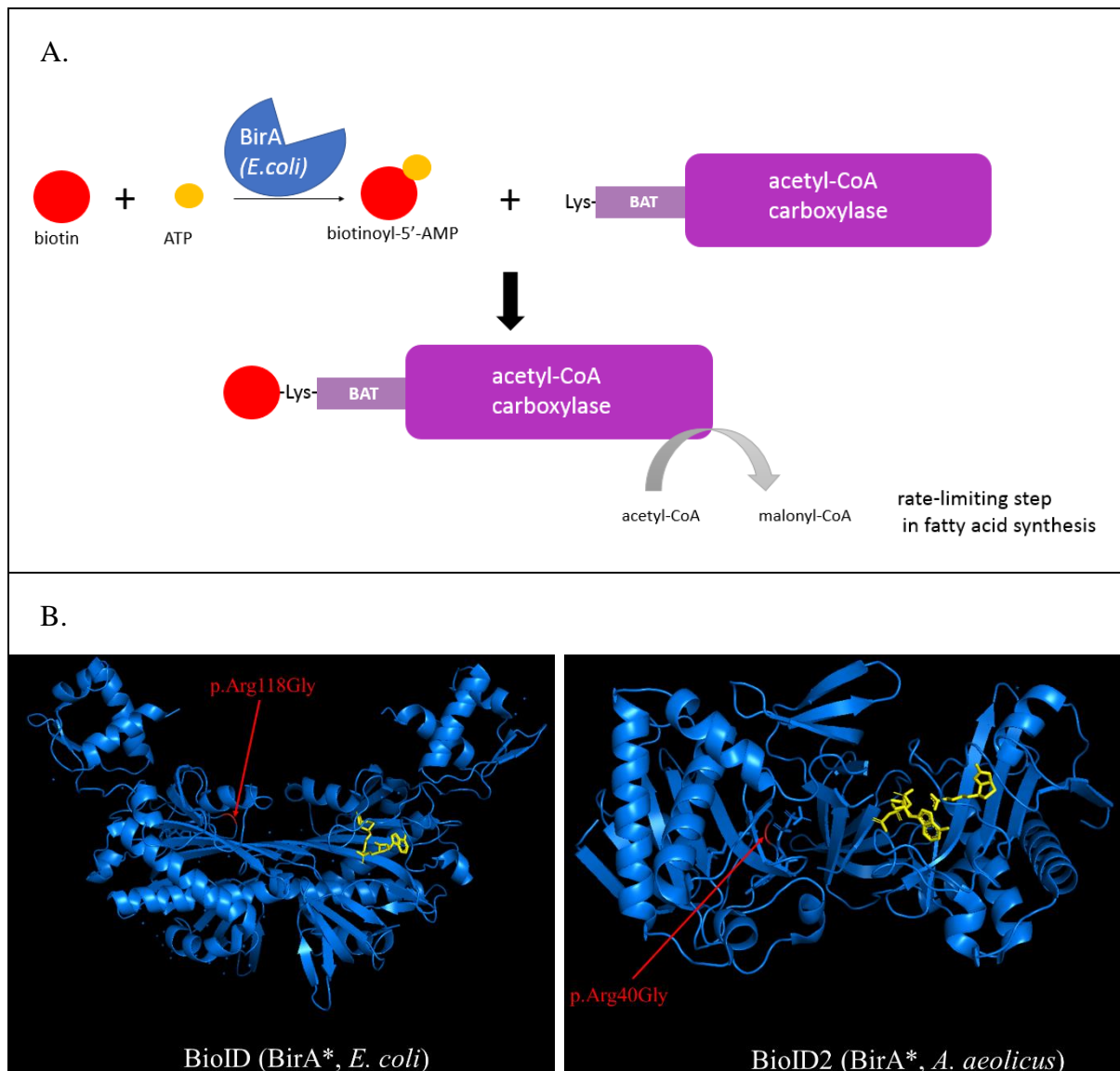


Figure 4-1. Principle of biotinylation and promiscuous biotin-ligases

A. Molecular mechanism of biotinylation in bacteria. The biotin ligase (BirA) specifically biotinylates the acetyl-CoA carboxylase at a lysine residue of the biotin acceptor tag (BAT). The reaction requires activation of the biotin molecule by ATP. The biotinylated acetyl-CoA carboxylase catalyses the formation of malonyl-CoA, an intermediate in the fatty acid synthesis.

B. Structures of the enzymes used in biotin proximity labelling. The biotin-ligase from *E. coli* (BioID) and from *A. aeolicus* (BioID2) were mutated to become promiscuous. The aa change is coloured in red and the mutation indicated by a red arrow. The activated biotin is coloured in yellow. The 3D structures were retrieved from PDB and visualized in Pymol. PDB codes: 2EWN (*E. coli*) and 3EFS (*A. aeolicus*)

Several variants have been developed based on BioID: BioID2, Split-BioID, and more recently TurboID and miniTurbo. Split-BioID is used to detect interactors of protein dimers and therefore is not suitable for my project, as C12orf65 is monomeric (De Munter et al., 2017). I decided to use BioID2 because it uses an improved mutant (p.Arg40Gly) biotin-ligase isolated from *Aquifex aeolicus* (Kim et al., 2016a). It was noticed that, in some cases, when using *E. coli* BirA, some fusion proteins were not efficiently targeted, and the authors considered the size of the biotin-ligase (321 aa, 35 kDa) as a possible cause. The *A. aeolicus* biotin-ligase is the smallest known (233 aa, 26 kDa) and lacks the DNA-binding domain, making it the best option to study C12orf65, also a small protein (166 aa, 19 kDa). Moreover, it provides a more accurate targeting of the fusion protein and requires less biotin.

Both BioID and BioID2 require long biotinylation times (16-24h), which prevents the study of cellular dynamics. To circumvent this problem, Alice Y.Ting's group developed two types of BirA mutants: TurboID (35 kDa) and miniTurbo (28 kDa) (Branon et al., 2018), which allow biotin labelling in 10 minutes. Both proteins have been heavily mutated: TurboID has 15 mutations relative to wild-type BirA and miniTurbo has 13 mutations and lacks the N-terminal domain. Although the biotinylation is as efficient in 10 minutes as the one achieved by BioID in 16 hours, a later study raised concerns of cellular toxicity due to protein instability and persistent biotinylation in the absence of exogenous biotin (May et al., 2020). Also, TurboID was too big to fuse with C12orf65, and miniTurbo showed reduced biotinylation in the mitochondria matrix when comparing to BioID ((Branon et al., 2018), figure 2C of the reference). As my protein of interest is small and resides in the mitochondria matrix, I considered BioID2 a better approach to study it. The fact that the BioID expertise was already available in the lab (through Dr. Thomas Nicholls and Yasmin Proctor-Kent) also contributed to this decision.

It is worth mentioning that the BioID approach (and its variants) is not the only proximity-labelling method. APEX (Martell et al., 2012) was initially developed as genetic tag for electron microscopy. APEX is a modified ascorbate peroxidase of 28 kDa, original from plants, that requires H₂O₂ to catalyse the oxidation of biotin-phenol to the biotin-phenoxyl radical. Those radicals exist for a short time (<1 msec) and covalently react with electron-rich amino acids like tyrosine, tryptophan, histidine and cysteine encountered on a <20 nm radius (Rhee et al., 2013). Biotinylation using APEX only requires 1 min and has already been used to map the human mitochondria proteome (Rhee et al., 2013). However, there are several points of concern that make it unsuitable for the study of C12orf65. First, both H₂O₂ and biotin-phenol

are toxic for cells (Che and Khavari, 2017). Mitochondria are already a source of ROS and the expression of a fusion protein is a possible stressful event for the cell. Adding extra toxicity was unnecessary, when BioID2 could be used instead. Second, in the study that uses APEX to map the mitochondria matrix (Rhee et al., 2013), the ascorbate peroxidase was fused to a mitochondria targeting sequence, not to a mitochondria protein. The MTS is unaffected by H₂O₂, but a mitochondrial bait could possibly be modified by this treatment, and its function compromised. In the case of C12orf65, if I study its interactors in order to understand its function, it is essential that the protein remains as physiological as possible. There is no standard function of C12orf65 that I could use to compare to a ROS-modified variant.

Finally, BioID2 and APEX use different amino acids as biotin acceptors. The amino acids used by BioID2 (lysine) is one of the most abundant amino acids in a protein structure (32%), while the ones used by APEX are among the rarest (5%) (Lodish H, 2000). Also, lysine is a positively charged amino acid, rendering it more solvent-exposed, while tyrosine is amphipathic (Cronan and Reed, 2000). Mitochondrially-targeted proteins are more positively charged comparing to proteins targeted to other cellular compartments, or dual targeted (Hartmann et al., 1991, Dinur-Mills et al., 2008, Jaussi, 1995). As a proof of concept, C12orf65 itself is positively charged, with a net charge +13.306 (<https://www.protpi.ch/Calculator/ProteinTool>). By using BioID2 instead of APEX, I increase the possibility of finding more relevant hits.

The aim was to gain insight into the function of C12orf65 by identifying its possible interacting partners. I am aware that BioID2 only helps identifying those partners but does not provide an answer about their exact proximity with C12orf65, or the order in which they interact. However, judging from the lack of information available on this protein, I considered finding the possible interactors as the priority. BioID2 can help identify weak and transient interactions, which is useful to determine the C12orf65 function (Kim et al., 2016b). My goal was to obtain a map of interactors that could be grouped according to different criteria (function, localization, molecular pathways) and, thus, draw a potential conclusion about the C12orf65 function. BioID does not give a definitive answer, but rather points towards a new direction of research, towards a new possible function that can be later investigated (Antonicka et al., 2020).

4.2 Results

In order to detect any possible biotinylated interactors, the C12orf65 protein had to be linked to the promiscuous biotin-ligase from *A. aeolicus* (BioID2). This was achieved by transfection of the pcDNA5/FRT/TO plasmid containing C12orf65-BioID2-HA into the FlpIn TRex HEK293 cell line (performed by Mr. Reece Farren, MRes). This cell line contains two stable integrated plasmids: the pcDNATM6/TR plasmid, for the Tet repressor, and the pFRT/lacZeo plasmid, for a single Flp Recombination Target (FRT) site. When the C12orf65-BioID2-HA/pcDNA5/FRT/TO is cotransfected with the pOG44 plasmid, the Flp recombinase expressed by the latter (O'Gorman et al., 1991) mediates the integration of the *C12orf65-BioID2-HA* in the host genome, between the two FRT sites (Sauer, 1994).

Successful integration was assessed by detection of the fusion protein in the host cells. The transfected cells were induced with 1 μ g/ml tetracycline overnight and the fusion protein was identified by immunoblotting, via the HA tag. I was able to confirm that five clones showed HA expression (Figure 4-2, panels A and B).

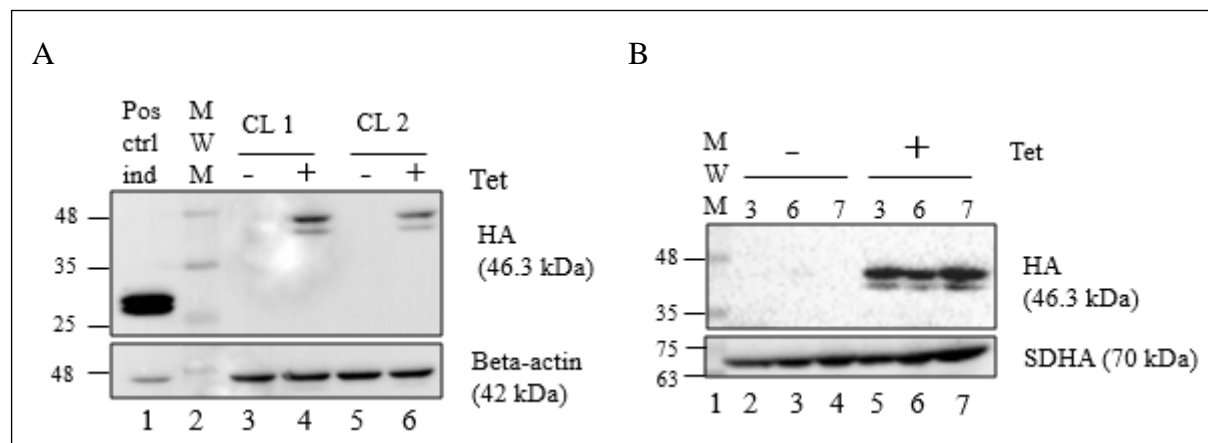


Figure 4-2. Determination of HA expression in C12orf65-BioID2-HA HEK cells

To induce expression of the C12orf65-BioID2-HA protein, HEK 293T cells were cultured overnight with tetracycline (1 μ g/ml final concentration, Tet). Cell lysates (50 μ g) were prepared from induced, non-induced clones (CL1, CL2, panel A and 3,6,7 panel B) and the positive control (pos ctrl ind) and separated by 10% SDS-PAGE. Western analysis determined the expression of the fusion protein using anti-HA antibodies. Beta-actin (42 kDa, panel A) and SDHA (70 kDa, panel B) were used as loading controls. MWM = molecular weight marker

The molecular weight of the fusion protein (46.3 kDa) was calculated using the SnapGene software (from Insightful Science; available at snapgene.com) by summing up the individual molecular weights of each component: C12orf65 (18.8 kDa), BioID2 (26.4 kDa) and HA tag (1.1 kDa). In all the five clones, the HA signal appears at the calculated molecular weight. I hypothesized that the two bands identified by the anti-HA antibody correspond to the cytosolic form (upper band, more intense) and mitochondrial form (lower band) of the fusion protein, as suggested by the presence of a cleavable 35 aa mitochondria-targeting sequence in the N-terminus of C12orf65 (according to UniProt database, code Q9H3J6). Apart from this cleavage event, there is no other fragment to suggest a proteolytic response of the host cell.

After identifying the five HA-expressing clones, I proceeded to their characterisation. As the C12orf65 function is not known, I was not able to determine whether the expression of the fusion protein would alter its function. Therefore, to assess whether C12orf65-BioID2-HA is physiological, I determined whether its characteristics overlap with what is already known about C12orf65. For this, I was interested in three main aspects:

1. Is C12orf65-BioID2-HA imported into mitochondria?
2. Is C12orf65-BioID2-HA targeted to the mitochondrial matrix?
3. Is C12orf65-BioID2-HA integrated in the mitochondrial ribosome?

To answer the first research question, cells were induced, and mitochondria were isolated from each of the five clones, lysed and analysed by western blot, using the anti-HA antibody. As control for cytosolic proteins, I kept the postmitochondrial supernatant (PMSN) and precipitated it with TCA. The percentage of PMSN loaded on SDS-PAGE, as compared to the total PMSN obtained, was equal to the percentage of mitochondria loaded, as compared to the total mitochondria obtained. To determine the isolation efficiency, I kept the final wash of mitochondria as one sample and precipitated it with TCA. To identify the cytosol, I used anti-GAPDH or anti-Beta-tubulin. For mitochondria identification, I used antibodies for different mitochondria compartments: anti-TOMM20, anti-VDAC1 (OMM), anti-SDHA (IMM) and anti-MRPS26, anti-MRPL28 (matrix).

As it can be observed in Figure 4-3, the HA signal accumulates in mitochondria for each of the five clones. The two bands are both present in the mitochondria fractions, but the HA signal is stronger in the lower band, suggesting that this band corresponds indeed to the C12orf65-BioID2-HA that lost its N-terminal sequence after mitochondria import. By contrast, in the

cytosolic fraction (panels A and B), the signal is stronger in the upper band, corresponding to the non-cleaved isoform.

For clones 1 and 2 (panel C), I was not able to resuspend the protein pellet resulted after TCA precipitation of PMSN. Instead, I used total cell lysate induced overnight as control, as this would contain both mitochondrial and cytosolic proteins. TCA precipitation also induced a curve in the migration front, corresponding to the PMSN sample (panel A, anti-Beta-tubulin; panel B, anti-HA). This disturbed shape persisted in the upper half of the SDS-PAGE, affecting the high-molecular weight proteins, but was corrected with gel migration and regained its linear form towards the end. As this observation stands only for PMSN samples and not for washes, I consider it is due to the high amount of proteins present. The lack of HA signal in the washes (except for lane 4, panel C) suggests that mitochondria were not lost during the procedure.

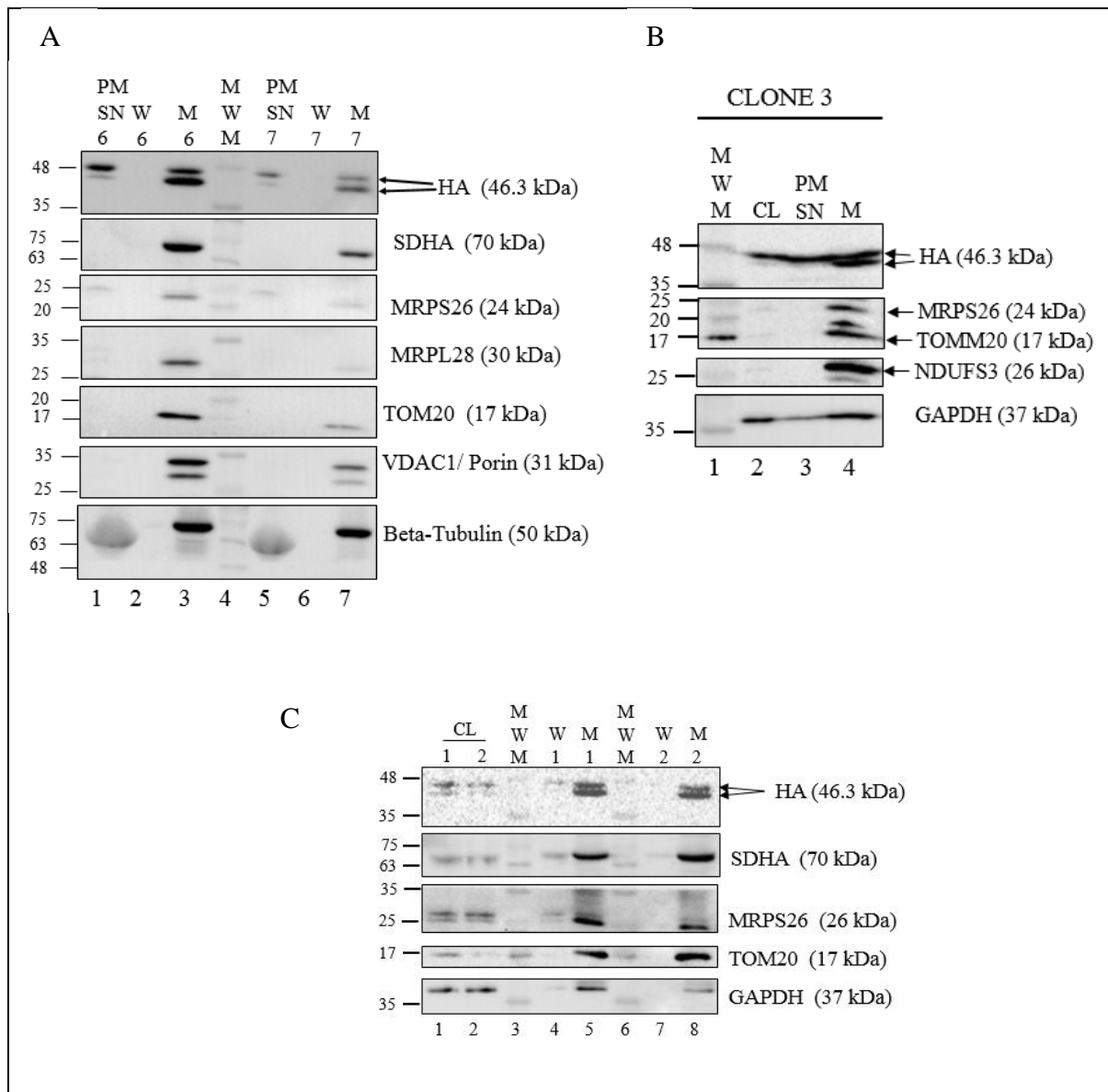


Figure 4-3. Mitochondria isolation from C12orf65-BioID2-HA HEK cells

To induce expression of the C12orf65-BioID2-HA protein, HEK 293T cells were cultured overnight with tetracycline (1 µg/ml final concentration). Mitochondria were isolated only from induced cells (clones 6 and 7, panel A; clone 3, panel B; clones 1 and 2, panel C) and separated by 10% SDS PAGE. Western analysis determined the expression of the fusion protein using anti-HA. The HA-positive, double band, indicated by two arrows, represents the two forms of the fusion protein: cytosolic (upper band) and mitochondrial (lower band). Beta-tubulin (50 kDa, panel A) and GAPDH (37 kDa, panels B and C) were used as cytosolic controls. M = mitochondria (1/3 of total sample volume, panel A; 50 µg panels B and C); PMSN = postmitochondrial supernatant, TCA precipitated (the volume loaded/total volume obtained = the mitochondria volume loaded/ total mitochondria obtained); W = wash, TCA precipitated (panels A and C, all sample loaded); CL = cell lysate (50 µg, panels B and C); MWM = molecular weight marker

After confirming the mitochondrial localization, the next step in C12orf65-BioID2-HA characterisation was to determine the mitochondrial compartment where it is targeted. The

isolated mitochondria were subfractionated by proteinase K treatment and consecutive centrifugations (Figure 4-4).

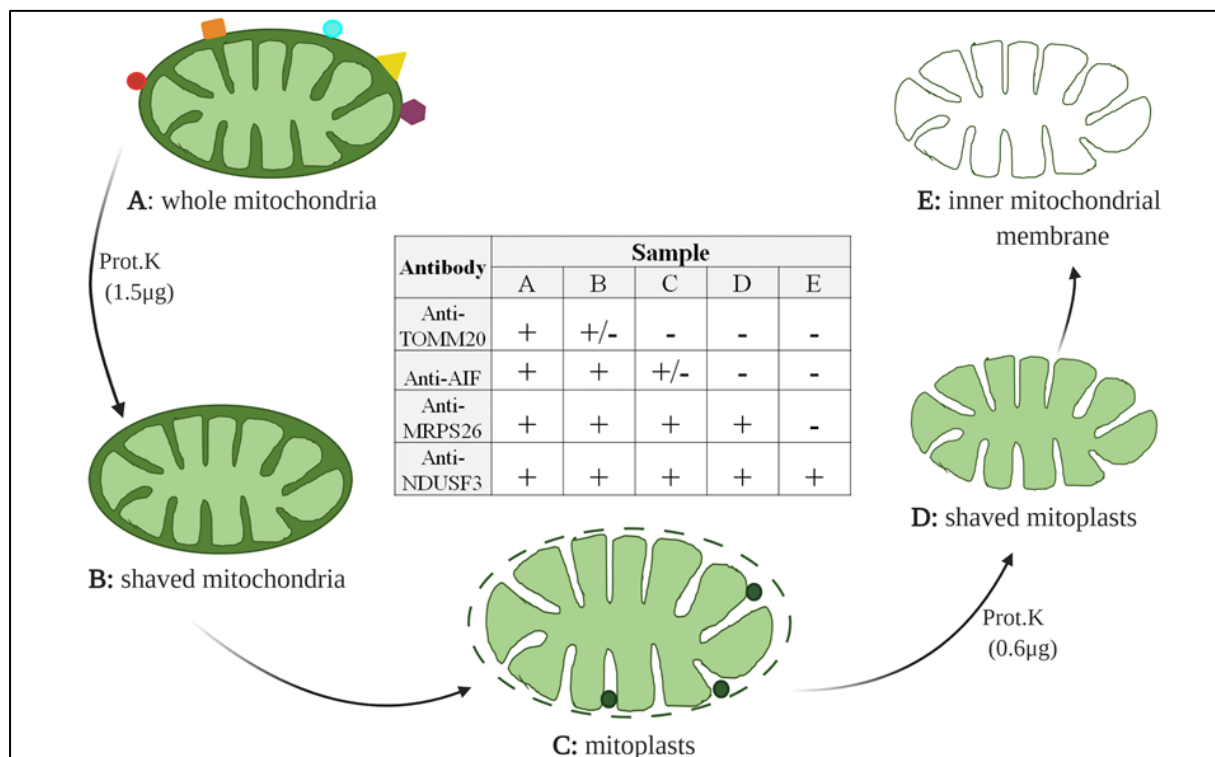


Figure 4-4. Cartoon depicting the steps of mitochondria subfractionation

Mitochondria were isolated (A) and subfractionated as described in 2.3.7. The resulting fractions (B-E) were identified by western blotting with the antibodies from the central table; geometric shapes of various colours - cytosolic proteins; dark green disks – intermembrane space proteins

Isolated mitochondria (A) were subjected first to a proteinase K treatment to remove the cytosolic proteins attached to the OMM (B), then to an osmotic shock to remove the OMM. The resulting mitoplasts (C) were treated with proteinase K to remove the intermembrane space proteins still attached to the IMM (D) then underwent an alkaline treatment to obtain the inner mitochondrial membrane (E). Each mitochondria subfraction was identified by western blotting with specific antibodies. The first experiment showed that the HA signal is present in fractions A-D (Figure 4-5) but not in the IMM fraction, identified with the anti-NDUFS3 antibody (lane 8). The proteinase K treatment removes the upper band of the HA signal and only the lower one is present up to fraction E, suggesting again that the fusion protein is cleaved after mitochondrial import. The presence of MRPS26 signal in the IMM (line 8) can be explained by the fact that the translating mitoribosome is attached to IMM via MRPL45 (Englmeier et

al., 2017) (Koripella et al., 2020). The band above MRPS26 (line 4) is NDUFS3, as the membrane was incubated first with anti-NDUFS3 antibody and then with anti-MRPS26.

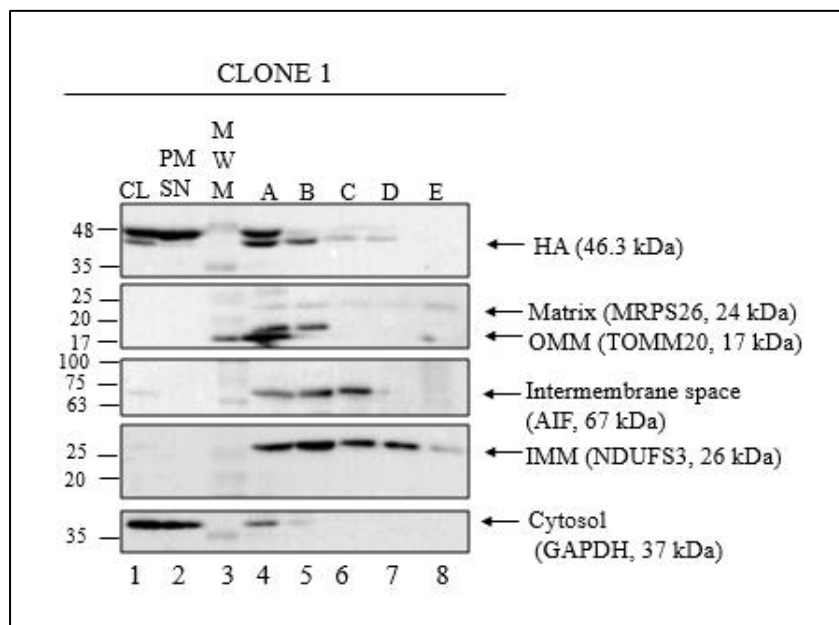


Figure 4-5. Example of mitochondria subfractionation of a C12orf65-BioID2-HA clone

To induce expression of the C12orf65-BioID2-HA protein in clone 1, HEK 293T cells were cultured overnight with tetracycline (1 µg/ml final concentration). Mitochondria were isolated and subfractioned, the samples were separated by 10% SDS-PAGE and each fraction was identified by western blot with its corresponding antibodies.

CL = cell lysate (60 µg); PMSN = postmitochondrial supernatant (volume PMSN loaded/total PMSN volume = volume of sample A/total mitochondria volume); MWM = molecular weight marker (kDa); starting material: 360 µg of isolated mitochondria; N=1

As all the five clones had the same growth rhythm and there were no morphological differences between them, I decided to subfractionate them all, to identify whether any of them has a better expression of the fusion protein in mitochondria. The distribution of the HA signal among mitochondria compartments is consistent among the other four clones, similar to clone 1: present in the matrix, not present in the IMM (Figure 4-6).

Clone 2 (bottom panel, left) had the lowest overall expression of HA and clone 6 (upper panel, left) had a strong HA expression in the PMSN. The clone with the lowest amount of cytosolic HA expression was clone 3 (bottom panel, right). The HA signal is almost non-distinguishable in the PMSN, and the upper band is fader comparing to the lower band. This is not caused by a technical error: by this stage, I was able to optimize the TCA precipitation and resuspension of the PMSN, as proved by the GAPDH signal (line 2). A weak HA signal was present in the

PMSN of clone 7 as well (upper panel, right) but the upper and lower bands had similar intensities in the isolated mitochondria. As my plan was to use the C12orf65-BioID2-HA cell model for identifying the interactors of C12orf65 by mass-spectrometry, it was imperative to use a clone in which the fusion protein is delivered to the matrix and does not accumulate in the cytosol, because this would increase the number of non-specific hits identified. Clone 3 was the closest to this ideal situation, so I continued my experiments with it.

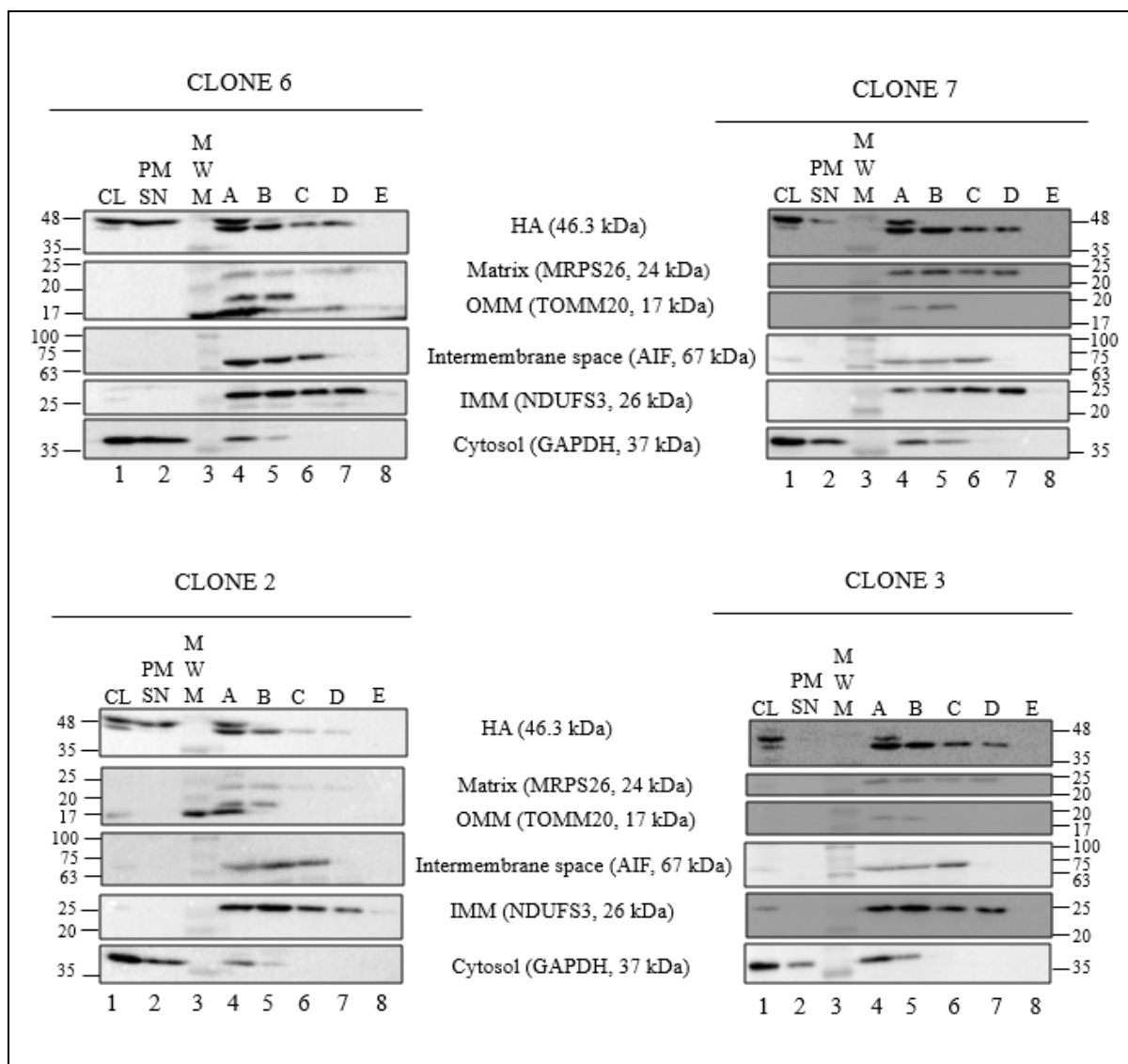


Figure 4-6. Comparison between mitochondria subfractionation of different C12orf65-BioID2-HA clones

For subfractionation, mitochondria were isolated from C12orf65-BioID2-HA HEK cells (clones 6,7,2,3) induced with tetracycline (1 μ g/ml final concentration, overnight); CL = cell lysate (60 μ g); PMSN = postmitochondrial supernatant (volume PMSN loaded/total PMSN volume = volume of sample A/total mitochondria volume); MWM = molecular weight marker (kDa); starting material: 360 μ g of isolated mitochondria; N=1 for each clone

Having established that C12orf65-BioID2-HA is targeted to mitochondrial matrix, I studied the interaction between this protein and the mitoribosome. Previous experiments have shown that C12orf65 does not associate with the ribosome (Iria Jimenez, unpublished data; Aleksandra Pajak, PhD thesis (Pajak, 2013)). To determine whether this is the case for the fusion protein, I separated the cell lysate on a 10-30% sucrose gradient and collected 11 fractions. As observed in Figure 4-7, the highest amount of proteins is identified in fractions 1-3 (Ponceau staining), corresponding to the soluble proteins, and decreases towards the bottom of the gradient. The HA signal is present in fractions 1-3 only, suggesting that the fusion protein is soluble in the matrix. MRPS26 and DAP3, used as markers for the small ribosomal subunit, both appear in fractions 4,5 and 6, typical for the assembled small subunit. MRPS26 also appears as soluble protein, prior to assembly (fractions 1-2). The fractions specific for the assembled large subunit are 6,7 and 8, and they are identified by the markers MRPL45 and ICT1. As with MRPS26, MRPL45 also consists of a free non-assembled pool (fractions 1-3). The other member of the mitochondria translation termination family, ICT1, appears in fractions 6 and 7 only, in accord with previous data proving it is a constituent of the mitoribosome large subunit (Brown et al., 2014, Richter et al., 2010b). Fractions 6 and 7 suggest isolation of the monosome, as the markers for the small and large subunit overlap.

The fact that C12orf65-BioID2-HA was not identified in any of the mitoribosomal fractions shows that the fusion protein is soluble in the matrix, like the C12orf65.

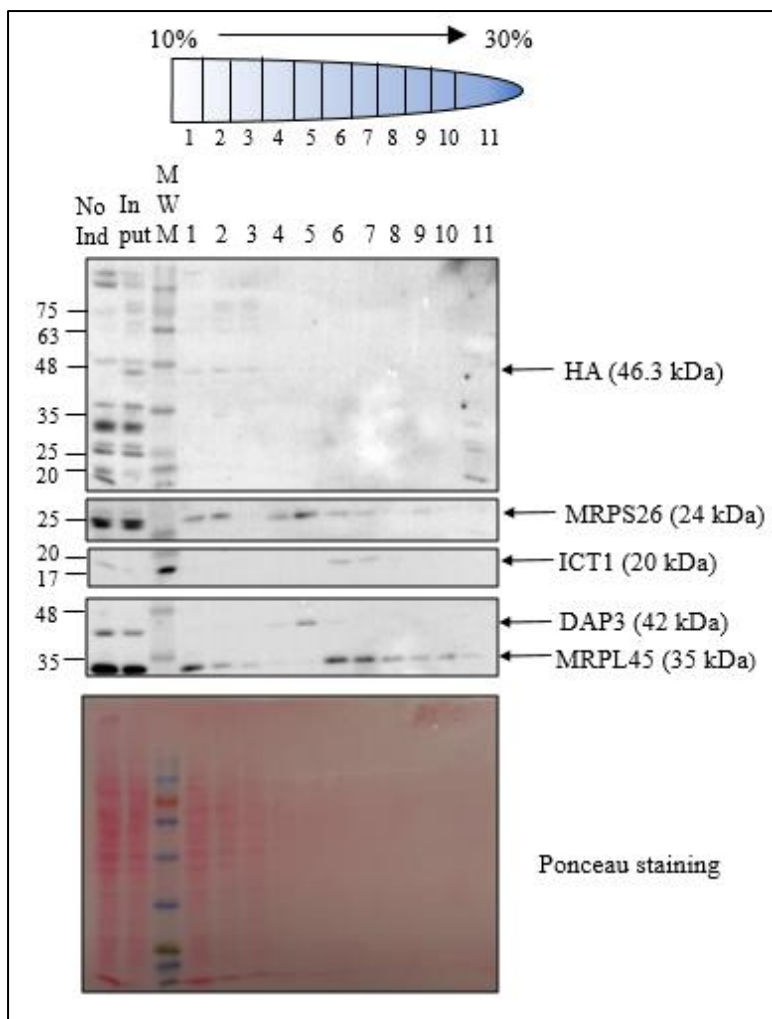


Figure 4-7. Sucrose gradient of C12orf65-BioID2-HA clone 3

To induce expression of the C12orf65-BioID2-HA protein, HEK 293T clone 3 cells were cultured overnight with tetracycline (1 μ g/ml final concentration). Cell lysate (700 μ g) was separated on a 10-30% sucrose gradient and the fractions were identified by 10% SDS-PAGE, using the indicated antibodies; a non-induced lysate (No Ind, 50 μ g) and an aliquot of the input loaded on top of the sucrose gradient (50 μ g) were used as negative and positive HA controls, respectively; 1/5 of total fraction volume (100 μ l) loaded for each fraction; MWM = molecular weight marker (kDa); N=1

4.3 Discussion

Characterization of the C12orf65-BioID2-HA HEK clones showed that the fusion protein resembles the wild-type C12orf65 in terms of localization and matrix solubility. These are encouraging results, because they indicate that the cell model is suitable to use in the mass-spectrometry experiments. BioID2 has already been successfully used in identifying novel bait interactors in: calcium regulation (Zheng et al., 2019), MAP (mitogen-activated protein)-kinase signaling (Prikas et al., 2020), inner mitochondria membrane from *Trypanosoma brucei* (Pyrih et al., 2020) and the parasitophorous vacuole membrane from *Plasmodium falciparum* (Nessel et al., 2020). In all those studies, however, the bait protein was bigger than the *A. aelicus* biotin-ligase (molecular weights provided by UniProt): 49 kDa - PAD2, (Zheng et al., 2019), 41 kDa - p38 α MAP-kinase, (Prikas et al., 2020), 55 kDa - ZapE1,(Pyrih et al., 2020), and 33 kDa - EXP2 (Nessel et al., 2020).

One point of concern was that, although it is the smallest isolated biotin ligase, *A. aeolius* BioID2 (26 kDa) is still bigger than C12orf65 (19 kDa); this could possibly prevent the fusion protein from being imported into the mitochondria, despite the N-terminal MTS present on C12orf65. The subfractionation experiments showed this is not the case.

Still, there was one obstacle that caused delays in my experiments: all the five C12orf65-BioID2-HA HEK clones showed a poor growth phenotype. The cells needed 2-3 weeks to recover and repopulate a flask after defrosting. They grew slowly when split, comparing to other FlpIn HEK cell lines, including the COX8-MTS-BioID2-HA HEK cell line which only expresses the BioID2 targeted to the mitochondria. Also, they would lose the C12orf65-BioID2-HA expression relatively quickly (3-4 months). Once tested positive for HA expression, I invested time in preparing multiple frozen stocks (5-6/clone) prior to conducting any experiment, in order to ensure the loss of expression will not affect my future work.

To stimulate cells growth, I added 10% extra FBS in the flask and I used conditioned media when refeeding them. The conditioned media was culture media that had already been used by other HEK cells and needed to be changed; instead of discarding it, I recovered it, filtered it and used to feed the poorly growing cells in a 1:1 ratio with fresh supplemented media. In this way, the cells would benefit from additional secreted metabolites, growth factors (epidermal growth factor, platelet-derived growth factor) and cytokines (interleukins) (Wickramasinghe,

1996). Those measures helped the cells recover and grow and I obtained enough material for the subfractionation experiment.

Another attempt to improve their growth was to reuse the flasks; after observing the growth rate after splitting, I noticed that the cells plated in a new flask grew slower comparing to the same cells plated in a reused flask. Reusing flasks, however, increased the risk of infections and caused the cells to grow on top of the others, forming clumps. I decided not to reuse a flask for more than three times.

This poor growth phenotype would suggest that the fusion protein interfered with cell physiology. Interestingly however, this phenotype appeared regardless of tetracycline-induction. If the fusion protein were the cause for poor growth, then I would have expected only the induced cells to be affected and to see products of protease cleavage identified with the HA antibody. The western blot results showed no such presence, neither in the cytoplasm nor in the mitochondria. A possible explanation could be that the structure of the fusion protein was not accessible to the proteases. However, cleavage of the N-terminus sequence suggests that at least the mitochondrial MPP is active and that the presequence is recognizable and accessible. It also suggests that delivery of the fusion protein to the matrix respects the canonical import pathway via Tom22/Tom40-Tim23 (Gakh et al., 2002).

The C12orf65-BioID2-HA cell line was suitable for the biotinylation experiment and mass-spectrometry analysis. The cells express HA when induced, the fusion protein is localized to the mitochondrial matrix, there is cleavage of the mitochondrial targeting sequence and there is no interference in the mitoribosome assembly. However, because of the poor growth phenotype, I decided to generate an additional cell line and introduce a linker between the C12orf65 bait and the biotin-ligase. The linker could improve cell growth by allowing the bait and the enzyme to be more dynamic. Also, by comparing the interactors identified using the clone described in this chapter with the ones identified using the clone containing the linker, the chances of identifying true interactors increase. The generation and characterization of the linker cell line are presented in the next chapter.

Chapter 5

**C12orf65-Linker-BioID2-HA, a second cell model to investigate
C12orf65 function using the BioID2 approach**

5.1 Introduction

Although a very useful method to detect nuclear envelope interactors when using lamin-A as a bait (Roux et al., 2012), Kyle J. Roux's group (Kim et al., 2016a) still considered that BioID could interfere with the bait localization. For this reason, they developed BioID2, which uses a 10 kDa smaller biotin-ligase and thus reduces steric hindrance, leading to a more precise localization of the fusion protein. In order to improve BioID2, the authors designed a flexible linker composed of 13 repeats of GGGGS, with a length of 25 nm. By introducing it between the bait protein and the biotin-ligase, they increased the biotinylation range, which lead to the identification of additional protein-protein interactions comparing to BioID2 alone. Using Nup43 as a bait, a component of the Nup107-160 subcomplex of the nuclear pore, they managed to detect two proteins of the central channel of the nuclear pore (Nup205 and Nup62) only after addition of the linker. The linker also seemed to confer more freedom of movement to the biotin-ligase, because the authors detected karyopherins as Nup43 interactors. Karyopherins are soluble proteins responsible for transporting different cargoes into (ex: transcription factors and histone deacetylases) or out (ex: tRNA, microRNA, mature mRNA molecules) of the nucleus (Mosammaparast and Pemberton, 2004). They are not constituents of the nuclear pore, so the authors presume they were biotinylated while passing through the pore central channel due to the occasional interaction with the biotin-ligase ((Kim et al., 2016a), Supplemental Table S2 of the reference).

After considering the above-mentioned article, I decided to use the linker for my BioID2 experiment for the following reasons:

1. To identify more possible C12orf65 interactors
2. To ensure the identification of any interactors, should the C12orf65-BioID2-HA protein be impaired by steric hindrance

The addition of the linker lead to the identification of soluble, transient, relatively distant interactors of the Nup43 protein. Those are the exact type of interactions that I am interested about in regard to C12orf65, as C12orf65 itself is a soluble protein, that only transiently interacts with the mitoribosome. However, Nup43 is a 42 kDa protein embedded in a nuclear envelope complex, while C12orf65 is less than half of this size and is soluble. The presence of an attached biotin ligase could at worst prevent Nup43 incorporation and destabilize the nuclear envelope complex, but it could not affect its function, because this protein does not have an

active function apart from the structural one. It is not the case, as the authors show correct Nup43-Linker-BioID2 localization. But, when applying this pessimistic scenario to C12orf65, I realized that, if C12orf65-BioID2-HA could not perform the mysterious function that C12orf65 normally performs, then I would virtually obtain no interacting partners. The presence of the linker would impose a spatial distance between my protein of interest and the biotin-ligase, allowing both to perform their functions unhindered.

The results obtained for C12orf65-BioID2-HA show that the fusion protein behaves similarly to the C12orf65, so I am inclined to expect significant hits both with and without linker. The only risk that the linker presence could create is an increased accessibility of the fusion protein to the action of proteases, leading to protein loss. However, Kim et al. did not find any abnormal proteolytic processing (Kim et al., 2016a), so I decided to develop a cell line expressing the C12orf65-Linker-BioID2-HA fusion protein. For this, I cloned the *C12orf65* DNA fragment into a pcDNA5 plasmid containing Linker-BioID2-HA and transfected HEK 293T cells. Following clonal expansion, I selected a positive HA clone to test localization of the fusion protein and assembly of the mitochondrial ribosome.

5.2 Results

With the aim of increasing the biotinylation range, a sequence linker formed of 13xGGGGS repeats (Amet et al., 2009) needed to be introduced between *C12orf65* and *BioID2*, in frame. This would provide an approx. 25 nm extension of the original 10 nm BioID2 range (Kim et al., 2016a). The linker had to be cloned in such a manner that it does not interfere with C12orf65 or with BioID2, which was possible by virtue of the pcDNA multiple cloning site (MCS). MCS contains the target sites of the restriction enzymes BamH1 and Xho1, which drove the entire cloning process (Figure 5-1).

The goal was to clone the human *C12orf65* gene upstream from the linker sequence in the Linker-BioID2-HA/pcDNA5/FRT/TO/ plasmid (Appendix-B, Figure Apx 2). For this, I digested the C12orf5-BioID2-HA/pcDNA5/FRT/TO plasmid using BamH1 and Xho1, which have cloning sites that flank the *C12orf65* fragment at 5' and respectively 3' end. The BamH1 (G/GATCC) and Xho1 (C/TCGAG) target sequences both produce compatible cohesive (sticky) ends (Newman and Schildkraut, 1995, Gingeras et al., 1978). The digestion produced a 500bp fragment corresponding to *C12orf65*, which was extracted from the agarose gel and used as insert in the ligation reaction (Figure 5-2). In order to obtain sticky ends compatible to

the *C12orf65* fragment, the Linker-BioID2-HA/pcDNA5/FRT/TO/ plasmid was also digested using BamH1 and Xho1 and was further dephosphorylated to prevent re-circularization (Figure 5-3).

Ligation of the *C12orf65* fragment into the Linker-BioID2-HA/pcDNA5/FRT/TO/ plasmid was possible due to the 5' phosphate contained by the insert. The experiment was performed as described in 2.4.9, using a vector and no insert as control reaction. Ligation was followed by transformation of competent cells (2.2.2) and the ampicillin-resistant clones were expanded and screened for the *C12orf65*-Linker-BioID2-HA/pcDNA5/FRT/TO/ plasmid. The new plasmid was isolated (2.4.1) and digested using BamH1 and Xho1 to determine the presence of the *C12orf65* fragment. Only one of the two initial Linker-BioID2-HA/pcDNA5/FRT/TO/ plasmid clones used for ligation proved successful and resulted in two new *C12orf65*-Linker-BioID2-HA/pcDNA5/FRT/TO/ plasmid clones, identified by the 500 bp fragment (Figure 5-4).

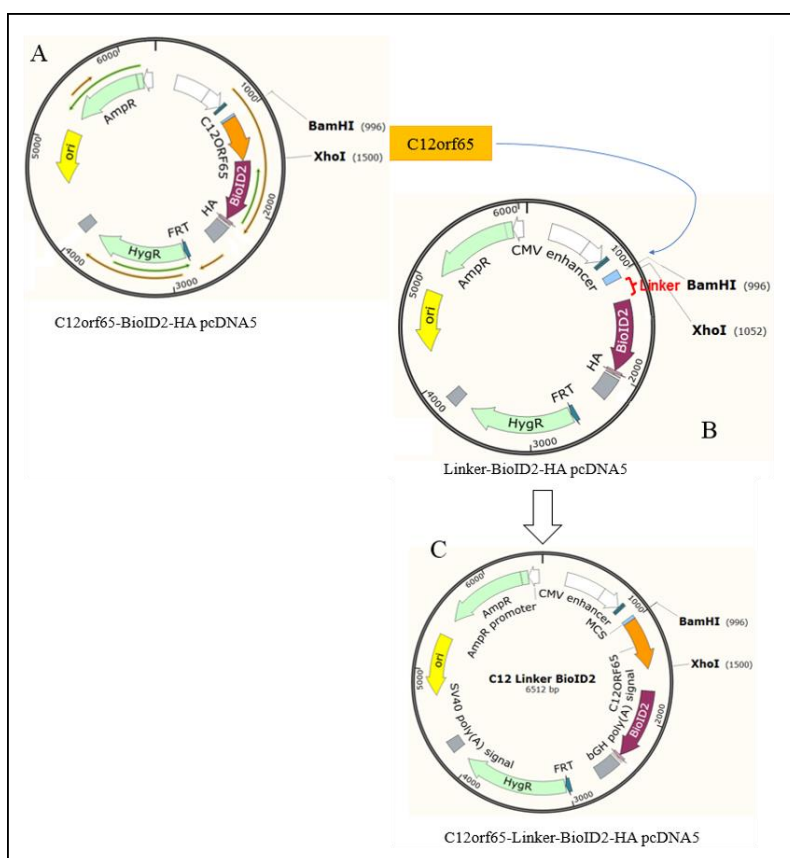


Figure 5-1. Cartoon depicting the cloning of C12orf65-Linker-BioID2-HA plasmid

The C12orf65-BioID2-HA pcDNA5 plasmid was digested to obtain the C12orf65 DNA fragment. The latter was inserted in frame in the Linker-BioID2-HA pcDNA5 plasmid, upstream from the linker and the biotin-ligase sequence.

Once the *C12orf65*-Linker-BioID2-HA plasmid was obtained, each clone was used to transfect the FlpIn TRex HEK293 cell line (2.1.7). The Flp recombinase expressed by the cotransfected pOG44 plasmid determined the insertion of the *C12orf65*-Linker-BioID2-HA into the host genome, by recognizing the FRT site situated on each of them.

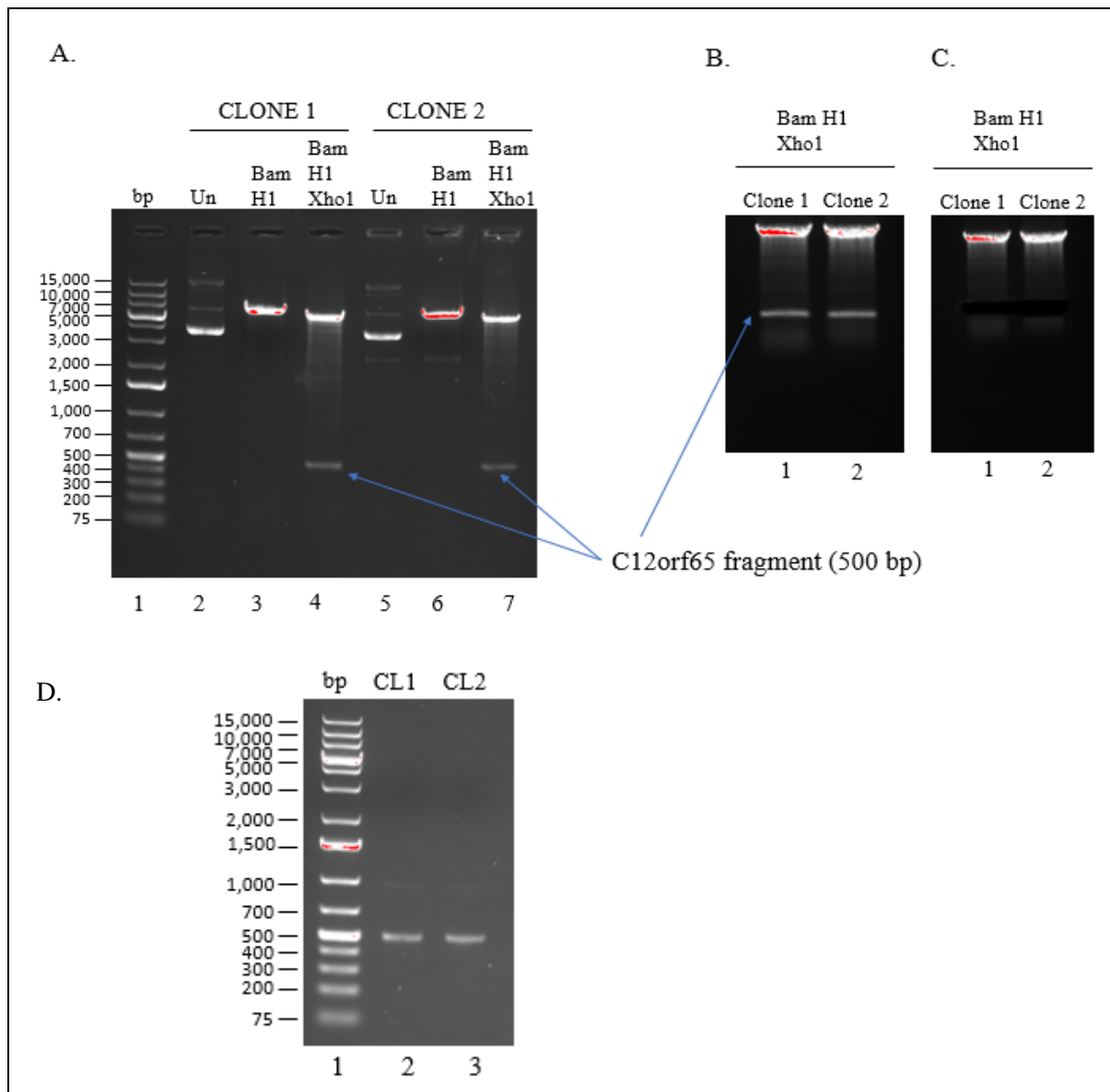


Figure 5-2. Production of the C12orf65 DNA fragment

C12orf65-BioID2-HA pcDNA5 plasmid (clones 1 and 2) was digested using BamH1 and Xho1 restriction enzymes. Electrophoresis gel from panel A (1% agarose) depicts the short digestion performed to test the efficiency of the restriction enzymes and the identification of the *C12orf65* fragment (500 bp). The undigested plasmid was used as negative control. Gel from panel B (1% agarose) depicts the electrophoresis of the double digest performed overnight and excision of the *C12orf65* fragment (panel C). Gel from panel D (1% agarose) depicts the electrophoresis of the *C12orf65* fragment isolated from the gel cut, the fragment appearing at 500 bp. The red coloration represents saturated signal. N=1

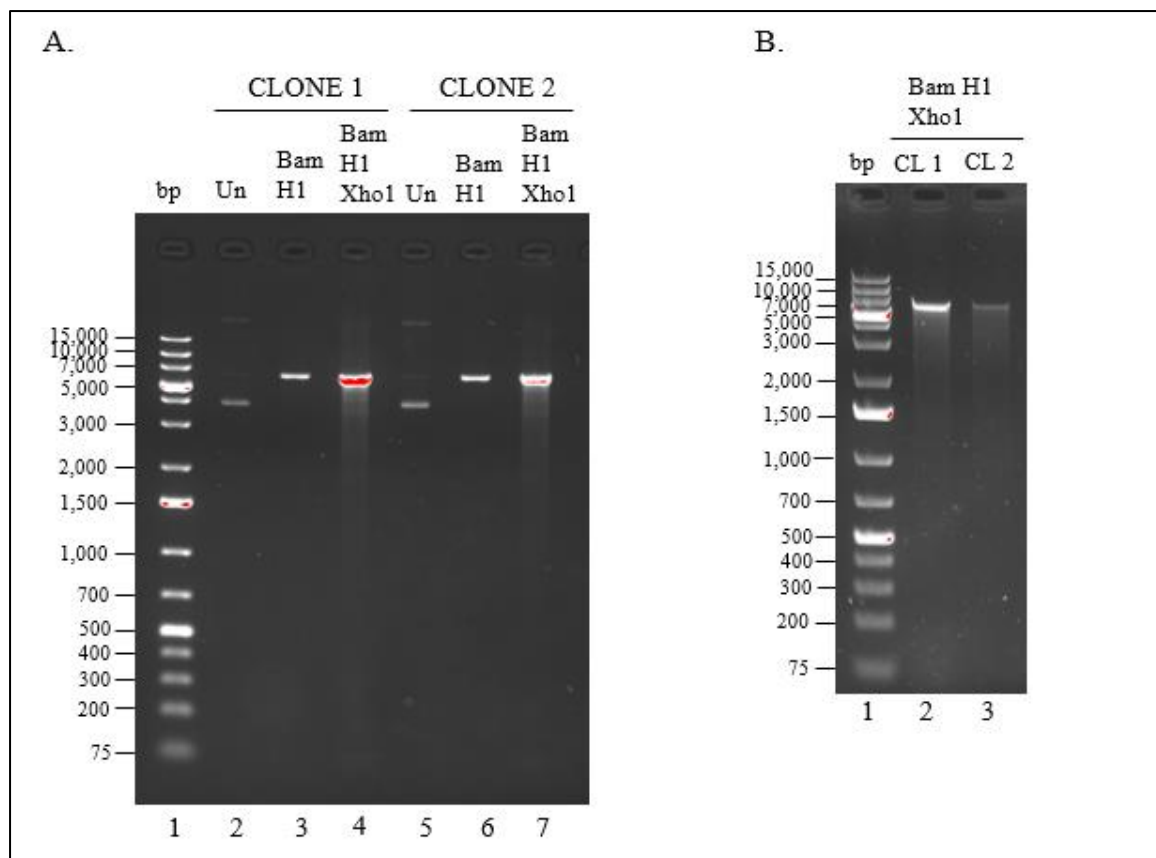


Figure 5-3. Digestion and dephosphorylation of the Linker-BioID2-HA pcDNA5 plasmid

A. Each clone of the Linker-BioID2-HA pcDNA5 plasmid was restriction digested using BamH1 and Xho1 (3 h). The undigested plasmid (Un) was used as negative control. The digestion products were identified on a 1% agarose gel. The red coloration represents saturated signal.

B. The products of the double digestion were dephosphorylated and purified by precipitation with phenol-chloroform, then visualised on a 1% agarose gel.

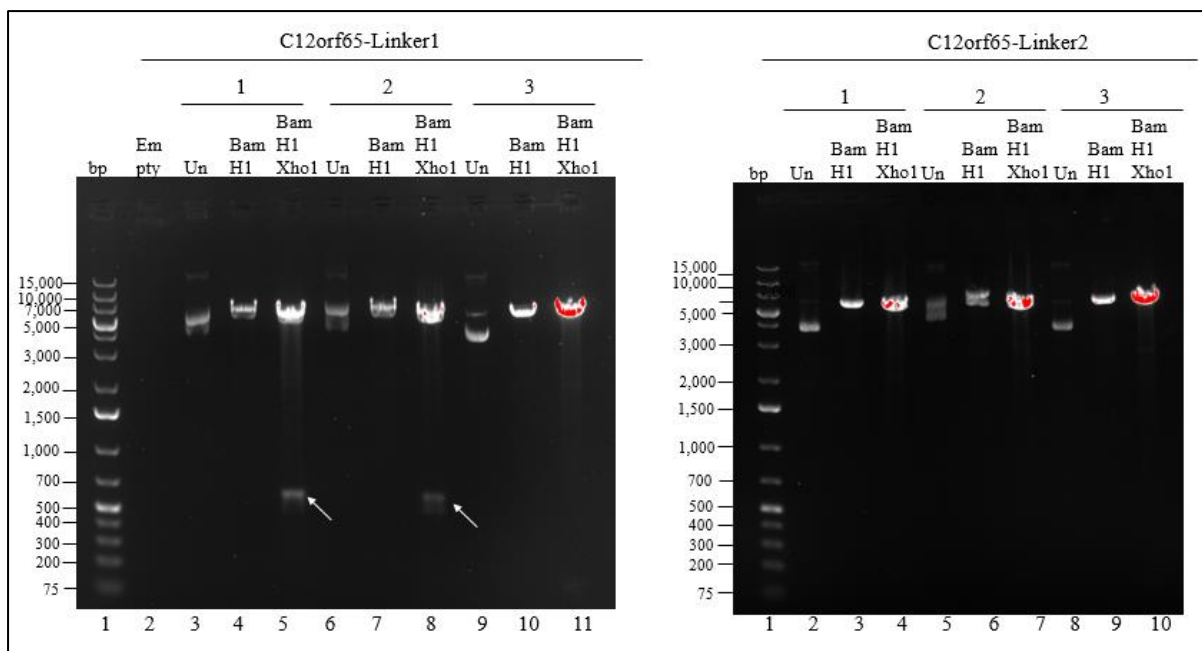


Figure 5-4. Digestion of the C12orf65-Linker-BioID2-HA pcDNA5 plasmid

Each clone of the C12orf65-Linker-BioID2-HA plasmid was restriction digested using BamH1 and Xho1 (10 min). The undigested plasmid (Un) was used as negative control. The digestion products were identified on a 1% agarose gel. The arrows indicate the presence of the C12orf65 fragment (500 bp). The red coloration represents saturated signal.

The transfected cells were selected by addition of Hygromycin^B (final concentration 100 µg/ml) and the Tet repressor was maintained with 10 µg/ml Blasticidin^S (final concentration). Once the non-transfected cells were killed by the antibiotic treatment (negative control), the small colonies of transfected cells were expanded and tested for the presence of the C12orf65-Linker-BioID2-HA fusion protein. Cells were induced with 1 µg/ml tetracycline overnight and the fusion protein was identified by immunoblotting, via the HA tag. I was able to confirm the presence of the HA signal in nine clones, with two of them showing leaky expression (lanes 3 and 5, right panel, Figure 5-5). The signal is composed of two bands, with the upper band being more pronounced, suggesting a cytosolic and a cleaved mitochondrial isoform, similar to what was observed for C12orf65-BioID2-HA. Both bands were present in the leaky clones, non-induced samples.

The molecular weight of the fusion protein (50.4 kDa) was calculated using the SnapGene software (from Insightful Science; available at snapgene.com) by summing up the individual molecular weight of C12orf65-BioID2-HA (46.3 kDa) and the molecular weight of the linker (4.1 kDa).

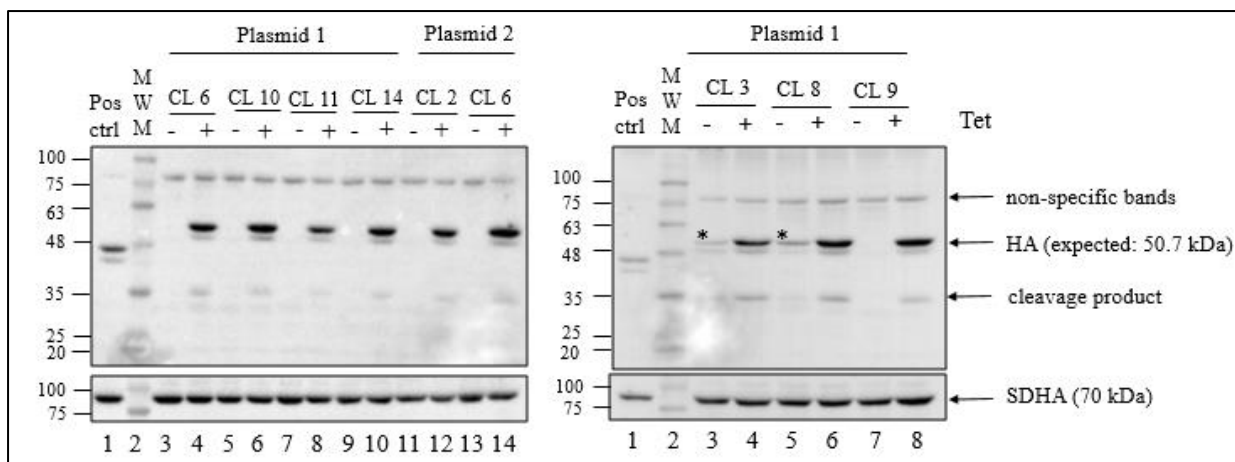


Figure 5-5. Determination of HA expression in C12orf65-Linker-BioID2-HA HEK cells

To induce expression of the C12orf65-Linker-BioID2-HA, HEK 293T cells transfected with either clone 1 or clone 2 of the C12orf65-Linker plasmid were cultured overnight with tetracycline (1 µg/ml final concentration, Tet). Cell lysates (50 µg) were prepared from induced and non-induced clones and separated by 10% SDS-PAGE. A C12orf65-BioID2-HA HEK lysate induced and previously tested was used as positive control for HA (pos ctrl). Western blot analysis determined the expression of fusion proteins (anti-HA). SDHA (70 kDa) was used as loading control. The bands marked (*) indicate leaky expression. The white discoidal zone present at the bottom of the upper panel is an artefact caused by a defect in the white light channel used to acquire the molecular weight. MWM = molecular weight marker. N=1 for each clone

In all the nine clones, the HA signal appears above the 48 kDa marker and above the C12orf65-BioID2-HA signal (positive control), which is consistent to the calculated molecular weight. Apart from this, probing with the HA antibody revealed two additional signals: one at approx. 75 kDa and a second one at 35 kDa. The 75 kDa signal was considered non-specific since it appears irrespectively of induction and can be observed in the positive control (lane 1, left panel). I ruled out the possibility of overlap with a previous antibody, because the anti-HA was the first one that the membrane was incubated with after blocking in 5% milk.

The 35 kDa signal was the one that caught my interest, since it suggested a cleavage event specific to the C12orf65-Linker-BioID2-HA HEK (referred as Linker) clones only. It was absent from the positive control (Figure 5-5, lane 1, both left and right panel) and has not been detected previously, for any of the C12orf65-BioID2-HA clones. Although much weaker than in the induced clones, this signal was present in the leaky Linker clones too. Being identified with the anti-HA antibody suggests that the possible cleaved product contains the HA tag and the biotin ligase part of the fusion protein. However, the molecular weight of this signal is higher than the size of BioID2 (approx. 26 kDa).

An important question was whether this 35 kDa product was transported to the mitochondria or remained in the cytosol. To address this, I selected the most robust Linker clone (clone 9) and used it for mitochondria isolation. The clone 9 cells were induced, mitochondria were isolated and lysed, then analysed by western blot, using the post mitochondrial supernatant as cytosolic control. The cytosol was identified using anti-GAPDH and mitochondria with anti-VDAC1. Probing with the anti-HA antibody showed that the possible cleavage product remains in the cytosol (Figure 5-6, panel A). This result was encouraging, because it showed that the Linker clone could be used for the BioID experiment and subsequent mass-spectrometry analysis without the risk of possible false interactors given by the cleavage product.

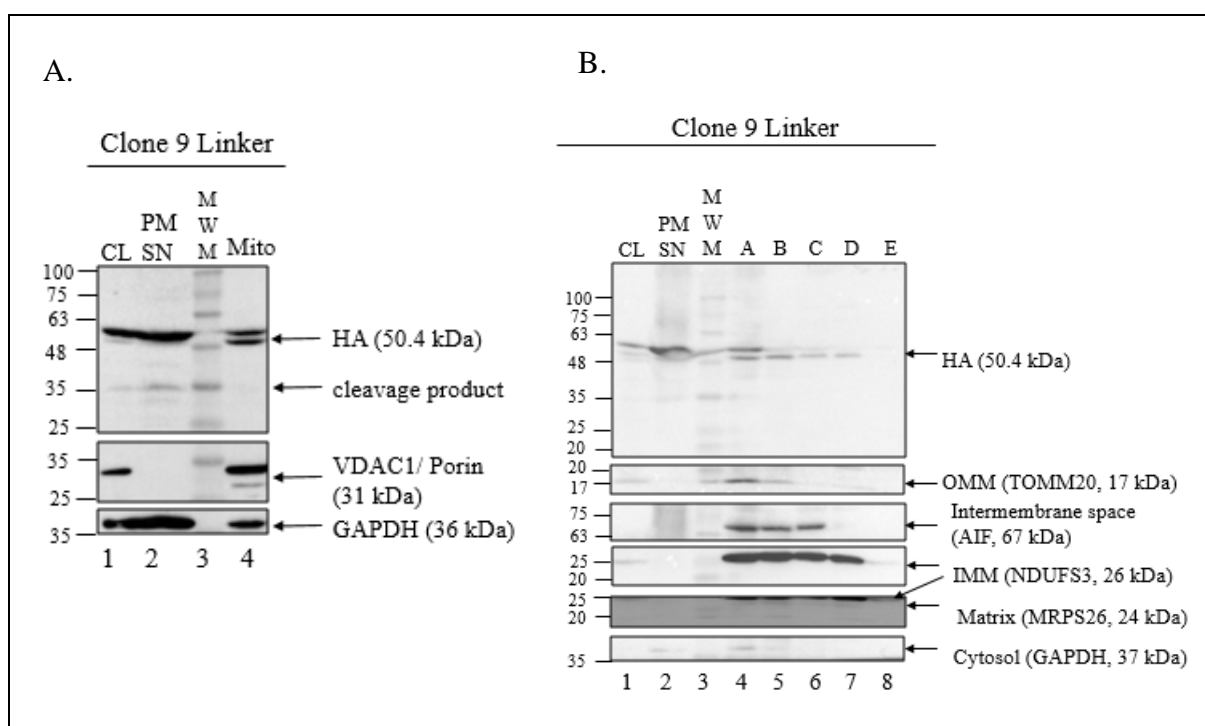


Figure 5-6. Isolation and subfractionation of mitochondria from C12orf65-Linker-BioID2-HA HEK cells

A. Mitochondria were isolated from C12orf65-Linker-BioID2-HA clone 9 HEK293T cells induced with tetracycline (1 μ g/ml final concentration, overnight). Samples were separated by 10% SDS-PAGE and probed with antibodies for the fusion protein (HA), mitochondria (VDAC1) and cytosol (GAPDH). Volumes of PMSN (TCA precipitated) and mitochondria loaded per well were 1/6 of total volumes obtained; N=1

B. Subfractionation of mitochondria isolated from C12orf65-BioID2-HA clone 9 HEK cells induced with tetracycline (1 μ g/ml), overnight; samples were separated by 10% SDS-PAGE and probed with the corresponding antibodies; PMSN = postmitochondrial supernatant, TCA precipitated (volume PMSN loaded/total PMSN volume = volume of sample A/total mitochondria volume); starting material: 360 μ g of isolated mitochondria; MWM = molecular weight marker (kDa); CL = cell lysate; N=1

Mitochondria isolation was also a first step in the Linker clone characterization. As for C12orf65-BioID2-HA, in order to use it for the identification of C12orf65 interactors, I had to determine whether the Linker clone is physiological, meaning that the Linker fusion protein behaves as what is known about C12orf65. As seen in Figure 5-6, panel A, the HA signal of the Linker clone is present in the mitochondria and the upper band corresponds to the cytosolic fraction of the protein. This result is reiterated by the subfractionation experiment (Figure 5-6, panel B) which shows that the Linker fusion protein is targeted to the mitochondria matrix. The lower band is the one present in the matrix, suggesting that the N-terminus is cleaved upon mitochondria import.

In the last step of characterization, I studied the interaction between the Linker protein and the mitoribosome. I induced the cells, separated the cell lysate on a 10-30% sucrose gradient and collected 11 fractions. I analyzed them by western blot and probed the membrane first with the anti-HA antibody, then with antibodies corresponding to the small mitoribosomal subunit (MRPS26, DAP3) and the large mitoribosomal subunit (MRPL45, ICT1). As shown in Figure 5-7, the HA signal appears predominantly in fractions 1-3, corresponding to the soluble proteins, and only a small amount appears in fraction 4. MRPS26 and DAP3 appear mostly in fractions 4 and 5, specific for the small subunit, while MRPL45 and ICT1 appear in fractions 6 and 7, specific for the large subunit. In the case of MRPL45, a pool of non-assembled protein can be observed in fraction 1. Fraction 6 suggests the presence of the monosome. These results show that the fusion protein does not affect the pattern of migration of the mitoribosome subunits, suggesting it does not interfere with subunits assembly.

The results obtained during the process of C12orf65-Linker-BioID2-HA characterization are consistent with the C12orf65-BioID2-HA results and with what is known so far about C12orf65: the fusion protein is targeted to the mitochondria matrix after cleavage of the N-terminal signal and does not integrate in the mitoribosome.

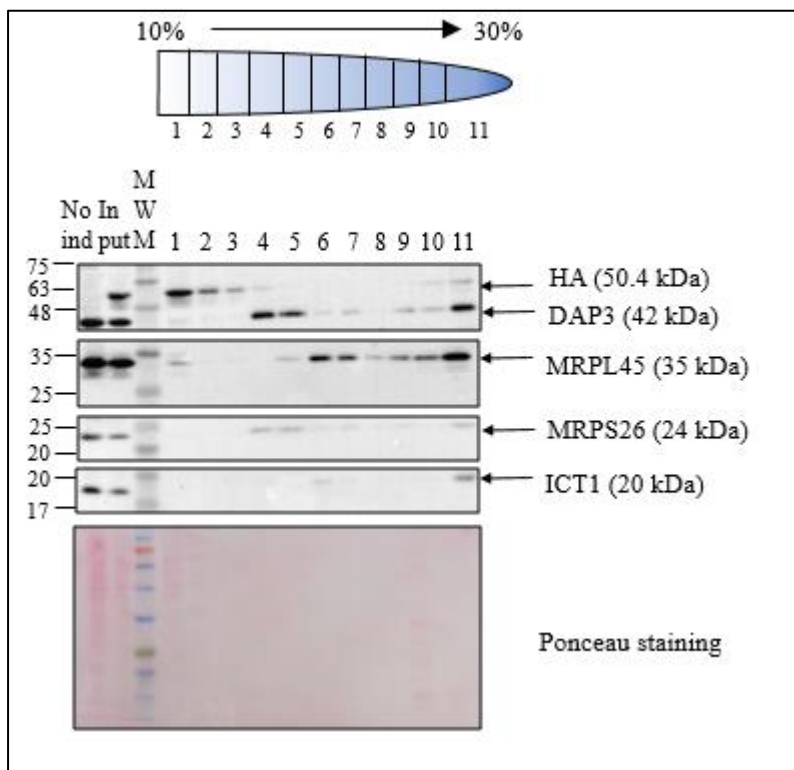


Figure 5-7. Sucrose gradient of C12orf65-Linker-BioID2-HA clone 9

C12orf65-Linker-BioID2-HA clone 9 HEK293T cells were induced (tetracycline 1 μ g/ml, overnight), lysed and the lysate (700 μ g) was separated on a 10-30% sucrose gradient. The fractions were analysed by 12% SDS-PAGE and identified using the indicated antibodies. A non-induced lysate (No Ind, 50 μ g) and an aliquot of the input loaded on top of the sucrose gradient (50 μ g) were used as negative and positive controls, respectively; 1/5 of total fraction volume (100 μ l) loaded for each fraction; MWM = molecular weight marker (kDa); N=1

5.3 Discussion

Characterization of C12orf65-Linker-BioID2-HA suggests, as in the case of C12orf65-BioID2-HA, that the fusion protein reproduces the results available so far on C12orf65: it is soluble, has a cleavable mitochondrial targeting sequence (Kogure et al., 2012), localizes to mitochondrial matrix and does not interfere with mitoribosome assembly (Pajak, 2013, Wesolowska, 2015). On this basis, the clone was suitable to be used for the mass-spectrometry experiment that would lead to identification of C12orf65 interactors.

Still, there are two differences between the C12orf65-Linker-BioID2-HA and the C12orf65-BioID2-HA that need to be addressed.

First, the phenotype differs because the Linker clone has a higher viability and growth rate and forms less clumps in culture. As mentioned in Chapter 4, the C12orf65-BioID2-HA clones had a slow growth rate and a poor recovery rate after defrosting, which led to increased risk of infections. This was not the case with C12orf65-Linker-BioID2-HA clone 9 ('Linker' clone). After transfection, the resulting Linker clones had indeed different speeds of growth and different recovery rates when moved from one dish to another. This provided the possibility to visually assess them and decide that clone 9, the fastest clone to grow that did not present leakage of expression, would be the best to use for further experiments (Figure 5-8). The phenotypic difference between the Linker clones can be attributed to the cell recovery after transfection.

Second, all the Linker clones show the presence of a cleavage product upon induction, which was not the case for C12orf65-BioID2-HA. This cleavage product, which appears in the non-induced leaky clones as well, is retained in the cytosol and is identified via the HA antibody, suggesting that the cleavage occurs between the C12orf65 and BioID2-HA moieties of the fusion protein. It could also be the reason why the Linker clones grew better than the C12orf65-BioID2-HA ones. Although BioID2 has been successfully used, the technique is ultimately based on the expression of a bacterial protein inside a HEK cell line. The bacterium (*A. aeolicus*) is different from any commensal or pathogenic bacteria that a human cell might encounter: it is thermophilic (best growth conditions: 95 °C), chemoautotrophic (grows on hydrogen, oxygen, carbon dioxide, and mineral salts) and not able to grow on organic substrates (sugars, amino acids, extracts from meat or yeast) (Deckert et al., 1998). Although only one protein from this bacterium is expressed in the cell, and it is in a mutant form, there is still a possibility for a cellular feedback, a recognition of BioID2 as 'non-self', followed by an attempt to degrade it.

The linker provides a physical separation between C12orf65 and BioID2, which could allow the action of proteases, with partial degradation of the fusion protein becoming the physiological response of cells to artificial expression. In C12orf65-BioID2-HA case, steric hindrance possibly impedes the action of proteases, imprisoning the cell in a feedback loop that exhausts it of energy, causing a slower growth. Without a degradation product present, the cell might continue to synthesize proteases, or redirect the already active ones, in an attempt to degrade the fusion protein, which would require a high amount of ATP.

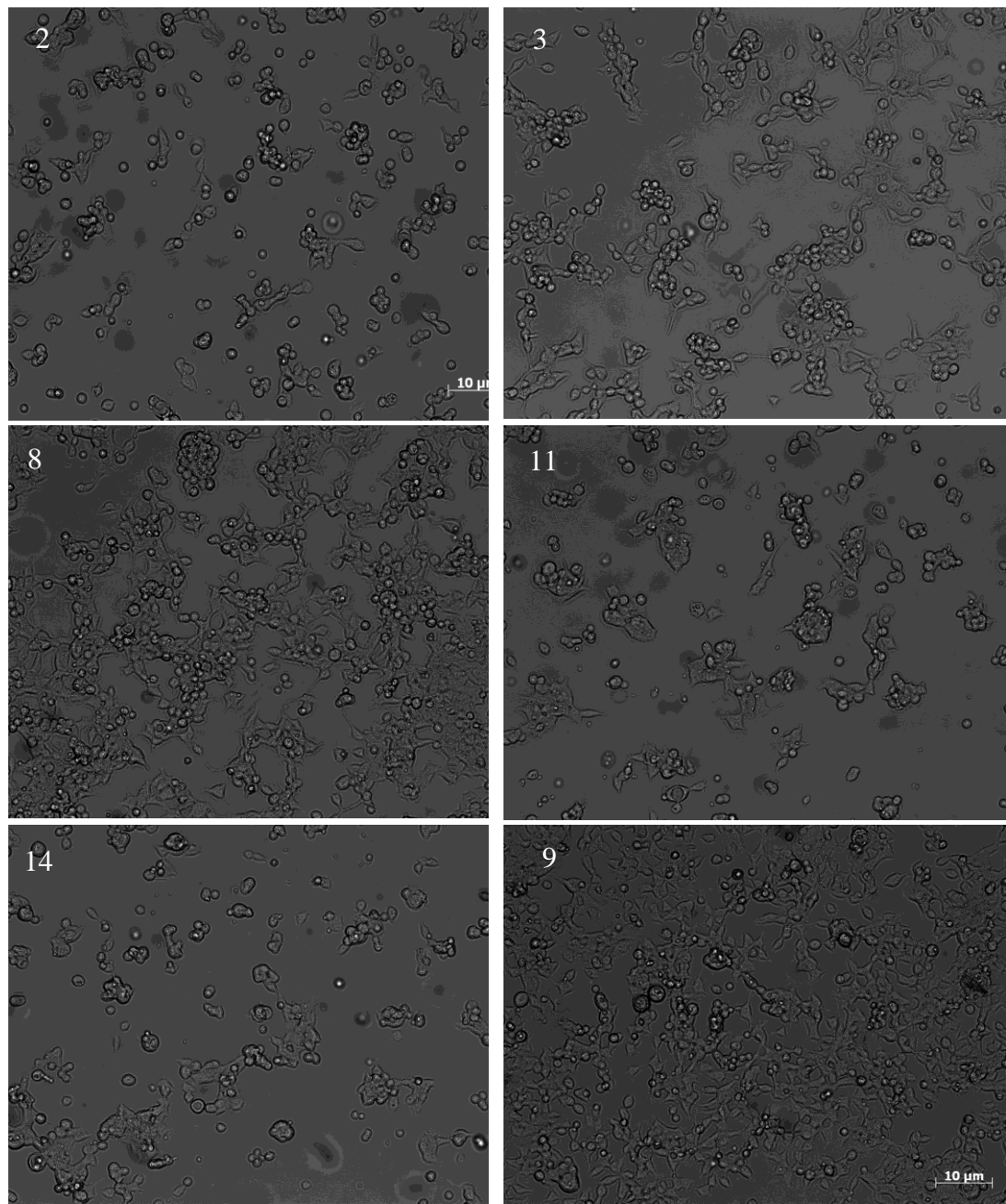


Figure 5-8. Examples of different phenotypes observed in Linker clones

HEK293T Linker clone cells were grown in a 6 well plate and photographed at the same time using a bright-field microscope. N=1 per clone

The size of the degradation product (35 kDa) in Linker clones is interesting. It was expected that the linker would be the main target of proteases, as it is flexible and easily accessible. Proteolytic cleavage would lead to the separation of C12orf65 and BioID2-HA, the latter being identified by the HA antibody. In this scenario, however, the BioID2-HA molecular weight would be approx. 27 kDa (the sum of 26 kDa - BioID2 and 1 kDa - HA,), which is far less than

what is seen on the western blot results. If the proteases cut right between C12orf65 and linker, adding the linker molecular weight (4 kDa) to the BioID2 moiety, the resulting product of degradation would still be light comparing to what is observed. The only possibility was that the proteases acted somewhere inside the C12orf65 moiety.

In order to see which is the most probable target site and which are the proteases responsible for cleavage, I used CleavPredict, an online tool developed by Cieplak and Strongin (Cieplak and Strongin, 2017). I preferred it to the typical cleavage sites predictor PeptideCutter from ExPASy (https://web.expasy.org/peptide_cutter/), frequently used in mass-spectrometry, because CleavPredict is specific to matrix metalloproteinases, while PeptideCutter uses bacterial and digestive enzymes. An extensive characterisation of the proteases expressed by HEK cells showed that matrix metalloproteinases are the typical proteases in this cell type, with MMP-2 being the most abundant, followed by MMP-1, -2, -3, -8, -9, -10 and -13 (Liu and Wu, 2006).

CleavPredict predicts the cleavage sites of 11 matrix metalloproteinases (MMP-2, -3, -8, -9, -10, -14, -15, -16, -24, -17, and -25) for a given primary protein sequence. For each MMP, the programme returns the predicted target sites, a prediction score for each site (the higher the score, the higher the probability that the target site is true) and the molecular weights for the N- and for the C-terminus cleavage products. Based on this, I imported the FASTA sequence of C12orf65 (UniProt ID Q9H3J6) and used it against each of the 11 MMPs on CleavPredict. For each predicted cleavage site, I summed the molecular weight of the C-terminus cleaved product to the molecular weight of BioID2-HA. To ensure that the molecular weights given by CleavPredict are correct, I checked the resulting aa sequences with ProtParam tool from ExPASy (<https://web.expasy.org/protparam/>).

I concluded that the cleavage site most probable is 110, because it would give me a C-terminus peptide of 10.8 kDa, which added to BioID2-HA gives the closest molecular weight to the 35 kDa. That would mean that approx. 30% of C12orf65 (166 aa length) before the linker sequence is cut (Figure 5-9).

The next step was to sort the possible MMPs that cleave at site 110 based on scores, highest to smallest, and check the intracellular localization of each (Table 5-1).

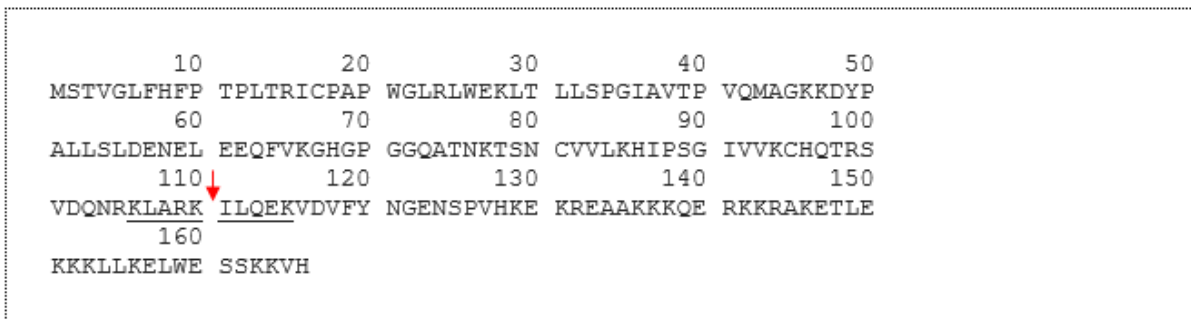


Figure 5-9. C12orf65 primary sequence

FASTA sequence of the C12orf65 isoform 1 (identifier: Q9H3J6-1), chosen as the canonical sequence. Red arrow indicates the position of the predicted cleavage site and the protease target sequence appears underlined.

Table 5-1. Predicted MMPs for C12orf65

Name	Score	Mass (kDa)	Localization (UniProt)
MMP-9	1.72	92	extracellular matrix
MMP-14	1.46	66	cell membrane, cytoplasm
MMP-8	1.05	53	stored in intracellular granules, extracellular matrix
MMP-15	1.03	76	cell membrane
MMP-2	0.88	72	isoform 2 is mitochondrial; extracellular matrix, nucleus
MMP-25	0.31	62.5	extracellular matrix; cell membrane

Based on this analysis, I considered that MMP-14 would be the best candidate to cleave at position 110, because it is cytoplasmic, has the second-highest prediction score and is the smallest after MMP-8. Based on its molecular weight, the MMP-14 has a radius of 2.5-3 nm (Erickson, 2009), which would fit in the 25 nm offered by the linker sequence, even if more than one molecule would attack the fusion protein at once. I eliminated MMP2 because there is no cleavage product observable in the mitochondria.

The fact that the potential cleavage site is deep inside the C12orf65 protein can be explained by two possibilities: the specificity of the protease target sequence and the inaccessibility of the late C-terminus aa. In the absence of the protein structure, I cannot draw any conclusions about the C-terminus. The only available C12orf65 structure, incomplete, comes from *Mus musculus* (Kogure et al., 2012), and lacks the aa from position 110 onwards (total length being 184 aa, UniProt ID Q80VP5)

Despite the cleavage product, C12orf65-Linker-BioID2-HA cell line proved to be a reliable model to use for the study of C12orf65 interactors. The robust growth rate meant it would provide a good amount of starting material and the biological characteristics of the fusion protein (matrix localization, MTS cleavage, canonical distribution of the 55S subunits on sucrose gradients) suggested it would help identify valid interactors. Therefore, the Linker clone was used for the BioID2 experiment, in which possible C12orf65 protein interactors were biotinylated and identified by mass-spectrometry, as detailed in the following chapter.

Chapter 6

Identification of C12orf65 protein interactors by BioID2

6.1 Introduction

Following characterisation of the fusion protein, the C12orf65-BioID2-HA and C12orf65-Linker-BioID2-HA HEK clones were used for biotinylation experiments and identification of C12orf65 protein interactors by mass-spectrometry. Using both BioID2 clones increases the chances to find valid interactions as opposed to random matrix proteins. Considering the successful application of the BioID2 technique to a wide variety of proteins in recent years, there was a high probability to identify C12orf65 interactors using the same technique, and understand its function starting from them.

BioID2 was developed from BioID, a technique that brought benefits to the study of protein-protein interactions (Roux et al., 2012). By fusing a protein of interest (bait) with a promiscuous mutant of *E. coli* biotin-ligase, researchers can identify interactors (preys or hits) that were previously obscure due to the limitations of traditional methods. Methods such as affinity purification and yeast-2-hybrid were not suitable for *in vivo* experiments and required a physical interaction between bait and prey (Kim and Roux, 2016). In contrast, BioID is applied in living cells and allows identification of both physical as well as transient interactions that occur under a 10 nm biotinylation range. The preys are captured via streptavidin interaction and analysed by mass-spectrometry (Roux et al., 2012). The technique circumvents the necessity of bait solubilization and has already been successfully used by several groups for interactors identification in different cell and organism models, last reviewed by Sears et al. (Sears et al., 2019).

BioID2 came as an improvement of BioID (Kim et al., 2016a) and used a different bacterium for generation of the mutant biotin ligase (*A. aeolicus*). This biotin ligase is 10 kDa smaller than the one used in BioID, which decreased the risk of steric hindrance with the bait. The addition of a linker formed by a sequence of 13x GGGGS repeats increased bait flexibility as well as the biotinylation range. The use of BioID2 spread rapidly in the scientific community, and, recently, the technique was applied to study various aspects of human cell biology, from cancer (Zheng et al., 2019) and immunology (Anczurowski et al., 2019, Prikas et al., 2020) to axonal regeneration (Gong et al., 2020) and cytosolic translation (Smejda et al., 2021).

The baits used in BioID2 are diverse, as they can be soluble or transmembrane proteins. Gong et al. used BioID2 to study the receptor protein tyrosine phosphatase PTPR σ , a transmembrane protein involved in axonal regeneration (Gong et al., 2020). PTPR σ substrates were not

completely characterized, but by fusing it with BioID2-HA, the authors were able to identify 100 interactors, including some previously reported (cortactin) with traditional methods. The identification of both known and unknown interactors indicates that the technique is reliable. Moreover, by using a bait protein with a clear function (dephosphorylation of tyrosine), the authors show that function is not affected by the presence of biotin-ligase.

The soluble proteins used as baits in BioID2 studies also had a known function, and few known interactors in human cells. BioID2 was employed to expand the level of knowledge currently available regarding them, rather than to indicate a function. For example, Zheng et al. succeeded in the identification of novel binding partners for PAD2 (protein arginine deiminase 2), a transcription factor involved in breast cancer, for which the mechanism of transport to the nucleus was unknown (Zheng et al., 2019). The two novel interactors (ANXA5 and Ran) helped uncover this mechanism and were further validated by immunoprecipitation. Moreover, BioID2 was efficiently utilized to study the MAP (Mitogen-activated protein) kinase p38 α (Prikas et al., 2020) interactors, leading to the identification of both new (XPA and MTA1) and previous known interactors. In this particular case, the interactors revealed an additional unexpected role for p38 α - transcription regulation (Prikas et al., 2020) as part of the DNA damage response caused by UV.

The use of BioID2 is not restricted to human cells. The technique was adapted to very different organisms, including *Drosophila* sp. (Mazina et al., 2020), plants (Arora et al., 2020, Huang et al., 2020) and an *in-vivo* BioID2 mouse model to study the cardiac diad (Feng et al., 2020). The study of parasitic protists has also benefitted from this approach. Several BioID2 protocols were developed for *Plasmodium falciparum* (Nessel et al., 2020), *Toxoplasma gondii* (Bradley et al., 2020) and *Trypanosoma brucei* (Pyrih et al., 2020). Notably, in *Plasmodium falciparum*, the initial protocol that involved BioID failed due to the size of BirA (35 kDa). The bait (EXP2, part of the PTEX complex involved in transport between the parasite and the host erythrocyte) was small (33 kDa) and the BirA from *A. aeolicus* (26 kDa) proved to be more suitable (Nessel et al., 2020).

In *Trypanosoma brucei*, BioID2 was used to study parasite's mitochondria and involved the fusion of the biotin-ligase with several mitochondrial baits: an ATPase located in IMM, a chaperone involved in Fe-S cluster assembly or an mtDNA ligase associated with mtDNA replication in this parasite. The authors identified new mitochondrial proteins with previously

unknown localization and revealed an interaction between the ATPase ZapE and mitochondrial insertase Oxa1 that leads to the destabilization of the respiratory chain.

Regarding the study of mitochondria, BioID2 lead to successful results not only in *Trypanosoma brucei*, but also in human cells. Two recent studies investigated protein interactions in the mitochondrial matrix of HEK cells using protein kinase A (Ould Amer and Hebert-Chatelain, 2020) and respectively C-Src kinase (Guedouari et al., 2021) as a bait. The publications report 21 mitochondrial interactors of protein kinase A and 51 for C-Src kinase, including both known and novel interactors for each case. TIMM44 was validated by coimmunoprecipitation as a physical interactor of protein kinase A (Ould Amer and Hebert-Chatelain, 2020), while ATP5 β and SLP2 were found to directly bind C-Src kinase (Guedouari et al., 2021). The two studies provide new insights into matrix phosphorylation and suggest new functions of mitochondrial kinases in altering cristae structure (via ATP5 β and SLP2). Importantly, in both cases, fusion with BioID2 did not affect the enzymatic function: the bait was correctly localized to mitochondria, cell respiration was not affected, and the biotin-ligase was functional.

When referring to mitochondria proximity mapping, the seminal work of Antonicka and colleagues (Antonicka et al., 2020) is the source of information for all mitochondria compartments. The authors used BioID (with the biotin-ligase from *E. coli*) to identify interactors for 100 mitochondrial baits that belong to OMM, IMM, IMS or matrix, as well as to characterize the mitochondrial environment by targeting the biotin-ligase to the matrix. All the bait-prey interactions described point towards a possible function for mitochondrial orphan proteins.

The mitochondrial protein C12orf65 is an interesting bait to use for BioID2 experiments, different from all the baits mentioned before. C12orf65 is soluble in the mitochondria matrix, as opposed to the membrane proteins PTPR σ (Gong et al., 2020) and EXP2 (Nessel et al., 2020). If it were part of a membrane complex, several physical interactors could have been identified so far, but this is not the case. C12orf65 is not an enzyme, like the protein kinase A and C-Src kinase (Ould Amer and Hebert-Chatelain, 2020, Guedouari et al., 2021), and has no dephosphorylation activity, like PTPR σ . Thus, there is no substrate that could be used to assess the physiology of C12orf65-BioID2 clones. For enzymes, the impact of BirA conjugation is determined by measuring the enzyme activity, but this is not possible for C12orf65. This protein does not belong to any well-described molecular cascade, like MAP kinase p38 α

(Prikas et al., 2020) or PAD2 (Zheng et al., 2019), and has no interactors identified by immunoprecipitation.

However, BioID2 can still be successfully applied to C12orf65. Although indirectly, the above-mentioned articles bring arguments in favour of its use, because they all have in common two positive aspects:

1. BioID2 correctly identifies protein-protein interactions
2. Bait function is not affected by fusion with BirA

When the bait had well-described interactors, they were also identified by BioID2 (Mazina et al., 2020, Gong et al., 2020, Pyrih et al., 2020, Huang et al., 2020). When BioID2 identified a novel interactor, it was further validated by coimmunoprecipitation (Zheng et al., 2019) (Ould Amer and Hebert-Chatelain, 2020, Guedouari et al., 2021) or immunofluorescence (Prikas et al., 2020). Although it is likely that C12orf65 interactors are transient and therefore not suitable to be validated by immunoprecipitation, they could still be ‘true’ interactors, that provide valuable insight into protein function. When Pyrih et al. identified a transient interaction between their bait and prey, they depleted the bait to show a functional interaction (Pyrih et al., 2020).

Regarding the conjugation with a bacterial biotin-ligase, there are no reports that BioID2 would affect the bait function (Gong et al., 2020, Ould Amer and Hebert-Chatelain, 2020, Guedouari et al., 2021). Although these results cannot be completely extrapolated to C12orf65, they provide a good indication that its function should not be affected. The addition of the 13x GGGGS repeats linker further decreases this possibility. The characterization of C12orf65-BioID2 and C12orf65-Linker-BioID2 clones (described in Chapter 4 and Chapter 5) indicated a natural behaviour of the bait: the fusion protein was targeted to the mitochondrial matrix after cleavage of the N-terminal sequence and the mitoribosome presented a normal distribution of the large and small subunits on the sucrose gradients.

Therefore, I proceeded to the investigation of C12orf65 specific interactors via mass-spectrometry. For this, I treated the clones with biotin (50 μ M, 17 h) prior to harvesting, isolated mitochondria, then pulled down the biotinylated proteins with magnetic beads coated with streptavidin. The prey proteins were digested off the beads and analysed by mass-spectrometry. Based on the results obtained when the method was developed, which show the biotin-ligase is capable of self-biotinylation (Kim et al., 2016a), it is possible to obtain

C12orf65 among the hits, together with its interactors (Figure 6-1). The non-specific interactors would be identified in the control cells (COX8-MTS-BioID2-HA).

As my research hypothesis is that C12orf65 rescues mitoribosomes that stall during translation, I would expect to find mitoribosomal proteins among the specific interactors. I could map those interactors on the mitoribosome structure and define the region where C12orf65 is most likely to bind.

The plan was to split the experimental work between my host lab in Newcastle and Prof. Hans Spelbrink's lab in Nijmegen, the Netherlands. My sponsor requested that all fellows have an exchange in another lab from the network (secondment). Because the mass-spectrometry facility in Nijmegen was performant and well-equipped, and Prof. Spelbrink's group had experience with BioID2, I decided to perform the streptavidin pull-down and mass-spectrometry there, thus fulfilling the request from my sponsor. Cell growth and mitochondria isolation were performed in Newcastle for all samples, and isolated mitochondria were sent to Nijmegen on carbonic ice.

Prior to the Nijmegen secondment, I performed a single BioID2 experiment in Newcastle, using Prof. Mattias Trost's mass-spectrometry facility, to check whether mitochondrial proteins (other than carboxylases) can be identified using this technique. After the Nijmegen secondment, because the results obtained there were not satisfactory, I repeated the BioID2 experiment two times in Newcastle, hoping to identify more interactors. The manner the samples were prepared for mass-spectrometry was not very different between the two centres. It included small adjustments required by the mass-spectrometrists based on the protocols developed in each centre (as described 2.6.2 in and 2.6.3). The biotinylated proteins identified in Newcastle and Nijmegen are detailed in the Results section of this chapter.

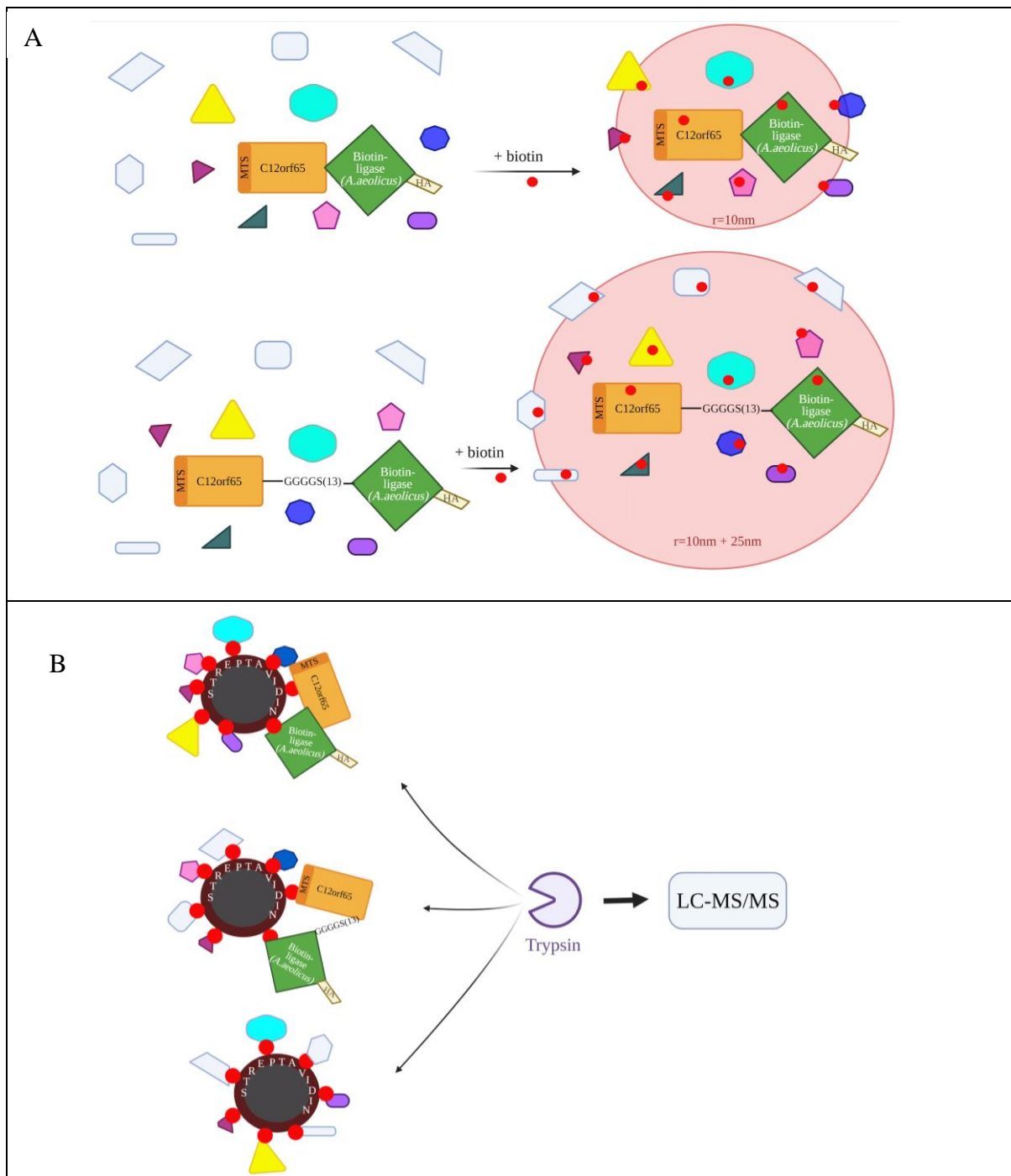


Figure 6-1. Application of the BioID2 principle to study C12orf65

C12orf65 (orange) was attached to the promiscuous biotin-ligase from *A. aeolicus* (green). The rationale was that, while C12orf65 performs its unknown function, the biotin ligase adds biotin to the proteins C12orf65 interacts with, proteins that can then be isolated and identified by mass-spectrometry.

A: Upon biotin treatment (red), this enzyme biotinylates the proteins with which C12orf65 transiently interacts along a 10 nm radius. Insertion of a linker (13xGGGGS repeats) increases the radius to 25 nm, allowing detection of additional proteins (light grey)
 B: Biotinylated proteins bind to streptavidin-coated magnetic beads and are digested with trypsin prior to mass-spectrometry analysis; figures made using www.biorender.com

6.2 Results

6.2.1 Non-specific biotinylation versus endogenously biotinylated proteins

After verifying that C12orf65-BioID2-HA and C12orf65-Linker-BioID2-HA are correctly distributed to the mitochondrial matrix and do not interfere with the mitoribosome, it was necessary to confirm that the biotin-ligase is functional. For this, I induced the cells with tetracycline (1 μ g/ml, 24 h) and fed them biotin (50 μ M, 16 h), then lysed them, and separated the lysate by western blot. I probed the membrane first with streptavidin coupled to horseradish peroxidase (HRP) to test for biotinylation, then with the anti-HA antibody to test for protein expression. I decided to use the streptavidin-HRP first to check for any potential self-biotinylation.

As shown in Figure 6-2, biotinylation occurred only upon biotin addition, identified by the smear signal resulted from the streptavidin-HRP incubation (lanes 4, 9 and 13). This smear contains distinct bands that appear at the same position with the bands resulted from HA incubation, indicating that the fusion proteins self-biotinylate.

Interestingly, streptavidin-HRP identifies a strong band at 35 kDa, corresponding to the C12orf65-Linker-BioID2-HA specific band described in the previous chapter, which seems to be a cleavage product that remains in the cytosol. This band only appears in the biotin-treated and induced sample and is also identified with the HA antibody (lane 13), suggesting that the cleavage product contains an active biotin-ligase. The HA antibody also identifies the 35 kDa band in the induced sample not treated with biotin (lane 12), which implies that biotinylation is dependent of additional biotin.

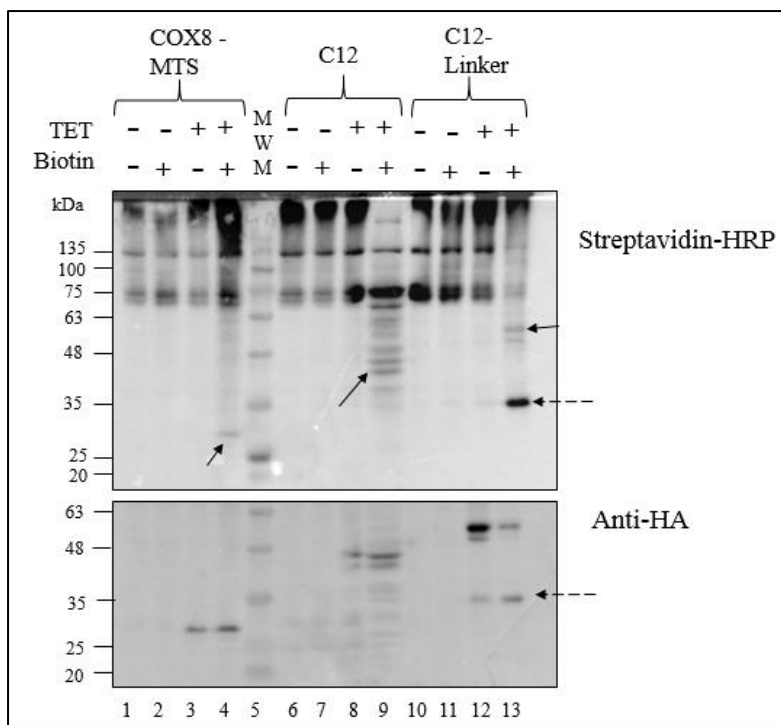


Figure 6-2. Biotin induces non-specific biotinylation in BioID2 clones

COX8-MTS, C12orf65 (C12) and C12orf65-Linker (C12-Linker) BioID2 clones were induced and fed with biotin prior to lysis and separation on SDS-PAGE. Full arrows indicate a possible self-biotinylation and dashed arrows indicate the possible cleavage product previously identified for C12orf65-Linker-BioID2-HA. Approx. 50 µg/well; 10% resolving gel; N=1

The strong bands above 75 kDa, visible with streptavidin-HRP on all samples, correspond to endogenous biotinylated proteins, most likely carboxylases. Carboxylases are enzymes that use biotin as cofactor to introduce a new CO₂ to organic compounds; in the presence of ATP and Mg²⁺, they transfer the CO₂ from a bicarbonate ion to biotin, and from biotin to their substrate (Knowles, 1989). Five such enzymes have been discovered in mammalian cells (Table 6-1): acetyl-CoA carboxylase (ACC) 1 (alpha) and 2 (beta), pyruvate carboxylase (PC), propionyl-CoA carboxylase (PCC), and 3-methylcrotonyl-CoA carboxylase (MCC). Apart from ACC1 which is cytosolic, all are mitochondrial (Kirkeby et al., 1993, Waldrop et al., 2012).

PCC and MCC are mitochondria catabolic enzymes: PCC degrades odd chain fatty acids and amino acids (isoleucine, threonine, methionine, and valine, (Kalousek et al., 1980)), while MCC is specific for leucine and isovaleric acid (Chu and Cheng, 2007). Each enzyme is formed by alpha and beta subunits, with only subunit alpha having biotin affinity; this explains why the non-specific streptavidin-HRP signal in Figure 6-2 does not appear between 48-63 kDa

(lines 1-3, 6-8, 10-12). The bands that appear at 75 kDa could correspond to the alpha subunit of PCC; although its absolute molecular weight is 80 kDa (according to the UniProt database), purification of the subunit from human cells showed that, in native state, it weighs less: 72 kDa (Kalousek et al., 1980). For MCC, the observed molecular weight is 80 kDa (Grünert et al., 2012).

Table 6-1. Mammalian biotin-dependent carboxylases

Name	Subunit	E.C. number	Cell compartment	MW (kDa)	Function	Reference
Acetyl-CoA carboxylase 1	-	6.4.1.2	cytosol, mitochondria	265	fatty acid biosynthesis	(Abu-Elheiga et al., 1995, Rath et al., 2021)
Acetyl-CoA carboxylase 2	-	6.4.1.2	mitochondria outer membrane	280	inhibits fatty acid β -oxidation	(Kim et al., 2007, Abu-Elheiga et al., 2000)
Propionyl-CoA carboxylase	alpha	6.4.1.3	mitochondria matrix	80	catabolism of odd, short chain fatty acids	(Frenkel and Kitchens, 1975)
	beta	6.4.1.3	mitochondria matrix	58	catabolism of odd, short chain fatty acids	(Kalousek et al., 1980)
Methyl crotonyl-CoA carboxylase	alpha	6.4.1.4	mitochondria matrix	80	L-leucine degradation	(Murín et al., 2006)
	beta	6.4.1.4	mitochondria matrix	61	L-leucine degradation	(Stadler et al., 2005)
Pyruvate carboxylase	-	6.4.1.1	mitochondria matrix	130	gluconeogenesis	(Böttger et al., 1969)

The strong streptavidin-HRP signal that accumulates at the top of the membrane, above 135 kDa, could represent acetyl-CoA carboxylases 1 and 2, with 265 and respectively 280 kDa (Witters et al., 1994). As they have big molecular weights, of close values, it is likely that the 10% resolving gel did not allow their separation, which resulted in the saturated blobs at the top of the membrane. ACC is a rate-limiting step enzyme for fatty acids synthesis: it converts acetyl-CoA to malonyl-CoA, which provides a two-carbon unit necessary for the synthesis. It was considered cytosol specific, but is currently listed as mitochondrial matrix protein in human Mitocarta 3.0 (Rath et al., 2021). ACC2 is anchored to the OMM and inhibits β -

oxidation by producing malonyl-CoA, which inhibits the carnitine palmitoyl transferase I involved in the transport of long-chain fatty acids to the mitochondria (Murthy and Pande, 1987).

Apart from carboxylases, there are several other proteins that can temporarily bind biotin: biotin transporters, biotinidase, and histones. As mammalian cells do not synthesize biotin, they have developed specific transporters that import it from the environment, like the sodium-dependent multivitamin transporter (*SLC5A6* gene, 68.6 kDa (Vadlapudi et al., 2012), (Schwantje et al., 2019)) or monocarboxylate transporter 1 (*SLC16A1* gene, 54 kDa, (Daberkow et al., 2003)). Biotinidase (EC 3.5.1.12, 61 kDa) is a biotin recycling factor and carrier, responsible for biotinylation of histones (Hymes and Wolf, 1999). As part of gene regulation, there are multiple lysine sites where biotin is attached via an amide bond (Stanley et al., 2001) to histones H2A (14.3 kDa, (Chew et al., 2006)), H3 (15 kDa, (Kobza et al., 2005)) and H4 (11.4 kDa, (Camporeale et al., 2004)). None of those temporarily biotinylated proteins was detected on the western blot from Figure 6-2, regardless of biotin addition. This could be explained by several possibilities: a low steady-state expression, the proteins had not bound biotin at the time when cells were lysed and harvested, or they contained biotin, but the amount was too low to be detected with the streptavidin-HRP.

6.2.2 Interactors identified in Newcastle

Once established that the biotin-ligase was capable of non-specific biotinylation, I proceeded to the first mass-spectrometry attempt (from here onwards, named NCL1). This first experiment was planned as an indicator of possible hits and as an occasion to identify points of optimization should that be necessary. It was performed only once (N=1) and included the three HEK clones: COX8-MTS-BioID2-HA (control, COX8), C12orf65-BioID2-HA (C12-BioID2) and C12orf65-Linker-BioID2-HA (C12-Linker-BioID2). For each clone, I had one sample induced only and another sample induced, and biotin treated.

As described in 2.6.1, the starting material for one sample came from 3*300 cm² flasks. Each clone was harvested at a different day and mitochondria isolation was performed at the same time for the induced and the corresponding induced and biotin treated sample. Isolated mitochondria were kept at -80°C until the start of the streptavidin pull-down (with 50 µl of Dynabeads MyOne Streptavidin C1). This step, as well as the following washes and preparations for mass-spectrometry analysis, was done for all the six samples at once.

In order to test HA expression, I separated the input, unbound and the first two washes by SDS-PAGE and probed the membrane with anti-HA antibody and with streptavidin-HRP. All clones showed HA expression (Figure 6-3), although weak, especially for C12-Linker-BioID2. This could be due to the low amount of sample loaded, as the total mitochondria lysate volume was high (2 ml) resulting in a diluted sample.

Streptavidin-HRP identified what most likely are mitochondrial endogenous carboxylases (top of the membrane, lanes 1-2 and 6-7 Figure 6-3 of A and B). Biotinylation smears were present in input and unbound for: COX8 control, C12-BioID2 and, although weak, C12-Linker-BioID2. The strong signal given by the streptavidin-HRP incubation in the ladder (line 5) is a technical artifact because the 75 and 20 sizes were particularly reactive. There was no signal at all in the first and second wash, proving that no biotinylated sample is lost.

After washes, the samples were treated with 1 mM TCEP to reduce the disulphide bonds, then alkylated with 5 mM (final concentration) chloroacetamide and the proteins attached to the beads were digested with trypsin (5 ng/μl). The resulting peptides were recovered by centrifugation and handed to the mass-spectrometry facility at Newcastle University. Dr. Frédérique Lamoliatte (Prof. Matthias Trost group) kindly performed the mass-spectrometry as well as data analysis for my samples. Peptides were analysed by nanoflow-LC-MS/MS using a Fusion Lumos Tribrid Orbitrap mass spectrometer (Thermo Scientific). Peptides were searched against the human Uniprot Swisprot Database containing isoforms and quantified using MaxQuant 1.6.5.0 (Cox and Mann, 2008).

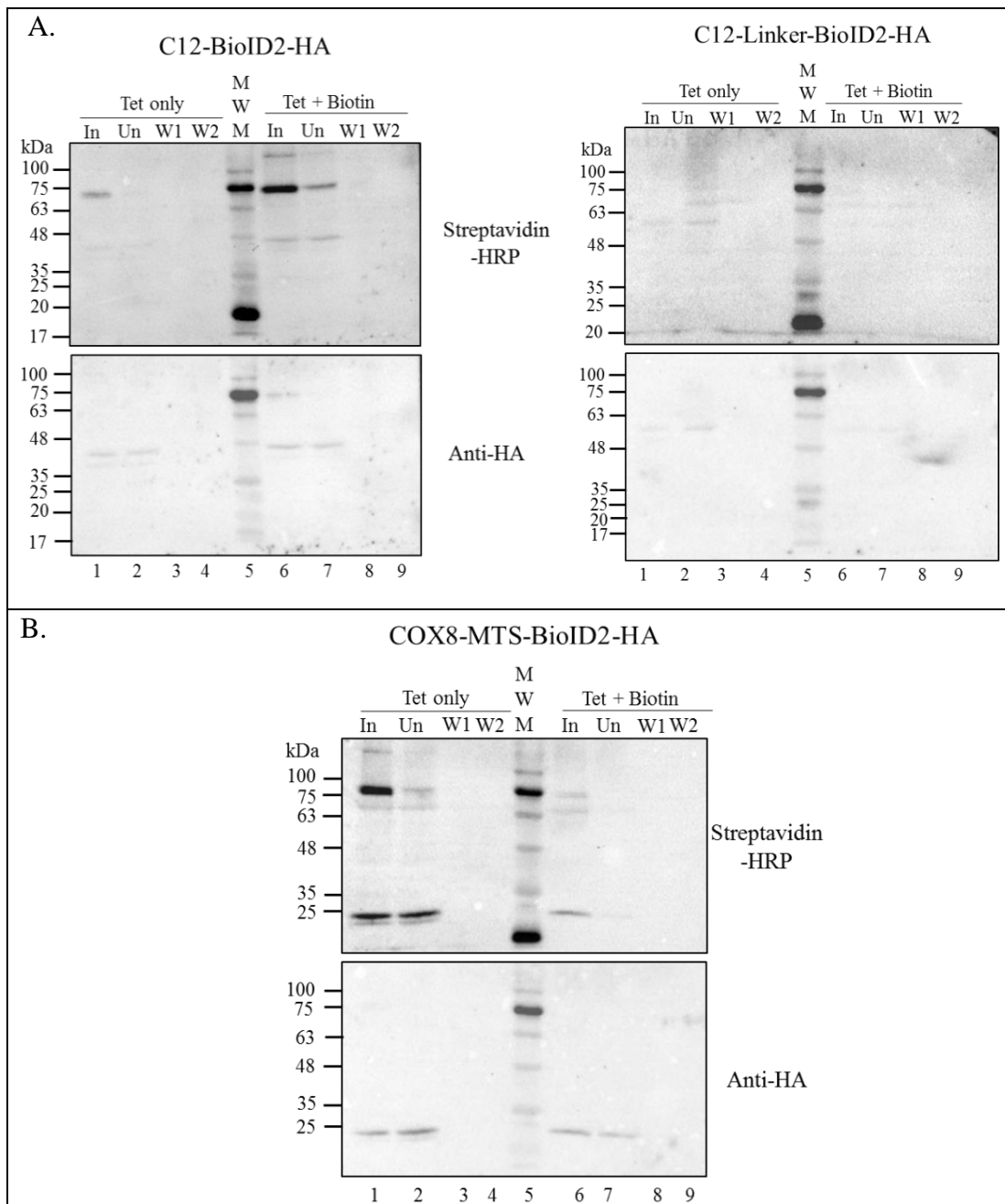


Figure 6-3. Western blot results for NCL1 affinity purification

COX8-MTS, C12orf65 (C12) and C12orf65-Linker (C12-Linker)- BioID2-HA clones were induced with 1 μ g/ml tetracycline and fed with 50 μ M biotin for 16 h prior to mitochondria isolation. Mitochondria were lysed (Input, In) and incubated with streptavidin beads. The unbound material (Un) was removed and the beads were washed extensively. Input unbound and the first two washes (W1, W2) were analysed by SDS-PAGE, using streptavidin-HRP to detect biotinylation and anti-HA to detect protein expression.

Approx. 20 μ g/well; 10% resolving gel, N=1

The identified proteins were filtered using the software Perseus, version 1.6.5.0, and the results were exported in Microsoft Excel. Five levels of filtering were used (Figure 6-4) in order to ensure that the identified hit is not a false-positive (Tyanova et al., 2016):

1. Only identified by site, to eliminate the proteins identified only by a post-translational modification
2. Reverse, to eliminate false positives (peptides randomly matched with a protein); During peptide identification, a decoy (reverse) database is created in MaxQuant. This decoy is composed from the reverse amino acid sequences of the protein sequence database used for search (target). True positives must align only with the target database. (Wang et al., 2009, Moore et al., 2002).
3. Potential contaminant (including keratins, streptavidin and trypsin)
4. Number of peptides/proteins ≥ 2
5. At least one of the six samples must have intensity > 0

The values used for subsequent data analysis were protein intensities, expressed as log2. An intensity of zero, to which log2 cannot be applied, means that the identified protein did not appear in that particular sample.

The total number of proteins identified for the six samples was 248, with 33 hits (13%) assigned as mitochondrial (Appendix-E, Table Apx 10) after comparison with Mitocarta 3.0 (Rath et al., 2021), 43 hits (17%) part of the cytosolic ribosome, 5 hits (2%) cytosolic translation factors and 9 hits (4%) in the endoplasmic reticulum (ER) (Figure 6 4A) (Appendix-E, Table Apx 11).

Contamination with cytosolic ribosomes and translation factors is not surprising, since translation of proteins that must be imported into mitochondria is localized close to the OMM (Vardi-Oknin and Arava, 2019). Also, mitochondria form contacts with ER, which explains the presence of ER hits (Lewis et al., 2016). The majority of hits (63%, ‘other’) are partially related to mitochondria (such as cytoskeleton subunits, glycolytic enzymes or peroxisomal proteins) or are not related at all (e.g. nucleus proteins including histones).

Most mitochondrial hits identified were matrix proteins (20, 61% of total mitochondrial proteins) followed by IMM proteins (6, 18% of total mitochondrial proteins), which is what was expected, considering that the BioID2 fusion proteins are targeted to the matrix (Figure 6-5B). Two hits belong to the IMS (catalase and peroxiredoxin 4) and three hits to the OMM

(VDAC1, VDAC2 and acetyl-CoA carboxylase 2). Two hits did not have an assigned mitochondrial compartment: peroxiredoxin 2 and thioredoxin.

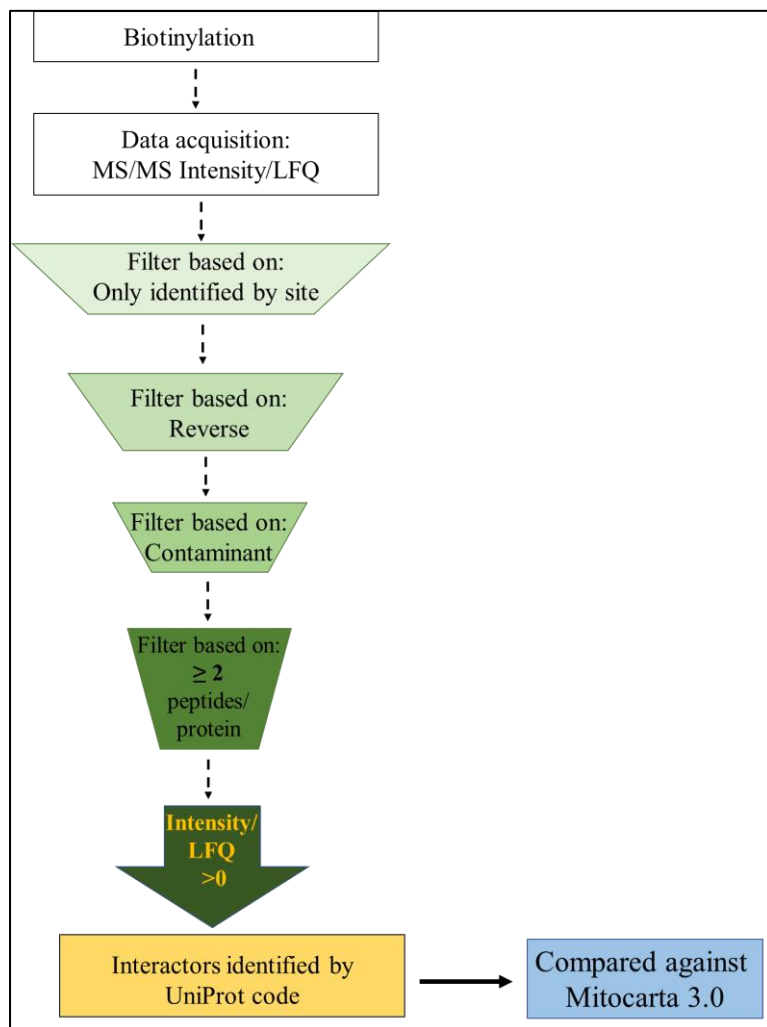


Figure 6-4. Filtering steps performed in Perseus version 1.6.5.0

Biotinylated proteins were analyzed by MS/MS based on their Intensity (NCL1) or LFQ (NCL2 and Nijmegen). Intensity was used in NCL1 because it was only one BioID2 experiment with 6 different samples. In Nijmegen (N=3 BioID2 experiments) and NCL2 (N=2) was used LFQ, which applies to two or more biological samples.

As anticipated, mitochondrial hits from all six samples included the endogenously biotinylated propionyl-CoA carboxylase, acetyl-CoA carboxylase, methylcrotonoyl-CoA carboxylase 1 and pyruvate carboxylase, proving that the streptavidin-pull down was successful. Hits were involved in lipid and amino acid metabolism, transport, TCA and OXPHOS (Figure 6-5C), but included chaperones (catalase, peroxiredoxin) and ROS scavengers as well. Mitochondrial topoisomerase 1 alpha (Top1, involved in mtDNA replication and transcription (Zhang et al., 2001)), and stress-70 protein (also known as Hspa9/mortalin, involved in Fe-S cluster biosynthesis (Shan and Cortopassi, 2016)) were grouped as ‘other’. Surprisingly, C12orf65 did

not figure among the hits, despite the known ability of the fusion protein to self-biotinylate. Proteins involved in translation were well represented (18% of mitochondrial hits), despite the low percentage of mitochondria proteins among the total hits.

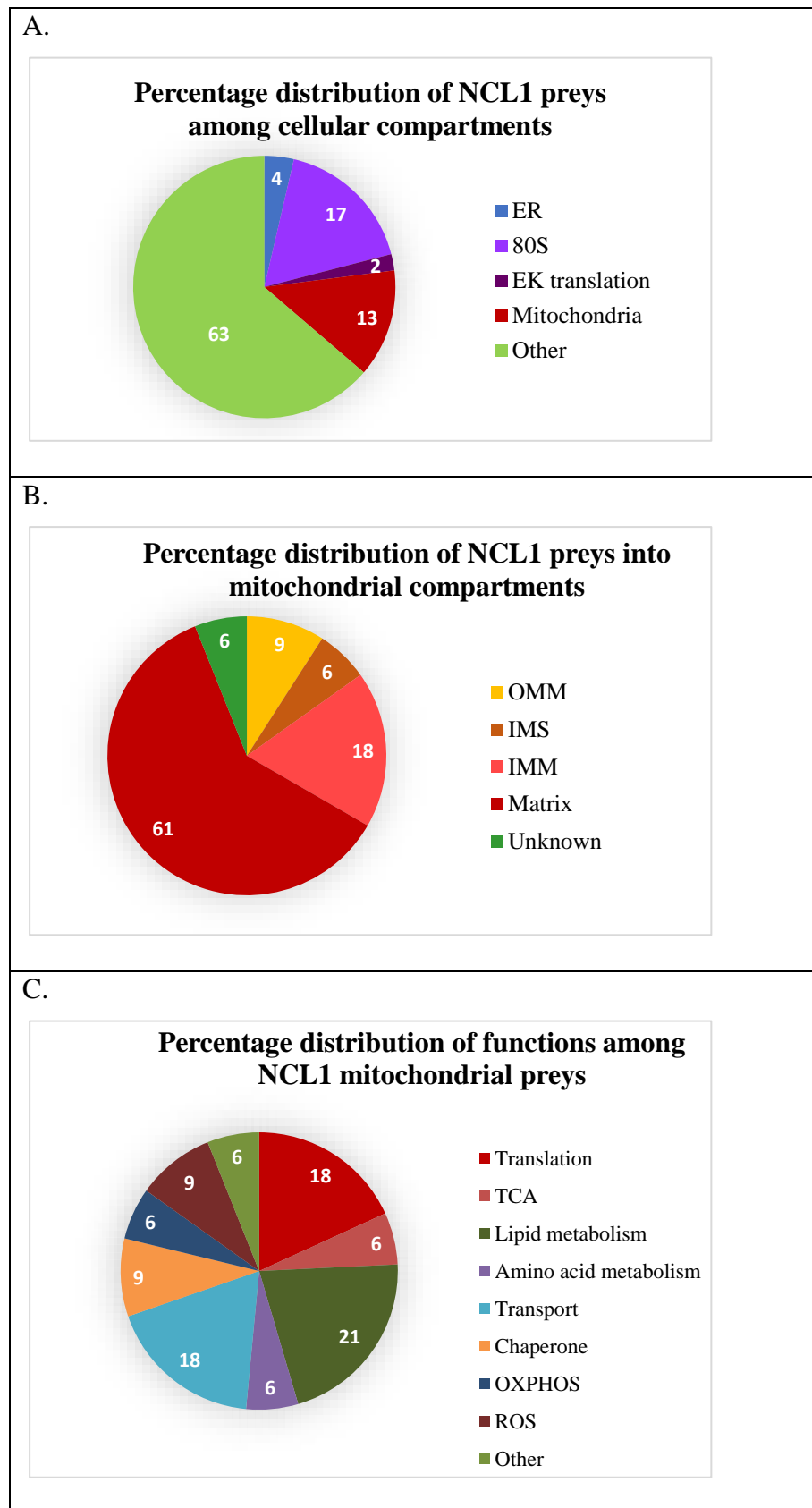


Figure 6-5. Analysis of BioID2 interactors identified in NCL1

Venn diagrams summarizing cellular (A) and mitochondrial (B) distribution of biotinylated proteins and their functions (C); N=1 biological repeat

There were three instances when a hit was assigned to multiple mitochondrial proteins by Mitocarta 3.0. This happened because the identified peptides could be attributed to different subunits or isoforms of one protein and were assigned different UniProt identification codes (Table 6-2). The issue is well-known for bottom-up proteomics due to its limited sequence coverage (Zhang et al., 2013, Aebersold and Mann, 2003). A low total number of peptides makes identification even harder. In my samples, in the first example, acetyl-CoA carboxylase isoforms 1 (alpha) and 2 (beta) have a 75% overall identity (Boone et al., 1999) and both of them appear in the current Mitocarta database, having been identified in different human tissues, so there is a reasonable explanation why the two could not be distinguished. In the second example, the electron transfer flavoprotein subunits alpha and beta belong to an enzyme that transfers electrons from mitochondrial primary flavoprotein dehydrogenases to the flavoprotein ubiquinone oxidoreductase (EC 1.5.5.1) from IMM, linking catabolism and respiratory chain (Henriques et al., 2021).

The two subunits do not have a high sequence homology (Roberts et al., 1996) and in my samples they were identified based on only three total peptides (Table 6-2). The same observation applies to the solute carrier family 25 (also known as the mitochondrial transporter family SLC25). The four possible members identified are all ADP/ATP translocases (Palmieri, 2013), they contain a similar signature motif of 20-30 aa (Palmieri, 2014), and were identified based on four total peptides.

Although I am aware that there are only three unique ‘Protein ID’ entries in my dataset, I decided to use the numbers given by the Mitocarta 3.0 identification to count the mitochondrial proteins. The peptides did not offer enough information to be assigned an irrefutable UniProt ID, and the proteins to which they were attributed belong to different mitochondria compartments. There are different possible scenarios explaining what I truly have in my trypsinized sample: it could be only one of the Mitocarta 3.0 proteins (in which case, which one?), all of them, or any random combination of isoforms. If I assume that all the Mitocarta 3.0 identified proteins are present in my sample, then, the numbers I have reported above are correct. If I assume that my sample contained less isoforms than the Mitocarta 3.0 search reported, then my total amount of mitochondrial proteins would decrease with an unknown number, but the numbers reported here would still be the maximum amount of mitochondrial proteins I could have in my data. Although it is unlikely that those hits are specific interactors

Table 6-2. NCL1 biotinylated proteins identified by multiple UniProt codes

Dataset entry #	UniProt ID	Name	Localization	Function	Peptides
1	Q13085	acetyl-CoA carboxylase 1	Matrix	Fatty acid synthesis	25
	O00763	acetyl-CoA carboxylase 2	OMM	Fatty acid oxidation	25
2	Q16134	electron transfer flavoprotein dehydrogenase EC 1.5.5.1	IMM	Glycine metabolism, Fatty acid oxidation	3
	P13804	electron transfer flavoprotein subunit alpha	Matrix	Glycine metabolism, Fatty acid oxidation	3
	P38117	electron transfer flavoprotein subunit beta	Matrix	Glycine metabolism, Fatty acid oxidation	3
3	P12235	solute carrier family 25 member 4	IMM	Small molecule transport	4
	P05141	solute carrier family 25 member 5	IMM	Small molecule transport	4
	Q9H0C2	solute carrier family 25 member 31	IMM	Small molecule transport	4
	P12236	solute carrier family 25 member 6	IMM	Small molecule transport	4

of C12orf65, because at least one of them truly exists in my samples, I considered that removing them would interfere with my results.

Regarding the mitochondrial hits involved in gene expression, I obtained five mitoribosomal proteins, the mtEF-Tu and the mtDNA Top1 (Table 6-3). The mitoribosomal proteins belonged to SSU as well as LSU and were bound to 12S and respectively 16S rRNA (Figure 6-6). The two proteins of the mtSSU (MRPS5 and AURKAIP1) appeared in all samples, including the COX8 control. Two of the mtLSU proteins (MRPL2 and MRPL15) appeared only in the C12orf65 clones, while MRPL34 appeared in the control as well. The mtDNA Top1 appeared in all samples including control, but mtEF-Tu lacked from C12-Linker samples.

Table 6-3. Biotinylated proteins from NCL1 involved in mitochondrial gene expression

COX8 control	C12-BioID2	CL12-Linker-BioID2	Function
Replication			
TOP1MT	TOP1MT	TOP1MT	mtDNA topoisomerase
Translation			
mtEF-TU	mtEF-TU	-	elongation factor Tu
MRPS5	MRPS5	MRPS5	28S protein
AURKAIP1	AURKAIP1	AURKAIP1	28S protein
-	MRPL2	MRPL2	39S protein
-	MRPL15	MRPL15	39S protein
MRPL34	MRPL34	MRPL34	39S protein

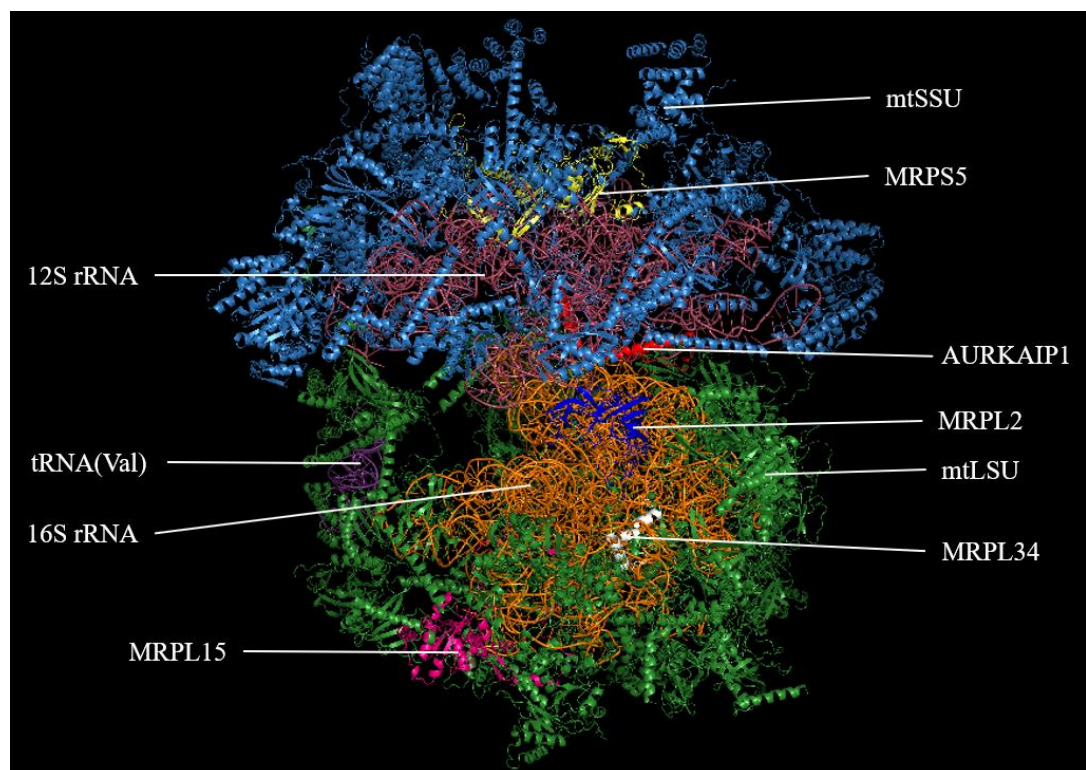


Figure 6-6. Biotinylated MRPs identified in NCL1

Structure of human mitochondrial ribosome (PDB entry 6zm5, (Itoh et al., 2021)) was imported in PyMOL Molecular Graphics System (Version 2.0 Schrödinger, LLC) and visualized as cartoon. The five MRPs identified by BioID2 were mapped on the structure by selecting their primary sequences and colouring it as: yellow (MRPS5), red (AURKAIP1), electric blue (MRPL2), white (MRPL34), magenta (MRPL15). mtSSU – sky blue (proteins), salmon (12S rRNA); mtLSU – forest green (proteins), orange (16S rRNA), dark purple (tRNA^{Val})

The studies from (Bogenhagen et al., 2018) show that MRPL15 is one of the earliest in the mtLSU assembly. It binds the 16S rRNA in the nucleoids, during rRNA processing (Bogenhagen et al., 2014) and, although appears at the surface of the mature mitoribosome, it maintains the extension inside the 16S rRNA. MRPL34, as an intermediary protein, binds to 16S rRNA in the regions that remain available after the binding of the early proteins. MRPL2 is a late assembly protein, despite the fact that it is deeply embedded in the 16S rRNA. (Bogenhagen et al., 2018) consider that the 16S rRNA is subjected to conformational changes caused by the early and late assembly proteins, changes that allow MRPL2 to bind.

Like MRPL15, MRPS5 is an early binding protein, but it does not interact with the 12S rRNA available immediately after transcription. The very first binding proteins are MRPS16, MRPS22, and MRPS18-2 (also named mS40), who bind the 5' domain of 12S rRNA, and MRPS34 and MRPS27, who bind the 3' domain of 12S rRNA. MRPS5 binds immediately after, it strongly interacts with MRPS22 and MRPS18-2, and links those very first proteins with the second set of early binding proteins (Bogenhagen et al., 2018). Like other early binding proteins, MRPS5 is present in the mitochondrial nucleoid and binds towards the SSU surface (Bogenhagen et al., 2014). In contrast, AURKAIP1 (also known as MRPS38) is a late assembly protein, that binds close to the interface with LSU (Bogenhagen et al., 2018) (Figure 6-7A).

Regarding the functions of the mitoribosomal hits, MRPL2 is part of the mitochondria-specific intersubunit bridges: it interacts with both 12S rRNA and with MRPS6. The positive residues Lys231 and Arg218 interact with the phosphate backbone of helices h24 and h23, respectively, while residues 171-174 interact with MRPS6 ((Amunts et al., 2015), Table S4 of the reference). MRPS5 forms the entry site of the mRNA channel (together with MRPS3), and provides positive (Arg189, Lys239, and Arg264) and aromatic (Phe229) residues that pave the channel (Amunts et al., 2015, Greber et al., 2015). Those residues are part of a specific mitochondrial extension of MRPS5 and are positioned between the entrance and the A site; they directly interact with the mRNA (Figure 6-7B), which they guide towards the A and P site (Kummer et al., 2018). MRPS5 has an important role in shaping the mRNA channel; the channel starts with a wide opening, but becomes narrower while the mRNA approaches the A site (Amunts et al., 2015, Kummer et al., 2018). AURKAIP1, MRPL34 and MRPL15 have not yet been assigned a specific role, other than being structural components of the 55S ribosome.

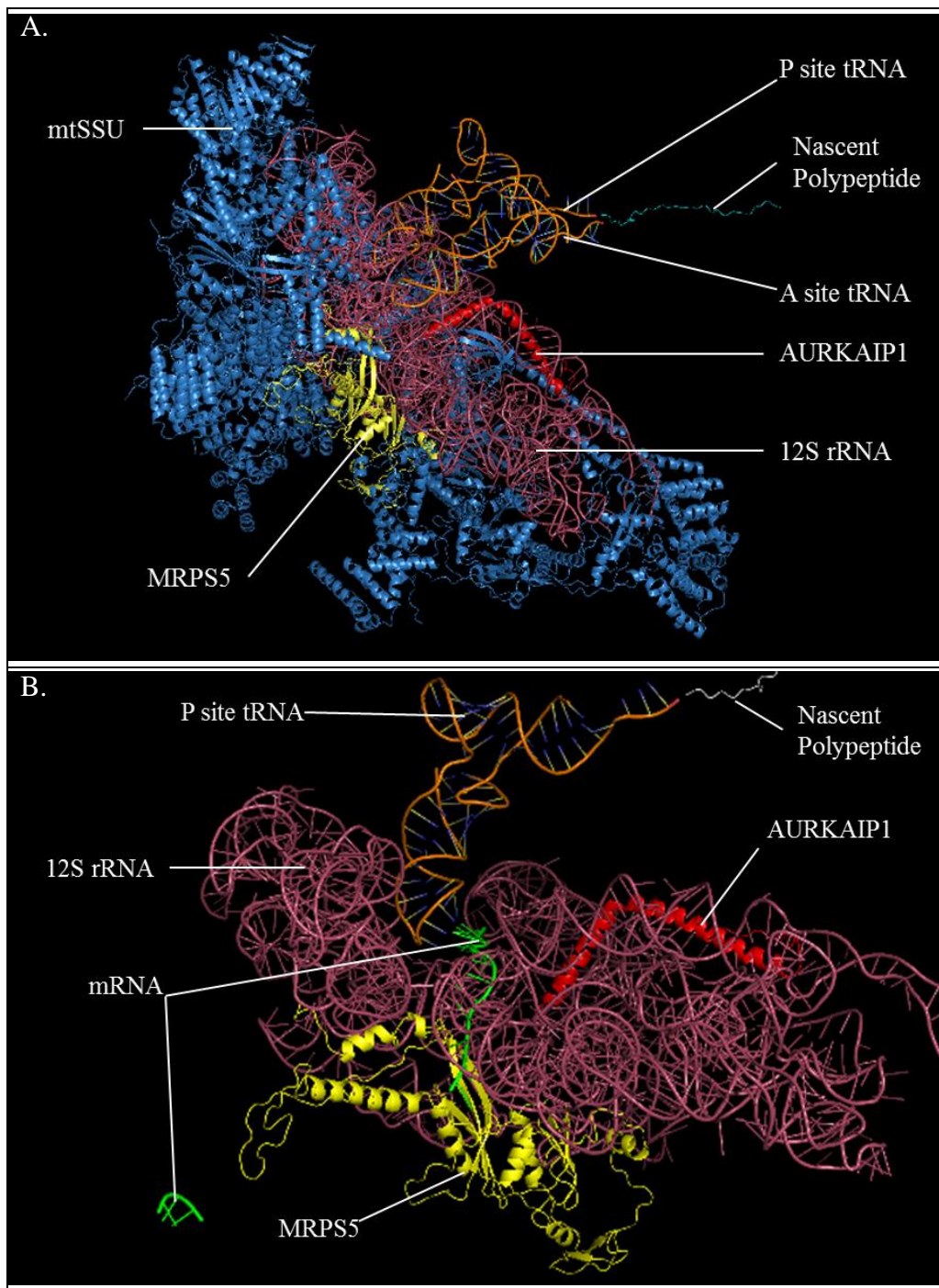


Figure 6-7. Localization of NCL1 hits on mtSSU

A. MRPS5 (yellow) and AURKAIP1 (red) both localize in proximity with P-site and A-site tRNA molecules, without interacting directly. MRPS5 is situated at the surface of mtLSU and interacts with other proteins (sky-blue), while AURKAIP1 is embedded in the 12S rRNA (salmon) and has reduced interaction with other proteins.

B. MRPS5 (yellow) binds mRNA (bright green) and guides it towards the P site tRNA. AURKAIP1 has no interaction with either mRNA or P-site tRNA. For figure clarity, A-site tRNA is not represented.

PDB entry 6zm5, (Itoh et al., 2021); figure made using the PyMOL software, visualized as cartoon

Although found in only one biological replicate, the hits involved in mitochondria gene expression, and, most importantly, the MRPs-constituted an encouraging result, that needed to be repeated. Finding mitoribosomal proteins among the hits aligns with the hypothesis that C12orf65 rescues stalled mitoribosomes. BioID2 studies transient or weak interactions that occur at various distances from C12orf65 (comprised in the biotinylation range), so I could not expect to obtain exactly the same translation hits in the same samples. But a repetition could clarify, for example, why mtEF-Tu is not present in the C12-Linker-BioID2 samples. It would be unlikely that a hit that appears in the C12-BioID2 samples does not appear in the Linker samples, because the biotinylation range increases in the Linker. A protein biotinylated by C12-BioID2, in theory, should be biotinylated by C12-Linker-BioID2 as well. As biotinylation happens in live cells, which are dynamic, the absence of mtEF-Tu could be due to chance: it simply was not at the right spot at the right time. But it could also be due to a less efficient mitochondria isolation.

6.2.3 Interactors identified in Nijmegen, the Netherlands

To clarify those aspects, and to increase the confidence of my hits, I repeated the BioID2 experiments in three biological replicates, of six samples each. For this, mitochondria isolation was performed in Newcastle, as described in 2.6.1, only from induced cells, with a pair of biotin-treated and non-treated samples obtained at the same time. Isolated mitochondria were sent on carbonic ice to Prof. Hans Spelbrink, collaborator from Radboud University in Nijmegen, the Netherlands. Here, as part of the secondment required by the Marie Curie ITN REMIX programme, I performed the streptavidin-pull down and mass-spectrometry analysis. His lab offered me the expertise in BioID experiments combined with an excellent mass-spectrometry facility. As the proteomics approach was similar (bottom-up, Orbitrap mass-spectrometer, the same software used for data acquisition and processing), I could compare the hits found in Nijmegen with the ones found in Newcastle.

All samples were kept at -80°C until needed for lysis. The pull-down experiments were performed three times, once for each biological repeat (COX8-MTS-BioID2 induced +/- biotin, C12-BioID2 induced +/- biotin, C12-Linker-BioID2 induced +/- biotin). There were only minor differences between the pull-down effectuated in Newcastle and the one effectuated in Nijmegen. For example, in Nijmegen, I was allowed to use Triton X-100 and do less washes than in Newcastle (2.6.3). After the washes, the beads and the proteins attached to them were resuspended in 8 M urea prepared in 50 mM ammonium bicarbonate and kept at -80°C until

digestion. In order to ensure identical conditions, all the 18 samples were digested at the same time. For optimal digestion, in Nijmegen I performed an additional pre-digestion with Lysyl endopeptidase C prior to addition of trypsin.

After digestion, I cleaned the samples from detergent and salts and concentrated them using the STAGE tips' technique (Rappsilber et al., 2003), in parallel with my colleague Alisa Potter. The 96-well plate used to deliver the samples to the mass-spectrometer was prepared by Alisa Potter, who used her samples on the same plate, so that my samples and her samples play the role of additional control for each other. Alisa was also the one who prepared the blank, BSA standard and C18 resin column, under the supervision of Dr. Alfredo Cabrera Orefice, who also did the peptide analysis.

Data analysis was performed in MaxQuant version 1.5.0.25, against the human reference proteome. First, I applied the filtering steps 1-4 described at 6.2.2. Because my samples were in triplicate, I worked with LFQ intensities and I applied a criterion of 70% minim valid values. The results obtained were disappointing: a total of 10 proteins, with only the carboxylases to represent mitochondrial proteins (Table 6-4).

Table 6-4. Biotinylated proteins identified in Nijmegen

Nº	UniProt ID	Name	Localization	Peptides
1	P05165	Propionyl-CoA carboxylase alpha chain, mitochondrial	mitochondrial matrix	51
2	P10412	Histone H1.4	nucleus	10
3	P11498	Pyruvate carboxylase, mitochondrial	mitochondrial matrix	57
4	P62241	40S ribosomal protein S8	80S ribosome	5
5	P62750	60S ribosomal protein L23a	80S ribosome	8
6	P81605	Dermcidin	secreted	3
7	Q02878	60S ribosomal protein L6	80S ribosome	14
8	Q86UE4	Protein LYRIC	ER	16
9	Q96RQ3	Methyl-crotonyl-CoA carboxylase subunit alpha, mitochondrial	mitochondrial matrix	34
10	Q9NWB6	Arginine and glutamate-rich protein 1	nucleus	6

I therefore proceeded to identifying the cause of those negative results. The fact that I was able to pull down endogenously biotinylated proteins proves that technically the affinity purification worked: the streptavidin coated beads bound biotinylated proteins. I ruled out any technical

issue with the mass-spectrometer, because Alisa's samples gave good results, and the BSA standard looked fine (Figure Apx 6).

Loosing sample during detergent removal and STAGE tips was plausible, but not for all 18 samples. The technique can be visually assessed by the presence of a white precipitate, which occurred in my samples. Western blot showed a low HA expression in the input, for all samples, which could suggest low biotinylation efficiency. However, this could not be correlated with the streptavidin-HRP signal: in some samples a smear is present even if the HA signal cannot be detected (Figure 6-8).

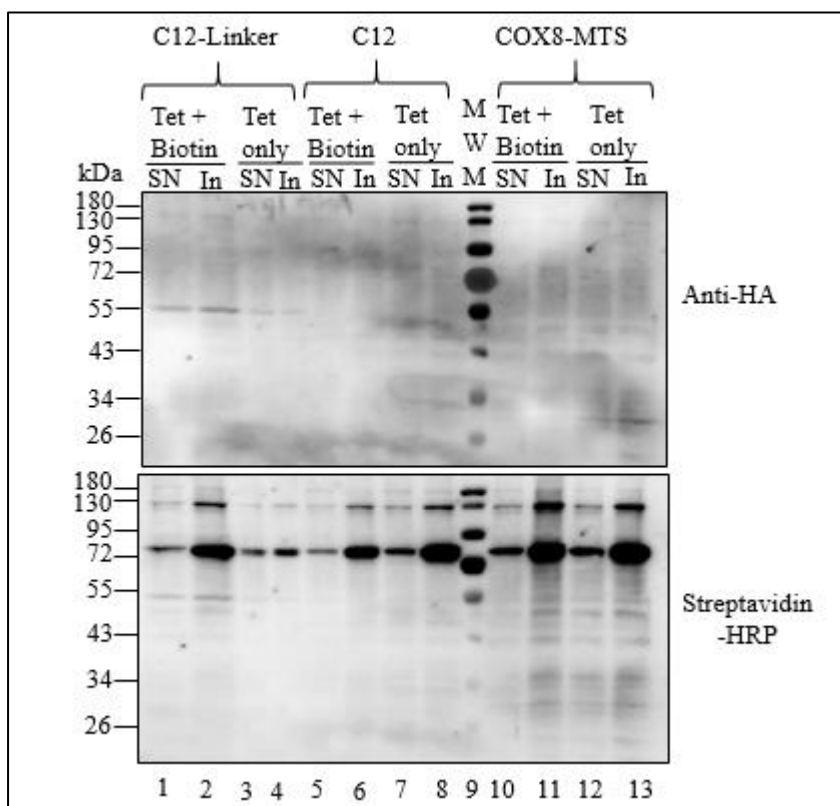


Figure 6-8. Western blot results for the Nijmegen affinity purification

COX8-MTS, C12 and C12-Linker- BioID2-HA cells were induced (1 μ g/ml tetracycline) and treated with biotin (50 μ M, 16 h). Mitochondria were isolated, then lysed and incubated with streptavidin beads. The input (In) and supernatant (SN) were analysed by SDS-PAGE, using streptavidin-HRP to detect biotinylation and anti HA to detect protein expression. Approx. 10 μ g/well; 10% resolving gel; representative image of 3 biological replicates

There was still the possibility that trypsinization was inefficient and the biotinylated proteins had remained on the beads. To test this, I resuspended 10% of the beads in 20 μ l of Laemmeli buffer with 1% beta-mercaptoethanol, boiled at 95°C for 10 min, then used the supernatant for

SDS-PAGE. The results showed no streptavidin-HRP signal (Figure Apx 5). If proteins remained undigested on the beads, I should have seen a smear or at least some bands at the top of the membrane, corresponding to endogenous carboxylases. But the lack of streptavidin-HRP signal from the beads, together with the presence of mitochondrial carboxylases in the hits, suggest that trypsinization was not defective.

There were two main issues which could be addressed:

1. Increasing the starting material
2. Increasing the volume of beads suspension used for pull-down

After returning to Newcastle, I repeated the BioID2 experiments using more starting material and a double volume of streptavidin beads per sample (100 μ l).

6.2.4 Interactors identified in Newcastle using an improved methodology

The final round of mass-spectrometry experiments that took place in Newcastle (from here onwards, named NCL2) comprised two biological replicates of six samples each: COX8-MTS-BioID2 induced +/- biotin, C12-BioID2 induced +/- biotin, C12-Linker-BioID2 induced +/- biotin. To increase the amount of starting material, I used a different type of flask for culture (Nunc TripleFlask), with an increased surface (500 cm^2) and a better cell adherence. Two such flasks were used for mitochondria isolation for one sample. Mitochondria isolation and streptavidin-pull down were performed as described in 2.6.1 and 2.6.2, with the exception that I used 100 μ l beads/sample.

The input and unbound were investigated by SDS-PAGE, and showed HA expression in all samples, as well as a biotinylation smear in the induced and biotinylated input samples (Figure 6-9, lanes 3, 8 and 12). The smear disappears in the supernatant, suggesting that the biotinylated proteins bound the streptavidin beads. The two intense bands at the top of the membranes, identified with the streptavidin-HRP, are the endogenous carboxylases identified in the previous experiments.

Dr. Akshada Gajbhiye (Prof. Matthias Trost group) was the specialist who performed the data acquisition and analysis for my samples. She helped optimize the experiment by using a lower Automatic Gain Control (AGC) target for MS (5E3 compared to 1E6) and a higher separation time on linear gradient during HPLC compared to the parameters used in Nijmegen (180 min at 300 nL/min instead of 30 min at 300 nL/min). This increased the peptide detection.

Identification of proteins and filtering of false positives was performed as described in 6.2.2. To investigate the self-biotinylation, the search included the amino acid sequence of *A. aeolicus* biotin ligase in addition to the human Uniprot Swisprot Database. Each sample group (control, C12-BioID2 or C12-Linker-BioID2) was analysed separately, using the log₂ LFQ intensity values from the duplicate measurements, with minimum two valid values per group.

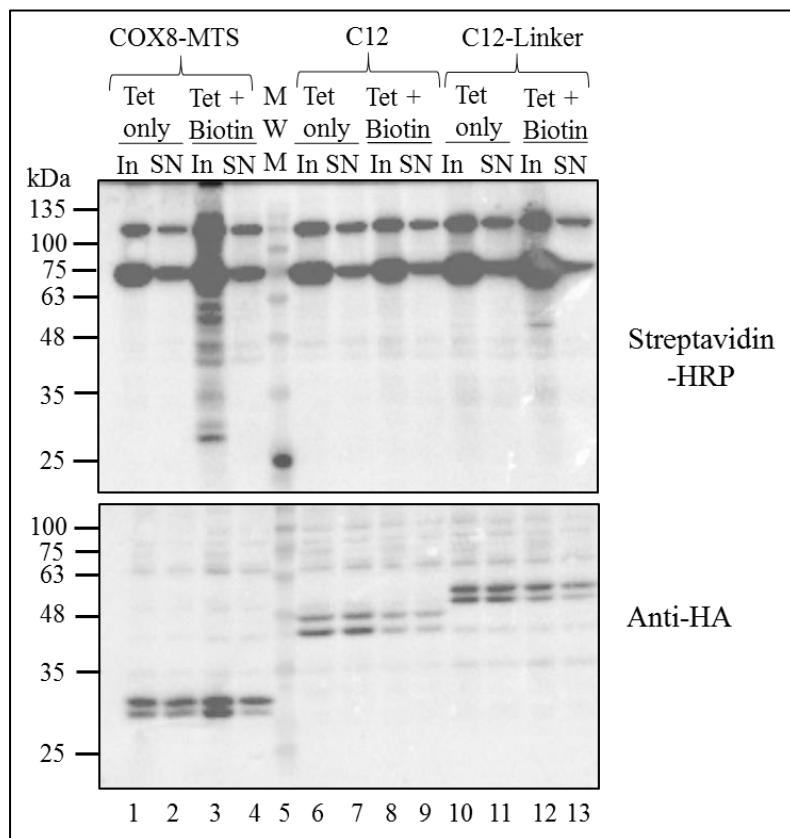


Figure 6-9. Western blot results for NCL2 affinity purification

Mitochondria isolated from COX8-MTS, C12 and C12-Linker- BioID2-HA clones were lysed and incubated with streptavidin beads. The input (In) and supernatant (SN) were analysed by SDS-PAGE, using streptavidin-HRP to detect biotinylation and anti-HA to detect protein expression. For induction was used 1 µg/ml tetracycline with or without 50 µM biotin (16 h).

Approx. 30 µg/well; 10% resolving gel; representative image of 2 biological replicates

For COX8-MTS I obtained 141 hits (including the bacterial biotin-ligase), the lowest number when compared to C12 and C12-Linker samples. Of the total number, 39% (56 hits) were mitochondrial proteins, as assigned after Mitocarta 3.0 filtering (Figure 6-10A, Table Apx 12 from Appendix-E). One third of total hits were either involved in cytoplasmic translation or had ER-related functions (Table Apx 13), and less than a third (27%) were hits non-related to mitochondria (including the bacterial biotin-ligase, histones, cytoskeleton proteins and

glycolytic enzymes). As seen for NCL1, there were five instances where the two isoforms of the same protein could not be distinguished, so both isoforms appeared as hits in my dataset- (Appendix-C, Table Apx 7). The majority of mitochondrial hits belong to the matrix compartment (32 hits, 57%) and IMM (15 hits, 27%) (Figure 6-10B). Three hits (5%) are found in OMM (VDAC1, VDAC2 and acetyl-CoA carboxylase 2) and four hits (7%) in the IMS (peroxiredoxin 4, PNPT1 and Ca-binding protein carrier Aralar 1 and 2). Two hits (4%) did not have an assigned mitochondrial compartment: SND1 endonuclease and HSD17B4. Both have primarily non-mitochondrial functions-SND1 is involved in RNA silencing in cancer (Tsuchiya et al., 2007), while HSD17B4 is an enzyme mainly associated with fatty acids catabolism in the peroxisome (Ferdinandusse et al., 2004).

In terms of functions, COX8-MTS hits were diverse: the majority were involved in lipid (20%), amino acid metabolism (12%) and TCA (9%) (Figure 6-10C). A percentage of 14% effectuate transport of small molecules, like calcium or ADP/ATP, and 11% are either OXPHOS subunits (RC III and V) or OXPHOS assembly factors. Four proteins (7%) were grouped as ‘other’ functions – peroxiredoxin 4, stress-70 protein, MIC60 and SND1. Peroxiredoxin 4 is responsible for ROS detoxification, (Tavender and Bulleid, 2010), while stress-70 protein (also known as mortalin, encoded by *Hspa9* gene) is involved in Fe-S cluster biosynthesis (Shan and Cortopassi, 2016). MIC60 is a MICOS complex subunit with a role in cristae maintenance (Ott et al., 2015).

There were few proteins involved in mitochondrial gene expression comparing to the total number of hits: four proteins involved in translation (7%) and four proteins (7%) involved in replication and transcription. The proteins involved in translation were mtEF-Tu, serine-tRNA ligase, isoleucine-tRNA ligase and MRPL34 (Table 6-5). The pull-down of the first three proteins is not surprising; as they are all soluble in the mitochondria matrix, they could have been non-specifically biotinylated by the biotin-ligase targeted to this compartment. Identification of MRPL34 is surprising relative to the protein position in the mitoribosome- it is strongly associated with the 16S rRNA in the mtLSU, not exposed to the surface. The other hits involved in gene expression are the mitochondrial Top1, TFAM, PNPT1 (also known as PNPase1) and SHMT2. PNPT1 is involved in 3' processing and polyadenylation of mt- mRNA molecules (Piwowarski et al., 2003) (Slomovic and Schuster, 2008). SHMT2 is also involved in tRNA modification: by using the cofactor 10-formyl tetrahydrofolate (THF), it produces formyl methionyl-tRNA molecules required for translation initiation (Minton et al., 2018, Morscher et al., 2018).

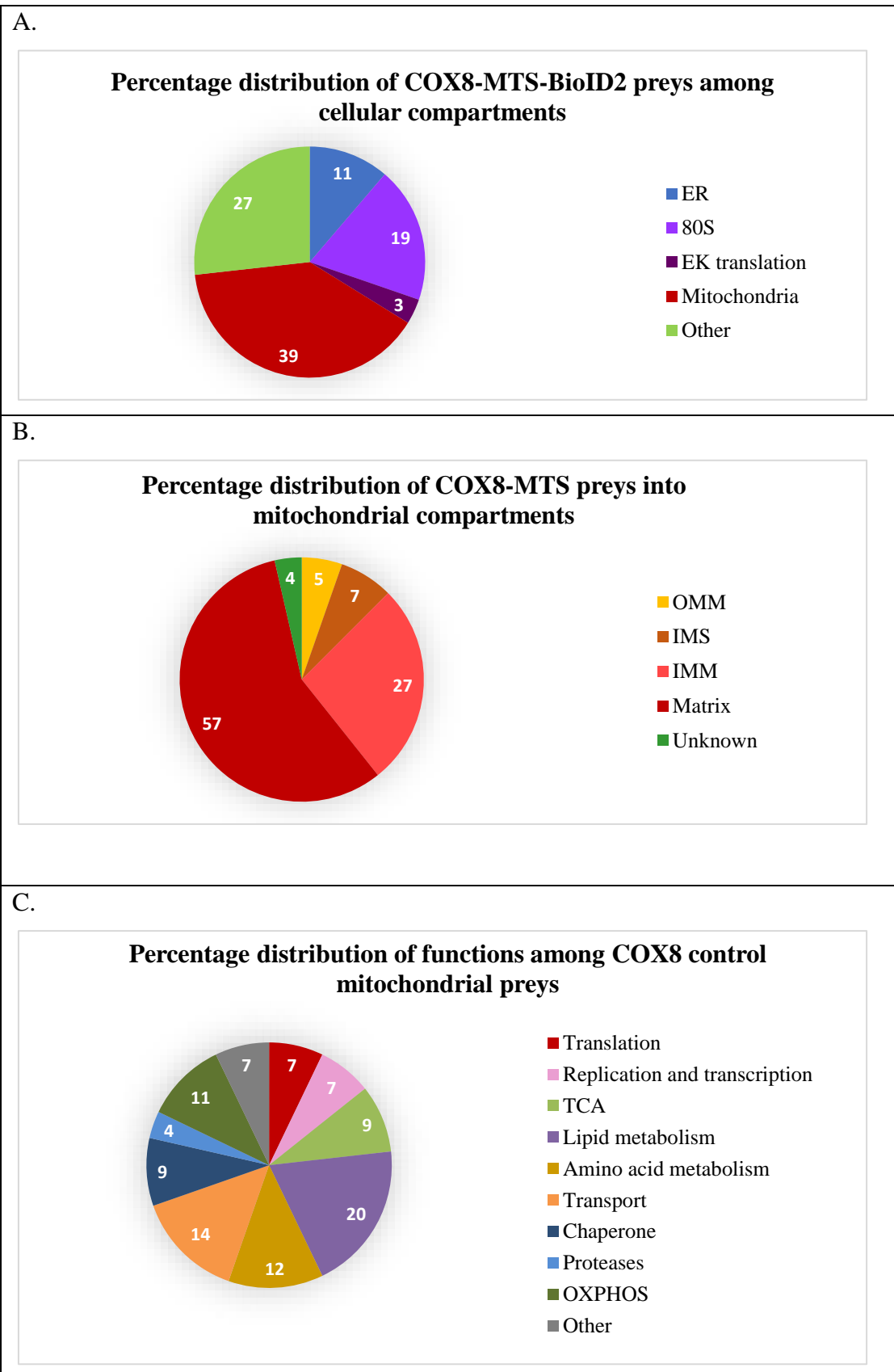


Figure 6-10. Analysis of COX8-MTS-BioID2-HA interactors identified in NCL2

Venn diagrams summarizing cellular (A) and mitochondrial (B) distribution of biotinylated proteins obtained for COX8-MTS control. (C) summarizes the proteins functions. N=2

Table 6-5. Biotinylated proteins from NCL2 involved in mitochondrial gene expression

COX8-MTS control	C12-BioID2	CL12-Linker-BioID2	Function
Replication			
TOP1MT	TOP1MT	TOP1MT	mtDNA topoisomerase
		POLDIP2	Associates with mtSSB and TFAM
Transcription, RNA processing and modification			
PNPT1	PNPT1	PNPT1	mtRNA stability and decay
SHMT2	SHMT2	SHMT2	Formyl methionyl-tRNA synthesis
-	HSD17B10	HSD17B10	Cleaves tRNA at 5' end part of ribonuclease P complex
-	LRPPRC	LRPPRC	3' polyadenylation of mRNA delivery of mRNA to 55S
-	-	TRMT10C	tRNA N1-methyltransferase methylation of MT-ND5 mRNA part of ribonuclease P complex
-	-	DHX30	ATP-dependent RNA helicase (LSU assembly)
TFAM	-	-	Transcription factor A
Translation			
mtEF-Tu	mtEF-Tu	mtEF-Tu	Elongation factor Tu
-	-	MRPS9	28S protein
-	-	MRPS23	28S protein
-	-	MRPS28	28S protein
-	MRPS31	MRPS31	28S protein
-	MRPL15	MRPL15	39S protein
MRPL34	MRPL34	MRPL34	39S protein
-	ATAD3A/ ATAD3B	ATAD3A/ ATAD3B	Interactor of mtDNA, mRNA and 39S
SARS2	SARS2	SARS2	Serine-tRNA ligase
IARS2	IARS2	IARS2	Isoleucine-tRNA ligase
-	-	AARS2	Alanine-tRNA ligase
-	-	TARS2	Threonine-tRNA ligase

For C12-BioID2 I obtained 162 hits (including the bacterial biotin-ligase) with 62 of them (38%) attributed to mitochondria by Mitocarta 3.0 (Figure 6-11A and Appendix-E, Table Apx 14). C12orf65 was not identified. The amount of proteins likely associated with mitochondria (cytosolic ribosomes, cytosolic translation and ER) was similar to the one from the COX8 control (one third of total hits, Table Apx 15). There was a small difference in the ratio between ER and 80S proteins: in C12-BioID2 there are slightly more ER proteins than 80S proteins (16% vs. 15%), while in the control is the other way around (19% 80S vs. 11% ER). The percentage of proteins non-associated with mitochondria is identical with the one from control (27%). This suggests the existence of a minimal background for the BioID2 experiments, present because the bacterial biotin- ligase was not affected by the fusion with C12orf65.

Of the mitochondrial proteins, 35 (57%) were localized to the matrix, followed by 18 (29%) localized in the IMM (Figure 6-11B). Four hits localized to OMM (6%): three already identified in the control (VDAC1, VDAC2, acetyl-CoA carboxylase 2) and one clone-specific (NADH-cytochrome b5 reductase 3). IMS was represented by three hits (3%)- peroxiredoxin 4, PNPT1 (also identified in the control) and adenylate kinase 2. NADH-cytochrome b5 reductase 3 (CYB5R3) is involved in synthesis of fatty acids and cholesterol (de Cabo et al., 2009), while adenylate kinase 2 (AK2) catalyses the transfer of phosphate group between ATP and AMP and *vice versa* (Bruns and Regina, 1977). Two hits could not be categorized ('Unknown', 2%): SND1 and HSD17B4, the same hits present in the control. Like in the control, there were five hits which could not be uniquely identified, as they could belong to two different isoforms of the same enzyme (Appendix-E, Table Apx 8). Three of them appeared in the control (acetyl-CoA carboxylase, glutamate-dehydrogenase and ADP/ATP translocase) but two were specific for C12-BioID2: ATAD3A/ATAD3B and pyruvate-dehydrogenase. ATAD3 (ATPase family AAA domain-containing protein 3) has three isoforms: ATAD3A, ATAD3B and ATAD3C (Desai et al., 2017b). Only isoforms A and B appeared in my C12-BioID2 and C12-Linker-BioID2 samples (Table Apx 14 and Table Apx 16). ATAD3A is associated with IMM and mitochondrial nucleoids, where it binds the D-loop of mtDNA and possibly contributes to segregation of nucleoids (He et al., 2007). A later study showed that ATAD3A interacts with mt-mRNA and the mitoribosome, with preference for the 39S subunit (He et al., 2012). I therefore counted it among the translation-involved hits. ATAD3B is a mitochondrial protein specific to human embryonic stem cells as well as cancer cells that suppresses ATAD3A function. By forming hetero-oligomers with ATAD3A, ATAD3B reduces ATAD3A interaction with the mitochondrial nucleoid (Merle et al., 2012).

There were twice more mitochondrial hits involved in translation for C12-BioID2 compared to the control (13% vs. 7%, Figure 6-11C), while the percentage of hits involved in replication and transcription remained the same (7%). The percentage of OXPHOS was also identical (11%), and it included subunits of complexes III, IV and V as well as AIF (apoptosis-inducing factor) who, apart from its role in apoptosis, participates in the assembly of complex I (Modjtahedi and Kroemer, 2016). One third of hits were involved in lipid metabolism, amino acid metabolism

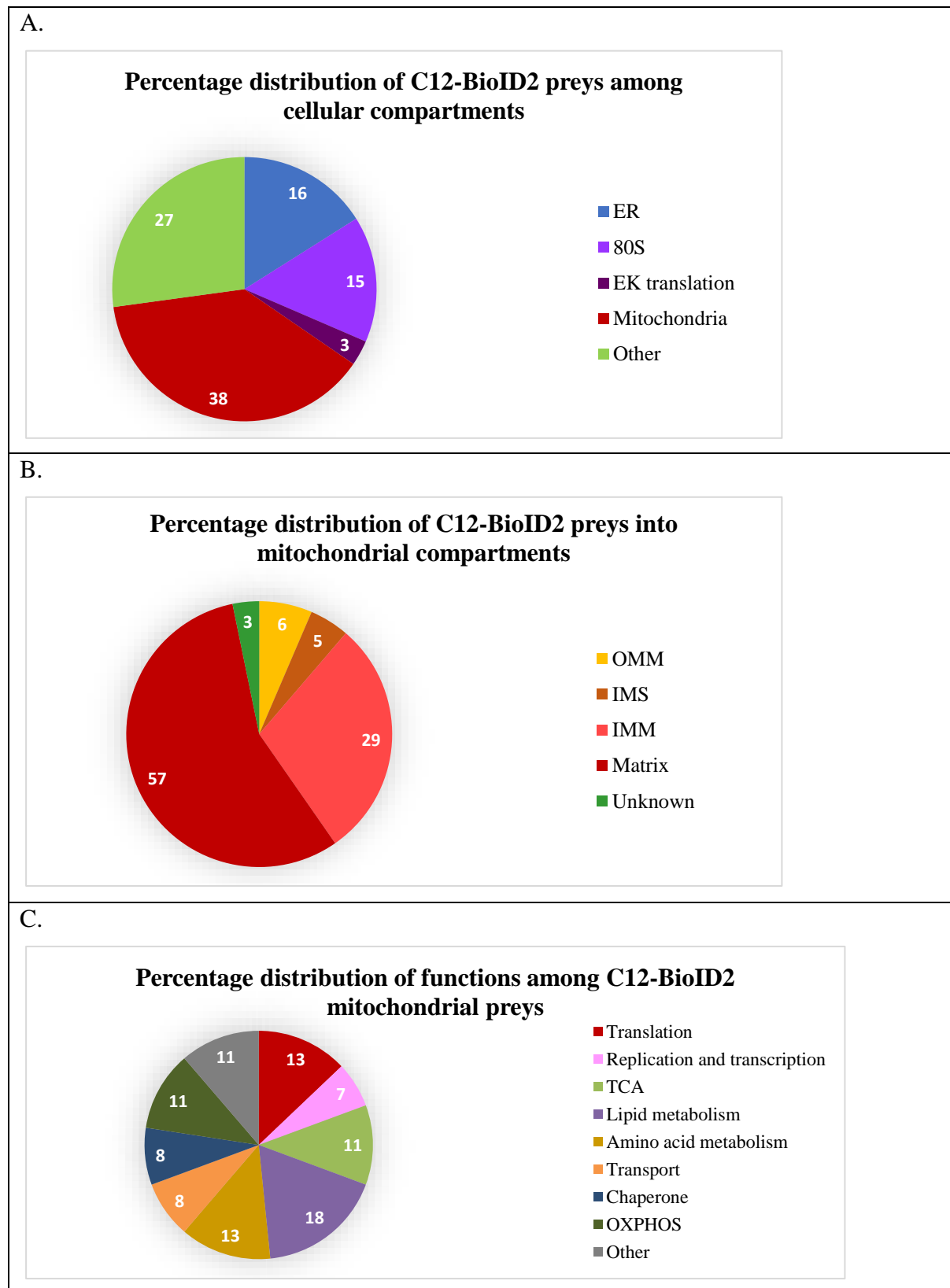


Figure 6-11. Analysis of C12orf65-BioID2-HA interactors identified in NCL2

Venn diagrams summarizing cellular (A) and mitochondrial (B) distribution of biotinylated proteins obtained for C12orf65-BioID2-HA samples. (C) summarizes the proteins functions. N=2

and TCA cycle, similar to what was noticed in the control. Those included the endogenous mitochondrial carboxylases described at 6.2.1. There were less proteins involved in transport compared to the control (8% vs. 14%), and only one protease identified (PMPCB, mitochondrial processing peptidase subunit beta). This protease was grouped as ‘Other’, together with other singular hits which function could not be assigned to any of the other types. Three of the ‘Other’ hits appeared in the control (peroxiredoxin, stress-70 protein and MIC60) but two were specific to C12-BioID2: MTHFD1L and AK2. MTHFD1L (monofunctional C1-tetrahydrofolatesynthase) is an enzyme of the one-carbon metabolism that synthesizes 10-formyl-THF (Walkup and Appling, 2005), the cofactor required by SHMT2 to produce formyl methionyl-tRNA (Minton et al., 2018). AK2 (adenylate kinase 2) is the IMS enzyme responsible for ATP/AMP phosphorylation (Bruns and Regina, 1977).

The hits involved in gene expression contained some C12-BioID2 specific proteins as well as proteins already encountered in the COX8 control. The common ones were the mitochondrial Top1, PNPT1 and SHMT2. The two specific hits were HSD17B10 and LRPPRC. TFAM, identified in the control, was not present in the C12orf65-BioID2 hits (Table 6-5).

HSD17B10 (3-hydroxyacyl-CoA dehydrogenase type-2, also named SDR5C1) is a protein with dual function, catalytic and non-catalytic, involved in tRNA processing and maturation. As part of the RNase P complex, it cleaves the 5' end of tRNA molecules (Holzmann et al., 2008). As part of MRPP1-MRPP2, a subcomplex of RNase P, it catalyses the methylation of tRNA molecules (m1G9 and m1A9) (Vilardo et al., 2012, Vilardo et al., 2018). The MRPP1-MRPP2 subcomplex was also found to serve as a platform for tRNA maturation: after the 5' end of tRNA is cleaved, the subcomplex remains attached to the tRNA, facilitating the removal of the 3' end by the RNase Z (ELAC2) and the subsequent addition of 3'-CCA by the nucleotidyl transferase TRNT1 (Reinhard et al., 2017).

LRPPRC is a pentatricopeptide repeat (PPR) motif-containing protein that was initially known to bind nuclear mRNA, but (Mili and Piñol-Roma, 2003) showed that the majority binds mitochondrial mRNA molecules. (Sterky et al., 2010) identified a unique isoform, mitochondrial specific, with a targeting signal that is cleaved when it enters the organelle. Mitochondrial LRPPRC acts in complex with SLIRP (Sasarman et al., 2010, Spåhr et al., 2016) to inhibit the 3' degradation of mRNA and promote the 3' polyadenylation by the mtPAP enzyme (Chujo et al., 2012). LRPPRC/SLIRP is RNA-dependent (Ruzzene et al., 2012), with specific binding sites in mRNA and 16S rRNA, but not in tRNA, possibly because it

disrupts mRNA secondary structures (Siira et al., 2017). Recently, cryo-EM experiments with translating human mitoribosomes showed that LRPPRC/SLIRP is associated with the mtSSU via an interaction with MRPS39 (PTCD3), a mitoribosomal protein that also contains a pentatricopeptide repeat (Aibara et al., 2020). For my results, I classified LRPPRC in the RNA processing group, because it is not strictly restricted to translation.

The C12-BioID2 hits that I classified as ‘translation’ were all directly implicated in translation: mitoribosomal proteins, amino acyl-tRNA ligases or mtEF-Tu. There were four hits common with the control -EF-Tu, MRPL34, serine-tRNA ligase and isoleucine-tRNA ligase- and three specific to C12-BioID2: MRPS31, MRPL15 and ATAD3, a 39S interactor from IMM (He et al., 2007).

MRPL15 and MRPL34 are both part of mtLSU, which they join at different time points during assembly. MRPL15 is an early protein, that binds directly to 16S rRNA (Bogenhagen et al., 2018). It is a relatively large protein (33 kDa) that protrudes towards the edge of the LSU, opposite from the SSU interface (Figure 6-12). In contrast, MRPL34 is an intermediary binding protein, three times smaller than MRPL15 (10 kDa) (Bogenhagen et al., 2018). None of the two proteins had been assigned a particular function within the mitoribosome.

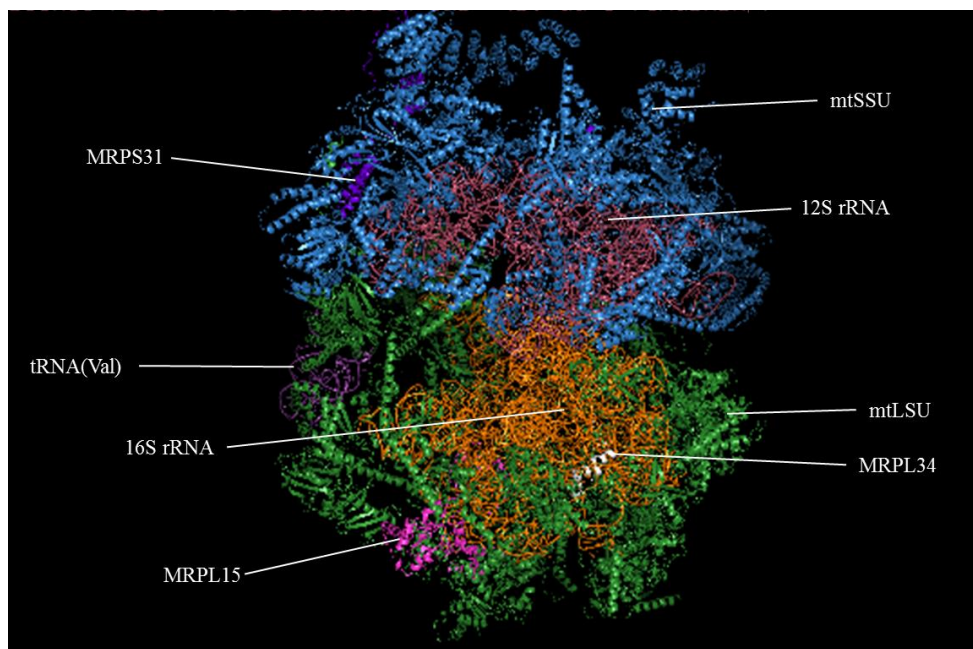


Figure 6-12. Biotinylated MRPs identified in C12orf65-BioID2-HA (NCL2) samples

The structure of human mitochondrial ribosome PDB entry 6zm5, (Itoh et al., 2021) was visualized in PyMOL. The three hits were coloured as it follows: MRPS31- bright blue purple; MRPL15- magenta; MRPL34-white; mtSSU – sky blue (protein) and salmon (12S rRNA); mtLSU – forest green (protein), orange (16S rRNA) and purple (tRNA(Val))

MRPS31 was the only mtSSU hit identified for C12-BioID2. It binds early during the subunit assembly but lacks any interaction with 12S rRNA, its assembly being mediated by MRPS7, MRPS29 and MRPS9. It is a large protein (45 kDa), exposed to the surface of the subunit (Figure 6-12), with no function assigned so far, apart from participating in the mitoribosome structure.

The C12-Linker-BioID2 samples delivered the highest amount of total hits (221, including the bacterial biotin-ligase) and the highest amount of mitochondrial proteins (93, 42%) identified by Mitocarta 3.0 filtering. Less than a third of total hits (29%) are part of the ER, 80S ribosome or cytosolic translation, lower than what was found for the control (33%) and for C12-BioID2 (34%). The hits not related to mitochondria were slightly increased (29%, compared to 27% in the control and C12-BioID2) (Figure 6-13A). As described for the previous clones and for the NCL1 experiment, there were examples of proteins from C12-Linker-BioID2 dataset which were attributed two UniProt codes, because there was not enough information to distinguish between two isoforms of the same protein. The six such hits were already found in control and C12-BioID2 clones, with no duplicate specific for C12-Linker (Table Apx 9).

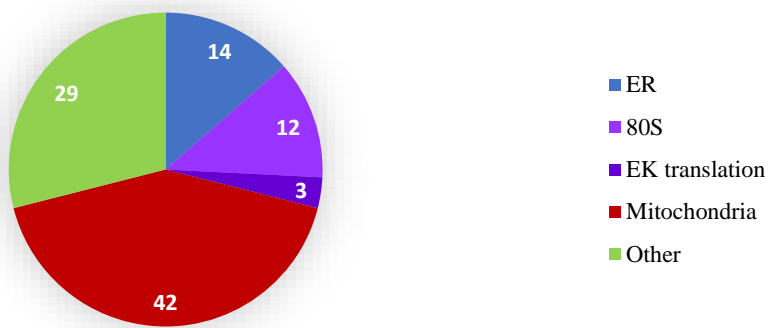
Of the mitochondrial proteins, 55 (60%) were localized to the matrix, the highest number among all clones (Figure 6-13B). This is what was expected, because the increase of biotinylation range provided by the linker allows more proteins to be biotinylated. Surprisingly, C12orf65 was still not present among them, which suggests there is an issue with the bait itself rather than a defect of the biotin-ligase. The second largest group contained proteins localized to IMM (25 hits, 27%), followed by OMM (6 hits, 6%) and IMS (4 hits, 4%). Two hits were listed in Mitocarta 3.0, but not assigned a mitochondrial compartment: SND1 and HSD17B4, present both in the control and C12-BioID2. OMM hits contained the same hits found in control and C12-BioID2 (VDAC1, VDAC2, acetyl-CoA carboxylase 2, CYB5R3) with two C12-Linker specific additions: TOM70 and AKAP1. AKAP1 (A-kinase anchoring protein 1) anchors the protein kinase A to OMM. The IMS hits have all been previously identified in both control and C12-BioID2 (peroxiredoxin 4, Ca-binding protein carrier Aralar 1 and 2) or in C12-bioID2 only (AK2).

The functions of C12-Linker-BioID2 mitochondrial hits were more diverse than those observed without the linker (Figure 6-13C). For example, it was the first time that translocases were identified: TOM70, TIM44 and TIM50. Also, the percentage of proteins with unique functions ('other') was the lowest (6%). They included proteins identified in the COX8 control

(peroxiredoxin 4, stress-70 protein and MIC60), proteins identified in C12-BioID2. (tetrahydrofolate synthase MTHFD1L, AK2) but also a linker specific hit: AKAP1.

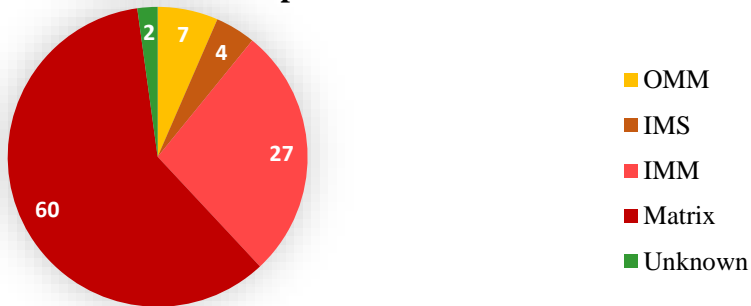
A.

Percentage distribution of C12-Linker-BioID2 preys among cellular compartments



B.

Percentage distribution of C12-Linker-BioID2 preys into mitochondrial compartments



C.

Percentage distribution of functions among C12-Linker-BioID2 mitochondrial preys

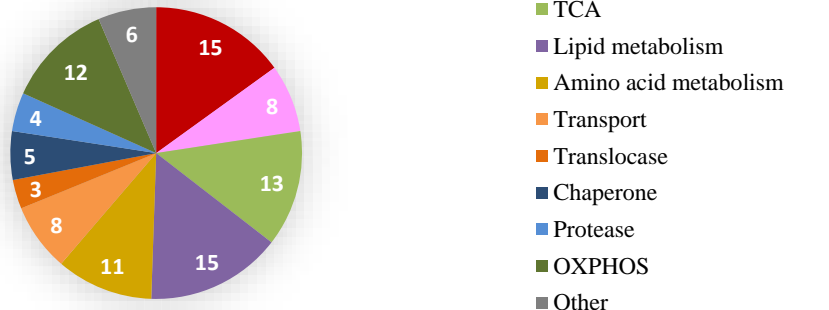


Figure 6-13. Analysis of C12orf65-Linker-BioID2-HA interactors identified in NCL2

Venn diagrams summarizing cellular (A) and mitochondrial (B) distribution of biotinylated proteins obtained for C12orf65-Linker-BioID2-HA samples. (C) summarizes the proteins functions. N=2

A positive aspect was the identification of the highest percentage of hits involved in translation (15%) more than double of what was noticed for the control (7%). There was also a small increase in the percentage of hits involved in replication and transcription (8% vs. 7% in the control), with some uniquely identified in the linker samples.

Two hits were involved in mtDNA replication: Top1 (identified both in the control and C12-BioID2) and POLDIP2 (polymerase delta-interacting protein 2) (Table 6-5). POLDIP2, unique for the linker samples, was initially known as binding partner of polymerase delta (nucleus), but was shown to reside in the mitochondrial matrix, where it associates with nucleoid components like mtSSB and TFAM (Cheng et al., 2005).

The hits involved in transcription and RNA maturation included PNPT1, involved in mRNA stability, and SHMT2, responsible for synthesis of formyl methionyl-tRNA. As both appeared in control and C12-BioID2, it is not surprising to find them among the C12-Linker hits. LRPPRC and HSD17B10, present only in C12-BioID2, were also identified, but without LRPPRC binding partner SLIRP.

Two hits appeared only in the C12-Linker dataset: TRMT10C and DHX30. TRMT10C is part of RNase P, like HSD17B10 identified in C12-BioID2. Rather than having nuclease activity, TRMT10C acts as N1-methyltransferase for mt-tRNA molecules (Holzmann et al., 2008, Metodiev et al., 2016) and for ND5 mRNA (Safra et al., 2017). Methylation of tRNA at position 9 is required for the correct formation of tRNA tertiary structure (Helm et al., 1998), while methylation of ND5 mRNA inhibits its translation (Safra et al., 2017). Absence of TRMT10C and HSD17B10 from the control suggests a possible interaction between C12orf65 and RNase P complex. DHX30 is an RNA-dependent helicase initially identified in the nucleoid (Wang and Bogenhagen, 2006) and later attributed to the mitochondrial RNA granules, where they play a role in the mitoribosome assembly (Antonicka and Shoubridge, 2015).

In terms of translation, C12-Linker hits were more abundant in MRPs compared to what was observed for control and C12 samples. The difference was not made by the mtLSU proteins, but by the mtSSU (Figure 6-14A). The mtLSU proteins identified were MRPL34 and MRPL15 (Table 6-5) which have been found in the control and respectively C12-BioID2. The fact that MRPL15 did not appear in the control increases the possibility to be a C12orf65 interactor. The functionality of this interaction is unknown, as the cryo-EM structures of 55S available so far do not describe a specific role for MRPL15.

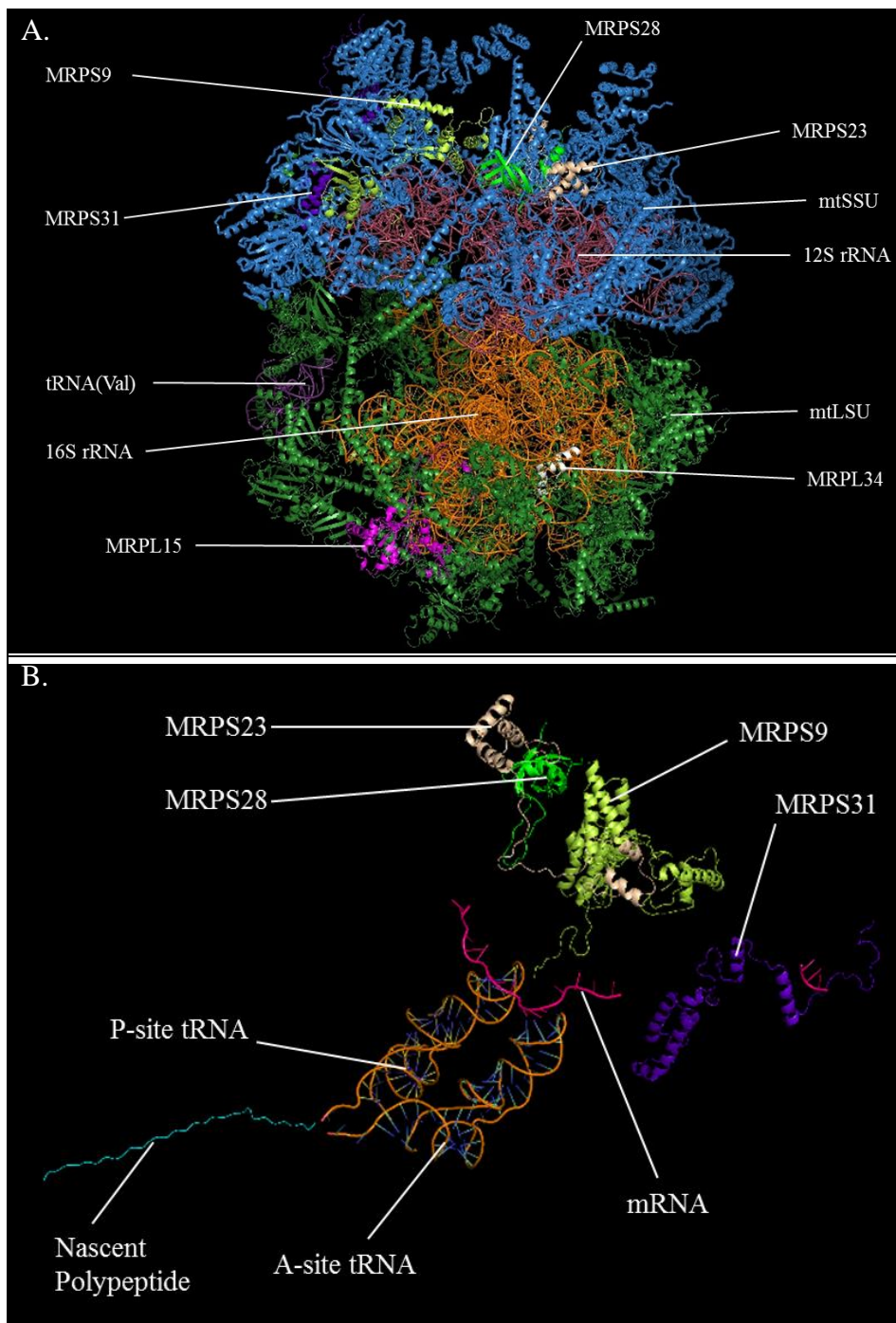


Figure 6-14. Biotinylated MRPs identified for C12orf65-Linker-BioID2-HA (NCL2)

A. BioID2 experiments using C12orf65-Linker-BioID2-HA HEK cells identified four hits in mtSSU: MRPS31 (bright blue purple), MRPS9 (lemon), MRPS28 (electric green) and MRPS23 (wheat). Two hits were identified in mtLSU: MRPL15 (magenta) and MRPL34 (white). mtSSU – sky blue (protein) and salmon (12S rRNA); mtLSU – forest green (protein), orange (16S rRNA) and purple (tRNA^{Val})

B. In the mtSSU, MRPS9 (lemon) binds the anticodon stem loop of the P-site tRNA. MRPS28 forms the mRNA (electric pink) exit channel. MRPS23 is tightly bound to MRPS28.

PDB entry 6zm5, (Itoh et al., 2021); figure made using the PyMOL software

The mtSSU hits identified were MRPS9, MRPS23, MRPS28 (also named bS1m) and MRPS31, the latter identified in C12-BioID2 as well. In terms of their role during 55S assembly, they are all early binding proteins. MRPS9 attaches to the major 3' domain of 12S rRNA and facilitates the recruitment of MRPS31 which has no individual connection with 12S rRNA. MRPS23 and MRPS28 (bS1m) form a module that interacts with MRPS9 and MRPS5 (Bogenhagen et al., 2018).

MRPS28 (bS1m) is one of the proteins that form the mRNA exit channel, providing positive amino acids to interact with mRNA (Amunts et al., 2015). MRPS23 is tightly associated to it, which explains why both hits were biotinylated (Figure 6-14B). On its turn, MRPS9 is the only 55S protein to interact with P-site tRNA: the C-terminal tail, positively charged (residues K396 and R397) interacts with the phosphate backbone of the anticodon stem loop (Kummer et al., 2018, Aibara et al., 2020).

Other C12-Linker hits involved in translation were matrix soluble: mtEF-Tu, serine-tRNA ligase, isoleucine-tRNA ligase (common with the control and C12-BioID2), as well as alanine- and threonine-tRNA ligase (Table 6-5).

The hits with the highest probability to be real interactors of C12orf65 are the ones that cannot be found in the control. The presence of such hits in C12-BioID2 and C12-Linker-BioID2 samples is promising. The fact that C12-Linker-BioID2 experiments produced hits that are only specific to this clone, and cannot be found in C12-BioID2, suggests that addition of the linker is an advantage. As those hits are not found in the control, they cannot be considered background. Rather, they are C12orf65 interactors that require either an increased steric flexibility of the biotin-ligase, as part of the fusion protein, or they are simply more distant interactors.

6.1 Discussion

6.1.1 Comparison between the mass-spectrometry experiments

The goal of the BioID2 experiments was to identify interactors of C12orf65, which could help elucidate its function. As the method identifies transient or weak interactions, as opposed to immunoprecipitation that identifies physical interactions (Kim and Roux, 2016), it was necessary to perform numerous biological repeats to identify true interactors. Ideally, the more a hit appears in the different datasets, the more likely it is to be a true C12orf65 interactor. But,

as the method requires a certain biotinylation range (10 nm or 35 nm with the linker) and takes place in live cells (Kim et al., 2016a), which are dynamic, it can happen that certain hits appear only in some biological replicates and not in the others. The COX8 control serves as a guide for non-specific biotinylation, helping distinguish C12orf65 interactors from the background.

To identify the proteins most likely to interact with C12orf65, I performed three rounds of BioID2 experiments: NCL1 (N=1), Nijmegen (N=3) and NCL2 (N=2). The Nijmegen results were disappointing in terms of hit identification, but they did provide a minimal background, indicating the hits that might be expected to appear in any of my BioID2 experiments (for example, endogenously biotinylated proteins).

For NCL1, only 13% of total hits were mitochondrial. The reasons why so few mitochondrial hits have been detected could be both technical and biological.

From a technical point of view, the method used for mitochondria isolation (differential centrifugation) is characterised by low purity. The methods that would offer a higher purity of mitochondria, like density gradient centrifugation or capture by affinity purification, are not suitable for a large quantity of starting material (Bury et al., 2020). They are applicable to brain tissue (Sims and Anderson, 2008, Hubbard et al., 2019) or to a small number of cultured cells (Hornig-Do et al., 2009). For mitochondria isolation from cell lines, differential centrifugation is the standard method (Liao et al., 2020) and the yield depends greatly on the homogenisation and amount of starting material. It is possible that during homogenisation, due to lack of experience, I accidentally broke the mitochondrial membranes, allowing the fusion protein to escape in the homogenate and biotinylate proteins there. With time, after becoming more confident with mitochondria isolation and after increasing the amount of cells used for the experiment, the mitochondrial yield increased up to 40% (NCL2).

From a biological point of view, it could be that not all fusion protein is imported in the mitochondria. In theory, the fusion protein is translated by the cytosolic ribosomes located in close proximity with the mitochondria (Vardi-Oknin and Arava, 2019) then imported in linear form and, after cleavage of the N-terminus sequence, folded in its three-dimensional structure (Wiedemann and Pfanner, 2017). In practice, if the import is not efficient, the cytosolic form could be assembled and, if functional, it could randomly biotinylate proteins outside mitochondria, leading to more non-specific hits. In Figure 6-2, the streptavidin-HRP shows a band at 35 kDa in the Linker clone, corresponding to what could be a cleavage product that contains the biotin-ligase. Since the enzyme is capable to self-biotinylate, the 35 kDa fragment

could only be biotinylated and subsequently identified via streptavidin-HRP if the enzyme were folded, and active, in the cytosol, as the fragment is not imported in the mitochondria (Figure 5-6).

When comparing NCL1 and NCL2, it can be noticed that in general NCL2 has a better mitochondria yield (approximatively 40%) than NCL1 (13%) illustrated by more abundant matrix hits. This was achieved after optimization of the BioID2 technique by increasing the amount of starting material and changing the type of flask used for culture, partially based on lessons learned from the Nijmegen run. Apart from endogenous carboxylases and chaperone proteins, there are four interesting hits common between NCL1 and NCL2, all of them involved in mitochondria gene expression: mitochondrial Top1, mtEF-Tu, MRPL15 and MRPL34. The four hits are consistent between samples in both rounds: Top1, mtEF-Tu and MRPL34 appear in all samples including control, while MRPL15 is specific to C12-BioID2 and C12-Linker-BioID2.

As both Top1 and mtEF-Tu are matrix soluble proteins, it is understandable that they appear in both control and when using C12orf65 as a prey. They belong to distinct mitochondria foci: Top1 is in the nucleoid (Zhang et al., 2001, Lee and Han, 2017), while mtEF-Tu, as translation factor, is most likely to reside in the recently discovered translation foci (Zorkau et al., 2021). As the biotin-ligase is capable of non-specific biotinylation, it is possible that both were randomly biotinylated.

Two particular proteins that are interesting are MRPL34 and MRPL15, from 39S. MRPL34 (UniProt ID Q9BQ48) is a small protein (10 kDa), formed by two alpha-helices in shape of letter ‘V’(Figure 6-15), situated in the centre of mtLSU, embedded in the 16S rRNA (Figure 6-6). Almost half of its primary structure is represented by the N-terminal transit peptide (46 out of total 92 aa) and all lysine residues are concentrated in the C-terminal half. It is therefore surprising that it appears with such consistency in two BioID2 rounds and especially in the control: the protein is not exposed to the subunit surface, so the chances of being randomly biotinylated while being a component of a mature 55S are low. It is more probable that MRPL34 is biotinylated as a free protein, prior to assembly.

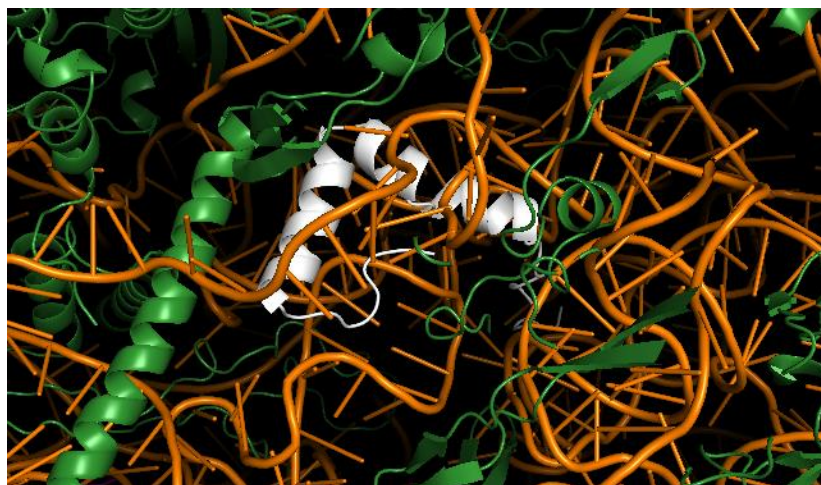


Figure 6-15. Structure of MRPL34 (close view)

MRPL34 (white) is not exposed to the mtLSU surface. This protein is intertwined inside the 16S rRNA (orange). The other proteins from mtLSU are coloured forest green. PDB entry 6zm5, (Itoh et al., 2021); figure made using the PyMOL software

Studies from Lightowlers' group (Richter et al., 2010b, Rozanska et al., 2017) and others (Bogenhagen et al., 2018, Lavdovskaia et al., 2018) show that some MRPs exist as a free, non-assembled pool, in the mitochondria matrix, in addition to being part of the 55S. This could be the case of MRPL34, especially as it is a late-assembly protein: it could remain in the matrix until the early-assembly proteins have finished binding the 16S rRNA. As mitoribosome assembly takes 2-3h (Bogenhagen et al., 2018) and biotinylation treatment lasted for 17h, MRPL34 could participate in 5-6 consecutive 55S assemblies while being randomly biotinylated. This comes under the assumption that biotinylation of MRPL34 would not interfere with 39S assembly. Recent publications that identified hits belonging to protein complexes did not report any damage of those complexes (Guedouari et al., 2021, Ould Amer and Hebert-Chatelain, 2020), so it is likely that biotinylated MRPL34 participates in the correct assembly of mtLSU.

Bogenhagen et al. found that MRPs are imported in excess in the matrix but are rapidly degraded if not used (Bogenhagen et al., 2018). If that was the case for MRPL34, I would not expect to find it among my hits. Therefore, I consider the consistent presence of this protein in NCL1 and NCL2 is caused by biotinylation in the non-assembled state. Separation of cellular components on sucrose gradient followed by SDS-PAGE could ascertain the amount of MRPL34 from free fractions as opposed to the one from mtLSU.

MRPL15, also consistent between NCL1 and NCL2, does not appear in the control, which suggests a specific C12orf65 interaction. MRPL15 (UniProt ID Q9P015) is larger (33 kDa) than MRPL34 and has a shorter mitochondrial targeting sequence (21 aa). It is an early-binding protein that extends towards the 16S rRNA, situated at the surface of the 39S subunit (Bogenhagen et al., 2018). So far there is no special function attributed to this protein during translation. If C12orf65 is involved in rescue of stalled mitochondrial ribosomes, as my hypothesis states, then I would expect to find MRPL hits involved in translation and recycling. The fact that I identified MRPL15 could be due to its size: the bigger a protein is, the more peptides it generates after trypsinization, which increases the chances of identification. Also, being situated at the surface of 39S provided exposed amino acids to biotinylation.

There are no mtSSU hits shared between NCL1 and NCL2. NCL1 only identified MRPS5 and AURKAIP1, which appeared in the control, while NCL2 identified MRPS9, MRPS23, MRPS28 (bS1m) and MRPS31, all specific to C12 samples. However, the hits share common characteristics. With the exception of AURKAIP1, all the MRPSs identified are early assembly proteins (Bogenhagen et al., 2018). In terms of function, all are associated with the active sites of translation: MRPS5 forms the entry site of the mRNA channel, while MRPS28 forms the exit site (Amunts et al., 2015). Also, MRPS9 interacts with the anticodon stem loop of the tRNA from the P site, while MRPS23 is a strong interactor of MRPS28. The mtSSU hits from NCL1 and NCL2 complement each other: they contour a region where C12orf65 could bind, and that region corresponds to active sites of translation. During rescue, if C12orf65 occupied the A site of the mitoribosome, the biotin-ligase would non-specifically biotinylate firstly the closest proteins- the P-site and mRNA interactors. The fact that MRPS5 is encountered in NCL1 control can be explained by its localization towards the surface of mtSSU, which makes it more accessible to biotinylation (Figure 6-7A). AURKAIP1, as late binding protein, could be biotinylated prior to assembly, which could explain why it appears in the control.

A striking difference between NCL1 and NCL2 is the absence of mtRNA-related hits from the former. There are no NCL1 hits involved in transcription, RNA processing or RNA modification. This can be explained by the increased mitochondria yield in NCL2, resulted from the increased amount of starting material as well as technical improvement of mitochondria isolation. Although it is difficult to make assumptions based on a single biological repeat, the absence of those hits from the database does not equal to their absence from the sample. Also, considering that BioID2 identifies protein-protein interactions, which

are dynamic, it could happen that no RNA-related hit occurred in the biotinylation range for NCL1. The hits from NCL2 cannot be dismissed because they failed to be identified in NCL1.

The C12orf65 specific hits identified in NCL2 are involved in processing and maturation of transcripts or mtLSU assembly (DHX30). HSD17B10 and TRMT10C are both part of the RNase P complex, which explains why they were both biotinylated. But LRPPRC appeared alone, which was unexpected since it forms a dimer with SLIRP. The interaction between the two is strong: both SLIRP and LRPPRC contain amino acids specific to each other, which belong to structural motifs that were predicted to bind RNA (Spåhr et al., 2016). LRPPRC binds RNA strongly and non-specifically, while SLIRP uses its RNA recognition motif to stabilize LRPPRC (Spåhr et al., 2016).

It was therefore expected to find both LRPPRC and SLIRP as BioID2 hits. However, the absence of SLIRP was reported by (Guedouari et al., 2021) and (Ould Amer and Hebert-Chatelain, 2020) in BioID2 experiments performed in HEK293T cells, similar to mine. This suggests a logical cause for SLIRP absence, other than simply dismissing it as technical artifact. SLIRP (UniProt ID Q9GZT3) has a very small molecular weight (12 kDa) comparing to LRPPRC (UniProt ID P42704, 158 kDa). This could mean that LRPPRC shields SLIRP from biotinylation. Or, if both proteins are biotinylated and SLIRP is captured on the streptavidin beads, the SLIRP peptides resulted from trypsinization could be outside the mass window of this experiment. One of mass-spectrometry disadvantages is that proteins with high molecular weight can hide the signal of low molecular weight proteins, because only a small fraction of peptides are detected, and an even smaller fraction are fragmented (Aebersold and Mann, 2003). Aibara et al. (Aibara et al., 2020) were able to identify SLIRP via mass-spectrometry with 46% sequence coverage, but they used highly purified mitoribosomes as starting material, which provides a limited range of protein masses, while I started from crude mitochondria. In addition, the SLIRP lysine residues from C-terminal half are involved in LRPPRC binding, which could rend them unavailable for biotinylation (Spåhr et al., 2016).

Another important common aspect of NCL1 and NCL2 is the absence of C12orf65 from the hits. This was also a surprising result, because previous studies report identification of the bait protein among interactors, due to BirA capacity to self-biotinylate (Kim et al., 2016a). To understand this, I explored several scenarios.

The absence of C12orf65 could be explained by a possible impairment of BirA function caused by the fusion with the bait. However, the identification of the bacterial biotin-ligase among the

NCL2 hits, as well as the western blot results that show a biotinylation smear (Figure 6-2), suggest this is not the case. In addition, the linker would provide the flexibility necessary to biotinylate C12orf65, so the protein should be identified at least in C12-Linker-BioID2 hits.

In theory, C12orf65 tertiary structure could prevent biotinylation if the lysine residues are not exposed to the protein surface. However, recent determination of human C12orf65 structure shows that the protein has an open conformation where the C-terminus, most abundant in lysine, forms an α -helix (Desai et al., 2020). C12orf65 is most likely biotinylated and bound to the streptavidin-coated beads, but the primary structure prevents it from being identified.

C12orf65 is composed of 166 aa from which the first 35 form the mitochondria targeting signal (Figure 6-16). The sequence after the signal is rich in lysine (23 residues) from which only K94 is listed as PTM site (ubiquitylation) by PhosphoSitePlus v6.5.9.3.

```
>sp|Q9H3J6|CL065_HUMAN
Probable peptide chain release factor C12orf65, mitochondrial
|PS=Homo sapiens OX=9606 GN=C12orf65 PE=2 SV=1

      10          20          30          40          50
MSTVGLFHFP TPLTRICPAP WGLRLWEKLT LLSPGIAVTP VQMAGKKDYP
      60          70          80          90         100
ALLSLDENEL EEQFVKGHGP GQQATNKTSN CVVLIKHIPSG IVVKCHQTRS
     110         120         130         140         150
VDQNRKLARK ILQEKVDFVY NGENSPVHKE KREAAKKKQE RKKRAKETLE
     160
KKKLLKELWE SSKKVH
```

Figure 6-16. Primary sequence of human C12orf65

Amino acid sequence of human C12orf65 was retrieved from UniProt (<https://www.uniprot.org/>) and annotated accordingly. MTS is highlighted in yellow. Red font-lysine residue; green font-arginine residue

This should provide an excellent biotinylation target. However, the unequal spread of residues through the sequence makes it difficult to obtain useful peptides after trypsinization. The lysine and arginine residues, both target sites for trypsin (Olsen et al., 2004), are abundant in the C-terminal half of the protein and in many cases are situated next to each other. For this reason, trypsinization results in no -or short-peptides, which are difficult to detect. For example, short hydrophobic peptides can remain captured in the HPLC column (Schweizer et al., 2007), while very hydrophobic peptides cannot be captured on the column (Mitulović and Mechtler, 2006). Trypsin does not cleave at biotinylated lysine residues (Kuroishi et al., 2010), so it is possible

that some cleavage sites are missed. But even considering randomly missed cleavages, the resulting peptides can still be too short to be detected.

From the peptides that get eluted from HPLC, some do not have optimal ionization, or, if they are ionized, they cannot be fragmented due to their amino acid composition. Certain amino acid residues can favour fragmentation (e.g. aspartic acid) while others lead to poor fragmentation (e.g. arginine) (Kapp et al., 2003). Applying those possibilities to a short protein like C12orf65, that cannot result in a high number of peptides, offers a reasonable explanation as to why this protein is missing from my hits. There are not enough peptides that could be detected in the BioID2 experiments.

6.1.2 Integration of C12orf65 BioID2 results in the context of current research

At the beginning of my project, the function of C12orf65 was not understood, despite pathogenic variants that suggested it is involved in mitochondria translation (Wesolowska et al., 2015, Antonicka et al., 2010). This protein contained the universally conserved GGQ motif, specific to translation release factors, but no codon recognition motif (Richter et al., 2010b). In addition, another translation termination factor (mtRF1a) was already proved to terminate mitochondrial translation (Soleimanpour-Lichaei et al., 2007). On this basis, I started from the hypothesis that C12orf65 is involved in translation quality control, more specifically in the rescue of stalled 55S ribosomes. The method I chose to test the hypothesis was BioID2, which would allow me to identify weak and transient binding partners of C12orf65 (Roux et al., 2012, Kim et al., 2016a). I reasoned that those interactors would indicate C12orf65 function, or at least illuminate the molecular pathways that involve C12orf65. As anticipated, I identified several factors involved in RNA processing and modification, as well as MRPS proteins that localize to the P site and mRNA channel of the 55S ribosome.

The interactors that I identified were also identified by Hana Antonicka (Antonicka et al., 2020). In a massive effort to map the protein-protein interactions from all mitochondrial compartments, the authors applied the BioID method to 100 mitochondrial baits, including C12orf65. To characterize the biotinylation background in the matrix, they used MTS from three proteins, including COX8, the same that I used as control. For C12orf65-BioID they identified approximatively 1,000 proteins, 5-6 times more than what I identified. This discrepancy can be explained by the different manner of sample preparation. The affinity purification that I performed started from isolated mitochondria, while Antonicka et al. used

cell lysate (Antonicka et al., 2020). Also, I did more washes prior to trypsinization (10 vs.6), which could reduce the non-specific binding and therefore the total number of hits identified by mass-spectrometry.

All the MRPS that I have identified, apart from AURKAIP1, figured among the 1,000 proteins. The authors defined a BFDR score to represent high-confident interactions ($BFDR \leq 0.01$) as opposed to random interactions or endogenously biotinylated proteins. Importantly, when comparing COX8-MTS interactions with C12orf65 interactions, most of the MRPs that I have identified only in C12 samples were listed in both COX8-MTS and C12-BioID preys, in both cases as high confident interactors, with $BFDR = 0$ (MRPS5, MRPS9, MRPS23, MRPS28, MRPS31, MRPL15). MRPL34, which in my experiments appeared as a non-specific interactor, was identified with a higher confidence score in C12-BioID ($BFDR=0$) than in COX8-MTS ($BFDR=0.27$).

The hits involved in RNA stability and maturation were also found by Antonicka et al. (Antonicka et al., 2020), all with high-confidence interacting score ($BFDR=0$). In addition, the authors did identify SLIRP as a high confident interactor of C12orf65, together with LRPPRC ($BFDR=0$). This could be possible because the authors used mass-spectrometers with a higher resolution (LTQ-Orbitrap Velos or Elite instrument) than the one used in Newcastle (Fusion Lumos Tribrid Orbitrap), which could also permit identification of more hits in COX8-MTS. Importantly, C12orf65 did not figure among their preys, neither when using C12orf65 as a bait, nor when using other mitochondrial proteins as baits. This strengthens the argument that the C12orf65 primary structure impedes identification via bottom-up proteomics.

During the writing of this thesis, Desai et al. published the cryo-EM structure of an elegant model of mitoribosome stalling in HEK29T cells, which allowed them to determinate the function of C12orf65 (renamed mtRF-R) (Desai et al., 2020). They identified an intermediate of the rescue process formed by mtLSU that contained the nascent polypeptide attached to the tRNA in the P site. The rescue factor was not C12orf65 alone, but a dimer of C12orf65 and MTRES1 (C6orf203), a protein previously known to bind double-stranded RNA (Gopalakrishna et al., 2019). To form this dimer, the α -helix situated closest to the C-terminus in C12orf65 (α 2) interacts with the S4-like domain of MTRES1. C12orf65 binds to the A-site of the LSU, while MTRES1 binds the anticodon stem-loop of tRNA from the P site. In agreement to the previous bioinformatic predictions, the GGQ motif of C12orf65 extends into the PTC of the 55S ribosome and interacts with the 3'-CCA extremity of the P-site tRNA. Using

bacterial LSU, the authors showed that C12orf65 and MTRES1 induce the hydrolysis of the nascent polypeptide.

MTRES1 was not identified in my BioID2 studies. One possible cause for this absence could be that I did not induce mitoribosome stalling in my HEK cells, and the C12orf65-MTRES1 dimer might not be stable with normal translation. Using MTRES1-FLAG as bait, Gopalakrishna et al. were able to immunoprecipitate C12orf65 in HEK293T cells without stalling, and without crosslinking (Gopalakrishna et al., 2019). However, Desai et al. show that the dimer is stabilized by the interaction with 16S rRNA, in particular with helix 69 to which both C12orf65 and MTRES1 make contact (Desai et al., 2020). They identify specific amino acid residues in C12orf65 as well as MTRES1, residues involved in the contact with each other, and Gopalakrishna et al. show that the interaction exists without stalling (Gopalakrishna et al., 2019). It is not known how stable a steady-state interaction would be and whether the structure of the dimer in native state would be identical to the structure of the dimer during stalling. Interaction with the mtLSU could induce a conformational change of the dimer.

The absence of MTRES1 could also be explained by the technical differences between the BioID2 technique and FLAG-immunoprecipitation followed by mass-spectrometry used by Gopalakrishna et al. (Gopalakrishna et al., 2019). BioID2 identification is based on biotinylation of prey at the lysine residues. Desai et al. show MTRES1 has a rather packed structure, which could hide the lysine residues from biotinylation (Desai et al., 2020). Also, a FLAG-immunoprecipitation is more specific than BioID2, because the hits must physically interact with the prey, which reduces the number of proteins and the mass-widow in mass-spectrometry analysis, increasing the chances of identification.

Last but not least, attaching the BirA to the C-terminus of C12orf65 could disrupt the interaction with MTRES1. Desai et al. (Desai et al., 2020) showed that the longest α -helix, the one at the very end of C-terminus, is responsible for MTRES1 binding. MTRES1 molecular weight (28 kDa) is only slightly bigger than BirA (25 kDa), so BirA could cause a steric hindrance preventing it from binding. It might be that the binding site between C12orf65 and MTRES1 is affected even with the linker insertion. This would explain the presence of a cleavage product in the C12orf65-Linker-BioID2-HA clones and why the clones without linker had a poor growing phenotype. To test whether MTRES1 is capable of binding C12orf65 in the BioID2 clones, an immunoprecipitation similar to Gopalakrishna et al. (Gopalakrishna et

al., 2019) could be performed, using HA as tag. MTRES1 could be identified by mass-spectrometry of the eluate.

The results obtained by Desai et al. (Desai et al., 2020) concomitantly support and contradict my results. They support them because they show C12orf65 binding to the same region where my hits are situated. For example, MRPS9, identified in the linker clone, interacts with the anticodon stem loop of the P-site tRNA (Aibara et al., 2020). MRPS28 (bS1m) and MRPS23, from the mRNA exit channel, and MRPS5 in the RNA entry channel (Amunts et al., 2015) are all situated close to the A site, where C12orf65 binds. The distance between the A and P sites (50 Å) (Aibara et al., 2020) permits their biotinylation even in the absence of the linker (within 10nm biotinylation range). Clearly, the BioID2 cannot map the interactions with the same precision as cryo-EM, but taken together, both results point towards active sites of mitochondria translation. The hits that I identified do not figure among the proteins involved in co-translational insertion, for example (Itoh et al., 2021). I did not identify MRPs that interact with Oxa1L to guide the co-translational insertion of mitochondria translated proteins in the IMM. I identified proteins that map to the region described by Desai et al., proteins that interact with P-site tRNA and mRNA (Desai et al., 2020),.

In the same time, Desai et al. contradict my results because the hits that I identified are mostly from the mtSSU, when they demonstrate that the C12orf65-MTRES1 dimer binds to the mtLSU (Desai et al., 2020). They further explain that the $\alpha 1$ and $\alpha 2$ helices of C12orf65 would clash with mtSSU and conclude that C12orf65-MTRES1 bind to the stalled mtLSU after it had been separated from mtSSU. In addition, the few mtLSU that I identified (MRPL34, MRPL15, MRPL2) are not reported to have any special role in translation, and do not figure among the MRPLs mentioned in this article.

This opened new research questions. Does C12orf65 or C12orf65/MTRES1 interact with an assembled, translating 55S ribosome, in the absence of stalling? Does it scan the translating mitoribosome to check for stalling and is removed by mtRF1a once a correct stop codon is found in the A site? This could be possible, since C12orf65 does not have a codon recognition domain, so mtRF1a would have a higher affinity for the stop codon. Where does C12orf65-or C12orf65/MTRES1- reside in the matrix? Is it ubiquitous, or does it reside in a specific matrix area and is only recruited when stalling happens?

The majority of MRPs that I identified are early-binding proteins, binding directly to rRNA. In NCL2, I identified several interactors involved in RNA maturation and ribosome assembly.

The post-transcriptional processing of RNA as well as biogenesis of 55S take place in RNA granules (Antonicka and Shoubridge, 2015). RNA granules are defined as punctate sub-compartments that associate with IMM and are very dynamic in composition (Rey et al., 2020). Recently, the RNA granules and mitochondria translation sites were shown to be spatially different (Zorkau et al., 2021). Under the experiments limitations, my BioID2 results raise the possibility that C12orf65 resides in the RNA granules, either alone or associated with MTRES1, from where it is recruited to the translation region. To test this hypothesis, a similar approach as used by Zorkau et al. (Zorkau et al., 2021) involving STED nanoscopy could be applied to C12orf65-FLAG expressing HEK cells in order to determine its exact localization.

Two of the hits identified in the BioID2 experiments (DHX30 and TRMT10C) were also found by Gopalakrishna et al. in the MTRES1-FLAG eluate (Gopalakrishna et al., 2019). TRMT10C is part of the RNase P complex (Metodiev et al., 2016), while DHX30 is involved in 55S assembly (Antonicka and Shoubridge, 2015). Since Desai et al. (Desai et al., 2020) show mtLSU is rescued after dissociation of mtSSU, if DHX30 and TRMT10C interact with MTRES1, they could be involved in mtLSU disassembly, most likely acting after C12orf65/MTRES1 hydrolyse the nascent polypeptide. An immunoprecipitation using HA tag could clarify whether they are close C12orf65-BioID2 interactors when stalling is not induced. Also, using the 55S stalling model from Desai et al. (Desai et al., 2020), the DHX30 and TRMT10C levels could be tested and compared with the levels without stalling. If stalling increased their expression, then the two proteins are more likely to be responsible for disassembly of the stalled mtLSU.

An important aspect remains the validation of the hits identified in this work and their physiological relevance. Previous studies in which the function of the bait protein was at least partially known validated the new BioID interactors using fluorescence microscopy or co-immunoprecipitation (Youn et al., 2018, Ould Amer and Hebert-Chatelain, 2020). When the bait protein was known to be part of a complex, the other members of the same complex were used to validate the interactors obtained by BioID: if the previously known interactors appeared among the newly discovered ones, then the BioID2 method was reliable (Gong et al., 2020). The authors would then choose some of these new interactors and test their co-localization with the bait protein via immunofluorescence, or their interaction via co-immunoprecipitation followed by western blot (Gong et al., 2020).

These approaches are insufficient to shed light on the functional interplay between C12orf65 and the hits. Even if they were validated by immunofluorescence or co-immunoprecipitation, the physiological relevance of the interaction would remain unknown. Since the function of C12orf65 was unknown at the beginning of the project, I decided to create a C12orf65 knockout (KO) cell model in which to observe the effect that the lack of C12orf65 has on the BioID2 hits, more specifically to explore changes in their protein level by western blotting.

Such a model would be of interest particularly for the hits involved in transcription and RNA processing. Previous attempts to downregulate C12orf65 in Lightowers lab lead to an upregulation of mt-RNAs (Pajak, 2013), a result that could not be reproduced (Wesolowska, 2015). Using a KO model would clarify the molecular behaviour of mitochondrial transcripts and identify any change in the BioID2 hits regulating those transcripts. In addition, the model would provide a basis for the study of mitoribosome assembly in the absence of C12orf65 and the role of other BioID2 hits (DHX30, ATAD3A, ATAD3B) in this process. In the following chapter, I describe an attempt to generate a C12orf65 KO cell model.

Chapter 7
Generation of a C12orf65 knockout cell line using
CRISPR-Cas9

7.1 Introduction

Using more than one method increases the chance of success when studying the function of a protein, especially if the protein is associated with such heterogenous phenotypes as in mitochondrial diseases. Although BioID2 is a new and powerful technique (Kim et al., 2016a), which represents the improved version of the original BioID (Roux et al., 2012), it is not always straightforward. Traditionally, in order to find out which is the role of a protein, researchers removed it from a cell/organism by disrupting the expression of the protein-coding gene (Alberts B, 2002).

This approach has already been tried in my host laboratory. Aleksandra Pajak treated HEK293T cells with siRNA-C12orf65 or siRNA-NT and noticed that, even after 6 days of treatment, the levels were not changed in COXII (mitochondria-encoded), NDUFB8 (nuclear-encoded, marker of complex I assembly) and MRPs. However, the steady state levels of mitochondrial mRNA and rRNA were higher in the siRNA-C12orf65 samples than in the control (Pajak, 2013). When Maria Wesolowska repeated the experiment, she found that, apart from *MT-ND1*, there was no difference in mitochondria transcripts levels between treatment and control. When investigating this issue, she observed that the lowest *C12orf65* transcript level was achieved after 3 days of treatment (40% of the control), but it increased for the 6 days treatment (90%) (Wesolowska, 2015).

Both experiments are based on transient depletion of C12orf65, and the level achieved is not consistent. In Pajak's thesis there is a lower transcript level after 6 days of treatment compared to 3 days, while in Wesolowska's thesis is the other way around. Moreover, in both cases the depletion seems insufficient to recapitulate the phenotype seen in *C12orf65* patients, which reported a drastic deficiency of complexes I, IV, and V (Antonicka et al., 2010).

The creation of an improved cell model with C12orf65 deficiency was therefore necessary. Although patient cells are a good model for genetics studies, they are not immortal, they are difficult to obtain, their use requires ethical approval and, most importantly, they are heterogenous in terms of pathogenic variant and tissue. In order to obtain a cell model with an identical variant that does not become senescent and is likely to give consistent results, scientists can immortalize primary cells that carry a genetic defect (Robin et al., 2015) or they can knockout (KO) the gene of interest in a largely used cell model (Pearce et al., 2017). Since

immortalization of patient cells is time-consuming due to the slow growth of mutant cells and it requires a careful selection of an appropriate control, I opted for the KO method.

I performed CRISPR-Cas9 against *C12orf65* in HEK293T cells because they grow rapidly, are easy to transfect and allow the use of an identical control, since both KO and control have the same origin. This method is relatively straightforward and commonly used in research. It was used in Lightowers lab to KO another member of the translation release factor family- mtRF1 (Shreya Ayyub, unpublished data). The aim was to obtain a *C12orf65* KO cell line to study the function of *C12orf65* and its link with the interactors identified by BioID2. Should the experiment be successful, the KO clone would not require retransfection, as in the case of siRNA, and would provide a reliable model for future rescue or double knockout experiments.

CRISPR (clustered regularly interspaced short palindromic repeats) and the CRISPR-associated (Cas) systems are a basic type of adaptive immunity from bacteria and archaea, that allow the cell to detect and silence foreign nucleic acids (viruses, plasmids). In this process, bacteria that contain CRISPR loci integrate short fragments from the invader genome into their own genome, at the end of the CRISPR loci, and use them as a record for previous infections. After the CRISPR loci are transcribed, the transcripts are processed into numerous short CRISPR-derived RNAs (crRNAs), each one containing a sequence that is complementary to the sequence of the invader. The foreign nucleic acid is silenced by Cas endonucleases, which act in conjunction with crRNAs (Bhaya et al., 2011, Wiedenheft et al., 2012).

In 2012, a collaboration between Jennifer Doudna and Emmanuelle Charpentier revealed the mechanisms of action behind the Cas9 enzyme, which constitute the base of current genetic engineering research. They reported that Cas9 is an endonuclease capable to cut both strands of DNA and requires an additional small noncoding RNA- triggering pre-crRNA (tracrRNA)- for its function (Figure 7-1).

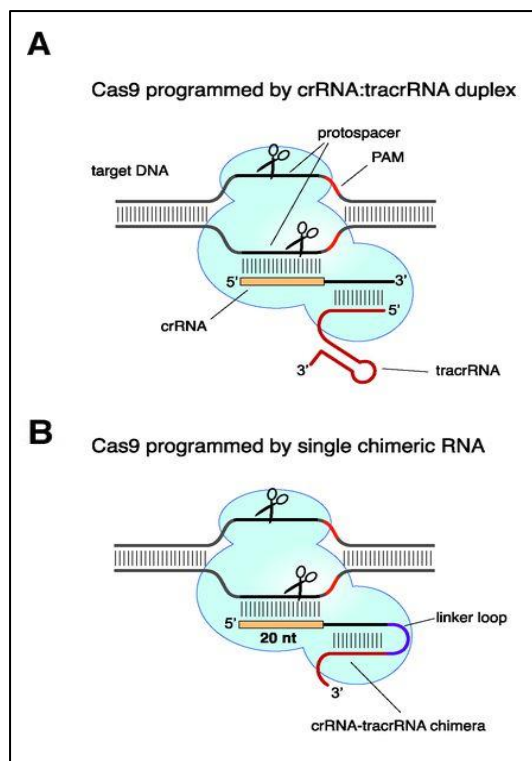


Figure 7-1. Mechanism of action for CRISPR-Cas9

A. In the WT system, crRNA forms base-pairs with the protospacer sequence in the target DNA and with the tracrRNA. The RNA duplex directs Cas9 to the target DNA, which is cleaved on both strands once the PAM motif is recognized.

B. In the genetically engineered system, Cas9 is activated by a chimera of crRNA linked to tracrRNA. The crRNA part of the chimera is designed to be complementary with the target DNA, which in addition must contain a PAM motif. (taken from (Jinek et al., 2012) with permission, RightsLink license number 4996690254172)

The tracrRNA is necessary both for maturation of crRNA and for activation of Cas9. The double stranded breaks (DSB) occur at a specific site, defined by the base-pairing of crRNA with the foreign DNA (protospacer) and the protospacer adjacent motif (PAM). PAM motif is situated in the target DNA, next to the region recognized by crRNA (Jinek et al., 2012).

Based on the tracrRNA:crRNA duplex, the authors designed a guide RNA (gRNA), a chimeric molecule that contains a target recognition sequence and a base-pairing sequence of tracrRNA with crRNA. The gRNA was used to programme Cas9 and successfully cleave the green-fluorescent protein coding sequence *in vitro*. With both plasmid and linear DNA, Cas9 produced blunt ends, making reannealing difficult, which opened the possibility of gene editing (Jinek et al., 2012). One year later, the group announced the successful use of CRISPR-

Cas technology in human HEK293T cells to induce DSB in the human clathrin light chain (*CLTA*) gene, using a gRNA specifically designed for it (Jinek et al., 2013).

In both eukaryotes, the formation of DSBs triggers two endogenous DNA repair mechanisms: non-homologous end joining (NHEJ) or homology-directed repair (HDR). NHEJ is highly conserved during evolution, from bacteria to mammals, but has the highest contribution in mammals (Hefferin and Tomkinson, 2005). The mechanism brings together the two DNA broken ends and joins them, ideally by direct ligation. However, as the DNA ends are usually non-ligatable, they are first processed by phosphoglycolate enzymes, then aligned against complementary sequences of 1-4 nucleotides. Those small sequences are compared, aligned and used as scaffold for bridging the gap, which can lead to mismatches, insertions or deletions. In mammalian cells, NHEJ is possible due to the Ku complex, a heterodimer of Ku70 and Ku80 with toroid shape that can accommodate both DNA strands in the middle hole. The interior wall of the channel is formed by positively charged amino acids, which allow interactions with the ribose-phosphate backbone of DNA (Walker et al., 2001). The Ku complex prevents degradation of the broken DNA by nucleases and bridges the two ends by recruiting the DNA-dependent kinase (Gottlieb and Jackson, 1993) and the DNA ligase IV/XRCC4 complex (Chen et al., 2000). The DNA ligase complex is capable to ligate the two ends even if they are incompatible (no potential of base-pairing) and to ligate over 1 nucleotide gaps, if the two ends have a 1-4 nucleotides complementary sequence (Gu et al., 2007). The DNA-polymerases Pol μ (Mahajan et al., 2002) and Pol λ (Lee et al., 2004) from the Pol X family are also associated with the Ku complex (Mahajan et al., 2002) (Ma et al., 2004) and incorporate nucleotides to fill in any gaps formed during processing of DNA ends (Hefferin and Tomkinson, 2005). The NHEJ process is therefore error-prone, allowing random indels to occur.

The other DNA repair mechanism, HDR, is based on homologous recombination. Homologous recombination involves the exchange of sequences between the DNA molecule that contains the DSB and another DNA molecule, identical and intact (homologous template). HDR is more precise, but also occurs at lower frequency comparing to NHEJ in mammals (Pardo et al., 2009). If NHEJ is specific to G0 and G1 phase of the cycle (non-dividing), HDR takes place only during the late S and G2 phases, when the cell is dividing, and the homologous DNA becomes available (Bolderson et al., 2009).

In gene editing, the KO experiments exploit the NHEJ pathway, while the knock-in experiments (substitution of a DNA sequence or insertion of exogenous DNA at a particular

locus) exploit the HDR (Zhang et al., 2017). The CRISPR-Cas9 system favors NHEJ over HDR, making it ideal for KO experiments (Liu et al., 2019a). The indels introduced by NHEJ in a coding gene are likely to result in a premature stop codon, leading to the removal of the aberrant transcript via nonsense-mediated decay (NMD).

NMD is a mRNA-surveillance mechanism well-conserved in eukaryotes, having been described in vertebrates (Maquat, 1995), nematodes (*Caenorhabditis elegans*), plants (*Arabidopsis sp.*) and yeast (*S. cerevisiae*) (Longman et al., 2013, Degtiar et al., 2015, Conti and Izaurralde, 2005). The mechanism is based on three universally conserved proteins: UPF1, UPF2 and UPF3. UPF2 and UPF3 interact with the exon junction complex (EJC), situated 20–24 bases upstream of the exon-exon junction (Le Hir et al., 2001), while UPF1 is an RNA helicase that associates with UPF2 /UPF3 as well as the translation release factors eRF1 and eRF3 (Conti and Izaurralde, 2005). UPF3 is mostly nuclear but travels to the cytoplasm as part of the EJC. UPF2 is perinuclear and serves as ligand between UPF3 and UPF1, while UPF1 is mainly cytoplasmatic, but capable to shuttle to the nucleus (Chang et al., 2007). In mammals, the NMD model suggests that, when a stop codon occurs upstream from the EJC, the translation release factors recruit UPF1, which interacts with UPF2 and UPF3. Normally, the stop codon is situated downstream from EJC and the complex is removed by the translating ribosomes. During NMD, the protein-kinase SMG1 phosphorylates UPF1, resulting in the recruitment of SMG5, SMG6 and SMG7 factors (Nickless et al., 2017). The protein SMG6 is an endonuclease that cleaves the transcripts near the premature stop codon (Huntzinger et al., 2008). The dimer SMG5-SMG7 recruits factors that hydrolyze the N7-methylated guanosine from the 5'cap (DCP1a, DCP2 (Lejeune et al., 2003)) and factors that remove the 3'polyA tail (POP2, a catalytic subunit of the CCR4–NOT deadenylase complex (Loh et al., 2013)). Without the two structures that would ensure its stability, the mRNA is degraded by the 5'-3' (Xrn1) and 3'-5' (PM/Sc1100) exonucleases (Lejeune et al., 2003, Chen and Shyu, 2003).

Not all NHEJ errors lead to NMD. If the ORF is not changed, the mutant transcript can be translated into a defective protein. When studying the effect of indels on HAP1 cells, which contain only one copy of each chromosome, Tuladhar et al. observed that both events occur randomly: some KO proteins were completely lost, while others presented with novel forms that could still be detected by western blot (Tuladhar et al., 2019). In some instances, even if the ORF is affected, the aberrant transcripts escape NMD. NMD escape is done by reinitiating transcription at a downstream start codon (Neu-Yilik et al., 2011), by stop codon readthrough or with the help of RNA-binding proteins (Dyle et al., 2020). In melanoma and colon cancer

cells, for example, the indels transcripts that evade NMD result in neoantigen proteins that act as ‘danger signal’, triggering the anti-tumoral response and infiltration of cytotoxic T lymphocytes (Litchfield et al., 2020, Maby et al., 2016).

The effect of indels cannot be accurately predicted. However, in mammals, mRNAs that contain a premature stop codon located 50-55 nucleotides upstream from the final exon-exon junction are generally degraded (Nagy and Maquat, 1998), because a normal stop codon would localize to the last exon (Popp and Maquat, 2016). In a FISH-experiment done on human osteosarcoma (U2OS) cells, (Trcek et al., 2013) studied NMD by comparing degradation rates of β -globin mRNA containing premature stop codons at codon 39 with normal mRNA. They concluded that 40% of the mutant transcripts escape NMD, while the majority are degraded either proximal to the nuclear envelope, with a half-life of <1 min, or in the cytoplasm, with a half-life >12 h.

It is therefore reasonable to use the CRISPR-Cas9 to induce DSBs in the *C12orf65* gene, because the NHEJ mechanism triggered could produce a premature stop codon, that would likely result in transcript degradation and subsequent protein loss. The choice of CRISPR-Cas9 over the other genome editing technologies (ZFNs, TALENs) was made because the system is efficient, target specific and in principle could be used to KO multiple genes at the same time. It only requires a different gRNA for each gene, without the need to redesign the Cas9 enzyme, allowing more scientists to use it concomitantly for different purposes. Also, CRISPR-Cas9 is easy to transfect and has been extensively used in HEK293T cells, the model that I am using (Ran et al., 2013).

The aim of the work presented in this chapter, therefore, was to obtain a human cell model devoid of *C12orf65* for the following reasons:

1. Investigate changes in the levels of *C12orf65* interactors identified by BioID2, in particular the ones involved in transcription and ribosome assembly and the MRPs
2. Investigate the mitoribosome assembly, OXPHOS assembly and the levels of mtDNA-encoded proteins and compare the results to what was described in patients (Antonicka et al., 2010, Wesolowska et al., 2015)
3. Understand the effect that the absence of *C12orf65* has on the level of mitochondrial transcripts, since previous investigations from the group provided different results
4. Compare the *C12orf65* KO phenotype with the mtRF1 KO phenotype described by Shreya Ayyub; similar results could indicate whether the two factors compensate for

each other, whether they are involved in the same molecular pathway or are involved in different pathways given the differences between their primary structures

This chapter describes the sequencing analysis performed to identify a possible C12orf65 KO HEK clone. Due to the outbreak of Covid-19 pandemic and lab closing, it was not possible to characterize the cells experimentally.

7.2 Results

When performing the KO experiment, I took into consideration two important aspects: gRNA target and gene essentiality. As my objective was a complete loss of the C12orf65 protein, I was interested to obtain homozygous mutants. In a previous case report, only the individuals with homozygous pathogenic *C12orf65* variants were affected; since those variants have a recessive inheritance pattern, the heterozygous parents were normal (Spiegel et al., 2014).

If *C12orf65* were essential, homozygous mutants would be lethal, and only the heterozygous would be selected. On the Online GEene Essentiality database (OGEE, <http://ogee.medgenius.info>), based on eight large-scale CRISPR/Cas9 and RNAi screenings, C12orf65 is classified as ‘conditional’, not ‘essential’. In addition, patients with *C12orf65* homozygous or compound heterozygous variants present with onset of symptoms at different ages, some of them reaching maturity, as reviewed by Perrone et al. (Perrone et al., 2020). It is therefore unlikely that a homozygous KO is lethal for the HEK cells.

To increase the probability of a premature stop codon, the DSB should occur early during translation. Cas9 induces DSBs approximatively 3bp upstream from the PAM motif (Ran et al., 2013), which is immediately adjacent to the gRNA target. The gRNA target and PAM motif were therefore assigned to the first coding exon of the *C12orf65* gene, upstream from the GGQ motif (Figure 7-2), to ensure any possible peptidyl-tRNA hydrolysis activity is lost.

1	GCGTGCAGATCAGGGATCGCATTGCGATCCTCCGCTGAGGTGATTGGATATCCCT	60
61	
121	CGTATGAGCACCGTGGGTTATTCATTTCTACACCACTGACCCGAATAIGCCCGC-M--S--T--V--G--L--F--H--F--P--T--P--L--T--R--I--C--P--A	180 19
181	GCATGGGACTCGGGCTTGGAGAAGCTGACGTGTTATCCCCAGGAATAGCTGTCAC 19 ---P--W--G--L--R--L--W--E--K--L--T--L--S--P--G--I--A--V--T	240 39
241	TCCGGTCCAGATGGCAGGCAAGAAGGACTACCCCTGCACTGCTTCCCTGGATGAGAATGA 39 ---P--V--Q--M--A--G--K--K--D--Y--P--A--L--L--S--L--D--E--N--E	300 59
301	ACTCGAAGAGCAGTTGTGAAAGGACACGGTCCAGGGGGCCAGGCAACCAACAAACAG 59 --L--E--E--Q--F--V--K--G--H--G--P--G--G--Q--A--T--N--K--T--S	360 79
361	CAACTGCGTGGTGTGAAAGCACATCCCTCAGGCATCGTTGAAAGTGCATCAGACAAG 79 --N--C--V--V--L--K--H--I--P--S--G--I--V--V--K--C--H--Q--T--R	420 99
421	ATCAGTTGATCAGAACAGAAAGCTAGCTGGAAAATCTACAAAGAGAAAGTAGATGTTT 99 --S--V--D--Q--N--R--K--L--A--R--K--I--L--Q--E--K--V--D--V--F	480 119
481	CTACAAATGGTAAAAACAGTCTGTCACAAAGAAAAACGAGAACGGCGAAGAAAAACA 119 --Y--N--G--E--N--S--P--V--H--K--E--K--R--E--A--A--K--K--K--Q	540 139
541	AGAAAGGAAAAAGAGCAAAGGAAACCTGGAAAAAGAAGCTACTTAAAGAACTGTG 139 --E--R--K--K--R--A--K--E--T--L--E--K--K--L--L--K--E--L--W	600 159
601	GGAGTCAAGTAAAAGTCCACTGAGAAAAGAATTAGAGATTCCAACTGACAGAATCTGC 159 --E--S--S--K--K--V--H--*--.....	660 166
661	CAGAAGCTCCAGGGATAATGGTGGCAGTTCCATCACCAGCATTATTATAGTGCTTCA	720

Figure 7-2. Localisation of the CRISPR-Cas9 target sequence on the reference C12orf65

The gRNA target sequence is highlighted in yellow background and the adjacent PAM motif in green. The GGQ motif is shown in red.

Grey background – 3' and respectively 5' UTR;

Blue font-first coding exon; black font-second coding exon

Sequence according to the Ensemble Genome Browser, release 102, transcript ID ENST00000253233.6

To avoid potential cleavage activity of random genes, the gRNA should be highly specific, as Cas9 on its own has no off-target effects (Lino et al., 2018, Zhang et al., 2015a). The gRNA that I used in my experiments has low off-target sites. When checking the 20 nucleotide sequence on the Off-Spotter online tool (Pliatsika and Rigoutsos, 2015) <https://cm.jefferson.edu/Off-Spotter/>, the only gene returned, with a region 100% identical to the query, was the coding sequence of human *C12orf65*. The tool also allows mismatches of 1-5 bp between the query sequence and a possible off-target. There were no off-targets

identified with 1-2 mismatches. The first off-target gene predicted, with 3 mismatches, was *XKR6* – *XK* (Kell blood group complex subunit-related family, member 6), on the reverse strand of chromosome 8 (ENSG00000171044). *XKR6* is not involved in mitochondria; it is a multi-pass protein from the plasma membrane involved in Hepatitis B virus infection, *XKR6* being one of the target genes for the genomic integration of the virus (Li et al., 2020a).

As described in 2.1.8, the transfection with the PX458 plasmid was done in three cell lines: HEK 293T FLP-In, C12orf65-FLAG HEK 293T FLP-In non-induced and C12orf65-FLAG HEK 293T FLP-In T-Rex induced at the moment of transfection. As control were used HEK 293T FLP-In transfected with the empty vector (no gRNA). For all cells, successful transfection was assessed by the expression of GFP, present in PX458 and the empty vector. Also, GFP was the criteria used during FACS sorting to obtain single cells. The induction of C12orf65-FLAG, maintained during cell sorting and clone growth, was thought as the equivalent of a rescue experiment: should both endogenous *C12orf65* alleles be mutated, the deleterious phenotype could be restored by expression of C12orf65-FLAG.

After selecting single-cell clones, I observed no difference in cell growth between induced cells and control: the initial single cells grew rapidly comparing to the non-induced and HEK 293T FLP-In transfected with the PX458 plasmid, and the difference was maintained as the clones were propagated. The induced and control single cell clones grew evenly at the bottom of the well/flask and were the first that needed to be moved in a bigger recipient. In contrast, single-cell colonies resulted from non-induced and HEK 293T FLP-In cells had a poor rhythm of growth and formed clumps.

When the cells from a 25 cm² flask became confluent, I isolated total DNA for sequencing. I amplified the *C12orf65* region approximatively 150 bp upstream and downstream from the PAM motif and used this PCR product for Sanger sequencing. Sequencing was performed only with the forward primer, which binds in the intronic region, 74 nucleotides upstream from the start of the first coding exon (Appendix-D, Figure Apx 7); this location was chosen to ensure that any sequencing artefacts that might raise during the process localize to the intronic and not to the coding region. I first analysed the results with Standard Nucleotide BLAST (blastn, NCBI) against *Homo sapiens* as organism (Boratyn et al., 2013), starting from approximatively 80 bases after the beginning of the sequence. Blastn showed no mutations in the two controls transfected with empty vector (12E and 4E) and matched them to human *C12orf65*, as expected (Appendix-D, Figure Apx 8-9 and 10-11). Although only one control was obligatory for sample

comparison, I decided to sequence two control cell lines to pre-empt technical difficulties, like sequencing fail. I isolated DNA and sequenced both controls at the same time. The second control further illustrates the precision of the technique: the gRNA target and PAM motif are intact not only for one, but for two controls. Then, I compared all the sequences against the control 4E using the online deconvolution software Indigo (<https://www.gear-genomics.com/indigo/>, (Rausch et al., 2020)). The software separates the alleles for each sample and compares each allele to a reference sequence. It identifies insertions, deletions and substitutions on each separate allele and provides the estimated allelic fraction (number of alleles with a particular change divided by total number of alleles). As indels are the main consequence of CRISPR-Cas9 experiments and the DSBs are not guaranteed to happen on every allele, I considered successful only the clones that harbour indels on both alleles (complete KO).

The first sample identified as such was clone 5N (non-induced C12orf65-FLAG HEK FlipIn cell line). The two alleles are in identical proportion. The first allele of 5N contains a 14 b deletion that starts three bases upstream from the PAM motif (CGG), consistent with the Cas9 cleavage site (Ran et al., 2013) (Figure 7-3). The protein product encoded by this mutated allele, as predicted by the online tool ExPasy available from the Swiss Institute of Bioinformatics (Gasteiger et al., 2003) (<https://web.expasy.org/translate/>), is truncated by a premature stop codon. The length of the aa chain is less than a third of the WT and the GGQ motif is lost (Figure 7-4A). The blastp analysis shows that only the first 22 aa are identical between this aa chain and the C12orf65 reference sequence (UniProt ID Q9H3J6) (Figure 7-4B). Therefore, the deletion is likely to result in activation of NMD. If the transcript escapes this process, the predicted polypeptide is most likely degraded.

The second allele of 5N also contains a 14 b deletion, which starts 5 b upstream from the PAM motif (Figure 7-5). In contrast to the first allele, the predicted protein product encoded by the second allele does not contain a stop codon and maintains the GGQ motif. However, when aligned to the reference C12orf65 sequence (UniProt ID Q9H3J6), this predicted polypeptide lacks five aa in the mitochondrial targeting signal (aa 1-35) (Figure 7-6). Even if it were synthetized, the predicted polypeptide may not enter mitochondria; more likely, it would accumulate in the cytosol and eventually be degraded.

Since the two alleles appear in 1:1 ratio, and each of them is mutated in such a way that the encoded polypeptide is lost, I considered sample 5N a successful KO.

>Alt1 (Estimated allelic Fraction: 0.49) = 5N
 AGCCAGCAGAGGCCACGTTCTTATGAGCACCGTGGGTTATTCATTTCTACACCACTGACCCGAATATGCC
 CGGCGCCATGGGGAGAAGCTGACGTTGTTATCCCCAGGAATAGCTGTCACTCCGGTCCAAATGGCAGGCAAGAA
 GGACTACCCCTGCACTGCTTCTTGGATGAGAATGAACCTGAAAAGCAGTTGTGAAAGGACACGGTCCAGGGG
 GCCAGGCAACCAACAAAACCAGCAACTGCGTGGTGTGATT
 >Ref wildtype: 7-300 forward = E4 (control)
 ATTCTCTAACAAAGGTTCTTCAGCCGAGAGGCCACGTTCTTATGAGCACCGTGGGTTATTCATTTCTAC
 TTACTGACCCGAATATGCCCGGCCATGGGACTCCGGCTTGGGAGAAGCTGACGTTGTATCCCAGGAAT
 AGCTGTCACTCCGGTCCAGATGGCAGGCAAGAAGGACTACCCCTGCACTGCTTCTTGGATGAGAATGAACCTG
 AAGAGCAGTTGTGAAAGGACACGGTCCAGGGGCCAGGCAACCAACAAAACCAGCAACTGCGTGGTGTGATT
 Alignment score: 650
 #-----
 Alt (5N) 1 -----AGCCAGCAGAGGCCACGTTCTTATGAGCACCGTGGGTTA
 Ref (4E) 7 ATTCTCTAACAAAGGTTCTTCAGCC-GCAGAGGCCACGTTCTTATGAGCACCGTGGGTTA
 Alt (5N) 41 TTTCATTTCCTACACCACTGACCCGAATATGCCCGGCCATGGGG-----
 Ref (4E) 66 TTTCATTTCCTACATTACTGACCCGAATATGCCCGGCCATGGGACTCCGGCTTTGG
 Alt (5N) 89 --GAAGCTGACGTTGTTATCCCCAGGAATAGCTGTCACTCCGGTCCAAATGGCAGGCAAG
 Ref (4E) 126 GAGAAGCTGACGTTGTTATCCCCAGGAATAGCTGTCACTCCGGTCCAGATGGCAGGCAAG
 Alt (5N) 147 AAGGACTACCCCTGCACTGCTTCTTGGATGAGAATGAACCTGAAAAGCAGTTGTGAAA
 Ref (4E) 186 AAGGACTACCCCTGCACTGCTTCTTGGATGAGAATGAACCTGAAAGAGCAGTTGTGAAA
 Alt (5N) 207 GGACACGGTCCAGGGGGCCAGGCAACCAACAAAACCAGCAACTGCGTGGTGTGATT
 Ref (4E) 246 GGACACGGTCCAGGGGGCCAGGCAACCAACAAAACCAGCAACTGCGTGGTGTGATT
 GGQ

Figure 7-3. The results of DNA sequencing of mutant cells from sample 5N- allele 1

After isolating total DNA from cells, the first exon of *C12orf65* was amplified and the PCR product sent to Sanger sequencing using the forward primer. An online deconvolution tool (<https://www.gear-genomics.com/indigo/>) was used to align sample 5N against no gRNA control (4E). The start codon is underlined and indicated by a black arrow. The 14 nucleotides deletion from 5N allele 1 is represented by a dotted line and emphasized by a red line. The gRNA target is highlighted in yellow, the PAM motif in green, and the sequence encoding for the GGQ motif – in red.

A.

-5'3' Frame 1

```
atg agc acc gtg ggt tta ttt cat ttt cct aca cca ctg acc cga ata tgc ccg gcg cca
M S T V G L F H F P T P L T R I C P A P
tgg gga gaa gct gac gtt gtt atc ccc agg aat agc tgt cac tcc ggt cca aat ggc agg
W G E A D V V I P R N S C H S G P N G R
caa gaa gga cta ccc tgc act gct ttc ctt gga tga gaa tga act cga aaa gca gtt tgt
Q E G L P C T A F L G - E - T R K A V C
gaa agg aca cgg tcc agg ggg cca ggc aac caa aac cag caa ctg cgt ggt gct gat
E R T R S R G P G N Q Q N Q L R G A D
```

B.

sp|Q9H3J6|MTRFR_HUMAN Mitochondrial translation release factor in rescue OS=Homo sapiens OX=9606 GN=MTRFR PE=1

SV=1

Sequence ID: Query_364099 Length: 166 Number of Matches: 1

Range 1: 1 to 22 [Graphics](#)

[▼ Next Match](#) [▲ Previous Match](#)

Score	Expect	Method	Identities	Positives	Gaps
54.7 bits(130)	3e-16	Composition-based stats.	22/22(100%)	22/22(100%)	0/22(0%)
Query 1	MSTVGLFHFPPTPLTRICPAPWG	22			
Subjct 1	MSTVGLFHFPPTPLTRICPAPWG	22			

Figure 7-4. Predicted polypeptide encoded by 5N allele 1

A. The predicted aa sequence encoded by sample 5N allele 1, obtained with the online translating tool Expasy available from the Swiss Institute of Bioinformatics. The dash represents a stop codon, the open reading frame is highlighted in red. The canonical start codon (ATG) is according to the C12orf65 reference sequence from the Ensemble Genome Browser release 102, transcript ID ENST00000253233.6.

B. Alignment (blastp, NCBI) between the aa sequence predicted from allele 1 of sample 5N (Subjct) and the reference aa sequence of C12orf65 (MTRFR, UniProt ID Q9H3J6)

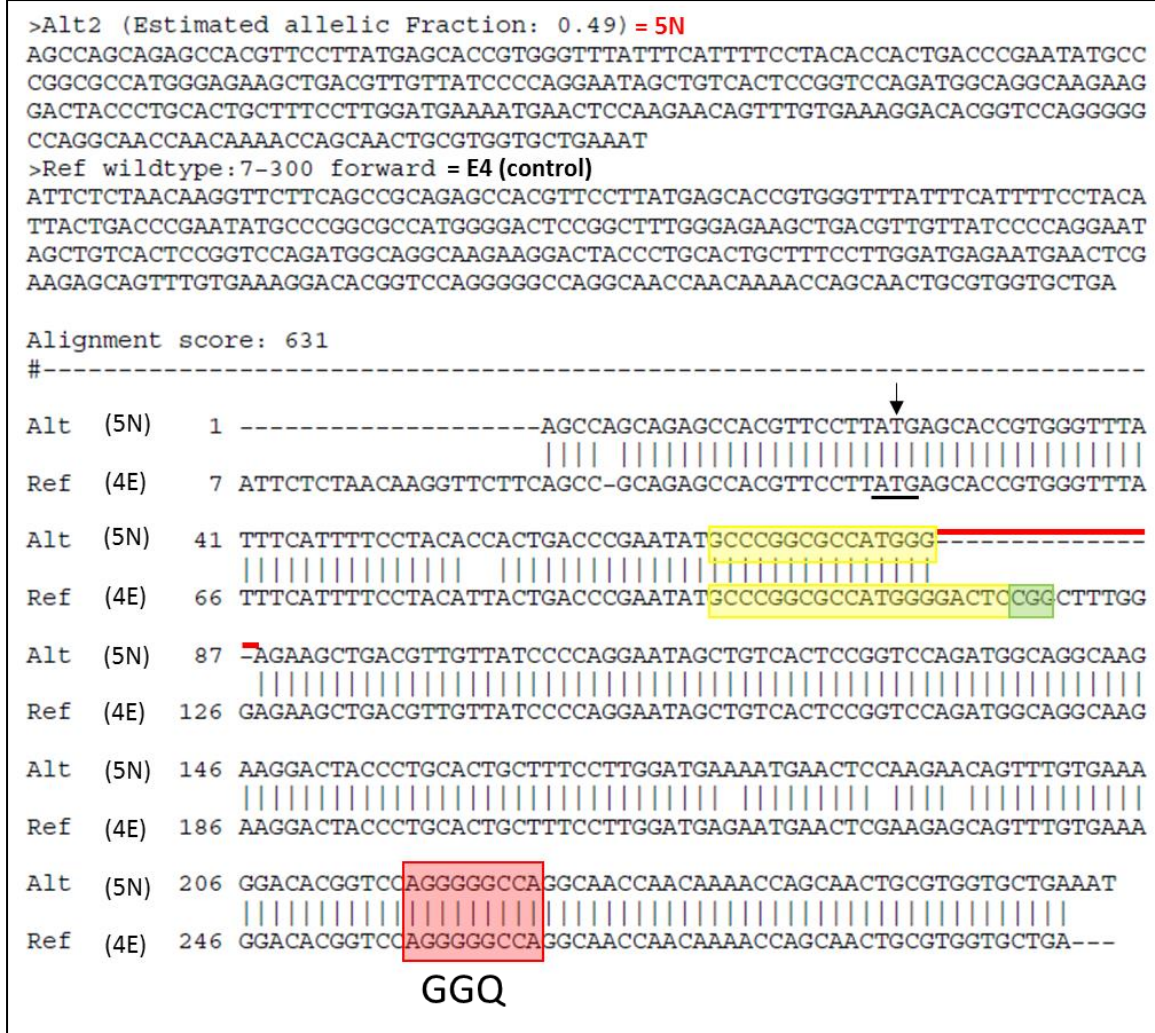


Figure 7-5. The results of DNA sequencing of mutant cells from sample 5N- allele 2

After isolating total DNA from cells, the first exon of *C12orf65* was amplified and the PCR product sent to Sanger sequencing using the forward primer. An online deconvolution tool (<https://www.gear-genomics.com/indigo/>) was used to align sample 5N against no gRNA control (4E). The start codon is underlined and indicated by a black arrow. The 14 nucleotides deletion from 5N allele 2 is represented by a dotted line and emphasized by a red line. The gRNA target is highlighted in yellow, the PAM motif in green, and the sequence encoding for the GGQ motif – in red.

A.

-5'3' Frame 1

atg	agc	acc	gtg	ggt	tta	ttt	cat	ttt	cct	aca	cca	ctg	acc	cga	ata	tgc	ccg	gct	cca
M	S	T	V	G	L	F	H	F	P	T	P	L	T	R	I	C	P	A	P
tgg	gag	aag	ctg	acg	ttg	tta	tcc	cca	gga	ata	gct	gtc	act	ccg	gtc	cag	atg	gca	ggc
W	E	K	L	T	L	L	S	P	G	I	A	V	T	P	V	Q	M	A	G
aag	aag	gac	tac	cct	gca	ctg	ctt	tcc	ttg	gat	gaa	aat	gaa	ctc	caa	gaa	cag	ttt	gtg
K	K	D	Y	P	A	L	L	S	L	D	E	N	E	L	Q	E	Q	F	V
aaa	gga	cac	ggg	cca	ggg	ggc	cag	gca	acc	aac	aaa	acc	agc	aac	tgc	gtg	gtg	ctg	aaa
K	G	H	G	P	G	G	Q	A	T	N	K	T	S	N	C	V	V	L	K

B.

sp|Q9H3J6|MTRFR_HUMAN Mitochondrial translation release factor in rescue OS=Homo sapiens OX=9606 GN=MTRFR PE=1
SV=1
Sequence ID: Query_22847 Length: 166 Number of Matches: 1

Range 1: 1 to 85 [Graphics](#) [▼ Next Match](#) [▲ Previous Match](#)

Score	Expect	Method	Identities	Positives	Gaps
162 bits(411)	3e-58	Compositional matrix adjust.	79/85(93%)	80/85(94%)	5/85(5%)

Query 1 MSTVGLFHFPPTPLTRICPAPW-----EKLTLLSPGIAVTPVQ^{MAGKKDYPALLSDENEL} 55
MSTVGLFHFPPTPLTRICPAPW EKLTLLSPGIAVTPVQ^{MAGKKDYPALLSDENEL}
Sbjct 1 MSTVGLFHFPPTPLTRICPAPWGLRLWEKLTLSPGIAVTPVQ^{MAGKKDYPALLSDENEL} 60

Query 56 QEQFVKGHGF **GGQ**ATNKTTSNCVVLK 80
+EQFVKGHGF GQGATNKTTSNCVVLK
Sbjct 61 EEQFVKGHGF **GGQ**ATNKTTSNCVVLK 85

Figure 7-6. Predicted polypeptide encoded by 5N allele 2

A. The predicted amino acid sequence encoded by sample 5N allele 2, obtained with the online translating tool Expasy available from the Swiss Institute of Bioinformatics. The open reading frame is highlighted in red, the GGQ motif is indicated by a black square. The canonical start codon (ATG) is according to the *C12orf65* reference sequence from the Ensemble Genome Browser release 102, transcript ID ENST00000253233.6.

B. Alignment (blastp, NCBI) between the aa sequence predicted from allele 2 of sample 5N (Sbjct) and the reference aa sequence of *C12orf65* (MTRFR, UniProt ID Q9H3J6); the red square indicates the GGQ motif and the '+' indicates amino acids with similar chemical properties.

The second sample identified was 15N (non-induced C12orf65-FLAG HEK FlipIn cell line). It contains an identical deletion of one cytosine in both alleles, located downstream from the sequence encoding the GGQ motif. Despite that, the mutations identified, and their consequences, are different for each allele.

The first allele of 15N contains intact canonical start codon, gRNA target and PAM sequence (Figure 7-7). Apart from the cytosine deletion, it contains two substitutions upstream from the gRNA target. This allele encodes a predicted polypeptide of 83 aa, with an intact mitochondrial targeting sequence and GGQ motif (Figure 7-8A). Apart from the last three aa, this polypeptide is identical to the C12orf65 reference sequence (UniProt ID Q9H3J6) (Figure 7-8B); therefore, there is a high probability that it is correctly synthetized, imported in the mitochondria and assembled.

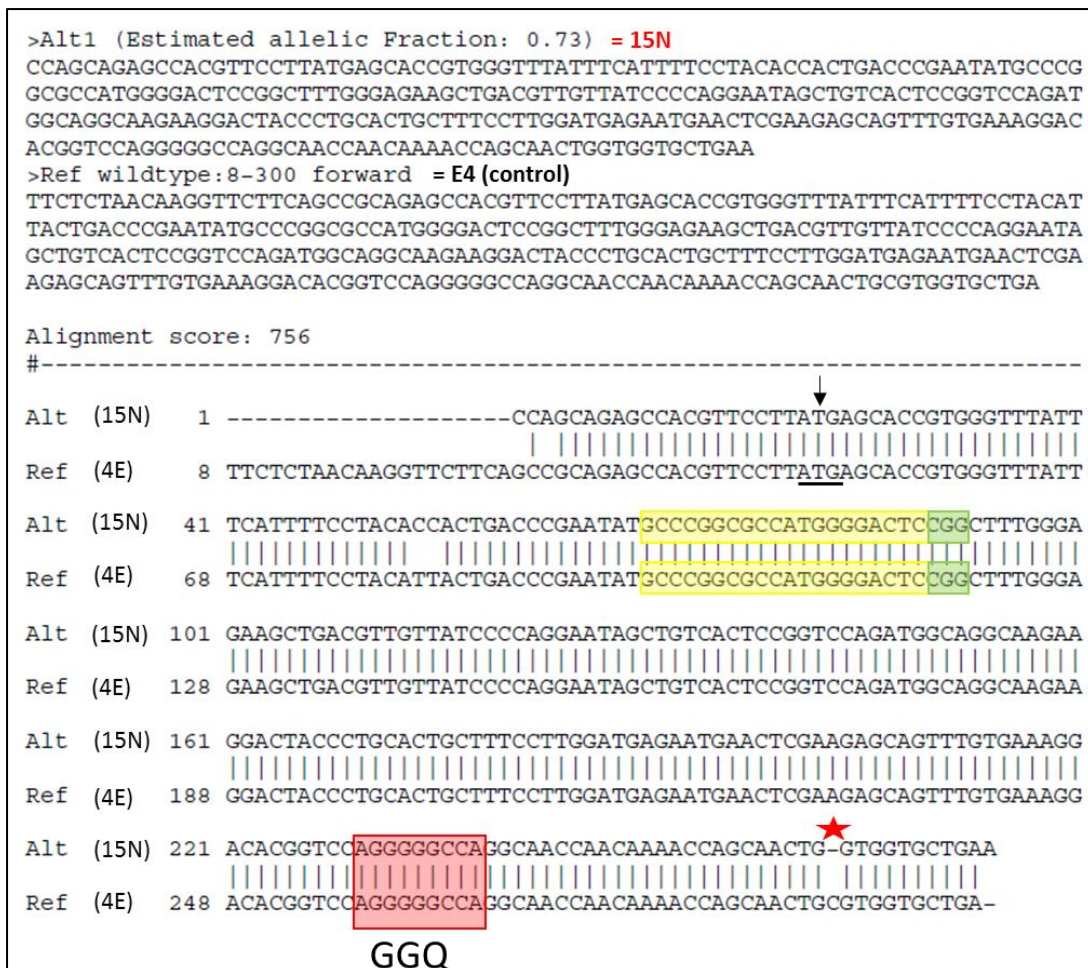


Figure 7-7. The results of DNA sequencing of mutant cells from sample 15N – allele 1

After isolating total DNA from cells, the first exon of *C12orf65* was amplified and the PCR product sent to Sanger sequencing using the forward primer. An online deconvolution tool (<https://www.gear-genomics.com/indigo/>) was used to align sample 15N against no gRNA control (4E). The start codon is underlined and indicated by a black arrow. The red star indicates a single nucleotide deletion. The gRNA target is highlighted in yellow, the PAM motif in green, and the sequence encoding for the GGQ motif – in red.

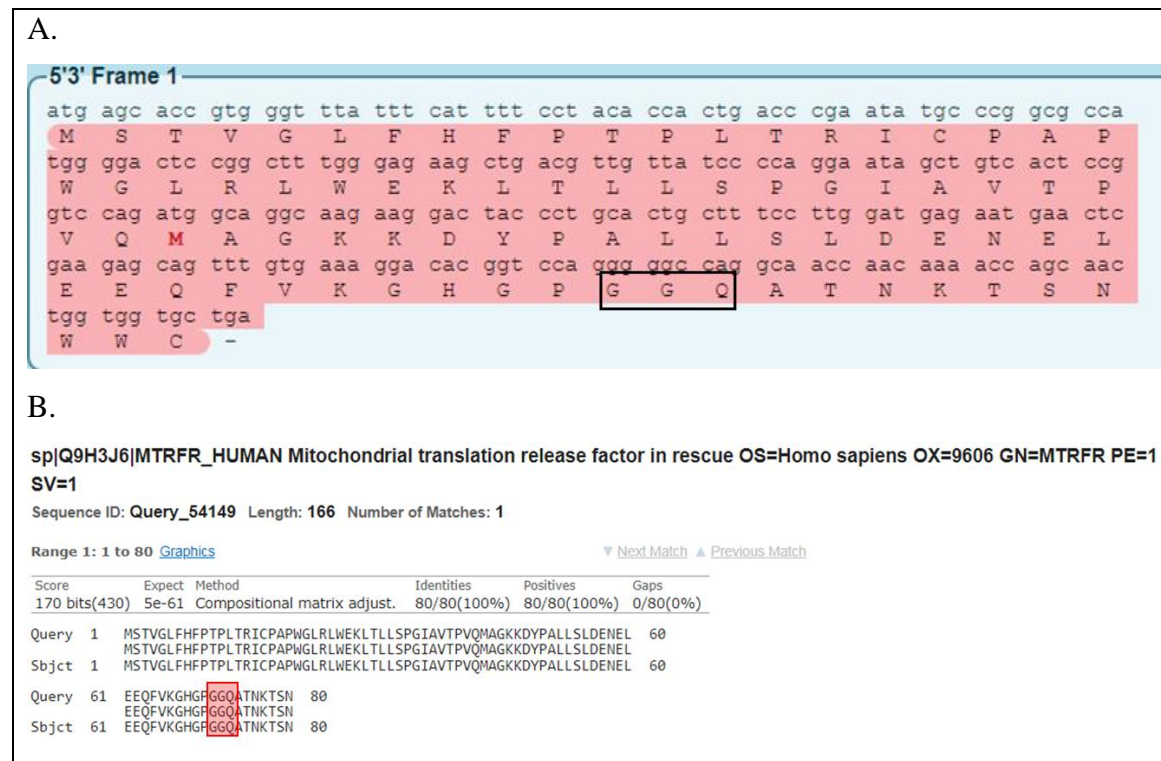


Figure 7-8. Predicted polypeptide encoded by 15N allele 1

A. The predicted amino acid sequence encoded by sample 15N allele 1, obtained with the online translating tool Expasy available from the Swiss Institute of Bioinformatics. The dash represents a stop codon, the open reading frame is highlighted in red, and the GGQ motif is shown in a black square. The canonical start codon (ATG) is according to the *C12orf65* reference sequence from the Ensemble Genome Browser release 102, transcript ID ENST00000253233.6.

B. Alignment (blastp, NCBI) between the aa sequence predicted from allele 1 of sample 15N (Sbjct) and the reference aa sequence of *C12orf65* (MTRFR, UniProt ID Q9H3J6); the GGQ motif is shown in a red square.

The second allele of sample 15N contains a substitution in the first start codon and several substitutions in the gRNA target (Figure 7-9A). Because of the substitution, the canonical start codon is not recognized by the pre-initiation complex at the start of translation. If the transcript is not degraded, the translation of the polypeptide encoded by this allele would start from the second codon, which would lead to a complete loss of the mitochondrial targeting sequence. The predicted polypeptide has no stop codon (Figure 7-9B) and is so different from the *C12orf65* reference sequence, that the blastp comparison between the two found no similarity and an alignment could not be performed. It is likely that this polypeptide, if synthesized, is degraded.

A.

```
>Alt2 (Estimated allelic Fraction: 0.23) = 15N
CCAGTTGAGCGACGTTCTTGTGAGCTCCGTGGGTTATTCATTTCATTTCTTCACCGCTGAGCGGGAGGTGCCAG
GGGACTTGGGACTCCGGCTTGGGAGAAGCTGACCTTGTATCCCCAGGAATAGATGTCACTCCAGTCAGAT
GCCATGCAAGAATGACTACCAGAACAGGAAACAGACAGCAACTGGTGGTGTGAA
>Ref wildtype:8-300 forward = E4 (control)
TTCTCTAACAGGTTCTTCAGCCGAGGCCACGTTCTTATGAGCACCGTGGGTTATTCATTTCTACAT
TACTGACCCGAATATGCCCGGCCATGGGACTCCGGCTTGGGAGAAGCTGACGTGTTATCCCAGGAATA
GCTGTCACTCCGGTCCAGATGGCAGGAAGGACTACCCCTGACTGCTTCTGGATGAGAATGAACTCGA
AGAGCAGTTGTGAAAGGACACGGTCAGGGGCCAGGCAACCAACAAACAGCAACTGCGTGGTGTGAA

Alignment score: 492
#-----
```

Alt (15N) 1 CCAGTTGAGCGACGTTCTTGTGAGCTCCGTGGGTTATT
Ref (4E) 8 TTCTCTAACAGGTTCTTCAGCCGAGGCCACGTTCTTATGAGCACCGTGGGTTATT
Alt (15N) 41 TCATTTCTTCCACCGCTGAGCGGGAGGTGCCAGGGACTTGGGACTCCGGCTTTGGGA
Ref (4E) 68 TCATTTCTTACATTACTGACCGAATATGCCGGCCATGGGACTCCGGCTTTGGGA
Alt (15N) 101 GAAGCTGACCTTGTATCCCCAGGAATAGATGTCACTCCAGTCCAGATGGCATGCAAGAA
Ref (4E) 128 GAAGCTGACGTTGTATCCCCAGGAATAGCTGTCACTCCGGTCCAGATGGCAGGCAAGAA
Alt (15N) 161 TGACTACCAGAACGCTTGTGGATGACAGTGAAGTCCACAGCATTGTGGAAGG
Ref (4E) 188 GGACTACCCTGCACTGCTTCTGGATGAGAATGAACTCGAACAGGAGCTTGTGAAAGG
Alt (15N) 221 ACACGGTCCAGGGGCCAGGCAACCAACAGACAGCAACTG-GTGGTGTGAA
Ref (4E) 248 ACACGGTCCAGGGGCCAGGCAACCAACAAACAGCAACTGCGTGGTGTGAA
GGQ

B.

-5'3' Frame 1

atg tca ctc cag tcc aga tgg cat gca aga atg act acc atg aac tgc ttt gct tgg atg	M S L Q S R W H A R M T T M N C F A W M
aca gtc aag tcc aac agc att tgg tgg aag gac acg gtc cag ggg gcc agg caa cca aca	T V K S N S I L W K D T V Q G A R Q P T
aga cca gca act ggt ggt gct gaa	R P A T G G A E

Figure 7-9. DNA sequencing and polypeptide prediction of sample 15N – allele 2

After isolating total DNA from cells, the first exon of *C12orf65* was amplified and the PCR product sent to Sanger sequencing using the forward primer.

A. An online deconvolution tool (<https://www.gear-genomics.com/indigo/>) was used to align sample 15N against no gRNA control (4E). The canonical start codon is mutated (underlined, indicated by a crossed arrow) and the next start codon is indicated by a black arrow and underlined. The red star indicates a single nucleotide deletion. The gRNA target is highlighted in yellow, the PAM motif in green, and the sequence encoding for the GGQ motif – in red. The yellow line indicates the gRNA target sequence affected by variants.

B. The predicted aa sequence encoded by sample 15N allele 2, obtained with the online translating tool Expasy available from the Swiss Institute of Bioinformatics. The open reading frame is highlighted in red. Because the canonical start codon is mutated, the second ATG was used for this translation, according to the *C12orf65* reference sequence from the Ensemble Genome Browser release 102, transcript ID ENST00000253233.6.

The single cytosine deletion present in both 15N alleles occurs towards the 3'end of the first coding exon, which raises the possibility of a defective exon/intron recognition, with alterations of the ORF should the intron be retained (Anna and Monika, 2018). This could lead to an aberrant protein product with a different C-terminal region, prone to being targeted by the ubiquitin–proteasome system (UPS) or lysosomal proteolysis (Vilchez et al., 2014). However, the predicted polypeptide encoded from allele 1 contains a stop codon. Also, this single base deletion appears close to the end of the sequence, so it could be a sequencing artifact. To further confirm the presence of this deletion, the sample 15N should be sequenced using the reverse primer.

Based on current sequencing results, the first allele, which might lead to a correct protein product, is three times more abundant than the second allele, encoding for a defective polypeptide. This makes the clone 15N unlikely to be a real KO.

Finally, another sample identified as a complete KO by the deconvolution software was 22F. In this case, the canonical start codon was intact for both alleles. The first allele contains a large insertion (64 b) that starts in the gRNA target sequence, 3 b upstream from the PAM motif, which is in agreement with the position where Cas9 cuts the DNA strands (Figure 7-10). The insertion is followed by five substitutions, which all occur upstream from the region that encodes the GGQ motif (Figure 7-11A). In the predicted polypeptide encoded by this allele, the GGQ motif is lost due to a premature stop codon. The alignment of this peptide with the C12orf65 reference (UniProt ID Q9H3J6) reveals a low similarity and a 5 b deletion in the mitochondrial targeting sequence (Figure 7-11B). If translated, this predicted polypeptide would probably not be functional and would be degraded.

The second allele of sample 22F contains a four nucleotides deletion in the gRNA target sequence and a one base substitution in the PAM motif (Figure 7-12). The deletion is localized 3 b upstream from the PAM motif, consistent to the Cas9 cleavage site. The substitution from the PAM motif is followed by numerous other substitutions which precede a large insertion (69 b). All these events occur upstream from the sequence that encodes the GGQ motif. The predicted aa sequence encoded by this allele is very short (36 residues) because it is truncated by a premature stop codon (Figure 7-13A). The polypeptide has the length of the mitochondrial targeting sequence of WT C12orf65 and has lost the GGQ motif. When compared to the C12orf65 reference, only the first 20 aa are identical, the rest cannot be aligned (Figure 7-13B).

Because it is so short, has an incomplete mitochondrial targeting sequence and lacks the GQG motif, the polypeptide encoded by the second allele of 22F is likely to be degraded.

Since both alleles of 22F are mutated, and each of them encodes for a truncated polypeptide with low similarity to the WT sequence, the C12orf65 is likely to be absent in this clone.

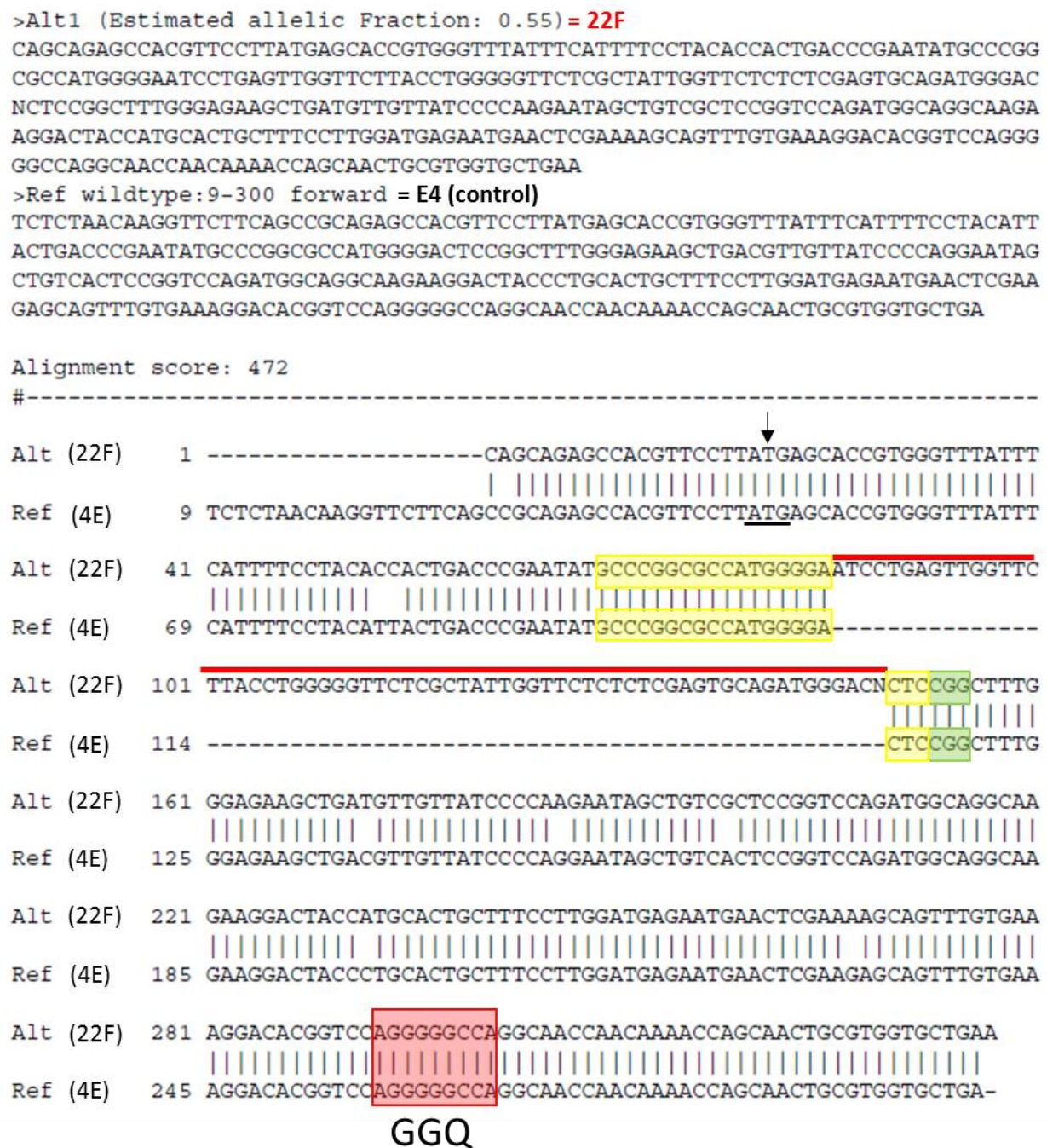


Figure 7-10. The results of DNA sequencing of mutant cells from sample 22F – allele 1

After isolating total DNA from cells, the first exon of *C12orf65* was amplified and the PCR product sent to Sanger sequencing using the forward primer. An online deconvolution tool (<https://www.gear-genomics.com/indigo/>) was used to align sample 22F against no gRNA control (4E). The start codon is underlined and indicated by a black arrow. The 64 nucleotides insertion from 22F allele 1 is represented by a dotted line in the control and emphasized by a red line. The gRNA target is highlighted in yellow, the PAM motif in green, and the sequence encoding for the GGQ motif – in red.

A.

5'3' Frame 1

atg	agc	acc	gtg	ggt	tta	ttt	cat	ttt	cct	aca	cca	ctg	acc	cga	ata	tgc	ccg	gcg	cca
M	S	T	V	G	L	F	H	F	P	T	P	L	T	R	I	C	P	A	P
tgg	gga	atc	ctg	agt	tgg	ttc	tta	cct	ggg	ggt	tct	cgc	tat	tgg	ttc	tct	ctc	gag	tgc
W	G	I	L	S	W	F	L	P	G	G	S	R	Y	W	F	S	L	E	C
aga	tgg	gac	nct	ccg	gct	ttg	gga	gaa	gct	gat	gtt	gtt	atc	ccc	aag	aat	agc	tgt	cgc
R	W	D	X	P	A	L	G	E	A	D	V	V	I	P	K	N	S	C	R
tcc	ggt	cca	gat	ggc	agg	caa	gaa	gga	cta	cca	tgc	act	gtc	ttc	ctt	gga	tga	gaa	tga
S	G	P	D	G	R	Q	E	G	L	P	C	T	A	F	L	G	-	E	-
act	cga	aaa	gca	gtt	tgt	gaa	agg	aca	cgg	tcc	agg	ggg	cca	ggc	aac	caa	caa	aac	cag
T	R	K	A	V	C	E	R	T	R	S	R	G	P	G	N	Q	Q	N	Q
caa	ctg	cgt	ggt	gct	gaa														
Q	L	R	G	A	E														

B.

sp|Q9H3J6|MTRFR_HUMAN Mitochondrial translation release factor in rescue OS=Homo sapiens OX=9606 GN=MTRFR PE=1 SV=1

Sequence ID: Query_48047 Length: 166 Number of Matches: 1

Range 1: 1 to 56 [Graphics](#) [▼ Next Match](#) [▲ Previous Match](#)

Score	Expect	Method	Identities	Positives	Gaps
57.8 bits(138)	6e-17	Compositional matrix adjust.	30/56(54%)	35/56(62%)	5/56(8%)

Query 1 MSTVGLFHFTPPLTRICPAPWGI-----LSWFLPGGSRYWFSLECRWDXPALGEAD 51
Sbjct 1 MSTVGLFHFTPPLTRICPAPWGI+L+PG+ + + D PAL D MSTVGLFHFTPPLTRICPAPWGLRLWEKLTLSPGIAVTPVQMGKKDYPALLSD 56

Figure 7-11. Predicted polypeptide encoded by 22F allele 1

A. The predicted aa sequence encoded by sample 22F allele 1, obtained with the online translating tool Expasy available from the Swiss Institute of Bioinformatics. The dash represents a stop codon, the open reading frame is highlighted in red. The canonical start codon (ATG) is according to the *C12orf65* reference sequence from the Ensemble Genome Browser release 102, transcript ID ENST00000253233.6.

B. Alignment (blastp, NCBI) between the aa sequence predicted from allele 1 of sample 22F (Sbjct) and the reference aa sequence of *C12orf65* (MTRFR, UniProt ID Q9H3J6); the '+' indicates amino acids with similar chemical properties.

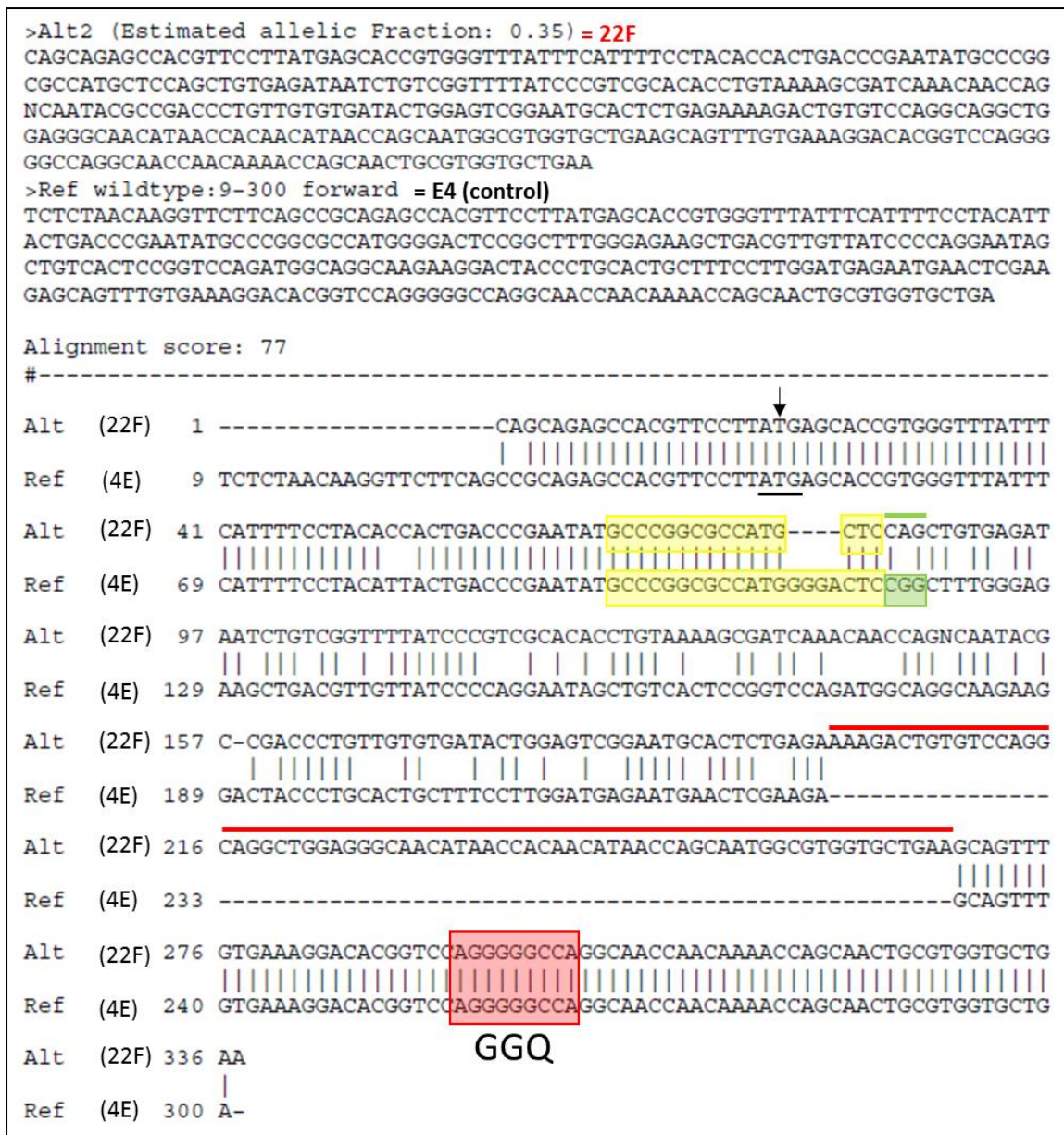


Figure 7-12. The results of DNA sequencing of mutant cells from sample 22F- allele 2

After isolating total DNA from cells, the first exon of *C12orf65* was amplified and the PCR product sent to Sanger sequencing using the forward primer. An online deconvolution tool (<https://www.gear-genomics.com/indigo/>) was used to align sample 22F against no gRNA control (4E). The start codon is underlined and indicated by a black arrow. The 69 nucleotides insertion from 22F allele 2 is represented by a dotted line in the control and emphasized by a red line. The gRNA target is highlighted in yellow, the PAM motif in green, and the sequence encoding for the GGQ motif – in red. The green line represents the mutated PAM motif.

A.

5'3' Frame 1

atg	agc	acc	gtg	ggt	tta	ttt	cat	ttt	cct	aca	cca	ctg	acc	cga	ata	tgc	ccg	gcg	cca
M	S	T	V	G	L	F	H	F	P	T	P	L	T	R	I	C	P	A	P
tgc	tcc	agc	tgt	gag	ata	atc	tgt	cggt	ttt	tat	ccc	gtc	gca	cac	ctg	taa	aag	cga	tca
C	S	S	C	E	I	I	C	R	F	Y	P	V	A	H	L	-	K	R	S
aac	aac	cag	nca	ata	cgc	cga	ccc	tgt	tgt	gtg	ata	ctg	gag	tcg	gaa	tgc	act	ctg	aga
N	N	Q	X	I	R	R	P	C	C	V	I	L	E	S	E	C	T	L	R
aaa	gac	tgt	gtc	cag	gca	ggc	tgg	agg	gca	aca	taa	cca	caa	cat	aac	cag	caa	tgg	cgt
K	D	C	V	Q	A	G	W	R	A	T	-	P	Q	H	N	Q	Q	W	R
ggt	gct	gaa	gca	gtt	tgt	gaa	agg	aca	cggt	tcc	agg	ggg	cca	ggc	aac	caa	caa	aac	cag
G	A	E	A	V	C	E	R	T	R	S	R	G	P	G	N	Q	Q	N	Q
caa	ctg	cgt	ggt	gct	gaa														
Q	L	R	G	A	E														

B.

sp|Q9H3J6|MTRFR_HUMAN Mitochondrial translation release factor in rescue OS=Homo sapiens OX=9606 GN=MTRFR PE=1
SV=1
Sequence ID: Query_32447 Length: 166 Number of Matches: 1
Range 1: 1 to 20 Graphics ▾ Next Match ▲ Previous Match
Score Expect Method Identities Positives Gaps
49.3 bits(116) 2e-14 Composition-based stats. 20/20(100%) 20/20(100%) 0/20(0%)
Query 1 MSTVGLFHFTPPLTRICPAP 20
Sbjct 1 MSTVGLFHFTPPLTRICPAP 20

Figure 7-13. Predicted polypeptide encoded by 22F allele 2

A. The predicted aa sequence encoded by sample 22F allele 2, obtained with the online translating tool Expasy available from the Swiss Institute of Bioinformatics. The dash represents a stop codon, the open reading frame is highlighted in red. The canonical start codon (ATG) is according to the *C12orf65* reference sequence from the Ensemble Genome Browser release 102, transcript ID ENST00000253233.6.

B. Alignment (blastp, NCBI) between the aa sequence predicted from allele 2 of sample 22F (Sbjct) and the reference aa sequence of C12orf65 (MTRFR, UniProt ID Q9H3J6)

7.3 Discussion

Based on sequencing only, two HEK clones appear as successful KO: 5N and 22F. A western blot analysis would be necessary to confirm the absence of the protein, but this was not possible because an anti-C12orf65 antibody was not available.

The HEK293T cell line is prone to aneuploidy and chromosome instability. In theory, *C12orf65*-FLAG transfected but non-induced samples (5N and 15N) should have three alleles, and FlpIn non-transfected samples (22F) should have two. According to ATCC, HEK293 is a hypotriploid line, with a modal chromosome number of 64, occurring in 30% of cells. In practice, it was found that stable transfection of HEK293 cells leads to a decreased modal number of chromosomes and that, in particular, chromosome 12 (C12) had 3 copies/cell

(Stepanenko et al., 2015). When analysing the karyotype of four different HEK293 derivates, Lin et al. found that HEK293T lacked a copy of C12 in 6/19 metaphases that they have assessed (Lin et al., 2014). This might explain the differences in estimated allelic fraction between the three clones, and why the two alleles of sample 5N appear in a 1:1 ratio.

Due to the outbreak of Covid-19, I could not perform any formal analysis of the two cell lines that I consider a successful KO. In this discussion, I will detail the experiments that I had planned for their characterization and use as biological models.

To assess whether NMD was efficient, I would measure mRNA expression of *C12orf65* by qPCR. Verification of protein levels by western blot could be challenging, as the current commercial antibodies only recognize the overexpressed *C12orf65*. A previous attempt to purify *C12orf65* antibodies in the lab was not conclusive: it was not certain whether the antibodies recognized the protein; they were unstable and the results could not be reproduced (Pajak, 2013). The only endogenous *C12orf65* western blot signals available in literature come from two Japanese groups (Kogure et al., 2012, Shimazaki et al., 2012). They both used Can Get Signal immunostain (Toyobo), which was not available.

To characterize the cell lines, I would measure cell viability and proliferation in normal glucose media and in galactose media (to force cell respiration), because those are the first indicators of health status. As mentioned before, I have already seen a lower growth rate and a clumps phenotype in the KO clones comparing to the control. But for a formal characterization, I would measure cell growth with Incucyte and viability with trypan blue for 3-6 days. This would allow me to compare the KO results with the siRNA results previously obtained by Dr. Pajak. I would also measure the oxygen consumption rate using Seahorse in order to test mitochondria respiration.

To investigate the BioID2 hits, I would first focus on the ones involved in transcription and RNA processing, like mtRNase P complex and LRPPRC-SLIRP, by checking the protein levels by western blot. I would expect these levels to be increased as a feedback mechanism to compensate for the impaired translation that the lack of *C12orf65* would induce. Second, I would investigate MRPs from the small subunit that interact with mRNA: MRPS5, MRPS9, MRPS23, MRPS28, and MRPS31. I would check their protein levels by western blot and their migration pattern on sucrose gradients to see whether they change in the absence of *C12orf65*.

To investigate mitochondria translation, I would first analyse the steady state levels of mtRNAs by Northern blot. Dr. Pajak and Dr. Wesolowska obtained different results with the

siRNA treatment and I consider that, as KO is stable, my clones would shift the balance towards an effect. Antonicka et al. reported a slight increase in mt-RNA in two patients with *C12orf65* variants that resulted in a premature stop codon (Antonicka et al., 2010). Later, Wesolowska et al. reported a similar modest increase of mt-RNAs in an adult patient with Leigh syndrome diagnosed in Newcastle (Wesolowska et al., 2015). KO and patients' cells are stable models, which do not need siRNA re-transfection, but the HEK293T cells and patients' fibroblasts are different as types of cell. For this reason, I cannot speculate on the outcome of mt-RNA measurement. Should I find a difference in 16S mt-LSU rRNA, 12S mt-SSU rRNA or mt-tRNA^{Val} levels, I would further explore the composition of the mitoribosome by separating the small and large subunits on sucrose gradients and probe them with specific antibodies on western blot.

Next, I would investigate the protein levels and OXPHOS activity by western blot and BN-PAGE. The literature available agrees that *C12orf65* defects lead to a decrease in OXPHOS activity and protein levels of respiratory subunits, but the results are contradictory in terms of specific proteins/complexes. They depend on the type of pathogenic variant and tissue analysed. Also, there are more *C12orf65* clinical reports than scientific articles, and some biochemical experiments are missing. Antonicka et al. reported decreased levels of mtDNA-encoded polypeptides and decreased activity of cytochrome c oxidase (RC IV), with assembly defects in RC I, III (milder) IV, and V (Antonicka et al., 2010). Wesolowska et al. reported a similar pattern: global reduction of mitochondrial polypeptides, reduced levels of RC I and IV, defects of assembly in complexes I, IV and V with milder defects for complex III, and an isolated CIV deficiency in muscle and fibroblasts (Wesolowska et al., 2015). Shimazaki et al. also reported a reduced mtDNA-encoded protein level with disruption of supercomplexes formed by I, III and IV, but the enzymatic activity was reduced in both complex I and IV, not only in IV (Shimazaki et al., 2012). In contrast, Tucci et al. describe a decreased activity and impaired assembly only in complex V, without mentioning any other complex (Tucci et al., 2014). Imagawa et al. (Imagawa et al., 2016) found an isolated complex IV deficiency, although they measured the activities of all respiratory complexes, and the pathogenic variant they present is identical with the one from Tucci et al. (Tucci et al., 2014).

Considering this cumulative evidence, I would expect to see a global decreased level of mitochondria-encoded proteins, which would impair complex assembly and enzymatic function in my KO clones.

In light of the new results from Desai et al. (Desai et al., 2020), I would check MTRES1 expression and protein levels to see whether they correlate with the C12orf65 levels. They have shown that the two proteins form a dimer in a HEK293T model with stalled mitoribosomes. It would be interesting to see what happens when mitochondria translation is not artificially stalled: would MTRES1 decrease with C12orf65? Would it increase, in an attempt to compensate for its partner loss? Or would it stay the same, assuming that the two do not interact unless the stalling happens?

The gene KO triggers the genetic compensation response. Genetic compensation response is a feedback phenomenon based on upregulation of the genes related to the mutant, which can take over the mutant function (El-Brolosy and Stainier, 2017, Ma Zhipeng, 2019). Based on experiments done in mouse and zebrafish mutants with a premature stop codon, it is proposed that the genetic compensation response is triggered by NMD, which produces fragments of degraded mRNA that base-pair with the related genes (El-Brolosy et al., 2019). The mechanism involves Upf3, an NSD factor that binds to the EJC close to the premature stop codon and recruits the COMPASS complex. COMPASS is a transcription activator that methylates histone 3 at the promoter regions of the compensatory genes, increasing their expression (Ma et al., 2019). Considering these, the *C12orf65* KO could trigger the upregulation of the other members of the mitochondria translation factor family: ICT1, mtRF1a and mtRF1. Current results from Lightowlers lab show that KO of mtRF1 leads to a significant increase in *C12orf65* transcripts, but not in *ICT1* or *mtRF1a* (Dr. Shreya Ayyub, unpublished data). Comparing the results obtained for the C12orf65 KO with the mtRF1 KO could allow the identification of a possible compensatory mechanism between the mitochondrial release factors.

On long term, once confirmed and characterized, the KO clones can be used for rescue experiments. Rescue of C12orf65 would serve as additional confirmation for the phenotype of the KO clones, while rescue of ICT1, mtRF1 or mtRF1a could shed light on their function.

Chapter 8

Final conclusions

At the start of my PhD, one of the key unanswered questions of mitochondrial biology was about the termination step of translation. Based on sequence comparison with bacterial release factors, four proteins had been included in the mitochondria translation release factor family: mtRF1a, mtRF1, ICT1 and C12orf65 (Richter et al., 2010a). Only mtRF1a was proven to terminate translation for all the 13 mtDNA-encoded proteins (Soleimanpour-Lichaei et al., 2007), despite the fact that all four members contain the GGQ motif necessary for peptide release (Richter et al., 2010b, Huynen et al., 2012). ICT1 was shown to be part of the mtLSU (Richter et al., 2010b) but the functions of mtRF1 and C12orf65 were not determined at the time.

My work focused on investigating the role of mtRF1 and C12orf65 in mitochondria translation. I started from the hypothesis that both factors are involved in quality control by rescuing mitoribosome stalled during translation. The rescue would occur in different situations for each factor. This chapter will summarize the results I obtained and discuss how they relate to the original hypothesis.

For mtRF1, it was already known that it is imported in the mitochondria (Soleimanpour-Lichaei et al., 2007). Previous studies from my host lab have proven that it is necessary for cell viability (Pajak, 2013). Based on its primary structure, that showed an extended codon recognition motif when compared to bacterial release factors, Huynen et al. performed 3D modelling that positioned the additional amino acids on the mitoribosome (Huynen et al., 2012). The 3D model predicted that the additional amino acids from the codon recognition motif would not fit in the A site if a codon was present there (Huynen et al., 2012), which led to the hypothesis that mtRF1 binds to mitoribosomes stalled on an empty A site. Therefore, mtRF1 would rescue mitoribosomes that became stalled due to a truncated mRNA that lacked a stop codon.

The technical approach chosen for mtRF1 study was aimed at isolation of the putative truncated mRNA target. First, I used DSP to cross-link mtRF1-FLAG to the mitoribosome. Second, I performed an immunoprecipitation with anti-FLAG agarose beads to isolate the cross-linked partners, together with the mRNA protected by the mitoribosome. I isolated RNA from the precipitate, reverse-transcribed it and identified it using qPCR.

I successfully cross-linked mtRF1-FLAG to the mitoribosome and isolated RNA from the immunoprecipitate. This shows that mtRF1 transiently interacts with the mitoribosome, as expected. Since mtRF1 is not part of the mitoribosome structure, if it is involved in rescue, it would occur near the mitoribosome. This close proximity allows cross-linking, which results

in mtLSU, mtSSU and mtRF1 being locked together. If mtRF1 had no functional relation with the mitoribosome, cross-linking would not be possible.

Isolation of RNA from the immunoprecipitate did not lead to conclusive results due to the high level of background. I was expecting to obtain RNA only from the induced cells, that expressed mtRF1-FLAG, because only in this case the binding to anti-FLAG coated beads should be possible. Unfortunately, I obtained a similar amount of RNA from non-induced and induced cells.

During qPCR, I used primers for 12S and 16S rRNA, corresponding to the small and respectively large mitoribosome subunit, and for COX2 mRNA. They showed similar expression levels for induced and non-induced samples, and the optimization attempts (elution with 3X FLAG, using two different batches of 3X FLAG peptide) did not change this result. Therefore, I could not identify the mRNA targets of mtRF1.

The focus of my project changed towards C12orf65. Similar to mtRF1, C12orf65 is localized to mitochondria and contains the GGQ motif (Antonicka et al., 2010). As distinct from mtRF1, it lacks the codon recognition motif, and pathogenic variants in *C12orf65* were discovered in patients with mitochondrial diseases (Antonicka et al., 2010, Buchert et al., 2013, Shimazaki et al., 2012, Tucci et al., 2014, Wesolowska et al., 2015). The lack of a stop codon recognition motif suggests that, if C12orf65 is involved in mitoribosome rescue, this function is independent from the codon in the A site. Stalling of mitoribosomes could have different causes, each scenario allowing the presence of a codon in the A site. It could be caused by insufficient aminoacyl-tRNA molecules (Pearce et al., 2017), deficient maturation of tRNA (Morscher et al., 2018), insufficient amino acids or particularities of the mRNA (Ayyub et al., 2020). For example, the mRNA secondary structure, loss of the stop codon causing translation to continue in the poly(A) tail (Ayyub et al., 2020), or codons encoding for successive proline residues (Lee et al., 2021) could all result in stalling. In my research hypothesis, C12orf65 is the factor that rescues stalled ribosomes in all those scenarios.

To study C12orf65 I used two techniques: CRISPR-Cas9 and BioID2. Using CRISPR-Cas9 I obtained two possible C12orf65 knockout HEK clones that presented a defect in proliferation. They were identified by Sanger sequencing and require further characterization to be confirmed as KO. The BioID2 technique allowed me to identify protein interactors of C12orf65. The advantage of BioID2 is that it permits identification of proteins within a 10-35 nm range (Kim et al., 2016a) from C12orf65, proteins that do not physically interact with C12orf65 and

therefore could not be identified by immunoprecipitation. The interactors identified in the present work included proteins involved in mitochondria translation (MRPs, aminoacyl-tRNA ligases) and RNA processing and modification (LRPPRC, RNase P, DHX30). Interestingly, the majority of MRPs belonged to the small subunit: MRPS5, MRPS9, MRPS23, MRPS28 (bS1m) and MRPS31. Mapping those proteins on the human 55S ribosome structure revealed that they are involved in formation of the mRNA channel (MRPS5, MRPS28) (Amunts et al., 2015) and interaction with the tRNA from the P site (MRPS9) (Aibara et al., 2020). Those results are consistent with C12orf65 being involved in mitoribosome rescue, because they show that C12orf65 interacts with the translation active site of the mitoribosome. Moreover, those hits are most probably to be biotinylated if C12orf65-BioID2 (or -Linker-BioID2) bound to the A site.

During the writing of the present thesis, the article published by Desai et al. (Desai et al., 2020) revealed the role of C12orf65. Using a model of mitoribosome stalling (Pearce et al., 2017), they showed that C12orf65 (renamed mtRF-R) forms a dimer with MTRES1 and both bind to the mtLSU after splitting from mtSSU: C12orf65 binds to the A site and MTRES1 to the P site. This is in agreement with my BioID2 results, since some of the hits are MRPs from the mRNA channel in the mtSSU, and one hit (MRPS9) interacts with the mt-tRNA from the P site.

The use of an appropriate stalling model had a key contribution to unveiling the function of C12orf65 and raised the possibility that a similar approach could be applied to mtRF1. However, all the current mitochondrial stalling models require a codon in the A site. The model used by Pearce et al. (Pearce et al., 2017) was based on knockout of PDE12 deadenylase, which caused the mitoribosomes to stall on codons encoding lysine (AAA and AAG). Another model, established by knockout of SHMT2, induces stalling at lysine (AAG) and leucine (UUG) codons (Morscher et al., 2018). Similarly, treating human cells with the arginine analogue canavanine resulted in stalling downstream from the arginine encoding codons, possibly because canavanine incorporation caused misfolding of the nascent polypeptide (Konovalova et al., 2015).

Obtaining a mitochondrial model of truncated mRNA is challenging, because alterations of RNA processing could affect tRNA and rRNA as well. For example, knockdown of human SUV3, a mitochondrial ATP-dependent helicase (Minczuk et al., 2002, Shu et al., 2004), results in mRNA species truncated at their 3'-ends (Szczesny et al., 2010). But this induces apoptosis in HeLa cells (Szczesny et al., 2007). Also, *in vivo* knockdown of SUV3 leads to decrease in mt-

tRNA and ultimately to pupal lethality in *D. melanogaster* (Clemente et al., 2015), while homozygous mSuv3-knockout leads to embryonic lethality in mice (Chen et al., 2013).

Therefore, I would not consider a mRNA stalling model as a further approach to study mtRF1. Instead, if I continued the investigation, I would apply the BioID2 technique to mtRF1, similarly to the C12orf65-BioID2 approach. The cross-linking experiments already show that mtRF1 and the mitoribosome interact, and BioID2 could help identify the region where this factor is most likely to bind. Also, I would use the C12orf65 KO model that I have obtained as a platform to modulate mtRF1 expression, by overexpressing or downregulating it. Alternatively, an *in vitro* translation system similar to the one established by Lee et al. (Lee et al., 2021) and including mtRF1 could be adapted to human mitochondria. DNA templates containing or not a stop codon could be chemically synthesized and transcribed, and a relatively large quantity of human mitoribosomes could be isolated as described by Aibara et al. (Aibara et al., 2018). In the translation system that lacks the stop codon, if the working hypothesis is correct, the release of the nascent polypeptide should occur after addition of mtRF1¹.

Concluding, the aims set for this thesis were only partially met. However, I am confident that the results obtained will contribute to a better understanding of mitochondria quality control. To the best of my knowledge, this is the first C12orf65 KO that was attempted and the first time mtRF1 was cross-linked to the mitoribosome, confirming a transient interaction. In addition, I optimized the BioID2 technique and identified C12orf65 interactors. The BioID2 technique and the C12orf65 KO model could be used in the future to study mtRF1.

¹ Shortly before my submission deadline, (Kummer et al., 2021) published an experiment similar to the one proposed here, in which they used porcine 55S ribosomes, human mitochondria release factors (including mtRF1) and a short oligo lacking a stop codon (CUGAUG) to produce an empty A site at the end of translation . They found that ICT1, not mtRF1, bound to the mitoribosome with an empty A site.

Appendices

Appendix-A Antibodies

Table Apx 1. Primary antibodies used for western blotting in Newcastle University

Antibody	Working dilution	Produced in	Dilution buffer	Manufacturer	Product code
Primary					
Anti-FLAG M2	1:1,000	mouse	5% milk TTBS	Sigma Aldrich	SLBT7654
Anti-HA	1:1,000	mouse	5% milk TTBS	Abcam	ab49969
Anti-HA	1:5,000	rabbit	5% BSA TTBS	Abcam	ab9110
Anti-MRPL3	1:1,000	goat	5% milk TTBS	Abcam	ab39268
Anti-MRPS22	1:1,000	rabbit	5% milk TTBS	Proteintech	10984-1-AP
Anti-DAP3	1:2,000	mouse	5% milk TTBS	Invitrogen	MA1.41279
Anti-MRPL11	1:1,000	rabbit	5% milk TTBS	Cell Signalling Technology	D68F2
Anti-MRPL45	1:1,000	rabbit	5% milk TTBS	Proteintech	15682-1-AP
Anti-MTRF1	1:1,000	rabbit	5% milk TTBS	custom made and affinity purified	
Anti-MRPS26	1:1,000	rabbit	5% milk TTBS	Proteintech	15989-1-AP
Anti-SDHA	1:2,000	mouse	5% milk TTBS	Abcam	ab14715
Anti-TOMM20	1:1,000	rabbit	5% milk TTBS	Abcam	ab78574
Anti-GAPDH	1:5,000	mouse	5% milk TTBS	Abcam	ab14715
Anti-MRPL28	1:1,000	rabbit	5% milk TTBS	Sigma Aldrich	HPA030594
Anti-alpha-tubulin	1:2,000	mouse	5% milk TTBS	Santa Cruz Biotechnology	Sc5286
Anti-VDAC1 (porin)	1:10,000	mouse	5% milk TTBS	Abcam	ab14734
Anti-AIF	1:2,000	rabbit	5% milk TTBS	Cell Signalling Technology	4642S
Anti-NDUFS3	1:2,000	mouse	5% milk TTBS	Abcam	ab110246

Table Apx 2. Secondary antibodies used for western blotting in Newcastle University

Antibody	Working dilution	Produced in	Dilution buffer	Manufacturer	Product code
Secondary, HRP-conjugated					
Anti-mouse	1:2,000	rabbit	5% milk TTBS	DAKO Cytomation	P0260
Anti-goat	1:2,000	rabbit	5% milk TTBS	DAKO Cytomation	P0217
Anti-rabbit	1:3,000	swine	5% milk TTBS or 5% BSA TTBS	DAKO Cytomation	P0449
Streptavidin-HRP	1:1,000	<i>S. avidinii</i>	5% BSA TTBS	Abcam	ab7403

Table Apx 3. Primary and secondary antibodies used for western blotting in Radboud University, Nijmegen, The Netherlands

	Antibody	Working dilution	Produced in	Dilution buffer	Manufacturer	Product code
Primary	Anti-HA	1:5,000	mouse	3% BSA TTBS	Sigma Aldrich	H3663
Secondary, HRP-conjugated	Anti-mouse	1:5,000	horse	3% BSA TTBS	Vector Laboratories	PI-2000
	Streptavidin -HRP	1:10,000	<i>S. avidinii</i>	3% BSA TTBS	Pierce	21126

Appendix-B Plasmid details

Appendix-B.1 C12orf65-BioID2-HA in pcDNA5/FRT/TO (6,305bp)

The restriction enzymes used for C12orf65 insertion into the BioID2-HA-pcDNA5/FRT/TO plasmid were BamH1, Xho1.

The BioID2-HA-pcDNA5/FRT/TO was provided by Dr. Thomas Nicholls, at the time part of Prof. Maria Falkenberg's group, University of Gothenburg, Sweden. Amplification of *C12orf65* fragment and insertion into BioID2-HA-pcDNA5/FRT/TO plasmid was performed by Mr. Reece Farren, MRes, under the supervision of Miss Yasmin Proctor-Kent.

Table Apx 4. Primers used for C12orf65 insert generation

Primer	Sequence from 5' to 3'	Tm
C12 Forward	gcg cat G [↓] GA TCC atg agc acc gtg ggt tta ttt cat	64°C
C12 Reverse	ggc cgc C [↓] TC GAG gtg gac ctt ttt act tga ctc cca ca	64°C

The nucleotides written in capital letters represent the target sites for BamH1 (GGA TCC) or Xho1 (CTC GAG) respectively. The arrow indicates the site where BamH1 or Xho1 cuts.

Table Apx 5. Primers used for sequencing of the C12orf65 region after ligation

Primer	Sequence from 5' to 3'	Tm
CMV Forward Seq	CGC AAA TGG GCG GTA GGC GTG	65°C
BIOID SEQ reverse	GTT CAG CAG GAA GCT GAA GTA CAG GCC G	66°C

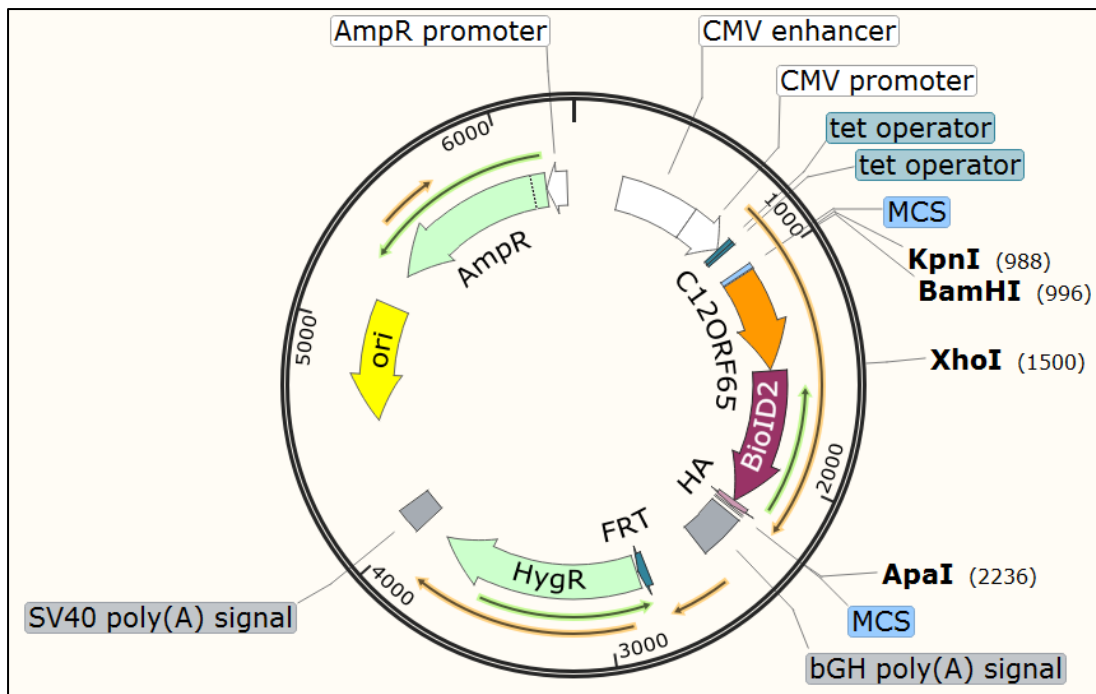


Figure Apx 1. Map of the C12orf65-BioID2-HA/pcDNA5/FRT/TO plasmid

Appendix-B.2 Linker-BioID2-HA in pcDNA5/FRT/TO (6,064bp)

The restriction enzymes used for Linker-BioID2-HA insertion into the pcDNA5/FRT/TO plasmid (performed by Mr. Reece Farren, MRes) were Xho1, Apa1. Sequencing of the Linker region after ligation was performed with the CMV Forward and BIOID Seq Reverse primers (Table Apx 5).

Table Apx 6. Primers used for generation of the *Linker-BioID2* insert

Primer	Sequence from 5' to 3'	Tm
Linker Forward	ata tat C [↓] TCGAGg gtg gag gcg ggt ctg gag	69°C
Linker Reverse	gca tat GGGCC [↓] C cta tgc gta atc cgg tac atc gta agg	68°C

The nucleotides written in capital letters represent the target sites for Xho1 (CTC GAG) or Apa1 (GGG CCC). The arrow indicates the site where BamH1 or Xho1 cuts.

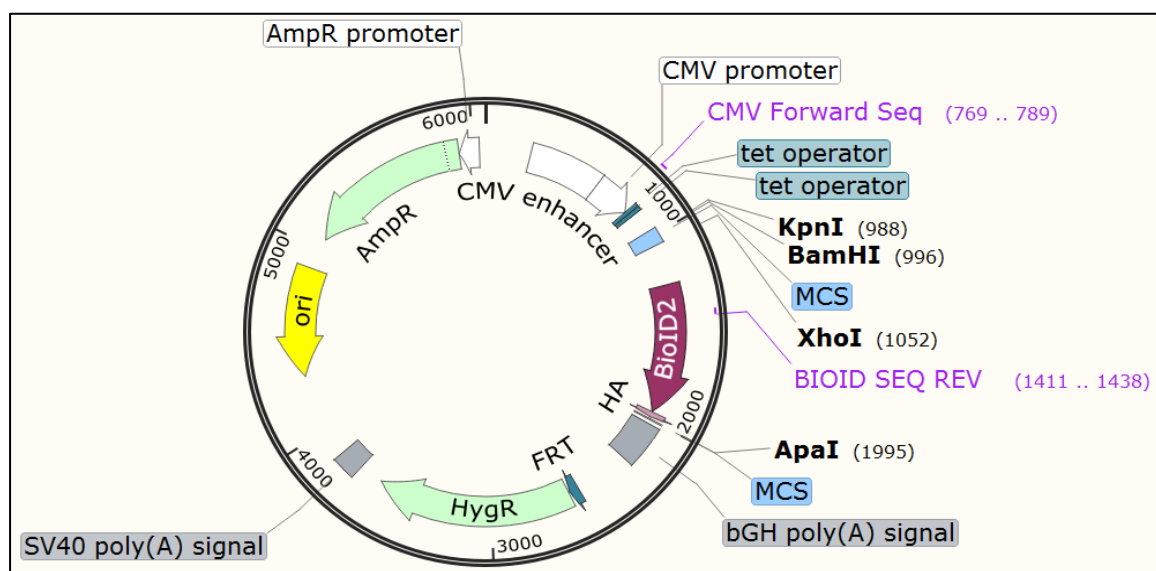


Figure Apx 2. Map of the Linker-BioID2-HA/pcDNA5/FRT/TO plasmid

Appendix-B.3 *C12orf65*-Linker-BioID2-HA in pcDNA5/FRT/TO (6,512bp)

The restriction enzymes used for *C12orf65* insertion into the Linker-BioID2-HA/pcDNA5/FRT/TO plasmid were: BamH1, Xho1. *C12orf65* fragment was obtained by digestion with the same enzymes. Fragment isolation and insertion into the plasmid was done by myself.

Sequencing after ligation was performed with the CMV Forward and BIOID Seq Reverse primers (Table Apx 5).

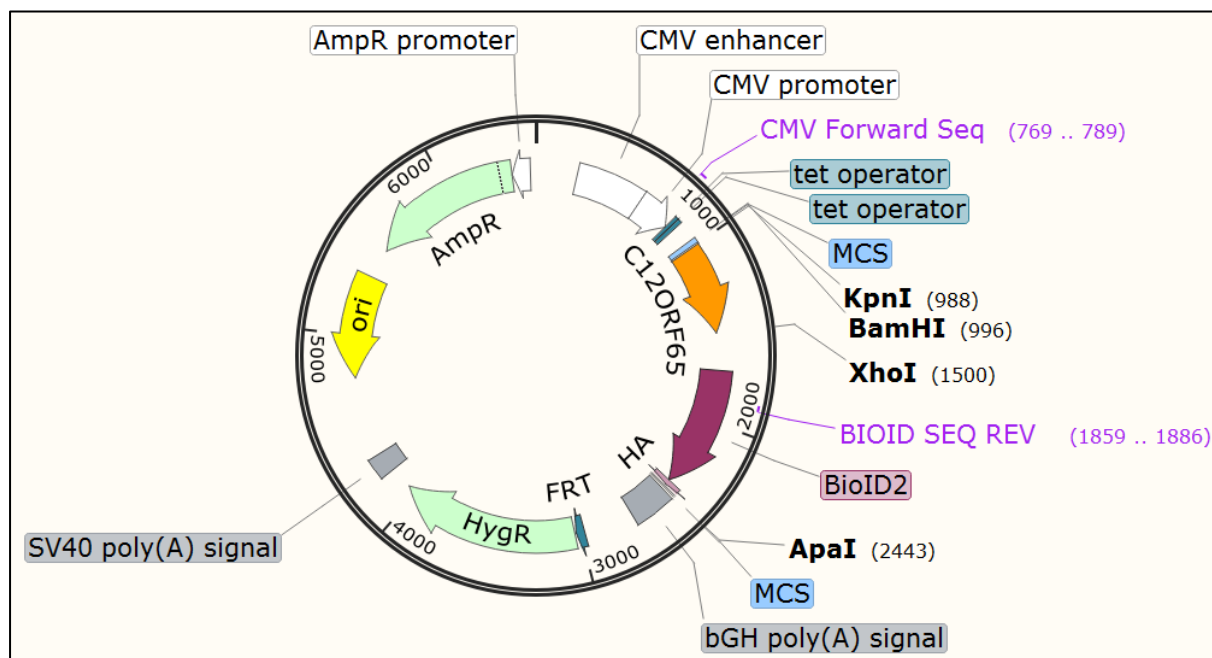


Figure Apx 3. Map of the C12orf65-Linker-BioID2-HA/pcDNA5/FRT/TO plasmid

Appendix-B.4 PX458 C12orf65 gRNA (9,290bp)

The restriction enzyme used for C12orf65 gRNA insertion (performed by Mr. Reece Farren, MRes) was BbsI (both ends).

Oligonucleotides used for construction of C12orf65 gRNA insert:

Oligo 1 (24-mer): CAC CGC CCG GCG CCA TGG GGA CTC
Oligo 2 (24-mer): AAA CGA GTC CCC ATG GCG CCG GGC

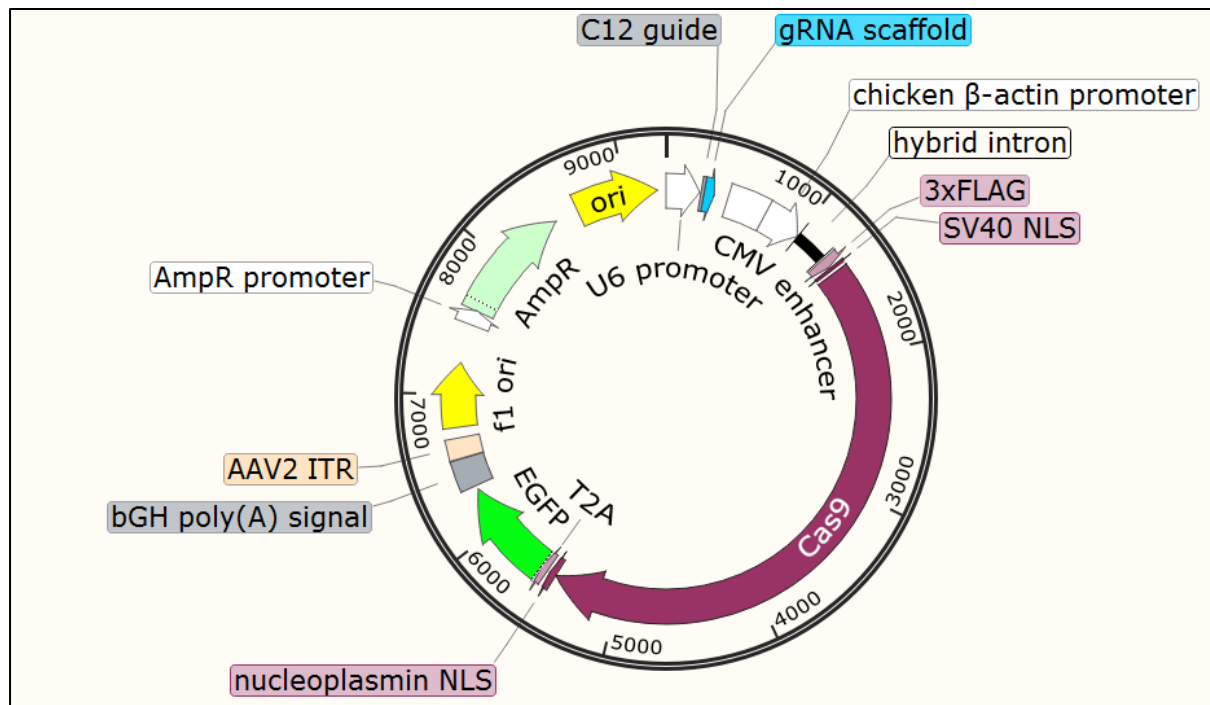


Figure Apx 4. Map of the C12orf65 gRNA PX458 plasmid

Appendix-C Details of mass-spectrometry experiments

Table Apx 7. Biotinylated proteins identified by multiple UniProt codes in COX8-MTS control (NCL2)

Dataset entry #	UniProt ID	Name	Localization	Function	Peptides
1	Q13085	acetyl-CoA carboxylase 1	Matrix	Fatty acid synthesis	58
	O00763	acetyl-CoA carboxylase 2	OMM	Fatty acid oxidation	58
2	P00367	Glutamate-dehydrogenase 1	Matrix	Glutamate metabolism	14
	P49448	Glutamate-dehydrogenase 2	Matrix	Glutamate metabolism	14
3	P12235	ADP/ATP translocase 1	IMM	Small molecule transport	7
	P12236	ADP/ATP translocase 3	IMM	Small molecule transport	7
4	Q96C36	Pyrroline-5-carboxylate reductase 2	matrix	Proline metabolism	4
	P32322	Pyrroline-5-carboxylate reductase	matrix	Proline metabolism	4
5	O75746	Calcium-binding mitochondrial carrier protein Aralar1	IMM	Small molecule transport	8
	Q9UJS0	Calcium-binding mitochondrial carrier protein Aralar2	IMM	Small molecule transport	8

Table Apx 8. Biotinylated proteins identified by multiple UniProt codes in C12orf65-BioID2 samples (NCL2)

Dataset entry #	UniProt ID	Name	Localization	Function	Peptides
1	Q13085	acetyl-CoA carboxylase 1	Matrix	Fatty acid synthesis	58
	O00763	acetyl-CoA carboxylase 2	OMM	Fatty acid oxidation	58
2	P00367	Glutamate-dehydrogenase 1	Matrix	Glutamate metabolism	14
	P49448	Glutamate-dehydrogenase 2	Matrix	Glutamate metabolism	14
3	P12235	ADP/ATP translocase 1	IMM	Small molecule transport	7
	P12236	ADP/ATP translocase 3	IMM	Small molecule transport	7
4	P08559	Pyruvate dehydrogenase E1 component subunit alpha, somatic form	Matrix	Carbohydrate metabolism	4
	P29803	Pyruvate dehydrogenase E1 component subunit alpha, testis-specific form	Matrix	Carbohydrate metabolism	4
5	Q9NVI7	ATAD3A (ATPase family AAA domain-containing protein 3A)	IMM	Mitochondria gene expression	8
	Q5T9A4	ATAD3B (ATPase family AAA domain-containing protein 3B)	IMM	Mitochondria gene expression	8

Table Apx 9. Biotinylated proteins identified by multiple UniProt codes in C12orf65-Linker- BioID2 samples (NCL2)

Dataset entry #	UniProt ID	Name	Localization	Function	Peptides
1	Q13085	acetyl-CoA carboxylase 1	Matrix	Fatty acid synthesis	58
	O00763	acetyl-CoA carboxylase 2	OMM	Fatty acid oxidation	58
2	P00367	Glutamate-dehydrogenase 1	Matrix	Glutamate metabolism	14
	P49448	Glutamate-dehydrogenase 2	Matrix	Glutamate metabolism	14
3	P12235	ADP/ATP translocase 1	IMM	Small molecule transport	7
	P12236	ADP/ATP translocase 3	IMM	Small molecule transport	7
4	P08559	Pyruvate dehydrogenase E1 component subunit alpha, somatic form	Matrix	Carbohydrate metabolism	4
	P29803	Pyruvate dehydrogenase E1 component subunit alpha, testis-specific form	Matrix	Carbohydrate metabolism	4
5	Q9NVI7	ATAD3A (ATPase family AAA domain-containing protein 3A)	IMM	Mitochondria gene expression	8
	Q5T9A4	ATAD3B (ATPase family AAA domain-containing protein 3B)	IMM	Mitochondria gene expression	8
6	O75746	Calcium-binding mitochondrial carrier protein Aralar1	IMM	Small molecule transport	8
	Q9UJS0	Calcium-binding mitochondrial carrier protein Aralar2	IMM	Small molecule transport	8

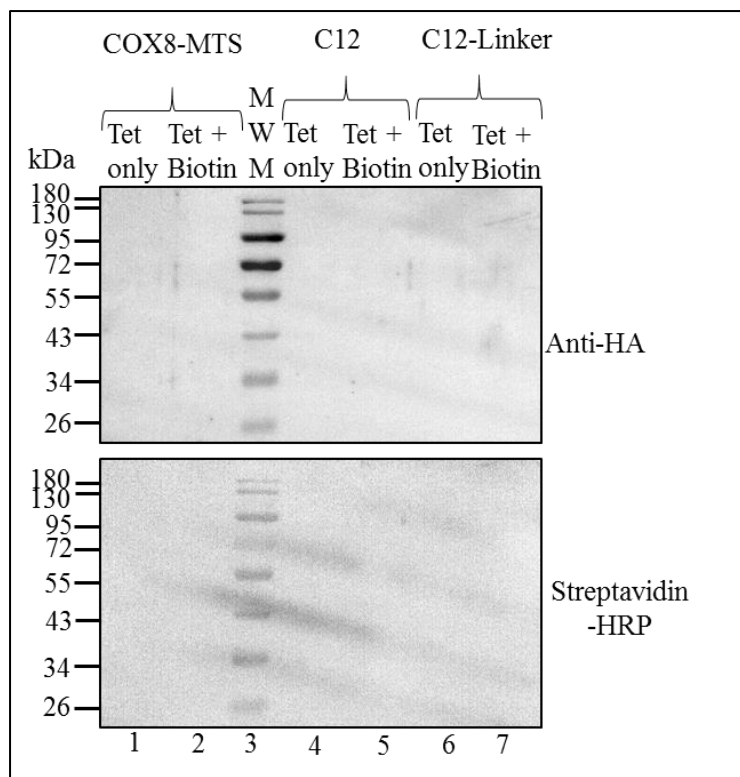


Figure Apx 5. Test of trypsinization efficiency performed in Nijmegen

After trypsinization, 10% of the magnetic beads were resuspended in 20 μ l of Laemmeli buffer with 1% beta-mercaptoethanol and boiled at 95°C for 10 min, to denature the proteins that had possibly remained attached. They were briefly centrifuged, and the supernatant was used for SDS-PAGE. Streptavidin -HRP was used to detect biotinylated proteins and anti-HA to detect the BioID2 bait. 10% gel

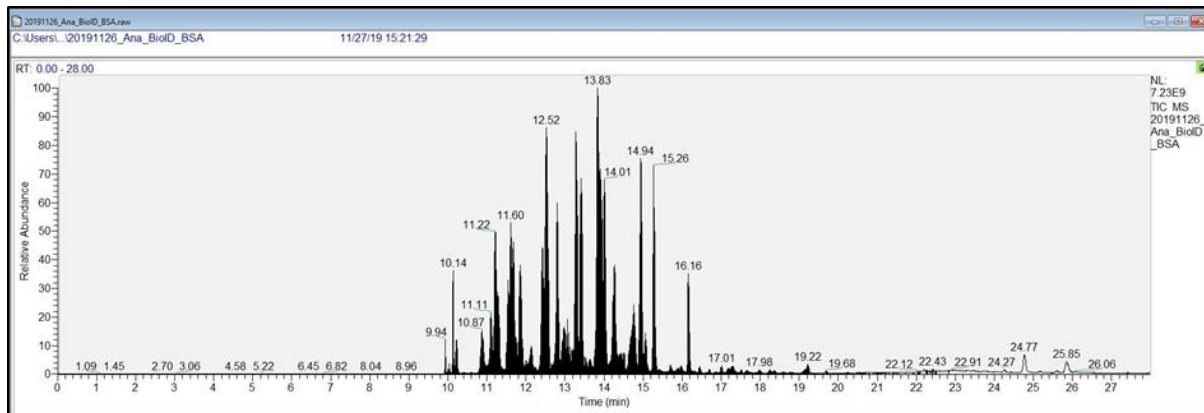


Figure Apx 6. Total ion chromatogram of BSA positive control

As standard for the mass-spectrometry calibration were used 5 μ l of a BSA tryptic digest (PierceTM BSA Protein Digest, MS grade, Thermo Fisher Scientific, catalogue number: 88341) prepared in 0.1% formic acid, final concentration 50 fmol/ μ l. BSA peptides were separated by a linear 30 min gradient of 5–35% acetonitrile containing 0.1% formic acid at a flow rate of 300 nl/min. The graph represents the relative abundance of peptides over 30 min.

Appendix-D Sequencing of KO control HEK clones



Figure Apx 7. Binding sites of the C12orf65 primers used for sequencing

After DNA extraction, a region of *C12orf65* was amplified and the PCR product (326 bp) was sent for Sanger sequencing, performed with the forward primer. The two primers (plum) bind approximatively 150 bp upstream and respectively downstream from the PAM motif (green), in the first coding exon (blue). Forward primer binds in the intronic region, 74 bp upstream from the start codon (turquoise). For visualization, human *C12orf65* sequence was downloaded from NCBI (Gene ID: 91574, updated on February 3rd, 2021) and the regions were mapped using SnapGene version 5.1.6. Coding exon 1 and the start codon were retrieved from the Ensemble Genome Browser, release 102, transcript ID ENST00000253233.6

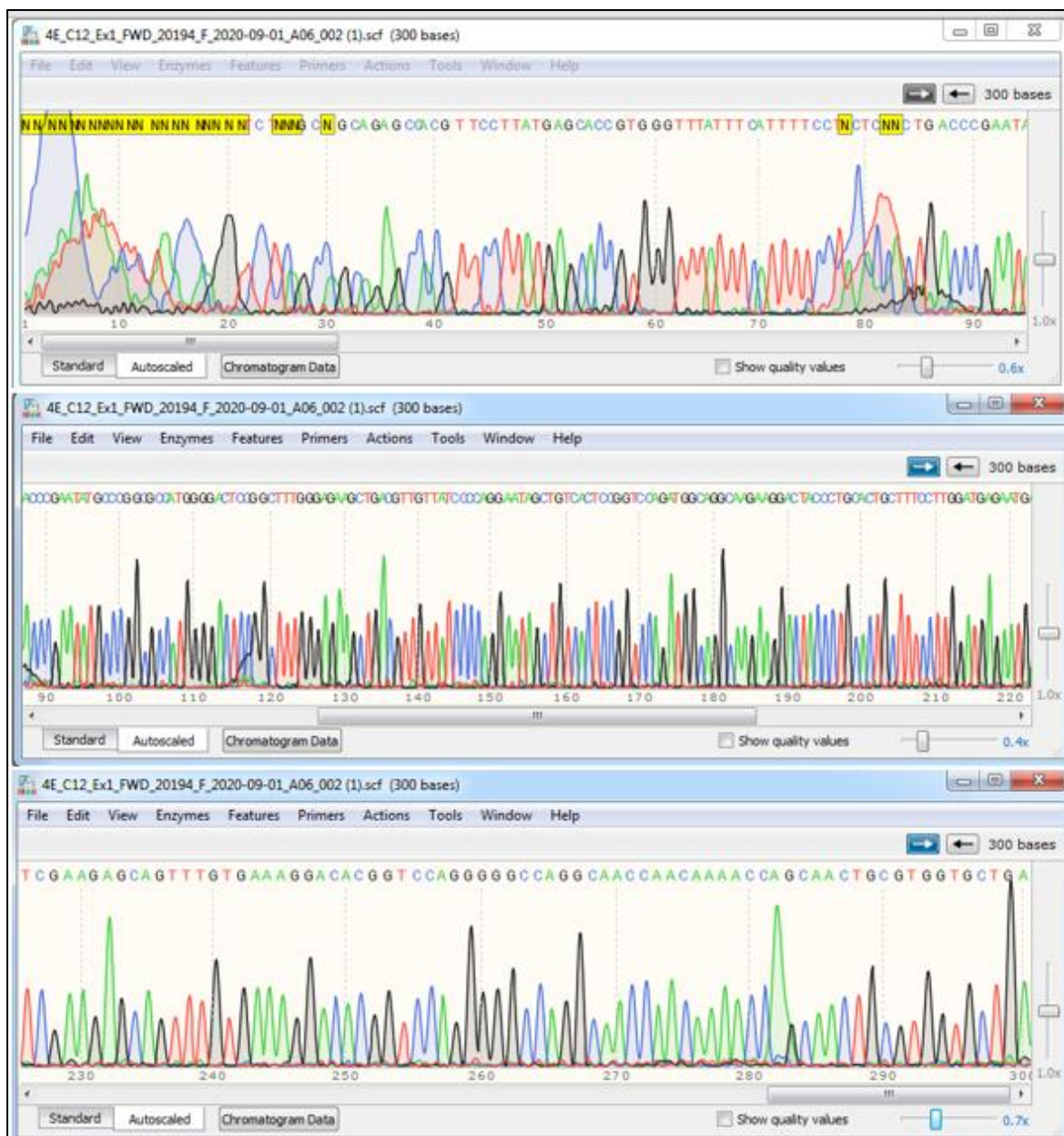


Figure Apx 8. Sequencing results of 4E, control sample for CRISPR-Cas9

For CRISPR-Cas9, HEK cells were transfected with PX458 (GFP) plasmid containing the gRNA to target coding ex 1 of *C12orf65*. Controls were transfected with the plasmid lacking gRNA. *C12orf65* was amplified and the PCR product was sequenced using the forward primer. Here, the chromatogram of control 4E shows consistent clear peaks, with minor artefacts at the beginning the sequence; visualised with SnapGene version 5.1.6

Homo sapiens chromosome 12 open reading frame 65 (C12orf65), transcript variant 1, mRNA					
Sequence ID: NM_152269.5 Length: 1554 Number of Matches: 1					
Range 1: 148 to 377 GenBank Graphics				▼ Next Match ▲ Previous	
Score 409 bits(221)	Expect 1e-111	Identities 226/230(98%)	Gaps 0/230(0%)	Strand Plus/Plus	
Query 1	TTTCCTNCTNNCTGACCGAATAT	GCCCCGGGCCATGGGACTCCGG	CTTGGGAGAA	60	
Sbjct 148	TTTCCTACACCACTGACCGAATAT	GCCCCGGGCCATGGGACTCCGG	CTTGGGAGAA	207	
Query 61	GCTGACGTTGTTATCCCCAGGAATAGCTGTCACTCCGGTCCAGATGGCAGGCAAGAAGGA			120	
Sbjct 208	GCTGACGTTGTTATCCCCAGGAATAGCTGTCACTCCGGTCCAGATGGCAGGCAAGAAGGA			267	
Query 121	CTACCCCTGCACTGCTTCTGGATGAGAATGAACCTGAAGAGCAGTTGTGAAAGGACA			180	
Sbjct 268	CTACCCCTGCACTGCTTCTGGATGAGAATGAACCTGAAGAGCAGTTGTGAAAGGACA			327	
Query 181	CGGTCCAGGGGGCCAGGCAACCAACAAAACCAGCAACTGCGTGGTGCTGA			230	
Sbjct 328	CGGTCCAGGGGGCCAGGCAACCAACAAAACCAGCAACTGCGTGGTGCTGA			377	

Figure Apx 9. Alignment of 4E control sequence against the human genome

Results of nucleotide alignment (Blastn, NCBI) of 4E (query) against the *H. sapiens* (taxid 9606) nucleotide collection. Top hit was C12orf65 (sbjct). The first 70 nucleotides of 4E were not included in the blastn. yellow- gRNA target; green- PAM motif



Figure Apx 10. Sequencing results of 12E, control sample for CRISPR-Cas9

Chromatogram of control 12E (transfected with plasmid without gRNA) visualised with SnapGene software version 5.1.6. The peaks are clear, and the background is low, apart from the beginning of the sequence.

Homo sapiens chromosome 12 open reading frame 65 (C12orf65), transcript variant 1, mRNA					
Sequence ID: NM_152269.5 Length: 1554 Number of Matches: 1					
Range 1: 162 to 376 GenBank Graphics				▼ Next Match ▲ Previous Match	
Score 394 bits(213)	Expect 3e-107	Identities 214/215(99%)	Gaps 0/215(0%)	Strand Plus/Plus	
Query 1	TGACCCGAATAT	GCCCCGGCGCCATGGGGACTCCGGCTTGGGAGAAGCTGACGTTTTAT			60
Sbjct 162	TGACCCGAATAT	GCCCCGGCGCCATGGGGACTCCGGCTTGGGAGAAGCTGACGTTTTAT			221
Query 61	CCCCAGGAATAGCTGTCACTCCGGTCCAGATGGCAGGAAGAAGGACTACCCTGCACTGC				120
Sbjct 222	CCCCAGGAATAGCTGTCACTCCGGTCCAGATGGCAGGAAGAAGGACTACCCTGCACTGC				281
Query 121	TTTCCTTGGATGAGAATGAACTCGAAGAGCAGTTGTGAAAGGACACGGTCCAGGGGGCC				180
Sbjct 282	TTTCCTTGGATGAGAATGAACTCGAAGAGCAGTTGTGAAAGGACACGGTCCAGGGGGCC				341
Query 181	AGGCAACCAACAAAACCANCAACTGCGTGGTGCTG				215
Sbjct 342	AGGCAACCAACAAAACCAGCAACTGCGTGGTGCTG				376

Figure Apx 11. Alignment of 12E control sequence against the human genome

The Blastn search of 12E (query) against the H. sapiens (taxid 9606) nucleotide collection returned C12orf65 (sbjct). The first 80 nucleotides were excluded from the alignment. The gRNA target is highlighted in yellow and the PAM motif in green.

Appendix-E List of hits identified using BioID2

This section contains the biotinylated hits identified by mass-spectrometry in Newcastle. For simplicity, I separated the mitochondrial proteins from the proteins that belong to the compartments adjacent to mitochondria (ER, cytosolic translation). Hits were assigned as ‘mitochondrial’ according to Mitocarta 3.0 inventory. Contaminants (keratin, trypsin) and ubiquitous non-mitochondrial proteins (histones, cytoskeleton proteins, secreted or cell membranal proteins) are excluded. LC MS/MS was performed and analysed by Dr. Frédérique Lamoliatte (NCL1) and Dr. Akshada Gajbhiye (NCL2).

NCL1 = first mass-spectrometry run in Newcastle (N=1)

NCL2 = second mass-spectrometry run in Newcastle (N=2)

n/a = hit Intensity/ LFQ was zero for that particular sample

bright blue font = mtDNA associated hits

orange font = hits involved in transcription, RNA processing and modification

dark red font = translation associated hits

Table Apx 10. NCL1 mitochondria

The table contains all the mitochondrial hits identified during the first mass-spectrometry run in Newcastle.

№	UniProt ID	Name	Localization	log2 (Intensity)							Peptides
				C12-BioID2 Tet	C12-BioID2 Tet + Biotin	C12-Linker-BioID2 Tet	C12-Linker-BioID2 Tet + Biotin	COX8-MTS Tet	COX8-MTS Tet + Biotin		
1	P00367	Glutamate dehydrogenase 1	Matrix	n/a	20.67	n/a	18.3915	n/a	n/a	2	
2	P05165	Propionyl-CoA carboxylase subunit alpha	Matrix	28.0152	30.9	24.681	28.6867	28.978	26.49	57	
3	P10809	Heat shock protein family D (Hsp60) member 1	Matrix	18.1017	22.71	n/a	18.3397	19.362	n/a	5	
4	Q969P6	DNA topoisomerase I mitochondrial	Matrix	24.72	25.77	15.3472	25.1495	23.727	n/a	28	
5	P11498	Pyruvate carboxylase	Matrix	29.0687	31.44	24.8062	29.1712	29.323	27.29	67	
6	P38646	Heat shock protein family A (Hsp70) member 9	Matrix	16.8588	22.72	n/a	18.0043	18.835	14.56	7	
7	P40926	Malate dehydrogenase 2	Matrix	19.6203	22.11	n/a	18.7187	n/a	n/a	2	
8	P49411	Tu translation elongation factor, mitochondrial	Matrix	19.2537	22.13	n/a	n/a	18.472	n/a	4	

№	UniProt ID	Name	Localization	log2 (Intensity)							Peptides
				C12-BioID2 Tet	C12-BioID2 Tet + Biotin	C12-Linker-BioID2 Tet	C12-Linker-BioID2 Tet + Biotin	COX8-MTS Tet	COX8-MTS Tet + Biotin		
9	P61604	Heat shock protein family E (Hsp10) member 1	Matrix	n/a	19.96	n/a	n/a	n/a	20.39	2	
10	P82675	Mitochondrial ribosomal protein S5	Matrix	20.8867	21.46	n/a	21.8202	20.262	n/a	5	
11	Q12931	Heat shock protein 75 kDa	Matrix	n/a	20.13	n/a	n/a	16.657	n/a	4	
12	Q13085	Acetyl-CoA carboxylase alpha	Matrix	22.4393	24.94	17.1149	24.177	21.451	n/a	25	
13	Q5T653	Mitochondrial ribosomal protein L2	Matrix	18.5255	19	n/a	19.3097	n/a	n/a	2	
14	P13804	Electron transfer flavoprotein subunit alpha	Matrix	21.4464	22.12	n/a	20.6776	20.064	n/a	3	
15	P38117	Electron transfer flavoprotein subunit beta	Matrix	21.4464	22.12	n/a	20.6776	20.064	n/a	3	
16	Q96RQ3	Methylcrotonoyl-CoA carboxylase 1	Matrix	26.3922	29.32	20.9744	26.1786	26.984	24.36	33	
17	Q9BQ48	Mitochondrial ribosomal protein L34	Matrix	21.9775	23.94	19.4733	23.469	21.919	19.89	5	

№	UniProt ID	Name	Localization	log2 (Intensity)							Peptides
				C12-BioID2 Tet	C12-BioID2 Tet + Biotin	C12-Linker-BioID2 Tet	C12-Linker-BioID2 Tet + Biotin	COX8-MTS Tet	COX8-MTS Tet + Biotin		
18	Q9NWT8	Aurora kinase A interacting protein 1	Matrix	23.8388	26.75	n/a	22.1766	24.371	n/a	2	
19	Q9P015	Mitochondrial ribosomal protein L15	Matrix	21.1124	21.85	n/a	22.8245	n/a	n/a	4	
20	Q96HJ9	Formation of mitochondrial complex V assembly factor 1 homolog	Matrix	23.8906	25.49	17.6542	24.486	22.478	14.82	14	
21	P12235	Solute carrier family 25 member 4	IMM	18.8523	22.13	n/a	17.4167	19.106	4	4	
22	P05141	Solute carrier family 25 member 5	IMM	18.8523	22.13	n/a	17.4167	19.106	4	4	
23	Q9H0C2	Solute carrier family 25 member 31	IMM	18.8523	22.13	n/a	17.4167	19.106	4	4	
24	P12236	Solute carrier family 25 member 6	IMM	18.8523	22.13	n/a	17.4167	19.106	4	4	
25	P25705	ATP synthase F1 subunit alpha	IMM	20.2667	23.71	n/a	19.7002	20.433	11	11	

№	UniProt ID	Name	Localization	log2 (Intensity)							Peptides
				C12-BioID2 Tet	C12-BioID2 Tet + Biotin	C12-Linker-BioID2 Tet	C12-Linker-BioID2 Tet + Biotin	COX8-MTS Tet	COX8-MTS Tet + Biotin		
26	Q16134	Electron transfer flavoprotein dehydrogenase, EC 1.5.5.1	IMM	21.4464	22.12	n/a	20.6776	20.064	3	3	
27	P04040	Catalase	IMS	21.0353	23.03	n/a	21.094	18.922	n/a	10	
28	Q13162	Peroxiredoxin 4	IMS	22.2843	23.58	15.4627	23.4376	20.011	18.79	6	
29	P21796	Voltage dependent anion channel 1	OMM	18.1983	21.44	n/a	18.0194	15.87	n/a	3	
30	P45880	Voltage dependent anion channel 2	OMM	n/a	21.29	n/a	17.4922	n/a	n/a	2	
31	O00763	Acetyl-CoA carboxylase beta	OMM	22.4393	24.94	17.1149	24.177	21.451	n/a	25	
32	P10599	Thioredoxin	Mitochondrial-unknown	23.0046	24.17	n/a	22.341	21.439	n/a	5	
33	P32119	Peroxiredoxin 2	Mitochondrial-unknown	19.5324	22.3	n/a	19.7924	17.265	n/a	5	

Table Apx 11. NCL1 adjacent

The table contains all the hits identified during the first mass-spectrometry run in Newcastle which belong to cytosolic ribosome, ER or are cytosolic translation factors.

№	UniProt ID	Name	Localization	log2 (Intensity)							
				C12-BioID2 Tet	C12-BioID2 Tet + Biotin	C12-Linker-BioID2 Tet	C12-Linker-BioID2 Tet + Biotin	COX8-MTS Tet	COX8-MTS Tet + Biotin	Peptides	
1											
2	Q9P2E9	Ribosome-binding protein 1	EK translation/ER binding	20.451	22.96	16.6184	22.59	n/a	21.02	12	
3	Q8NE71	ATP-binding cassette sub-family F member 1	EK translation	24.2355	26.57	17.0554	25.3972	23.298	20.31	33	
4	Q5VTE0	Putative elongation factor 1-alpha-like 3	EK translation	21.5008	23.15	n/a	22.4737	19.041	n/a	6	
5	O60841	Eukaryotic translation initiation factor 5B	EK translation	25.6347	27.72	18.0482	27.1885	24.648	24.34	51	
6	Q96EY4	Translation machinery-associated protein 16	EK translation	n/a	18.76	n/a	16.581	n/a	n/a	2	

№	UniProt ID	Name	Localization	log2 (Intensity)							Peptides
				C12-BioID2 Tet	C12-BioID2 Tet + Biotin	C12-Linker-BioID2 Tet	C12-Linker-BioID2 Tet + Biotin	COX8-MTS Tet	COX8-MTS Tet + Biotin		
7	P39023	60S ribosomal protein L3	80S ribosome	22.6296	22.33	17.4009	24.8979	19.089	23.99		14
8	P46777	60S ribosomal protein L5	80S ribosome	22.8535	23.62	18.4281	26.1033	21.409	15.03		17
9	P62913	60S ribosomal protein L11	80S ribosome	17.8392	20.48	n/a	19.324	17.441	n/a		2
10	P62987	Ubiquitin-60S ribosomal protein L40	80S ribosome	18.4392	20.02	n/a	20.2044	17.524	n/a		3
11	P62979	Ubiquitin-40S ribosomal protein S27a	80S ribosome	21.0192	23.82	n/a	22.8571	19.135	n/a		5
12	P26373	60S ribosomal protein L13	80S ribosome	25.4806	24.72	17.7828	25.9759	22.095	15.4		11
13	P62917	60S ribosomal protein L8	80S ribosome	26.2945	26.79	18.7188	26.3071	23.888	20.98		11
14	P83881	60S ribosomal protein L36a	80S ribosome	23.6923	26.16	17.8985	23.377	22.413	15.64		10
15	Q969Q0	60S ribosomal protein L36a-like	80S ribosome	20.8661	23.29	15.1415	20.6761	19.758	n/a		8
16	Q9Y3U8	60S ribosomal protein L36	80S ribosome	25.8429	26.8	17.279	26.5689	22.798	20.53		6
17	P62241	40S ribosomal protein S8	80S ribosome	24.5278	25.62	16.6629	24.566	22.016	n/a		13

№	UniProt ID	Name	Localization	log2 (Intensity)						Peptides	
				C12-BioID2 Tet	C12-BioID2 Tet + Biotin	C12-Linker-BioID2 Tet	C12-Linker-BioID2 Tet + Biotin	COX8-MTS Tet	COX8-MTS Tet + Biotin		
263	18	P46778	60S ribosomal protein L21	80S ribosome	24.3441	24.89	16.7958	25.8634	22.305	20.11	7
	19	P49207	60S ribosomal protein L34	80S ribosome	22.7359	24.78	16.3038	22.5667	19.798	n/a	5
	20	P61353	60S ribosomal protein L27	80S ribosome	24.0873	26.23	17.7556	25.6278	23.322	20.52	10
	21	Q02878	60S ribosomal protein L6	80S ribosome	27.0152	28.59	22.6721	27.9187	25.395	26.12	22
	22	Q07020	60S ribosomal protein L18	80S ribosome	22.9564	23.99	n/a	23.46	19.609	n/a	6
	23	P62266	40S ribosomal protein S23	80S ribosome	25.734	27.24	20.2865	26.2245	23.257	20.56	7
	24	P18621	60S ribosomal protein L17	80S ribosome	24.2869	24.13	n/a	26.1884	20.271	21.2	13
	25	P27635	60S ribosomal protein L10	80S ribosome	20.6027	21.82	19.2284	22.0735	19.283	22.96	5
	26	P35268	60S ribosomal protein L22	80S ribosome	21.763	22.85	n/a	22.7925	17.268	n/a	4
	27	P36578	60S ribosomal protein L4	80S ribosome	26.0096	26.18	16.3263	27.156	23.262	22.25	27
	28	P42766	60S ribosomal protein L35	80S ribosome	22.8883	25.79	17.3698	24.3857	20.091	23.92	9

№	UniProt ID	Name	Localization	log2 (Intensity)							Peptides
				C12-BioID2 Tet	C12-BioID2 Tet + Biotin	C12-Linker-BioID2 Tet	C12-Linker-BioID2 Tet + Biotin	COX8-MTS Tet	COX8-MTS Tet + Biotin		
29	P46776	60S ribosomal protein L27a	80S ribosome	23.1556	24.54	n/a	26423.7359	19.371	n/a		4
30	P46779	60S ribosomal protein L28	80S ribosome	24.2954	23.45	15.3324	25.8878	21.883	15.31		13
31	P47914	60S ribosomal protein L29	80S ribosome	27.2811	29.72	22.4847	27.1917	25.555	21.78		6
32	P50914	60S ribosomal protein L14	80S ribosome	21.6676	23.21	15.6179	24.0816	19.259	n/a		6
33	P61254	60S ribosomal protein L26	80S ribosome	28.4895	29.19	22.9607	28.9559	26.436	23.37		17
34	P61313	60S ribosomal protein L15	80S ribosome	21.2057	22.09	n/a	22.2859	19.709	n/a		2
35	P61513	60S ribosomal protein L37a	80S ribosome	24.2566	24.12	17.8328	24.9638	21.699	n/a		6
36	P61927	60S ribosomal protein L37	80S ribosome	19.0023	22.08	n/a	20.4839	n/a	n/a		2
37	P62424	60S ribosomal protein L7a	80S ribosome	24.167	25.65	17.3858	26.2278	21.135	22.12		12
38	P62750	60S ribosomal protein L23a	80S ribosome	24.8725	26.83	19.8297	24.221	23.375	n/a		10
39	P62899	60S ribosomal protein L31	80S ribosome	21.698	27.01	16.9063	27.1291	20.865	n/a		4

№	UniProt ID	Name	Localization	log2 (Intensity)							Peptides
				C12-BioID2 Tet	C12-BioID2 Tet + Biotin	C12-Linker-BioID2 Tet	C12-Linker-BioID2 Tet + Biotin	COX8-MTS Tet	COX8-MTS Tet + Biotin		
40	P62910	60S ribosomal protein L32	80S ribosome	23.1848	25.97	n/a	23.3712	22.466	n/a	8	
41	P83731	60S ribosomal protein L24	80S ribosome	24.0299	26.64	21.7971	25.7819	23.334	23.38	9	
42	P84098	60S ribosomal protein L19	80S ribosome	24.2978	24.77	n/a	24.5995	21.554	n/a	5	
43	Q02543	60S ribosomal protein L18a	80S ribosome	23.2331	22.75	16.9686	24.5568	21.465	n/a	6	
44	Q9UNX3	60S ribosomal protein L26-like 1	80S ribosome	22.4801	23.97	15.3919	23.4329	19.667	n/a	16	
45	P42677	40S ribosomal protein S27	80S ribosome	n/a	20.83	n/a	21.5422	n/a	n/a	2	
46	P62753	40S ribosomal protein S6	80S ribosome	24.4753	25.18	21.0255	25.1644	23.144	19.05	12	
47	P62847	40S ribosomal protein S24	80S ribosome	19.6259	20.43	n/a	21.869	n/a	n/a	3	
48	Q5JNZ5	Putative 40S ribosomal protein S26-like 1	80S ribosome	23.1342	23.84	n/a	23.9562	21.811	n/a	3	
49	P62861	40S ribosomal protein S30	80S ribosome	21.7133	25.17	n/a	22.6074	20.879	n/a	3	
50	P14625	Endoplasmin	ER	n/a	21.7	n/a	n/a	n/a	n/a	2	

№	UniProt ID	Name	Localization	log2 (Intensity)							Peptides
				C12-BioID2 Tet	C12-BioID2 Tet + Biotin	C12-Linker-BioID2 Tet	C12-Linker-BioID2 Tet + Biotin	COX8-MTS Tet	COX8-MTS Tet + Biotin		
51	P30101	Protein disulfide-isomerase A3	ER	16.8441	20.64	n/a	n/a	n/a	n/a	2	
52	Q14697	Neutral alpha-glucosidase AB	ER	19.2905	21.65	n/a	18.7526	17.988	n/a	4	
53	Q86UP2	Kinectin	ER	n/a	25.78	n/a	16.8429	n/a	16.22	35	
54	Q86UE4	Protein LYRIC	ER	24.7085	28.61	21.1159	24.4321	n/a	16.04	32	
55	O76094	Signal recognition particle subunit SRP72	ER	20.7826	22.4	n/a	21.8972	19.941	n/a	7	
56	P11021	Endoplasmic reticulum chaperone BiP	ER	18.6878	21.33	n/a	19.6103	n/a	n/a	3	
57	Q15643	Thyroid receptor-interacting protein 11	ER	22.5818	21.98	n/a	20.7823	20.02	n/a	2	

Table Apx 12. NCL2 COX8 mitochondria

The table contains all the mitochondrial hits identified for COX8-MTS control during the second Newcastle mass-spectrometry run.

Nº	UniProt ID	Name	Localization	log2 (LFQ)				Peptides
				COX8- MTS Tet 1	COX8- MTS Tet 2	COX8- MTS Tet + Biotin 1	COX8- MTS Tet + Biotin 2	
1	O75390	Citrate synthase	Matrix	19.42	n/a	n/a	19.7813	3
2	O75439	Peptidase, mitochondrial processing subunit beta	Matrix	20.51	n/a	n/a	20.3267	6
3	P00367	Glutamate dehydrogenase 1	Matrix	21.38	n/a	n/a	22.6697	14
4	P49448	Glutamate dehydrogenase 2	Matrix	21.38	n/a	n/a	22.6697	14
5	P05165	Propionyl-CoA carboxylase subunit alpha	Matrix	32.12	25.56	25.9885	31.881	62
6	P05166	Propionyl-CoA carboxylase subunit beta	Matrix	20.95	n/a	n/a	22.5331	16
7	P10809	Heat shock protein family D (Hsp60) member 1	Matrix	22.5	n/a	n/a	25.3014	26
8	P11177	Pyruvate dehydrogenase E1 subunit beta	Matrix	19.56	n/a	n/a	19.202	3
9	Q969P6	DNA topoisomerase I mitochondrial	Matrix	21.18	n/a	20.6747	21.8203	16
10	P11498	Pyruvate carboxylase	Matrix	32.33	26.47	27.0832	32.0158	73
11	P23368	Malic enzyme 2	Matrix	19.45	n/a	n/a	20.0258	6
12	P24752	Acetyl-CoA acetyltransferase 1	Matrix	20.47	n/a	n/a	20.2576	9
13	P30084	Enoyl-CoA hydratase, short chain 1	Matrix	18.68	n/a	n/a	19.0294	3
14	P34897	Serine hydroxymethyltransferase 2 (SHMT2)	Matrix	20.72	n/a	n/a	24.7554	15
15	P38117	Electron transfer flavoprotein subunit beta	Matrix	19.96	n/a	n/a	20.5626	4
16	P38646	Heat shock protein family A (Hsp70) member 9	Matrix	22.62	n/a	n/a	22.8708	15

№	UniProt ID	Name	Localization	log2 (LFQ)				Peptides
				COX8-MTS Tet 1	COX8-MTS Tet 2	COX8-MTS Tet + Biotin 1	COX8-MTS Tet + Biotin 2	
17	P40926	Malate dehydrogenase 2	Matrix	21.25	n/a	n/a	21.6501	8
18	P49411	Tu translation elongation factor, mitochondrial	Matrix	23.5	n/a	n/a	23.7058	13
19	P54886	Aldehyde dehydrogenase 18 family member A1	Matrix	20.94	n/a	n/a	21.6665	9
20	P61604	Heat shock protein family E (Hsp10) member 1	Matrix	18.27	n/a	n/a	24.1608	5
21	Q00059	Transcription factor A, mitochondrial	Matrix	19.34	n/a	n/a	20.4105	5
22	Q12931	Heat shock protein 75 kDa	Matrix	22.71	n/a	n/a	23.2436	15
23	Q13085	Acetyl-CoA carboxylase alpha	Matrix	23.65	n/a	22.109	22.8715	58
24	Q5JRX3	Pitrilysin metallopeptidase 1	Matrix	19.57	n/a	n/a	19.7586	4
25	Q96C36	Pyrroline-5-carboxylate reductase 2	Matrix	18.86	n/a	n/a	19.8802	4
26	P32322	Pyrroline-5-carboxylate reductase 1	Matrix	18.86	n/a	n/a	19.8802	4
27	Q96RQ3	Methylcrotonoyl-CoA carboxylase 1	Matrix	30.91	25.44	26.2017	30.6087	43
28	Q99798	Aconitase 2	Matrix	20.84	n/a	n/a	20.9274	6
29	Q9BQ48	Mitochondrial ribosomal protein L34	Matrix	22.69	n/a	21.5704	23.5299	4
30	Q9HCC0	Methylcrotonoyl-CoA carboxylase 2	Matrix	18.86	n/a	n/a	19.1432	3
31	Q9NP81	Seryl-tRNA synthetase 2, mitochondrial	Matrix	19.46	n/a	n/a	19.5841	5
32	Q9NSE4	Isoleucyl-tRNA synthetase 2, mitochondrial	Matrix	20.18	n/a	n/a	21.1474	9
33	O95831	Apoptosis inducing factor mitochondria associated 1	IMM	19.72	n/a	n/a	19.53	7
34	P06576	ATP synthase F1 subunit beta	IMM	22.18	n/a	n/a	24.5746	15
35	P12235	Solute carrier family 25 member 4	IMM	21.64	n/a	n/a	21.7543	7

№	UniProt ID	Name	Localization	log2 (LFQ)				Peptides
				COX8-MTS Tet 1	COX8-MTS Tet 2	COX8-MTS Tet + Biotin 1	COX8-MTS Tet + Biotin 2	
36	P12236	Solute carrier family 25 member 6	IMM	21.64	n/a	n/a	21.7543	7
37	P22695	Ubiquinol-cytochrome c reductase core protein 2	IMM	21.36	n/a	n/a	21.4089	8
38	P25705	ATP synthase F1 subunit alpha	IMM	24.3	21.58	n/a	25.273	25
39	P31930	Ubiquinol-cytochrome c reductase core protein 1	IMM	21.07	n/a	n/a	21.3148	7
40	P35232	Prohibitin	IMM	20.84	n/a	n/a	20.9962	5
41	P40939	Hydroxyacyl-CoA dehydrogenase trifunctional multienzyme complex subunit alpha	IMM	21.81	n/a	n/a	22.6161	19
42	P48047	ATP synthase peripheral stalk subunit OSCP	IMM	20.28	n/a	n/a	20.5457	5
43	P55084	Hydroxyacyl-CoA dehydrogenase trifunctional multienzyme complex subunit beta	IMM	20.17	n/a	n/a	20.5469	8
44	Q16891	MIC60 subunit	IMM	19.62	n/a	n/a	20.8973	5
45	Q99623	Prohibitin 2	IMM	21.66	n/a	n/a	22.1421	15
46	O75746	Solute carrier family 25 member 12	IMM	20.19	n/a	n/a	20.2071	8
47	Q9UJS0	Solute carrier family 25 member 13	IMM	20.19	n/a	n/a	20.2071	8
48	Q13162	Peroxiredoxin 4	IMS	21.57	n/a	n/a	20.105	10
49	Q9NRP2	Calcium-binding mitochondrial carrier protein Aralar2	IMS	20.19	n/a	n/a	20.2071	8
50	Q7Z7K0	Calcium-binding mitochondrial carrier protein Aralar1	IMS	20.19	n/a	n/a	20.2071	8

№	UniProt ID	Name	Localization	log2 (LFQ)				Peptides
				COX8-MTS Tet 1	COX8-MTS Tet 2	COX8-MTS Tet + Biotin 1	COX8-MTS Tet + Biotin 2	
51	Q8TCS8	Polyribonucleotide nucleotidyltransferase 1 (PNPT1)	IMS	19.57	n/a	n/a	20.4062	5
52	P21796	Voltage dependent anion channel 1	OMM	22.72	n/a	n/a	21.471	11
53	P45880	Voltage dependent anion channel 2	OMM	22.05	n/a	n/a	21.0905	4
54	O00763	Acetyl-CoA carboxylase beta	OMM	23.65	n/a	22.109	22.8715	58
55	P51659	Hydroxysteroid 17-beta dehydrogenase 4	Mitochondrial - unknown	21.92	n/a	n/a	22.3043	15
56	Q7KZF4	Staphylococcal nuclease and tudor domain containing 1	Mitochondrial - unknown	20.62	n/a	n/a	21.3895	11

Table Apx 13. NCL2 COX8 adjacent

The table contains all the ER, 80S or cytosolic translation hits identified for COX8-MTS control during the second Newcastle mass-spectrometry run.

№	UniProt ID	Name	Localization	log2 (LFQ)				
				COX8-MTS Tet 1	COX8-MTS Tet 2	COX8-MTS Tet + Biotin 1	COX8-MTS Tet + Biotin 2	Peptides
1	-	<i>A. aeolicus</i> biotin-ligase	Exogenous, induced	19.994	n/a	23.2474	27.6279	18
2	O60841	Eukaryotic translation initiation factor 5B	EK translation	26.629	23.02	24.2312	25.1835	33
3	Q5VTE0	Putative elongation factor 1-alpha-like 3	EK translation	22.188	23.09	22.218	22.0706	8
4	Q96GA3	Protein LTV1 homolog	EK translation	21.871	n/a	n/a	22.8165	7
5	Q8NE71	ATP-binding cassette sub-family F member 1	EK translation	23.692	n/a	n/a	19.9396	13
6	Q96EY4	Translation machinery-associated protein 16	EK translation	20.06	n/a	n/a	22.2508	4
7	P61353	60S ribosomal protein L27	80S ribosome	23.762	22.57	24.2458	23.2676	9
8	Q02878	60S ribosomal protein L6	80S ribosome	26.156	24.98	26.0261	24.5487	12
9	P62854	40S ribosomal protein S26	80S ribosome	23.895	n/a	n/a	23.2076	4
10	P62266	40S ribosomal protein S23	80S ribosome	27.064	20.55	21.9457	24.3877	8
11	P46777	60S ribosomal protein L5	80S ribosome	21.068	n/a	n/a	22.0952	8
12	P62979	Ubiquitin-40S ribosomal protein S27a	80S ribosome	22.988	n/a	n/a	23.1151	4
13	P30050	60S ribosomal protein L12	80S ribosome	20.388	n/a	n/a	19.8331	3
14	P50914	60S ribosomal protein L14	80S ribosome	21.777	n/a	n/a	22.0126	3
15	P62917	60S ribosomal protein L8	80S ribosome	21.004	n/a	n/a	19.8209	4
16	P35268	60S ribosomal protein L22	80S ribosome	20.398	n/a	n/a	22.17	5

№	UniProt ID	Name	Localization	log2 (LFQ)				Peptides
				COX8-MTS Tet 1	COX8-MTS Tet 2	COX8-MTS Tet + Biotin 1	COX8-MTS Tet + Biotin 2	
17	P46776	60S ribosomal protein L27a	80S ribosome	23.902	n/a	n/a	23.144	5
18	P62906	60S ribosomal protein L10a	80S ribosome	19.843	n/a	n/a	19.8223	5
19	P62910	60S ribosomal protein L32	80S ribosome	21.197	n/a	n/a	21.7092	5
20	P84098	60S ribosomal protein L19	80S ribosome	23.182	n/a	n/a	22.4041	5
21	Q9Y3U8	60S ribosomal protein L36	80S ribosome	23.678	n/a	n/a	22.2101	5
22	P26373	60S ribosomal protein L13	80S ribosome	21.429	n/a	n/a	22.516	6
23	P47914	60S ribosomal protein L29	80S ribosome	26.866	22.11	23.3434	24.5451	6
24	P83731	60S ribosomal protein L24	80S ribosome	23.64	n/a	22.8931	21.6888	6
25	P83881	60S ribosomal protein L36a	80S ribosome	25.359	n/a	18.9247	21.1773	6
26	P18621	60S ribosomal protein L17	80S ribosome	21.672	n/a	n/a	24.5671	7
27	P42766	60S ribosomal protein L35	80S ribosome	27.452	21.33	22.3582	25.4473	7
28	P61254	60S ribosomal protein L26	80S ribosome	25.426	n/a	20.0025	24.9994	10
29	P62750	60S ribosomal protein L23a	80S ribosome	26.611	23.21	24.6243	26.4884	11
30	P36578	60S ribosomal protein L4	80S ribosome	24.033	n/a	n/a	24.3547	15
31	P62861	40S ribosomal protein S30	80S ribosome	27.294	23.87	24.668	26.5125	5
32	P62753	40S ribosomal protein S6	80S ribosome	22.035	n/a	21.5469	20.6426	7
33	P62241	40S ribosomal protein S8	80S ribosome	24.559	n/a	n/a	22.5112	10
34	Q96AG4	Leucine-rich repeat-containing protein 59	ER	21.046	n/a	n/a	22.8766	8
35	P55072	Transitional endoplasmic reticulum ATPase	ER	19.154	n/a	n/a	20.2882	14
36	Q86UE4	Protein LYRIC	ER	26.156	21.17	24.4044	28.2718	34
37	P13667	Protein disulfide-isomerase A4	ER	18.942	n/a	n/a	19.6175	5
38	P23284	Peptidyl-prolyl cis-trans isomerase B	ER	20.371	n/a	n/a	20.1806	5

№	UniProt ID	Name	Localization	log2 (LFQ)				Peptides
				COX8-MTS Tet 1	COX8-MTS Tet 2	COX8-MTS Tet + Biotin 1	COX8-MTS Tet + Biotin 2	
39	P27824	Calnexin	ER	20.33	n/a	n/a	20.5689	5
40	P16615	Sarcoplasmic/endoplasmic reticulum calcium ATPase 2	ER	21.591	n/a	n/a	21.0086	6
41	P13674	Prolyl 4-hydroxylase subunit alpha-1	ER	20.794	n/a	n/a	21.3376	7
42	Q9BSJ8	Extended synaptotagmin-1	ER	19.75	n/a	n/a	21.4858	7
43	Q9P2E9	Ribosome-binding protein 1	ER	n/a	n/a	21.2726	20.9362	8
44	P04843	Dolichyl-diphosphooligosaccharide--protein glycosyltransferase subunit 1	ER	20.821	n/a	n/a	20.891	9
45	P30101	Protein disulfide-isomerase A3	ER	20.603	n/a	n/a	21.2294	9
46	Q14697	Neutral alpha-glucosidase AB	ER	22.253	n/a	n/a	22.1994	10
47	O76094	Signal recognition particle subunit SRP72	ER	20.84	n/a	21.3751	21.804	12
48	P14625	Endoplasmin	ER	21.992	n/a	n/a	22.8002	17
49	P11021	Endoplasmic reticulum chaperone BiP	ER	21.505	n/a	n/a	22.6537	18

Table Apx 14. NCL2 C12-BioID2 mitochondria

The table contains all the mitochondrial hits identified for C12orf65-BioID2-HA during the second Newcastle mass-spectrometry run.

№	UniProt ID	Name	Localization	log2 (LFQ)				
				C12-BioID2 Tet 1	C12-BioID2 Tet 2	C12-BioID2 Tet + Biotin 1	C12-BioID2 Tet + Biotin 2	Peptides
1	O75390	Citrate synthase	Matrix	n/a	20.442	20.628	19.8804	3
2	O75439	Peptidase, mitochondrial processing subunit beta	Matrix	n/a	20.502	19.8011	20.2712	6
3	P00367	Glutamate dehydrogenase 1	Matrix	22.55	21.942	22.3543	22.2456	14
4	P49448	Glutamate dehydrogenase 2	Matrix	22.55	21.942	22.3543	22.2456	14
5	P04181	Ornithine aminotransferase	Matrix	n/a	19.425	19.7635	20.0155	3
6	P05165	Propionyl-CoA carboxylase subunit alpha	Matrix	31.432	32.668	30.9044	32.1216	62
7	P05166	Propionyl-CoA carboxylase subunit beta	Matrix	22.554	23.407	21.4115	23.2987	16
8	P08559	Pyruvate dehydrogenase E1 subunit alpha 1	Matrix	n/a	21.109	20.0417	20.7474	4
9	P29803	Pyruvate dehydrogenase E1 subunit alpha 2	Matrix	n/a	21.109	20.0417	20.7474	4
10	P10809	Heat shock protein family D (Hsp60) member 1	Matrix	21.84	23.313	24.2591	24.0429	26
11	P11177	Pyruvate dehydrogenase E1 subunit beta	Matrix	n/a	19.388	19.4728	19.6051	3
12	Q969P6	DNA topoisomerase I mitochondrial	Matrix	20.961	23.108	21.7273	23.6419	16
13	P11498	Pyruvate carboxylase	Matrix	32.391	32.991	31.7474	32.4023	73
14	P24752	Acetyl-CoA acetyltransferase 1	Matrix	19.713	20.641	20.7829	20.1216	9
15	P30084	Enoyl-CoA hydratase, short chain 1	Matrix	n/a	18.889	n/a	18.5756	3
16	P34897	Serine hydroxymethyltransferase 2 (SHMT2)	Matrix	n/a	20.107	20.8212	21.7213	15

№	UniProt ID	Name	Localization	log2 (LFQ)				Peptides
				C12-BioID2 Tet 1	C12-BioID2 Tet 2	C12-BioID2 Tet + Biotin 1	C12-BioID2 Tet + Biotin 2	
17	P36957	Dihydrolipoamide S-succinyltransferase	Matrix	n/a	19.829	19.7187	20.9393	4
18	P38117	Electron transfer flavoprotein subunit beta	Matrix	n/a	20.759	n/a	20.8932	4
19	P38646	Heat shock protein family A (Hsp70) member 9	Matrix	21.559	22.688	22.8389	23.8546	15
20	P40926	Malate dehydrogenase 2	Matrix	20.267	21.884	21.1914	21.9872	8
21	P42704	Leucine-rich PPR motif-containing protein (LRPPRC)	Matrix	n/a	n/a	20.6866	21.6117	23
22	P49411	Tu translation elongation factor, mitochondrial	Matrix	23.549	23.64	23.2257	23.6829	13
23	P54886	Aldehyde dehydrogenase 18 family member A1	Matrix	21.138	20.712	20.8694	20.3686	9
24	P61604	Heat shock protein family E (Hsp10) member 1	Matrix	n/a	19.224	20.46	18.8367	5
25	Q12931	Heat shock protein 75 kDa	Matrix	22.525	23.191	22.6226	23.0768	15
26	Q13085	Acetyl-CoA carboxylase alpha	Matrix	27.083	24.178	27.0087	23.7236	58
27	Q6UB35	Methylenetetrahydrofolate dehydrogenase (NADP+ dependent) 1 like	Matrix	19.945	20.178	20.7182	21.452	9
28	Q92665	Mitochondrial ribosomal protein S31	Matrix	n/a	17.848	18.4163	18.5751	4
29	Q96RQ3	Methylcrotonoyl-CoA carboxylase 1	Matrix	30.765	31.503	30.3018	30.7238	43
30	Q99714	Hydroxysteroid 17-beta dehydrogenase 10 (HSD17B10)	Matrix	n/a	20.641	n/a	21.3066	7
31	Q99798	Aconitase 2	Matrix	n/a	20.567	n/a	20.7333	6
32	Q9BQ48	Mitochondrial ribosomal protein L34	Matrix	21.149	20.732	22.1772	23.684	4

№	UniProt ID	Name	Localization	log2 (LFQ)				Peptides
				C12-BioID2 Tet 1	C12-BioID2 Tet 2	C12-BioID2 Tet + Biotin 1	C12-BioID2 Tet + Biotin 2	
33	Q9NP81	Seryl-tRNA synthetase 2, mitochondrial	Matrix	n/a	19.576	19.9261	20.2061	5
34	Q9NSE4	Isoleucyl-tRNA synthetase 2, mitochondrial	Matrix	n/a	n/a	20.3205	19.9439	9
35	Q9P015	Mitochondrial ribosomal protein L15	Matrix	n/a	n/a	20.0066	20.9837	4
36	O95831	Apoptosis inducing factor mitochondria associated 1	IMM	19.328	n/a	20.3164	21.1104	7
37	P00505	Glutamic-oxaloacetic transaminase 2	IMM	n/a	n/a	20.1127	19.6654	4
38	P06576	ATP synthase F1 subunit beta	IMM	n/a	22.069	23.7311	24.0946	15
39	P12235	Solute carrier family 25 member 4	IMM	21.24	20.229	21.4682	20.7766	7
40	P12236	Solute carrier family 25 member 6	IMM	21.24	20.229	21.4682	20.7766	7
41	P13073	Cytochrome c oxidase subunit 4I1	IMM	n/a	20.597	n/a	20.144	5
42	P22695	Ubiquinol-cytochrome c reductase core protein 2	IMM	n/a	20.676	20.7785	22.1642	8
43	P25705	ATP synthase F1 subunit alpha	IMM	24.624	24.774	24.765	25.2608	25
44	P35232	Prohibitin	IMM	n/a	21.418	21.8247	21.7111	5
45	P36542	ATP synthase F1 subunit gamma	IMM	21.384	20.841	n/a	20.8975	4
46	P40939	Hydroxyacyl-CoA dehydrogenase trifunctional multienzyme complex subunit alpha	IMM	22.428	22.585	21.472	22.5084	19
47	P48047	ATP synthase peripheral stalk subunit OSCP	IMM	21.612	20.969	20.4929	21.4752	5
48	P55084	Hydroxyacyl-CoA dehydrogenase trifunctional multienzyme complex subunit beta	IMM	20.261	20.541	20.7208	20.7633	8
49	Q16891	MIC60 subunit	IMM	n/a	n/a	20.4603	20.2541	5

№	UniProt ID	Name	Localization	log2 (LFQ)				Peptides
				C12-BioID2 Tet 1	C12-BioID2 Tet 2	C12-BioID2 Tet + Biotin 1	C12-BioID2 Tet + Biotin 2	
50	Q99623	Prohibitin 2	IMM	22.837	22.221	22.6654	22.9855	15
51	Q9H9B4	Sideroflexin 1	IMM	n/a	19.481	n/a	19.5176	3
52	Q9NVI7	ATPase family AAA domain containing 3A (ATAD3)	IMM	n/a	n/a	19.2168	20.2248	8
53	Q5T9A4	ATPase family AAA domain containing 3B (ATAD3)	IMM	n/a	n/a	19.2168	20.2248	8
54	P54819	Adenylate kinase 2	IMS	n/a	n/a	18.546	18.6585	4
55	Q13162	Peroxiredoxin 4	IMS	n/a	19.54	21.5887	20.4051	10
56	Q8TCS8	Polyribonucleotide nucleotidyltransferase 1 (PNPT1)	IMS/matrix	n/a	19.444	19.8109	n/a	5
57	P00387	Cytochrome b5 reductase 3	OMM	n/a	19.564	n/a	20.2251	3
58	P21796	Voltage dependent anion channel 1	OMM	23.119	22.605	22.8376	22.1229	11
59	P45880	Voltage dependent anion channel 2	OMM	22.186	21.854	21.7944	21.3142	4
60	O00763	Acetyl-CoA carboxylase beta	OMM	27.083	24.178	27.0087	23.7236	58
61	P51659	Hydroxysteroid 17-beta dehydrogenase 4	Mitochondrial - unknown	22.235	22.208	22.4365	22.5855	15
62	Q7KZF4	Staphylococcal nuclease and tudor domain containing 1	Mitochondrial - unknown	21.992	21.174	21.0415	21.71	11

Table Apx 15. NCL2 C12-BioID2 adjacent

The table contains all the ER, 80S ribosome or cytosolic translation hits identified for C12orf65-BioID2-HA during the second Newcastle mass-spectrometry run.

№	UniProt ID	Name	Localization	log2 (LFQ)				Peptides
				C12-BioID2 Tet 1	C12-BioID2 Tet 2	C12-BioID2 Tet + Biotin 1	C12-BioID2 Tet + Biotin 2	
1	-	<i>A. aeolicus</i> biotin-ligase	Exogenous, induced	n/a	n/a	20.616	23.114	18
2	Q8NE71	ATP-binding cassette sub-family F member 1	EK translation	23.056	20.41	23.439	21.275	13
3	Q5VTE0	Putative elongation factor 1-alpha-like 3	EK translation	22.776	22.8	22.612	22.949	8
4	O60841	Eukaryotic translation initiation factor 5B	EK translation	26.374	26.21	26.096	26.153	33
5	O76021	Ribosomal L1 domain-containing protein 1	EK translation	19.556	n/a	20.26	n/a	4
6	Q96EY4	Translation machinery-associated protein 16	EK translation	n/a	20.13	n/a	22.115	4
7	P61353	60S ribosomal protein L27	80S ribosome	25.021	24.85	25.318	24.554	9
8	Q02878	60S ribosomal protein L6	80S ribosome	25.107	23.72	25.969	24.705	12
9	P62854	40S ribosomal protein S26	80S ribosome	20.452	17.89	n/a	22.289	4
10	P62266	40S ribosomal protein S23	80S ribosome	22.308	21.78	22.974	24.159	8
11	P05388	60S acidic ribosomal protein P0	80S ribosome	n/a	n/a	19.085	19.943	4
12	P46777	60S ribosomal protein L5	80S ribosome	20.758	20.16	21.162	22.719	8
13	P62979	Ubiquitin-40S ribosomal protein S27a	80S ribosome	23.641	22.5	24.383	22.577	4

№	UniProt ID	Name	Localization	log2 (LFQ)				Peptides
				C12-BioID2 Tet 1	C12-BioID2 Tet 2	C12-BioID2 Tet + Biotin 1	C12-BioID2 Tet + Biotin 2	
14	Q9Y3U8	60S ribosomal protein L36	80S ribosome	19.605	n/a	19.742	24.02	5
15	P26373	60S ribosomal protein L13	80S ribosome	21.141	20.03	20.15	22.688	6
16	P83881	60S ribosomal protein L36a	80S ribosome	26.562	22.71	25.875	22.177	6
17	P62241	40S ribosomal protein S8	80S ribosome	23.762	21.99	23.546	23.256	10
18	P27635	60S ribosomal protein L10	80S ribosome	20.179	19.16	n/a	20.351	4
19	P62424	60S ribosomal protein L7a	80S ribosome	20.065	n/a	20.859	21.896	4
20	P35268	60S ribosomal protein L22	80S ribosome	21.052	20.64	19.304	22.784	5
21	P46776	60S ribosomal protein L27a	80S ribosome	19.534	19.48	21.168	22.009	5
22	P62906	60S ribosomal protein L10a	80S ribosome	20.307	19.96	20.627	20.566	5
23	P62910	60S ribosomal protein L32	80S ribosome	n/a	20.1	n/a	21.888	5
24	P47914	60S ribosomal protein L29	80S ribosome	29.096	26.25	28.55	25.105	6
25	P83731	60S ribosomal protein L24	80S ribosome	21.934	n/a	22.786	22.088	6
26	P18621	60S ribosomal protein L17	80S ribosome	21.583	19.26	n/a	24.063	7
27	P42766	60S ribosomal protein L35	80S ribosome	21.932	24.7	24.483	26.748	7
28	P61254	60S ribosomal protein L26	80S ribosome	20.661	21.27	20.721	25.247	10
29	P62750	60S ribosomal protein L23a	80S ribosome	27.477	27.38	27.765	27.084	11
30	P36578	60S ribosomal protein L4	80S ribosome	21.164	20.6	19.222	24.758	15
31	P62861	40S ribosomal protein S30	80S ribosome	28.759	28.15	28.876	27.489	5
32	O76094	Signal recognition particle subunit SRP72	ER	21.773	22.6	22.188	23.123	12
33	P11021	Endoplasmic reticulum chaperone BiP	ER	22.249	22.47	23.269	23.213	18
34	Q86UE4	Protein LYRIC	ER	27.366	28.21	27.693	28.436	34
35	P14625	Endoplasmin	ER	22.463	22.76	23.575	23.712	17

№	UniProt ID	Name	Localization	log2 (LFQ)				
				C12-BioID2 Tet 1	C12-BioID2 Tet 2	C12-BioID2 Tet + Biotin 1	C12-BioID2 Tet + Biotin 2	Peptides
36	Q96AG4	Leucine-rich repeat-containing protein 59	ER	20.63	20.41	n/a	22.823	8
37	Q9P035	Very-long-chain (3R)-3-hydroxyacyl-CoA dehydratase 3	ER	20.104	20.03	20.228	19.935	3
38	O95573	Long-chain-fatty-acid-CoA ligase 3	ER	19.441	n/a	n/a	19.74	4
39	P51571	Translocon-associated protein subunit delta	ER	n/a	20.37	20.569	20.463	4
40	P13667	Protein disulfide-isomerase A4	ER	n/a	19.78	21.247	19.956	5
41	P23284	Peptidyl-prolyl cis-trans isomerase B	ER	20.805	21.15	20.475	21.167	5
42	P27824	Calnexin	ER	20.39	21.07	21.191	20.851	5
43	Q15084	Protein disulfide-isomerase A6	ER	n/a	20.09	20.663	20.534	5
44	Q9UGP8	Translocation protein SEC63 homolog	ER	n/a	19.52	n/a	20.002	5
45	P16615	Sarcoplasmic/endoplasmic reticulum calcium ATPase 2	ER	21.846	n/a	21.563	21.269	6
46	P39656	Dolichyl-diphosphooligosaccharide-protein glycosyltransferase 48 kDa subunit	ER	19.824	19.68	n/a	20.292	6
47	P13674	Prolyl 4-hydroxylase subunit alpha-1	ER	n/a	n/a	20.406	21.456	7
48	Q9BSJ8	Extended synaptotagmin-1	ER	n/a	19.67	20.236	20.438	7
49	Q9P2E9	Ribosome-binding protein 1	ER	n/a	19.78	n/a	20.286	8
50	P04843	Dolichyl-diphosphooligosaccharide-protein glycosyltransferase subunit 1	ER	22.003	21.79	21.967	21.62	9
51	P30101	Protein disulfide-isomerase A3	ER	21.418	21.01	22.295	21.814	9

№	UniProt ID	Name	Localization	log2 (LFQ)					Peptides
				C12-BioID2 Tet 1	C12-BioID2 Tet 2	C12-BioID2 Tet + Biotin 1	C12-BioID2 Tet + Biotin 2		
52	Q14697	Neutral alpha-glucosidase AB	ER	22.124	22.15	22.81	22.18	10	
53	P05023	Sodium/potassium-transporting ATPase subunit alpha-1	ER	n/a	20.44	n/a	21.255	9	
54	Q07065	Cytoskeleton-associated protein 4	ER	22.367	22.82	22.805	24.44	20	
55	P14618	Pyruvate kinase PKM	ER	19.969	20.95	20.306	19.96	5	
56	P0DMV8	Heat shock 70 kDa protein 1A	ER	20.974	n/a	21.508	22.271	9	

Table Apx 16. NCL2 C12-Linker-BioID2 mitochondria

The table contains all the mitochondrial hits identified for C12orf65-Linker-BioID2-HA during the second Newcastle mass-spectrometry run.

Nº	UniProt ID	Name	Localization	log2 (LFQ)				Peptides
				C12-Linker-BioID2 Tet 1	C12-Linker-BioID2 Tet 2	C12-Linker-BioID2 Tet + Biotin 1	C12-Linker-BioID2 Tet + Biotin 2	
1	P24752	Acetyl-CoA acetyltransferase 1	Matrix	21.4766	21.8428	22.4988	22.1655	9
2	P30084	Enoyl-CoA hydratase, short chain 1	Matrix	18.9973	n/a	19.2913	19.4814	3
3	P38117	Electron transfer flavoprotein subunit beta	Matrix	20.2783	20.8497	n/a	20.7059	4
4	Q99714	Hydroxysteroid 17-beta dehydrogenase 10 (HSD17B10)	Matrix	21.3735	21.9124	21.4886	21.7537	7
5	P05165	Propionyl-CoA carboxylase subunit alpha	Matrix	32.2826	33.4313	31.549	32.4095	62
6	P05166	Propionyl-CoA carboxylase subunit beta	Matrix	21.8516	23.8362	21.3897	22.9508	16
7	P11310	Acyl-CoA dehydrogenase medium chain	Matrix	n/a	20.3177	19.451	19.4438	4
8	P22033	Methylmalonyl-CoA mutase	Matrix	n/a	19.2006	19.418	19.699	4
9	Q13011	Enoyl-CoA hydratase 1	Matrix	20.1061	19.7667	21.6679	19.4778	5
10	Q13085	Acetyl-CoA carboxylase alpha	Matrix	25.7617	23.2175	25.4296	22.538	58
11	P09622	Dihydrolipoamide dehydrogenase	Matrix	21.1203	21.6765	n/a	21.3501	4
12	P36957	Dihydrolipoamide S- succinyltransferase	Matrix	19.4658	20.1287	20.6344	20.0846	4
13	P00367	Glutamate dehydrogenase 1	Matrix	23.1562	22.4721	23.3247	22.7396	14

№	UniProt ID	Name	Localization	log2 (LFQ)				Peptides
				C12-Linker-BioID2 Tet 1	C12-Linker-BioID2 Tet 2	C12-Linker-BioID2 Tet + Biotin 1	C12-Linker-BioID2 Tet + Biotin 2	
14	P49448	Glutamate dehydrogenase 2	Matrix	23.1562	22.4721	23.3247	22.7396	14
15	P04181	Ornithine aminotransferase	Matrix	n/a	20.4643	20.1706	19.9212	3
16	P11182	Dihydrolipoamide branched chain transacylase E2	Matrix	n/a	19.0884	19.058	n/a	5
17	P54886	Delta-1-pyrroline-5-carboxylate synthase	Matrix	21.4637	21.3808	22.0626	21.7944	9
18	Q96RQ3	Methylcrotonoyl-CoA carboxylase 1	Matrix	30.8288	30.9589	29.9925	30.4519	43
19	MCCB	Methylcrotonoyl-CoA carboxylase 2	Matrix	19.3539	19.2835	19.2703	19.3336	3
20	P34897	Serine hydroxymethyltransferase 2 (SHMT2)	Matrix	19.6284	22.0722	21.2868	22.3828	15
21	O75390	Citrate synthase	Matrix	19.9495	21.5152	21.675	20.9013	3
22	P07954	Fumarate hydratase	Matrix	n/a	19.4425	19.8024	19.6259	3
23	P11498	Pyruvate carboxylase	Matrix	32.3058	32.5607	31.2057	31.9794	73
24	P23368	Malic enzyme 2	Matrix	n/a	19.6974	19.9816	19.8711	6
25	P40926	Malate dehydrogenase 2	Matrix	21.4233	22.6494	20.955	21.6621	8
26	Q99798	Aconitase 2	Matrix	20.4368	21.1265	21.1557	20.8192	6
27	Q9P2R7	Succinate-CoA ligase ADP-forming subunit beta	Matrix	20.336	20.436	20.097	20.151	4
28	O75439	Peptidase, mitochondrial processing subunit beta	Matrix	20.5267	21.8029	21.2373	21.2423	6
29	O76031	Caseinolytic mitochondrial matrix peptidase chaperone subunit X (ATP-dependent Clp protease)	Matrix	n/a	20.5547	20.0538	20.4333	8

№	UniProt ID	Name	Localization	log2 (LFQ)				Peptides
				C12-Linker-BioID2 Tet 1	C12-Linker-BioID2 Tet 2	C12-Linker-BioID2 Tet + Biotin 1	C12-Linker-BioID2 Tet + Biotin 2	
30	P08559	Pyruvate dehydrogenase E1 subunit alpha 1	Matrix	20.4668	21.4269	n/a	n/a	4
31	P29803	Pyruvate dehydrogenase E1 subunit alpha 2	Matrix	20.4668	21.4269	n/a	n/a	4
32	P10809	Heat shock protein family D (Hsp60) member 1	Matrix	23.5681	25.1931	24.9701	24.7713	26
33	P11177	Pyruvate dehydrogenase E1 subunit beta	Matrix	19.5269	20.2411	20.1483	20.0618	3
34	P36776	Lon peptidase 1, mitochondrial	Matrix	n/a	20.2449	20.1928	20.1195	5
35	P38646	Heat shock protein family A (Hsp70) member 9	Matrix	22.9935	24.5696	24.4212	24.4966	15
36	P61604	Heat shock protein family E (Hsp10) member 1	Matrix	19.6175	20.6719	20.9713	20.5678	5
37	Q12931	Heat shock protein 75 kDa	Matrix	23.3225	24.2107	23.7458	23.9348	15
38	Q5JRX3	Pitrysin metallopeptidase 1	Matrix	19.4238	19.4967	19.5552	20.1104	4
39	Q6UB35	Monofunctional C1-tetrahydrofolate synthase	Matrix	20.6192	21.1252	21.217	21.4407	9
40	Q969P6	DNA topoisomerase I mitochondrial	Matrix	19.786	24.4672	21.5607	24.2776	16
41	P42704	Leucine-rich PPR motif-containing protein (LRPPRC)	Matrix	19.825	22.4267	21.6486	23.2911	23
42	P49411	Tu translation elongation factor, mitochondrial	Matrix	24.3759	24.2148	24.4057	24.0031	13
43	P82933	Mitochondrial ribosomal protein S9	Matrix	n/a	19.8957	n/a	19.8248	7

№	UniProt ID	Name	Localization	log2 (LFQ)				Peptides
				C12-Linker-BioID2 Tet 1	C12-Linker-BioID2 Tet 2	C12-Linker-BioID2 Tet + Biotin 1	C12-Linker-BioID2 Tet + Biotin 2	
44	Q5JTZ9	Alanyl-tRNA synthetase 2, mitochondrial	Matrix	n/a	18.5914	n/a	19.0091	5
45	Q7L0Y3	TRNA methyltransferase 10C, mitochondrial RNase P subunit (TRMT10C)	Matrix	n/a	19.6235	19.1688	19.638	5
46	Q7L2E3	DExH-box helicase 30 (DHX30)	Matrix	19.4786	n/a	19.9884	18.5676	3
47	Q92665	Mitochondrial ribosomal protein S31	Matrix	n/a	20.5159	19.252	19.8225	4
48	Q9BQ48	Mitochondrial ribosomal protein L34	Matrix	21.0234	21.1779	22.7464	24.1901	4
49	Q9BW92	Threonyl-tRNA synthetase 2, mitochondrial	Matrix	n/a	n/a	19.1554	19.128	3
50	Q9NP81	Seryl-tRNA synthetase 2, mitochondrial	Matrix	20.1683	20.4119	20.0006	20.7599	5
51	Q9NSE4	Isoleucyl-tRNA synthetase 2, mitochondrial	Matrix	20.3644	20.4236	20.2992	20.1719	9
52	Q9P015	Mitochondrial ribosomal protein L15	Matrix	20.4424	19.1357	21.1454	20.5975	4
53	Q9Y2Q9	Mitochondrial ribosomal protein S28	Matrix	n/a	18.9851	n/a	18.911	3
54	Q9Y2S7	DNA polymerase delta interacting protein 2 (POLDIP2)	Matrix	n/a	n/a	18.9585	18.5498	3
55	Q9Y3D9	Mitochondrial ribosomal protein S23	Matrix	n/a	19.5996	19.3284	19.4884	5
56	P40939	Hydroxyacyl-CoA dehydrogenase trifunctional multienzyme complex subunit alpha	IMM	22.6932	22.7956	22.9144	22.6706	19

№	UniProt ID	Name	Localization	log2 (LFQ)				Peptides
				C12-Linker-BioID2 Tet 1	C12-Linker-BioID2 Tet 2	C12-Linker-BioID2 Tet + Biotin 1	C12-Linker-BioID2 Tet + Biotin 2	
57	P55084	Hydroxyacyl-CoA dehydrogenase trifunctional multienzyme complex subunit beta	IMM	20.6912	21.3402	21.1358	21.4962	8
60	Q9H9B4	Sideroflexin 1	IMM	19.074	19.7701	20.4508	20.6972	3
61	O75746	Solute carrier family 25 member 12	IMM	20.0141	20.5929	20.7195	20.9363	8
62	Q9UJS0	Solute carrier family 25 member 13	IMM	20.0141	20.5929	20.7195	20.9363	8
63	O94925	Glutaminase	IMM	n/a	18.4293	18.339	n/a	6
64	P00505	Glutamic-oxaloacetic transaminase 2	IMM	19.6415	20.6554	19.3178	20.0989	4
65	P12235	Solute carrier family 25 member 4	IMM	21.657	20.3286	22.4379	21.3619	7
66	P12236	Solute carrier family 25 member 6	IMM	21.657	20.3286	22.4379	21.3619	7
67	O95831	Apoptosis inducing factor mitochondria associated 1	IMM	20.5346	21.1641	22.4057	22.0137	7
68	P06576	ATP synthase F1 subunit beta	IMM	22.5716	24.9245	24.9927	24.9781	15
69	P09669	Cytochrome c oxidase subunit 6C	IMM	n/a	21.1415	19.4379	20.0449	3
70	P13073	Cytochrome c oxidase subunit 4I1	IMM	n/a	21.6018	21.6128	20.6872	5
71	P22695	Ubiquinol-cytochrome c reductase core protein 2	IMM	21.1414	22.4287	22.0446	22.7028	8
72	P25705	ATP synthase F1 subunit alpha	IMM	24.8114	26.1092	25.8943	26.0611	25
73	P31930	Ubiquinol-cytochrome c reductase core protein 1	IMM	21.2005	22.5342	21.8993	22.2309	7
74	P36542	ATP synthase F1 subunit gamma	IMM	20.9854	21.16	21.3112	21.514	4
75	P48047	ATP synthase peripheral stalk subunit OSCP	IMM	20.8153	22.2332	20.7891	21.7904	5

№	UniProt ID	Name	Localization	log2 (LFQ)				Peptides
				C12-Linker-BioID2 Tet 1	C12-Linker-BioID2 Tet 2	C12-Linker-BioID2 Tet + Biotin 1	C12-Linker-BioID2 Tet + Biotin 2	
76	P35232	Prohibitin	IMM	20.82	22.3847	22.7499	22.5726	5
77	Q16891	MIC60 subunit	IMM	n/a	21.5741	22.1582	21.974	5
78	Q99623	Prohibitin 2	IMM	22.8711	23.4453	23.4174	23.8999	15
79	Q9NVI7	ATPase family AAA domain containing 3A (ATAD3)	IMM	n/a	20.6037	20.6157	21.028	8
80	Q5T9A4	ATPase family AAA domain containing 3B (ATAD3)	IMM	n/a	20.6037	20.6157	21.028	8
81	Q9UJS0	Calcium-binding mitochondrial carrier protein Aralar2	IMS	20.0141	20.5929	20.7195	20.9363	8
82	O75746	Calcium-binding mitochondrial carrier protein Aralar1	IMS	20.0141	20.5929	20.7195	20.9363	8
83	P54819	Adenylate kinase 2	IMS	18.9866	21.3118	20.821	20.6927	4
84	Q13162	Peroxiredoxin 4	IMS	19.7094	20.1378	24.8463	20.4284	10
85	Q8TCS8	Polyribonucleotide nucleotidyltransferase 1 (PNPT1)	IMS/matrix	n/a	19.3041	n/a	19.4197	5
86	P00387	Cytochrome b5 reductase 3	OMM	19.7688	20.9521	n/a	20.1525	3
87	O00763	Acetyl-CoA carboxylase beta	OMM	25.7617	23.2175	25.4296	22.538	58
88	O94826	Translocase of outer mitochondrial membrane 70	OMM	n/a	19.3961	19.2572	19.5846	3
89	P21796	Voltage dependent anion channel 1	OMM	23.7377	24.3708	23.7966	23.4675	11
90	P45880	Voltage dependent anion channel 2	OMM	22.9034	22.7093	22.3498	22.6143	4
91	Q92667	A-kinase anchoring protein 1	OMM	n/a	21.6118	22.8945	22.832	10

№	UniProt ID	Name	Localization	log2 (LFQ)				Peptides
				C12-Linker-BioID2 Tet 1	C12-Linker-BioID2 Tet 2	C12-Linker-BioID2 Tet + Biotin 1	C12-Linker-BioID2 Tet + Biotin 2	
92	P51659	Hydroxysteroid 17-beta dehydrogenase 4	Mitochondrial - unknown	22.3643	22.385	22.3525	22.6383	15
93	Q7KZF4	Staphylococcal nuclease and tudor domain containing 1	Mitochondrial - unknown	21.2807	21.2985	21.7941	21.3659	11

Table Apx 17. NCL2 C12-Linker-BioID2 adjacent

The table contains all the ER, 80S ribosome or cytosolic translation hits identified for C12orf65-Linker-BioID2-HA during the second Newcastle mass-spectrometry run

№	UniProt ID	Name	Localization	log2 (LFQ)				Peptides
				C12-Linker-BioID2 Tet 1	C12-Linker-BioID2 Tet 2	C12-Linker-BioID2 Tet + Biotin 1	C12-Linker-BioID2 Tet + Biotin 2	
1	-	<i>A. aeolicus</i> biotin-ligase	Exogenous, induced	19.7921	22.2883	22.8754	24.3698	18
2	P26641	Elongation factor 1-gamma	EK translation	n/a	19.5397	19.2125	20.2894	3
3	Q96EY4	Translation machinery-associated protein 16	EK translation	19.5245	20.7543	20.0714	21.2638	4
4	Q5VTE0	Putative elongation factor 1-alpha-like 3	EK translation	22.3024	23.3003	22.8713	23.2967	8
5	O60841	Eukaryotic translation initiation factor 5B	EK translation	25.177	24.2707	25.5526	24.3752	33
6	Q14684	Ribosomal RNA processing protein 1 homolog B	EK translation	22.0429	21.3432	20.4844	21.7681	8
7	Q8NE71	ATP-binding cassette sub-family F member 1	EK translation	22.5521	19.7116	23.6955	19.6433	13
8	P61353	60S ribosomal protein L27	80S ribosome	23.8832	24.7387	25.032	24.3882	9
9	Q02878	60S ribosomal protein L6	80S ribosome	24.3947	23.7948	26.4985	24.6122	12
10	P62854	40S ribosomal protein S26	80S ribosome	n/a	20.1211	19.9772	22.1079	4
11	P62266	40S ribosomal protein S23	80S ribosome	20.984	22.0695	24.3243	24.5029	8
12	P05388	60S acidic ribosomal protein P0	80S ribosome	n/a	20.5369	19.8841	20.7153	4

№	UniProt ID	Name	Localization	log2 (LFQ)				Peptides
				C12-Linker-BioID2 Tet 1	C12-Linker-BioID2 Tet 2	C12-Linker-BioID2 Tet + Biotin 1	C12-Linker-BioID2 Tet + Biotin 2	
13	P46777	60S ribosomal protein L5	80S ribosome	n/a	21.4381	21.1845	21.9734	8
14	P62979	Ubiquitin-40S ribosomal protein S27a	80S ribosome	22.9827	22.9464	23.8373	22.5613	4
15	P50914	60S ribosomal protein L14	80S ribosome	n/a	21.3258	20.8947	21.8381	3
16	P27635	60S ribosomal protein L10	80S ribosome	n/a	n/a	20.0915	20.712	4
17	P62424	60S ribosomal protein L7a	80S ribosome	20.5392	20.2343	20.9841	21.5349	4
18	P35268	60S ribosomal protein L22	80S ribosome	n/a	20.2393	22.0237	22.449	5
19	P46776	60S ribosomal protein L27a	80S ribosome	19.4651	20.0895	21.1076	23.0019	5
20	P62906	60S ribosomal protein L10a	80S ribosome	19.2531	20.9397	20.5477	20.8163	5
21	P62910	60S ribosomal protein L32	80S ribosome	n/a	19.0573	20.1093	n/a	5
22	Q9Y3U8	60S ribosomal protein L36	80S ribosome	n/a	19.9543	20.9308	23.9367	5
23	P26373	60S ribosomal protein L13	80S ribosome	19.8704	19.7527	20.1614	21.9311	6
24	P47914	60S ribosomal protein L29	80S ribosome	28.1061	25.1359	28.039	24.7348	6
25	P83731	60S ribosomal protein L24	80S ribosome	n/a	20.8383	24.1876	22.025	6
26	P83881	60S ribosomal protein L36a	80S ribosome	26.4598	22.979	25.6684	22.9455	6
27	P18621	60S ribosomal protein L17	80S ribosome	19.7066	20.4381	20.3831	24.5515	7
28	P42766	60S ribosomal protein L35	80S ribosome	21.0605	26.0589	26.2129	26.3105	7
29	P61254	60S ribosomal protein L26	80S ribosome	19.9886	21.116	22.2971	24.7076	10
30	P62750	60S ribosomal protein L23a	80S ribosome	26.6091	25.9466	26.7817	26.6661	11
31	P36578	60S ribosomal protein L4	80S ribosome	20.6089	21.4276	21.7248	24.245	15
32	P62861	40S ribosomal protein S30	80S ribosome	27.963	27.3533	27.7704	26.6823	5
33	P62753	40S ribosomal protein S6	80S ribosome	n/a	19.7573	22.0416	20.992	7
34	P62241	40S ribosomal protein S8	80S ribosome	22.7258	22.6182	24.4169	22.9064	10

№	UniProt ID	Name	Localization	log2 (LFQ)				Peptides
				C12-Linker-BioID2 Tet 1	C12-Linker-BioID2 Tet 2	C12-Linker-BioID2 Tet + Biotin 1	C12-Linker-BioID2 Tet + Biotin 2	
35	P14625	Endoplasmin	ER	22.0632	23.5203	23.5407	23.877	17
36	P11021	Endoplasmic reticulum chaperone BiP	ER	21.9918	23.5163	23.1081	23.8068	18
37	P55072	Transitional endoplasmic reticulum ATPase	ER	19.1699	21.8228	22.7609	24.0553	14
38	Q86UE4	Protein LYRIC	ER	27.3747	28.7998	27.8379	28.965	34
39	Q96AG4	Leucine-rich repeat-containing protein 59	ER	21.332	23.6322	22.2362	23.3793	8
40	P04439	HLA class I histocompatibility antigen, A alpha chain	ER	n/a	20.0243	n/a	19.802	3
41	P08240	Signal recognition particle receptor subunit alpha	ER	n/a	18.2183	18.5751	18.602	3
42	Q08379	Golgin subfamily A member 2	ER	n/a	18.0199	n/a	18.3988	4
43	Q9P035	Very-long-chain (3R)-3-hydroxyacyl-CoA dehydratase 3	ER	n/a	20.1447	20.0804	19.9758	3
44	P51571	Translocon-associated protein subunit delta	ER	19.9927	20.8168	20.3511	20.3772	4
45	P13667	Protein disulfide-isomerase A4	ER	19.8865	20.7989	20.8928	20.3673	5
46	P23284	Peptidyl-prolyl cis-trans isomerase B	ER	21.2955	22.2572	21.0003	21.2805	5
47	P27824	Calnexin	ER	20.076	22.7352	21.5202	21.4236	5

№	UniProt ID	Name	Localization	log2 (LFQ)				Peptides
				C12-Linker-BioID2 Tet 1	C12-Linker-BioID2 Tet 2	C12-Linker-BioID2 Tet + Biotin 1	C12-Linker-BioID2 Tet + Biotin 2	
48	Q15084	Protein disulfide-isomerase A6	ER	19.3929	21.09	n/a	20.6757	5
49	Q9UGP8	Translocation protein SEC63 homolog	ER	n/a	19.5258	19.7724	20.076	5
50	P16615	Sarcoplasmic/endoplasmic reticulum calcium ATPase 2	ER	21.4174	20.9579	21.8203	20.689	6
51	P39656	Dolichyl-diphosphooligosaccharide--protein glycosyltransferase 48 kDa subunit	ER	18.8982	19.895	19.9413	19.895	6
52	Q9Y4L1	Hypoxia up-regulated protein 1	ER	n/a	20.3828	20.3461	20.6457	6
53	P13674	Prolyl 4-hydroxylase subunit alpha-1	ER	20.1192	21.0713	20.3609	21.0282	7
54	Q9BSJ8	Extended synaptotagmin-1	ER	19.97	20.1299	20.6067	20.2892	7
55	P04843	Dolichyl-diphosphooligosaccharide--protein glycosyltransferase subunit 1	ER	21.3672	22.1124	22.2607	22.2189	9
56	P30101	Protein disulfide-isomerase A3	ER	20.2268	22.7854	22.2448	22.2261	9
57	Q14697	Neutral alpha-glucosidase AB	ER	22.4684	22.1131	22.7428	22.4237	10
58	O76094	Signal recognition particle subunit SRP72	ER	20.4866	21.3136	21.7822	22.4225	12
59	Q07065	Cytoskeleton-associated protein 4	ER	20.8158	23.7402	22.8136	23.5328	20

№	UniProt ID	Name	Localization	log2 (LFQ)				Peptides
				C12-Linker-BioID2 Tet 1	C12-Linker-BioID2 Tet 2	C12-Linker-BioID2 Tet + Biotin 1	C12-Linker-BioID2 Tet + Biotin 2	
60	P14618	Pyruvate kinase PKM	ER	20.401	19.7927	19.8942	19.6909	5
61	P0DMV8	Heat shock 70 kDa protein 1A	ER	n/a	21.6802	22.3328	22.2423	9
62	P46459	Vesicle-fusing ATPase	ER	n/a	19.1182	19.4878	n/a	3
63	P05023	Sodium/potassium-transporting ATPase subunit alpha-1	ER	n/a	21.4611	20.3582	21.2829	9
64	Q9P2E9	Ribosome-binding protein 1	ER	n/a	21.0849	21.0985	21.3333	8

References

ABE, Y., SHODAI, T., MUTO, T., MIHARA, K., TORII, H., NISHIKAWA, S.-I., ENDO, T. & KOHDA, D. 2000. Structural Basis of Presequence Recognition by the Mitochondrial Protein Import Receptor Tom20. *Cell*, 100, 551-560.

ABU-ELHEIGA, L., BRINKLEY, W. R., ZHONG, L., CHIRALA, S. S., WOLDEGIORGIS, G. & WAKIL, S. J. 2000. The subcellular localization of acetyl-CoA carboxylase 2. *Proc Natl Acad Sci U S A*, 97, 1444-9.

ABU-ELHEIGA, L., JAYAKUMAR, A., BALDINI, A., CHIRALA, S. S. & WAKIL, S. J. 1995. Human acetyl-CoA carboxylase: characterization, molecular cloning, and evidence for two isoforms. *Proceedings of the National Academy of Sciences*, 92, 4011-4015.

ADEVA, M. M., SOUTO, G., BLANCO, N. & DONAPETRY, C. 2012. Ammonium metabolism in humans. *Metabolism*, 61, 1495-511.

AEBERSOLD, R. & MANN, M. 2003. Mass spectrometry-based proteomics. *Nature*, 422, 198-207.

AGARONYAN, K., MOROZOV, Y. I., ANIKIN, M. & TEMIakov, D. 2015. Replication-transcription switch in human mitochondria. *Science*, 347, 548-551.

AIBARA, S., ANDRÉLL, J., SINGH, V. & AMUNTS, A. 2018. Rapid Isolation of the Mitoribosome from HEK Cells. *J Vis Exp*.

AIBARA, S., SINGH, V., MODELSKA, A. & AMUNTS, A. 2020. Structural basis of mitochondrial translation. *Elife*, 9.

AL SHAHRANI, M., HEALES, S., HARGREAVES, I. & ORFORD, M. 2017. Oxidative Stress: Mechanistic Insights into Inherited Mitochondrial Disorders and Parkinson's Disease. *Journal of clinical medicine*, 6, 100.

ALAM, T. I., KANKI, T., MUTA, T., UKAJI, K., ABE, Y., NAKAYAMA, H., TAKIO, K., HAMASAKI, N. & KANG, D. 2003. Human mitochondrial DNA is packaged with TFAM. *Nucleic Acids Res*, 31, 1640-5.

ALBERTS B, J. A., LEWIS J, ET AL. 2002. Studying Gene Expression and Function. *Molecular Biology of the Cell. 4th edition*. New York Garland Science.

ALKALAEVA, E. Z., PISAREV, A. V., FROLOVA, L. Y., KISSELEV, L. L. & PESTOVA, T. V. 2006. In vitro reconstitution of eukaryotic translation reveals cooperativity between release factors eRF1 and eRF3. *Cell*, 125, 1125-36.

ALMENDRO-VEDIA, V., NATALE, P., VALDIVIESO GONZÁLEZ, D., LILLO, M. P., ARAGONES, J. L. & LÓPEZ-MONTERO, I. 2021. How rotating ATP synthases can modulate membrane structure. *Archives of Biochemistry and Biophysics*, 708, 108939.

ALTMANN, R. 1890. Die Elementarorganismen und ihre Beziehungen zu den Zellen. *Veit*. Leipzig.

AMET, N., LEE, H. F. & SHEN, W. C. 2009. Insertion of the designed helical linker led to increased expression of tf-based fusion proteins. *Pharm Res*, 26, 523-8.

AMUNTS, A., BROWN, A., BAI, X.-C., LLÁCER, J. L., HUSSAIN, T., EMSLEY, P., LONG, F., MURSHUDOV, G., SCHERES, S. H. W. & RAMAKRISHNAN, V. 2014. Structure of the Yeast Mitochondrial Large Ribosomal Subunit. *Science*, 343, 1485-1489.

AMUNTS, A., BROWN, A., TOOTS, J., SCHERES, S. H. W. & RAMAKRISHNAN, V. 2015. The structure of the human mitochondrial ribosome. *Science*, 348, 95-98.

ANAND, R., WAI, T., BAKER, M. J., KLAUDT, N., SCHAUSS, A. C., RUGARLI, E. & LANGER, T. 2014. The i-AAA protease YME1L and OMA1 cleave OPA1 to balance mitochondrial fusion and fission. *The Journal of cell biology*, 204, 919-929.

ANCZUROWSKI, M., SUGATA, K., MATSUNAGA, Y., YAMASHITA, Y., WANG, C.-H., GUO, T., MURATA, K., SAIJO, H., KAGOYA, Y., SASO, K., BUTLER, M. O. & HIRANO, N. 2019. Chaperones of the class I peptide-loading complex facilitate the constitutive presentation of endogenous antigens on HLA-DP84GGPM87. *Journal of Autoimmunity*, 102, 114-125.

ANDERSON, J. S. & PARKER, R. P. 1998. The 3' to 5' degradation of yeast mRNAs is a general mechanism for mRNA turnover that requires the SKI2 DEVH box protein and 3' to 5' exonucleases of the exosome complex. *Embo j*, 17, 1497-506.

ANDERSON, S., BANKIER, A. T., BARRELL, B. G., DE BRUIJN, M. H., COULSON, A. R., DROUIN, J., EPERON, I. C., NIERLICH, D. P., ROE, B. A., SANGER, F., SCHREIER, P. H., SMITH, A. J., STADEN, R. & YOUNG, I. G. 1981. Sequence and organization of the human mitochondrial genome. *Nature*, 290, 457-65.

ANDERSSON, S. G. E., ZOMORODIPOUR, A., ANDERSSON, J. O., SICHERITZ-PONTÉN, T., ALSMARK, U. C. M., PODOWSKI, R. M., NÄSLUND, A. K., ERIKSSON, A.-S., WINKLER, H. H. & KURLAND, C. G.

1998. The genome sequence of *Rickettsia prowazekii* and the origin of mitochondria. *Nature*, 396, 133.

ANDREWS, R. M., KUBACKA, I., CHINNERY, P. F., LIGHTOWLERS, R. N., TURNBULL, D. M. & HOWELL, N. 1999. Reanalysis and revision of the Cambridge reference sequence for human mitochondrial DNA. *Nature Genetics*, 23, 147-147.

ANGER, A. M., ARMACHE, J.-P., BERNINGHAUSEN, O., HABECK, M., SUBKLEWE, M., WILSON, D. N. & BECKMANN, R. 2013. Structures of the human and *Drosophila* 80S ribosome. *Nature*, 497, 80-85.

ANNA, A. & MONIKA, G. 2018. Splicing mutations in human genetic disorders: examples, detection, and confirmation. *Journal of applied genetics*, 59, 253-268.

ANTONICKA, H., LIN, Z.-Y., JANER, A., WERAARPACHAI, W., GINGRAS, A.-C. & SHOUBRIDGE, E. A. 2020. A high-density human mitochondrial proximity interaction network. *bioRxiv*, 2020.04.01.020479.

ANTONICKA, H., OSTERGAARD, E., SASARMAN, F., WERAARPACHAI, W., WIBRAND, F., PEDERSEN, A. M. B., RODENBURG, R. J., VAN DER KNAAP, M. S., SMEITINK, J. A. M., CHRZANOWSKA-LIGHTOWLERS, Z. M. & SHOUBRIDGE, E. A. 2010. Mutations in C12orf65 in patients with encephalomyopathy and a mitochondrial translation defect. *American journal of human genetics*, 87, 115-122.

ANTONICKA, H., SASARMAN, F., KENNAWAY, N. G. & SHOUBRIDGE, E. A. 2006. The molecular basis for tissue specificity of the oxidative phosphorylation deficiencies in patients with mutations in the mitochondrial translation factor EFG1. *Human Molecular Genetics*, 15, 1835-1846.

ANTONICKA, H. & SHOUBRIDGE, E. A. 2015. Mitochondrial RNA Granules Are Centers for Posttranscriptional RNA Processing and Ribosome Biogenesis. *Cell Rep*, 10, 920-932.

ARCHIBALD, JOHN M. 2015. Endosymbiosis and Eukaryotic Cell Evolution. *Current Biology*, 25, R911-R921.

ARORA, D., ABEL, N. B., LIU, C., VAN DAMME, P., YPERMAN, K., EECKHOUT, D., VU, L. D., WANG, J., TORNKVIST, A., IMPENS, F., KORBEI, B., VAN LEENE, J., GOOSSENS, A., DE JAEGER, G., OTT, T., MOSCHOU, P. N. & VAN DAMME, D. 2020. Establishment of Proximity-Dependent Biotinylation Approaches in Different Plant Model Systems. *The Plant Cell*, 32, 3388-3407.

ASANO, K., SUZUKI, T., SAITO, A., WEI, F.-Y., IKEUCHI, Y., NUMATA, T., TANAKA, R., YAMANE, Y., YAMAMOTO, T., GOTO, T., KISHITA, Y., MURAYAMA, K., OHTAKE, A., OKAZAKI, Y., TOMIZAWA, K., SAKAGUCHI, Y. & SUZUKI, T. 2018. Metabolic and chemical regulation of tRNA modification associated with taurine deficiency and human disease. *Nucleic acids research*, 46, 1565-1583.

ASIN-CAYUELA, J., SCHWEND, T., FARGE, G. & GUSTAFSSON, C. M. 2005. The Human Mitochondrial Transcription Termination Factor (mTERF) Is FullyActive *in Vitro* in the Non-phosphorylatedForm *. *Journal of Biological Chemistry*, 280, 25499-25505.

AYYUB, S. A., GAO, F., LIGHTOWLERS, R. N. & CHRZANOWSKA-LIGHTOWLERS, Z. M. 2020. Rescuing stalled mammalian mitoribosomes - what can we learn from bacteria? *J Cell Sci*, 133.

AYYUB, S. A. & VARSHNEY, U. 2020. Translation initiation in mammalian mitochondria- a prokaryotic perspective. *RNA Biol*, 17, 165-175.

BAINES, H. L., STEWART, J. B., STAMP, C., ZUPANIC, A., KIRKWOOD, T. B. L., LARSSON, N.-G., TURNBULL, D. M. & GREAVES, L. C. 2014. Similar patterns of clonally expanded somatic mtDNA mutations in the colon of heterozygous mtDNA mutator mice and ageing humans. *Mechanisms of Ageing and Development*, 139, 22-30.

BAN, N., BECKMANN, R., CATE, J. H. D., DINMAN, J. D., DRAGON, F., ELLIS, S. R., LAFONTAINE, D. L. J., LINDAHL, L., LILJAS, A., LIPTON, J. M., MCALEAR, M. A., MOORE, P. B., NOLLER, H. F., ORTEGA, J., PANSE, V. G., RAMAKRISHNAN, V., SPAHN, C. M. T., STEITZ, T. A., TCHORZEWSKI, M., TOLLERVEY, D., WARREN, A. J., WILLIAMSON, J. R., WILSON, D., YONATH, A. & YUSUPOV, M. 2014. A new system for naming ribosomal proteins. *Current Opinion in Structural Biology*, 24, 165-169.

BANERJEE, R., GLADKOVA, C., MAPA, K., WITTE, G. & MOKRANJAC, D. 2015. Protein translocation channel of mitochondrial inner membrane and matrix-exposed import motor communicate via two-domain coupling protein. *eLife*, 4, e11897.

BARRELL, B. G., BANKIER, A. T. & DROUIN, J. 1979. A different genetic code in human mitochondria. *Nature*, 282, 189-194.

BARTLETT, K. & EATON, S. 2004. Mitochondrial β -oxidation. *European Journal of Biochemistry*, 271, 462-469.

BARTSAKOULIA, M., MÝLLER, J. S., GOMEZ-DURAN, A., YU-WAI-MAN, P., BOCZONADI, V. & HORVATH, R. 2016. Cysteine Supplementation May be Beneficial in a Subgroup of Mitochondrial Translation Deficiencies. *J Neuromuscul Dis*, 3, 363-379.

BAUERSCHMITT, H., FUNES, S. & HERRMANN, J. M. 2008. The Membrane-bound GTPase Guf1 Promotes Mitochondrial Protein Synthesis under Suboptimal Conditions *^{sup}</sup>. *Journal of Biological Chemistry*, 283, 17139-17146.

BAYRHUBER, M., MEINS, T., HABECK, M., BECKER, S., GILLER, K., VILLINGER, S., VONRHEIN, C., GRIESINGER, C., ZWECKSTETTER, M. & ZETH, K. 2008. Structure of the human voltage-dependent anion channel. *Proceedings of the National Academy of Sciences*, 105, 15370-15375.

BECKER, T., ARMACHE, J. P., JARASCH, A., ANGER, A. M., VILLA, E., SIEBER, H., MOTAAL, B. A., MIELKE, T., BERNINGHAUSEN, O. & BECKMANN, R. 2011a. Structure of the no-go mRNA decay complex Dom34-Hbs1 bound to a stalled 80S ribosome. *Nat Struct Mol Biol*, 18, 715-20.

BECKER, T., WENZ, L.-S., KRÜGER, V., LEHMANN, W., MÜLLER, J. M., GORONCY, L., ZUFALL, N., LITHGOW, T., GUIARD, B., CHACINSKA, A., WAGNER, R., MEISINGER, C. & PFANNER, N. 2011b. The mitochondrial import protein Mim1 promotes biogenesis of multispansing outer membrane proteins. *Journal of Cell Biology*, 194, 387-395.

BECKETT, D., KOVALEVA, E. & SCHATZ, P. J. 1999. A minimal peptide substrate in biotin holoenzyme synthetase-catalyzed biotinylation. *Protein Sci*, 8, 921-9.

BEHM-ANSMANT, I., GROSJEAN, H., MASSENET, S., MOTORIN, Y. & BRANLANT, C. 2004. Pseudouridylation at Position 32 of Mitochondrial and Cytoplasmic tRNAs Requires Two Distinct Enzymes in *Saccharomyces cerevisiae*. *Journal of Biological Chemistry*, 279, 52998-53006.

BELOSTOTSKY, R., BEN-SHALOM, E., RINAT, C., BECKER-COHEN, R., FEINSTEIN, S., ZELIGSON, S., SEGEL, R., ELPELEG, O., NASSAR, S. & FRISHBERG, Y. 2011. Mutations in the Mitochondrial Seryl-tRNA Synthetase Cause Hyperuricemia, Pulmonary Hypertension, Renal Failure in Infancy and Alkalosis, HUPRA Syndrome. *American Journal of Human Genetics*, 88, 193-200.

BERG JM, T. J., STRYER L. 2002. Section 18.3, The Respiratory Chain Consists of Four Complexes: Three Proton Pumps and a Physical Link to the Citric Acid Cycle. In: FREEMAN, W. H. (ed.) *Biochemistry*. New York.

BHANGOO, M. K., TZANKOV, S., FAN, A. C. Y., DEJGAARD, K., THOMAS, D. Y. & YOUNG, J. C. 2007. Multiple 40-kDa Heat-Shock Protein Chaperones Function in Tom70-dependent Mitochondrial Import. *Molecular Biology of the Cell*, 18, 3414-3428.

BHARADWAJ, M. S., ZHOU, Y., MOLINA, A. J., CRISWELL, T. & LU, B. 2014. Examination of bioenergetic function in the inner mitochondrial membrane peptidase 2-like (Immp2l) mutant mice. *Redox Biol*, 2, 1008-15.

BHARGAVA, K. & SPREMULLI, L. L. 2005. Role of the N- and C-terminal extensions on the activity of mammalian mitochondrial translational initiation factor 3. *Nucleic acids research*, 33, 7011-7018.

BHARGAVA, K., TEMPLETON, P. & SPREMULLI, L. L. 2004. Expression and characterization of isoform 1 of human mitochondrial elongation factor G. *Protein Expr Purif*, 37, 368-76.

BHAYA, D., DAVISON, M. & BARRANGOU, R. 2011. CRISPR-Cas systems in bacteria and archaea: versatile small RNAs for adaptive defense and regulation. *Annu Rev Genet*, 45, 273-97.

BILBILLE, Y., GUSTILO, E. M., HARRIS, K. A., JONES, C. N., LUSIC, H., KAISER, R. J., DELANEY, M. O., SPREMULLI, L. L., DEITERS, A. & AGRIS, P. F. 2011. The Human Mitochondrial tRNAMet: Structure/Function Relationship of a Unique Modification in the Decoding of Unconventional Codons. *Journal of Molecular Biology*, 406, 257-274.

BIRRELL, J. A., MORINA, K., BRIDGES, H. R., FRIEDRICH, T. & HIRST, J. 2013. Investigating the function of [2Fe-2S] cluster N1a, the off-pathway cluster in complex I, by manipulating its reduction potential. *Biochem J*, 456, 139-46.

BLAHA, G., STANLEY, R. E. & STEITZ, T. A. 2009. Formation of the First Peptide Bond: The Structure of EF-P Bound to the 70S Ribosome. *Science*, 325, 966-970.

BLAIR, N. F., CREMER, P. D. & TCHAN, M. C. 2015. Urea cycle disorders: a life-threatening yet treatable cause of metabolic encephalopathy in adults. *Practical Neurology*, 15, 45.

BOCZONADI, V. & HORVATH, R. 2014. Mitochondria: Impaired mitochondrial translation in human disease. *The International Journal of Biochemistry & Cell Biology*, 48, 77-84.

BOCZONADI, V., JENNINGS, M. J. & HORVATH, R. 2018a. The role of tRNA synthetases in neurological and neuromuscular disorders. *FEBS Lett*, 592, 703-717.

BOCZONADI, V., RICCI, G. & HORVATH, R. 2018b. Mitochondrial DNA transcription and translation: clinical syndromes. *Essays in biochemistry*, 62, 321-340.

BOCZONADI, V., SMITH, P. M., PYLE, A., GOMEZ-DURAN, A., SCHARA, U., TULINIUS, M., CHINNERY, P. F. & HORVATH, R. 2013. Altered 2-thiouridylation impairs mitochondrial translation in reversible infantile respiratory chain deficiency. *Human molecular genetics*, 22, 4602-4615.

BOEHM, E., ZAGANELLI, S., MAUNDRELL, K., JOURDAIN, A. A., THORE, S. & MARTINOU, J. C. 2017. FASTKD1 and FASTKD4 have opposite effects on expression of specific mitochondrial RNAs, depending upon their endonuclease-like RAP domain. *Nucleic Acids Res*, 45, 6135-6146.

BOGENHAGEN, D. F. 2012. Mitochondrial DNA nucleoid structure. *Biochimica et Biophysica Acta (BBA) - Gene Regulatory Mechanisms*, 1819, 914-920.

BOGENHAGEN, DANIEL F., MARTIN, DWIGHT W. & KOLLER, A. 2014. Initial Steps in RNA Processing and Ribosome Assembly Occur at Mitochondrial DNA Nucleoids. *Cell Metabolism*, 19, 618-629.

BOGENHAGEN, D. F., OSTERMEYER-FAY, A. G., HALEY, J. D. & GARCIA-DIAZ, M. 2018. Kinetics and Mechanism of Mammalian Mitochondrial Ribosome Assembly. *Cell reports*, 22, 1935-1944.

BOGORAD, L. 1975. Evolution of organelles and eukaryotic genomes. *Science*, 188, 891-898.

BOHNERT, M., REHLING, P., GUIARD, B., HERRMANN, J. M., PFANNER, N. & VAN DER LAAN, M. 2010. Cooperation of Stop-Transfer and Conservative Sorting Mechanisms in Mitochondrial Protein Transport. *Current Biology*, 20, 1227-1232.

BOLDERSON, E., RICHARD, D. J., ZHOU, B.-B. S. & KHANNA, K. K. 2009. Recent Advances in Cancer Therapy Targeting Proteins Involved in DNA Double-Strand Break Repair. *Clinical Cancer Research*, 15, 6314-6320.

BONEN, L., CUNNINGHAM, R. S., GRAY, M. W. & DOOLITTLE, W. F. 1977. Wheat embryo mitochondrial 18S ribosomal RNA: evidence for its prokaryotic nature. *Nucleic Acids Research*, 4, 663-671.

BOONE, A. N., RODRIGUES, B. & BROWNSEY, R. W. 1999. Multiple-site phosphorylation of the 280 kDa isoform of acetyl-CoA carboxylase in rat cardiac myocytes: evidence that cAMP-dependent protein kinase mediates effects of beta-adrenergic stimulation. *Biochem J*, 341 (Pt 2), 347-54.

BORATYN, G. M., CAMACHO, C., COOPER, P. S., COULOURIS, G., FONG, A., MA, N., MADDEN, T. L., MATTEN, W. T., MCGINNIS, S. D., MEREZHUK, Y., RAYTSELIS, Y., SAYERS, E. W., TAO, T., YE, J. & ZARETSKAYA, I. 2013. BLAST: a more efficient report with usability improvements. *Nucleic Acids Research*, 41, W29-W33.

BORNA, N. N., KISHITA, Y., KOHDA, M., LIM, S. C., SHIMURA, M., WU, Y., MOGUSHI, K., YATSUKA, Y., HARASHIMA, H., HISATOMI, Y., FUSHIMI, T., ICHIMOTO, K., MURAYAMA, K., OHTAKE, A. & OKAZAKI, Y. 2019. Mitochondrial ribosomal protein PTCD3 mutations cause oxidative phosphorylation defects with Leigh syndrome. *Neurogenetics*, 20, 9-25.

BOROWSKI, L. S., SZCZESNY, R. J., BRZEZNIAK, L. K. & STEPIEN, P. P. 2010. RNA turnover in human mitochondria: More questions than answers? *Biochimica et Biophysica Acta (BBA) - Bioenergetics*, 1797, 1066-1070.

BORST, P., RUTTENBERG, G. J. C. M. & KROON, A. M. 1967. Mitochondrial DNA I. Preparation and properties of mitochondrial DNA from chick liver. *Biochimica et Biophysica Acta (BBA) - Nucleic Acids and Protein Synthesis*, 149, 140-155.

BOTELHO, S. C., ÖSTERBERG, M., REICHERT, A. S., YAMANO, K., BJÖRKHOLM, P., ENDO, T., VON HEIJNE, G. & KIM, H. 2011. TIM23-mediated insertion of transmembrane α -helices into the mitochondrial inner membrane. *The EMBO Journal*, 30, 1003-1011.

BÖTTGER, I., WIELAND, O., BRDICZKA, D. & PETTE, D. 1969. Intracellular Localization of Pyruvate Carboxylase and Phosphoenolpyruvate Carboxykinase in Rat Liver. *European Journal of Biochemistry*, 8, 113-119.

BOWMAKER, M., YANG, M. Y., YASUKAWA, T., REYES, A., JACOBS, H. T., HUBERMAN, J. A. & HOLT, I. J. 2003. Mammalian mitochondrial DNA replicates bidirectionally from an initiation zone. *J Biol Chem*, 278, 50961-9.

BRADLEY, P. J., RAYATPISHEH, S., WOHLSCHEGEL, J. A. & NADIPURAM, S. M. 2020. Using BioID for the Identification of Interacting and Proximal Proteins in Subcellular Compartments in *Toxoplasma gondii*. *Methods Mol Biol*, 2071, 323-346.

BRAND, M. D. 2016. Mitochondrial generation of superoxide and hydrogen peroxide as the source of mitochondrial redox signaling. *Free Radical Biology and Medicine*, 100, 14-31.

BRANDT, U. 1998. The chemistry and mechanics of ubihydroquinone oxidation at center P (Qo) of the cytochrome bc1 complex. *Biochim Biophys Acta*, 1365, 261-8.

BRANON, T. C., BOSCH, J. A., SANCHEZ, A. D., UDESHI, N. D., SVINKINA, T., CARR, S. A., FELDMAN, J. L., PERRIMON, N. & TING, A. Y. 2018. Efficient proximity labeling in living cells and organisms with TurboID. *Nature biotechnology*, 36, 880-887.

BRICKER, D. K., TAYLOR, E. B., SCHELL, J. C., ORSAK, T., BOUTRON, A., CHEN, Y.-C., COX, J. E., CARDON, C. M., VAN VRANKEN, J. G., DEPHOURE, N., REDIN, C., BOUDINA, S., GYGI, S. P., BRIVET, M., THUMMEL, C. S. & RUTTER, J. 2012. A mitochondrial pyruvate carrier required for pyruvate uptake in yeast, *Drosophila*, and humans. *Science (New York, N.Y.)*, 337, 96-100.

BROWN, A., AMUNTS, A., BAI, X.-C., SUGIMOTO, Y., EDWARDS, P. C., MURSHUDOV, G., SCHERES, S. H. W. & RAMAKRISHNAN, V. 2014. Structure of the large ribosomal subunit from human mitochondria. *Science*, 346, 718-722.

BROWN, A., RATHORE, S., KIMANIUS, D., AIBARA, S., BAI, X. C., RORBACH, J., AMUNTS, A. & RAMAKRISHNAN, V. 2017. Structures of the human mitochondrial ribosome in native states of assembly. *Nat Struct Mol Biol*, 24, 866-869.

BROWN, T. A., TKACHUK, A. N., SHTENGEL, G., KOPEK, B. G., BOGENHAGEN, D. F., HESS, H. F. & CLAYTON, D. A. 2011. Superresolution fluorescence imaging of mitochondrial nucleoids reveals their spatial range, limits, and membrane interaction. *Mol Cell Biol*, 31, 4994-5010.

BRUNS, G. A. & REGINA, V. M. 1977. Adenylate kinase 2, a mitochondrial enzyme. *Biochem Genet*, 15, 477-86.

BRZEZNIAK, L. K., BIJATA, M., SZCZESNY, R. J. & STEPIEN, P. P. 2011. Involvement of human ELAC2 gene product in 3' end processing of mitochondrial tRNAs. *RNA Biol*, 8, 616-26.

BUCHERT, R., UEBE, S., RADWAN, F., TAWAMIE, H., ISSA, S., SHIMAZAKI, H., HENNEKE, M., EKICI, A. B., REIS, A. & ABOU JAMRA, R. 2013. Mutations in the mitochondrial gene C12ORF65 lead to syndromic autosomal recessive intellectual disability and show genotype phenotype correlation. *European Journal of Medical Genetics*, 56, 599-602.

BUGIARDINI, E., MITCHELL, A. L., ROSA, I. D., HORNING-DO, H. T., PITMANN, A. M., POOLE, O. V., HOLTON, J. L., SHAH, S., WOODWARD, C., HARGREAVES, I., QUINLIVAN, R., AMUNTS, A., WIESNER, R. J., HOULDEN, H., HOLT, I. J., HANNA, M. G., PITCEATHLY, R. D. S. & SPINAZZOLA, A. 2019. MRPS25 mutations impair mitochondrial translation and cause encephalomyopathy. *Hum Mol Genet*, 28, 2711-2719.

BURGER, G., GRAY, M. W. & FRANZ LANG, B. 2003. Mitochondrial genomes: anything goes. *Trends in Genetics*, 19, 709-716.

BURY, A. G., VINCENT, A. E., TURNBULL, D. M., ACTIS, P. & HUDSON, G. 2020. Mitochondrial isolation: when size matters. *Wellcome open research*, 5, 226-226.

BUSKIRK, A. R. & GREEN, R. 2017. Ribosome pausing, arrest and rescue in bacteria and eukaryotes. *Philosophical Transactions of the Royal Society B: Biological Sciences*, 372, 20160183.

BYKHOVSKAYA, Y., CASAS, K., MENGECHA, E., INBAL, A. & FISCHEL-GHOUDSIAN, N. 2004. Missense mutation in pseudouridine synthase 1 (PUS1) causes mitochondrial myopathy and sideroblastic anemia (MLASA). *American journal of human genetics*, 74, 1303-1308.

CAI, Y. C., BULLARD, J. M., THOMPSON, N. L. & SPREMULLI, L. L. 2000. Interaction of mitochondrial elongation factor Tu with aminoacyl-tRNA and elongation factor Ts. *J Biol Chem*, 275, 20308-14.

CALVO, S. E., CLAUSER, K. R. & MOOTHA, V. K. 2016. MitoCarta2.0: an updated inventory of mammalian mitochondrial proteins. *Nucleic Acids Res*, 44, D1251-7.

CAMARA, A. K. S., ZHOU, Y., WEN, P.-C., TAJKHORSHID, E. & KWOK, W.-M. 2017. Mitochondrial VDAC1: A Key Gatekeeper as Potential Therapeutic Target. *Frontiers in Physiology*, 8, 460.

CAMPOREALE, G., SHUBERT, E. E., SARATH, G., CERNY, R. & ZEMPLENI, J. 2004. K8 and K12 are biotinylated in human histone H4. *Eur J Biochem*, 271, 2257-63.

CARDENAS-RODRIGUEZ, M., CHATZI, A. & TOKATLIDIS, K. 2018. Iron-sulfur clusters: from metals through mitochondria biogenesis to disease. *Journal of biological inorganic chemistry : JBIC : a publication of the Society of Biological Inorganic Chemistry*, 23, 509-520.

CARR-SCHMID, A., PFUND, C., CRAIG, E. A. & KINZY, T. G. 2002. Novel G-protein complex whose requirement is linked to the translational status of the cell. *Molecular and cellular biology*, 22, 2564-2574.

CARROLL, C. J., ISOHANNI, P., PÖYHÖNEN, R., EURO, L., RICHTER, U., BRILHANTE, V., GÖTZ, A., LAHTINEN, T., PAETAU, A., PIJKO, H., BATTERSBY, B. J., TYYNISMAA, H. & SUOMALAINEN, A. 2013. Whole-exome sequencing identifies a mutation in the mitochondrial ribosome protein MRPL44 to underlie mitochondrial infantile cardiomyopathy. *Journal of Medical Genetics*, 50, 151-159.

CARROLL, J., FEARNLEY, I. M., SHANNON, R. J., HIRST, J. & WALKER, J. E. 2003. Analysis of the subunit composition of complex I from bovine heart mitochondria. *Mol Cell Proteomics*, 2, 117-26.

CAVALIER-SMITH, T. 1975. The origin of nuclei and of eukaryotic cells. *Nature*, 256, 463-468.

CHACINSKA, A., PFANNSCHMIDT, S., WIEDEMANN, N., KOZJAK, V., SANJUÁN SZKLARZ, L. K., SCHULZE-SPECKING, A., TRUSCOTT, K. N., GUIARD, B., MEISINGER, C. & PFANNER, N. 2004. Essential role of Mia40 in import and assembly of mitochondrial intermembrane space proteins. *The EMBO Journal*, 23, 3735-3746.

CHADANI, Y., ONO, K., KUTSUKAKE, K. & ABO, T. 2011. Escherichia coli YaeJ protein mediates a novel ribosome-rescue pathway distinct from SsrA- and ArfA-mediated pathways. *Molecular Microbiology*, 80, 772-785.

CHADANI, Y., ONO, K., OZAWA, S.-I., TAKAHASHI, Y., TAKAI, K., NANAMIYA, H., TOZAWA, Y., KUTSUKAKE, K. & ABO, T. 2010. Ribosome rescue by Escherichia coli ArfA (YhdL) in the absence of trans-translation system. *Molecular Microbiology*, 78, 796-808.

CHAE, H. Z., ROBISON, K., POOLE, L. B., CHURCH, G., STORZ, G. & RHEE, S. G. 1994. Cloning and sequencing of thiol-specific antioxidant from mammalian brain: alkyl hydroperoxide reductase and thiol-specific antioxidant define a large family of antioxidant enzymes. *Proc Natl Acad Sci U S A*, 91, 7017-21.

CHANG, D. D. & CLAYTON, D. A. 1984. Precise identification of individual promoters for transcription of each strand of human mitochondrial DNA. *Cell*, 36, 635-43.

CHANG, Y.-F., IMAM, J. & WILKINSON, M. 2007. The nonsense-mediated decay RNA surveillance pathway. *Annual review of biochemistry*, 76, 51-74.

CHAPMAN-SMITH, A. & CRONAN, J. E., JR. 1999. Molecular biology of biotin attachment to proteins. *J Nutr*, 129, 477s-484s.

CHE, Y. & KHAVARI, P. A. 2017. Research Techniques Made Simple: Emerging Methods to Elucidate Protein Interactions through Spatial Proximity. *Journal of Investigative Dermatology*, 137, e197-e203.

CHEN, C.-Y. A. & SHYU, A.-B. 2003. Rapid Deadenylation Triggered by a Nonsense Codon Precedes Decay of the RNA Body in a Mammalian Cytoplasmic Nonsense-Mediated Decay Pathway. *Molecular and Cellular Biology*, 23, 4805-4813.

CHEN, L., TRUJILLO, K., SUNG, P. & TOMKINSON, A. E. 2000. Interactions of the DNA ligase IV-XRCC4 complex with DNA ends and the DNA-dependent protein kinase. *J Biol Chem*, 275, 26196-205.

CHEN, P. L., CHEN, C. F., CHEN, Y., GUO, X. E., HUANG, C. K., SHEW, J. Y., REDDICK, R. L., WALLACE, D. C. & LEE, W. H. 2013. Mitochondrial genome instability resulting from SUV3 haploinsufficiency leads to tumorigenesis and shortened lifespan. *Oncogene*, 32, 1193-1201.

CHEN, Q., VAZQUEZ, E. J., MOGHADDAS, S., HOPPEL, C. L. & LESNEFSKY, E. J. 2003. Production of reactive oxygen species by mitochondria: central role of complex III. *J Biol Chem*, 278, 36027-31.

CHEN, S. S., SPERLING, E., SILVERMAN, J. M., DAVIS, J. H. & WILLIAMSON, J. R. 2012. Measuring the dynamics of *E. coli* ribosome biogenesis using pulse-labeling and quantitative mass spectrometry. *Molecular BioSystems*, 8, 3325-3334.

CHENG, X., KANKI, T., FUKUOH, A., OHGAKI, K., TAKEYA, R., AOKI, Y., HAMASAKI, N. & KANG, D. 2005. PDIP38 associates with proteins constituting the mitochondrial DNA nucleoid. *J Biochem*, 138, 673-8.

CHEW, Y. C., CAMPOREALE, G., KOTHAPALLI, N., SARATH, G. & ZEMPLENI, J. 2006. Lysine residues in N-terminal and C-terminal regions of human histone H2A are targets for biotinylation by biotinidase. *J Nutr Biochem*, 17, 225-33.

CHOI-RHEE, E., SCHULMAN, H. & CRONAN, J. E. 2004. Promiscuous protein biotinylation by *Escherichia coli* biotin protein ligase. *Protein Sci*, 13, 3043-50.

CHRISTIAN, B. E. & SPREMULLI, L. L. 2010. Preferential selection of the 5'-terminal start codon on leaderless mRNAs by mammalian mitochondrial ribosomes. *The Journal of biological chemistry*, 285, 28379-28386.

CHRISTIAN, B. E. & SPREMULLI, L. L. 2012. Mechanism of protein biosynthesis in mammalian mitochondria. *Biochimica et biophysica acta*, 1819, 1035-1054.

CHRZANOWSKA-LIGHTOWLERS, Z. M. A., PAJAK, A. & LIGHTOWLERS, R. N. 2011. Termination of protein synthesis in mammalian mitochondria. *The Journal of biological chemistry*, 286, 34479-34485.

CHRZANOWSKA-LIGHTOWLERS, Z. M. A., TEMPERLEY, R. J., SMITH, P. M., SENECA, S. H. & LIGHTOWLERS, R. N. 2004. Functional polypeptides can be synthesized from human mitochondrial transcripts lacking termination codons. *The Biochemical journal*, 377, 725-731.

CHU, C.-H. & CHENG, D. 2007. Expression, purification, characterization of human 3-methylcrotonyl-CoA carboxylase (MCCC). *Protein Expression and Purification*, 53, 421-427.

CHUJO, T., OHIRA, T., SAKAGUCHI, Y., GOSHIMA, N., NOMURA, N., NAGAO, A. & SUZUKI, T. 2012. LRPPRC/SLIRP suppresses PNPase-mediated mRNA decay and promotes polyadenylation in human mitochondria. *Nucleic acids research*, 40, 8033-8047.

CHUNG, H. K. & SPREMULLI, L. L. 1990. Purification and characterization of elongation factor G from bovine liver mitochondria. *J Biol Chem*, 265, 21000-4.

CIEPLAK, P. & STRONGIN, A. Y. 2017. Matrix metalloproteinases - From the cleavage data to the prediction tools and beyond. *Biochimica et biophysica acta. Molecular cell research*, 1864, 1952-1963.

CIPOLAT, S., DE BRITO, O. M., DAL ZILIO, B. & SCORRANO, L. 2004. OPA1 requires mitofusin 1 to promote mitochondrial fusion. *Proceedings of the National Academy of Sciences of the United States of America*, 101, 15927-15932.

CIPOLAT, S., RUDKA, T., HARTMANN, D., COSTA, V., SERNEELS, L., CRAESSAERTS, K., METZGER, K., FREZZA, C., ANNAERT, W., D'ADAMIO, L., DERKS, C., DEJAEGERE, T., PELLEGRINI, L., D'HOOGE, R., SCORRANO, L. & DE STROOPER, B. 2006. Mitochondrial Rhomboid PARL Regulates Cytochrome c Release during Apoptosis via OPA1-Dependent Cristae Remodeling. *Cell*, 126, 163-175.

CLÉMENT, M. V. & PERVAIZ, S. 2001. Intracellular superoxide and hydrogen peroxide concentrations: a critical balance that determines survival or death. *Redox Rep*, 6, 211-4.

CLEMENTE, P., PAJAK, A., LAINE, I., WIBOM, R., WEDELL, A., FREYER, C. & WREDENBERG, A. 2015. SUV3 helicase is required for correct processing of mitochondrial transcripts. *Nucleic Acids Research*, 43, 7398-7413.

COGLIATI, S., FREZZA, C., SORIANO, MARIA E., VARANITA, T., QUINTANA-CABRERA, R., CORRADO, M., CIPOLAT, S., COSTA, V., CASARIN, A., GOMES, LIGIA C., PERALES-CLEMENTE, E., SALVIATI, L., FERNANDEZ-SILVA, P., ENRIQUEZ, JOSE A. & SCORRANO, L. 2013. Mitochondrial Cristae Shape Determines Respiratory Chain Supercomplexes Assembly and Respiratory Efficiency. *Cell*, 155, 160-171.

CONNELL, S. R., TOPF, M., QIN, Y., WILSON, D. N., MIELKE, T., FUCINI, P., NIERHAUS, K. H. & SPAHN, C. M. 2008. A new tRNA intermediate revealed on the ribosome during EF4-mediated back-translocation. *Nat Struct Mol Biol*, 15, 910-5.

CONTI, E. & IZAURRALDE, E. 2005. Nonsense-mediated mRNA decay: molecular insights and mechanistic variations across species. *Current Opinion in Cell Biology*, 17, 316-325.

COX, J. & MANN, M. 2008. MaxQuant enables high peptide identification rates, individualized p.p.b.-range mass accuracies and proteome-wide protein quantification. *Nat Biotechnol*, 26, 1367-72.

COXHEAD, J., KURZAWA-AKANBI, M., HUSSAIN, R., PYLE, A., CHINNERY, P. & HUDSON, G. 2016. Somatic mtDNA variation is an important component of Parkinson's disease. *Neurobiology of aging*, 38, 217.e1-217.e6.

CRICK, F. H. C. 1966. Codon—anticodon pairing: The wobble hypothesis. *Journal of Molecular Biology*, 19, 548-555.

CRONAN, J. E. 2005. Targeted and proximity-dependent promiscuous protein biotinylation by a mutant *Escherichia coli* biotin protein ligase. *J Nutr Biochem*, 16, 416-8.

CRONAN, J. E. & REED, K. E. 2000. [27] Biotinylation of proteins in vivo: A useful posttranslational modification for protein analysis. *Methods in Enzymology*. Academic Press.

D'SOUZA, A. R. & MINCZUK, M. 2018. Mitochondrial transcription and translation: overview. *Essays in biochemistry*, 62, 309-320.

DABERKOW, R. L., WHITE, B. R., CEDERBERG, R. A., GRIFFIN, J. B. & ZEMPLINI, J. 2003. Monocarboxylate Transporter 1 Mediates Biotin Uptake in Human Peripheral Blood Mononuclear Cells. *The Journal of Nutrition*, 133, 2703-2706.

DE CABO, R., SIENDONES, E., MINOR, R. & NAVAS, P. 2009. CYB5R3: a key player in aerobic metabolism and aging? *Aging*, 2, 63-68.

DE LOS RIOS, P., BEN-ZVI, A., SLUTSKY, O., AZEM, A. & GOLOUBINOFF, P. 2006. Hsp70 chaperones accelerate protein translocation and the unfolding of stable protein aggregates by entropic pulling. *Proceedings of the National Academy of Sciences*, 103, 6166-6171.

DE MUNTER, S., GÖRNEMANN, J., DERUA, R., LESAGE, B., QIAN, J., HEROES, E., WAELKENS, E., VAN EYNDE, A., BEULLENS, M. & BOLLEN, M. 2017. Split-BioID: a proximity biotinylation assay for dimerization-dependent protein interactions. *FEBS Lett*, 591, 415-424.

DE SILVA, D., TU, Y. T., AMUNTS, A., FONTANESI, F. & BARRIENTOS, A. 2015. Mitochondrial ribosome assembly in health and disease. *Cell Cycle*, 14, 2226-50.

DE VALDIVIA, E. I. G. & ISAKSSON, L. A. 2005. Abortive translation caused by peptidyl-tRNA drop-off at NGG codons in the early coding region of mRNA. *FEBS Journal*, 272, 5306-5316.

DECKERT, G., WARREN, P. V., GAASTERLAND, T., YOUNG, W. G., LENOX, A. L., GRAHAM, D. E., OVERBEEK, R., SNEAD, M. A., KELLER, M., AUJAY, M., HUBER, R., FELDMAN, R. A., SHORT, J. M., OLSEN, G. J. & SWANSON, R. V. 1998. The complete genome of the hyperthermophilic bacterium *Aquifex aeolicus*. *Nature*, 392, 353-358.

DEGOUL, F., NELSON, I., LESTIENNE, P., FRANCOIS, D., ROMERO, N., DUBOC, D., EYMARD, B., FARDEAU, M., PONSOT, G., PATURNEAU-JOUAS, M. & ET AL. 1991. Deletions of mitochondrial DNA in Kearns-Sayre syndrome and ocular myopathies: genetic, biochemical and morphological studies. *J Neurol Sci*, 101, 168-77.

DEGTiar, E., FRIDMAN, A., GOTTLIEB, D., VEXLER, K., BEREZIN, I., FARHI, R., GOLANI, L. & SHAUL, O. 2015. The feedback control of UPF3 is crucial for RNA surveillance in plants. *Nucleic Acids Res*, 43, 4219-35.

DEL DOTTO, V., FOGAZZA, M., CARELLI, V., RUGOLO, M. & ZANNA, C. 2018. Eight human OPA1 isoforms, long and short: What are they for? *Biochim Biophys Acta Bioenerg*, 1859, 263-269.

DEMO, G., SVIDRITSKIY, E., MADIREDDY, R., DIAZ-AVALOS, R., GRANT, T., GRIGORIEFF, N., SOUSA, D. & KOROSTELEV, A. A. 2017. Mechanism of ribosome rescue by ArfA and RF2. *eLife*, 6, e23687.

DENNERLEIN, S., ROZANSKA, A., WYDRO, M., CHRZANOWSKA-LIGHTOWLERS, Z. M. & LIGHTOWLERS, R. N. 2010. Human ERAL1 is a mitochondrial RNA chaperone involved in the assembly of the 28S small mitochondrial ribosomal subunit. *Biochem J*, 430, 551-8.

DEPONTE, M. 2013. Glutathione catalysis and the reaction mechanisms of glutathione-dependent enzymes. *Biochimica et Biophysica Acta (BBA) - General Subjects*, 1830, 3217-3266.

DESAI, N., BROWN, A., AMUNTS, A. & RAMAKRISHNAN, V. 2017a. The structure of the yeast mitochondrial ribosome. *Science (New York, N.Y.)*, 355, 528-531.

DESAI, N., YANG, H., CHANDRASEKARAN, V., KAZI, R., MINCZUK, M. & RAMAKRISHNAN, V. 2020. Elongational stalling activates mitoribosome-associated quality control. *Science*, 370, 1105-1110.

DESAI, R., FRAZIER, A. E., DURIGON, R., PATEL, H., JONES, A. W., DALLA ROSA, I., LAKE, N. J., COMPTON, A. G., MOUNTFORD, H. S., TUCKER, E. J., MITCHELL, A. L. R., JACKSON, D., SESAY, A., DI RE, M., VAN DEN HEUVEL, L. P., BURKE, D., FRANCIS, D., LUNKE, S., MCGILLIVRAY, G., MANDELSTAM, S., MOCHEL, F., KEREN, B., JARDEL, C., TURNER, A. M., IAN ANDREWS, P., SMEITINK, J., SPELBRINK, J. N., HEALES, S. J., KOHDA, M., OHTAKE, A., MURAYAMA, K., OKAZAKI, Y., LOMBÈS, A., HOLT, I. J., THORBURN, D. R. & SPINAZZOLA, A. 2017b. ATAD3 gene cluster deletions cause cerebellar dysfunction associated with altered mitochondrial DNA and cholesterol metabolism. *Brain : a journal of neurology*, 140, 1595-1610.

DEVER, T. E. & GREEN, R. 2012. The elongation, termination, and recycling phases of translation in eukaryotes. *Cold Spring Harb Perspect Biol*, 4, a013706.

DI NOTTIA, M., MONTANARI, A., VERRIGNI, D., OLIVA, R., TORRACO, A., FERNANDEZ-VIZARRA, E., DIODATO, D., RIZZA, T., BIANCHI, M., CATTERUCCIA, M., ZEVIANI, M., DIONISI-VICI, C., FRANCISCI, S., BERTINI, E. & CARROZZO, R. 2017. Novel mutation in mitochondrial Elongation Factor EF-Tu associated to dysplastic leukoencephalopathy and defective mitochondrial DNA translation. *Biochimica et Biophysica Acta*, 1863, 961-967.

DICKINSON, A., YEUNG, K. Y., DONOGHUE, J., BAKER, M. J., KELLY, R. D., MCKENZIE, M., JOHNS, T. G. & ST. JOHN, J. C. 2013. The regulation of mitochondrial DNA copy number in glioblastoma cells. *Cell Death & Differentiation*, 20, 1644-1653.

DIMITROVA, L. N., KUROHA, K., TATEMATSU, T. & INADA, T. 2009. Nascent Peptide-dependent Translation Arrest Leads to Not4p-mediated Protein Degradation by the Proteasome. *J Biol Chem*, 284, 10343-10352.

DIMMER, K. S., PAPIĆ, D., SCHUMANN, B., SPERL, D., KRUMPE, K., WALTHER, D. M. & RAPAPORT, D. 2012. A crucial role for Mim2 in the biogenesis of mitochondrial outer membrane proteins. *Journal of Cell Science*, 125, 3464-3473.

DING, C., WU, Z., HUANG, L., WANG, Y., XUE, J., CHEN, S., DENG, Z., WANG, L., SONG, Z. & CHEN, S. 2015. Mitofillin and CHCHD6 physically interact with Sam50 to sustain cristae structure. *Scientific reports*, 5, 16064-16064.

DINUR-MILLS, M., TAL, M. & PINES, O. 2008. Dual targeted mitochondrial proteins are characterized by lower MTS parameters and total net charge. *PLoS one*, 3, e2161-e2161.

DLASKOVÁ, A., ENGSTOVÁ, H., ŠPAČEK, T., KAHANCOVÁ, A., PAVLUCH, V., SMOLKOVÁ, K., ŠPAČKOVÁ, J., BARTOŠ, M., HLAVATÁ, L. P. & JEŽEK, P. 2018. 3D super-resolution microscopy reflects mitochondrial cristae alternations and mtDNA nucleoid size and distribution. *Biochim Biophys Acta Bioenerg*, 1859, 829-844.

DONTSOVA, O. A. & DINMAN, J. D. 2005. 5S rRNA: Structure and Function from Head to Toe. *International journal of biomedical science : IJBS*, 1, 1-7.

DU, C., FANG, M., LI, Y., LI, L. & WANG, X. 2000. Smac, a mitochondrial protein that promotes cytochrome c-dependent caspase activation by eliminating IAP inhibition. *Cell*, 102, 33-42.

DUDKINA, N. V., HEINEMEYER, J., KEEGSTRA, W., BOEKEMA, E. J. & BRAUN, H.-P. 2005. Structure of dimeric ATP synthase from mitochondria: An angular association of monomers induces the strong curvature of the inner membrane. *FEBS Letters*, 579, 5769-5772.

DURIGON, R., WANG, Q., CEH PAVIA, E., GRANT, C. M. & LU, H. 2012. Cytosolic thioredoxin system facilitates the import of mitochondrial small Tim proteins. *EMBO reports*, 13, 916-922.

DYLE, M. C., KOLAKADA, D., CORTAZAR, M. A. & JAGANNATHAN, S. 2020. How to get away with nonsense: Mechanisms and consequences of escape from nonsense-mediated RNA decay. *WIREs RNA*, 11, e1560.

ECKELMAN, B. P., SALVESEN, G. S. & SCOTT, F. L. 2006. Human inhibitor of apoptosis proteins: why XIAP is the black sheep of the family. *EMBO reports*, 7, 988-994.

ECKMANN, C. R., RAMMELT, C. & WAHLE, E. 2011. Control of poly(A) tail length. *Wiley Interdisciplinary Reviews: RNA*, 2, 348-361.

EDWARDSON, S., SHAAG, A., KOLESNIKOVA, O., GOMORI, JOHN M., TARASSOV, I., EINBINDER, T., SAADA, A. & ELPELEG, O. 2007. Deleterious Mutation in the Mitochondrial Arginyl-Transfer RNA Synthetase Gene Is Associated with Pontocerebellar Hypoplasia. *American Journal of Human Genetics*, 81, 857-862.

EL-BROLOSY, M. A., KONTARAKIS, Z., ROSSI, A., KUENNE, C., GÜNTHER, S., FUKUDA, N., KIKHI, K., BOEZIO, G. L. M., TAKACS, C. M., LAI, S.-L., FUKUDA, R., GERRI, C., GIRALDEZ, A. J. & STAINIER, D. Y. R. 2019. Genetic compensation triggered by mutant mRNA degradation. *Nature*, 568, 193-197.

EL-BROLOSY, M. A. & STAINIER, D. Y. R. 2017. Genetic compensation: A phenomenon in search of mechanisms. *PLOS Genetics*, 13, e1006780.

ELLIOTT, H. R., SAMUELS, D. C., EDEN, J. A., RELTON, C. L. & CHINNERY, P. F. 2008. Pathogenic Mitochondrial DNA Mutations Are Common in the General Population. *The American Journal of Human Genetics*, 83, 254-260.

ENGLMEIER, R., PFEFFER, S. & FÖRSTER, F. 2017. Structure of the Human Mitochondrial Ribosome Studied In Situ by Cryoelectron Tomography. *Structure*, 25, 1574-1581.e2.

ERICKSON, H. P. 2009. Size and shape of protein molecules at the nanometer level determined by sedimentation, gel filtration, and electron microscopy. *Biological procedures online*, 11, 32-51.

ERNSTER, L. & SCHATZ, G. 1981. Mitochondria: a historical review. *Journal of Cell Biology*, 91, 227s-255s.

ESAKI, M., KANAMORI, T., NISHIKAWA, S.-I., SHIN, I., SCHULTZ, P. G. & ENDO, T. 2003. Tom40 protein import channel binds to non-native proteins and prevents their aggregation. *Nature Structural & Molecular Biology*, 10, 988-994.

FALKENBERG, M. 2018. Mitochondrial DNA replication in mammalian cells: overview of the pathway. *Essays in biochemistry*, 62, 287-296.

FANG, F., LIU, Z., FANG, H. ET AL. 2017. The clinical and genetic characteristics in children with mitochondrial disease in China. *Science China Life Sciences*, 60, 746-757.

FANG, X. J., ZHANG, W., LYU, H., WANG, Z. X., WANG, W. W. & YUAN, Y. 2017. Compound Heterozygote Mutation of C12orf65 Causes Distal Motor Neuropathy and Optic Atrophy. *Chin Med J (Engl)*, 130, 242-244.

FEAGA, H. A., QUICKEL, M. D., HANKEY-GIBLIN, P. A. & KEILER, K. C. 2016. Human Cells Require Non-stop Ribosome Rescue Activity in Mitochondria. *PLOS Genetics*, 12, e1005964.

FENG, W., LIU, C., SPINOZZI, S., WANG, L., EVANS, S. M. & CHEN, J. 2020. Identifying the Cardiac Dyad Proteome In Vivo by a BiOID2 Knock-In Strategy. *Circulation*, 141, 940-942.

FERDINANDUSSE, S., DENIS, S., VAN ROERMUND, C. W., WANDERS, R. J. & DACREMONT, G. 2004. Identification of the peroxisomal beta-oxidation enzymes involved in the degradation of long-chain dicarboxylic acids. *J Lipid Res*, 45, 1104-11.

FERNIE, A. R., CARRARI, F. & SWEETLOVE, L. J. 2004. Respiratory metabolism: glycolysis, the TCA cycle and mitochondrial electron transport. *Current Opinion in Plant Biology*, 7, 254-261.

FEY, J., WEIL, J. H., TOMITA, K., COSSET, A., DIETRICH, A., SMALL, I. & MARÉCHAL-DROUARD, L. 2002. Role of editing in plant mitochondrial transfer RNAs. *Gene*, 286, 21-24.

FINEL, M. 1987. Studies on the oligomeric state of isolated cytochrome oxidase using cross-linking reagents. *Biochimica et Biophysica Acta (BBA) - Bioenergetics*, 894, 174-179.

FINSTERER, J. 2020. The Leigh phenotype resulting from C12orf65 variants. *Genet Mol Biol*, 43, e20200177.

FISHER, R. P. & CLAYTON, D. A. 1988. Purification and characterization of human mitochondrial transcription factor 1. *Mol Cell Biol*, 8, 3496-509.

FISHER, R. P., TOPPER, J. N. & CLAYTON, D. A. 1987. Promoter selection in human mitochondria involves binding of a transcription factor to orientation-independent upstream regulatory elements. *Cell*, 50, 247-258.

FONTANESI, F., TIGANO, M., FU, Y., SFEIR, A. & BARRIENTOS, A. 2020. Chapter 2 - Human mitochondrial transcription and translation. In: GASPARRE, G. & PORCELLI, A. M. (eds.) *The Human Mitochondrial Genome*. Academic Press.

FREISTROFFER, D. V., PAVLOV, M. Y., MACDOUGALL, J., BUCKINGHAM, R. H. & EHRENBERG, M. 1997. Release factor RF3 in E.coli accelerates the dissociation of release factors RF1 and RF2 from the ribosome in a GTP-dependent manner. *Embo j*, 16, 4126-33.

FRENKEL, E. P. & KITCHENS, R. L. 1975. Intracellular localization of hepatic propionyl-CoA carboxylase and methylmalonyl-CoA mutase in humans and normal and vitamin B12 deficient rats. *Br J Haematol*, 31, 501-13.

FREYER, C., PARK, C. B., EKSTRAND, M. I., SHI, Y., KHVOROSTOVA, J., WIBOM, R., FALKENBERG, M., GUSTAFSSON, C. M. & LARSSON, N. G. 2010. Maintenance of respiratory chain function in mouse hearts with severely impaired mtDNA transcription. *Nucleic Acids Res*, 38, 6577-88.

FROLOVA, L. Y., TSIVKOVSKII, R. Y., SIVOLOBOVA, G. F., OPARINA, N. Y., SERPINSKY, O. I., BLINOV, V. M., TATKOV, S. I. & KISSELEV, L. L. 1999. Mutations in the highly conserved GQQ motif of class 1 polypeptide release factors abolish ability of human eRF1 to trigger peptidyl-tRNA hydrolysis. *RNA (New York, N.Y.)*, 5, 1014-1020.

FUKAI, T. & USHIO-FUKAI, M. 2020. Cross-Talk between NADPH Oxidase and Mitochondria: Role in ROS Signaling and Angiogenesis. *Cells*, 9, 1849.

FUSTÉ, J. M., WANROOIJ, S., JEMT, E., GRANYCOME, C. E., CLUETT, T. J., SHI, Y., ATANASSOVA, N., HOLT, I. J., GUSTAFSSON, C. M. & FALKENBERG, M. 2010. Mitochondrial RNA polymerase is needed for activation of the origin of light-strand DNA replication. *Mol Cell*, 37, 67-78.

GAGNON, M. G., SEETHARAMAN, S. V., BULKLEY, D. & STEITZ, T. A. 2012. Structural Basis for the Rescue of Stalled Ribosomes: Structure of YaeJ Bound to the Ribosome. *Science*, 335, 1370-1372.

GAKH, O., CAVADINI, P. & ISAYA, G. 2002. Mitochondrial processing peptidases. *Biochimica et Biophysica Acta (BBA) - Molecular Cell Research*, 1592, 63-77.

GALMICHE, L., SERRE, V., BEINAT, M., ASSOULINE, Z., LEBRE, A.-S., CHRETIEN, D., NIETSCHKE, P., BENES, V., BODDAERT, N., SIDI, D., BRUNELLE, F., RIO, M., MUNNICH, A. & RÖTIG, A. 2011. Exome sequencing identifies MRPL3 mutation in mitochondrial cardiomyopathy. *Human Mutation*, 32, 1225-1231.

GAO, Y., BAI, X., ZHANG, D., HAN, C., YUAN, J., LIU, W., CAO, X., CHEN, Z., SHANGGUAN, F., ZHU, Z., GAO, F. & QIN, Y. 2016. Mammalian elongation factor 4 regulates mitochondrial translation essential for spermatogenesis. *Nat Struct Mol Biol*, 23, 441-9.

GARDEITCHIK, T., MOHAMED, M., RUZZENENTE, B., KARALL, D., GUERRERO-CASTILLO, S., DALLOYAUX, D., VAN DEN BRAND, M., VAN KRAAIJ, S., VAN ASBECK, E., ASSOULINE, Z., RIO, M., DE LONLAY, P., SCHOLL-BUERGI, S., WOLTHUIS, D., HOISCHEN, A., RODENBURG, R. J., SPERL, W., URBAN, Z., BRANDT, U., MAYR, J. A., WONG, S., DE BROUWER, A. P. M., NIJTMANS, L., MUNNICH, A., RÖTIG, A., WEVERS, R. A., METODIEV, M. D. & MORAVA, E. 2018. Bi-allelic Mutations in the Mitochondrial Ribosomal Protein MRPS2 Cause Sensorineural Hearing Loss, Hypoglycemia, and Multiple OXPHOS Complex Deficiencies. *Am J Hum Genet*, 102, 685-695.

GARZA-SÁNCHEZ, F., SCHaub, R. E., JANSSEN, B. D. & HAYES, C. S. 2011. tmRNA regulates synthesis of the ArfA ribosome rescue factor. *Molecular Microbiology*, 80, 1204-1219.

GASPARI, M., FALKENBERG, M., LARSSON, N. G. & GUSTAFSSON, C. M. 2004. The mitochondrial RNA polymerase contributes critically to promoter specificity in mammalian cells. *Embo j*, 23, 4606-14.

GASTEIGER, E., GATTIKER, A., HOOGLAND, C., IVANYI, I., APPEL, R. D. & BAIROCH, A. 2003. ExPASy: The proteomics server for in-depth protein knowledge and analysis. *Nucleic Acids Res*, 31, 3784-8.

GEBERT, N., CHACINSKA, A., WAGNER, K., GUIARD, B., KOEHLER, C. M., REHLING, P., PFANNER, N. & WIEDEMANN, N. 2008. Assembly of the three small Tim proteins precedes docking to the mitochondrial carrier translocase. *EMBO reports*, 9, 548-554.

GELFAND, R. & ATTARDI, G. 1981. Synthesis and turnover of mitochondrial ribonucleic acid in HeLa cells: the mature ribosomal and messenger ribonucleic acid species are metabolically unstable. *Molecular and cellular biology*, 1, 497-511.

GHEZZI, D., BARUFFINI, E., HAACK, TOBIAS B., INVERNIZZI, F., MELCHIONDA, L., DALLABONA, C., STROM, TIM M., PARINI, R., BURLINA, ALBERTO B., MEITINGER, T., PROKISCH, H., FERRERO, I. & ZEVIANI, M. 2012. Mutations of the Mitochondrial-tRNA Modifier MTO1 Cause Hypertrophic Cardiomyopathy and Lactic Acidosis. *American Journal of Human Genetics*, 90, 1079-1087.

GINGERAS, T. R., MYERS, P. A., OLSON, J. A., HANBERG, F. A. & ROBERTS, R. J. 1978. A new specific endonuclease present in *Xanthomonas holcicola*, *Xanthomonas papavericola* and *Brevibacterium luteum*. *J Mol Biol*, 118, 113-22.

GLASGOW, R. I. C., THOMPSON, K., BARBOSA, I. A., HE, L., ALSTON, C. L., DESHPANDE, C., SIMPSON, M. A., MORRIS, A. A. M., NEU, A., LÖBEL, U., HALL, J., PROKISCH, H., HAACK, T. B., HEMPEL, M., MCFARLAND, R. & TAYLOR, R. W. 2017. Novel GFM2 variants associated with early-onset

neurological presentations of mitochondrial disease and impaired expression of OXPHOS subunits. *Neurogenetics*, 18, 227-235.

GLICK, B. S., BRANDT, A., CUNNINGHAM, K., MÜLLER, S., HALLBERG, R. L. & SCHATZ, G. 1992. Cytochromes *c* and *b* are sorted to the intermembrane space of yeast mitochondria by a stop-transfer mechanism. *Cell*, 69, 809-822.

GOLDSTEIN, J. C., WATERHOUSE, N. J., JUIN, P., EVAN, G. I. & GREEN, D. R. 2000. The coordinate release of cytochrome *c* during apoptosis is rapid, complete and kinetically invariant. *Nature Cell Biology*, 2, 156-162.

GOMES, F., PALMA, F. R., BARROS, M. H., TSUCHIDA, E. T., TURANO, H. G., ALEGRIA, T. G. P., DEMASI, M. & NETTO, L. E. S. 2017. Proteolytic cleavage by the inner membrane peptidase (IMP) complex or Oct1 peptidase controls the localization of the yeast peroxiredoxin Prx1 to distinct mitochondrial compartments. *J Biol Chem*, 292, 17011-17024.

GONG, Y., ABUDUREYIMU, S., KADOMATSU, K. & SAKAMOTO, K. 2020. Identification of PTPR σ -interacting proteins by proximity-labeling assay. *The Journal of Biochemistry*.

GONZÁLEZ-HALPHEN, M. V.-A. E. V.-M. M. M. J. M. G.-R. 2002. A case of Kearns-Sayre syndrome with the 4,977-bp common deletion associated with a novel 7,704-bp deletion. *Neurological Sciences*, 23, 247-250.

GOODENBOUR, J. M. & PAN, T. 2006. Diversity of tRNA genes in eukaryotes. *Nucleic Acids Research*, 34, 6137-6146.

GOPALAKRISHNA, S., PEARCE, S. F., DINAN, A. M., SCHOBER, F. A., CIPULLO, M., SPÅHR, H., KHAWAJA, A., MAFFEZZINI, C., FREYER, C., WREDENBERG, A., ATANASSOV, I., FIRTH, A. E. & RORBACH, J. 2019. C6orf203 is an RNA-binding protein involved in mitochondrial protein synthesis. *Nucleic acids research*, 47, 9386-9399.

GORALSKI, T. D. P., KIRIMANJESWARA, G. S. & KEILER, K. C. 2018. A New Mechanism for Ribosome Rescue Can Recruit RF1 or RF2 to Nonstop Ribosomes. *mBio*, 9, e02436-18.

GORMAN, G. S., SCHAEFER, A. M., NG, Y., GOMEZ, N., BLAKELY, E. L., ALSTON, C. L., FEENEY, C., HORVATH, R., YU-WAI-MAN, P., CHINNERY, P. F., TAYLOR, R. W., TURNBULL, D. M. & MCFARLAND, R. 2015. Prevalence of nuclear and mitochondrial DNA mutations related to adult mitochondrial disease. *Annals of neurology*, 77, 753-759.

GORNICKA, A., BRAGOSZEWSKI, P., CHROSCICKI, P., WENZ, L.-S., SCHULZ, C., REHLING, P. & CHACINSKA, A. 2014. A discrete pathway for the transfer of intermembrane space proteins across the outer membrane of mitochondria. *Molecular Biology of the Cell*, 25, 3999-4009.

GOTTESMAN, S., ROCHE, E., ZHOU, Y. & SAUER, R. T. 1998. The ClpXP and ClpAP proteases degrade proteins with carboxy-terminal peptide tails added by the SsrA-tagging system. *Genes & Development*, 12, 1338-1347.

GOTTLIEB, T. M. & JACKSON, S. P. 1993. The DNA-dependent protein kinase: Requirement for DNA ends and association with Ku antigen. *Cell*, 72, 131-142.

GÖTZ, A., TYYNISMAA, H., EURO, L., ELLONEN, P., HYÖTYLÄINEN, T., OJALA, T., HÄMÄLÄINEN, RIIKKA H., TOMMISKA, J., RAIPIO, T., ORESIC, M., KARIKOSKI, R., TAMMELA, O., SIMOLA, KALLE O. J., PAETAU, A., TYNI, T. & SUOMALAINEN, A. 2011. Exome Sequencing Identifies Mitochondrial Alanyl-tRNA Synthetase Mutations in Infantile Mitochondrial Cardiomyopathy. *The American Journal of Human Genetics*, 88, 635-642.

GOUJON, M., MCWILLIAM, H., LI, W., VALENTIN, F., SQUIZZATO, S., PAERN, J. & LOPEZ, R. 2010. A new bioinformatics analysis tools framework at EMBL-EBI. *Nucleic Acids Research*, 38, W695-W699.

GRAILLE, M., CHAILLET, M. & VAN TILBEURGH, H. 2008. Structure of Yeast Dom34: A PROTEIN RELATED TO TRANSLATION TERMINATION FACTOR Erf1 AND INVOLVED IN No-Go DECAY*. *Journal of Biological Chemistry*, 283, 7145-7154.

GRAY, M. W. 2014. The Pre-Endosymbiont Hypothesis: A New Perspective on the Origin and Evolution of Mitochondria. *Cold Spring Harbor Perspectives in Biology*, 6, a016097.

GRAY, M. W., BURGER, G. & LANG, B. F. 2001. The origin and early evolution of mitochondria. *Genome biology*, 2, REVIEWS1018-REVIEWS1018.

GREAVES, L. C., REEVE, A. K., TAYLOR, R. W. & TURNBULL, D. M. 2012. Mitochondrial DNA and disease. *The Journal of Pathology*, 226, 274-286.

GREBER, B. J., BIERI, P., LEIBUNDGUT, M., LEITNER, A., AEBERSOLD, R., BOEHRINGER, D. & BAN, N. 2015. The complete structure of the 55S mammalian mitochondrial ribosome. *Science*, 348, 303-308.

GREBER, B. J., BOEHRINGER, D., LEIBUNDGUT, M., BIERI, P., LEITNER, A., SCHMITZ, N., AEBERSOLD, R. & BAN, N. 2014a. The complete structure of the large subunit of the mammalian mitochondrial ribosome. *Nature*, 515, 283-286.

GREBER, B. J., BOEHRINGER, D., LEITNER, A., BIERI, P., VOIGTS-HOFFMANN, F., ERZBERGER, J. P., LEIBUNDGUT, M., AEBERSOLD, R. & BAN, N. 2014b. Architecture of the large subunit of the mammalian mitochondrial ribosome. *Nature*, 505, 515-9.

GRIPARIC, L., VAN DER WEL, N. N., OROZCO, I. J., PETERS, P. J. & VAN DER BLIEK, A. M. 2004. Loss of the Intermembrane Space Protein Mgm1/OPA1 Induces Swelling and Localized Constrictions along the Lengths of Mitochondria. *Journal of Biological Chemistry*, 279, 18792-18798.

GRÜNERT, S. C., STUCKI, M., MORSCHER, R. J., SUORMALA, T., BÜRER, C., BURDA, P., CHRISTENSEN, E., FICICIOGLU, C., HERWIG, J., KÖLKER, S., MÖSLINGER, D., PASQUINI, E., SANTER, R., SCHWAB, K. O., WILCKEN, B., FOWLER, B., YUE, W. W. & BAUMGARTNER, M. R. 2012. 3-methylcrotonyl-CoA carboxylase deficiency: clinical, biochemical, enzymatic and molecular studies in 88 individuals. *Orphanet journal of rare diseases* [Online], 7. Available: <http://europemc.org/abstract/MED/22642865>

<https://www.ncbi.nlm.nih.gov/pmc/articles/pmid/22642865/pdf/?tool=EBI>

<https://www.ncbi.nlm.nih.gov/pmc/articles/pmid/22642865/?tool=EBI>

<https://doi.org/10.1186/1750-1172-7-31>

<https://europemc.org/articles/PMC3495011>

<https://europemc.org/articles/PMC3495011?pdf=render> [Accessed 2012/05//].

GU, J., LU, H., TIPPIN, B., SHIMAZAKI, N., GOODMAN, M. F. & LIEBER, M. R. 2007. XRCC4:DNA ligase IV can ligate incompatible DNA ends and can ligate across gaps. *The EMBO journal*, 26, 1010-1023.

GUAN, M. X. 2011. Mitochondrial 12S rRNA mutations associated with aminoglycoside ototoxicity. *Mitochondrion*, 11, 237-45.

GUEDOUARI, H., OULD AMER, Y., PICHAUD, N. & HEBERT-CHATELAIN, E. 2021. Characterization of the interactome of c-Src within the mitochondrial matrix by proximity-dependent biotin identification. *Mitochondrion*, 57, 257-269.

GUSTAFSSON, C. M., FALKENBERG, M. & LARSSON, N. G. 2016. Maintenance and Expression of Mammalian Mitochondrial DNA. *Annu Rev Biochem*, 85, 133-60.

GUTMANN, S., HAEBEL, P. W., METZINGER, L., SUTTER, M., FELDEN, B. & BAN, N. 2003. Crystal structure of the transfer-tRNA domain of transfer-messenger RNA in complex with SmpB. *Nature*, 424, 699-703.

GUYOMAR, C. & GILLET, R. 2019. When transfer-messenger RNA scars reveal its ancient origins. *Annals of the New York Academy of Sciences*, 1447, 80-87.

HAMMARSUND, M., WILSON, W., CORCORAN, M., MERUP, M., EINHORN, S., GRANDÉR, D. & SANGFELT, O. 2001. Identification and characterization of two novel human mitochondrial elongation factor genes, hEFG2 and hEFG1, phylogenetically conserved through evolution. *Human Genetics*, 109, 542-550.

HANDA, Y., HIKAWA, Y., TOCHIO, N., KOGURE, H., INOUE, M., KOSHIBA, S., GÜNTERT, P., INOUE, Y., KIGAWA, T., YOKOYAMA, S. & NAMEKI, N. 2010. Solution Structure of the Catalytic Domain of the Mitochondrial Protein ICT1 That Is Essential for Cell Vitality. *Journal of Molecular Biology*, 404, 260-273.

HANDA, Y., INAHO, N. & NAMEKI, N. 2011. YaeJ is a novel ribosome-associated protein in *Escherichia coli* that can hydrolyze peptidyl-tRNA on stalled ribosomes. *Nucleic Acids Res*, 39, 1739-1748.

HAQUE, M. E., SPREMULLI, L. L. & FECKO, C. J. 2010. Identification of protein-protein and protein-ribosome interacting regions of the C-terminal tail of human mitochondrial inner membrane protein Oxa1L. *The Journal of biological chemistry*, 285, 34991-34998.

HARTL, F.-U., SCHMIDT, B., WACHTER, E., WEISS, H. & NEUPERT, W. 1986. Transport into mitochondria and intramitochondrial sorting of the Fe/S protein of ubiquinol-cytochrome c reductase. *Cell*, 47, 939-951.

HARTMANN, C., CHRISTEN, P. & JAUSSI, R. 1991. Mitochondrial protein charge. *Nature*, 352, 762-763.

HAWLITSCHKE, G., SCHNEIDER, H., SCHMIDT, B., TROPSCHUG, M., HARTL, F.-U. & NEUPERT, W. 1988. Mitochondrial protein import: Identification of processing peptidase and of PEP, a processing enhancing protein. *Cell*, 53, 795-806.

HE, J., COOPER, H. M., REYES, A., DI RE, M., SEMBONGI, H., LITWIN, T. R., GAO, J., NEUMAN, K. C., FEARNLEY, I. M., SPINAZZOLA, A., WALKER, J. E. & HOLT, I. J. 2012. Mitochondrial nucleoid interacting proteins support mitochondrial protein synthesis. *Nucleic Acids Research*, 40, 6109-6121.

HE, J., MAO, C. C., REYES, A., SEMBONGI, H., DI RE, M., GRANYCOME, C., CLIPPINGDALE, A. B., FEARNLEY, I. M., HARBOUR, M., ROBINSON, A. J., REICHELT, S., SPELBRINK, J. N., WALKER, J. E. & HOLT, I. J. 2007. The AAA+ protein ATAD3 has displacement loop binding properties and is involved in mitochondrial nucleoid organization. *J Cell Biol*, 176, 141-6.

HEFFERIN, M. L. & TOMKINSON, A. E. 2005. Mechanism of DNA double-strand break repair by non-homologous end joining. *DNA Repair (Amst)*, 4, 639-48.

HEIDARY, G., CALDERWOOD, L., COX, G. F., ROBSON, C. D., TEOT, L. A., MULLON, J. & ANSELM, I. 2014. Optic atrophy and a Leigh-like syndrome due to mutations in the c12orf65 gene: report of a novel mutation and review of the literature. *J Neuroophthalmol*, 34, 39-43.

HEIGHTON, J. N., BRADY, L. I., NEWMAN, M. C. & TARNOPOLSKY, M. A. 2017. Clinical and demographic features of chronic progressive external ophthalmoplegia in a large adult-onset cohort. *Mitochondrion*.

HELM, M., BRULÉ, H., DEGOUL, F., CEPANEC, C., LEROUX, J. P., GIEGÉ, R. & FLORENTZ, C. 1998. The presence of modified nucleotides is required for cloverleaf folding of a human mitochondrial tRNA. *Nucleic acids research*, 26, 1636-1643.

HENRIQUES, B. J., KATRINE JENTOFT OLSEN, R., GOMES, C. M. & BROSS, P. 2021. Electron transfer flavoprotein and its role in mitochondrial energy metabolism in health and disease. *Gene*, 776, 145407.

HENRY, V. J., BANDROWSKI, A. E., PEPIN, A.-S., GONZALEZ, B. J. & DESFEUX, A. 2014. OMICtools: an informative directory for multi-omic data analysis. *Database : the journal of biological databases and curation*, 2014, bau069.

HENSEN, F., POTTER, A., VAN ESVELD, S. L., TARRÉS-SOLÉ, A., CHAKRABORTY, A., SOLÀ, M. & SPELBRINK, J. N. 2019. Mitochondrial RNA granules are critically dependent on mtDNA replication factors Twinkle and mtSSB. *Nucleic Acids Research*, 47, 3680-3698.

HERBST, A., PAK, J. W., MCKENZIE, D., BUA, E., BASSIOUNI, M. & AIKEN, J. M. 2007. Accumulation of mitochondrial DNA deletion mutations in aged muscle fibers: evidence for a causal role in muscle fiber loss. *The journals of gerontology. Series A, Biological sciences and medical sciences*, 62, 235-245.

HERMANSON, G. T. 2013. Chapter 5 - Homobifunctional Crosslinkers. In: HERMANSON, G. T. (ed.) *Bioconjugate Techniques (Third Edition)*. Boston: Academic Press.

HERRMANN, J. M. & RIEMER, J. 2010. The Intermembrane Space of Mitochondria. *Antioxidants & Redox Signaling*, 13, 1341-1358.

HERRMANN, J. M., WOELLHAF, M. W. & BONNEFOY, N. 2013. Control of protein synthesis in yeast mitochondria: The concept of translational activators. *Biochimica et Biophysica Acta (BBA) - Molecular Cell Research*, 1833, 286-294.

HILLEN, H. S., MOROZOV, Y. I., SARFALLAH, A., TEMIAKOV, D. & CRAMER, P. 2017a. Structural Basis of Mitochondrial Transcription Initiation. *Cell*, 171, 1072-1081.e10.

HILLEN, H. S., PARSHIN, A. V., AGARONYAN, K., MOROZOV, Y. I., GRABER, J. J., CHERNEV, A., SCHWINGHAMMER, K., URLAUB, H., ANIKIN, M., CRAMER, P. & TEMIAKOV, D. 2017b. Mechanism of Transcription Anti-termination in Human Mitochondria. *Cell*, 171, 1082-1093.e13.

HIMENO, H., NAMEKI, N., KURITA, D., MUTO, A. & ABO, T. 2015. Ribosome rescue systems in bacteria. *Biochimie*, 114, 102-112.

HINNEBUSCH, A. G. 2014. The Scanning Mechanism of Eukaryotic Translation Initiation. *Annual Review of Biochemistry*, 83, 779-812.

HOLMES, J. B., AKMAN, G., WOOD, S. R., SAKHUJA, K., CERRITELLI, S. M., MOSS, C., BOWMAKER, M. R., JACOBS, H. T., CROUCH, R. J. & HOLT, I. J. 2015. Primer retention owing to the absence of RNase H1 is catastrophic for mitochondrial DNA replication. *Proc Natl Acad Sci U S A*, 112, 9334-9.

HOLT, I. J., LORIMER, H. E. & JACOBS, H. T. 2000. Coupled leading- and lagging-strand synthesis of mammalian mitochondrial DNA. *Cell*, 100, 515-24.

HOLT, I. J. & REYES, A. 2012. Human Mitochondrial DNA Replication. *Cold Spring Harbor Perspectives in Biology*, 4, a012971.

HOLZMANN, J., FRANK, P., LÖFFLER, E., BENNETT, K. L., GERNER, C. & ROSSMANITH, W. 2008. RNase P without RNA: identification and functional reconstitution of the human mitochondrial tRNA processing enzyme. *Cell*, 135, 462-74.

HOPPINS, S. C. & NARGANG, F. E. 2004. The Tim8-Tim13 Complex of *Neurospora crassa* Functions in the Assembly of Proteins into Both Mitochondrial Membranes. *Journal of Biological Chemistry*, 279, 12396-12405.

HORNIG-DO, H.-T., GÜNTHER, G., BUST, M., LEHNARTZ, P., BOSIO, A. & WIESNER, R. J. 2009. Isolation of functional pure mitochondria by superparamagnetic microbeads. *Analytical Biochemistry*, 389, 1-5.

HORST, M., OPPLIGER, W., ROSPERT, S., SCHÖNFELD, H.-J., SCHATZ, G. & AZEM, A. 1997. Sequential action of two hsp70 complexes during protein import into mitochondria. *The EMBO Journal*, 16, 1842-1849.

HUANG, A., TANG, Y., SHI, X., JIA, M., ZHU, J., YAN, X., CHEN, H. & GU, Y. 2020. Proximity labeling proteomics reveals critical regulators for inner nuclear membrane protein degradation in plants. *Nature Communications*, 11, 3284.

HUBBARD, W. B., HARWOOD, C. L., PRAJAPATI, P., SPRINGER, J. E., SAATMAN, K. E. & SULLIVAN, P. G. 2019. Fractionated mitochondrial magnetic separation for isolation of synaptic mitochondria from brain tissue. *Sci Rep*, 9, 9656.

HUNTZINGER, E., KASHIMA, I., FAUSER, M., SAULIÈRE, J. & IZAURRALDE, E. 2008. SMG6 is the catalytic endonuclease that cleaves mRNAs containing nonsense codons in metazoan. *RNA (New York, N.Y.)*, 14, 2609-2617.

HUTCHISON, C. A., NEWBOLD, J. E., POTTER, S. S. & EDGE, M. H. 1974. Maternal inheritance of mammalian mitochondrial DNA. *Nature*, 251, 536-538.

HUTER, P., ARENZ, S., BOCK, L. V., GRAF, M., FRISTER, J. O., HEUER, A., PEIL, L., STAROSTA, A. L., WOHLGEMUTH, I., PESKE, F., NOVÁČEK, J., BERNINGHAUSEN, O., GRUBMÜLLER, H., TENSON, T., BECKMANN, R., RODNINA, M. V., VAIANA, A. C. & WILSON, D. N. 2017a. Structural Basis for Polyproline-Mediated Ribosome Stalling and Rescue by the Translation Elongation Factor EF-P. *Molecular Cell*, 68, 515-527.e6.

HUTER, P., MÜLLER, C., ARENZ, S., BECKERT, B. & WILSON, D. N. 2017b. Structural Basis for Ribosome Rescue in Bacteria. *Trends in Biochemical Sciences*, 42, 669-680.

HUTER, P., MÜLLER, C., BECKERT, B., ARENZ, S., BERNINGHAUSEN, O., BECKMANN, R. & WILSON, D. N. 2017c. Structural basis for ArfA-RF2-mediated translation termination on mRNAs lacking stop codons. *Nature*, 541, 546-549.

HYUNEN, M. A., DUARTE, I., CHRZANOWSKA-LIGHTOWLERS, Z. M. A. & NABUURS, S. B. 2012. Structure based hypothesis of a mitochondrial ribosome rescue mechanism. *Biology Direct*, 7, 14.

HYUNEN, M. A., MÜHLMEISTER, M., GOTTHARDT, K., GUERRERO-CASTILLO, S. & BRANDT, U. 2016. Evolution and structural organization of the mitochondrial contact site (MICOS) complex and the mitochondrial intermembrane space bridging (MIB) complex. *Biochimica et Biophysica Acta (BBA) - Molecular Cell Research*, 1863, 91-101.

HYMES, J. & WOLF, B. 1999. Human Biotinidase Isn't Just for Recycling Biotin. *The Journal of Nutrition*, 129, 485S-489S.

HYVÄRINEN, A. K., KUMANTO, M. K., MARJAVAARA, S. K. & JACOBS, H. T. 2010. Effects on mitochondrial transcription of manipulating mTERF protein levels in cultured human HEK293 cells. *BMC Mol Biol*, 11, 72.

IEVA, R., SCHREMPP, SANDRA G., OPALIŃSKI, Ł., WOLLWEBER, F., HÖß, P., HEIßWOLF, ANNA K., GEBERT, M., ZHANG, Y., GUIARD, B., ROSPERT, S., BECKER, T., CHACINSKA, A., PFANNER, N. & VAN DER LAAN, M. 2014. Mgr2 Functions as Lateral Gatekeeper for Preprotein Sorting in the Mitochondrial Inner Membrane. *Molecular Cell*, 56, 641-652.

IKON, N. & RYAN, R. O. 2017. Cardiolipin and mitochondrial cristae organization. *Biochimica et biophysica acta. Biomembranes*, 1859, 1156-1163.

IMAGAWA, E., FATTAL-VALEVSKI, A., EYAL, O., MIYATAKE, S., SAADA, A., NAKASHIMA, M., TSURUSAKI, Y., SAITSU, H., MIYAKE, N. & MATSUMOTO, N. 2016. Homozygous p.V116* mutation in C12orf65 results in Leigh syndrome. *J Neurol Neurosurg Psychiatry*, 87, 212-6.

ITO-HARASHIMA, S., KUROHA, K., TATEMATSU, T. & INADA, T. 2007. Translation of the poly(A) tail plays crucial roles in nonstop mRNA surveillance via translation repression and protein destabilization by proteasome in yeast. *Genes & Development*, 21, 519-524.

ITO, K., CHADANI, Y., NAKAMORI, K., CHIBA, S., AKIYAMA, Y. & ABO, T. 2011. Nascentome Analysis Uncovers Futile Protein Synthesis in Escherichia coli. *PLOS ONE*, 6, e28413.

ITO, K., UNO, M. & NAKAMURA, Y. 2000. A tripeptide 'anticodon' deciphers stop codons in messenger RNA. *Nature*, 403, 680-684.

ITOH, Y., ANDRÉLL, J., CHOI, A., RICHTER, U., MAITI, P., BEST, R. B., BARRIENTOS, A., BATTERSBY, B. J. & AMUNTS, A. 2021. Mechanism of membrane-tethered mitochondrial protein synthesis. *Science*, 371, 846-849.

IVERSON, T. M. 2013. Catalytic mechanisms of complex II enzymes: a structural perspective. *Biochimica et biophysica acta*, 1827, 648-657.

JANOSI, L., HARA, H., ZHANG, S. & KAJI, A. 1996. Ribosome recycling by ribosome recycling factor (RRF) — An important but overlooked step of protein biosynthesis. *Advances in Biophysics*, 32, 121-201.

JANS, D. C., WURM, C. A., RIEDEL, D., WENZEL, D., STAGGE, F., DECKERS, M., REHLING, P. & JAKOBS, S. 2013. STED super-resolution microscopy reveals an array of MINOS clusters along human mitochondria. *Proc Natl Acad Sci U S A*, 110, 8936-41.

JAUSSI, R. 1995. Homologous Nuclear-Encoded Mitochondrial and Cytosolic Isoproteins. *European Journal of Biochemistry*, 228, 551-561.

JIANG, S., KOOLMEISTER, C., MISIC, J., SIIRA, S., KÜHL, I., SILVA RAMOS, E., MIRANDA, M., JIANG, M., POSSE, V., LYTOVCHENKO, O., ATANASSOV, I., SCHÖBER, F. A., WIBOM, R., HULTENBY, K., MILENKOVIĆ, D., GUSTAFSSON, C. M., FILIPOVSKA, A. & LARSSON, N.-G. 2019. TEFM regulates both transcription elongation and RNA processing in mitochondria. *EMBO reports*, 20, e48101.

JIMÉNEZ-MENÉDEZ, N., FERNÁNDEZ-MILLÁN, P., RUBIO-COSIALS, A., ARNAN, C., MONTOYA, J., JACOBS, H. T., BERNADÓ, P., COLL, M., USÓN, I. & SOLÀ, M. 2010. Human mitochondrial mTERF wraps around DNA through a left-handed superhelical tandem repeat. *Nat Struct Mol Biol*, 17, 891-3.

JIN, H., KELLEY, A. C., LOAKES, D. & RAMAKRISHNAN, V. 2010. Structure of the 70S ribosome bound to release factor 2 and a substrate analog provides insights into catalysis of peptide release. *Proc Natl Acad Sci U S A*, 107, 8593-8.

JINEK, M., CHYLINSKI, K., FONFARA, I., HAUER, M., DOUDNA, J. A. & CHARPENTIER, E. 2012. A Programmable Dual-RNA-Guided DNA Endonuclease in Adaptive Bacterial Immunity. *Science*, 337, 816-821.

JINEK, M., EAST, A., CHENG, A., LIN, S., MA, E. & DOUDNA, J. 2013. RNA-programmed genome editing in human cells. *Elife*, 2, e00471.

JOHN, G. B., SHANG, Y., LI, L., RENKEN, C., MANNELLA, C. A., SELKER, J. M. L., RANGELL, L., BENNETT, M. J. & ZHA, J. 2005. The mitochondrial inner membrane protein mitofillin controls cristae morphology. *Molecular biology of the cell*, 16, 1543-1554.

JOHNSON, K. A., BHUSHAN, S., STÅHL, A., HALLBERG, B. M., FROHN, A., GLASER, E. & ENEQVIST, T. 2006. The closed structure of presequence protease PreP forms a unique 10 000 Å³ chamber for proteolysis. *The EMBO Journal*, 25, 1977-1986.

JONCKHEERE, A. I., SMEITINK, J. A. M. & RODENBURG, R. J. T. 2012. Mitochondrial ATP synthase: architecture, function and pathology. *Journal of inherited metabolic disease*, 35, 211-225.

JONES, A. J., BLAZA, J. N., VARGHESE, F. & HIRST, J. 2017. Respiratory Complex I in Bos taurus and *Paracoccus denitrificans* Pumps Four Protons across the Membrane for Every NADH Oxidized. *J Biol Chem*, 292, 4987-4995.

JONES, C. N., MILLER, C., TENENBAUM, A., SPREMULLI, L. L. & SAADA, A. 2009. Antibiotic effects on mitochondrial translation and in patients with mitochondrial translational defects. *Mitochondrion*, 9, 429-437.

JORES, T., KLINGER, A., GROß, L. E., KAWANO, S., FLINNER, N., DUCHARDT-FERNER, E., WÖHNERT, J., KALBACHER, H., ENDO, T., SCHLEIFF, E. & RAPAPORT, D. 2016. Characterization of the targeting signal in mitochondrial β -barrel proteins. *Nature Communications*, 7, 12036.

JOURDAIN, A. A., BOEHM, E., MAUNDRELL, K. & MARTINOU, J.-C. 2016. Mitochondrial RNA granules: Compartmentalizing mitochondrial gene expression. *The Journal of cell biology*, 212, 611-614.

JOURDAIN, ALEXIS A., KOPPEN, M., RODLEY, CHRISTOPHER D., MAUNDRELL, K., GUEGUEN, N., REYNIER, P., GUARAS, ADELA M., ENRIQUEZ, JOSÉ A., ANDERSON, P., SIMARRO, M. & MARTINOU, J.-C. 2015. A Mitochondria-Specific Isoform of FASTK Is Present In Mitochondrial RNA Granules and Regulates Gene Expression and Function. *Cell Reports*, 10, 1110-1121.

JOURDAIN, A. A., POPOW, J., DE LA FUENTE, M. A., MARTINOU, J.-C., ANDERSON, P. & SIMARRO, M. 2017. The FASTK family of proteins: emerging regulators of mitochondrial RNA biology. *Nucleic acids research*, 45, 10941-10947.

JU, Y. S., ALEXANDROV, L. B., GERSTUNG, M., MARTINCORENA, I., NIK-ZAINAL, S., RAMAKRISHNA, M., DAVIES, H. R., PAPAEMMANUIL, E., GUNDEM, G., SHLIEN, A., BOLLI, N., BEHJATI, S., TARPEY, P. S., NANGALIA, J., MASSIE, C. E., BUTLER, A. P., TEAGUE, J. W., VASSILIOU, G. S., GREEN, A. R., DU, M.-Q., UNNIKRISHNAN, A., PIMANDA, J. E., TEH, B. T., MUNSHI, N., GREAVES, M., VYAS, P., EL-NAGGAR, A. K., SANTARIUS, T., COLLINS, V. P., GRUNDY, R., TAYLOR, J. A., HAYES, D. N., MALKIN, D., GROUP, I. B. C., GROUP, I. C. M. D., GROUP, I. P. C., FOSTER, C. S., WARREN, A. Y., WHITAKER, H. C., BREWER, D., EELES, R., COOPER, C., NEAL, D., VISAKORPI, T., ISAACS, W. B., BOVA, G. S., FLANAGAN, A. M., FUTREAL, P. A., LYNCH, A. G., CHINNERY, P. F., MCDERMOTT, U., STRATTON, M. R. & CAMPBELL, P. J. 2014. Origins and functional consequences of somatic mitochondrial DNA mutations in human cancer. *eLife*, 3, e02935.

KADENBACH, B. & HÜTTEMANN, M. 2015. The subunit composition and function of mammalian cytochrome c oxidase. *Mitochondrion*, 24, 64-76.

KALOUSEK, F., DARIGO, M. D. & ROSENBERG, L. E. 1980. Isolation and characterization of propionyl-CoA carboxylase from normal human liver. Evidence for a protomeric tetramer of nonidentical subunits. *J Biol Chem*, 255, 60-5.

KANG, P.-J., OSTERMANN, J., SHILLING, J., NEUPERT, W., CRAIG, E. A. & PFANNER, N. 1990. Requirement for hsp70 in the mitochondrial matrix for translocation and folding of precursor proteins. *Nature*, 348, 137-143.

KAPP, E. A., SCHÜTZ, F., REID, G. E., EDDES, J. S., MORITZ, R. L., O'HAIR, R. A. J., SPEED, T. P. & SIMPSON, R. J. 2003. Mining a Tandem Mass Spectrometry Database To Determine the Trends and Global Factors Influencing Peptide Fragmentation. *Analytical Chemistry*, 75, 6251-6264.

KARCHER, A., SCHELE, A. & HOPFNER, K. P. 2008. X-ray structure of the complete ABC enzyme ABCE1 from *Pyrococcus abyssi*. *J Biol Chem*, 283, 7962-71.

KARLBERG, O., CANBÄCK, B., KURLAND, C. G. & ANDERSSON, S. G. 2000. The dual origin of the yeast mitochondrial proteome. *Yeast (Chichester, England)*, 17, 170-187.

KARNKOWSKA, A., VACEK, V., ZUBÁČOVÁ, Z., TREITLI, S. C., PETRŽELKOVÁ, R., EME, L., NOVÁK, L., ŽÁRSKÝ, V., BARLOW, L. D., HERMAN, E. K., SOUKAL, P., HROUDOVÁ, M., DOLEŽAL, P., STAIRS, C. W., ROGER, A. J., ELIÁŠ, M., DACKS, J. B., VLČEK, Č. & HAMPL, V. 2016. A Eukaryote without a Mitochondrial Organelle. *Current Biology*, 26, 1274-1284.

KASIVISWANATHAN, R., COLLINS, T. R. L. & COPELAND, W. C. 2012. The interface of transcription and DNA replication in the mitochondria. *Biochimica et biophysica acta*, 1819, 970-978.

KEILER, K. C. & FEAGA, H. A. 2014. Resolving nonstop translation complexes is a matter of life or death. *Journal of bacteriology*, 196, 2123-2130.

KEMPER, C., HABIB, S. J., ENGL, G., HECKMEYER, P., DIMMER, K. S. & RAPAPORT, D. 2008. Integration of tail-anchored proteins into the mitochondrial outer membrane does not require any known import components. *Journal of Cell Science*, 121, 1990-1998.

KHAWAJA, A., ITOH, Y., REMES, C., SPÅHR, H., YUKHNOVETS, O., HÖFIG, H., AMUNTS, A. & RORBACH, J. 2020. Distinct pre-initiation steps in human mitochondrial translation. *Nature Communications*, 11, 2932.

KIERZEK, E., MALGOWSKA, M., LISOWIEC, J., TURNER, D. H., GDANIEC, Z. & KIERZEK, R. 2013. The contribution of pseudouridine to stabilities and structure of RNAs. *Nucleic Acids Research*, 42, 3492-3501.

KILBRIDE, S. M. & PREHN, J. H. M. 2013. Central roles of apoptotic proteins in mitochondrial function. *Oncogene*, 32, 2703-2711.

KIM, D. I., BIRENDRA, K. C., ZHU, W., MOTAMEDCHABOKI, K., DOYE, V. & ROUX, K. J. 2014. Probing nuclear pore complex architecture with proximity-dependent biotinylation. *Proceedings of the National Academy of Sciences of the United States of America*, 111, E2453-E2461.

KIM, D. I., JENSEN, S. C., NOBLE, K. A., KC, B., ROUX, K. H., MOTAMEDCHABOKI, K. & ROUX, K. J. 2016a. An improved smaller biotin ligase for BioID proximity labeling. *Molecular biology of the cell*, 27, 1188-1196.

KIM, D. I., JENSEN, S. C. & ROUX, K. J. 2016b. Identifying Protein-Protein Associations at the Nuclear Envelope with BioID. *Methods in molecular biology (Clifton, N.J.)*, 1411, 133-146.

KIM, D. I. & ROUX, K. J. 2016. Filling the Void: Proximity-Based Labeling of Proteins in Living Cells. *Trends in cell biology*, 26, 804-817.

KIM, K. W., YAMANE, H., ZONDLO, J., BUSBY, J. & WANG, M. 2007. Expression, purification, and characterization of human acetyl-CoA carboxylase 2. *Protein Expr Purif*, 53, 16-23.

KING, M. P. & ATTARDI, G. 1989. Human Cells Lacking mtDNA: Repopulation with Exogenous Mitochondria by Complementation. *Science*, 246, 500.

KIRKEBY, S., MOE, D., BØG-HANSEN, T. C. & VAN NOORDEN, C. J. 1993. Biotin carboxylases in mitochondria and the cytosol from skeletal and cardiac muscle as detected by avidin binding. *Histochemistry*, 100, 415-21.

KIRKMAN, H. N., ROLFO, M., FERRARIS, A. M. & GAETANI, G. F. 1999. Mechanisms of Protection of Catalase by NADPH: KINETICS AND STOICHIOMETRY*. *Journal of Biological Chemistry*, 274, 13908-13914.

KNOWLES, J. R. 1989. The mechanism of biotin-dependent enzymes. *Annu Rev Biochem*, 58, 195-221.

KOBZA, K., CAMPOREALE, G., RUECKERT, B., KUEH, A., GRIFFIN, J. B., SARATH, G. & ZEMPLENI, J. 2005. K4, K9 and K18 in human histone H3 are targets for biotinylation by biotinidase. *Febs j*, 272, 4249-59.

KOC, E., CIMEN, H., KUMCUOGLU, B., ABU, N., AKPINAR, G., HAQUE, M., SPREMULLI, L. & KOC, H. 2013. Identification and characterization of CHCHD1, AURKAIP1, and CRIF1 as new members of the mammalian mitochondrial ribosome. *Frontiers in Physiology*, 4.

KOC, E. C. & KOC, H. 2012. Regulation of mammalian mitochondrial translation by post-translational modifications. *Biochimica et Biophysica Acta (BBA) - Gene Regulatory Mechanisms*, 1819, 1055-1066.

KOC, E. C. & SPREMULLI, L. L. 2002. Identification of mammalian mitochondrial translational initiation factor 3 and examination of its role in initiation complex formation with natural mRNAs. *J Biol Chem*, 277, 35541-9.

KOCH, J. R. & SCHMID, F. X. 2014. Mia40 Combines Thiol Oxidase and Disulfide Isomerase Activity to Efficiently Catalyze Oxidative Folding in Mitochondria. *Journal of Molecular Biology*, 426, 4087-4098.

KOGURE, H., HANNA, Y., NAGATA, M., KANAI, N., GÜNTERT, P., KUBOTA, K. & NAMEKI, N. 2013. Identification of residues required for stalled-ribosome rescue in the codon-independent release factor YaeJ. *Nucleic Acids Research*, 42, 3152-3163.

KOGURE, H., HIKAWA, Y., HAGIHARA, M., TOCHIO, N., KOSHIBA, S., INOUE, Y., GÜNTERT, P., KIGAWA, T., YOKOYAMA, S. & NAMEKI, N. 2012. Solution structure and siRNA-mediated knockdown analysis of the mitochondrial disease-related protein C12orf65. *Proteins*, 80, 2629-42.

KOMINE, Y., KITABATAKE, M., YOKOGAWA, T., NISHIKAWA, K. & INOKUCHI, H. 1994. A tRNA-like structure is present in 10Sa RNA, a small stable RNA from *Escherichia coli*. *Proceedings of the National Academy of Sciences*, 91, 9223-9227.

KOMULAINEN, T., HAUTAKANGAS, M.-R., HINTTALA, R., PAKANEN, S., VÄHÄSARJA, V., LEHENKARI, P., OLSEN, P., VIEIRA, P., SAARENPÄÄ-HEIKKILÄ, O., PALMIO, J., TUOMINEN, H., KINNUNEN, P., MAJAMAA, K., RANTALA, H. & UUSIMAA, J. 2015. Mitochondrial DNA Depletion and Deletions in Paediatric Patients with Neuromuscular Diseases: Novel Phenotypes. *JIMD Reports*, 23, 91-100.

KONDADI, A. K., ANAND, R. & REICHERT, A. S. 2019. Functional Interplay between Cristae Biogenesis, Mitochondrial Dynamics and Mitochondrial DNA Integrity. *International journal of molecular sciences*, 20, 4311.

KONECKI, D. S., AUNE, K. C., TATE, W. & CASKEY, C. T. 1977. Characterization of reticulocyte release factor. *Journal of Biological Chemistry*, 252, 4514-4520.

KONOVALOVA, S., HILANDER, T., LOAYZA-PUCH, F., ROOIJERS, K., AGAMI, R. & TYYNISMAA, H. 2015. Exposure to arginine analog canavanine induces aberrant mitochondrial translation products, mitoribosome stalling, and instability of the mitochondrial proteome. *The International Journal of Biochemistry & Cell Biology*, 65, 268-274.

KORHONEN, J. A., GASPARI, M. & FALKENBERG, M. 2003. TWINKLE Has 5'-3' DNA Helicase Activity and Is Specifically Stimulated by Mitochondrial Single-stranded DNA-binding Protein *. *Journal of Biological Chemistry*, 278, 48627-48632.

KORHONEN, J. A., PHAM, X. H., PELLEGRINI, M. & FALKENBERG, M. 2004. Reconstitution of a minimal mtDNA replisome in vitro. *The EMBO Journal*, 23, 2423-2429.

KORIPELLA, R. K., SHARMA, M. R., BHARGAVA, K., DATTA, P. P., KAUSHAL, P. S., KESHAVAN, P., SPREMULLI, L. L., BANAVALI, N. K. & AGRAWAL, R. K. 2020. Structures of the human mitochondrial ribosome bound to EF-G1 reveal distinct features of mitochondrial translation elongation. *Nature Communications*, 11, 3830.

KORIPELLA, R. K., SHARMA, M. R., HAQUE, M. E., RISTEFF, P., SPREMULLI, L. L. & AGRAWAL, R. K. 2019. Structure of Human Mitochondrial Translation Initiation Factor 3 Bound to the Small Ribosomal Subunit. *iScience*, 12, 76-86.

KOROSTELEV, A., ASAHARA, H., LANCASTER, L., LAURBERG, M., HIRSCHI, A., ZHU, J., TRAKHANOV, S., SCOTT, W. G. & NOLLER, H. F. 2008. Crystal structure of a translation termination complex formed with release factor RF2. *Proceedings of the National Academy of Sciences*, 105, 19684-19689.

KOROSTELEV, A., ZHU, J., ASAHARA, H. & NOLLER, H. F. 2010. Recognition of the amber UAG stop codon by release factor RF1. *Embo j*, 29, 2577-85.

KOTRYS, A. V., CYSEWSKI, D., CZARNOMSKA, S. D., PIETRAS, Z., BOROWSKI, L. S., DZIEMBOWSKI, A. & SZCZESNY, R. J. 2019. Quantitative proteomics revealed C6orf203/MTRES1 as a factor preventing stress-induced transcription deficiency in human mitochondria. *Nucleic acids research*, 47, 7502-7517.

KOZAK, M. 1986. Point mutations define a sequence flanking the AUG initiator codon that modulates translation by eukaryotic ribosomes. *Cell*, 44, 283-92.

KOZJAK-PAVLOVIC, V. 2017. The MICOS complex of human mitochondria. *Cell Tissue Res*, 367, 83-93.

KRUMPE, K., FRUMKIN, I., HERZIG, Y., RIMON, N., ÖZBALCI, C., BRÜGGER, B., RAPAPORT, D. & SCHULDINER, M. 2012. Ergosterol content specifies targeting of tail-anchored proteins to mitochondrial outer membranes. *Molecular Biology of the Cell*, 23, 3927-3935.

KRUSE, B., NARASIMHAN, N. & ATTARDI, G. 1989. Termination of transcription in human mitochondria: identification and purification of a DNA binding protein factor that promotes termination. *Cell*, 58, 391-7.

KÜHLBRANDT, W. 2015. Structure and function of mitochondrial membrane protein complexes. *BMC Biol*, 13, 89.

KUKAT, C., DAVIES, K. M., WURM, C. A., SPÅHR, H., BONEKAMP, N. A., KÜHL, I., JOOS, F., POLOSA, P. L., PARK, C. B., POSSE, V., FALKENBERG, M., JAKOBS, S., KÜHLBRANDT, W. & LARSSON, N. G. 2015. Cross-strand binding of TFAM to a single mtDNA molecule forms the mitochondrial nucleoid. *Proc Natl Acad Sci U S A*, 112, 11288-93.

KUKAT, C., WURM, C. A., SPÅHR, H., FALKENBERG, M., LARSSON, N. G. & JAKOBS, S. 2011. Super-resolution microscopy reveals that mammalian mitochondrial nucleoids have a uniform size and frequently contain a single copy of mtDNA. *Proc Natl Acad Sci U S A*, 108, 13534-9.

KUMAR, K. R., BLAIR, N. F. & SUE, C. M. 2015. An Update on the Hereditary Spastic Paraplegias: New Genes and New Disease Models. *Mov Disord Clin Pract*, 2, 213-223.

KUMMER, E. & BAN, N. 2020. Structural insights into mammalian mitochondrial translation elongation catalyzed by mtEFG1. *The EMBO Journal*, 39, e104820.

KUMMER, E. & BAN, N. 2021. Mechanisms and regulation of protein synthesis in mitochondria. *Nat Rev Mol Cell Biol*, 22, 307-325.

KUMMER, E., LEIBUNDGUT, M., RACKHAM, O., LEE, R. G., BOEHRINGER, D., FILIPOVSKA, A. & BAN, N. 2018. Unique features of mammalian mitochondrial translation initiation revealed by cryo-EM. *Nature*, 560, 263-267.

KUMMER, E., SCHUBERT, K. N., SCHOENHUT, T., SCAIOLA, A. & BAN, N. 2021. Structural basis of translation termination, rescue, and recycling in mammalian mitochondria. *Molecular Cell*.

KUROISHI, T., CERNY, R. L. & ZEMPLENI, J. 2010. Mass spectrometric analysis of biotinylated peptides and histones. *The FASEB Journal*, 24, 107.2-107.2.

KUTIK, S., STOJANOVSKI, D., BECKER, L., BECKER, T., MEINECKE, M., KRÜGER, V., PRINZ, C., MEISINGER, C., GUIARD, B., WAGNER, R., PFANNER, N. & WIEDEMANN, N. 2008. Dissecting membrane insertion of mitochondrial beta-barrel proteins. *Cell*, 132, 1011-24.

KWON, K. & BECKETT, D. 2000. Function of a conserved sequence motif in biotin holoenzyme synthetases. *Protein Sci*, 9, 1530-9.

KWON, K., STREAKER, E. D., RUPARELIA, S. & BECKETT, D. 2000. Multiple disordered loops function in corepressor-induced dimerization of the biotin repressor. *J Mol Biol*, 304, 821-33.

LACKEY, S. W. K., TAYLOR, R. D., GO, N. E., WONG, A., SHERMAN, E. L. & NARGANG, F. E. 2014. Evidence Supporting the 19 β-Strand Model for Tom40 from Cysteine Scanning and Protease Site Accessibility Studies. *Journal of Biological Chemistry*, 289, 21640-21650.

LAKSHMIPATHY, U. & CAMPBELL, C. 1999. The human DNA ligase III gene encodes nuclear and mitochondrial proteins. *Mol Cell Biol*, 19, 3869-76.

LANE, M. D., ROMINGER, K. L., YOUNG, D. L. & LYNEN, F. 1964. THE ENZYMATIC SYNTHESIS OF HOLOTRANSCARBOXYLASE FROM APOTRANSCARBOXYLASE AND (+)-BIOTIN. II. INVESTIGATION OF THE REACTION MECHANISM. *J Biol Chem*, 239, 2865-71.

LANG, B. F., BURGER, G., O'KELLY, C. J., CEDERGREN, R., GOLDING, G. B., LEMIEUX, C., SANKOFF, D., TURMEL, M. & GRAY, M. W. 1997. An ancestral mitochondrial DNA resembling a eubacterial genome in miniature. *Nature*, 387, 493-497.

LARSSON, N. G., OLDFORS, A., GARMAN, J. D., BARSH, G. S. & CLAYTON, D. A. 1997. Down-regulation of mitochondrial transcription factor A during spermatogenesis in humans. *Hum Mol Genet*, 6, 185-91.

LAURBERG, M., ASAHIARA, H., KOROSTELEV, A., ZHU, J., TRAKHANOV, S. & NOLLER, H. F. 2008. Structural basis for translation termination on the 70S ribosome. *Nature*, 454, 852-857.

LAVDOVSKAIA, E., DENKS, K., NADLER, F., STEUBE, E., LINDEN, A., URLAUB, H., RODNINA, M. V. & RICHTER-DENNERLEIN, R. 2020. Dual function of GTPBP6 in biogenesis and recycling of human mitochondrial ribosomes. *Nucleic Acids Research*, 48, 12929-12942.

LAVDOVSKAIA, E., KOLANDER, E., STEUBE, E., MAI, M. M.-Q., URLAUB, H. & RICHTER-DENNERLEIN, R. 2018. The human Obg protein GTPBP10 is involved in mitoribosomal biogenesis. *Nucleic acids research*, 46, 8471-8482.

LE HIR, H., GATFIELD, D., IZAURRALDE, E. & MOORE, M. J. 2001. The exon-exon junction complex provides a binding platform for factors involved in mRNA export and nonsense-mediated mRNA decay. *The EMBO journal*, 20, 4987-4997.

LEE, H.-F., LEE, H.-J., CHI, C.-S., TSAI, C.-R., CHANG, T.-K. & WANG, C.-J. 2007. The neurological evolution of Pearson syndrome: Case report and literature review. *European Journal of Paediatric Neurology*, 11, 208-214.

LEE, H. H., KIM, Y.-S., KIM, K. H., HEO, I., KIM, S. K., KIM, O., KIM, H. K., YOON, J. Y., KIM, H. S., KIM, D. J., LEE, S. J., YOON, H. J., KIM, S. J., LEE, B. G., SONG, H. K., KIM, V. N., PARK, C.-M. & SUH, S. W. 2018. Structural and Functional Insights into Dom34, a Key Component of No-Go mRNA Decay. *Molecular Cell*, 27, 938-950.

LEE, J. W., BLANCO, L., ZHOU, T., GARCIA-DIAZ, M., BEBENEK, K., KUNKEL, T. A., WANG, Z. & POVIRK, L. F. 2004. Implication of DNA polymerase lambda in alignment-based gap filling for nonhomologous DNA end joining in human nuclear extracts. *J Biol Chem*, 279, 805-11.

LEE, M., MATSUNAGA, N., AKABANE, S., YASUDA, I., UEDA, T. & TAKEUCHI-TOMITA, N. 2021. Reconstitution of mammalian mitochondrial translation system capable of correct initiation and long polypeptide synthesis from leaderless mRNA. *Nucleic acids research*, 49, 371-382.

LEE, R. G., GAO, J., SIIRA, S. J., SHEARWOOD, A.-M., ERMER, J. A., HOFFEREK, V., MATHEWS, J. C., ZHENG, M., REID, G. E., RACKHAM, O. & FILIPOVSKA, A. 2020. Cardiolipin is required for membrane docking of mitochondrial ribosomes and protein synthesis. *Journal of Cell Science*, 133.

LEE, S. R. & HAN, J. 2017. Mitochondrial Nucleoid: Shield and Switch of the Mitochondrial Genome. *Oxidative medicine and cellular longevity*, 2017, 8060949-8060949.

LEJEUNE, F., LI, X. & MAQUAT, L. E. 2003. Nonsense-Mediated mRNA Decay in Mammalian Cells Involves Decapping, Deadenyling, and Exonucleolytic Activities. *Molecular Cell*, 12, 675-687.

LESZCZYNIECKA, M., BHATIA, U., CUETO, M., NIRMALA, N. R., TOWBIN, H., VATTAY, A., WANG, B., ZABLUDOFF, S. & PHILLIPS, P. E. 2006. MAP1D, a novel methionine aminopeptidase family member is overexpressed in colon cancer. *Oncogene*, 25, 3471-3478.

LI, L. Y., LUO, X. & WANG, X. 2001. Endonuclease G is an apoptotic DNase when released from mitochondria. *Nature*, 412, 95-9.

LI, M., SHEN, Y., CHEN, Y., GAO, H., ZHOU, J., WANG, Q., FAN, C., ZHANG, W., LI, J., CONG, H., GU, J., GAN, Y. & TU, H. 2020a. Characterization of hepatitis B virus infection and viral DNA integration in non-Hodgkin lymphoma. *Int J Cancer*, 147, 2199-2209.

LI, X., XIONG, X., ZHANG, M., WANG, K., CHEN, Y., ZHOU, J., MAO, Y., LV, J., YI, D., CHEN, X.-W., WANG, C., QIAN, S.-B. & YI, C. 2017. Base-Resolution Mapping Reveals Distinct m(1)A Methylome in Nuclear- and Mitochondrial-Encoded Transcripts. *Molecular cell*, 68, 993-1005.e9.

LI, Y., IVICA, N. A., DONG, T., PAPAGEORGIOU, D. P., HE, Y., BROWN, D. R., KLEYMAN, M., HU, G., CHEN, W. W., SULLIVAN, L. B., DEL ROSARIO, A., HAMMOND, P. T., VANDER HEIDEN, M. G. & CHEN, J. 2020b. MFSD7C switches mitochondrial ATP synthesis to thermogenesis in response to heme. *Nat Commun*, 11, 4837.

LIAO, P.-C., BERGAMINI, C., FATO, R., PON, L. A. & PALLOTTI, F. 2020. Isolation of mitochondria from cells and tissues. *Methods in cell biology*, 155, 3-31.

LIGHTOWLERS, R. N. & CHRZANOWSKA-LIGHTOWLERS, Z. M. A. 2010. Terminating human mitochondrial protein synthesis: A shift in our thinking. *RNA Biology*, 7, 282-286.

LILL, R. 2009. Function and biogenesis of iron-sulphur proteins. *Nature*, 460, 831-8.

LILL, R. & MÜHLENHOFF, U. 2008. Maturation of Iron-Sulfur Proteins in Eukaryotes: Mechanisms, Connected Processes, and Diseases. *Annual Review of Biochemistry*, 77, 669-700.

LIN, Y.-C., BOONE, M., MEURIS, L., LEMMENS, I., VAN ROY, N., SOETE, A., REUMERS, J., MOISSE, M., PLAISANCE, S., DRMANAC, R., CHEN, J., SPELEMAN, F., LAMBRECHTS, D., VAN DE PEER, Y., TAVERNIER, J. & CALLEWAERT, N. 2014. Genome dynamics of the human embryonic kidney 293 lineage in response to cell biology manipulations. *Nature Communications*, 5, 4767.

LINK, T. A. & IWATA, S. 1996. Functional implications of the structure of the 'Rieske' iron-sulfur protein of bovine heart mitochondrial cytochrome bc1 complex. *Biochim Biophys Acta*, 1275, 54-60.

LINO, C. A., HARPER, J. C., CARNEY, J. P. & TIMLIN, J. A. 2018. Delivering CRISPR: a review of the challenges and approaches. *Drug delivery*, 25, 1234-1257.

LIONAKI, E., DE MARCOS LOUSA, C., BAUD, C., VOUGIOUKALAKI, M., PANAYOTOU, G. & TOKATLIDIS, K. 2008. The Essential Function of Tim12 in Vivo Is Ensured by the Assembly Interactions of Its C-terminal Domain. *Journal of Biological Chemistry*, 283, 15747-15753.

LITCHFIELD, K., READING, J. L., LIM, E. L., XU, H., LIU, P., AL-BAKIR, M., WONG, Y. N. S., ROWAN, A., FUNT, S. A., MERGHOUB, T., PERKINS, D., LAUSS, M., SVANE, I. M., JÖNSSON, G., HERRERO, J., LARKIN, J., QUEZADA, S. A., HELLMANN, M. D., TURAJLIC, S. & SWANTON, C. 2020. Escape from nonsense-mediated decay associates with anti-tumor immunogenicity. *Nature Communications*, 11, 3800.

LITONIN, D., SOLOGUB, M., SHI, Y., SAVKINA, M., ANIKIN, M., FALKENBERG, M., GUSTAFSSON, C. M. & TEMIAKOV, D. 2010. Human mitochondrial transcription revisited: only TFAM and TFB2M are

required for transcription of the mitochondrial genes in vitro. *The Journal of biological chemistry*, 285, 18129-18133.

LIU, C.-H. & WU, P.-S. 2006. Characterization of matrix metalloproteinase expressed by human embryonic kidney cells. *Biotechnology Letters*, 28, 1725-1730.

LIU, M., REHMAN, S., TANG, X., GU, K., FAN, Q., CHEN, D. & MA, W. 2019a. Methodologies for Improving HDR Efficiency. *Frontiers in Genetics*, 9.

LIU, X., SHEN, S., WU, P., LI, F., LIU, X., WANG, C., GONG, Q., WU, J., YAO, X., ZHANG, H. & SHI, Y. 2019b. Structural insights into dimethylation of 12S rRNA by TFB1M: indispensable role in translation of mitochondrial genes and mitochondrial function. *Nucleic Acids Res*, 47, 7648-7665.

LIU, Y., XU, R., GU, H., ZHANG, E., QU, J., CAO, W., HUANG, X., YAN, H., HE, J. & CAI, Z. 2021. Metabolic reprogramming in macrophage responses. *Biomarker Research*, 9, 1.

LODISH H, B. A., ZIPURSKY SL, ET AL. 2000. *Molecular Cell Biology. 4th edition.*, New York:.

LOH, B., JONAS, S. & IZAURRALDE, E. 2013. The SMG5-SMG7 heterodimer directly recruits the CCR4-NOT deadenylase complex to mRNAs containing nonsense codons via interaction with POP2. *Genes Dev*, 27, 2125-38.

LONGMAN, D., HUG, N., KEITH, M., ANASTASAKI, C., PATTON, E. E., GRIMES, G. & CÁCERES, J. F. 2013. DHX34 and NBAS form part of an autoregulatory NMD circuit that regulates endogenous RNA targets in human cells, zebrafish and *Caenorhabditis elegans*. *Nucleic Acids Res*, 41, 8319-31.

LÓPEZ-GALLARDO, E., LÓPEZ-PÉREZ, M. J., MONTOYA, J. & RUIZ-PESINI, E. 2009. CPEO and KSS differ in the percentage and location of the mtDNA deletion. *Mitochondrion*, 9, 314-317.

LOPEZ SANCHEZ, M. I. G., KRÜGER, A., SHIRIAEV, D. I., LIU, Y. & RORBACH, J. 2021. Human Mitoribosome Biogenesis and Its Emerging Links to Disease. *International journal of molecular sciences*, 22, 3827.

LV, Z. Y., XU, X. M., CAO, X. F., WANG, Q., SUN, D. F., TIAN, W. J., YANG, Y., WANG, Y. Z. & HAO, Y. L. 2017. Mitochondrial mutations in 12S rRNA and 16S rRNA presenting as chronic progressive external ophthalmoplegia (CPEO) plus: A case report. *Medicine (Baltimore)*, 96, e8869.

MA, Y., LU, H., TIPPIN, B., GOODMAN, M. F., SHIMAZAKI, N., KOIWAI, O., HSIEH, C. L., SCHWARZ, K. & LIEBER, M. R. 2004. A biochemically defined system for mammalian nonhomologous DNA end joining. *Mol Cell*, 16, 701-13.

MA, Z., ZHU, P., SHI, H., GUO, L., ZHANG, Q., CHEN, Y., CHEN, S., ZHANG, Z., PENG, J. & CHEN, J. 2019. PTC-bearing mRNA elicits a genetic compensation response via Upf3a and COMPASS components. *Nature*, 568, 259-263.

MA ZHIPENG, C. J. 2019. Nonsense mutations and genetic compensation response. *Hereditas(Beijing)*, 41, 359-364.

MABY, P., GALON, J. & LATOUCHE, J.-B. 2016. Frameshift mutations, neoantigens and tumor-specific CD8+ T cells in microsatellite unstable colorectal cancers. *OncolImmunology*, 5, e1115943.

MAHAJAN, K. N., NICK MCELHINNY, S. A., MITCHELL, B. S. & RAMSDEN, D. A. 2002. Association of DNA polymerase mu (pol mu) with Ku and ligase IV: role for pol mu in end-joining double-strand break repair. *Mol Cell Biol*, 22, 5194-202.

MAITI, P., ANTONICKA, H., GINGRAS, A. C., SHOUBRIDGE, E. A. & BARRIENTOS, A. 2020. Human GTPBP5 (MTG2) fuels mitoribosome large subunit maturation by facilitating 16S rRNA methylation. *Nucleic Acids Res*, 48, 7924-7943.

MAJAMAA, K., MOILANEN, J. S., UIMONEN, S., REMES, A. M., SALMELA, P. I., KÄRPPÄ, M., MAJAMAA-VOLTTI, K. A., RUSANEN, H., SORRI, M., PEUHKURINEN, K. J. & HASSINEN, I. E. 1998. Epidemiology of A3243G, the mutation for mitochondrial encephalomyopathy, lactic acidosis, and strokelike episodes: prevalence of the mutation in an adult population. *Am J Hum Genet*, 63, 447-54.

MALHOTRA, K., SATHAPPA, M., LANDIN, J. S., JOHNSON, A. E. & ALDER, N. N. 2013. Structural changes in the mitochondrial Tim23 channel are coupled to the proton-motive force. *Nature Structural & Molecular Biology*, 20, 965-972.

MANAM, S. & VAN TUYLE, G. C. 1987. Separation and characterization of 5'- and 3'-tRNA processing nucleases from rat liver mitochondria. *Journal of Biological Chemistry*, 262, 10272-10279.

MAQUAT, L. E. 1995. When cells stop making sense: effects of nonsense codons on RNA metabolism in vertebrate cells. *Rna*, 1, 453-65.

MARGULIS, L. 1970. Origin of eukaryotic cells. *Yale University Press*.

MARTELL, J. D., DEERINCK, T. J., SANCAK, Y., POULOS, T. L., MOOTHA, V. K., SOSINSKY, G. E., ELLISMAN, M. H. & TING, A. Y. 2012. Engineered ascorbate peroxidase as a genetically encoded reporter for electron microscopy. *Nature biotechnology*, 30, 1143-1148.

MARTENS, P. A. & CLAYTON, D. A. 1979. Mechanism of mitochondrial DNA replication in mouse L-cells: localization and sequence of the light-strand origin of replication. *J Mol Biol*, 135, 327-51.

MARTIN, J., MAHLKE, K. & PFANNER, N. 1991. Role of an energized inner membrane in mitochondrial protein import. Delta psi drives the movement of presequences. *Journal of Biological Chemistry*, 266, 18051-18057.

MATTSON, G., CONKLIN, E., DESAI, S., NIELANDER, G., SAVAGE, M. D. & MORGENSEN, S. 1993. A practical approach to crosslinking. *Mol Biol Rep*, 17, 167-83.

MAY, D. G., SCOTT, K. L., CAMPOS, A. R. & ROUX, K. J. 2020. Comparative Application of BiOID and Turboid for Protein-Proximity Biotinylation. *Cells*, 9.

MAZINA, M. Y., ZIGANSHIN, R. H., MAGNITOV, M. D., GOLOVNIN, A. K. & VOROBYEVA, N. E. 2020. Proximity-dependent biotin labelling reveals CP190 as an EcR/Usp molecular partner. *Scientific Reports*, 10, 4793.

MEINECKE, M., WAGNER, R., KOVERMANN, P., GUIARD, B., MICK, D. U., HUTU, D. P., VOOS, W., TRUSCOTT, K. N., CHACINSKA, A., PFANNER, N. & REHLING, P. 2006. Tim50 Maintains the Permeability Barrier of the Mitochondrial Inner Membrane. *Science*, 312, 1523-1526.

MELIN, J., SCHULZ, C., WROBEL, L., BERNHARD, O., CHACINSKA, A., JAHN, O., SCHMIDT, B. & REHLING, P. 2014. Presequence Recognition by the Tom40 Channel Contributes to Precursor Translocation into the Mitochondrial Matrix. *Molecular and Cellular Biology*, 34, 3473-3485.

MENEZES, M. J., GUO, Y., ZHANG, J., RILEY, L. G., COOPER, S. T., THORBURN, D. R., LI, J., DONG, D., LI, Z., GLESSNER, J., DAVIS, R. L., SUE, C. M., ALEXANDER, S. I., ARBUCKLE, S., KIRWAN, P., KEATING, B. J., XU, X., HAKONARSON, H. & CHRISTODOULOU, J. 2015. Mutation in mitochondrial ribosomal protein S7 (MRPS7) causes congenital sensorineural deafness, progressive hepatic and renal failure and lactic acidemia. *Hum Mol Genet*, 24, 2297-307.

MENGER, K. E., RODRÍGUEZ-LUIS, A., CHAPMAN, J. & NICHOLLS, T. J. 2021. Controlling the topology of mammalian mitochondrial DNA. *Open biology*, 11, 210168-210168.

MERLE, N., FÉRAUD, O., GILQUIN, B., HUBSTENBERGER, A., KIEFFER-JACQUINOT, S., ASSARD, N., BENNACEUR-GRISCELLI, A., HONNORAT, J. & BAUDIER, J. 2012. ATAD3B is a human embryonic stem cell specific mitochondrial protein, re-expressed in cancer cells, that functions as dominant negative for the ubiquitous ATAD3A. *Mitochondrion*, 12, 441-448.

MERRIKH, H., ZHANG, Y., GROSSMAN, A. D. & WANG, J. D. 2012. Replication-transcription conflicts in bacteria. *Nature reviews. Microbiology*, 10, 449-458.

METODIEV, M. D., THOMPSON, K., ALSTON, C. L., MORRIS, A. A. M., HE, L., ASSOULINE, Z., RIO, M., BAHI-BUISSON, N., PYLE, A., GRIFFIN, H., SIIRA, S., FILIPOVSKA, A., MUNNICH, A., CHINNERY, P. F., MCFARLAND, R., RÖTIG, A. & TAYLOR, R. W. 2016. Recessive Mutations in TRMT10C Cause Defects in Mitochondrial RNA Processing and Multiple Respiratory Chain Deficiencies. *Am J Hum Genet*, 98, 993-1000.

MILI, S. & PIÑOL-ROMA, S. 2003. LRP130, a pentatricopeptide motif protein with a noncanonical RNA-binding domain, is bound in vivo to mitochondrial and nuclear RNAs. *Mol Cell Biol*, 23, 4972-82.

MILLER, C., SAADA, A., SHAUL, N., SHABTAI, N., BEN-SHALOM, E., SHAAG, A., HERSHKOVITZ, E. & ELPELEG, O. 2004. Defective mitochondrial translation caused by a ribosomal protein (MRPS16) mutation. *Annals of Neurology*, 56, 734-738.

MINCZUK, M., HE, J., DUCH, A. M., ETTEMA, T. J., CHLEBOWSKI, A., DZIONEK, K., NIJTMANS, L. G., HUYNEN, M. A. & HOLT, I. J. 2011. TEFM (c17orf42) is necessary for transcription of human mtDNA. *Nucleic Acids Res*, 39, 4284-99.

MINCZUK, M., PIWOWARSKI, J., PAPWORTH, M. A., AWISZUS, K., SCHALINSKI, S., DZIEMBOWSKI, A., DMOCHOWSKA, A., BARTNIK, E., TOKATLIDIS, K., STEPIEN, P. P. & BOROWSKI, P. 2002. Localisation of the human hSuv3p helicase in the mitochondrial matrix and its preferential unwinding of dsDNA. *Nucleic Acids Res*, 30, 5074-86.

MINTON, D. R., NAM, M., MCLAUGHLIN, D. J., SHIN, J., BAYRAKTAR, E. C., ALVAREZ, S. W., SVIDERSKIY, V. O., PAPAGIANNAKOPOULOS, T., SABATINI, D. M., BIRSOY, K. & POSSEMATO, R. 2018. Serine Catabolism by SHMT2 Is Required for Proper Mitochondrial Translation Initiation and Maintenance of Formylmethionyl-tRNAs. *Mol Cell*, 69, 610-621.e5.

MIQUEL, J., ECONOMOS, A. C., FLEMING, J. & JOHNSON, J. E. 1980. Mitochondrial role in cell aging. *Experimental Gerontology*, 15, 575-591.

MIRALLES FUSTÉ, J., SHI, Y., WANROOIJ, S., ZHU, X., JEMT, E., PERSSON, Ö., SABOURI, N., GUSTAFSSON, C. M. & FALKENBERG, M. 2014. In vivo occupancy of mitochondrial single-stranded DNA binding protein supports the strand displacement mode of DNA replication. *PLoS Genet*, 10, e1004832.

MITCHELL, P. 1961. Coupling of Phosphorylation to Electron and Hydrogen Transfer by a Chemi-Osmotic type of Mechanism. *Nature*, 191, 144-148.

MITULOVIĆ, G. & MECHTLER, K. 2006. HPLC techniques for proteomics analysis—a short overview of latest developments. *Briefings in Functional Genomics*, 5, 249-260.

MOCZKO, M., BÖMER, U., KÜBRICH, M., ZUFALL, N., HÖNLINGER, A. & PFANNER, N. 1997. The intermembrane space domain of mitochondrial Tom22 functions as a trans binding site for preproteins with N-terminal targeting sequences. *Molecular and Cellular Biology*, 17, 6574-6584.

MODJTAHEDI, N. & KROEMER, G. 2016. CHCHD4 links AIF to the biogenesis of respiratory chain complex I. *Mol Cell Oncol*, 3, e1074332.

MOHAMED, W. K. E., ARNOUX, M., CARDOSO, T. H. S., ALMUTERY, A. & TLILI, A. 2020. Mitochondrial mutations in non-syndromic hearing loss at UAE. *Int J Pediatr Otorhinolaryngol*, 138, 110286.

MOLL, I., HIROKAWA, G., KIEL, M. C., KAJI, A. & BLÄSI, U. 2004. Translation initiation with 70S ribosomes: an alternative pathway for leaderless mRNAs. *Nucleic acids research*, 32, 3354-3363.

MONTOYA, J., CHRISTIANSON, T., LEVENS, D., RABINOWITZ, M. & ATTARDI, G. 1982. Identification of initiation sites for heavy-strand and light-strand transcription in human mitochondrial DNA. *Proceedings of the National Academy of Sciences of the United States of America*, 79, 7195-7199.

MONTOYA, J., GAINES, G. L. & ATTARDI, G. 1983. The pattern of transcription of the human mitochondrial rRNA genes reveals two overlapping transcription units. *Cell*, 34, 151-9.

MONTOYA, J., OJALA, D. & ATTARDI, G. 1981. Distinctive features of the 5'-terminal sequences of the human mitochondrial mRNAs. *Nature*, 290, 465-470.

MOORE, R. E., YOUNG, M. K. & LEE, T. D. 2002. Qscore: An algorithm for evaluating SEQUEST database search results. *Journal of the American Society for Mass Spectrometry*, 13, 378-386.

MOORE, S. D. & SAUER, R. T. 2005. Ribosome rescue: tmRNA tagging activity and capacity in *Escherichia coli*. *Mol Microbiol*, 58, 456-66.

MORA, L., HEURGUÉ-HAMARD, V., DE ZAMAROCZY, M., KERVESTIN, S. & BUCKINGHAM, R. H. 2007. Methylation of Bacterial Release Factors RF1 and RF2 Is Required for Normal Translation Termination in Vivo*. *Journal of Biological Chemistry*, 282, 35638-35645.

MOROZOV, Y. I., AGARONYAN, K., CHEUNG, A. C. M., ANIKIN, M., CRAMER, P. & TEMIAKOV, D. 2014. A novel intermediate in transcription initiation by human mitochondrial RNA polymerase. *Nucleic acids research*, 42, 3884-3893.

MORSCHER, R. J., DUCKER, G. S., LI, S. H.-J., MAYER, J. A., GITAI, Z., SPERL, W. & RABINOWITZ, J. D. 2018. Mitochondrial translation requires folate-dependent tRNA methylation. *Nature*, 554, 128-132.

MOSAMMAPARAST, N. & PEMBERTON, L. F. 2004. Karyopherins: from nuclear-transport mediators to nuclear-function regulators. *Trends Cell Biol*, 14, 547-56.

MOSSMANN, D., VÖGTLÉ, F. N., TASKIN, ASLI A., TEIXEIRA, PEDRO F., RING, J., BURKHART, JULIA M., BURGER, N., PINHO, CATARINA M., TADIC, J., LORETH, D., GRAFF, C., METZGER, F., SICKMANN, A., KRETZ, O., WIEDEMANN, N., ZAHEDI, RENÉ P., MADEO, F., GLASER, E. & MEISINGER, C. 2014. Amyloid- β Peptide Induces Mitochondrial Dysfunction by Inhibition of Preprotein Maturation. *Cell Metabolism*, 20, 662-669.

MÜHLENHOFF, U., GERBER, J., RICHHARDT, N. & LILL, R. 2003. Components involved in assembly and dislocation of iron-sulfur clusters on the scaffold protein Isu1p. *The EMBO journal*, 22, 4815-4825.

MURÍN, R., VERLEYSDONK, S., RAPP, M. & HAMPRECHT, B. 2006. Immunocytochemical localization of 3-methylcrotonyl-CoA carboxylase in cultured ependymal, microglial and oligodendroglial cells. *J Neurochem*, 97, 1393-402.

MURPHY, MICHAEL P. 2008. How mitochondria produce reactive oxygen species. *Biochemical Journal*, 417, 1-13.

MURTHY, M. S. & PANDE, S. V. 1987. Some differences in the properties of carnitine palmitoyltransferase activities of the mitochondrial outer and inner membranes. *Biochemical Journal*, 248, 727-733.

NAGAIKE, T., SUZUKI, T., TOMARI, Y., TAKEMOTO-HORI, C., NEGAYAMA, F., WATANABE, K. & UEDA, T. 2001. Identification and characterization of mammalian mitochondrial tRNA nucleotidyltransferases. *J Biol Chem*, 276, 40041-9.

NAGY, E. & MAQUAT, L. E. 1998. A rule for termination-codon position within intron-containing genes: when nonsense affects RNA abundance. *Trends Biochem Sci*, 23, 198-9.

NAKAMURA, Y., ITO, K. & ISAKSSON, L. A. 1996. Emerging Understanding of Translation Termination. *Cell*, 87, 147-150.

NAM, S. C. & KANG, C. 2005. DNA light-strand preferential recognition of human mitochondria transcription termination factor mTERF. *J Biochem Mol Biol*, 38, 690-4.

NAOÉ, M., OHWA, Y., ISHIKAWA, D., OHSHIMA, C., NISHIKAWA, S.-I., YAMAMOTO, H. & ENDO, T. 2004. Identification of Tim40 That Mediates Protein Sorting to the Mitochondrial Intermembrane Space. *Journal of Biological Chemistry*, 279, 47815-47821.

NASS, M. M. K. & NASS, S. 1963. INTRAMITOCHONDRIAL FIBERS WITH DNA CHARACTERISTICS : I. Fixation and Electron Staining Reactions. *J Cell Biol*, 19, 593-611.

NEEVE, V. C. M., PYLE, A., BOCZONADI, V., GOMEZ-DURAN, A., GRIFFIN, H., SANTIBANEZ-KOREF, M., GAISER, U., BAUER, P., TZSCHACH, A., CHINNERY, P. F. & HORVATH, R. 2013. Clinical and functional characterisation of the combined respiratory chain defect in two sisters due to autosomal recessive mutations in MTFMT. *Mitochondrion*, 13, 743-748.

NELSON, D. L. C., MICHAEL M. 2017. *Lehninger principles of biochemistry* (7th edition).

NELSON, D. R., FELIX, C. M. & SWANSON, J. M. 1998. Highly conserved charge-pair networks in the mitochondrial carrier family 11Edited by A. R. Fersht. *Journal of Molecular Biology*, 277, 285-308.

NESSEL, T., BECK, J. M., RAYATPISHEH, S., JAMI-ALAHMADI, Y., WOHLSCHELEGEL, J. A., GOLDBERG, D. E. & BECK, J. R. 2020. EXP1 is required for organisation of EXP2 in the intraerythrocytic malaria parasite vacuole. *Cellular Microbiology*, 22, e13168.

NEU-YILIK, G., AMTHOR, B., GEHRING, N. H., BAHRI, S., PAIDASSI, H., HENTZE, M. W. & KULOZIK, A. E. 2011. Mechanism of escape from nonsense-mediated mRNA decay of human beta-globin transcripts with nonsense mutations in the first exon. *RNA (New York, N.Y.)*, 17, 843-854.

NEWMAN, M. S., TERESA; DORNER, LYDIA F.; & SCHILDKRAUT, I. A., ANEEL K. 1995. Structure of Bam HI Endonuclease Bound to DNA: Partial Folding and Unfolding on DNA Binding. *Science*, 269, 656-663.

NGO, H. B., KAISER, J. T. & CHAN, D. C. 2011. The mitochondrial transcription and packaging factor Tfam imposes a U-turn on mitochondrial DNA. *Nat Struct Mol Biol*, 18, 1290-6.

NICHOLLS, T. J. & MINCZUK, M. 2014. In D-loop: 40years of mitochondrial 7S DNA. *Experimental Gerontology*, 56, 175-181.

NICKLESS, A., BAILIS, J. M. & YOU, Z. 2017. Control of gene expression through the nonsense-mediated RNA decay pathway. *Cell & Bioscience*, 7, 26.

NISHIHARA, H., OMOTO, M., TAKAO, M., HIGUCHI, Y., KOGA, M., KAWAI, M., KAWANO, H., IKEDA, E., TAKASHIMA, H. & KANDA, T. 2017. Autopsy case of the C12orf65 mutation in a patient with signs of mitochondrial dysfunction. *Neurol Genet*, 3, e171.

NOZAKI, Y., MATSUNAGA, N., ISHIZAWA, T., UEDA, T. & TAKEUCHI, N. 2008. HMRF1L is a human mitochondrial translation release factor involved in the decoding of the termination codons UAA and UAG. *Genes to Cells*, 13, 429-438.

O'GORMAN, S., FOX, D. T. & WAHL, G. M. 1991. Recombinase-mediated gene activation and site-specific integration in mammalian cells. *Science*, 251, 1351-5.

ODGREN, P. R., TOUKATLY, G., BANGS, P. L., GILMORE, R. & FEY, E. G. 1996. Molecular characterization of mitofillin (HMP), a mitochondria-associated protein with predicted coiled coil and intermembrane space targeting domains. *J Cell Sci*, 109 (Pt 9), 2253-64.

OJALA, D., MONTOYA, J. & ATTARDI, G. 1981. tRNA punctuation model of RNA processing in human mitochondria. *Nature*, 290, 470-4.

OKADO-MATSUMOTO, A. & FRIDOVICH, I. 2001. Subcellular Distribution of Superoxide Dismutases (SOD) in Rat Liver: Cu,Zn-SOD IN MITOCHONDRIA*. *Journal of Biological Chemistry*, 276, 38388-38393.

OLICHON, A., EMORINE, L. J., DESCLOUDS, E., PELLOQUIN, L., BRICHESE, L., GAS, N., GUILLOU, E., DELETTRE, C., VALETTE, A., HAMEL, C. P., DUCOMMUN, B., LENAERS, G. & BELENGUER, P. 2002. The human dynamin-related protein OPA1 is anchored to the mitochondrial inner membrane facing the inter-membrane space. *FEBS Letters*, 523, 171-176.

OLSEN, J. V., ONG, S. E. & MANN, M. 2004. Trypsin cleaves exclusively C-terminal to arginine and lysine residues. *Mol Cell Proteomics*, 3, 608-14.

OSTERMANN, J., HORWICH, A. L., NEUPERT, W. & HARTL, F. U. 1989. Protein folding in mitochondria requires complex formation with hsp60 and ATP hydrolysis. *Nature*, 341, 125-130.

OTT, C., DORSCH, E., FRAUNHOLZ, M., STRAUB, S. & KOZJAK-PAVLOVIC, V. 2015. Detailed Analysis of the Human Mitochondrial Contact Site Complex Indicate a Hierarchy of Subunits. *PLOS ONE*, 10, e0120213.

OTT, C., ROSS, K., STRAUB, S., THIEDE, B., GÖTZ, M., GOOSMANN, C., KRISCHKE, M., MUELLER, M. J., KROHNE, G., RUDEL, T. & KOZJAK-PAVLOVIC, V. 2012. Sam50 Functions in Mitochondrial Intermembrane Space Bridging and Biogenesis of Respiratory Complexes. *Molecular and Cellular Biology*, 32, 1173.

OULD AMER, Y. & HEBERT-CHATELAIN, E. 2020. Insight into the Interactome of Intramitochondrial PKA Using Biotinylation-Proximity Labeling. *Int J Mol Sci*, 21.

PAJAK, A. 2013. *Characterisation of human mtRF1 and C12orf65 : what are their roles in mitochondrial protein synthesis?* PhD, Newcastle.

PALADE, G. E. 1952. The fine structure of mitochondria. *The Anatomical Record*, 114, 427-451.

PALADE, G. E. 1953. AN ELECTRON MICROSCOPE STUDY OF THE MITOCHONDRIAL STRUCTURE. *Journal of Histochemistry & Cytochemistry*, 1, 188-211.

PALMIERI, F. 2013. The mitochondrial transporter family SLC25: identification, properties and physiopathology. *Mol Aspects Med*, 34, 465-84.

PALMIERI, F. 2014. Mitochondrial transporters of the SLC25 family and associated diseases: a review. *J Inher Metab Dis*, 37, 565-75.

PARDO, B., GÓMEZ-GONZÁLEZ, B. & AGUILERA, A. 2009. DNA Repair in Mammalian Cells. *Cellular and Molecular Life Sciences*, 66, 1039-1056.

PARK, J., RYU, H., JANG, W., CHAE, H., KIM, M., KIM, Y., KIM, J., LEE, J. W., CHUNG, N., CHO, B., SUH, B. K 2015. Novel 5.712 kb mitochondrial DNA deletion in a patient with Pearson syndrome: A case report. *Molecular Medicine Reports* 11, 3741-3745.

PARK, K., BOTELHO, S. C., HONG, J., ÖSTERBERG, M. & KIM, H. 2013. Dissecting Stop Transfer versus Conservative Sorting Pathways for Mitochondrial Inner Membrane Proteins in Vivo. *Journal of Biological Chemistry*, 288, 1521-1532.

PASCHEN, S. A., WAIZENEGGER, T., STAN, T., PREUSS, M., CYRKLAFF, M., HELL, K., RAPAPORT, D. & NEUPERT, W. 2003. Evolutionary conservation of biogenesis of β -barrel membrane proteins. *Nature*, 426, 862-866.

PATEL, M. S., NEMERIA, N. S., FUREY, W. & JORDAN, F. 2014. The pyruvate dehydrogenase complexes: structure-based function and regulation. *J Biol Chem*, 289, 16615-23.

PAUMARD, P., VAILLIER, J., COULARY, B., SCHAEFFER, J., SOUBANNIER, V., MUELLER, D. M., BRÈTHES, D., DI RAGO, J. P. & VELOURS, J. 2002. The ATP synthase is involved in generating mitochondrial cristae morphology. *Embo J*, 21, 221-30.

PEARCE, S., NEZICH, C. L. & SPINAZZOLA, A. 2013. Mitochondrial diseases: Translation matters. *Molecular and Cellular Neuroscience*, 55, 1-12.

PEARCE, S. F., RORBACH, J., HAUTE, L. V., D'SOUZA, A. R., REBELO-GUIMAR, P., POWELL, C. A., BRIERLEY, I., FIRTH, A. E. & MINCZUK, M. 2017. Maturation of selected human mitochondrial tRNAs requires deadenylation. *eLife*, 6, e27596.

PELEH, V., CORDAT, E. & HERRMANN, J. M. 2016. Mia40 is a trans-site receptor that drives protein import into the mitochondrial intermembrane space by hydrophobic substrate binding. *eLife*, 5, e16177.

PERKINS, G., RENKEN, C., MARTONE, M. E., YOUNG, S. J., ELLISMAN, M. & FREY, T. 1997. Electron tomography of neuronal mitochondria: three-dimensional structure and organization of cristae and membrane contacts. *J Struct Biol*, 119, 260-72.

PERKINS, G. A., SONG, J. Y., TARSA, L., DEERINCK, T. J., ELLISMAN, M. H. & FREY, T. G. 1998. Electron tomography of mitochondria from brown adipocytes reveals crista junctions. *J Bioenerg Biomembr*, 30, 431-42.

PERLI, E., PISANO, A., GLASGOW, R. I. C., CARBO, M., HARDY, S. A., FALKOUS, G., HE, L., CERBELLI, B., PIGNATARO, M. G., ZACARA, E., RE, F., DELLA MONICA, P. L., MOREA, V., BONNEN, P. E., TAYLOR, R. W., D'AMATI, G. & GIORDANO, C. 2019. Novel compound mutations in the mitochondrial translation elongation factor (TSFM) gene cause severe cardiomyopathy with myocardial fibro-adipose replacement. *Sci Rep*, 9, 5108.

PERRONE, E., CAVOLE, T. R., OLIVEIRA, M. G., VIRMOND, L. D. A., SILVA, M. D. F. B., SOARES, M. D. F. F., IGLESIAS, S. B. D. O., FALCONI, A., SILVA, J. S., NAKANO, V., MILANEZI, M. F., MENDES, C. S. C., CURIATI, M. A. & MICHELETTI, C. 2020. Leigh syndrome in a patient with a novel C12orf65 pathogenic variant: case report and literature review. *Genetics and molecular biology*, 43, e20180271-e20180271.

PETRONILLI, V., COSTANTINI, P., SCORRANO, L., COLONNA, R., PASSAMONTI, S. & BERNARDI, P. 1994. The voltage sensor of the mitochondrial permeability transition pore is tuned by the oxidation-reduction state of vicinal thiols. Increase of the gating potential by oxidants and its reversal by reducing agents. *Journal of Biological Chemistry*, 269, 16638-16642.

PETROV, A. S., WOOD, E. C., BERNIER, C. R., NORRIS, A. M., BROWN, A. & AMUNTS, A. 2018. Structural Patching Fosters Divergence of Mitochondrial Ribosomes. *Molecular Biology and Evolution*, 36, 207-219.

PETRY, S., BRODERSEN, D. E., MURPHY, F. V. I. V., DUNHAM, C. M., SELMER, M., TARRY, M. J., KELLEY, A. C. & RAMAKRISHNAN, V. 2005. Crystal Structures of the Ribosome in Complex with Release Factors RF1 and RF2 Bound to a Cognate Stop Codon. *Cell*, 123, 1255-1266.

PFEFFER, S., WOELLHAF, M. W., HERRMANN, J. M. & FÖRSTER, F. 2015. Organization of the mitochondrial translation machinery studied in situ by cryoelectron tomography. *Nature Communications*, 6, 6019.

PIEL, R. B., 3RD, DAILEY, H. A., JR. & MEDLOCK, A. E. 2019. The mitochondrial heme metabolon: Insights into the complex(ity) of heme synthesis and distribution. *Molecular genetics and metabolism*, 128, 198-203.

PIERCE, S. B., CHISHOLM, K. M., LYNCH, E. D., LEE, M. K., WALSH, T., OPITZ, J. M., LI, W., KLEVIT, R. E. & KING, M.-C. 2011. Mutations in mitochondrial histidyl tRNA synthetase HARS2 cause ovarian dysgenesis and sensorineural hearing loss of Perrault syndrome. *Proceedings of the National Academy of Sciences of the United States of America*, 108, 6543-6548.

PIERCE, SARAH B., GERSAK, K., MICHAELSON-COHEN, R., WALSH, T., LEE, MING K., MALACH, D., KLEVIT, RACHEL E., KING, M.-C. & LEVY-LAHAD, E. 2013. Mutations in LARS2, Encoding Mitochondrial Leucyl-tRNA Synthetase, Lead to Premature Ovarian Failure and Hearing Loss in Perrault Syndrome. *American Journal of Human Genetics*, 92, 614-620.

PISAREV, A. V., HELLEN, C. U. T. & PESTOVA, T. V. 2007. Recycling of eukaryotic post-termination ribosomal complexes. *Cell*, 131, 286-299.

PISAREV, A. V., SKABKIN, M. A., PISAREVA, V. P., SKABKINA, O. V., RAKOTONDRAFARA, A. M., HENTZE, M. W., HELLEN, C. U. & PESTOVA, T. V. 2010. The role of ABCE1 in eukaryotic posttermination ribosomal recycling. *Mol Cell*, 37, 196-210.

PISAREVA, V. P., SKABKIN, M. A., HELLEN, C. U. T., PESTOVA, T. V. & PISAREV, A. V. 2011. Dissociation by Pelota, Hbs1 and ABCE1 of mammalian vacant 80S ribosomes and stalled elongation complexes. *EMBO J*, 30, 1804-1817.

PIWOWARSKI, J., GRZECHNIK, P., DZIEMBOWSKI, A., DMOCHOWSKA, A., MINCZUK, M. & STEPIEN, P. P. 2003. Human Polynucleotide Phosphorylase, hPNPase, is Localized in Mitochondria. *Journal of Molecular Biology*, 329, 853-857.

PLIATSIKA, V. & RIGOUTSOS, I. 2015. "Off-Spotter": very fast and exhaustive enumeration of genomic lookalikes for designing CRISPR/Cas guide RNAs. *Biology Direct*, 10, 4.

POHJOISMÄKI, J. L., HOLMES, J. B., WOOD, S. R., YANG, M. Y., YASUKAWA, T., REYES, A., BAILEY, L. J., CLUETT, T. J., GOFFART, S., WILLCOX, S., RIGBY, R. E., JACKSON, A. P., SPELBRINK, J. N., GRIFFITH, J. D., CROUCH, R. J., JACOBS, H. T. & HOLT, I. J. 2010. Mammalian mitochondrial DNA replication intermediates are essentially duplex but contain extensive tracts of RNA/DNA hybrid. *J Mol Biol*, 397, 1144-55.

POLACEK, N. & MANKIN, A. S. 2005. The ribosomal peptidyl transferase center: structure, function, evolution, inhibition. *Crit Rev Biochem Mol Biol*, 40, 285-311.

POPOV-ČELEKETIĆ, D., MAPA, K., NEUPERT, W. & MOKRANJAC, D. 2008. Active remodelling of the TIM23 complex during translocation of preproteins into mitochondria. *The EMBO Journal*, 27, 1469-1480.

POPP, M. W. & MAQUAT, L. E. 2016. Leveraging Rules of Nonsense-Mediated mRNA Decay for Genome Engineering and Personalized Medicine. *Cell*, 165, 1319-1322.

POSSE, V. & GUSTAFSSON, C. M. 2017. Human Mitochondrial Transcription Factor B2 Is Required for Promoter Melting during Initiation of Transcription. *The Journal of biological chemistry*, 292, 2637-2645.

POSSE, V., SHAHZAD, S., FALKENBERG, M., HÄLLBERG, B. M. & GUSTAFSSON, C. M. 2015. TEFM is a potent stimulator of mitochondrial transcription elongation in vitro. *Nucleic acids research*, 43, 2615-2624.

PRIKAS, E., POLJAK, A. & ITTNER, A. 2020. Mapping p38 α mitogen-activated protein kinase signaling by proximity-dependent labeling. *Protein Sci*, 29, 1196-1210.

PUEBLA-OSORIO, N., LACEY, D. B., ALT, F. W. & ZHU, C. 2006. Early embryonic lethality due to targeted inactivation of DNA ligase III. *Mol Cell Biol*, 26, 3935-41.

PULMAN, J., RUZZENENTE, B., BIANCHI, L., RIO, M., BODDAERT, N., MUNNICH, A., RÖTIG, A. & METODIEV, M. D. 2019. Mutations in the MRPS28 gene encoding the small mitoribosomal subunit protein bS1m in a patient with intrauterine growth retardation, craniofacial dysmorphism and multisystemic involvement. *Hum Mol Genet*, 28, 1445-1462.

PYLE, A., RAMESH, V., BARTSAKOULIA, M., BOCZONADI, V., GOMEZ-DURAN, A., HERCZEGFALVI, A., BLAKELY, E. L., SMERTENKO, T., DUFF, J., EGLON, G., MOORE, D., YU-WAI-MAN, P., DOUROUDIS, K., SANTIBANEZ-KOREF, M., GRIFFIN, H., LOCHMÜLLER, H., KARCAGI, V., TAYLOR, R. W., CHINNERY, P. F. & HORVATH, R. 2014. Behr's Syndrome is Typically Associated with Disturbed Mitochondrial Translation and Mutations in the C12orf65 Gene. *J Neuromuscul Dis*, 1, 55-63.

PYRIH, J., RAŠKOVÁ, V., ŠKODOVÁ-SVERÁKOVÁ, I., PÁNEK, T. & LUKEŠ, J. 2020. ZapE/Afg1 interacts with Oxa1 and its depletion causes a multifaceted phenotype. *PLoS One*, 15, e0234918.

QIU, J., WENZ, L.-S., ZERBES, RALF M., OELJEKLAUS, S., BOHNERT, M., STROUD, DAVID A., WIRTH, C., ELLENRIEDER, L., THORNTON, N., KUTIK, S., WIESE, S., SCHULZE-SPECKING, A., ZUFALL, N., CHACINKA, A., GUIARD, B., HUNTE, C., WARSCHIED, B., VAN DER LAAN, M., PFANNER, N., WIEDEMANN, N. & BECKER, T. 2013. Coupling of Mitochondrial Import and Export Translocases by Receptor-Mediated Supercomplex Formation. *Cell*, 154, 596-608.

RACKHAM, O., BUSCH, JAKOB D., MATIC, S., SIIRA, STEFAN J., KUZNETSOVA, I., ATANASSOV, I., ERMER, JUDITH A., SHEARWOOD, A.-MARIE J., RICHMAN, TARA R., STEWART, JAMES B., MOURIER, A., MILENKOVIC, D., LARSSON, N.-G. & FILIPOVSKA, A. 2016. Hierarchical RNA Processing Is Required for Mitochondrial Ribosome Assembly. *Cell Reports*, 16, 1874-1890.

RAFF, R. A. & MAHLER, H. R. 1972. The Non symbiotic Origin of Mitochondria. *Science*, 177, 575-582.

RAHMAN, B., KAWANO, S., YUNOKI-ESAKI, K., ANZAI, T. & ENDO, T. 2014. NMR analyses on the interactions of the yeast Tim50 C-terminal region with the presequence and Tim50 core domain. *FEBS Letters*, 588, 678-684.

RAN, F. A., HSU, P. D., WRIGHT, J., AGARWALA, V., SCOTT, D. A. & ZHANG, F. 2013. Genome engineering using the CRISPR-Cas9 system. *Nature protocols*, 8, 2281-2308.

RAPPSILBER, J., ISHIHAMA, Y. & MANN, M. 2003. Stop and go extraction tips for matrix-assisted laser desorption/ionization, nanoelectrospray, and LC/MS sample pretreatment in proteomics. *Anal Chem*, 75, 663-70.

RATH, S., SHARMA, R., GUPTA, R., AST, T., CHAN, C., DURHAM, T. J., GOODMAN, R. P., GRABAREK, Z., HAAS, M. E., HUNG, W. H. W., JOSHI, P. R., JOURDAIN, A. A., KIM, S. H., KOTRYS, A. V., LAM, S., MCCOY, J. G., MEISEL, J. D., MIRANDA, M., PANDA, A., PATGIRI, A., ROGERS, R., SADRE, S., SHAH, H., SKINNER, O. S., TO, T. L., WALKER, M. A., WANG, H., WARD, P. S., WENGROD, J., YUAN, C. C., CALVO, S. E. & MOOTHA, V. K. 2021. MitoCarta3.0: an updated mitochondrial proteome now with sub-organelle localization and pathway annotations. *Nucleic Acids Res*, 49, D1541-d1547.

RAUSCH, T., FRITZ, M. H.-Y., UNTERGASSER, A. & BENES, V. 2020. Tracy: basecalling, alignment, assembly and deconvolution of sanger chromatogram trace files. *BMC Genomics*, 21, 230.

RAVN, K., SCHÖNEWOLF-GREULICH, B., HANSEN, R. M., BOHR, A.-H., DUNO, M., WIBRAND, F. & OSTERGAARD, E. 2015. Neonatal mitochondrial hepatoencephalopathy caused by novel GFM1 mutations. *Molecular Genetics and Metabolism Reports*, 3, 5-10.

REBELO-GUIMAR, P., POWELL, C. A., VAN HAUTE, L. & MINCZUK, M. 2019. The mammalian mitochondrial epitranscriptome. *Biochimica et biophysica acta. Gene regulatory mechanisms*, 1862, 429-446.

REDZA-DUTORDOIR, M. & AVERILL-BATES, D. A. 2016. Activation of apoptosis signalling pathways by reactive oxygen species. *Biochim Biophys Acta*, 1863, 2977-2992.

REECE, J. B., URRY, L. A., CAIN, M. L., WASSERMAN, S. A., MINORSKY, P. V., AND JACKSON, R. B 2011. An accounting of ATP production by cellular respiration. *Campbell biology* San Francisco: CA: Pearson.

REEDY, C. J., ELVEKROG, M. M. & GIBNEY, B. R. 2008. Development of a heme protein structure-electrochemical function database. *Nucleic acids research*, 36, D307-D313.

REHLING, P., MODEL, K., BRANDNER, K., KOVERMANN, P., SICKMANN, A., MEYER, H. E., KÜHLBRANDT, W., WAGNER, R., TRUSCOTT, K. N. & PFANNER, N. 2003. Protein Insertion into the Mitochondrial Inner Membrane by a Twin-Pore Translocase. *Science*, 299, 1747-1751.

REINHARD, L., SRIDHARA, S. & HÄLLBERG, B. M. 2017. The MRPP1/MRPP2 complex is a tRNA-maturation platform in human mitochondria. *Nucleic Acids Res*, 45, 12469-12480.

REY, T., ZAGANELLI, S., CUILLERY, E., VARTHOLOMAIOU, E., CROISIER, M., MARTINOU, J. C. & MANLEY, S. 2020. Mitochondrial RNA granules are fluid condensates positioned by membrane dynamics. *Nat Cell Biol*, 22, 1180-1186.

REYES, A., KAZAK, L., WOOD, S. R., YASUKAWA, T., JACOBS, H. T. & HOLT, I. J. 2013. Mitochondrial DNA replication proceeds via a 'bootlace' mechanism involving the incorporation of processed transcripts. *Nucleic Acids Res*, 41, 5837-50.

RHEE, H.-W., ZOU, P., UDESHI, N. D., MARTELL, J. D., MOOTHA, V. K., CARR, S. A. & TING, A. Y. 2013. Proteomic mapping of mitochondria in living cells via spatially restricted enzymatic tagging. *Science (New York, N.Y.)*, 339, 1328-1331.

RICHARD M. KLEIN, A. C. 1967. A consideration of the evolutionary and taxonomic significance of some biochemical, micromorphological and physiological characters in the Thallophytes. *The Quarterly Review of Biology*, 42, 105-296.

RICHMAN, T. R., ERMER, J. A., DAVIES, S. M., PERKS, K. L., VIOLA, H. M., SHEARWOOD, A. M., HOOL, L. C., RACKHAM, O. & FILIPOVSKA, A. 2015. Mutation in MRPS34 compromises protein synthesis and causes mitochondrial dysfunction. *PLoS Genet*, 11, e1005089.

RICHMAN, T. R., SPÅHR, H., ERMER, J. A., DAVIES, S. M. K., VIOLA, H. M., BATES, K. A., PAPADIMITRIOU, J., HOOL, L. C., RODGER, J., LARSSON, N.-G., RACKHAM, O. & FILIPOVSKA, A. 2016. Loss of the RNA-binding protein TACO1 causes late-onset mitochondrial dysfunction in mice. *Nature communications*, 7, 11884-11884.

RICHTER, C., PARK, J. W. & AMES, B. N. 1988. Normal oxidative damage to mitochondrial and nuclear DNA is extensive. *Proceedings of the National Academy of Sciences*, 85, 6465-6467.

RICHTER, R., PAJAK, A., DENNERLEIN, S., ROZANSKA, A., LIGHTOWLERS, ROBERT N. & CHRZANOWSKA-LIGHTOWLERS, ZOFIA M. A. 2010a. Translation termination in human mitochondrial ribosomes. *Biochemical Society Transactions*, 38, 1523-1526.

RICHTER, R., RORBACH, J., PAJAK, A., SMITH, P. M., WESSELS, H. J., HUYNEN, M. A., SMEITINK, J. A., LIGHTOWLERS, R. N. & CHRZANOWSKA-LIGHTOWLERS, Z. M. 2010b. A functional peptidyl-tRNA hydrolase, ICT1, has been recruited into the human mitochondrial ribosome. *The EMBO journal*, 29, 1116-1125.

RILEY, L. G., COOPER, S., HICKEY, P., RUDINGER-THIRION, J., MCKENZIE, M., COMPTON, A., LIM, S. C., THORBURN, D., RYAN, M. T., GIEGÉ, R., BAHLO, M. & CHRISTODOULOU, J. 2010. Mutation of the Mitochondrial Tyrosyl-tRNA Synthetase Gene, YARS2, Causes Myopathy, Lactic Acidosis, and Sideroblastic Anemia—MLASA Syndrome. *American Journal of Human Genetics*, 87, 52-59.

RINGEL, R., SOLOGUB, M., MOROZOV, Y. I., LITONIN, D., CRAMER, P. & TEMIAKOV, D. 2011. Structure of human mitochondrial RNA polymerase. *Nature*, 478, 269-73.

RIZZUTO, R., DE STEFANI, D., RAFFAELLO, A. & MAMMUCARI, C. 2012. Mitochondria as sensors and regulators of calcium signalling. *Nat Rev Mol Cell Biol*, 13, 566-78.

ROBBERSON, D. L., KASAMATSU, H. & VINOGRAD, J. 1972. Replication of mitochondrial DNA. Circular replicative intermediates in mouse L cells. *Proc Natl Acad Sci U S A*, 69, 737-41.

ROBERTS, D. L., FRERMAN, F. E. & KIM, J. J. 1996. Three-dimensional structure of human electron transfer flavoprotein to 2.1-A resolution. *Proceedings of the National Academy of Sciences of the United States of America*, 93, 14355-14360.

ROBIN, E. D. & WONG, R. 1988. Mitochondrial DNA molecules and virtual number of mitochondria per cell in mammalian cells. *Journal of Cellular Physiology*, 136, 507-513.

ROBIN, J. D., WRIGHT, W. E., ZOU, Y., COSSETTE, S. C., LAWLOR, M. W. & GUSSONI, E. 2015. Isolation and immortalization of patient-derived cell lines from muscle biopsy for disease modeling. *Journal of visualized experiments : JoVE*, 52307-52307.

RODNINA, M. V. 2013. The ribosome as a versatile catalyst: reactions at the peptidyl transferase center. *Current Opinion in Structural Biology*, 23, 595-602.

RODNINA, M. V. 2018. Translation in Prokaryotes. *Cold Spring Harbor Perspectives in Biology*, 10.

ROISE, D., HORVATH, S. J., TOMICH, J. M., RICHARDS, J. H. & SCHATZ, G. 1986. A chemically synthesized pre-sequence of an imported mitochondrial protein can form an amphiphilic helix and perturb natural and artificial phospholipid bilayers. *The EMBO Journal*, 5, 1327-1334.

ROJO, E. E., STUART, R. A. & NEUPERT, W. 1995. Conservative sorting of F0-ATPase subunit 9: export from matrix requires delta pH across inner membrane and matrix ATP. *The EMBO Journal*, 14, 3445-3451.

ROLL-MECAK, A., SHIN, B.-S., DEVER, T. E. & BURLEY, S. K. 2001. Engaging the ribosome: universal IFs of translation. *Trends in Biochemical Sciences*, 26, 705-709.

ROOIJERS, K., LOAYZA-PUCH, F., NIJTMANS, L. G. & AGAMI, R. 2013. Ribosome profiling reveals features of normal and disease-associated mitochondrial translation. *Nature communications*, 4, 2886-2886.

ROPP, P. A. & COPELAND, W. C. 1996. Cloning and Characterization of the Human Mitochondrial DNA Polymerase, DNA Polymerase γ . *Genomics*, 36, 449-458.

RORBACH, J., BOESCH, P., GAMMAGE, P. A., NICHOLLS, T. J., PEARCE, S. F., PATEL, D., HAUSER, A., PEROCCHI, F. & MINCZUK, M. 2014. MRM2 and MRM3 are involved in biogenesis of the large subunit of the mitochondrial ribosome. *Mol Biol Cell*, 25, 2542-55.

RORBACH, J., GAO, F., POWELL, C. A., D'SOUZA, A., LIGHTOWLERS, R. N., MINCZUK, M. & CHRZANOWSKA-LIGHTOWLERS, Z. M. 2016. Human mitochondrial ribosomes can switch their structural RNA composition. *Proceedings of the National Academy of Sciences of the United States of America*, 113, 12198-12201.

RORBACH, J., RICHTER, R., WESSELS, H. J., WYDRO, M., PEKALSKI, M., FARHOUD, M., KÜHL, I., GAISNE, M., BONNEFOY, N., SMEITINK, J. A., LIGHTOWLERS, R. N. & CHRZANOWSKA-LIGHTOWLERS, Z. M. A. 2008. The human mitochondrial ribosome recycling factor is essential for cell viability. *Nucleic acids research*, 36, 5787-5799.

ROSSMANITH, W. 2011. Localization of human RNase Z isoforms: dual nuclear/mitochondrial targeting of the ELAC2 gene product by alternative translation initiation. *PLoS one*, 6, e19152-e19152.

RÖTIG, A. 2011. Human diseases with impaired mitochondrial protein synthesis. *Biochimica et Biophysica Acta (BBA) - Bioenergetics*, 1807, 1198-1205.

ROUX, K. J., KIM, D. I., RAIDA, M. & BURKE, B. 2012. A promiscuous biotin ligase fusion protein identifies proximal and interacting proteins in mammalian cells. *J Cell Biol*, 196, 801-10.

ROZANSKA, A., RICHTER-DENNERLEIN, R., RORBACH, J., GAO, F., LEWIS, R. J., CHRZANOWSKA-LIGHTOWLERS, Z. M. & LIGHTOWLERS, R. N. 2017. The human RNA-binding protein RBFA promotes the maturation of the mitochondrial ribosome. *The Biochemical journal*, 474, 2145-2158.

RUBIO-COSIALS, A., SYDOW, J. F., JIMÉNEZ-MENÉNDEZ, N., FERNÁNDEZ-MILLÁN, P., MONTOYA, J., JACOBS, H. T., COLL, M., BERNADÓ, P. & SOLÀ, M. 2011. Human mitochondrial transcription factor A induces a U-turn structure in the light strand promoter. *Nature Structural & Molecular Biology*, 18, 1281-1289.

RUSSELL, O. M., GORMAN, G. S., LIGHTOWLERS, R. N. & TURNBULL, D. M. 2020. Mitochondrial Diseases: Hope for the Future. *Cell*, 181, 168-188.

RUZZENENTE, B., METODIEV, M. D., WREDENBERG, A., BRATIC, A., PARK, C. B., CÁMARA, Y., MILENKOVIC, D., ZICKERMANN, V., WIBOM, R., HULTENBY, K., ERDJUMENT-BROMAGE, H., TEMPST, P., BRANDT, U., STEWART, J. B., GUSTAFSSON, C. M. & LARSSON, N.-G. 2012. LRPPRC is necessary for polyadenylation and coordination of translation of mitochondrial mRNAs. *The EMBO journal*, 31, 443-456.

RYGIEL, K. A., TUPPEN, H. A., GRADY, J. P., VINCENT, A., BLAKELY, E. L., REEVE, A. K., TAYLOR, R. W., PICARD, M., MILLER, J. & TURNBULL, D. M. 2016. Complex mitochondrial DNA rearrangements in individual cells from patients with sporadic inclusion body myositis. *Nucleic Acids Res*, 44, 5313-5329.

SAADA, A., SHAAG, A., ARNON, S., DOLFIN, T., MILLER, C., FUCHS-TELEM, D., LOMBES, A. & ELPELEG, O. 2007. Antenatal mitochondrial disease caused by mitochondrial ribosomal protein (MRPS22) mutation. *Journal of Medical Genetics*, 44, 784-786.

SAFRA, M., SAS-CHEN, A., NIR, R., WINKLER, R., NACHSHON, A., BAR-YAACOV, D., ERLACHER, M., ROSSMANITH, W., STERN-GINOSSAR, N. & SCHWARTZ, S. 2017. The m1A landscape on cytosolic and mitochondrial mRNA at single-base resolution. *Nature*, 551, 251-255.

SAPP, J. 2007. *Mitochondria and Their Host: Morphology to Molecular Phylogeny*, Springer-Verlag Berlin Heidelberg.

SARASTE, M. & WALKER, J. E. 1982. Internal sequence repeats and the path of polypeptide in mitochondrial ADP/ATP translocase. *FEBS Letters*, 144, 250-254.

SASARMAN, F., BRUNEL-GUITTON, C., ANTONICKA, H., WAI, T., SHOUBRIDGE, E. A. & CONSORTIUM, L. 2010. LRPPRC and SLIRP interact in a ribonucleoprotein complex that regulates posttranscriptional gene expression in mitochondria. *Molecular biology of the cell*, 21, 1315-1323.

SATIAPUTRA, J., SHEARWIN, K. E., BOOKER, G. W. & POLYAK, S. W. 2016. Mechanisms of biotin-regulated gene expression in microbes. *Synthetic and Systems Biotechnology*, 1, 17-24.

SATO, M. & SATO, K. 2013. Maternal inheritance of mitochondrial DNA by diverse mechanisms to eliminate paternal mitochondrial DNA. *Biochimica et Biophysica Acta (BBA) - Molecular Cell Research*, 1833, 1979-1984.

SAUER, B. 1994. Site-specific recombination: developments and applications. *Curr Opin Biotechnol*, 5, 521-7.

SCHÄGGER, H. & PFEIFFER, K. 2000. Supercomplexes in the respiratory chains of yeast and mammalian mitochondria. *The EMBO Journal*, 19, 1777-1783.

SCHÄGGER, H. & PFEIFFER, K. 2001. The Ratio of Oxidative Phosphorylation Complexes I-V in Bovine Heart Mitochondria and the Composition of Respiratory Chain Supercomplexes*. *Journal of Biological Chemistry*, 276, 37861-37867.

SCHEPER, G. C., VAN DER KLOK, T., VAN ANDEL, R. J., VAN BERKEL, C. G. M., SISSLER, M., SMET, J., MURAVINA, T. I., SERKOV, S. V., UZIEL, G., BUGIANI, M., SCHIFFMANN, R., KRÄGELOH-MANN, I., SMEITINK, J. A. M., FLORENTZ, C., VAN COSTER, R., PRONK, J. C. & VAN DER KNAAP, M. S. 2007. Mitochondrial aspartyl-tRNA synthetase deficiency causes leukoencephalopathy with brain stem and spinal cord involvement and lactate elevation. *Nature Genetics*, 39, 534.

SCHULLER, A. P. & GREEN, R. 2018. Roadblocks and resolutions in eukaryotic translation. *Nature reviews. Molecular cell biology*, 19, 526-541.

SCHWANTJE, M., DE SAIN-VAN DER VELDEN, M., JANS, J., VAN GASSEN, K., DORREPAAL, C., KOOP, K. & VISSER, G. 2019. Genetic defect of the sodium-dependent multivitamin transporter: A treatable disease, mimicking biotinidase deficiency. *JIMD Reports*, 48, 11-14.

SCHWARTZBACH, C. J. & SPREMULLI, L. L. 1989. Bovine mitochondrial protein synthesis elongation factors: Identification and initial characterization of an elongation factor Tu-elongation factor Ts complex*. *Journal of Biological Chemistry*, 264, 19125-19131.

SCHWEERS, R. L., ZHANG, J., RANDALL, M. S., LOYD, M. R., LI, W., DORSEY, F. C., KUNDU, M., OPFERMAN, J. T., CLEVELAND, J. L., MILLER, J. L. & NEY, P. A. 2007. NIX is required for programmed mitochondrial clearance during reticulocyte maturation. *Proc Natl Acad Sci U S A*, 104, 19500-5.

SCHWEIZER, M., CHEVALOT, I., BLANCHARD, F., FOURNIER, F., HARSCOAT-SCHIAVO, C., VANDERESSE, R. & MARC, I. 2007. Prediction of short peptides composition by RP-HPLC coupled to ESI mass spectrometry. *Food Chemistry*, 105, 1606-1613.

SCORRANO, L., ASHIYA, M., BUTTLE, K., WEILER, S., OAKES, S. A., MANNELLA, C. A. & KORSMEYER, S. J. 2002. A distinct pathway remodels mitochondrial cristae and mobilizes cytochrome c during apoptosis. *Dev Cell*, 2, 55-67.

SCOTT, I. & YOULE, R. J. 2010. Mitochondrial fission and fusion. *Essays in Biochemistry*, 47, 85-98.

SEARS, R. M., MAY, D. G. & ROUX, K. J. 2019. BioID as a Tool for Protein-Proximity Labeling in Living Cells. *Methods in molecular biology (Clifton, N.J.)*, 2012, 299-313.

SERERO, A., GIGLIONE, C., SARDINI, A., MARTINEZ-SANZ, J. & MEINNEL, T. 2003. An Unusual Peptide Deformylase Features in the Human Mitochondrial N-terminal Methionine Excision Pathway*. *Journal of Biological Chemistry*, 278, 52953-52963.

SERRE, V., ROZANSKA, A., BEINAT, M., CHRETIEN, D., BODDAERT, N., MUNNICH, A., RÖTIG, A. & CHRZANOWSKA-LIGHTOWLERS, Z. M. 2013. Mutations in mitochondrial ribosomal protein MRPL12 leads to growth retardation, neurological deterioration and mitochondrial translation deficiency(). *Biochim Biophys Acta*, 1832, 1304-1312.

SHAN, Y. & CORTOPASSI, G. 2016. Mitochondrial Hspa9/Mortalin regulates erythroid differentiation via iron-sulfur cluster assembly. *Mitochondrion*, 26, 94-103.

SHARMA, M. R., KOC, E. C., DATTA, P. P., BOOTH, T. M., SPREMULLI, L. L. & AGRAWAL, R. K. 2003. Structure of the Mammalian Mitochondrial Ribosome Reveals an Expanded Functional Role for Its Component Proteins. *Cell*, 115, 97-108.

SHIMAZAKI, H., TAKIYAMA, Y., ISHIURA, H., SAKAI, C., MATSUSHIMA, Y., HATAKEYAMA, H., HONDA, J., SAKOE, K., NAOI, T., NAMEKAWA, M., FUKUDA, Y., TAKAHASHI, Y., GOTO, J., TSUJI, S., GOTO, Y. & NAKANO, I. 2012. A homozygous mutation of C12orf65 causes spastic paraplegia with optic atrophy and neuropathy (SPG55). *J Med Genet*, 49, 777-84.

SHIMIZU, S., NARITA, M., TSUJIMOTO, Y. & TSUJIMOTO, Y. 1999. Bcl-2 family proteins regulate the release of apoptogenic cytochrome c by the mitochondrial channel VDAC. *Nature*, 399, 483-487.

SHIMIZU, Y. 2012. ArfA Recruits RF2 into Stalled Ribosomes. *Journal of Molecular Biology*, 423, 624-631.

SHIOTA, T., IMAI, K., QIU, J., HEWITT, V. L., TAN, K., SHEN, H.-H., SAKIYAMA, N., FUKASAWA, Y., HAYAT, S., KAMIYA, M., ELOFSSON, A., TOMII, K., HORTON, P., WIEDEMANN, N., PFANNER, N., LITHGOW, T. & ENDO, T. 2015. Molecular architecture of the active mitochondrial protein gate. *Science*, 349, 1544-1548.

SHOEMAKER, C. J., EYLER, D. E. & GREEN, R. 2010. Dom34:Hbs1 promotes subunit dissociation and peptidyl-tRNA drop off to initiate no-go decay. *Science (New York, N.Y.)*, 330, 369-372.

SHOEMAKER, C. J. & GREEN, R. 2011. Kinetic analysis reveals the ordered coupling of translation termination and ribosome recycling in yeast. *Proc Natl Acad Sci U S A*, 108, E1392-E1398.

SHOEMAKER, C. J. & GREEN, R. 2012. Translation drives mRNA quality control. *Nat Struct Mol Biol*, 19, 594-601.

SHOFFNER, J. M., LOTT, M. T., LEZZA, A. M., SEIBEL, P., BALLINGER, S. W. & WALLACE, D. C. 1990. Myoclonic epilepsy and ragged-red fiber disease (MERRF) is associated with a mitochondrial DNA tRNA(Lys) mutation. *Cell*, 61, 931-7.

SHU, Z., VIJAYAKUMAR, S., CHEN, C. F., CHEN, P. L. & LEE, W. H. 2004. Purified human SUV3p exhibits multiple-substrate unwinding activity upon conformational change. *Biochemistry*, 43, 4781-90.

SIEVERS, F., WILM, A., DINEEN, D., GIBSON, T. J., KARPLUS, K., LI, W., LOPEZ, R., MCWILLIAM, H., REMMERT, M., SÖDING, J., THOMPSON, J. D. & HIGGINS, D. G. 2011. Fast, scalable generation of high-quality protein multiple sequence alignments using Clustal Omega. *Molecular Systems Biology*, 7, 539.

SIIRA, S. J., SPÅHR, H., SHEARWOOD, A.-M. J., RUZZENENTE, B., LARSSON, N.-G., RACKHAM, O. & FILIPOVSKA, A. 2017. LRPPRC-mediated folding of the mitochondrial transcriptome. *Nature communications*, 8, 1532-1532.

SIMS, N. R. & ANDERSON, M. F. 2008. Isolation of mitochondria from rat brain using Percoll density gradient centrifugation. *Nat Protoc*, 3, 1228-39.

SISSLER, M., GONZÁLEZ-SERRANO, L. E. & WESTHOF, E. 2017. Recent Advances in Mitochondrial Aminoacyl-tRNA Synthetases and Disease. *Trends in Molecular Medicine*, 23, 693-708.

SJÖSTRAND, F. S. 1956. The Ultrastructure of Cells as Revealed by the Electron Microscope. In: BOURNE, G. H. & DANIELLI, J. F. (eds.) *International Review of Cytology*. Academic Press.

SKABKIN, M. A., SKABKINA, O. V., DHOTE, V., KOMAR, A. A., HELLEN, C. U. T. & PESTOVA, T. V. 2010. Activities of Ligatin and MCT-1/DENR in eukaryotic translation initiation and ribosomal recycling. *Genes & Development*, 24, 1787-1801.

SLOMOVIC, S., LAUFER, D., GEIGER, D. & SCHUSTER, G. 2005. Polyadenylation and degradation of human mitochondrial RNA: the prokaryotic past leaves its mark. *Molecular and cellular biology*, 25, 6427-6435.

SLOMOVIC, S. & SCHUSTER, G. 2008. Stable PNPase RNAi silencing: its effect on the processing and adenylation of human mitochondrial RNA. *Rna*, 14, 310-23.

SMEJDA, M., KĄDZIOŁKA, D., RADZUK, N., KRUTYHOŁOWA, R., CHRAMIEC-GŁĄBIK, A., KĘDRACKA-KROK, S., JANKOWSKA, U., BIELA, A. & GLATT, S. 2021. Same but different — Molecular comparison of human KTI12 and PSTK. *Biochimica et Biophysica Acta (BBA) - Molecular Cell Research*, 1868, 118945.

SOLEIMANPOUR-LICHAEI, H. R., KÜHL, I., GAISNE, M., PASSOS, J. F., WYDRO, M., RORBACH, J., TEMPERLEY, R., BONNEFOY, N., TATE, W., LIGHTOWLERS, R. & CHRZANOWSKA-LIGHTOWLERS, Z. 2007. mtRF1a is a human mitochondrial translation release factor decoding the major termination codons UAA and UAG. *Molecular cell*, 27, 745-757.

SONG, S., PURSELL, Z. F., COPELAND, W. C., LONGLEY, M. J., KUNKEL, T. A. & MATHEWS, C. K. 2005. DNA precursor asymmetries in mammalian tissue mitochondria and possible contribution to mutagenesis through reduced replication fidelity. *Proc Natl Acad Sci U S A*, 102, 4990-5.

SONG, Z., GHOCHANI, M., MCCAFFERY, J. M., FREY, T. G. & CHAN, D. C. 2009. Mitofusins and OPA1 mediate sequential steps in mitochondrial membrane fusion. *Molecular biology of the cell*, 20, 3525-3532.

SPÅHR, H., ROZANSKA, A., LI, X., ATANASSOV, I., LIGHTOWLERS, R. N., CHRZANOWSKA-LIGHTOWLERS, ZOFIA M. A., RACKHAM, O. & LARSSON, N.-G. 2016. SLIRP stabilizes LRPPRC via an RRM-PPR protein interface. *Nucleic Acids Research*, 44, 6868-6882.

SPELBRINK, J. N., LI, F.-Y., TIRANTI, V., NIKALI, K., YUAN, Q.-P., TARIQ, M., WANROOIJ, S., GARRIDO, N., COMI, G., MORANDI, L., SANTORO, L., TOSCANO, A., FABRIZI, G.-M., SOMER, H., CROXEN, R., BEESON, D., POULTON, J., SUOMALAINEN, A., JACOBS, H. T., ZEVIANI, M. & LARSSON, C. 2001. Human mitochondrial DNA deletions associated with mutations in the gene encoding Twinkle, a phage T7 gene 4-like protein localized in mitochondria. *Nature Genetics*, 28, 223-231.

SPENCER, A. C. & SPREMULLI, L. L. 2004. Interaction of mitochondrial initiation factor 2 with mitochondrial fMet-tRNA. *Nucleic Acids Research*, 32, 5464-5470.

SPIEGEL, R., MANDEL, H., SAADA, A., LERER, I., BURGER, A., SHAAG, A., SHALEV, S. A., JABALY-HABIB, H., GOLDSHER, D., GOMORI, J. M., LOSSOS, A., ELPELEG, O. & MEINER, V. 2014. Delineation of C12orf65-related phenotypes: a genotype-phenotype relationship. *Eur J Hum Genet*, 22, 1019-25.

SRINIVASULA, S. M., HEGDE, R., SALEH, A., DATTA, P., SHIOZAKI, E., CHAI, J., LEE, R.-A., ROBBINS, P. D., FERNANDES-ALNEMRI, T., SHI, Y. & ALNEMRI, E. S. 2001. A conserved XIAP-interaction motif in caspase-9 and Smac/DIABLO regulates caspase activity and apoptosis. *Nature*, 410, 112-116.

STADLER, S. C., POLANETZ, R., MEIER, S., MAYERHOFER, P. U., HERRMANN, J. M., ANSLINGER, K., ROSCHER, A. A., RÖSCHINGER, W. & HOLZINGER, A. 2005. Mitochondrial targeting signals and mature peptides of 3-methylcrotonyl-CoA carboxylase. *Biochem Biophys Res Commun*, 334, 939-46.

STANLEY, J. S., GRIFFIN, J. B. & ZEMPLENI, J. 2001. Biotinylation of histones in human cells. Effects of cell proliferation. *Eur J Biochem*, 268, 5424-9.

STEENWEG, M. E., GHEZZI, D., HAACK, T., ABBINK, T. E. M., MARTINELLI, D., VAN BERKEL, C. G. M., BLEY, A., DIOGO, L., GRILLO, E., TE WATER NAUDÉ, J., STROM, T. M., BERTINI, E., PROKISCH, H., VAN DER KNAAP, M. S. & ZEVIANI, M. 2012. Leukoencephalopathy with thalamus and brainstem involvement and high lactate 'LTBL' caused by EARS2 mutations. *Brain*, 135, 1387-1394.

STEPANENKO, A., ANDREIEVA, S., KORETS, K., MYKYTENKO, D., HULEYUK, N., VASSETZKY, Y. & KAVSAN, V. 2015. Step-wise and punctuated genome evolution drive phenotype changes of tumor cells. *Mutation Research/Fundamental and Molecular Mechanisms of Mutagenesis*, 771, 56-69.

STERKY, F. H., RUZZENENTE, B., GUSTAFSSON, C. M., SAMUELSSON, T. & LARSSON, N. G. 2010. LRPPRC is a mitochondrial matrix protein that is conserved in metazoans. *Biochem Biophys Res Commun*, 398, 759-64.

STEWART, J. B. & CHINNERY, P. F. 2015. The dynamics of mitochondrial DNA heteroplasmy: implications for human health and disease. *Nat Rev Genet*, 16, 530-42.

STILLER, SEBASTIAN B., HÖPKER, J., OELJEKLAUS, S., SCHÜTZE, C., SCHREMPF, SANDRA G., VENT-SCHMIDT, J., HORVATH, SUSANNE E., FRAZIER, ANN E., GEBERT, N., VAN DER LAAN, M., BOHNERT, M., WARSCHIED, B., PFANNER, N. & WIEDEMANN, N. 2016. Mitochondrial OXA Translocase Plays a Major Role in Biogenesis of Inner-Membrane Proteins. *Cell Metabolism*, 23, 901-908.

STRAUSS, M., HOFHAUS, G., SCHRÖDER, R. R. & KÜHLBRANDT, W. 2008. Dimer ribbons of ATP synthase shape the inner mitochondrial membrane. *The EMBO journal*, 27, 1154-1160.

SUN, F., HUO, X., ZHAI, Y., WANG, A., XU, J., SU, D., BARTLAM, M. & RAO, Z. 2005. Crystal structure of mitochondrial respiratory membrane protein complex II. *Cell*, 121, 1043-57.

SZCZEPANOWSKA, K. & TRIFUNOVIC, A. 2017. Origins of mtDNA mutations in ageing. *Essays Biochem*, 61, 325-337.

SZCZESNY, R. J., BOROWSKI, L. S., BRZEZNIAK, L. K., DMOCHOWSKA, A., GEWARTOWSKI, K., BARTNIK, E. & STEPIEN, P. P. 2010. Human mitochondrial RNA turnover caught in flagranti: involvement of hSuv3p helicase in RNA surveillance. *Nucleic acids research*, 38, 279-298.

SZCZESNY, R. J., OBRIOT, H., PACZKOWSKA, A., JEDRZEJCZAK, R., DMOCHOWSKA, A., BARTNIK, E., FORMSTECHER, P., POLAKOWSKA, R. & STEPIEN, P. P. 2007. Down-regulation of human RNA/DNA helicase SUV3 induces apoptosis by a caspase- and AIF-dependent pathway. *Biol Cell*, 99, 323-32.

TAKEUCHI, N., KAWAKAMI, M., OMORI, A., UEDA, T., SPREMULLI, L. L. & WATANABE, K. 1998. Mammalian mitochondrial methionyl-tRNA transformylase from bovine liver. Purification, characterization, and gene structure. *J Biol Chem*, 273, 15085-90.

TAVENDER, T. J. & BULLEID, N. J. 2010. Peroxiredoxin IV protects cells from oxidative stress by removing H₂O₂ produced during disulphide formation. *Journal of Cell Science*, 123, 2672-2679.

TAYLOR, F. J. R. 1974. II. IMPLICATIONS AND EXTENSIONS OF THE SERIAL ENDOSYMBIOSIS THEORY OF THE ORIGIN OF EUKARYOTES. *TAXON*, 23, 229-258.

TEMPERLEY, R., RICHTER, R., DENNERLEIN, S., LIGHTOWLERS, R. N. & CHRZANOWSKA-LIGHTOWLERS, Z. M. 2010a. Hungry Codons Promote Frameshifting in Human Mitochondrial Ribosomes. *Science*, 327, 301-301.

TEMPERLEY, R. J., SENECA, S. H., TONSKA, K., BARTNIK, E., BINDOFF, L. A., LIGHTOWLERS, R. N. & CHRZANOWSKA-LIGHTOWLERS, Z. M. A. 2003. Investigation of a pathogenic mtDNA

microdeletion reveals a translation-dependent deadenylation decay pathway in human mitochondria. *Human Molecular Genetics*, 12, 2341-2348.

TEMPERLEY, R. J., WYDRO, M., LIGHTOWLERS, R. N. & CHRZANOWSKA-LIGHTOWLERS, Z. M. 2010b. Human mitochondrial mRNAs—like members of all families, similar but different. *Biochimica et Biophysica Acta (BBA) - Bioenergetics*, 1797, 1081-1085.

TERZIOGLU, M., RUZZENENTE, B., HARMEL, J., MOURIER, A., JEMT, E., LÓPEZ, M. D., KUKAT, C., STEWART, J. B., WIBOM, R., MEHARG, C., HABERMANN, B., FALKENBERG, M., GUSTAFSSON, C. M., PARK, C. B. & LARSSON, N. G. 2013. MTERF1 binds mtDNA to prevent transcriptional interference at the light-strand promoter but is dispensable for rRNA gene transcription regulation. *Cell Metab*, 17, 618-26.

THORSNESS, P. E. & FOX, T. D. 1990. Escape of DNA from mitochondria to the nucleus in *Saccharomyces cerevisiae*. *Nature*, 346, 376.

TOMECKI, R., DMOCHOWSKA, A., GEWARTOWSKI, K., DZIEMBOWSKI, A. & STEPIEN, P. P. 2004. Identification of a novel human nuclear-encoded mitochondrial poly(A) polymerase. *Nucleic Acids Research*, 32, 6001-6014.

TRCEK, T., SATO, H., SINGER, R. H. & MAQUAT, L. E. 2013. Temporal and spatial characterization of nonsense-mediated mRNA decay. *Genes & development*, 27, 541-551.

TRUSCOTT, K. N., KOVERMANN, P., GEISSLER, A., MERLIN, A., MEIJER, M., DRIESSEN, A. J. M., RASSOW, J., PFANNER, N. & WAGNER, R. 2001. A presequence- and voltage-sensitive channel of the mitochondrial preprotein translocase formed by Tim23. *Nature Structural Biology*, 8, 1074-1082.

TSAI, C.-L. & BARONDEAU, D. P. 2010. Human Frataxin Is an Allosteric Switch That Activates the Fe-S Cluster Biosynthetic Complex. *Biochemistry*, 49, 9132-9139.

TSUBOI, M., MORITA, H., NOZAKI, Y., AKAMA, K., UEDA, T., ITO, K., NIERHAUS, K. H. & TAKEUCHI, N. 2009. EF-G2mt Is an Exclusive Recycling Factor in Mammalian Mitochondrial Protein Synthesis. *Molecular Cell*, 35, 502-510.

TSUCHIYA, N., OCHIAI, M., NAKASHIMA, K., UBAGAI, T., SUGIMURA, T. & NAKAGAMA, H. 2007. SND1, a Component of RNA-Induced Silencing Complex, Is Up-regulated in Human Colon Cancers and Implicated in Early Stage Colon Carcinogenesis. *Cancer Research*, 67, 9568-9576.

TSUKIHARA, T., AOYAMA, H., YAMASHITA, E., TOMIZAKI, T., YAMAGUCHI, H., SHINZAWA-ITO, K., NAKASHIMA, R., YAONO, R. & YOSHIKAWA, S. 1996. The Whole Structure of the 13-Subunit Oxidized Cytochrome c Oxidase at 2.8 Å. *Science*, 272, 1136-1144.

TU, Y. T. & BARRIENTOS, A. 2015. The Human Mitochondrial DEAD-Box Protein DDX28 Resides in RNA Granules and Functions in Mitoribosome Assembly. *Cell Rep*, 10, 854-864.

TUCCI, A., LIU, Y. T., PREZA, E., PITCEATHLY, R. D., CHALASANI, A., PLAGNOL, V., LAND, J. M., TRABZUNI, D., RYTEN, M., JAUNMUKTANE, Z., REILLY, M. M., BRANDNER, S., HARGREAVES, I., HARDY, J., SINGLETON, A. B., ABRAMOV, A. Y. & HOULDEN, H. 2014. Novel C12orf65 mutations in patients with axonal neuropathy and optic atrophy. *J Neurol Neurosurg Psychiatry*, 85, 486-92.

TUCKER, E. J., HERSHMAN, S. G., KÖHRER, C., BELCHER-TIMME, C. A., PATEL, J., GOLDBERGER, O. A., CHRISTODOULOU, J., SILBERSTEIN, J. M., MCKENZIE, M., RYAN, M. T., COMPTON, A. G., JAFFE, J. D., CARR, S. A., CALVO, S. E., RAJBHANDARY, U. L., THORBURN, D. R. & MOOTHA, V. K. 2011. Mutations in MTFMT underlie a human disorder of formylation causing impaired mitochondrial translation. *Cell Metabolism*, 14, 428-434.

TULADHAR, R., YEU, Y., TYLER PIAZZA, J., TAN, Z., RENE CLEMENCEAU, J., WU, X., BARRETT, Q., HERBERT, J., MATHEWS, D. H., KIM, J., HYUN HWANG, T. & LUM, L. 2019. CRISPR-Cas9-based mutagenesis frequently provokes on-target mRNA misregulation. *Nature Communications*, 10, 4056.

TYANOVA, S., TEMU, T., SINITCYN, P., CARLSON, A., HEIN, M. Y., GEIGER, T., MANN, M. & COX, J. 2016. The Perseus computational platform for comprehensive analysis of (prote)omics data. *Nature Methods*, 13, 731-740.

UDAGAWA, T., SHIMIZU, Y. & UEDA, T. 2004. Evidence for the Translation Initiation of Leaderless mRNAs by the Intact 70 S Ribosome without Its Dissociation into Subunits in Eubacteria*. *Journal of Biological Chemistry*, 279, 8539-8546.

UZZELL, T. & SPOLSKY, C. 1974. Mitochondria and plastids as endosymbionts: a revival of special creation? *American Scientist*, 62, 334-343.

VADLAPUDI, A. D., VADLAPATLA, R. K. & MITRA, A. K. 2012. Sodium dependent multivitamin transporter (SMVT): a potential target for drug delivery. *Current drug targets*, 13, 994-1003.

VAKIFAHMETOGLU-NORBERG, H., OUCHIDA, A. T. & NORBERG, E. 2017. The role of mitochondria in metabolism and cell death. *Biochemical and Biophysical Research Communications*, 482, 426-431.

VALENTE, L., TIRANTI, V., MARSANO, R. M., MALFATTI, E., FERNANDEZ-VIZARRA, E., DONNINI, C., MEREGHETTI, P., DE GIOIA, L., BURLINA, A., CASTELLAN, C., COMI, G. P., SAVASTA, S., FERRERO, I. & ZEVIANI, M. 2007. Infantile Encephalopathy and Defective Mitochondrial DNA Translation in Patients with Mutations of Mitochondrial Elongation Factors EFG1 and EFTu. *The American Journal of Human Genetics*, 80, 44-58.

VALKO, M., LEIBFRITZ, D., MONCOL, J., CRONIN, M. T. D., MAZUR, M. & TELSER, J. 2007. Free radicals and antioxidants in normal physiological functions and human disease. *The International Journal of Biochemistry & Cell Biology*, 39, 44-84.

VAN BELZEN, N., DIESVELD, M. P. G., VAN DER MADE, A. C. J., NOZAWA, Y., DINJENS, W. N. M., VLIETSTRA, R., TRAPMAN, J. & BOSMAN, F. T. 1995. Identification of mRNAs that Show Modulated Expression During Colon Carcinoma Cell Differentiation. *European Journal of Biochemistry*, 234, 843-848.

VAN VRANKEN, J. G., JEONG, M. Y., WEI, P., CHEN, Y. C., GYGI, S. P., WINGE, D. R. & RUTTER, J. 2016. The mitochondrial acyl carrier protein (ACP) coordinates mitochondrial fatty acid synthesis with iron sulfur cluster biogenesis. *Elife*, 5.

VARANITA, T., SORIANO, MARIA E., ROMANELLO, V., ZAGLIA, T., QUINTANA-CABRERA, R., SEMENZATO, M., MENABÒ, R., COSTA, V., CIVILETTO, G., PESCE, P., VISCOMI, C., ZEVIANI, M., DI LISA, F., MONGILLO, M., SANDRI, M. & SCORRANO, L. 2015. The Opa1-Dependent Mitochondrial Cristae Remodeling Pathway Controls Atrophic, Apoptotic, and Ischemic Tissue Damage. *Cell Metabolism*, 21, 834-844.

VARDI-OKNIN, D. & ARAVA, Y. 2019. Characterization of Factors Involved in Localized Translation Near Mitochondria by Ribosome-Proximity Labeling. *Frontiers in Cell and Developmental Biology*, 7.

VÁZQUEZ-ACEVEDO, M., ANTARAMIAN, A., CORONA, N. & GONZÁLEZ-HALPHEN, D. 1993. Subunit structures of purified beef mitochondrial cytochromebc1 complex from liver and heart. *Journal of Bioenergetics and Biomembranes*, 25, 401-410.

VENKATARAMAN, K., ZAFAR, H. & KARZAI, A. W. 2014. Distinct tmRNA sequence elements facilitate RNase R engagement on rescued ribosomes for selective nonstop mRNA decay. *Nucleic acids research*, 42, 11192-11202.

VILARDO, E., NACHBAGAUER, C., BUZET, A., TASCHNER, A., HOLZMANN, J. & ROSSMANITH, W. 2012. A subcomplex of human mitochondrial RNase P is a bifunctional methyltransferase--extensive moonlighting in mitochondrial tRNA biogenesis. *Nucleic acids research*, 40, 11583-11593.

VILARDO, E., NACHBAGAUER, C., BUZET, A., TASCHNER, A., HOLZMANN, J. & ROSSMANITH, W. 2018. A subcomplex of human mitochondrial RNase P is a bifunctional methyltransferase - extensive moonlighting in mitochondrial tRNA biogenesis. *Nucleic Acids Res*, 46, 11126-11127.

VILCHEZ, D., SAEZ, I. & DILLIN, A. 2014. The role of protein clearance mechanisms in organismal ageing and age-related diseases. *Nature Communications*, 5, 5659.

VINOTHKUMAR, K. R., ZHU, J. & HIRST, J. 2014. Architecture of mammalian respiratory complex I. *Nature*, 515, 80-84.

VOGEL, F., BORNHÖVD, C., NEUPERT, W. & REICHERT, A. S. 2006. Dynamic subcompartmentalization of the mitochondrial inner membrane. *J Cell Biol*, 175, 237-47.

VÖGTLER, F. N., WORTELKAMP, S., ZAHEDI, R. P., BECKER, D., LEIDHOLD, C., GEVAERT, K., KELLERMANN, J., VOOS, W., SICKMANN, A., PFANNER, N. & MEISINGER, C. 2009. Global Analysis of the Mitochondrial N-Proteome Identifies a Processing Peptidase Critical for Protein Stability. *Cell*, 139, 428-439.

VOLEMAN, L. & DOLEŽAL, P. 2019. Mitochondrial dynamics in parasitic protists. *PLoS pathogens*, 15, e1008008-e1008008.

WAGNER, K., GEBERT, N., GUIARD, B., BRANDNER, K., TRUSCOTT, K. N., WIEDEMANN, N., PFANNER, N. & REHLING, P. 2008. The Assembly Pathway of the Mitochondrial Carrier Translocase Involves Four Preprotein Translocases. *Molecular and Cellular Biology*, 28, 4251-4260.

WAI, T., AO, A., ZHANG, X., CYR, D., DUFORT, D. & SHOUBRIDGE, E. A. 2010. The role of mitochondrial DNA copy number in mammalian fertility. *Biology of reproduction*, 83, 52-62.

WALBERG, M. W. & CLAYTON, D. A. 1981. Sequence and properties of the human KB cell and mouse L cell D-loop regions of mitochondrial DNA. *Nucleic Acids Res*, 9, 5411-21.

WALDROP, G. L., HOLDEN, H. M. & ST MAURICE, M. 2012. The enzymes of biotin dependent CO₂ metabolism: what structures reveal about their reaction mechanisms. *Protein science : a publication of the Protein Society*, 21, 1597-1619.

WALKER, J. R., CORPINA, R. A. & GOLDBERG, J. 2001. Structure of the Ku heterodimer bound to DNA and its implications for double-strand break repair. *Nature*, 412, 607-14.

WALKUP, A. S. & APPLING, D. R. 2005. Enzymatic characterization of human mitochondrial C1-tetrahydrofolate synthase. *Arch Biochem Biophys*, 442, 196-205.

WANG, G., WU, W. W., ZHANG, Z., MASILAMANI, S. & SHEN, R.-F. 2009. Decoy Methods for Assessing False Positives and False Discovery Rates in Shotgun Proteomics. *Analytical Chemistry*, 81, 146-159.

WANG, T., MA, F. & QIAN, H.-L. 2021. Defueling the cancer: ATP synthase as an emerging target in cancer therapy. *Molecular Therapy - Oncolytics*, 23, 82-95.

WANG, Y. & BOGENHAGEN, D. F. 2006. Human mitochondrial DNA nucleoids are linked to protein folding machinery and metabolic enzymes at the mitochondrial inner membrane. *J Biol Chem*, 281, 25791-802.

WANROOIJ, S., FUSTÉ, J. M., FARGE, G., SHI, Y., GUSTAFSSON, C. M. & FALKENBERG, M. 2008. Human mitochondrial RNA polymerase primes lagging-strand DNA synthesis in vitro. *Proc Natl Acad Sci U S A*, 105, 11122-7.

WATT, I. N., MONTGOMERY, M. G., RUNSWICK, M. J., LESLIE, A. G. W. & WALKER, J. E. 2010. Bioenergetic cost of making an adenosine triphosphate molecule in animal mitochondria. *Proceedings of the National Academy of Sciences of the United States of America*, 107, 16823-16827.

WEI, Q., WANG, S., YAO, J., LU, Y., CHEN, Z., XING, G. & CAO, X. 2013. Genetic mutations of GJB2 and mitochondrial 12S rRNA in nonsyndromic hearing loss in Jiangsu Province of China. *J Transl Med*, 11, 163.

WEIXLBAUMER, A., JIN, H., NEUBAUER, C., VOORHEES, R. M., PETRY, S., KELLEY, A. C. & RAMAKRISHNAN, V. 2008. Insights into Translational Termination from the Structure of RF2 Bound to the Ribosome. *Science*, 322, 953-956.

WERAARPACHAI, W., ANTONICKA, H., SASARMAN, F., SEEGER, J., SCHRANK, B., KOLESAR, J. E., LOCHMÜLLER, H., CHEVRETTE, M., KAUFMAN, B. A., HORVATH, R. & SHOUBRIDGE, E. A. 2009. Mutation in TACO1, encoding a translational activator of COX I, results in cytochrome c oxidase deficiency and late-onset Leigh syndrome. *Nature Genetics*, 41, 833-837.

WESOLOWSKA, M., GORMAN, G. S., ALSTON, C. L., PAJAK, A., PYLE, A., HE, L., GRIFFIN, H., CHINNERY, P. F., MILLER, J. A., SCHAEFER, A. M., TAYLOR, R. W., LIGHTOWLERS, R. N. & CHRZANOWSKA-LIGHTOWLERS, Z. M. 2015. Adult Onset Leigh Syndrome in the Intensive Care Setting: A Novel Presentation of a C12orf65 Related Mitochondrial Disease. *J Neuromuscul Dis*, 2, 409-419.

WESOLOWSKA, M. T. 2015. *Developing mitoribosomal profiling to investigate quality control of human mitochondrial protein synthesis*. PhD, Newcastle University.

WESOLOWSKA, M. T., RICHTER-DENNERLEIN, R., LIGHTOWLERS, R. N. & CHRZANOWSKA-LIGHTOWLERS, Z. M. A. 2014. Overcoming stalled translation in human mitochondria. *Frontiers in Microbiology*, 5.

WICKRAMASINGHE, S. N. 1996. Culture of animal cells. A manual of basic technique, 3rd edn. R. Ian Freshney, Wiley-Liss, Inc: New York. xxiv + 486 pages (1994). *Cell Biochemistry and Function*, 14, 75-76.

WIDLAK, P., LI, L. Y., WANG, X. & GARRARD, W. T. 2001. Action of recombinant human apoptotic endonuclease G on naked DNA and chromatin substrates: cooperation with exonuclease and DNase I. *J Biol Chem*, 276, 48404-9.

WIEDEMANN, N. & PFANNER, N. 2017. Mitochondrial Machineries for Protein Import and Assembly. *Annual Review of Biochemistry*, 86, 685-714.

WIEDEMANN, N., PFANNER, N. & RYAN, M. T. 2001. The three modules of ADP/ATP carrier cooperate in receptor recruitment and translocation into mitochondria. *The EMBO Journal*, 20, 951-960.

WIEDEMANN, N., TRUSCOTT, K. N., PFANNSCHMIDT, S., GUIARD, B., MEISINGER, C. & PFANNER, N. 2004. Biogenesis of the protein import channel Tom40 of the mitochondrial outer membrane: intermembrane space components are involved in an early stage of the assembly pathway. *J Biol Chem*, 279, 18188-94.

WIEDENHEFT, B., STERNBERG, S. H. & DOUDNA, J. A. 2012. RNA-guided genetic silencing systems in bacteria and archaea. *Nature*, 482, 331-338.

WIESNER, R. J., RÜEGG, J. C. & MORANO, I. 1992. Counting target molecules by exponential polymerase chain reaction: Copy number of mitochondrial DNA in rat tissues. *Biochemical and Biophysical Research Communications*, 183, 553-559.

WIKSTROM, M. K. F. 1977. Proton pump coupled to cytochrome c oxidase in mitochondria. *Nature*, 266, 271-273.

WILSON, W. C., HORNING-DO, H.-T., BRUNI, F., CHANG, J. H., JOURDAIN, A. A., MARTINOU, J.-C., FALKENBERG, M., SPÅHR, H., LARSSON, N.-G., LEWIS, R. J., HEWITT, L., BASLÉ, A., CROSS, H. E., TONG, L., LEBEL, R. R., CROSBY, A. H., CHRZANOWSKA-LIGHTOWLERS, Z. M. A. & LIGHTOWLERS, R. N. 2014. A human mitochondrial poly(A) polymerase mutation reveals the complexities of post-transcriptional mitochondrial gene expression. *Human Molecular Genetics*, 23, 6345-6355.

WITTERS, L. A., WIDMER, J., KING, A. N., FASSIHI, K. & KUHAJDA, F. 1994. Identification of human acetyl-CoA carboxylase isozymes in tissue and in breast cancer cells. *Int J Biochem*, 26, 589-94.

WONG, H.-S., BENOIT, B. & BRAND, M. D. 2019. Mitochondrial and cytosolic sources of hydrogen peroxide in resting C2C12 myoblasts. *Free Radical Biology and Medicine*, 130, 140-150.

WONG, T. W. & CLAYTON, D. A. 1985. In vitro replication of human mitochondrial DNA: accurate initiation at the origin of light-strand synthesis. *Cell*, 42, 951-8.

XING, G., CHEN, Z. & CAO, X. 2007. Mitochondrial rRNA and tRNA and hearing function. *Cell Res*, 17, 227-39.

XU, W., BARRIENTOS, T. & ANDREWS, N. C. 2013. Iron and copper in mitochondrial diseases. *Cell metabolism*, 17, 319-328.

YAHALOMI, D., ATKINSON, S. D., NEUHOF, M., CHANG, E. S., PHILIPPE, H., CARTWRIGHT, P., BARTHOLOMEW, J. L. & HUCHON, D. 2020. A cnidarian parasite of salmon (Myxozoa: Henneguya) lacks a mitochondrial genome. *Proc Natl Acad Sci U S A*, 117, 5358-5363.

YAKUBOVSKAYA, E., MEJIA, E., BYRNES, J., HAMBARDJIEVA, E. & GARCIA-DIAZ, M. 2010. Helix Unwinding and Base Flipping Enable Human MTERF1 to Terminate Mitochondrial Transcription. *Cell*, 141, 982-993.

YAMANO, K., YATSUKAWA, Y.-I., ESAKI, M., HOBBS, A. E. A., JENSEN, R. E. & ENDO, T. 2008. Tom20 and Tom22 Share the Common Signal Recognition Pathway in Mitochondrial Protein Import. *Journal of Biological Chemistry*, 283, 3799-3807.

YANG, D., OYAIKU, Y., OYAIKU, H., OLSEN, G. J. & WOESE, C. R. 1985. Mitochondrial origins. *Proceedings of the National Academy of Sciences*, 82, 4443-4447.

YANG, F., GAO, Y., LI, Z., CHEN, L., XIA, Z., XU, T. & QIN, Y. 2014. Mitochondrial EF4 links respiratory dysfunction and cytoplasmic translation in *Caenorhabditis elegans*. *Biochim Biophys Acta*, 1837, 1674-83.

YANG, M. Y., BOWMAKER, M., REYES, A., VERGANI, L., ANGELI, P., GRINGERI, E., JACOBS, H. T. & HOLT, I. J. 2002. Biased incorporation of ribonucleotides on the mitochondrial L-strand accounts for apparent strand-asymmetric DNA replication. *Cell*, 111, 495-505.

YANG, Q.-H., CHURCH-HAJDUK, R., REN, J., NEWTON, M. L. & DU, C. 2003. Omi/HtrA2 catalytic cleavage of inhibitor of apoptosis (IAP) irreversibly inactivates IAPs and facilitates caspase activity in apoptosis. *Genes & development*, 17, 1487-1496.

YASSIN, A. S., HAQUE, M. E., DATTA, P. P., ELMORE, K., BANAVALI, N. K., SPREMULLI, L. L. & AGRAWAL, R. K. 2011. Insertion domain within mammalian mitochondrial translation initiation factor 2

serves the role of eubacterial initiation factor 1. *Proceedings of the National Academy of Sciences of the United States of America*, 108, 3918-3923.

YASUKAWA, T., REYES, A., CLUETT, T. J., YANG, M. Y., BOWMAKER, M., JACOBS, H. T. & HOLT, I. J. 2006. Replication of vertebrate mitochondrial DNA entails transient ribonucleotide incorporation throughout the lagging strand. *Embo J*, 25, 5358-71.

YE, H., CANDE, C., STEPHANOU, N. C., JIANG, S., GURBUXANI, S., LAROCHELLE, N., DAUGAS, E., GARRIDO, C., KROEMER, G. & WU, H. 2002. DNA binding is required for the apoptogenic action of apoptosis inducing factor. *Nature Structural Biology*, 9, 680-684.

YOSHIKAWA, S., MURAMOTO, K., SHINZAWA-ITO, K., AOYAMA, H., TSUKIHARA, T., OGURA, T., SHIMOKATA, K., KATAYAMA, Y. & SHIMADA, H. 2006. Reaction mechanism of bovine heart cytochrome c oxidase. *Biochimica et Biophysica Acta (BBA) - Bioenergetics*, 1757, 395-400.

YOUN, J. Y., DUNHAM, W. H., HONG, S. J., KNIGHT, J. D. R., BASHKUROV, M., CHEN, G. I., BAGCI, H., RATHOD, B., MACLEOD, G., ENG, S. W. M., ANGERS, S., MORRIS, Q., FABIAN, M., CÔTÉ, J. F. & GINGRAS, A. C. 2018. High-Density Proximity Mapping Reveals the Subcellular Organization of mRNA-Associated Granules and Bodies. *Mol Cell*, 69, 517-532.e11.

YOUNG, D. J., EDGAR, C. D., MURPHY, J., FREDEBOHM, J., POOLE, E. S. & TATE, W. P. 2010. Bioinformatic, structural, and functional analyses support release factor-like MTRF1 as a protein able to decode nonstandard stop codons beginning with adenine in vertebrate mitochondria. *Rna*, 16, 1146-55.

YOUNG, J. C., HOOGENRAAD, N. J. & HARTL, F. U. 2003. Molecular Chaperones Hsp90 and Hsp70 Deliver Preproteins to the Mitochondrial Import Receptor Tom70. *Cell*, 112, 41-50.

YU, Z., O'FARRELL, P. H., YAKUBOVICH, N. & DELUCA, S. Z. 2017. The Mitochondrial DNA Polymerase Promotes Elimination of Paternal Mitochondrial Genomes. *Current Biology*, 27, 1033-1039.

YUSUPOVA, G. Z., YUSUPOV, M. M., CATE, J. H. & NOLLER, H. F. 2001. The path of messenger RNA through the ribosome. *Cell*, 106, 233-41.

ZENG, F. & JIN, H. 2018. Conformation of methylated GGQ in the Peptidyl Transferase Center during Translation Termination. *Scientific reports*, 8, 2349-2349.

ZHANG, H., BARCELÓ, J. M., LEE, B., KOHLHAGEN, G., ZIMONJIC, D. B., POPESCU, N. C. & POMMIER, Y. 2001. Human mitochondrial topoisomerase I. *Proc Natl Acad Sci U S A*, 98, 10608-13.

ZHANG, J.-P., LI, X.-L., LI, G.-H., CHEN, W., ARAKAKI, C., BOTIMER, G. D., BAYLINK, D., ZHANG, L., WEN, W., FU, Y.-W., XU, J., CHUN, N., YUAN, W., CHENG, T. & ZHANG, X.-B. 2017. Efficient precise knockin with a double cut HDR donor after CRISPR/Cas9-mediated double-stranded DNA cleavage. *Genome Biology*, 18, 35.

ZHANG, X.-H., TEE, L. Y., WANG, X.-G., HUANG, Q.-S. & YANG, S.-H. 2015a. Off-target Effects in CRISPR/Cas9-mediated Genome Engineering. *Molecular Therapy - Nucleic Acids*, 4, e264.

ZHANG, Y., FONSLOW, B. R., SHAN, B., BAEK, M.-C. & YATES, J. R., 3RD 2013. Protein analysis by shotgun/bottom-up proteomics. *Chemical reviews*, 113, 2343-2394.

ZHANG, Y., MANDAVA, C. S., CAO, W., LI, X., ZHANG, D., LI, N., ZHANG, Y., ZHANG, X., QIN, Y., MI, K., LEI, J., SANYAL, S. & GAO, N. 2015b. HflX is a ribosome-splitting factor rescuing stalled ribosomes under stress conditions. *Nature Structural & Molecular Biology*, 22, 906-913.

ZHANG, Y. & SPREMULLI, L. L. 1998. Identification and cloning of human mitochondrial translational release factor 1 and the ribosome recycling factor. *Biochim Biophys Acta*, 1443, 245-50.

ZHANG, Z., HUANG, L., SHULMEISTER, V. M., CHI, Y. I., KIM, K. K., HUNG, L. W., CROFTS, A. R., BERRY, E. A. & KIM, S. H. 1998. Electron transfer by domain movement in cytochrome bc1. *Nature*, 392, 677-684.

ZHENG, L., NAGAR, M., MAURAIS, A. J., SLADE, D. J., PARELKAR, S. S., COONROD, S. A., WEERAPANA, E. & THOMPSON, P. R. 2019. Calcium Regulates the Nuclear Localization of Protein Arginine Deiminase 2. *Biochemistry*, 58, 3042-3056.

ZHENG, W., KHRAPKO, K., COLLER, H. A., THILLY, W. G. & COPELAND, W. C. 2006. Origins of human mitochondrial point mutations as DNA polymerase γ -mediated errors. *Mutation Research/Fundamental and Molecular Mechanisms of Mutagenesis*, 599, 11-20.

ZHOU, A., ROHOU, A., SCHEP, D. G., BASON, J. V., MONTGOMERY, M. G., WALKER, J. E., GRIGORIEFF, N. & RUBINSTEIN, J. L. 2015. Structure and conformational states of the bovine mitochondrial ATP synthase by cryo-EM. *Elife*, 4, e10180.

ZHU, P., LIU, Y., ZHANG, F., BAI, X., CHEN, Z., SHANGGUAN, F., ZHANG, B., ZHANG, L., CHEN, Q., XIE, D., LAN, L., XUE, X., LIANG, X. J., LU, B., WEI, T. & QIN, Y. 2018. Human Elongation Factor 4 Regulates Cancer Bioenergetics by Acting as a Mitochondrial Translation Switch. *Cancer Res*, 78, 2813-2824.

ZICKERMANN, V., WIRTH, C., NASIRI, H., SIEGMUND, K., SCHWALBE, H., HUNTE, C. & BRANDT, U. 2015. Mechanistic insight from the crystal structure of mitochondrial complex I. *Science*, 347, 44-49.

ZORKAU, M., ALBUS, C. A., BERLINGUER-PALMINI, R., CHRZANOWSKA-LIGHTOWLERS, Z. M. A. & LIGHTOWLERS, R. N. 2021. High-resolution imaging reveals compartmentalization of mitochondrial protein synthesis in cultured human cells. *Proceedings of the National Academy of Sciences*, 118, e2008778118.

ZOU, H., HENZEL, W. J., LIU, X., LUTSCHG, A. & WANG, X. 1997. Apaf-1, a human protein homologous to *C. elegans* CED-4, participates in cytochrome c-dependent activation of caspase-3. *Cell*, 90, 405-13.